AD-A124 884   ENHANCED TRACKING OF AIRBORNE TARGETS USING A   1/4
CORRELATOR/KALMAN FILTER(U) AIR FORCE INST OF TECH
WRIGHT-PATTERSON AFB OH SCHOOL OF ENGINEERING
UNCLASSIFIED   P P MILLNER DEC 82 AFIT/GE/EE/82D-50   F/G 12/1   NL

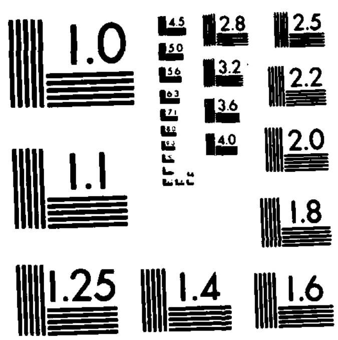

MICROCOPY RESOLUTION TEST CHART
NATIONAL BUREAU OF STANDARDS-1963-A

ENHANCED TRACKING OF AIRBORNE TARGETS USING A CORRELATOR/KALMAN FILTER

THESIS

AFIT/GE/EE/82D-50 Paul P. Millner
CPT US Army

DEPARTMENT OF THE AIR FORCE
AIR UNIVERSITY (ATC)
AIR FORCE INSTITUTE OF TECHNOLOGY

Wright-Patterson Air Force Base, Ohio

UNCLASSIFIED

SECURITY CLASSIFICATION OF THIS PAGE (When Data Entered)

REPORT DOCUMENTATION PAGE		READ INSTRUCTIONS BEFORE COMPLETING FORM
1. REPORT NUMBER AFIT/GE/EE/82D-50	2. GOVT ACCESSION NO. AD-A124 884	3. RECIPIENT'S CATALOG NUMBER
4. TITLE (and Subtitle) ENHANCED TRACKING OF AIRBORNE TARGETS USING A CORRELATOR/KALMAN FILTER		5. TYPE OF REPORT & PERIOD COVERED MS Thesis 6. PERFORMING ORG. REPORT NUMBER
7. AUTHOR(s) Paul P. Millner, Captain, US Army		8. CONTRACT OR GRANT NUMBER(s)
9. PERFORMING ORGANIZATION NAME AND ADDRESS Air Force Institute of Technology (AFIT-EN) Wright-Pattersnon AFB, Ohio 45433		10. PROGRAM ELEMENT, PROJECT, TASK AREA & WORK UNIT NUMBERS
11. CONTROLLING OFFICE NAME AND ADDRESS		12. REPORT DATE December 1982 13. NUMBER OF PAGES 357
14. MONITORING AGENCY NAME & ADDRESS(if different from Controlling Office)		15. SECURITY CLASS. (of this report) Unclassified 15a. DECLASSIFICATION/DOWNGRADING SCHEDULE

16. DISTRIBUTION STATEMENT (of this Report)

Approved for public release; distribution unlimited

17. DISTRIBUTION STATEMENT (of the abstract entered in Block 20, if different from Report)

18. SUPPLEMENTARY NOTES

~~Approved for public release; IAW AFR 190-17~~

4 JAN 1983

Approved for public release: IAW AFR 190-17.

LYNN E. WOLAVER
Dean for Research and Professional Development
Air Force Institute of Technology (ATC)
Wright-Patterson AFB OH 45433

19. KEY WORDS (Continue on reverse side if necessary and identify by block number)

Kalman Filter
Adaptive Estimation
Target Tracking
Forward Looking Infrared Systems
Correlators
Fast Fourier Transforms

20. ABSTRACT (Continue on reverse side if necessary and identify by block number)

Over the past four years considerable work has been accomplished at the Air Force Institute of Technology to improve the tracking capability of the high energy laser weapon against airborne targets. In this research, many of the prior concepts are incorporated into a correlator/Kalman filter to develop a tracker capable of providing precise target position estimates in a dynamic short-range environment using a Foward

DD FORM 1473, 1 JAN 73 EDITION OF 1 NOV 65 IS OBSOLETE

Looking Infrared sensor (FLIR) to provide measurement data. Digital signal processing is employed on the FLIR data to identify the underlying target intensity shape function when the target under consideration has either single or multiple "hot spots". The estimated target shape function is then used as the template in a correlation algorithm, where spatial and frequency domain correlation techniques were explored, to determine the offsets between the template and the incoming measurement. These offsets are used as "pseudomeasurements" in a linear Kalman filter which exploits knowledge of the process dynamics and statistical knowledge of the correlator errors to enhance the position estimates.

AFIT/GE/EE/82D-50

ENHANCED TRACKING OF AIRBORNE TARGETS USING A CORRELATOR/KALMAN FILTER

THESIS

AFIT/GE/EE/82D-50 Paul P. Millner
CPT US Army

Approved for public release; distribution unlimited

AFIT/GE/EE/82D-50

ENHANCED TRACKING OF AIRBORNE TARGETS USING A CORRELATOR/KALMAN FILTER

THESIS

Presented to the Faculty of the School of Engineering
of the Air Force Institute of Technology
Air University
in Partial Fulfillment of the
Requirements for the Degree of
Master of Science

by
Paul P. Millner, B.S.
CPT US Army
Graduate Electrical Engineering
December 1982

Approved for public release; distribution unlimited.

Preface

This study is part of a continuing effort to design a tracking system for use in a ground based laser system under development by the Air Force Weapons Laboratory. A correlator/Kalman filter which uses infrared sensor data was synthesized and tested.

I wish to express my appreciation to my thesis advisor, Dr. Peter S. Maybeck, for his expert guidance and enthusiastic support during this project.

Contents

		Page
Preface		ii
List of Figures		v
List of Tables		vii
List of Symbols		viii
Abstract		x
I.	Introduction	1
	1.1 Background	1
	1.2 Problem Overview	4
	1.3 Plan of Attack	11
	1.4 Overview	12
II.	Truth Model	14
	2.1 Introduction	14
	2.2 Target Model	14
	2.3 Trajectory Description	21
	2.4 Measurement Model	29
	2.5 Projection of Multiple Hot Spots	36
III.	Kalman Filter	49
	3.1 Introduction	49
	3.2 Acceleration and Atmospheric Models	50
	3.3 State Space Model	51
	3.4 State Propagation	55
	3.5 Measurement Update Equation	59
	3.6 $\underline{Q}_D$ Estimation	60
IV.	Methods of Correlation	64
	4.1 Introduction	64
	4.2 Image Resolution	65
	4.3 Correlation Methods	66
	4.4 Maximum Correlation Detection	77
	4.5 Analysis of Correlation Methods	83

Contents

		Page
V.	Performance Analysis	98
5.1	Introduction	98
5.2	Tracking Ability	98
5.3	Variation of Truth Model Parameters . .	100
5.4	Variation of Data Processing Parameters	101
5.5	Variation of Filter Parameters	102
5.6	Plotting Results	104
5.7	Analysis of Filter Performance	115
5.8	Evaluation of Correlation Methods . . .	117
5.9	Evaluation of Harnly and Jensen EKF . .	118
5.10	Evaluations Using Trajectory 1	134
5.11	Evaluation for Rolling Maneuvers. . . .	136
5.12	Evaluation for a Two-G Pullup Maneuver.	139
5.13	Evaluation for a Five-G Pullup Maneuver	141
5.14	Adaptive $\underline{Q}_{fd}$ Estimation Evaluation . .	143
5.15	Maneuvers Out of the x-y Plane	145
5.16	Summary of Test Cases	148
VI.	Conclusions and Recommendations	150
6.1	Introduction	150
6.2	Conclusions	150
6.3	Recommendations	152
Bibliography	. . . .	155
Appendix A:	Intensity Centroid Projection Model for Multiple Hot Spots	157
Appendix B:	Derivation of $\underline{Q}_{fd}$ for the Kalman Filter, Chapter III	164
Appendix C:	Plots of Tracking Errors	169
Appendix D:	Computer Software (Correlator/Kalman Filter)	284
Appendix E:	Computer Software (Trajectory Model) .	351
Vita	. . . .	357

List of Figures

Figure		Page
1	Data Processing Algorithm	5
2	Research Plan of Attack Flow Diagram	11
3	Inertial Coordinate Frame	19
4	Azimuth Geometry	19
5	Elevation Geometry	20
6	Trajectory 1	23
7	Trajectory 2	24
8	Trajectory 4	27
9	Out-of-Plane Coordinate Frame Rotations	28
10	Image Intensity Characteristics	30
11	Image Projection	32
12	Semimajor Axis Projection	33
13	$\vec{e}_{\beta}$-$\vec{e}_{z\alpha}$ Plane	38
14	$\vec{e}_{\beta}$-$\vec{e}_{z\alpha}$ Plane Translation	38
15	$\vec{e}_{\beta}$-$\vec{e}_{z\alpha}$ and H-Frame Unit Vectors	39
16	Initial Ellipsoidal Centers	40
17	Roll Maneuver Geometry	41
18	Hot Spot Offsets	42
19	Distance Translated in $\vec{e}_{\beta}$-$\vec{e}_{z\alpha}$ Plane	43
20	π Radians Roll	47
21	2π Radians Roll	48
22	Functions to be Correlated	67
23	Arrays to be Correlated	69
24	FLIR and Template Arrays	70

List of Figures

Figure		Page
25	Input-Output Relationships	72
26	FFT Correlation (Threshold = .3)	79
27	FFT Correlation (Threshold = .5)	80
28	Thresholding (FFT Correlation Method) . .	81
29	Thresholding (Phase Correlation Method) .	82
30	Histogram of Errors - Direct Method (2-Level Quantization, 1 Hot Spot) . . .	86
31	Histogram of Errors - Direct Method (6-Level Quantization, 1 Hot Spot) . . .	87
32	Histogram of Errors - FFT Method (Threshold = .3, 1 Hot Spot).	88
33	Histogram of Errors - Phase Method (Thresold = .7, 1 Hot Spot)	89
34	Histogram of Errors - Direct Method (2-Level Quantization, 3 Hot Spots) . . .	91
35	Histogram of Errors - Direct Method (G-Level Quantization, 3 Hot Spots) . . .	92
36	Histogram of Errors - FFT Method (Threshold = .3, 3 Hot Spots)	93
37	Histogram of Errors - Phase Method (Thresold = .7, 3 Hot Spots)	94
38(a-j)	Case 1	105-114
39(a-d)	Case A	119-122
40(a-d)	Case B	125-128
41(a-d)	Case C	130-133
A-1	Project on ont the FLIR Plane	163
(C-2)-(C-20)	Case 2-Case 20	170-283

List of Tables

Table		Page
I	Correlation Errors (Single Hot Spot Target)	85
II	Correlation Errors (Three Hot Spot Target)	90
III	Correlator Performance Results	116
IV	Harnly-Jensen EKF Performance	123
V	Trajectory 1 Evaluations	135
VI	Roll Maneuver Elevations	138
VII	Trajectory 2 (Two-g Pullup) Evaluations	140
VIII	Trajectory 2 (Five-g Pullup) Evaluations	142
IX	$\underline{Q}_{fd}$ Estimation Evaluation	144
X	Out of Plane Maneuvers	147
XI	Summary of Test Cases	149

List of Symbols

Symbol	
t	time
$\underline{u}$	deterministic velocity input function
$\underline{v}$	velocity vector
$v_{\perp LOS}$	target velocity component perpendicular to the FLIR image plane line of sight
$\alpha(t)$	azimuth
$\beta(t)$	elevation
γ	angle between velocity vector and image plane
ω	roll rate
ϕ	roll angle
δ	distance from aircraft center of mass to intensity function centroid
σ_g	dispersion of Gaussian intensity function
w	white noise
x_{peak}	horizontal coordinate of Gaussian intensity function maximum
y_{peak}	vertical coordinate of Gaussian intensity function maximum
$\underline{x}$	state vector
$\underline{z}$	measurement vector
I_{max}	maximum intensity received from target
r	range
r_h	horizontal range
T_{df}	correlation time assumed for target acceleration
T_{af}	correlation time assumed for atmospheric jitter

List of Symbols

Symbol	
σ^2_{df}	assumed target acceleration noise variance
σ^2_{af}	assumed target acceleration atmospheric jitter variance
$\hat{\underline{x}}_f(t_i^-)$	propagated filter state estimate vector before measurement incorporation at time t_i
$\hat{\underline{x}}_f(t_i^+)$	filter state estimate vector after measurement incorporation at time t_i
$\underline{P}(t_i^-)$	conditional filter state covariance matrix propagated from time t_{i-1} to time t_i
$\underline{\Phi}_f$	filter state transition matrix
$\underline{F}_f$	filter plant matrix
$\underline{G}_f$	filter noise distribution matrix
$\underline{H}_f$	linear combination of the filter state variables which contribute to the respective measurement elements
$\underline{v}_f$	additive noise corruption
$\underline{Q}_f$	noise covariance kernal descriptor
$^c\sqrt{\ }$	Cholesky square root

subscripts

a	atmospherics
d	dynamics
f	filter
t	true
B	body
H	horizontal

Abstract

Over the past four years considerable work has been accomplished at the Air Force Institute of Technology to improve the tracking capability of the high energy laser weapon against airborne targets. In this research, many of the prior concepts are incorporated into a correlator/Kalman filter to develop a tracker capable of providing precise target position estimates in a dynamic short-range environment using a Forward Looking Infrared sensor (FLIR) to provide measurement data. Digital signal processing is employed on the FLIR data to identify the underlying target intensity shape function when the target under consideration has either single or multiple hot spots. The estimated target shape function is then used as the template in a correlation algorithm, where spatial and frequency domain correlation techniques were explored, to determine the offsets between the template and the incoming measurement. These offsets are used as "pseudomeasurements" in a linear Kalman filter which exploits knowledge of the process dynamics and statistical knowledge of the correlator errors to enhance the position estimates.

ENHANCED TRACKING OF AIRBORNE TARGETS
USING A CORRELATOR/KALMAN FILTER

I. Introduction

The rapid growth in laser technology since the early 1960's has led researchers in a wide variety of disciplines to investigate possible applications of this device. The unique characteristics of the laser make it a highly desirable weapon system, with one prospective military application involving the use of laser energy to destroy airborne targets (1:14-17, 2:16-19). Since the directed energy is transmitted at the speed of light from the source to its destination, the energy arrives at the target almost instantaneously, eliminating the need for lead computation. Additionally, the laser can potentially deposit large amounts of energy on a target in a short period of time, thereby destroying or disabling the target without firing an expensive missile for each engagement opportunity as in conventional systems.

In actual implementation, this system requires a high energy laser, a very accurate pointing system, and a very accurate estimate of the target position. The precise pointing control and target position estimates are required to concentrate the directed energy on a specific part of the target, instead of "painting" the entire target with energy, and to maintain the laser beam on the target long enough to disable the target.

1.1 Background

This study is a continuation of other research projects conducted at the Air Force Institute of Technology

(AFIT) over the past four years which have investigated possible solutions to the target tracking problems associated with directed energy weapons. Currently, the Air Force Weapons Laboratory (AFWL) uses correlation trackers to provide precise target position estimates to feedback controllers in the presence of disturbances. These disturbances include any effect which can cause relative motion between the beam and the target, such as true target motion, atmospheric jitter, and sensor measurement errors (3:2). A correlation tracker compares new target information received from a sensor with a template, consisting of either predetermined or previous real-time data. Correlation techniques are then used to estimate the relative position offsets from one data frame to the next. This relative position information is then used to drive the tracking servo error voltages in azimuth and elevation to keep the target image centered within the sensor's field-of-view (FOV). Although various sensors capable of providing target position information are available, the one currently of the most interest due to its passive nature, and the one which will be used in this research, is the Forward Looking Infra-Red sensor (FLIR) (4).

The correlation algorithm is well suited to many practical applications because this methods requires no a priori information. However, in many tracking situations certain target parameters such as shape, size, and acceleration characteristics are either known or could be estimated, which would enhance the tracker's ability to estimate the true target position. The effects of atmospheric disturbances on radiated waveforms are known and statistical data could be used to separate the true target motion from apparent motion due to disturbances. This separation is crucial since the directed energy beam does not undergo the same distortion as the infrared wavefront eminating from the target. Additionally, statistical data on FLIR noise and background noise is available, and can be used to provide a better estimate of the target's true position (5:222). The desire to exploit this knowledge, unused by the correlation trackers, led researchers at AFIT to investigate the possibility of designing an extended Kalman filter as an alternative to correlation trackers. This method was selected because the reduced computational loading incurred with implementing this filter, when compared to other nonlinear filters is great enough to warrant an evaluation of its performance.

An extended Kalman filter can incorporate estimates of target parameters such as size, shape, and acceleration, as well as statistical information on the effects of atmospheric distortion on radiated wavefronts, and sensor errors, to aid in separating the true target motion from the apparent motion created by disturbances. In initial research efforts, the extended Kalman filter outperformed the correlation tracker against targets exhibiting a single point source of infrared radiation, or "hot spot", when the intensity function was relatively well-known by the filter, and the internal filter structure was designed to depict the tracking environment to be encountered (5,6). The performance enhancement achieved by the extended Kalman filter under these controlled conditions led to further efforts to design a filter capable of accurate tracking in an environment when the target intensity pattern on the FLIR image plane is not well known a priori (7,8). Additionally, as in realistic situations, the tracker has to be capable of tracking targets exhibiting both single and multiple hot spots which change in time, so the target intensity pattern must be identified in real time.

In the thesis by Captain S.K. Rogers (8), a digital processing algorithm was developed which is capable of identifying the target intensity pattern in real time for a single or multiple hot spot target when neither the functional form of the target intensity nor the number of hot spots is known a priori. This algorithm, shown in the upper path of Figure 1 and detailed in section 1.2, was implemented by Rogers in two trackers. The first tracker used the estimated target shape intensity directly in the measurement model of an extended Kalman filter while the second tracker used the estimated target shape as a template in an enhanced correlator to provide target measurement information to a linear Kalman filter. A linear Kalman filter can be utilized in this tracker because the outputs of the correlation algorithm are offset distances which are linear functions of the chosen state variables (see Chapter 3). Both trackers exhibited significant performance potential against targets having benign dynamics, with the extended filter having larger mean errors and the correlator filter having larger standard deviations (8,9). However, the reduced computational burden associated with the actual implementation of the correlator/Kalman filter, and the enhanced potential of using this filter with optical processing alternatives, strongly urges further investigation of this approach (9).

1.2 Problem Overview

The purpose of this research is to expand on the Rogers' work by investigating the feasibility of utilizing a linear Kalman filter in cascade with a correlation algorithm, using either the correlation method employed by Rogers or an alternative method as developed in Chapter 4. Alternative correlation methods were explored to determine if either a reduction in the

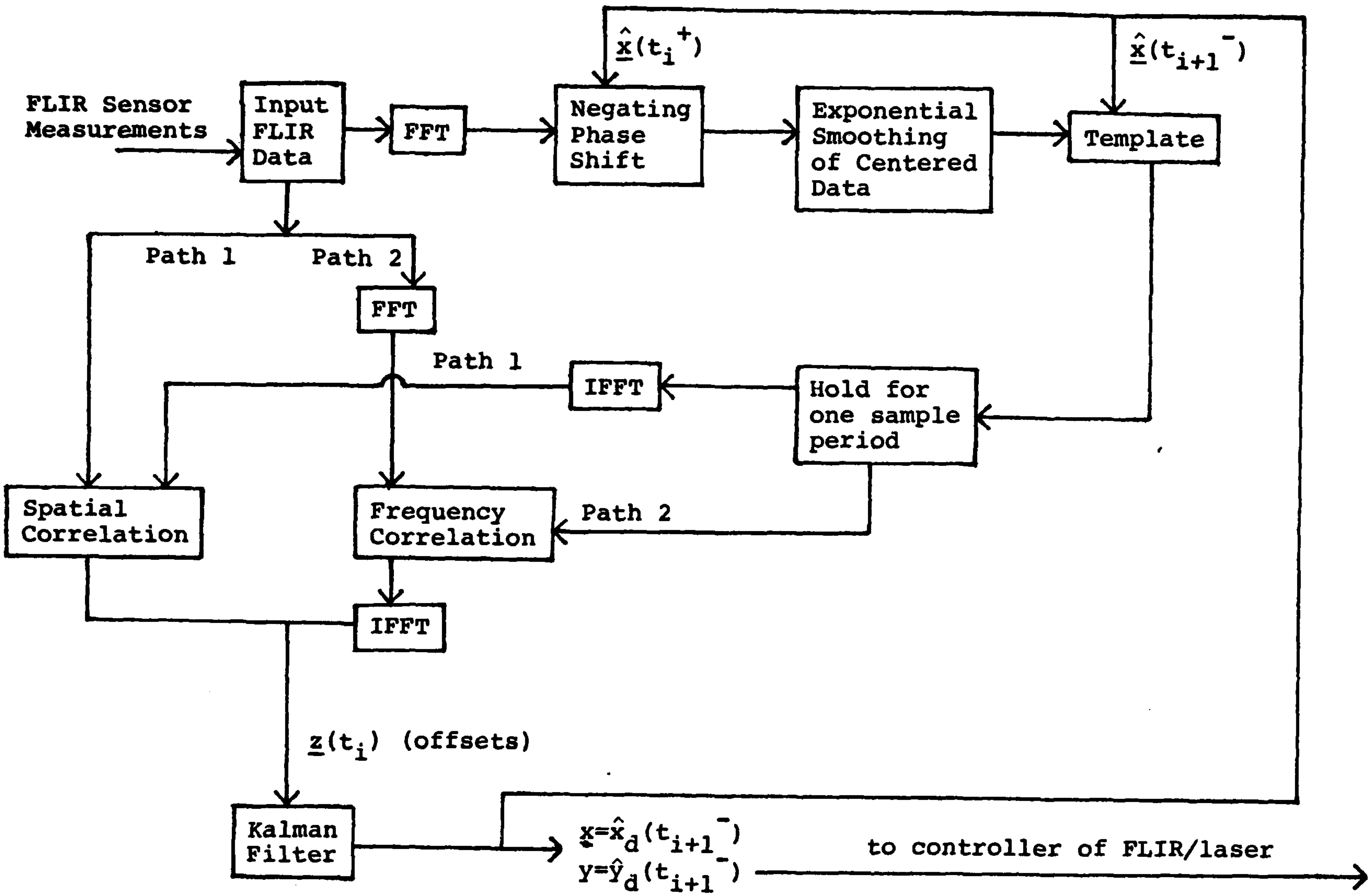

Figure 1. Data Processing Algorithm

computational loading of the correlator could be achieved without a degradation in performance, or another method is available which reduces the mean errors and standard deviations of the correlator without a substantial computational increase. The ability of the correlator/ Kalman filter to track targets exhibiting single and multiple hot spots over a varying range of dynamic profiles will be evaluated. These dynamic profiles were specifically designed to evaluate the ability of the filter to track changes in the target dynamics as well as changes in the target's intensity pattern. The target scenarios and reasons for selection of those scenarios are detailed in Chapter 2. In the single hot spot case, the performance achieved by the extended Kalman filter employed by Harnly and Jensen (6) will serve as the standard against which the correlator/Kalman filter performance will be evaluated.

As shown in Figure 1., measurement information of target position for the correlator/Kalman filter is generated by the FLIR sensor. In this research the FLIR tracking window is 8 pixels wide by 8 pixels high where a pixel length of 20 μ radians is used, although an expansion of this window is possible. The measurement information presented to the tracking algorithm is the average intensity over each of the 64 square pixel elements within the 8 x 8 tracking window. The concept of the correlator/Kalman filter is to generate an accurate reference image of the target's intensity function on the FLIR image plane to serve as a template for correlation with new data received from the sensor. In Figure 1., either path 1 or path 2 is followed depending on the correlation method being used. The results of the correlation of these two data arrays namely, the indicated angular position offsets of the target centroid, Equation (1-3), from the center of the FLIR field-of-view

(FOV), can then be used in the measurement model portion of a linear Kalman filter to estimate target offsets from the center of the FOV. The linear Kalman filter processes the measurement vector, $\underline{z}(t_i)$, using

$$\underline{x}(t_i^+) = \underline{x}(t_i^-) + \underline{K}(t_i)\ \{\underline{z}(t_i) - \underline{H}\ \underline{x}(t_i^-)\} \qquad (1\text{-}1)$$

where

$\underline{x}(t_i^+)$ = state estimate vector after measurement incorporation at time t_i

$\underline{x}(t_i^-)$ = state estimate vector propagated from previous measurement update to time t_i

$\underline{K}(t_i)$ = Kalman filter gain

$\underline{z}(t_i)$ = measurement vector of the estimated offset distance in the horizontal and vertical direction from the center of the FLIR plane to the centroid of the intensity function

$\underline{H}(t_i)$ = linear combination of the states which contribute to the respective measurements

A detailed development of the Kalman filter equations is given in Chapter 3. These estimated offsets are to be regulated to zero by using the estimates as inputs to a pointing controller that points the laser beam and the center of the FLIR FOV appropriately. The state estimates are also used to aid in estimating the shape function in the data processing algorithm.

The primary focus of the Rogers thesis was to generate an accurate estimate of the target's intensity shape function and to evaluate its performance in a benign tracking environment where the target did not leave the FLIR FOV in one sample period. Thus, a four-state estimate vector, $\underline{x}(t_i)$, consisting of estimates of the x and y positions due to true target dynamics and the x and y positions due to atmospherics was utilized (10). The position estimates are along the FLIR horizontal and vertical axes respectively. However, in order to track targets over a wide dynamic range the capability to to predict future target position is required; thus, in this research the four-state estimate vector is replaced by an eight-state estimate vector, consisting of estimates of the target's position due to dynamics and atmospherics in the x and y directions as well as estimates of the target's velocity and acceleration in both the x and y directions.

In the lower path of Figure 1, the Kalman filter incorporates the measurement information, using Equation (1-1) at time t_i, and utilizes its internal dynamics model to propagate its estimate of where the true target position will be at the next sample period, t_{i+1}, using

$$\underline{x}(t_{i+1}^-) = \underline{\Phi}(t_{i+1}, t_i)x(t_i^+) \qquad (1\text{-}2)$$

where

$\underline{\Phi}(t_{i+1},t_i)$ = filter state transition matrix as defined in Equation (3-11)

The FLIR is located so as to zero out the estimated target dynamics position components which are the first two states of $\underline{x}(t_{i+1}^-)$. The atmospheric disturbances which can cause apparent translational offsets of the intensity function on the FLIR image plane are also accounted for by $\underline{x}(t_{i+1}^-)$ and the correlator template is positioned with this estimate. The incoming measurement array is then correlated with the template to determine the position offset between the two arrays. Errors in the correlation algorithm are reduced by processing the position offset estimates with the Kalman filter which exploits statistical knowledge of the correlator errors to produce a better position estimate for actual tracking purposes (9:13-14). The Kalman filter then uses its internal dynamics model to propagate its best estimate of the states at the next sample time, $\underline{x}(t_{i+2})$.

The upper path of Figure 1 is designed to generate the template for correlation with the incoming FLIR data array. The fundamental concept of the algorithm is to utilize the fact that the actual target image will change rather slowly relative to a given sample period while background noises will typically change more rapidly. This path generates an estimated representation of the average value of the target intensity pattern over each pixel, which would be observed if the measurements were noise-free and the filter state estimates were perfect. The location of the centroid of the target intensity pattern is the sum of the effects caused by true target dynamics plus apparent translational motion caused by atmospheric disturbances. In the x-direction the centroid of the target's intensity profile is defined by

$$x_{centroid} = x_{dynamics} + x_{atmospherics} \qquad (1\text{-}3)$$

and control action is applied to zero out the estimated $x_{dynamics}$, and similiarly in the y-direction. Thus, under these conditions the target's intensity profile will be offset from the center of the FLIR FOV by the predicted atmospheric states, $x_a(t_i^-)$ and $y_a(t_i^-)$.

To generate the estimated target intensity pattern from the noise-corrupted FLIR data, interframe smoothing is employed to attenuate the noise. The raw FLIR data is put through an FFT to allow for efficient data processing and possible spatial frequency filtering. In order to center the target in the original spatial domain, the appropriate negating phase shift is applied to this transformed image. The offset estimate for the frame at t_i is provided by $x_{centoid}(t_i^+)$ and $y_{centroid}(t_i^+)$ based on Equation (1-3) as obtained from the Kalman filter. The phase shift is computed according to the shifting property of the two-dimensional discrete Fourier transform (8:Equation (2-7)), with the output of the "Negating Phase Shift" appearing as the result of passing a centered target image through a FFT.

This result can then be averaged with the most recent N such centered and transformed data frames to attenuate the background noise and accenuate the underlying target pattern. Instead of explicitly storing N data sets, finite-memory averaging is approximated by using exponential smoothing

$$\hat{\underline{G}}(t_i) = \alpha\underline{G}(t_i) + (1-\alpha)\hat{\underline{G}}(t_{i-1}) \qquad (1\text{-}4)$$

where

$\underline{G}(t_i)$ = current data frame value of $\underline{G}$

$\hat{\underline{G}}(t_i)$ = current estimate of $\underline{G}$

$\hat{\underline{G}}(t_{i-1})$ = previous smoothed estimates of $\underline{G}$

α = smoothing parameter; $0\leq\alpha\leq1$

Thus, a smaller α corresponds to a longer finite memory being approximated as appropriate for slowly changing target patterns (9:8-11).

At time t_i, the output of the "Exponential Smoothing of Centered Data" block is a representation of the FFT of the estimated target intensity pattern corresponding to a centered image. This pattern is then evaluated using $\underline{x}(t_{i+1}^-)$ which, due to the previous controller action, corresponds to offsetting this FFT by the phase shift corresponding to the atmospheric state components of $\underline{x}(t_{i+1}^-)$ as generated by the Kalman filter. The intensity function, $h(x(t_{i+1}^-), t_{i+1})$, is then ready for use as the template in the correlation process at the next sample time t_{i+1}, and is placed in a one period storage location awaiting the next measurement. Note the previous contents of this location which corresponds to the estimated intensity function generated by the smoothing algorithm at t_{i-1}, was used as the template at t_i, i.e. $h(x(t_i^-), t_i)$, to generate $\underline{x}(t_i^+)$ and $\underline{x}(t_{i+1}^-)$. Depending on the correlation method used, the correlation of the template and the incoming data array is either accomplished in the frequency or spatial domain. For a detailed development of the upper path of Figure 1, see reference 8.

1.3 Plan of Attack

This section presents a general overview of the flow of this research as depicted in Figure 2.

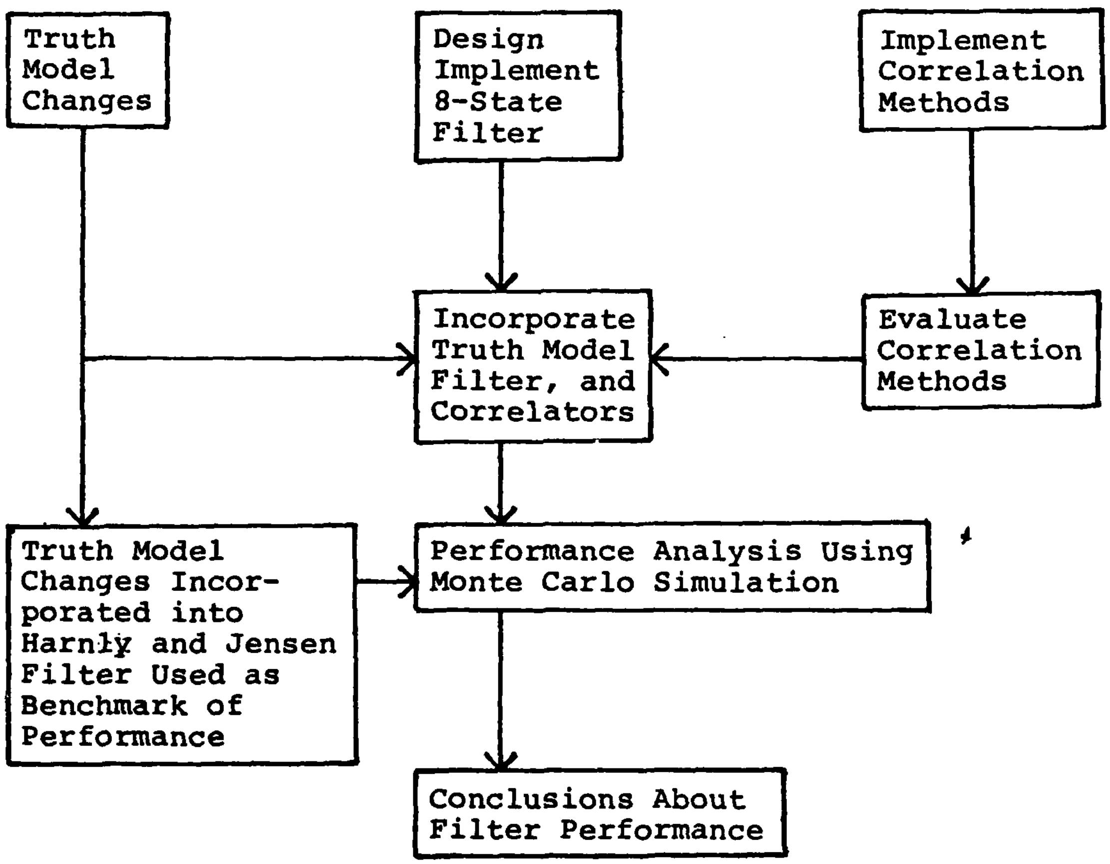

Figure 2. Research Plan of Attack Flow Diagram

The computer simulation developed by Captain Rogers (8) was used as the basic computer program to which changes were made to evaluate the performance of the correlator/Kalman filter in realistic tracking environments. This approach required that realistic target trajectories be incorporated into the truth model in place of the benign target trajectory model used by Rogers. Additionally, a model was developed to account for the movement of both single and multiple hot spots relative to the aircraft center of mass and to project the hot spot or spots onto the FLIR image plane for measurement data. The four-state Kalman filter used by Rogers was replaced by the eight-state Kalman filter which is developed in Chapter 3. Finally, based on a literature search of available correlation methods, alternative correlation methods were selected based on the criteria previously discussed, for evaluation against the correlation method used by Rogers, see Chapter 4. As a result of this evaluation, one alternative method, along with the method developed by Rogers, was implemented in cascade with the Kalman filter.

The truth model, Kalman filter, and correlator models were incorporated into a computer simulation for a performance analysis using a Monte Carlo simulation. Additionally, the truth model changes were incorporated into an extended Kalman filter developed by Harnly and Jensen (6) to track only single hot spot targets with intensity functions well described as bivariate Gaussian to provide a benchmark of performance for the proposed algorithm.

1.4 Overview

Chapters II, III, and IV, discuss in detail the mathematical models used in the computer simulation. Chapter II presents the truth model which represents the environment from which measurements are taken. Chapter III describes the eight-state linear Kalman filter used in the computer simulation. Chapter IV presents a mathematical development of the methods of correlation used and an analysis of the performance of these correlation methods. Chapter V presents a performance analysis of the linear correlator/Kalman filter and the Harnly and Jensen filter against targets exhibiting a wide range of dynamic profiles and both single and multiple hot spot intensity shapes on the FLIR image plane. Chapter VI presents the conclusions and recommendations.

II. Truth Model

2.1 Introduction

The truth model is the best mathematical representation of the real world process to be simulated that is available to, and can be implemented by, the researcher. In this study, the truth model portrays the motion of the target, an air-to-air missile or a multiple engine aircraft, in inertial space and the intensity function emitted by the target which is distorted by atmospheric disturbances. The resulting infrared image is then projected onto the two-dimensional FLIR image plane. With this distorted target intensity pattern projected onto the FLIR image plane, spatially correlated and temporally uncorrelated noise which accounts for background and inherent FLIR noises, are added to create the corrupted measurement array, $\underline{z}(t_i)$, for incorporation by the correlator/Kalman filter.

This chapter outlines the truth model used in this study. For details of how the components of the model were developed, consult the cited references.

2.2 Target Model

This section develops the equations which represent the trajectory of the target being tracked in inertial space and translates that into motion on the two-dimensional FLIR image plane, which is represented by movement of the target intensity patttern within the FLIR field-of-view. Although this motion consists of several components, in this research the apparent target motion due to boresight errors, FLIR system vibrations, etc., are assumed to be negligible compared to the motion due to target dynamics and atmospheric jitter. Thus, the continuous time target model describes the apparent target motion due to actual target dynamics and atmospherics by means of differential equations, as well as stochastically to represent the statistical properties of the physical processes of concern and to account for the unmodeled physical effects.

As developed by Harnly and Jensen (6), the continuous target dynamics model accounts for the true location of the target center of mass on the two-dimensional FLIR image plane in the horizontal direction, α, and in the vertical direction, β. A deterministic model was used to provide a time history of the target location so that specific trajectories could be generated for tracker evaluation although a stochastic model could be used. Thus,

$$\dot{x}_1(t) = \dot{\alpha}(t) = \text{horizontal velocity}$$

$$\dot{x}_2(t) = \dot{\beta}(t) = \text{elevation velocity}$$

or

$$\dot{\underline{x}}_D(t) = \underline{u}(t) = \left[\dot{\alpha}(t)\,\dot{\beta}(t)\right]^T \tag{2-1}$$

While a target trajectory could also have been generated by simply reading in time histories of α and β , a deterministic model of the form of Equation (2-1) was selected so a switch from the deterministic form to either a first-order Gauss-Markov process, a Brownian motion stochastic process, or the sum of a deterministic and stochastic model could readily be implemented if desired. The atmospheric disturbances, as developed by Mercier (10), were modeled as third-order Gauss-Markov processes, described by the output of a shaping filter with a frequency domain transfer function of

$$\frac{x_A}{w_3} = \frac{K(14.14)(659.5)^2}{(s+14.14)(s+659.5)^2} \tag{2-2}$$

driven by a unit strength white Gaussian noise w_3. A duplicate independent model is used to generate y_A

in the vertical FLIR plane direction. Physically, this corresponds to jitter in each of the two FLIR image plane coordinate directions being modeled as the output of a linear third order system driven by white Gaussian noise, developed to match the power spectral density characteristics of the observed physical jitter phenomenon. The atmospheric jitter is then represented in both FLIR plane directions by a stochastic differential equation of the form

$$\underline{\dot{x}}_A(t) = \underline{F}_A(t)\underline{x}_A(t)+\underline{G}_A(t)\underline{w}_A(t) \tag{2-3}$$

where

$\underline{\dot{x}}_A(t)$ = six atmospheric noise states

$\underline{F}_A(t)$ = atmospheric plant matrix

$\underline{G}_A(t)$ = atmospheric noise distribution matrix

$\underline{w}_A(t)$ = two-dimensional vector of white Gaussian noise inputs with statistics:

$$E\{\underline{w}_A(t)\} = \underline{0}$$

and

$$E\{\underline{w}_A(t)\underline{w}_A^T(t+\tau)\} = \underline{Q}_A(t)\delta(\tau)$$

After augmenting the atmospheric states to the dynamic states, Equations (2-1) and (2-3), and writing the equations in an equivalent discrete time form (6), the solution to the discretized truth model propagation of the motion of the target intensity function has the form

$$\underline{x}(t_{i+1}) = \underline{\Phi}(t_{i+1},t_i)\underline{x}(t_i)+\begin{bmatrix}\underline{B}_d(t_i)\\ \hline \underline{0}\end{bmatrix}\underline{u}_d(t_i)+\begin{bmatrix}\underline{0}\\ \hline \underline{C}\sqrt{\underline{Q}_{Ad}}\end{bmatrix}\underline{w}_{Ad}(t_i) \tag{2-4}$$

where

$\underline{x}(t_i)$ = state vector of the two dynamic states and six atmospheric states

$\underline{B}_d(t_i)$ = input matrix for dynamics = $\int_{t_i}^{t_{i+1}} \underline{\Phi}(t_{i+1},t_i)\underline{B}(\tau)d\tau$

$\underline{u}_d(t_i)$ = piecewise constant function (constant between sample times) evaluated at the interval midpoint as an approximation to the integral of $\dot{\alpha}(t)$ and $\dot{\beta}(t)$ from t_i to t_{i+1}. Explicitly,

$$\underline{u}_d(t_i) = \begin{bmatrix} \dot{\alpha}(t_i + \frac{\Delta t}{2}) \\ \\ \dot{\beta}(t_i + \frac{\Delta t}{2}) \end{bmatrix}$$

$$\Delta t = t_{i+1} - t_i$$

$\underline{w}_{Ad}(t_i)$ = discrete-time white Gaussian noise with statistics:

$$E\{\underline{w}_{Ad}(t_i)\} = \underline{0}$$

$$E\{\underline{w}_{Ad}(t_i)\underline{w}_{Ad}^T(t_j)\} = \underline{I}\delta_{ij}$$

and

$${}^c\sqrt{\underline{Q}_{Ad}(t_i)}\ \ {}^c\sqrt{\underline{Q}_{Ad}(t_i)}^T = \underline{Q}_{Ad}(t_i) =$$

$$= \int_{t_i}^{t_{i+1}} \underline{\Phi}_A(t_{i+1},\tau)\underline{G}_A(\tau)\underline{Q}_A(\tau)\underline{G}_A^T(\tau)\ \underline{\Phi}_A^T(t_{i+1},\tau)d\tau$$

where ${}^c\sqrt{\underline{Q}_{Ad}}$ represents the Cholesky square root of $\underline{Q}_{Ad}$. See reference (12) for development.

Thus,

$$E\{{}^{C}\sqrt{\underline{Q}_{Ad}}\ \underline{w}_{Ad}(t_i)\} = \underline{0}$$

$$E\{{}^{C}\sqrt{\underline{Q}_{Ad}}\ \underline{w}_{Ad}(t_i)\underline{w}_{Ad}^{T}(t_j)\,{}^{C}\sqrt{\underline{Q}_{Ad}}^{T}\} = \underline{Q}_{Ad}\delta_{ij}$$

Explicitly, the state transition matrix is

$$\underline{\Phi}(t_{i+1},t_i) = \begin{bmatrix} 1 & 0 & 0 & 0 & 0 & 0 & 0 & 0 \\ 0 & 1 & 0 & 0 & 0 & 0 & 0 & 0 \\ 0 & 0 & e^{-A\Delta t} & 0 & 0 & 0 & 0 & 0 \\ 0 & 0 & 0 & e^{-B\Delta t} & \Delta t e^{-B\Delta t} & 0 & 0 & 0 \\ 0 & 0 & 0 & 0 & e^{-B\Delta t} & 0 & 0 & 0 \\ 0 & 0 & 0 & 0 & 0 & e^{-A\Delta t} & 0 & 0 \\ 0 & 0 & 0 & 0 & 0 & 0 & e^{-B\Delta t} & \Delta t e^{-B\Delta t} \\ 0 & 0 & 0 & 0 & 0 & 0 & 0 & e^{-B\Delta t} \end{bmatrix}$$

The three by three submatrics in $\underline{\Phi}(t_{i+1},t_i)$ are identical and propagate the atmospheric disturbances in azimuth and elevation with poles A and B as shown in Equation (2-2).

$$\underline{B}_d(t_i) = \begin{bmatrix} \Delta t & 0 \\ 0 & \Delta t \\ 0 & 0 \\ 0 & 0 \\ 0 & 0 \\ 0 & 0 \\ 0 & 0 \\ 0 & 0 \end{bmatrix}$$

For a detailed development of Equation (2-4) consult ref. 6.

The last step in the target dynamics model is to define the azimuth velocity, $\dot{\alpha}(t)$, and elevation velocity, $\dot{\beta}(t)$, in the FLIR image plane. To simulate this motion, the target velocity was initially calculated in an inertial frame, with its origin at the center of the FLIR image plane, and then projected onto the two-dimensional FLIR image plane. The relationship between the FLIR frame and inertial frame is shown in Figure 3.

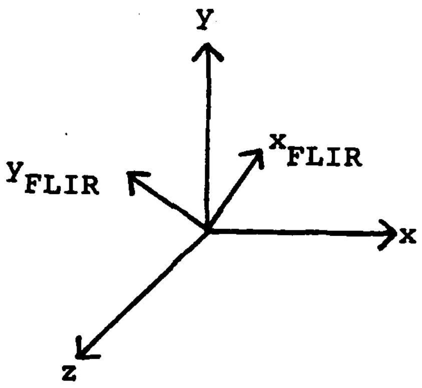

Figure 3. Inertial Coordinate Frame

The geometry involved in the azimuth direction is as shown in Figure 4.

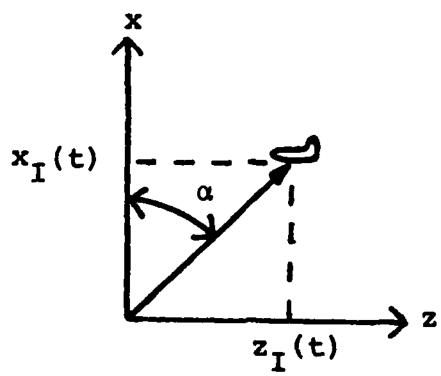

Figure 4. Azimuth Geometry

From Figure 4,

$$\alpha(t) = \tan^{-1} \frac{z_I(t)}{x_I(t)} \tag{2-5}$$

and

$$\dot{\alpha}(t) = \frac{x_I(t)\dot{z}_I(t) - z_I(t)\dot{x}_I(t)}{z_I^2(t) + x_I^2(t)} \tag{2-6}$$

Equation (2-6) yields an azimuth velocity in radians/ sec which is converted to FLIR image plane units, pixels/ sec, by dividing $\dot{\alpha}(t)$ by 20×10^{-6} radians/pixel (6:33).

Similiarly, Figure 5 shows the geometry involved in computing the elevation velocity.

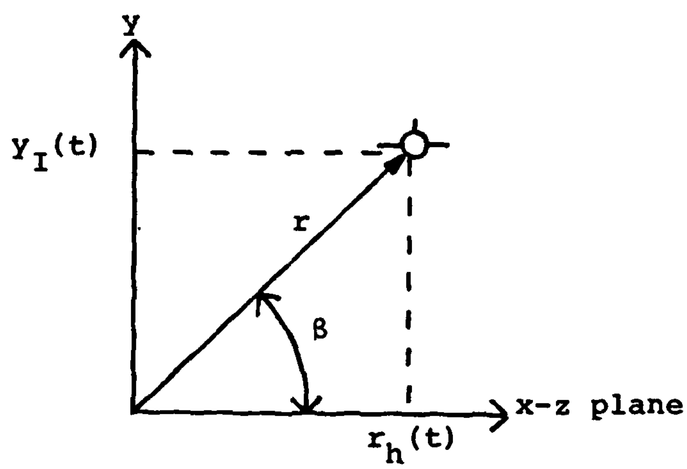

Figure 5. Elevation Geometry

where

$$r = \text{range} = \{x_I^2(t)+y_I^2(t)+z_I^2(t)\}^{\frac{1}{2}}$$

$$r_h = \text{horizontal range} = \{x_I^2(t)+z_I^2(t)\}^{\frac{1}{2}}$$

From Figure 5, the tangent function can be used to find β:

$$\beta = \tan^{-1}\frac{y(t)}{r_h(t)} \tag{2-7}$$

and

$$\dot{\beta}(t) = \frac{r_h(t)\dot{y}_I(t)-y_I(t)\dot{r}_h(t)}{r_h^2(t)+y_I^2(t)}$$

$$= \frac{r_h(t)\dot{y}_I(t)-y_I(t)\left[\dfrac{x_I(t)\dot{x}_I(t)+z_I(t)\dot{z}_I(t)}{r_h(t)}\right]}{r^2(t)} \tag{2-8}$$

The elevation velocity is then converted to pixels/sec also.

By inserting Equations (2-6) and (2-8) into Equation (2-4), deterministic time histories for the truth model propagation can be generated to produce the desired trajectories for the target.

2.3 Trajectory Description

A thorough evaluation of the filter's tracking performance requires that specific trajectories be designed to test the ability of the filter to maintain an accurate estimate of the target's true position under various circumstances. A benign crossing trajectory was selected to serve as the baseline for the filter's performance, as this should be an easy trajectory for the filter to track. For the multiple hot spot case, a rolling trajectory was designed to evaluate how well the data processing algorithm can reconstruct the target intensity pattern when the target's intensity pattern exhibits changes on the FLIR plane relative to the aircraft center of mass. Several trajectories were designed to evaluate the filter's ability to maintain track on a target performing highly dynamic maneuvers. Note, as will be discussed later, under these circumstances while the center of the target intensity pattern relative to the aircraft center of mass does not change, the orientation of the elliptical intensity pattern as projected onto the FLIR image plane will change. Finally, a trajectory was designed to evaluate the ability of the algorithm to estimate the target position when the target is performing a high-g maneuver and the dynamic shape of the intensity pattern is also changing simultaneously.

The benign trajectory which served as the baseline for filter performance was simulated by having the target fly a cross-range trajectory parallel to the x-y plane. The flight path referred to as trajectory 1, is depicted in Figure 6.

(NOT USED)

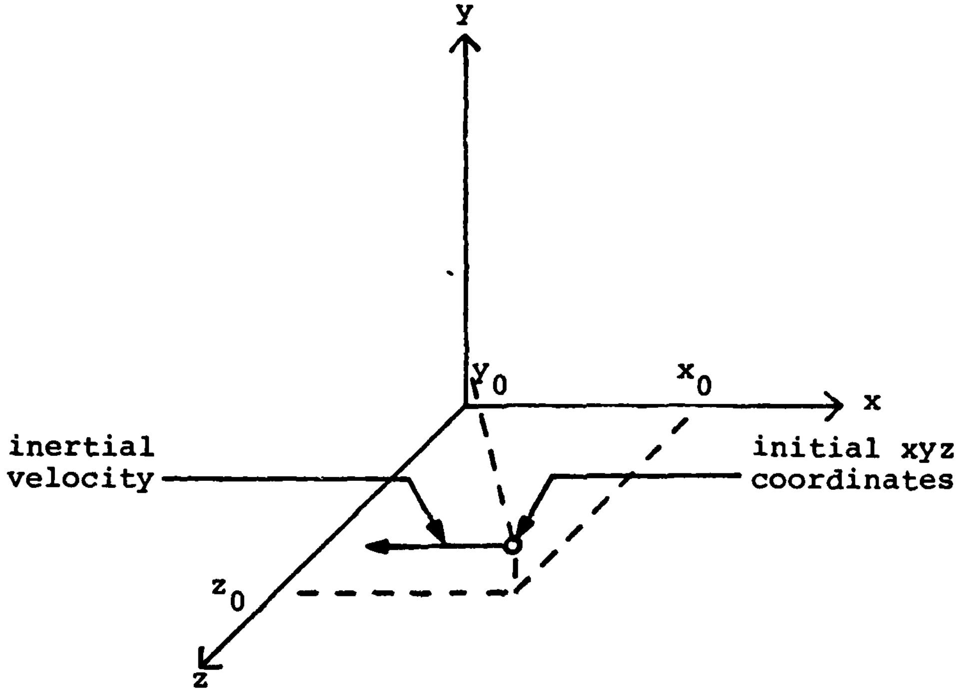

Figure 6. Trajectory 1

The inertial location of the target at t_0 is

$$x_I(t_0) = 5000.0 \text{ m}$$
$$y_I(t_0) = 500.0 \text{ m}$$
$$z_I(t_0) = 20000.0 \text{ m}$$

The trajectory throughout the simulation is given by

$$\dot{x}_I(t) = -1000. \text{ m/sec}$$
$$\dot{y}_I(t) = 0. \text{ m/sec}$$
$$\dot{z}_I(t) = 0. \text{ m/sec}$$

Trajectory 1 was used to evaluate the performance of the filter against a multiple hot spot target flying either a wings level trajectory or a roll maneuver. Roll rates of .5 radians/sec and 1.0 radians/sec were used as being representative of realistic performance.

To evaluate the performance of the filter against a target performing a maneuver, the target was initialized with the same inertial location and velocity as shown in Figure 6. Two seconds into the simulation, a constant g pullup maneuver was initiated which lasted for three seconds, and the simulation was terminated. The flight path, trajectory 2, is depicted in Figure 7.

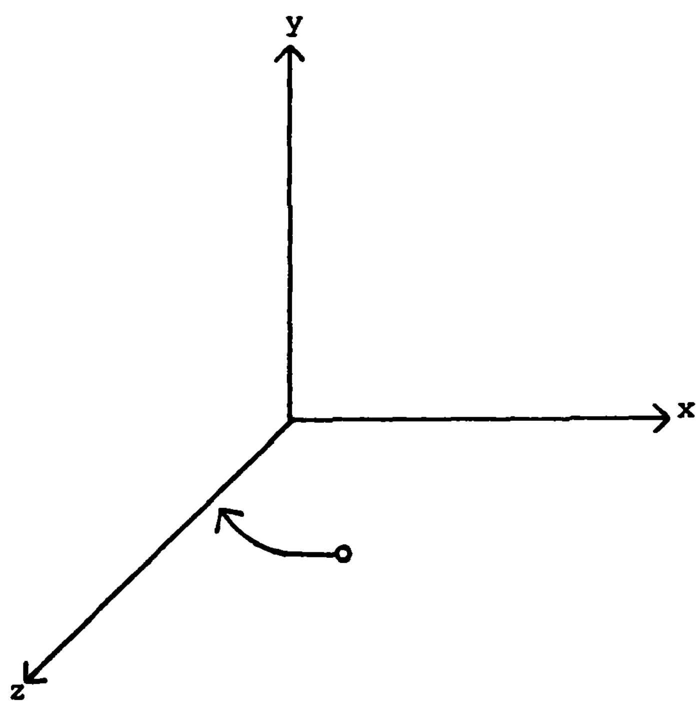

Figure 7. Trajectory 2

The trajectory prior to the pull-up manuever is desc· bed by

$$\dot{x}_I(t) = -1000 \text{ m/sec}$$

$$\dot{y}_I(t) = 0.$$

$$\dot{z}_I(t) = 0.$$

and is initiated at inertial coordinates

$$x_I(t_0) = 5000 \text{ m}$$

$$y_I(t_0) = 500 \text{ m}$$

$$z_I(t_0) = 20000 \text{ m}$$

At t_i=2.0 sec, the pull-up maneuver is initiated at the inertial coordinates

$$x_I(t_2) = 3000 \text{ m}$$

$$y_I(t_2) = 500 \text{ m}$$

$$z_I(t_2) = 20000 \text{ m}$$

The velocity equations are then

$$\dot{x}_I(t) = -1000 \cos\{\omega(t-2)\}\text{m/sec}$$

$$\dot{y}_I(t) = 1000 \sin\{\omega(t-2)\}\text{m/sec}$$

$$\dot{z}_I(t) = 0. \text{ m/sec}$$

and the inertial position of the target can be determined by

$$x_I(t) = x_I(t_0)-2000-\{1000/\omega\}\sin\{\omega(t-2)\} \text{ m}$$

$$y_I(t) = y_I(t_0)+\{1000/\omega\}\{1-\cos \omega(t-2)\} \text{ m}$$

$$z_I(t) = 20000 \text{ m}$$

The trajectory 2 equation can be modified so that instead of the target performing a pull-up maneuver in the inertial y-direction the target motion is in the negative inertial z-direction. In this case, the target turns in toward the FLIR image plane, and three distinct ellipsoidal intensity patterns are projected onto the FLIR plane. With the x equations being as previously described, the motion of the target is defined by:

$$\dot{y}_I(t) = 0.0 \text{ m/sec}$$

$$\dot{z}_I(t) = -1000.0 \sin\{\omega(t-2)\} \text{ m/sec}$$

The inertial position is given by:

$$y_I(t) = 500.0 \text{ m}$$

$$z_I(t) = z_I(t_0) - \{1000/\omega\}\{1-\cos \omega(t-2)\} \text{ m}$$

ω is set at various constant values in different simulations, to evaluate the performance of the tracker against targets exhibiting varying degrees of maneuverability. In this research, the performance of the tracker against targets performing 2 and 5 g turns was evaluated. (ω = 0.0196 and 0.049 radians/sec respectively). Note that this trajectory represents a step change to a constant g maneuver. Although realistically such changes do not occur, for ease of implementation this method was used. However, this also implies that the filter is being required to track a harsher maneuver than the more realistic pull-up maneuver, in which ω builds up smoothly from zero to a constant rate, and thus better performance should be achieved in the more realistic environment.

Trajectory 3 was motivated by the desire to evaluate not only how the filter responds when the target being tracked initiates a maneuver, but also how the filter responds when the target terminates the maneuver.

Trajectory 3 is initially the same as trajectory 2, with a two-g pull-up maneuver being initiated at $t = 2.0$ sec. With this maneuver the target has an inertial velocity at $t = 3.5$ sec of

$$\dot{x}_I(t = 3.5) = -999.58 \text{ m/sec}$$

$$\dot{y}_I(t = 3.5) = 29.069 \text{ m/sec}$$

$$\dot{z}_I(t = 3.5) = 0. \text{ m/sec}$$

The target terminates the pull-up maneuver at $t = 3.5$ sec and continues at this constant velocity for the remainder of the simulation.

The final trajectory, trajectory 4, was designed as the most realistic trajectory, and also to evaluate the performance of the filter when the dynamic shape of the target intensity pattern is changing. Trajectory 4 is initialized identically to trajectory 2. However, at $t = 2$ sec, a two-g turn is initiated, with the target turning toward the FLIR plane displaying motion in all inertial directions (see Figure 8).

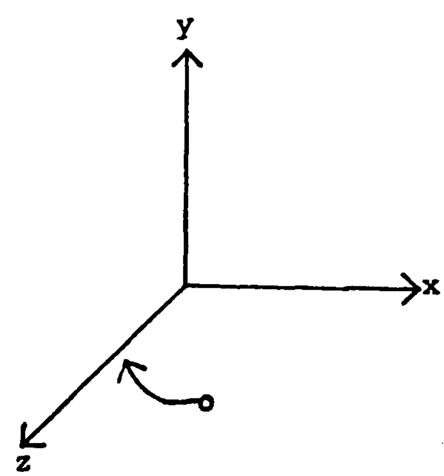

Figure 8. Trajectory 4.

This maneuver can be derived by the two coordinate system transformations shown in Figure 9.

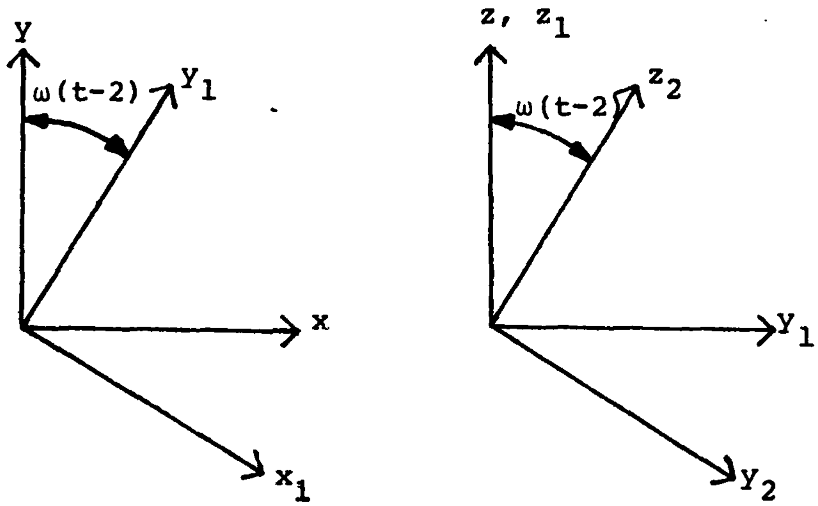

Figure 9. Out-of-Plane Coordinate Frame Rotations

Explicitly writing out the coordinate transformations yields:

$$\begin{matrix} \dot{x}_I(t) \\ \dot{y}_I(t) \\ \dot{z}_I(t) \end{matrix} = \begin{bmatrix} 1 & 0 & 0 \\ 0 & A & B \\ 0 & -B & A \end{bmatrix} \begin{bmatrix} A & B & 0 \\ -B & A & 0 \\ 0 & 0 & 1 \end{bmatrix} \begin{bmatrix} V \\ 0 \\ 0 \end{bmatrix}$$

where

$A = \cos \omega\,(t-2)$

$B = \sin \omega\,(t-2)$

Performing the matrix multiplication gives the velocity equations as:

$$\dot{x}_I(t) = -v\{\cos \omega(t-2)\} \text{ m/sec}$$

$$\dot{y}_I(t) = v\{\cos \omega(t-2)\}\sin \omega(t-2) \text{ m/sec}$$

$$\dot{z}_I(t) = -v\{\sin^2 \omega(t-2)\} \text{ m/sec}$$

and the inertial target position is:

$$x_I(t) = x_I(t_0)-2000-\{(1000/\omega)(\sin \omega(t-2)\}$$

$$y_I(t) = y_I(t_0)+\{\left(\frac{1000}{2\omega}\right)(\sin^2\omega(t-2))\}$$

$$z_I(t) = z_I(t_0)-1000\{\left(\frac{t-2}{2}\right)-\frac{1}{4\omega}\sin(2\omega(t-2))\}$$

where in this simulation v = -1000 m/sec. The out-of-plane angle associated with this maneuver can be found by

$$\text{op angle} = \tan^{-1} \frac{z_I(t)}{y_I(t)}$$

2.4 Measurement Model

With the motion of the target defined, the next step is to define the intensity function generated by the target and project that function onto the FLIR image plane. For distant targets, the intensity pattern projection onto the FLIR image plane is well approximated by a bivariate Gaussian function with circular equal intensity contours (5:223). However, for closer range targets, Harnly and Jensen, ref 6, found an elliptically shaped pattern was a better representation of the true intensity pattern. This intensity function is

$$I(x,y) = I_{max}\exp\left[-0.5\{(x-x_{peak})(y-y_{peak})\}\{\underline{P}\}^{-1}\begin{Bmatrix}x-x_{peak}\\ y-y_{peak}\end{Bmatrix}\right] \quad (2\text{-}9)$$

where the variables, as shown in Figure 10, are

I_{max} = maximum target intensity

x_{peak}, y_{peak} = coordinates of peak intensity function

σ_v, σ_{pv} = eigenvalues of $\underline{P}$; cooresponding to the ellipse semimajor axis along the velocity vector and the semiminor axis perpendicular to the velocity vector respectively.

$v_{\perp LOS}$ = velocity component of the target perpendicular to the line of sight from the FLIR image plane to the target

θ = orientation angle of $\underline{v}_{\perp LOS}$ in the FLIR plane, aligned with the semimajor axis of the intensity pattern

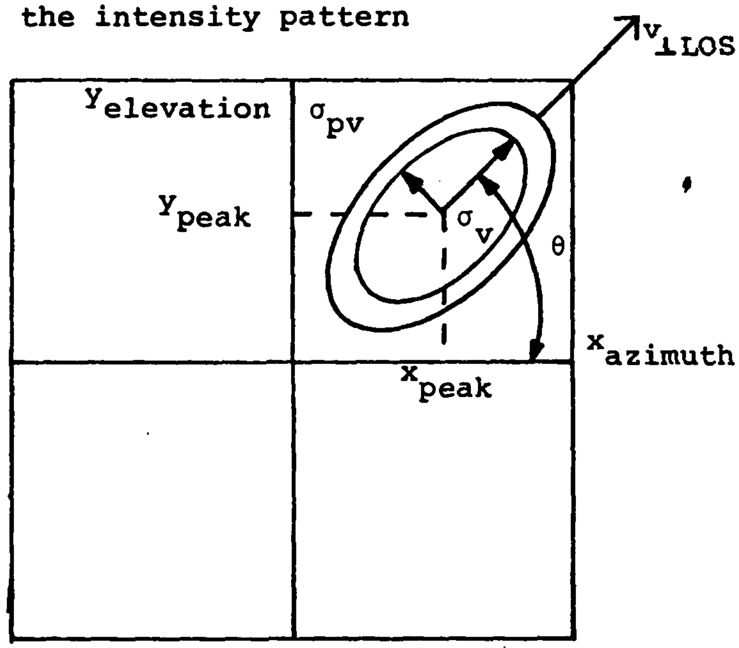

Figure 10. Image Intensity Characteristics

For this research, a pixel dimension of 20 μ rads is used. The movement of the point of maximum intensity on the FLIR image plane defined by x_{peak} and y_{peak} is determined by $\alpha(t)$ and $\beta(t)$, expressed in μ rads, respectively after the effects of tracker controller action have been accounted for. Therefore, the 8x8 FLIR FOV will be 160 μ rads wide in azimuth and 160 μ rads wide in elevation. Because of this small FOV, angular displacement of the target from the FLIR FOV can be approximated by linear displacement on the FLIR image plane. Similiarly, angular velocity closely approximates linear velocity in the FLIR image plane (6:24). Thus, angular measurements were used.

The intensity pattern on the FLIR image plane is produced in several steps. From the simulation of the inertial position and velocity of the missile, the azimuth velocity (x velocity in Figure 11), elevation velocity (y velocity in Figure 11), and speed (the magnitude of the velocity vector in inertial space), were computed in rad/sec. The azimuth and elevation velocity then define the missile velocity component perpendicular to the line of sight, $v_{\perp LOS}$, and the ratio of $v_{\perp LOS}$ and speed is the cosine of the out of place angle, γ. Figure 11 shows the geometry involved (6:24). Explicitly, the relationships are:

$$\cos\theta = \frac{\dot{\alpha}(t)}{|v_{\perp LOS}|}$$

$$\sin\theta = \frac{\dot{\beta}(t)}{|v_{\perp LOS}|}$$

where

$$|v_{\perp LOS}| = \{\dot{\alpha}^2(t)+\dot{\beta}^2(t)\}^{\frac{1}{2}}$$

and

$$\cos \gamma = \frac{|v_{LOS}|}{|v|}$$

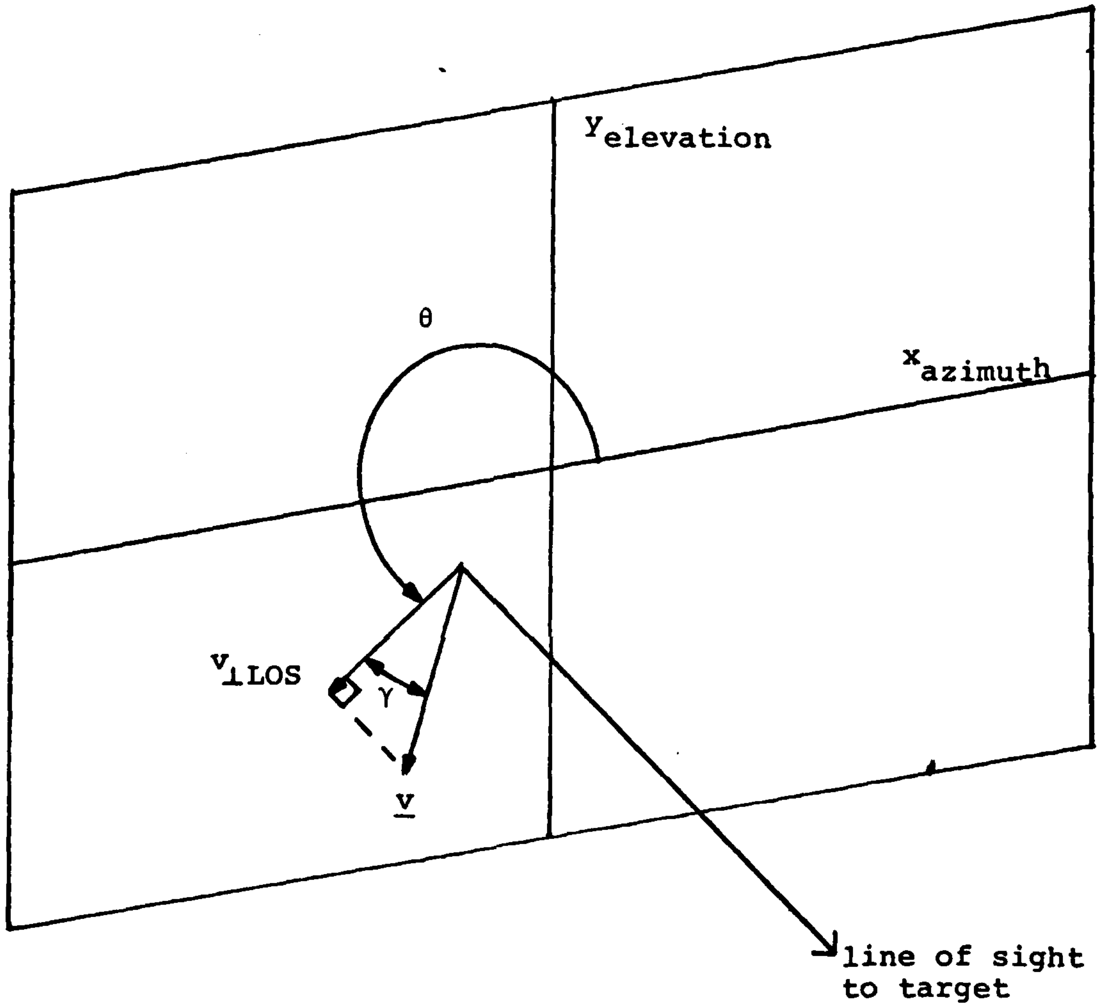

Figure 11. Image Projection

With cos γ determined, the semimajor axis of the missile can be projected onto the FLIR image plane. Referring to Figure 12, where δ is the length of the semimajor axis in meters, the length of the semimajor axis parallel to the FLIR plane is:

$$\sigma_p' = \delta \cos \gamma \text{ m}$$

By approximating linear distance on the FLIR plane as the angular displacement, this distance can be expressed as

$$\sigma_p = \psi/.00002 \quad \text{pixels} \qquad (2\text{-}10)$$

where

$$\psi \approx \frac{\sigma_p'}{r}$$

.00002 = conversion factor from radians to pixels

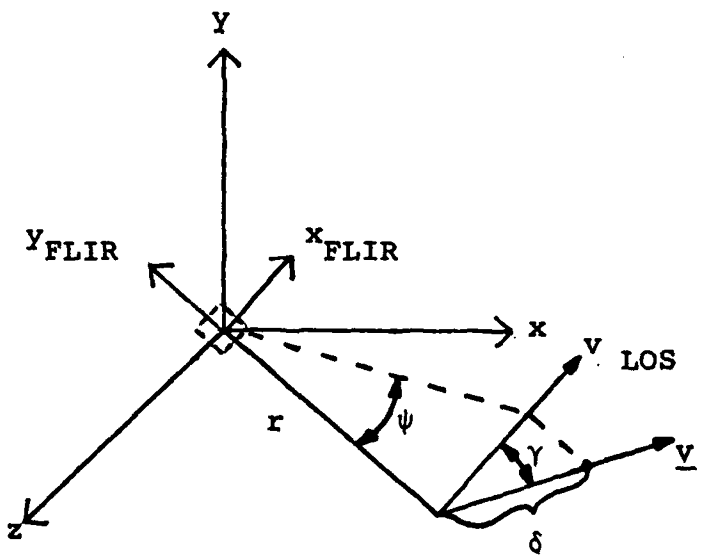

Figure 12. Semimajor Axis Projection

To make use of information already computed in the simulation and with cos $\gamma = 1$ at $t = 0$ for the trajectories used, Equation (2-10) becomes

$$\sigma_v = \frac{(\cos \gamma)(\sigma_{vI})(r_I)}{r} \text{ pixels} \qquad (2\text{-}11)$$

where

r_I = initial target range

σ_{vI} = initial length of semimajor axis in pixels

The radius of the circular missile IR cross-section is retained as the semiminor axis and similiar to the development of Equation (2-11) the distance on the FLIR image plane is given by

$$\sigma_{pv} = \frac{(\sigma_{pvI})(r_I)}{r} \text{ pixels} \qquad (2\text{-}12)$$

where

σ_{pvI} = initial length of semiminor axis in pixels

With these parameters established, the intensity at any point in the image plane can be computed. This calculation is performed in the image ellipse coordinate system. The intensity function is then (6:27)

$$I(x,y) = I_{max} \exp\left\{-0.5 \begin{bmatrix}\Delta x \Delta y\end{bmatrix} \begin{bmatrix}\sigma_v^2 & 0 \\ 0 & \sigma_{pv}^2\end{bmatrix}^{-1} \begin{bmatrix}\Delta x \\ \Delta y\end{bmatrix}\right\} \qquad (2\text{-}13)$$

where

$\Delta x = (x - x_{peak}) \cos \theta + (y - y_{peak}) \sin \theta$

$\Delta y = (y - y_{peak}) \cos \theta - (x - x_{peak}) \sin \theta$

θ = rotation angle between FLIR axis and image ellipse coordinate axis

The average intensity for any pixel, as measured by the FLIR, is the integral of the apparent target intensity function over the pixel area divided by the area of the pixel, corrupted by FLIR and background noise. To approximate this integral, the intensity function was averaged over twenty five equally spaced points within each pixel. To complete the simulation, noise corresponding to FLIR and background noise was added to each pixel. For one of the 64 pixels in the l-th row and m-th column the average intensity as measured by the FLIR is repesented as:

$$z_{lm}(t_i) = \frac{1}{25} \sum_{k=1}^{5} \sum_{j=1}^{5} I_{max} \exp\left\{ -0.5 \begin{bmatrix} \Delta x_{lk} & \Delta x_{mj} \end{bmatrix} \begin{bmatrix} \sigma_v^2 & 0 \\ 0 & \sigma_{vp}^2 \end{bmatrix}^{-1} \begin{bmatrix} \Delta x_{lk} \\ \Delta y_{mj} \end{bmatrix} \right\}$$

$$+ n_{lm}(t_i) \qquad (2\text{-}14)$$

The noise term, $n_{lm}(t_i)$, is based on the research of Harnly and Jensen, ref 6, who documented the existence of spatial correlations of background noise in each data frame with nonnegligible spatial correlations between each pixel and its closest two neighboring pixels in each direction (6:19). The 64 measurements are first arranged into a vector. Then, the covariance matrix, "$\underline{R}$", for the zero-mean white Gaussian noise, n, consisting of components seen in (2-14), is of dimension 64x64. With the spatial correlation matrix, $\underline{R}$, known, realizations of the noise vector can be produced by performing a Cholesky square root decomposition of $\underline{R}$ and post-multiplying it by a vector of independent, white Gaussian noises, each of zero mean and variance of one. The noise vector is

$$\underline{v}(t_i) = {}^{C}\sqrt{\underline{R}}\ \underline{v}'(t_i) \tag{2-15}$$

where

$\underline{v}'(t_i)$ = white Gaussian noise vector with independent scalar noises and statistics

$$E\{\underline{v}'(t_i)\} = 0$$

$$E\{\underline{v}'(t_i)\underline{v}'^{T}(t_j)\} = \underline{I}\delta_{ij}$$

The model given in Equation (2-15) is used because the noise $\underline{v}'$ is readily simulated via repeated independent calls to a Gaussian random number generator. Thus, the covariance of $\underline{v}(t_i)$ is equal to the correlation matrix.

$$E\{\underline{v}(t_i)\underline{v}^{T}(t_j)\} = E\{{}^{C}\sqrt{R}\ \underline{v}'(t_i)v'^{T}(t_j){}^{C}\sqrt{R}^{T}\} = \underline{R}\delta_{ij}$$

As justified in the analysis by Harnly and Jensen, temporal correlation of the background and FLIR noises are assumed negligible. The noise array vector is then added to the input array, as in Equation (2-14), to create the measurement array for the correlator/Kalman filter.

Equation (2-14) represents the measurement array for a single hot spot target. For multiple hot spot targets, three Gaussian hot spots with elliptical constant intensity contours and parallel semimajor axes were used in this study. The measurement is then the summation of three double summation terms of the form given in (2-14) instead of one, plus the noise as in (2-14).

2.5 Projection of Multiple Hot Spots

The location of the aircraft center of mass (COM) in FLIR coordinates can be determined, as previously described, and the method for projecting the intensity pattern onto the FLIR plane is the same for multiple and single hot spot cases because the assumption is made that the semimajor axes of the ellipsoids are parallel. Thus, by calculating the angular orientation of one of the hot spots the orientation of all of the hot spots is known. Therefore, the only remaining information required for the projection is the coordinates of the center of each ellipsoid in the FLIR image plane. This requires that the distance from the COM of the aircraft to the center of each ellipsoid be known in inertial frame coordinates and transformed into FLIR frame coordinates. For single hot spot targets, the center of the intensity ellipsoid is assumed to coincide with the aircraft COM and no additional calculations are required.

With the orientation of the FLIR image plane relative to an inertial frame being as shown in Figure 13, and the angles α and β known, as calculated in the trajectory model, unit vectors in the directions referred to as $\vec{e}_\beta$ and $\vec{e}_{z\alpha}$ can be determined. Notice that in FLIR frame coordinates $\vec{e}_\beta = \vec{e}_{y\ FLIR}$ and $\vec{e}_{z\alpha} = -\vec{e}_{x\ FLIR}$. This coordinate frame was selected instead of using $\vec{e}_{x\ FLIR}$ directly for ease in implementing the required coordinate frame transformations (Appendix A).

The $\vec{e}_\beta$-$\vec{e}_{z\alpha}$ plane is then translated in inertial space so that the origin of this plane coincides with the aircraft COM (Figure 14).

From the trajectory model, the velocity vector of the aircraft is known. Since the location of the hot spots in a body fixed frame can be readily determined, the velocity vector, which by assumption will always point out the nose of the aircraft, can be used to define

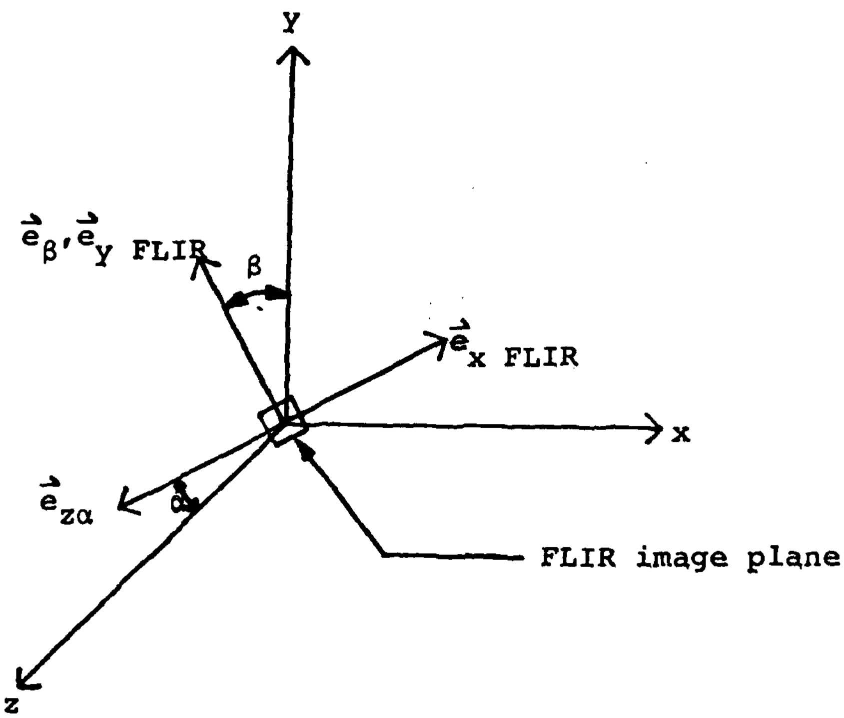

Figure 13. $\vec{e}_\beta$-$\vec{e}_{z\alpha}$ Plane

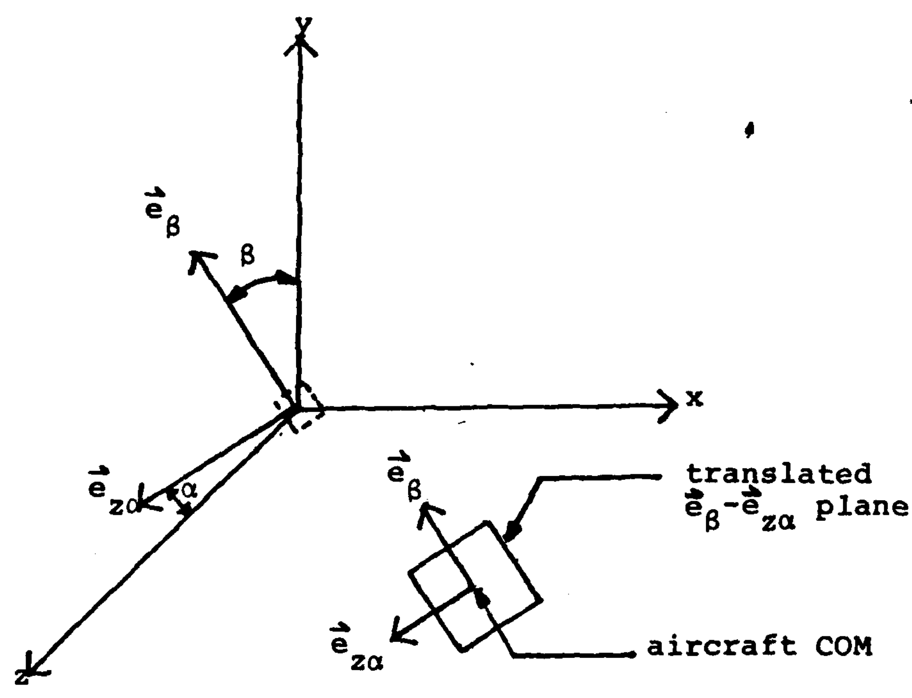

Figure 14. $\vec{e}_\beta$-$\vec{e}_{z\alpha}$ Plane Translation

one axis of a coordinate frame with its origin lying at the aircraft COM, referred to as the H-frame. Thus, $\vec{e}_{Hx}$ is defined to be a unit vector in the direction of the velocity vector and forms one axis of the H-frame. Performing a cross-product of the velocity vector with a unit vector in the inertial y direction, $\vec{j}$, will produce a vector normal to $\vec{j}$ and $\underline{v}$, which is normalized to form a unit in the direction of the second axis of the H-frame, $\vec{e}_{Hy}$. Note that this axis will always lie in the horizontal plane. The third axis of the H-frame is subsequently calculated by crossing the two H-frame axis vectors, to produce a vector normal to the $\vec{e}_{Hx}$-$\vec{e}_{Hy}$ plane, which when normalized becomes $\vec{e}_{Hz}$. The unit vectors of the translated $\vec{e}_{\beta}$-$\vec{e}_{z\alpha}$ frame and the H-frame with origins located at the aircraft COM, are shown in Figure 15.

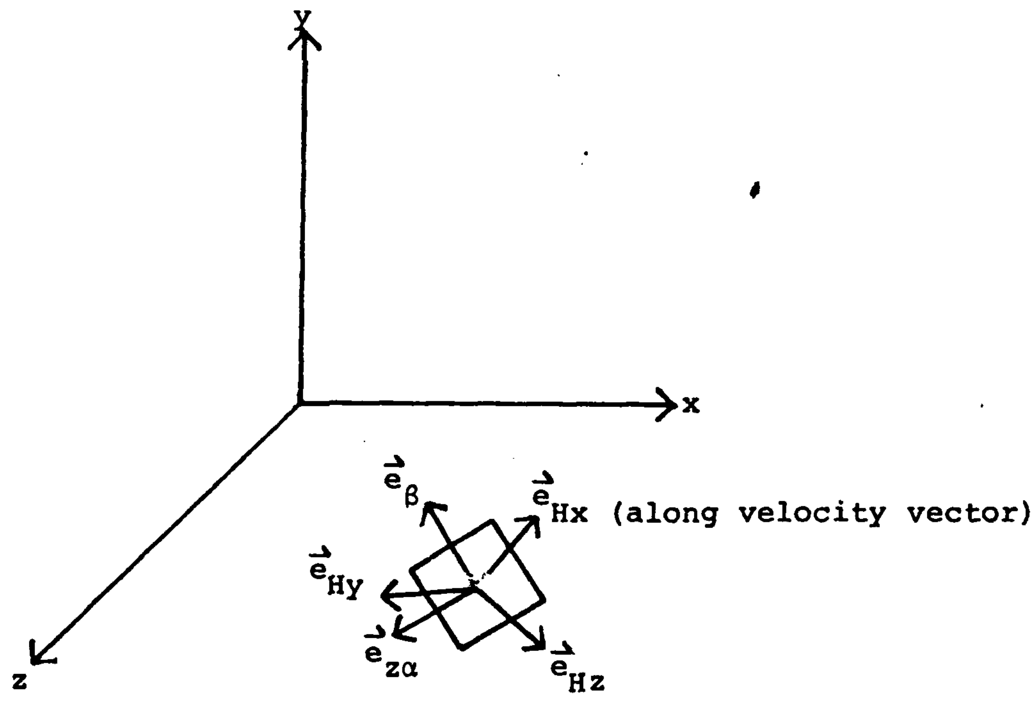

Figure 15. $\vec{e}_{\beta}$-$\vec{e}_{z\alpha}$ and H-Frame Unit Vectors

Let the body frame, B, have the x-axis out the aircraft nose, the y-axis out the aircraft right wing, and the z-axis out the aircraft belly, and assume that initially the aircraft is oriented such that the aircraft body frame lies with the plane of the aircraft wings in the $\vec{e}_{Hx}$-$\vec{e}_{Hy}$ plane. Specifically for the three hot spot target model used, the initial location of the intensity functions are shown in Figure 16.

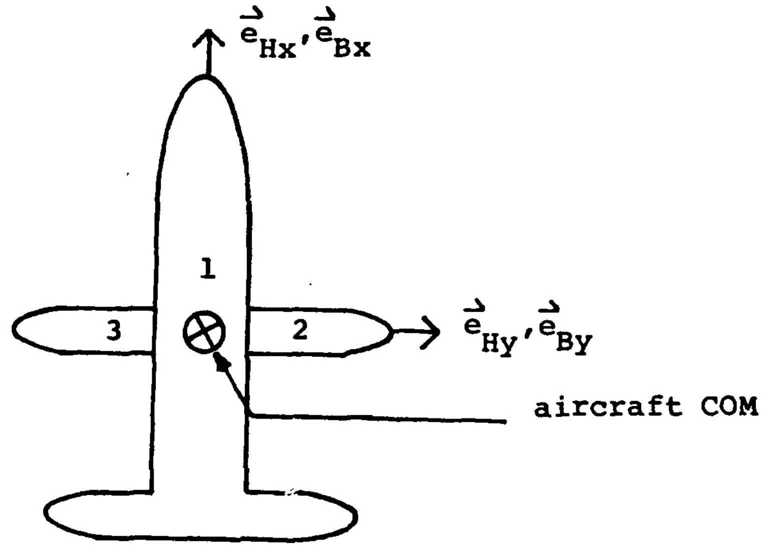

Figure 16. Initial Ellipsoidal Centers

where

$\vec{e}_{Hz}$, $\vec{e}_{\beta z}$ into the page

1, 2, and 3, location of the center of each intensity ellipsoid, in relation to the aircraft COM.

By assumption, the center of ellipsoid 1 will lie along the $\vec{e}_{Hx}$ axis. The ellipsoidal centers along the $\vec{e}_{Hy}$ axis will remain along that axis unless the aircraft performs a roll maneuver, in which case their location can be determined as shown in Figure 17. In order to simulate a roll maneuver in this thesis, a constant roll-rate, ω, was used. Using a constant roll-rate implies a step change from a wing-level trajectory to a constant roll-rate rather than a smooth build up to the desired rate. This method was used for ease in implementing the simulation. However, this also requires the filter to track a maneuver which is harsher than realistically would be encountered and thus the results obtained are for a worst case scenario.

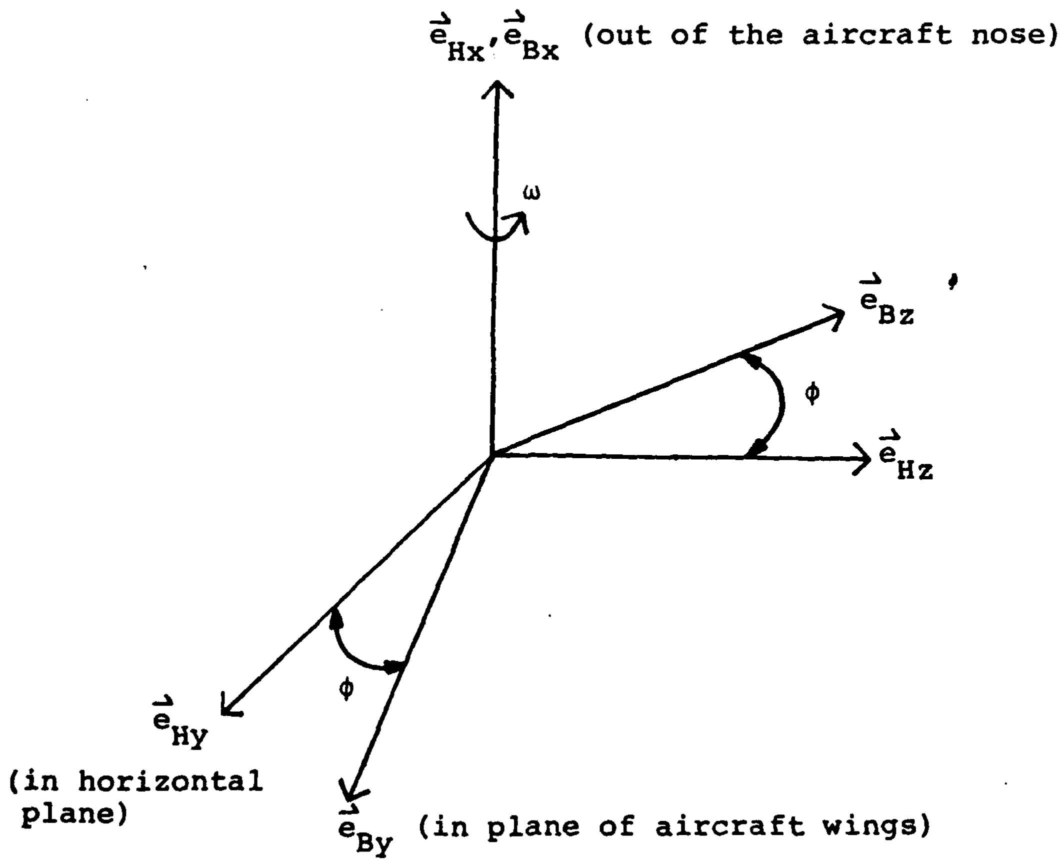

Figure 17. Roll Maneuver Geometry

Since the intensity funciton centroids are offset in the $\vec{e}_{Bx}$-$\vec{e}_{By}$ plane, the only calculation required to determine the direction of the ellipsoidal centers is

$$\vec{e}_{By} = \cos\phi\,\vec{e}_{Hy} + \sin\phi\,\vec{e}_{Hz} \qquad (2\text{-}16)$$

where

ϕ is the roll angle measured from $\vec{e}_{Hy}$ to $\vec{e}_{By}$. In simulations for this thesis, ϕ is the result of a constant roll rate ω, $\phi = \omega t$

Thus, the location of the three hot spots relative to the H-frame can always be determined.

The final step is to convert this distance to the equivalent offset distance on the FLIR image plane. Let δ represent the distance in meters from the aircraft COM to the center of ellipsoid 2, lying in the positive e_{By} direction. This is depicted in Figure 18.

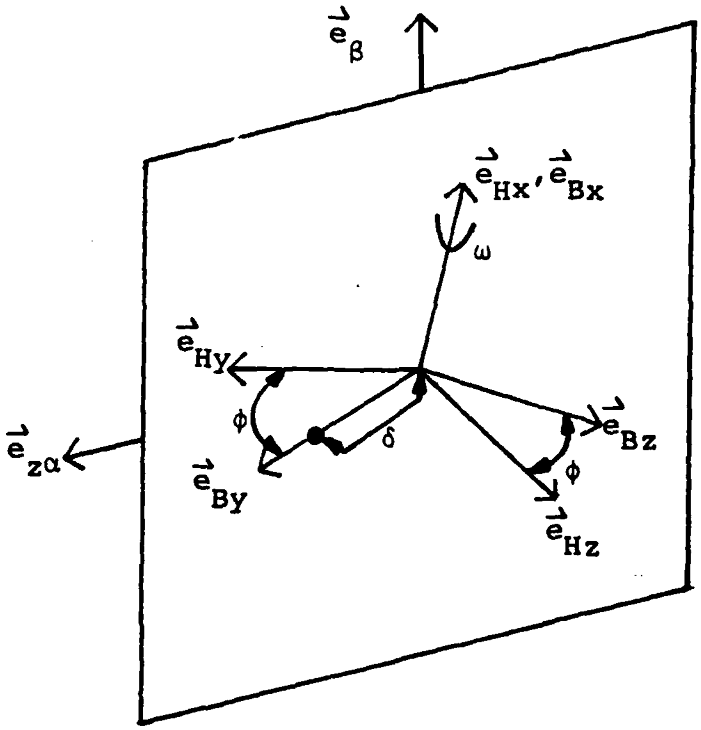

Figure 18. Hot Spot Offset

By taking the following dot products, $\delta\{\vec{e}_{By}\cdot\vec{e}_{z\alpha}\}$ and $\delta\{\vec{e}_{By}\cdot\vec{e}_{\beta}\}$, the projection of the ellipsoidal displacement onto the translated $\vec{e}_{\beta}$-$\vec{e}_{z\alpha}$ plane is determined, as shown in Figure 19.

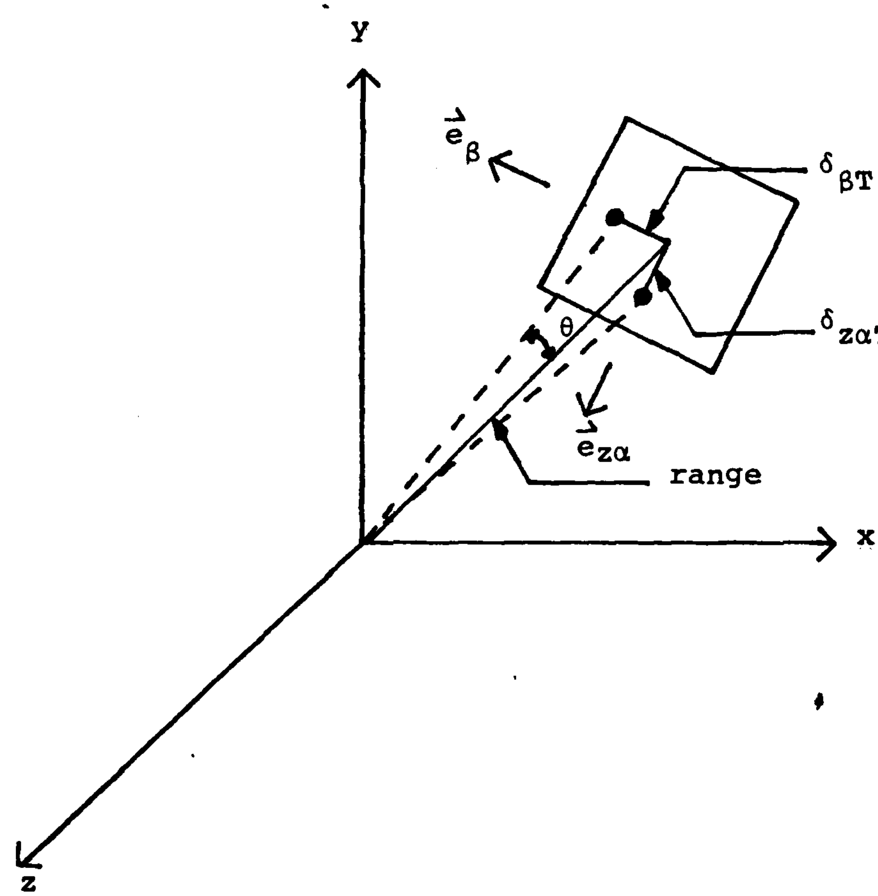

Figure 19. Distance Translated in $\vec{e}_{\beta}$-$\vec{e}_{z\alpha}$ Plane

where

$$\delta_{\beta T} = \delta(\vec{e}_{By}\cdot\vec{e}_{\beta}) = \text{distance along translated } \vec{e}_{\beta} \text{ axis}$$

in meters.

$\delta_{z\alpha T} = \delta(\vec{e}_{By} \cdot \vec{e}_z)$ = distance along translated $\vec{e}_{z\alpha}$ axis in meters

With $\delta_{\beta T}$ and $\delta_{z\alpha T}$ known, this distance is converted into distance on the FLIR image plane. Since the translated $\vec{e}_\beta$-$\vec{e}_{z\alpha}$ plane is normal to the range vector, the angular displacement of the hot spot from the center of the FLIR FOV can be used to approximate the linear displacement in the FLIR plane. In the $\vec{e}_\beta$ direction,

$$\delta_\beta = \tan\theta \approx \theta = \frac{\delta_{\beta T}}{r} \tag{2-17}$$

where

θ = displacement angle as shown in Figure 19.

r = range

Equation (2-17) gives the distance, δ_β, in radians, which is converted to pixels by dividing by .00002 radians/pixel. Displacement in the $\vec{e}_\beta$ direction is added in the y_{FLIR} direction to the coordinates of the aircraft COM to determine the y_{FLIR} location of the hot spot. Displacement in the $\vec{e}_{z\alpha}$ direction is likewise calculated and subtracted from the coordinates of the aircraft COM to determine the x_{FLIR} location of the hot spot because of the axis orientation shown in Figure 13. Thus, the coordinates of the ellipsoidal centers in the FLIR image plane are known. To demonstrate this projection, a sample trajectory was run with initial coordinates

$$x_I = y_I = z_I = 10,000 \text{ m}$$

and constant velocity

$$\dot{x}_I(t) = \dot{y}_I(t) = \dot{z}_I(t) = -500.0 \text{ m/sec} \qquad (2\text{-}19)$$

The target is moving directly at the FLIR image plane therefore,

$$\dot{\alpha}(t) = \dot{\beta}(t) = 0$$

for the entire trajectory. Hot spots were initially positioned 1 meter forward of the aircraft COM in the $\vec{e}_{Hx}$ direction and (±) .5 meters in the $\vec{e}_{Hy}$ direction. Two simulations were used to demonstrate this projection model, The first run, see Figure 20, shows that for a roll of π radians, hot spot 1 stays centered in the $\vec{e}_{\beta}$-$\vec{e}_{z\alpha}$ plane, while hot spots 2 and 3 roll through π radians and remain positioned π radians apart on the $\vec{e}_{\beta}$-$\vec{e}_{z\alpha}$ plane. As the aircraft approaches the tracker location, the distance from the aircraft COM to the hot spots as projected onto the FLIR plane will increase which accounts for the offset semicircles seen in Figure 20. The second run also initialized as in (2-18) with velocity components as in (2-19), was used to show the proper displacement on the $\vec{e}_{\beta}$-$\vec{e}_{z\alpha}$ plane. During this run, shown in Figure 21, the aircraft conducted a 2 π roll about its velocity vector with the hot spots positioned as in the first run. Substituting the initial conditions from Equation (2-18) into Equation (2-17) yields the initial offset distance for hot spots 2 and 3 from the aircraft COM.

$$\delta_{z\alpha} = \left[\frac{(\pm)(.5)}{\{(3)(10000^2)\}^{\frac{1}{2}}}\right]\left[\frac{1}{.00002}\right] = (\pm)\ 1.44 \text{ pixels}$$

For a 5 second simulation Equation (2-19) can also be used to determine the inertial position of the aircraft at t = 5.0. Thus, Equation (2-17) can again be used to determine final offsets of the hot spots.

$$\delta_{z\alpha} = \left[\frac{(\pm)(.5)}{\{(3)(7500^2)\}^{\frac{1}{2}}} \right] \left[\frac{1}{.00002} \right] = (\pm)\ 1.93 \text{ pixels}$$

As shown in Figure 21, hot spots 2 and 3 roll through 2 π radians with initial and final offset distance as calculated and hot spot 1 remains centered in the plane. For a detailed description of the projection model equations, see Appendix A.

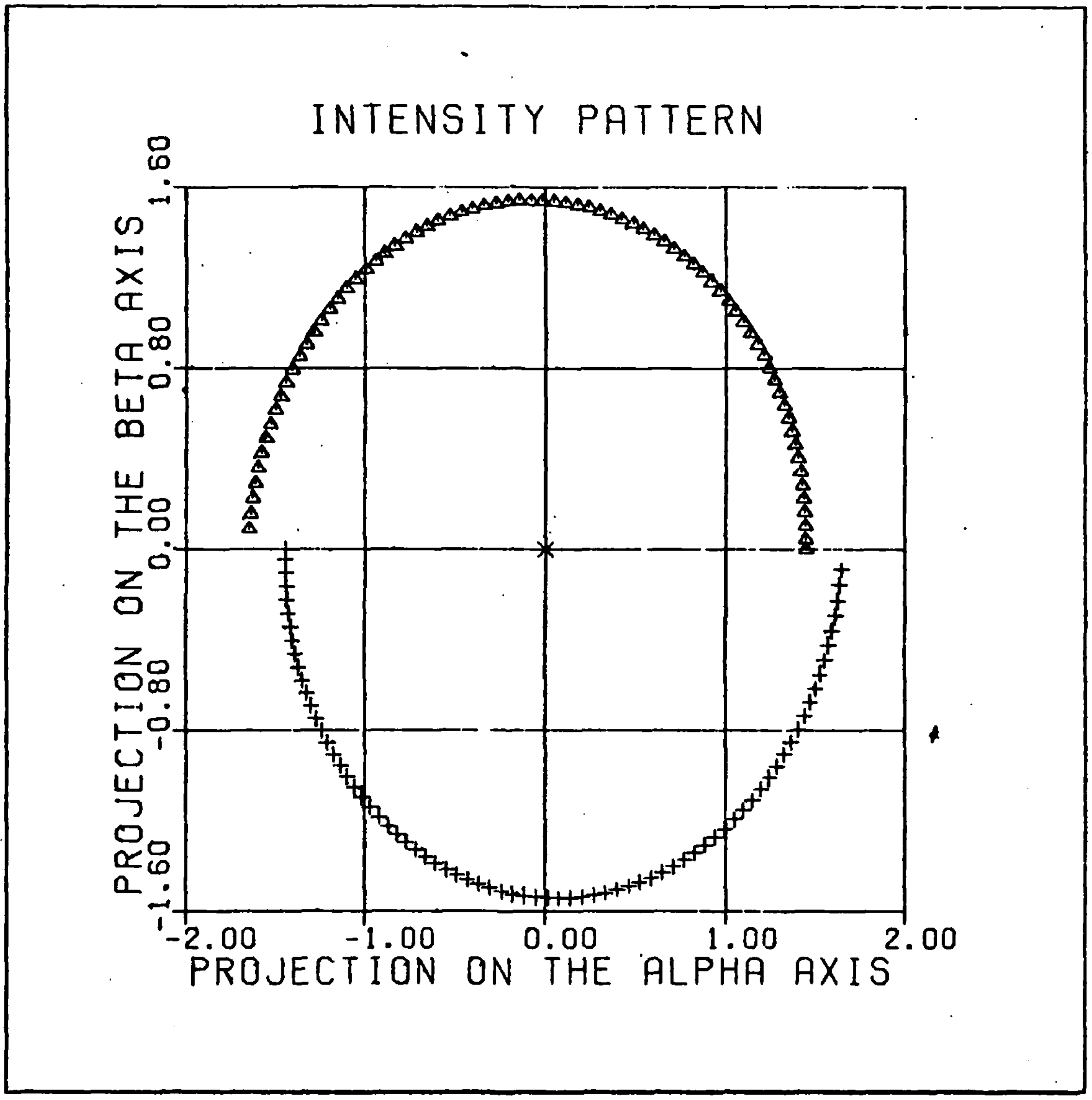

Figure 20. π Radians Roll

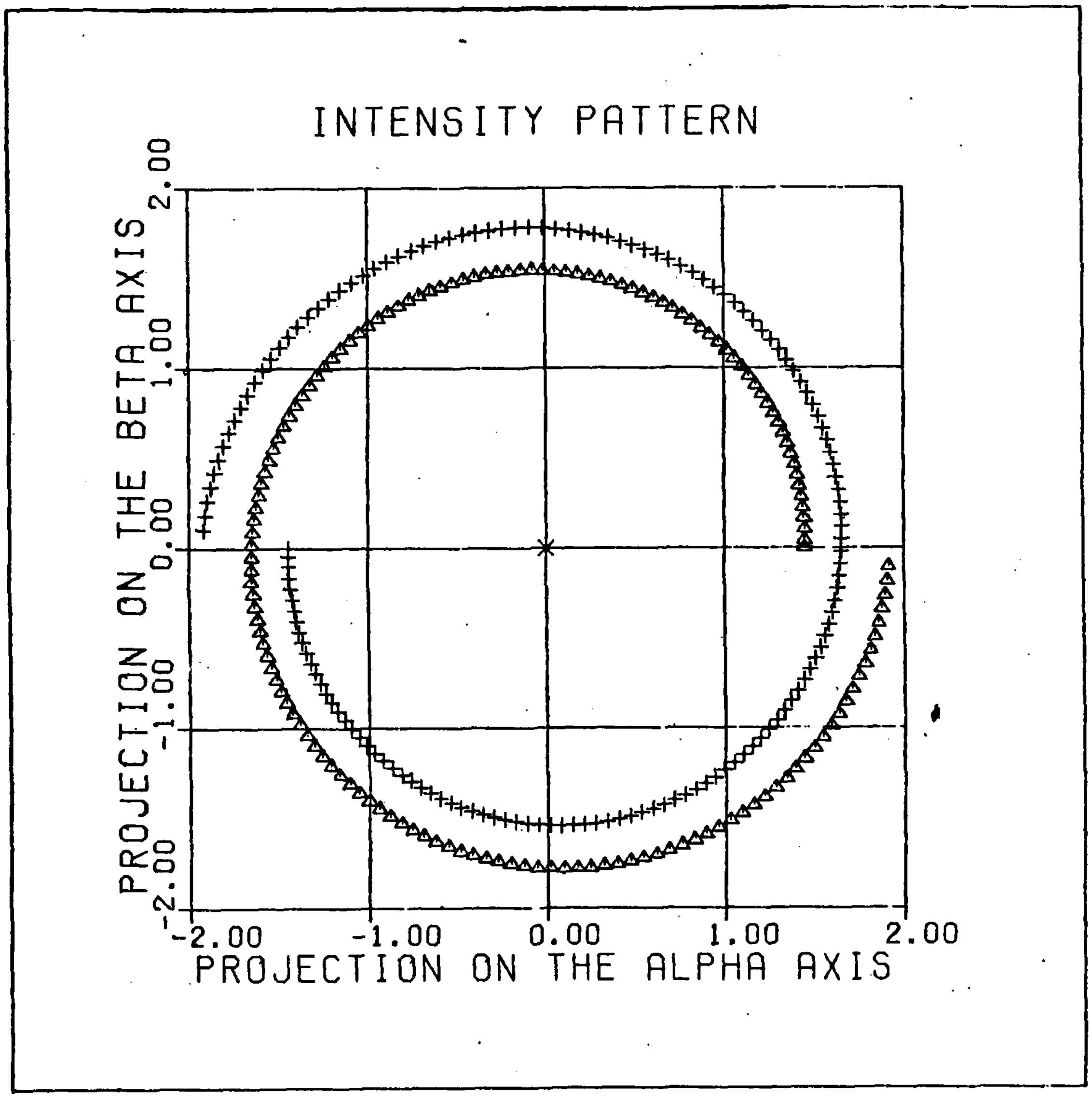

Figure 21. 2π Radians Roll

III. Kalman Filter

3.1 Introduction

The primary focus of Rogers' thesis (8) was to develop an algorithm capable of indentifying, in real-time, the intensity function of the target. As such, the ability of the Kalman filter to track a realistic, highly dynamic target was not of primary concern, so a four-state Kalman filter, consisting of estimates for the x and y position due to true target dynamics and the x and y position due to atmospherics, which sum together to form the apparent target centroid location as,

$$x_{centroid} = x_{dynamics} + x_{atmospherics} \tag{3-1}$$

and similarly in the y-direction, was used. Such a model is acceptable if the target is not highly dynamic and does not leave the FLIR FOV in one sample period. However, in practical applications a missile can travel many times the width of the FLIR FOV in one sample period. For example, a typical missile at a range of 10 km can travel approximately 80 pixels per sample period and a FLIR with an 8x8 pixel FOV and no predictive capability will not be able to keep the target within its FOV, resulting in loss of target track (6:69). Therefore, the tracker must have a predicted target position for the next sample period.

Although a six-state filter which additionally estimates target velocity in both directions might be appropriate in certain situations, previous research efforts have shown that in order to achieve accurate target position information acceleration estimates in both directions must be incorporated into the filter model as well, resulting in an eight-state filter (6).

Of the acceleration models most commonly used, first order Gauss-Markov and constant turn-rate models have yielded the best results, with the constant turn-rate model proving more representative of the tracking scenarios being investigated (7,16). However, the performance enhancement achieved by using the non-linear constant turn-rate model is not so significant as to justify the increased computational burden associated with its implementation over the linear Gauss-Markov model (11). Therefore, a first-order Gauss-Markov acceleration model was selected for this study. As in Rogers' four-state filter, this filter uses the Gauss-Markov model developed by Mercier for the atmospheric jitter process (10).

3.2 Acceleration and Atmospheric Models

Target acceleration and atmospheric jitter are modeled as stationary, first-order Gauss-Markov processes, generated as the outputs of first-order lags driven by white Gaussian noises. The differential equation describing such a process is

$$\dot{x}(t) = -\frac{1}{T}x(t) + w(t) \tag{3-2}$$

and

$$E\{w(t)\} = 0$$

$$E\{w(t)w(t+\tau)\} = \frac{2\sigma^2}{T}\,\delta(\tau)$$

where

$x(t)$ = the Gauss-Markov process with initial conditions determined from a priori knowledge of the process

T = correlation time of $x(t)$

$w(t)$ = white Gaussian noise process

σ = root mean square value of $x(t)$

Throughout the development of this chapter, the subscripts a, d, and f, will be used to represent atmospherics, dynamics, and filter, respectively. For the atmospheric position, the correlation time constant, T_{af}, as developed by Mercier (10) will be used. The acceleration time constant, T_{df}, is a parameter to be established during the off-line filter tuning process although on-time estimation techniques could be employed (13:Chapter 10). Equation (3-2) serves as the stochastic model upon which the filter is based.

3.3 State Space Model

The eight-state filter will now be put into state space notation. The dynamics model in each direction is

$$\dot{x}_{df}(t) = v_{df}(t)$$

$$\dot{v}_{df}(t) = a_{df}(t)$$

$$\dot{a}_{df}(t) = -\frac{1}{T_{df}} a_{df}(t) + w_{df}(t) \qquad (3\text{-}3)$$

and

$$E\{w_{df}(t)\} = 0$$

$$E\{w_{df}(t) w_{df}(t+\tau)\} = \frac{2\sigma^2_{df}}{T_{df}} \delta(\tau)$$

where

T_{df} = correlation time assumed for target acceleration

σ^2_{df} = assumed target acceleration process variance

The atmospheric disturbance model in each direction is

$$\dot{x}_{af}(t) = -\frac{1}{T_{af}} x_{af}(t)+w_{af}(t) \qquad (3\text{-}4)$$

and

$$E\{w_{af}(t)\} = 0$$

$$E\{w_{af}(t)w_{af}(t+\tau)\} = \frac{2\sigma^2_{af}\delta(\tau)}{T_{af}}$$

where

T_{af} = correlation time assumed for atmospheric jitter

σ^2_{af} = assumed atmospheric jitter process variance

Augmenting the atmospheric states to the dynamic states, the propagation equation upon which the Kalman filter is based is formed:

$$\underline{\dot{x}}_f(t) = \underline{F}_f(t)\underline{x}_f(t)+\underline{G}_f(t)\underline{w}_f(t) \qquad (3\text{-}5)$$

where

$\underline{F}_f(t)$ = time-invariant filter plant matrix

$\underline{x}_f(t)$ = filter state vector

x_1 = azimuth position

x_2 = elevation position

x_3 = azimuth velocity = $\dot{x}_1$

x_4 = elevation velocity = $\dot{x}_2$

x_5 = azimuth acceleration = $\dot{x}_3$

x_6 = elevation acceleration = $\dot{x}_4$

x_7 = azimuth atmospheric disturbance

x_8 = elevation atmospheric disturbance

$\underline{G}_f$ = constant 8x4 noise distribution matrix

$\underline{w}_f(t)$ = 4-dimensional white Gaussian noise composed of $w_1 = w_{dfx}$ and $w_2 = w_{dfy}$ as in (3-3) and $w_3 = w_{afx}$ and $w_4 = w_{afy}$ as in (3-4).

Substituting Equations (3-3) and (3-4) into Equation (3-5) yields:

$$\dot{\underline{x}}_f(t) = \begin{bmatrix} 0 & 0 & 1 & 0 & 0 & 0 & 0 & 0 \\ 0 & 0 & 0 & 1 & 0 & 0 & 0 & 0 \\ 0 & 0 & 0 & 0 & 1 & 0 & 0 & 0 \\ 0 & 0 & 0 & 0 & 0 & 1 & 0 & 0 \\ 0 & 0 & 0 & 0 & \frac{-1}{T_{df}} & 0 & 0 & 0 \\ 0 & 0 & 0 & 0 & 0 & \frac{-1}{T_{df}} & 0 & 0 \\ 0 & 0 & 0 & 0 & 0 & 0 & \frac{-1}{T_{af}} & 0 \\ 0 & 0 & 0 & 0 & 0 & 0 & 0 & \frac{-1}{T_{af}} \end{bmatrix} \underline{x}_f(t)$$

$$+ \begin{bmatrix} 0 & 0 & 0 & 0 \\ 0 & 0 & 0 & 0 \\ 0 & 0 & 0 & 0 \\ 0 & 0 & 0 & 0 \\ 1 & 0 & 0 & 0 \\ 0 & 1 & 0 & 0 \\ 0 & 0 & 1 & 0 \\ 0 & 0 & 0 & 1 \end{bmatrix} \begin{bmatrix} w_1(t) \\ w_2(t) \\ w_3(t) \\ w_4(t) \end{bmatrix} \tag{3-6}$$

where $w_1(t)$ through $w_4(t)$ are zero-mean, independent white Gaussian noises with

$$E\{\underline{w}_f(t)\underline{w}_f^T(t+\tau)\} = \underline{Q}_f\delta(\tau)$$

and

$$
\underline{Q}_f = \begin{bmatrix} \frac{2\sigma_{df}^2}{T_{df}} & 0 & 0 & 0 \\ 0 & \frac{2\sigma_{df}^2}{T_{df}} & 0 & 0 \\ 0 & 0 & \frac{2\sigma_{af}^2}{T_{af}} & 0 \\ 0 & 0 & 0 & \frac{2\sigma_{af}^2}{T_{af}} \end{bmatrix} \quad (3\text{-}7)
$$

3.4 State Propagation

The Kalman filter must propagate its state estimate vector and conditional covariance matrix from one sample time to the next. The standard propagation equations for the case of zero control inputs over a sample interval are:

$$
\hat{\underline{x}}_f(t_{i+1}^-) = \underline{\Phi}_f(t_{i+1},t_i)\hat{\underline{x}}_f(t_i^+) \quad (3\text{-}8)
$$

$$
\underline{P}_f(t_{i+1}^-) = \underline{\Phi}_f(t_{i+1},t_i)\underline{P}_f(t_i^+)\Phi_f^T(t_{i+1},t_i) + \quad (3\text{-}9)
$$

$$
+ \int_{t_i}^{t_{i+1}} \underline{\Phi}_f(t_{i+1},\tau)\underline{G}_f(\tau)\underline{Q}_f(\tau)\underline{G}_f^T(\tau)\Phi_f^T(t_{i+1},\tau)\,d\tau
$$

where

$\underline{\Phi}_f(t_{i+1},t_i)$ = filter state transition matrix

$\underline{P}_f(t_i^+)$ = conditional state covariance matrix from measurement update at time t_i

$\underline{P}_f(t_{i+1}^-)$ = conditional state covariance matrix propagated from time t_i to t_{i+1}

$\underline{Q}_f$ = noise covariance kernel description as defined in Equation (3-7)

The filter state transition matrix, $\underline{\Phi}_f(t_{i+1},t_i)$, must satisfy the differential equation

$$\dot{\underline{\Phi}}_f(t,t_i) = \underline{F}_f\underline{\Phi}_f(t,t_i) \tag{3-10}$$

over the interval (t_i,t_{i+1}), with initial condition

$$\underline{\Phi}_f(t_i,t_i) = \underline{I} \text{ (identity matrix)}$$

In this application, the plant matrix $\underline{F}_f$ is constant and the fixed sample period results in a constant state transition matrix, $\underline{\Phi}_f(t_{i+1},t_i)$, for all sample periods. Thus,

$$\underline{\Phi}_f(t_{i+1},t_i) = \begin{bmatrix} 1 & 0 & \Delta t & 0 & A & 0 & 0 & 0 \\ 0 & 1 & 0 & \Delta t & 0 & A & 0 & 0 \\ 0 & 0 & 1 & 0 & B & 0 & 0 & 0 \\ 0 & 0 & 0 & 1 & 0 & B & 0 & 0 \\ 0 & 0 & 0 & 0 & e^{\frac{-\Delta t}{T_{df}}} & 0 & 0 & 0 \\ 0 & 0 & 0 & 0 & 0 & e^{\frac{-\Delta t}{T_{df}}} & 0 & 0 \\ 0 & 0 & 0 & 0 & 0 & 0 & e^{\frac{-\Delta t}{T_{af}}} & 0 \\ 0 & 0 & 0 & 0 & 0 & 0 & 0 & e^{\frac{-\Delta t}{T_{af}}} \end{bmatrix} \tag{3-11}$$

where

$$A = T_{df}^{\,2}\left[\frac{\Delta t}{T_{df}} - 1 + e^{\frac{-\Delta t}{T_{df}}}\right]$$

$$B = T_{df}\left[1 - e^{\frac{-\Delta t}{T_{df}}}\right]$$

$$\Delta t = (t_{i+1} - t_i)$$

The solution to the integral term of Equation (3-9), $\underline{Q}_{fd}$, which represents the growth in uncertainty due to dynamic driving noise since the last measurement update becomes

$$\underline{Q}_{fd} = \begin{bmatrix} Q_{11} & 0 & Q_{13} & 0 & Q_{15} & 0 & 0 & 0 \\ 0 & Q_{11} & 0 & Q_{13} & 0 & Q_{15} & 0 & 0 \\ Q_{13} & 0 & Q_{33} & 0 & Q_{35} & 0 & 0 & 0 \\ 0 & Q_{13} & 0 & Q_{33} & 0 & Q_{35} & 0 & 0 \\ Q_{15} & 0 & Q_{35} & 0 & Q_{55} & 0 & 0 & 0 \\ 0 & Q_{15} & 0 & Q_{35} & 0 & Q_{55} & 0 & 0 \\ 0 & 0 & 0 & 0 & 0 & 0 & Q_{77} & 0 \\ 0 & 0 & 0 & 0 & 0 & 0 & 0 & Q_{77} \end{bmatrix} \tag{3-12}$$

where

$$Q_{11} = \sigma_{df}^2 \left[\frac{(2)(T_{df})(\Delta t)^3}{3} - (2)(T_{df})^2(\Delta t)^2 - (4)(T_{df})^3(\Delta t)(e^{\frac{-\Delta t}{T_{df}}}) + (2)(T_{df})^3(\Delta t) - (T_{df})^4(e^{\frac{-2\Delta t}{T_{df}}}) + T_{df}{}^4 \right]$$

$$Q_{13} = \sigma_{df}^2 \left[(T_{df})(\Delta t)^2 + (2)(T_{df})^2(\Delta t)(e^{\frac{-\Delta t}{T_{df}}}) + T_{df}{}^3 - (2)(T_{df})^3(e^{\frac{-\Delta t}{T_{df}}}) - (2)(T_{df})^2(\Delta t) + (T_{df})^3(e^{\frac{-2\Delta t}{T_{df}}}) \right]$$

$$Q_{15} = \sigma_{df}^2 \left[(-2)(T_{df})(\Delta t)(e^{\frac{-\Delta t}{T_{df}}}) + T_{df}{}^2 - (T_{df})^2(e^{\frac{-2\Delta t}{T_{df}}}) \right]$$

$$Q_{33} = \sigma^2_{df}\left[(2)(T_{df})(\Delta t)-(3)(T_{df})^2+(4)(T_{df})^2(e^{\frac{-\Delta t}{T_{df}}})-(T_{df})^2(e^{\frac{-2\Delta t}{T_{df}}})\right]$$

$$Q_{35} = \sigma^2_{df}\left[T_{df}-(2)(T_{df})(e^{\frac{-\Delta t}{T_{df}}})+(T_{df})(e^{\frac{-2\Delta t}{T_{df}}})\right]$$

$$Q_{55} = \sigma^2_{df}\left[1-e^{\frac{-2\Delta t}{T_{df}}}\right]$$

$$Q_{77} = \sigma^2_{df}\left[1-e^{\frac{-2\Delta t}{T_{af}}}\right]$$

Note that $Q_{22} = Q_{11}$, $Q_{44} = Q_{33}$, $Q_{66} = Q_{55}$, $Q_{88} = Q_{77}$, $Q_{24} = Q_{13}$, $Q_{26} = Q_{15}$, $Q_{46} = Q_{35}$. For development of the noise covariance matrix, Equation (3-12), see Appendix B.

The matrix of Equation (3-12) is constant for a given sample time and fixed T_{df} and T_{af}. The values of σ^2_{df} and σ^2_{af} of the Equation (3-7) can either be determined offline during a filter tuning process or adaptively in real-time although in this instance σ^2_{af} was always determined offline. This tuning process is used to select the values of these parameters which optimize tracking performance, optimum in the sense that the mean square tracking errors are minimized, for specific scenarios. Equations (3-8) and (3-9) propagate the filter states and conditional covariance forward to the next sample time. Once the predicted states for the next sample time are calculated, the estimates of the target's position in azimuth and elevation are fed back to the controller. The controller then positions the center of the FLIR field-of-view at that predicted location by the next sample time. Since the filter assumes that the FLIR is centered on the true target position, the state estimate prior to the measurement update is

$$\underline{\hat{x}}'(t_{i+1}^-) = \left[0 \;\; 0 \;\; \hat{x}_{vel}\hat{y}_{vel}\hat{x}_{acc}\hat{x}_{atmos}\hat{y}_{atmos}\right]^T \qquad (3\text{-}13)$$

i.e., $\hat{\underline{x}}(t_{i+1}^-)$ of Equation (3-8) with the first two components zeroed out.

3.5 Measurement Update Equation

The two-dimensional discrete-time measurement vector generated by the correlation algorithm, $\underline{z}(t_i)$, is a linear combination of the state variables of interest, i.e. the apparent target intensity function's true position corrupted by uncertain measurement disturbance, $\underline{v}(t_i)$. Thus,

$$\underline{z}(t_i) = \underline{H}_f \underline{x}_f(t_i) + \underline{v}_f(t_i) \qquad (3\text{-}14)$$

where

$\underline{z}(t_i) = \begin{bmatrix} x_c \\ y_c \end{bmatrix}$ = the estimated x and y coordinates of the centroid of the target intensity function as estimated by the correlation algorithm

$\underline{H}_f(t_i) = \begin{bmatrix} 1 & 0 & 0 & 0 & 0 & 0 & 1 & 0 \\ 0 & 1 & 0 & 0 & 0 & 0 & 0 & 1 \end{bmatrix}$ = linear combination of the state variables which contribute to the measurement elements

$\underline{v}_f(t_i)$ = additive noise assumed to be white Gaussian with statistics:

$$E\left[\underline{v}_f(t_i)\right] = \underline{0}$$

$$E\left[\underline{v}_f(t_i)\underline{v}_f^T(t_j)\right] = \underline{R}_f(t_i)\delta_{ij}$$

The measurement information, $\underline{z}(t_i)$, is incorporated by the Kalman filter using the standard update equations:

$$\underline{K}_f(t_i) = \underline{P}_f(t_i^-)\underline{H}_f^T(t_i)\{\underline{H}_f(t_i)\underline{P}_f(t_i^-)\underline{H}_f^T(t_i)+\underline{R}_f(t_i)\}^{-1}$$

$$\hat{\underline{x}}_f(t_i^+) = \hat{\underline{x}}_f(t_i^-)+\underline{K}_f(t_i)\{\underline{z}_f(t_i)-\underline{H}_f(t_i)\hat{\underline{x}}_f(t_i^-)\}$$

$$\underline{P}_f(t_i^+) = \underline{P}_f(t_i^-)-\underline{K}_f(t_i)\underline{H}_f(t_i)\underline{P}_f(t_i^-) \tag{3-15}$$

where

$\hat{\underline{x}}_f(t_i^-),\underline{P}_f(t_i^-)$ = state estimate and conditional covariance obtained from Equations (3-8) and (3-9)

$\underline{K}_f(t_i)$ = Kalman filter gain

$\underline{R}_f(t_i)$ = measurement uncertainty covariance matrix as determined from a statistical analysis of measurement errors (see Chapter 4) and assumed constant for off-line tuning

For a detailed development of the Kalman filter equations, see reference 12.

3.6 Q_D Estimation

Online parameter estimation techniques are often used to improve the quality of the state estimates when uncertain parameters exist within the system model or noise covariances. Although a variety of estimation techniques are available (13: Chapter 10), a self-tuning $\underline{Q}_D$ adaptation technique was chosen since all of the information required to implement this estimator is available from the Kalman filter equations, and the computational loading incurred by implementing this method is substantially less than the other estimation techniques referenced.

The estimator is developed as follows:

$$\underline{P}_f(t_i^-) = \underline{\Phi}_f(t_i,t_{i-1})\underline{P}_f(t_{i-1}^+)\underline{\Phi}_f^T(t_i,t_{i-1})+\underline{Q}_{fd}(t_{i-1}) \quad (3\text{-}16)$$

and

$$\underline{P}_f(t_i^+) = \underline{P}_f(t_i^-)-\underline{K}_f(t_i)\underline{H}_f(t_i)\underline{P}_f(t_i^-) \quad (3\text{-}17)$$

Solving Equation (3-16) for $\underline{P}(t_i^-)$ yields

$$\underline{P}_f(t_i^-) = \underline{P}_f(t_i^+)+\underline{K}_f(t_i)\underline{H}_f(t_i)\underline{P}_f(t_i^-) \quad (3\text{-}18)$$

where the $\underline{K}_f(t_i)\underline{H}_f(t_i)\underline{P}_f(t_i^-)$, term is preserved intact because it will be estimated on the basis of observed residuals. Setting Equation (3-18) equal to Equation (3-16) and solving for $\underline{Q}_{fd}(t_i)$ yields

$$\underline{Q}_{fd}(t_i) = \underline{K}_f(t_i)\underline{H}_f(t_i)\underline{P}_f(t_i^-)+\underline{P}_f(t_i^+)-\Phi_f(t_i,t_{i-1}) \cdot$$

$$\cdot\ \underline{P}_f(t_{i-1}^+)\underline{\Phi}_f^T(t_i,t_{i-1}) \quad (3\text{-}19)$$

The only term in Equation (3-19)not readily available from the filter is the first term. To obtain this information, rewrite the state update equation, Equation (3-15), as

$$\hat{\underline{x}}_f(t_i^+)-\hat{\underline{x}}_f(t_i^-) = \underline{K}_f(t_i)\underline{r}_f(t_i) = \Delta\underline{x}(t_i) \quad (3\text{-}20)$$

An estimate of $E\{\Delta\underline{x}(t_i)\Delta\underline{x}^T(t_i)\}$ may be obtained by invoking ergodicity to replace the ensemble average with a single sample time average:

$$E\{\Delta\underline{x}(t_i)\Delta\underline{x}^T(t_i)\} \triangleq \frac{1}{N}\sum_{j=i-N+1}^{i}\{\Delta\underline{x}(t_j)\Delta\underline{x}^T(t_j)\} \quad (3\text{-}21)$$

Assuming steady state filter operation, the residual sequence, $\Delta\underline{x}(t_i)$, can be shown to be a white Gaussian sequence with zero mean and covariance $\underline{K}_f(t_i)\underline{H}_f(t_i)\underline{P}_f(t_i^-)$ (12:229):

$$\underline{K}_f(t_i)\underline{H}_f(t_i)\underline{P}_f(t_i^-) \approx \frac{1}{N}\sum_{j=1-N+1}^{i}\{\Delta\underline{x}(t_j)\Delta\underline{x}^T(t_j)\} \qquad (3\text{-}22)$$

Substituting Equation (3-22) into Equation (3-19) gives $\hat{\underline{Q}}_{fd}(t_i)$ as:

$$\hat{\underline{Q}}_{fd}(t_i) = \frac{1}{N}\sum_{j=1-N+1}^{i}\{\Delta\underline{x}(t_j)\Delta\underline{x}^T(t_j)\}+\underline{P}_f(t_i^+)$$

$$-\underline{\Phi}_f(t_i,t_{i-1})\underline{P}_f(t_{i-1}^+)\underline{\Phi}_f^T(t_i,t_{i-1}) \qquad (3\text{-}23)$$

However, rather than averaging over just the first term, this can be approximated by averaging the entire relation over the most recent N sample periods:

$$\hat{\underline{Q}}_{fd}(t_i) = \frac{1}{N}\sum_{j=i-N+1}^{i}\Big[\{\Delta\underline{x}(t_j)\ \underline{x}^T(t_j)\}+\underline{P}_f(t_j^+)$$

$$-\underline{\Phi}_f(t_j,t_{j-1})\underline{P}_f(t_{j-1}^+)\underline{\Phi}_f^T(t_j,t_{j-1})\Big] \qquad (3\text{-}24)$$

This can also be viewed an an approximated maximum likelihood estimate of $\underline{Q}_d$ to be achieved simultaneously with state estimation (13:Chapter 10).

To reduce data storage requirements, a fading memory approximation to finite memory averaging was employed (6:86):

$$\hat{\underline{Q}}_{fd}(t_i) = \hat{\underline{Q}}_{fd}(t_{i-1})+(1- \ )\underline{Q}_{fd1}(t_i) \qquad (3\text{-}25)$$

where

$\underline{Q}_{fd1}(t_i)$ = the single summation term in (3-24) corresponding to time $t_j = t_i$

α = a parameter which essentially controls how long old estimates of $\hat{\underline{Q}}_{fd}$ are maintained, i.e., the length of the effective memory in the fading memory

In Equation (3-24), setting $\alpha = 1$ would use only the old $\hat{\underline{Q}}_{fd}(t_{i-1})$ and ignore the current data, while setting $\alpha = 0$ would result in ignoring all previous $\hat{\underline{Q}}_{fd}$ estimates. Therefore, a low α value implies that little useful information is believed to be contained in the previous estimates, while a high α responds slowly to current estimates. Typical values for α are

$$0.7<\alpha<1.0$$

Note this is the same fading memory technique employed in the "Exponential Smoothing of Data" algorithm shown in Equation (1-4).

IV. Methods of Correlation

4.1 Introduction

The extended Kalman filter has been shown to perform well in comparison to standard correlation trackers when the filter was provided valid a priori information about the analytic form of the intensity function (8). However, without this a priori information the benefit of implementing a high-dimensional measurement extended Kalman filter is greatly reduced. Additionally, the correlation algorithm is computationally easier to implement. Consequently, this section explores four correlation methods for possible implementation as data preprocessors to generate a two-dimensional FLIR target image centroid "measurement" to the linear Kalman filter described in Chapter 3.

The correlator in this tracking system is used to generate estimates of position within a noise-corrupted data frame using the estimated intensity function, $h(\hat{\underline{x}}_f(t_i^-), t_i)$, generated by the data processing algorithm as its template. The template has been positioned with $\hat{\underline{x}}_f(t_i^-)$, as propagated by the Kalman filter from time t_{i-1}. Additionally, controller action is taken to zero out the first two components of $\hat{\underline{x}}_f(t_i^-)$, i.e. the filter's estimation of where the true target dynamcis will place the target at the next sample time, or

$$\hat{\underline{x}}_f{}'(t_i^-) = \{0 \;\; 0 \;\; \hat{x}_{vel} \;\; \hat{y}_{vel} \;\; \hat{x}_{acc} \;\; \hat{y}_{acc} \;\; \hat{x}_{atmos} \;\; \hat{y}_{atmos}\}^T$$

where the components are evaluated at t_i^-. The incoming noise-corrupted measurement is then received at t_i and is correlated with the template to determine the point of maximum resemblance between the two data arrays. The distance from the center of the template to the point of maximum correlation, as estimated by the correlation process, in the x and y FLIR directions can be considered as an indication of the error in the Kalman filter's estimate, $\hat{\underline{x}}_f(t_i^-)$, of the target position, or as a pseudomeasurement of this position, Thus, the offset distances in the x_{FLIR} and y_{FLIR} directions are incorporated by the Kalman filter as measurement data to provide a better estimate, $\hat{\underline{x}}_f(t_i^+)$, of the true target position. The filter propagates the state estimate forward to the next sample time and the template is repositioned at that location with $\hat{\underline{x}}_f(t_{i+1}^-)$ for correlation with the next measurement. This method will enhance the performance achieved by standard correlation trackers because: a) the data processing algorithm, which provides the correlation template, yields a better representation of the target's true intensity function than raw data used by correlators, b) the Kalman filter statistically characterizes known errors in the correlation process to provide a better estimate, and c) the Kalman filter exploits knowledge of target dynamics and atmospherics to position the template for incorporation of the next measurement, whereas this information is not used in standard correlation methods.

In this chapter, several methods of computing the correlation between the two data arrays are considered and a performance analysis of the most promising methods is detailed. This analysis considers the performance of the correlation algorithms against targets exhibiting both single and multiple hot spots.

4.2 Image Resolution

A fundamental requirement for any of the correlation methods under consideration is that the images to be correlated must have the same spatial resolution. In this research, these two images are the 8x8 FLIR tracking window, and the 24x24 template array. The area of a pixel in the tracking window is the same as the area of a pixel in the template, thus the two images to be correlated have the same spatial resolution, and no image preprocessing is required. The 24x24 template is generated by the data processing algorithm (8), which assumes that the finite data array is one period of an infinitely periodic two-dimensional sequence. Padding the tracking window with 8 rows and columns of zeros creates a 24x24 array which is assumed to be one period by the Discrete Fourier Transform (DFT). This padding insures that the infinite periodicity assumption will not affect the results within the 8x8 tracking window. If the spread parameter of the intensity pattern, σ_g^2, is such that the height of the target intensity function is approaching zero near the edge of the tracking window, then padding the tracking window with zeros will not adversely affect the results of the data processing algorithm. In the situation where σ_g^2 is such that significant intensity magnitudes exist outside of the 8x8 array, then to pad with zeros would introduce an artifical edge in the intensity function. Thus, padding with zeros is desired when possible as this will accenuate the true intensity function without discarding useful data. However, since for this application a full FLIR frame consists of 300x400 pixels, the 8x8 data array could be padded with noise corrupted data when the spread parameter of the target intensity function is such that there are significant intensity magnitudes outside of the 8x8 tracking window (8:77-78).

4.3 Correlation Methods

a. Direct Method. The direct method is the classical approach to determining when two signals match. Consider the two functions shown in Figure 22.

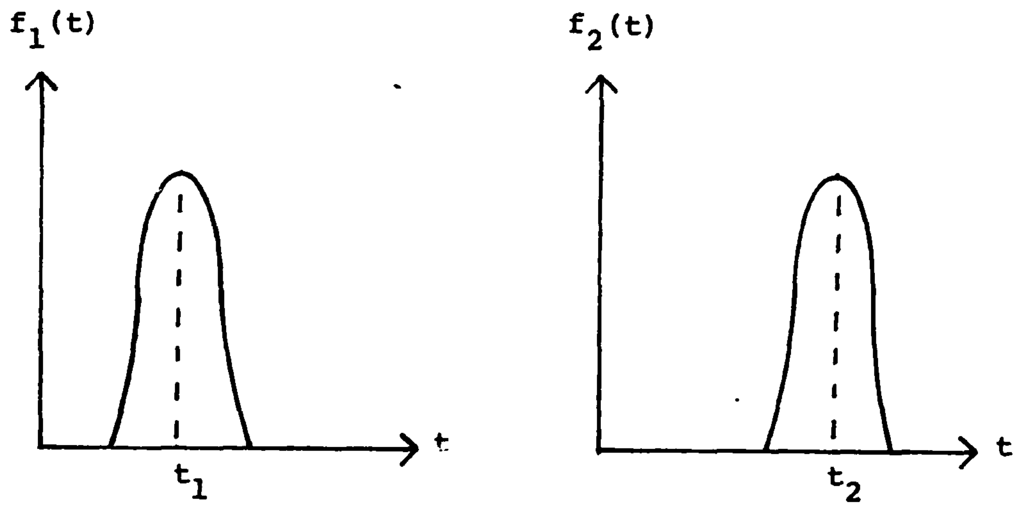

Figure 22. Functions to be Correlated

The correlation integral is defined as

$$C(\tau) = \int_{-\infty}^{\infty} f_1(t)f_2(t+\tau)dt \qquad (4\text{-}1)$$

Where τ is allowed to take on values from $-\infty$ to $+\infty$. The correlation peak is defined to be the point where the two signals most closely match, which occurs in Figure 22 at $\tau = t_2-t_1$.

For discrete signals, Equation (4-1) is approximated by

$$C(p) = T\sum_{n=-\infty}^{\infty} f_1(t) f_2(t+\tau) \qquad (4-2)$$

where

$$f_1(t) = f_1(t)\Big|_{t=nT}$$

$$f_2(t) = f_2(t+\tau)\Big|_{\substack{t=nT \\ \tau=pT}}$$

T = sample time

As T becomes small, the result of Equation (4-2) approaches (4-1) and the p which maximizes C(p) is defined as the corelation point. With the two-images to be correlated as shown in Figure 23, the two-dimensional discrete correlation algorithm is (14:17-20):

$$R(p,q) = \frac{1}{KL} \sum_{y=1}^{L} \sum_{x=1}^{K} \underline{G}_1(x,y)\underline{G}_2(x+p,y+q) \qquad (4-3)$$

for

$$0 \le p \le X-K$$

$$0 \le q \le Y-L$$

(Note: In this instance since the $\underline{G}_1$ array is of smaller dimension than the $\underline{G}_2$ array negative values of p and q are not required which corresponds to the tracking window being of smaller dimension than the template.)

Since in this research the 8x8 tracking window is padded either with zeros or noise corrupted data, the corrdinates of the pixels in the tracking window to be correlated range from 9-16 in the x and y FLIR directions. Equation (4-3) then becomes {14:20}

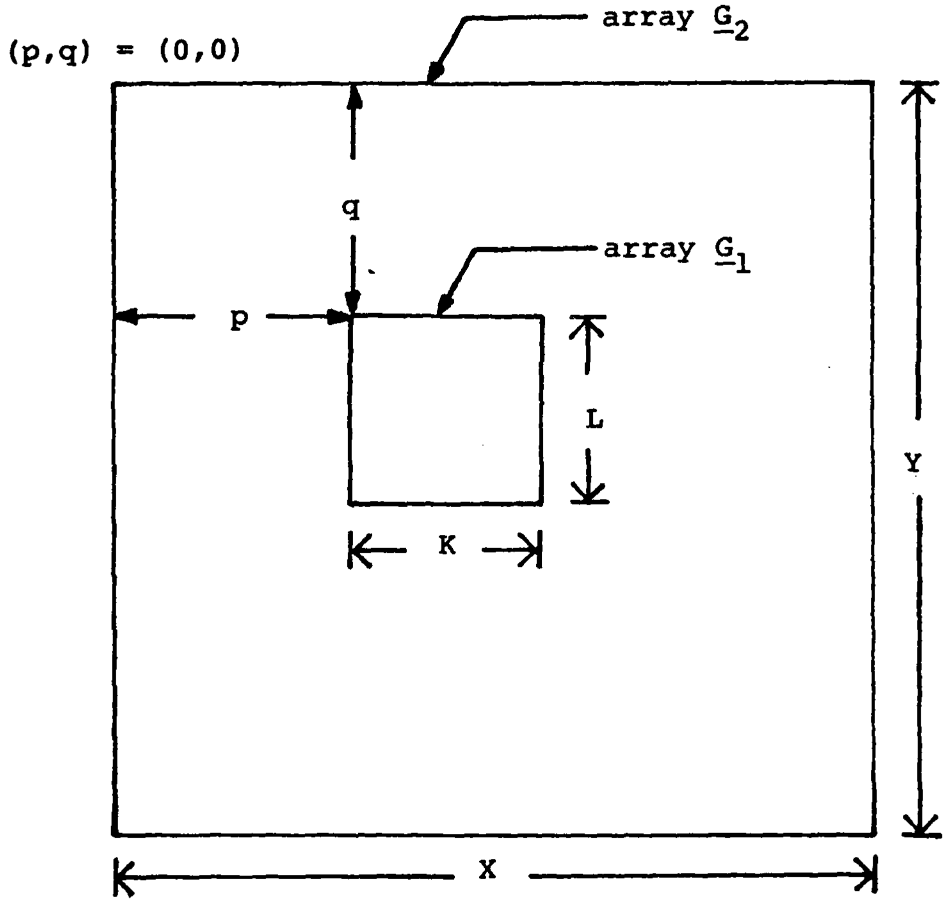

Figure 23. Arrays to be Correlated

$$R(p,q) = \frac{1}{(8)(8)} \sum_{y=1}^{8} \sum_{x=1}^{8} \underline{G}_1(x+8,y+8)\underline{G}_2(x+p,y+q) \qquad (4\text{-}4)$$

for

$4 \leq p \leq 12$

$4 \leq q \leq 12$

where

$\underline{G}_1$ = 8x8 tracking window within padded data array

$\underline{G}_2$ = 24x24 template

This is pictured in Figure 24.

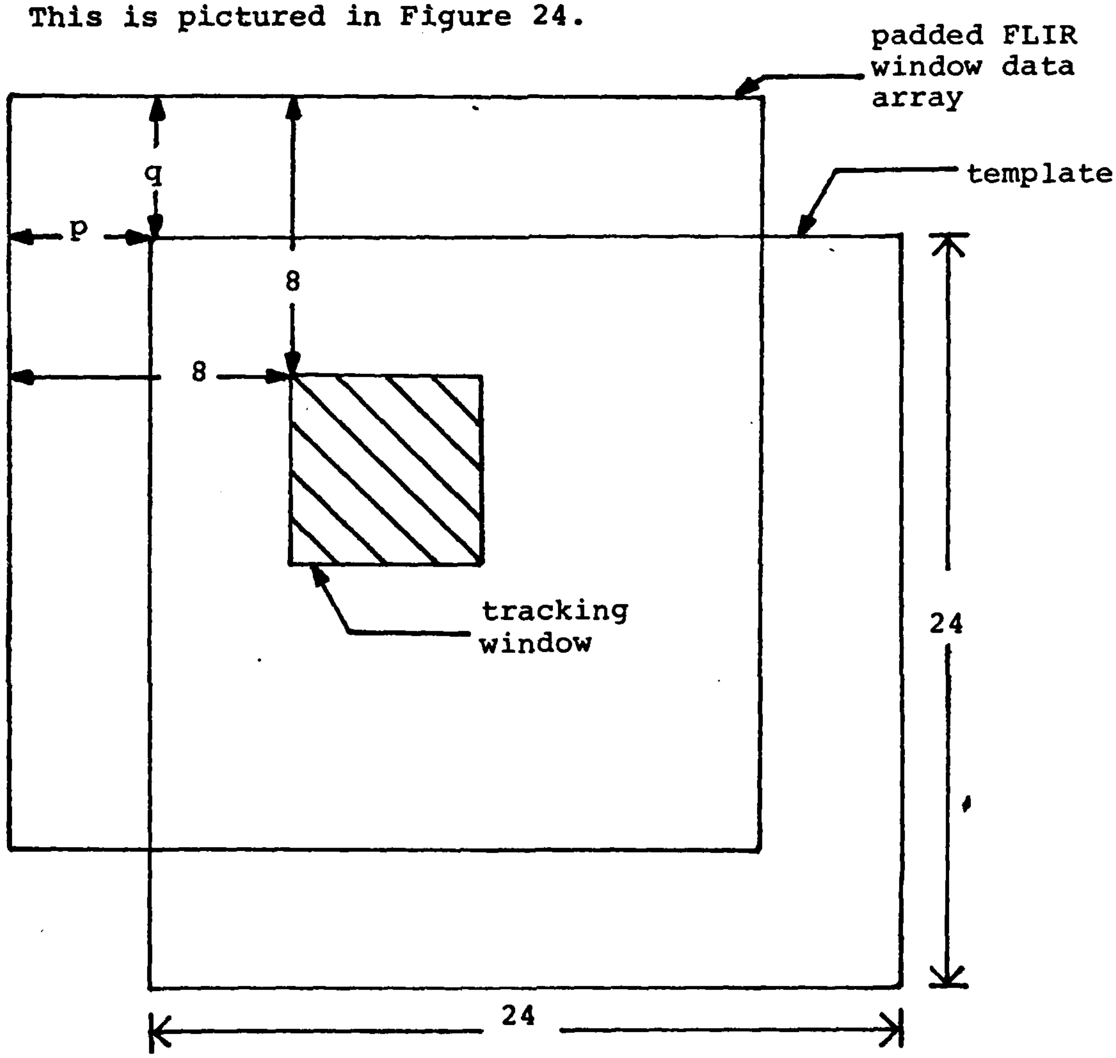

Figure 24. FLIR and Template Arrays

Equation (4-4) is referred to as the direct correlation method (14-20). Notice the range over which p and q are allowed to vary. A total correlation of the two arrays would have p and q range from 0 to 16. However, if the target intensity function is outside of the 8x8 tracking window no useful measurement information will be contained in the incoming data, and the tracker is considered to have lost the target unless the size of the tracking window is expanded (a possibility not explored in this research). Recall that the template which contains the estimated intensity function offset by the atmospheric states is generated via the data processing algorithm from the measurement arrays which have been padded with 8 rows and columns of either zeros or noise-corrupted data. Therefore, to perform a correlation outside of the p and q region shown is equivalent to correlating the incoming data array with either zeros or smoothed noise. In either case, a correlation match in this area indicates the incoming array contains no useful information, i.e. target track has been lost. For this reason, correlation in the region outside of the chosen p and q bounds was not performed, thereby reducing the computational loading of the algorithm.

Equation (4-4) can be normalized so that the calculation of correlation points is insensitive to magnitude values and depends solely on the pattern of the 8x8 arrays within the template (14:20). The normalized correlation function, $R_N(p,q)$ is:

$$R_N(p,q) = \frac{\sum_{y=1}^{8} \sum_{x=1}^{8} \underline{G}_1(x+8,y+8)\,\underline{G}_2(x+p,y+q)}{\left[\left[\sum_{y=1}^{8} \sum_{x=1}^{8} \underline{G}_1^2(x+8,y+8)\right]\left[\sum_{y=1}^{8} \sum_{x=1}^{8} \underline{G}_2^2(x+p,y+q)\right]\right]^{\frac{1}{2}}} \tag{4-5}$$

for

$4 \leq p \leq 12$

$4 \leq q \leq 12$

Thus, Equation (4-5) defines the normalized direct correlation method implemented in this research.

Actual implementation of Equation (4-5) requires the signals of template and the FLIR data be digitized. The process of digitizing a continuous signal consists of two distinct steps. The first is the sampling of the signal at discrete intervals, the second is quantization. The truth model provides the sampled signal in this instance. Two separate quantizers were implemented to evaluate the merits of using a low-level quantizer which is readily implemented versus the performance enhancement achieved by using a higher-level quantizer, with its associated increased computational burden. The input-output relationship for the two quantizers chosen is shown in Figure 25.

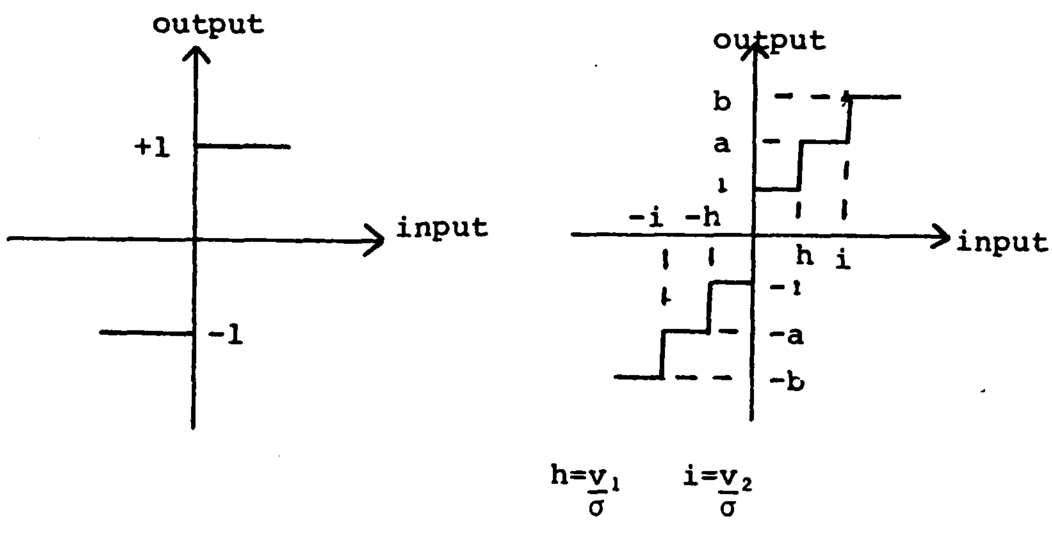

2-level quantizer 6-level quantizer

Figure 25. Input-Output Relationships

For the two-level quantizer, a pixel within the array is assigned a value of +1 if the intensity for that pixel is above the mean intensity level, and the pixel is assigned a value of -1 if the signal is below the mean intensity level. The mean intensity values, $\overline{G}_1$ and $\overline{G}_2(p,q)$ are determined by:

$$\overline{G}_1 = \frac{1}{(8)(8)} \sum_{y=1}^{8} \sum_{x=1}^{8} G_1(x+8,y+8)$$

$$\overline{G}_2(p,q) = \frac{1}{(8)(8)} \sum_{y=1}^{8} \sum_{x=1}^{8} G_2(x+p,y+q)$$

Thus, Equation (4-5) becomes (14:32)

$$R_N(p,q) = \frac{\sum_{y=1}^{8} \sum_{x=1}^{8} g_1(x+8,y+8)\,g_2(x+p,y+q)}{64} \tag{4-6}$$

for

$4 \leq p \leq 12$

$4 \leq q \leq 12$

where

$g_1(x+8,y+8)$ = value assigned to $\underline{G}_1(x+8,y+8)$ element after quantization

$g_2(x+p,Y=q)$ = value assigned to $\underline{G}_2(x+p,y+q)$ element after quantization

As shown in Figure 25b, the six-level quantization process requires the additional calculation of the variances of the input signal, σ, for $G_1(x+8,y+8)$ and $G_2(x+p,y+q)$. Optimum values in the sense that they minimize the variance of R, (i.e. minimize the loss in the signal to noise ratio due to quantization(14:28)), based on research detailed in ref 14 are a = ±3 and b = ±6 for $v_1/\sigma = \pm 0.6$ and $v_2/\sigma = \pm 1.4$. Thus, the quantized value, g, is assigned by:

$$\frac{v}{\sigma} \leq -1.4; \; g = -6$$

$$-1.4 \leq \frac{v}{\sigma} \leq -0.6; \; g = -3$$

$$-0.6 \leq \frac{v}{\sigma} \leq 0; \; g = -1$$

$$0 \leq \frac{v}{\sigma} \leq 0.6; \; g = 1$$

$$0 \leq \frac{v}{\sigma} \leq 1.4; \; g = 3$$

$$1.4 \leq \frac{v}{\sigma}; \; g = 6$$

where

v = (Intensity value for a particular pixel-mean intensity value for the data array.)

For the six-level quantizer Equation (4-5) becomes:

$$R_N(p,q) = \frac{\sum_{y=1}^{8} \sum_{x=1}^{8} \{g_1(x+8,y+8)\, g_2(x+p,y+q)\}}{\left[\left[\sum_{x=1}^{8} \sum_{y=1}^{8} g_1^2(x+8,y+8)\right]\left[\sum_{x=1}^{8} \sum_{y=1}^{8} g_2^2(x+p,y+q)\right]\right]^{\frac{1}{2}}} \tag{4-7}$$

for

$$4 \leq p \leq 12$$

$$4 \leq q \leq 12$$

The values of p and q which maximize R_N is the correlation point.

b. Fast Fourier Transform (FFT) Method. Since the arrays to be correlated are two-dimensional, rotating one array 180° and taking a convolution is equivalent to performing a correlation. The convolution has the useful property that its discrete Fourier Transform is a simple product of the Fourier Transform of the two image arrays (15:5). This method substantially reduces the number of steps required to calculate the correlation. The FFT can be used to calculate the cross-correlation as shown below.

$$\mathrm{FFT}\{\underline{G}_1(x,y)\} = \underline{G}_1\{f_x,f_y\} \tag{4-8}$$

$$\mathrm{FFT}\{\underline{G}_2(x,y)\} = \underline{G}_2\{f_x,f_y\} \tag{4-9}$$

$$\mathrm{FFT}\{\underline{G}_1(x,y)\cdot\underline{G}_2(x,y)\} = \underline{G}_1\{f_x,f_y\}\cdot\underline{G}_2^*\{f_x,f_y\} \tag{4-10}$$

where

$\underline{G}_1(x,y)\cdot\underline{G}_2(x,y)$ = cross-correlation of two-dimensional spatial sequences $\underline{G}_1(x,y)$ and $\underline{G}_2(x,y)$

$\underline{G}_2^*\{f_x,f_y\}$ = complex conjugate of Fourier transform of sequence $\underline{G}_2(x,y)$

FFT = Fast Fourier Transform

By taking the inverse FFT, FFT^{-1}, of Equation (4-10), the cross-correlation of the two-dimensional sequences $\underline{G}_1(x,y)$ and $\underline{G}_2(x,y)$ is obtained (8:53,54)

$$R(x,y) = \underline{G}_1(x,y)\cdot\underline{G}_2(x,y) = \mathrm{FFT}^{-1}\{\underline{G}_1(f_x,f_y)\cdot\underline{G}_2^*(f_x,f_y)\} \tag{4-11}$$

where

R(x,y) is the result of the correlation

c. Phase Correlation Method. While the FFT method is the simpliest and most readily implemented correlation technique, it possesses the undesirable characteristic of detecting false peaks, especially if the FLIR image is of high brightness while the template is of lesser brightness. The problem stems from the relative magnitude of the intensity of the sub-elements (14:22).

The phase correlation method, which reduces the false peak effects of the cross-correlation, is given by (14:22):

$$R_N'(x,y) = FFT^{-1}\left[\frac{\underline{G}_1(f_x,f_y)\cdot\underline{G}_2^*(f_x,f_y)}{\left|\underline{G}_1(f_x,f_y)\cdot\underline{G}_2^*(f_x,f_y)\right|}\right] \qquad (4\text{-}12)$$

where

$\left|\underline{G}_1(f_x,f_y)\cdot\underline{G}_2^*(f_x,f_y)\right|$ = magnitude of $\underline{G}_1(f_x,f_y)\cdot\underline{G}_2^*(f_x,f_y)$

$R_N'(x,y)$ = result of normalized correlation process

This is essentially a point by point normalization in the frequency domain. Due to the normalization, the magnitude effects which lead to the false peaks using the FFT method are reduced and more dependence is placed on the pattern of the data points within the two arrays. However, some of the computational advantage realized by using the FFT method will be lost. The computational loading incurred by using this method will be examined during the performance analysis.

d. Sequential Similiarity Detection Algorithm (SSDA).

Another method considered was the Sequential Similiarity Detection Algorithm. In this method, the absolute value of the difference between corresponding pixels of $\underline{G}_1$ and $\underline{G}_2$, for each p and q, is calculated and the result is defined to be the SSDA registration surface shown in Equation (4-13).

$$E\{p,q\} = \sum_{x=1}^{K} \sum_{y=1}^{L} \left| \underline{G}_1(x,y) - \underline{G}_2(x+p,y+q) \right| \tag{4-13}$$

for

$$0 \leq p \leq X \leq K$$

$$0 \leq q \leq Y \leq L$$

where

$\left| \underline{G}_1(x,y) - \underline{G}_2(x+p,y+q) \right|$ = absolute value of the difference

The registration point, which corresponds to the correlation point in the previous methods, is defined as the point for which E(p,q) is a minimum. Note this is not a true correlation technique since Equation (4-13) is not directly related to Equation (4-1). This method was not implemented as analysis has shown that two-level quantization of the SSDA method is equivalent to two-level quantization using the direct method, and for all higher quantization levels, the direct method out performs the SSDA (14:46). However, for actual implementation of a two-level quantizer, hardware considerations may cause the designer to select this method.

4.4 Maximum Correlation Detection

The magnitude of the components of the sequence R(x,y) is a measure of the degree of resemblance between the template and the FLIR image data where the peak location is used to indicate the amount of offset between the two arrays that result in the highest degree of resemblance. Thresholding is a technique often used to suppress lower peaks in the correlation. (Note: In the direct method, the quantization process accomplishes essentially the same function thus thresholding was only employed for the frequency domain correlation methods.) During the thresholding procedure, each element of the R(x,y) sequence is examined to determine if the value for that element is below some preselected fraction of the maximum valued element in the sequence. If the element value is below that minimum point, then that element is considered to have poor correlation and is set to zero. The result is that such elements will have no effect on the computed offset between the template and FLIR data. Figures 26 and 27 show the effects of thresholding as a result of setting the threshold value to .3 and .5 of the maximum valued element respectively. These cases were conducted under indentical conditions using the FFT method where the data array was offset from the template by +.15 pixels in the x and y FLIR directions. After the thresholding process has edited the results of the correlation, a center of mass calculation was used to determine the peak of correlation between the two arrays, see Equation (4-14). These plots show the errors in the calculated offset between the two arrays for 1000 cases where a zero error in the plot indicates the correct offset was achieved. As shown in Figure 27, a higher threshold locates the true offset more often but false peaks become prominent. Physically this can be explained by examining the correlation function of this method. For demonstration purposes,

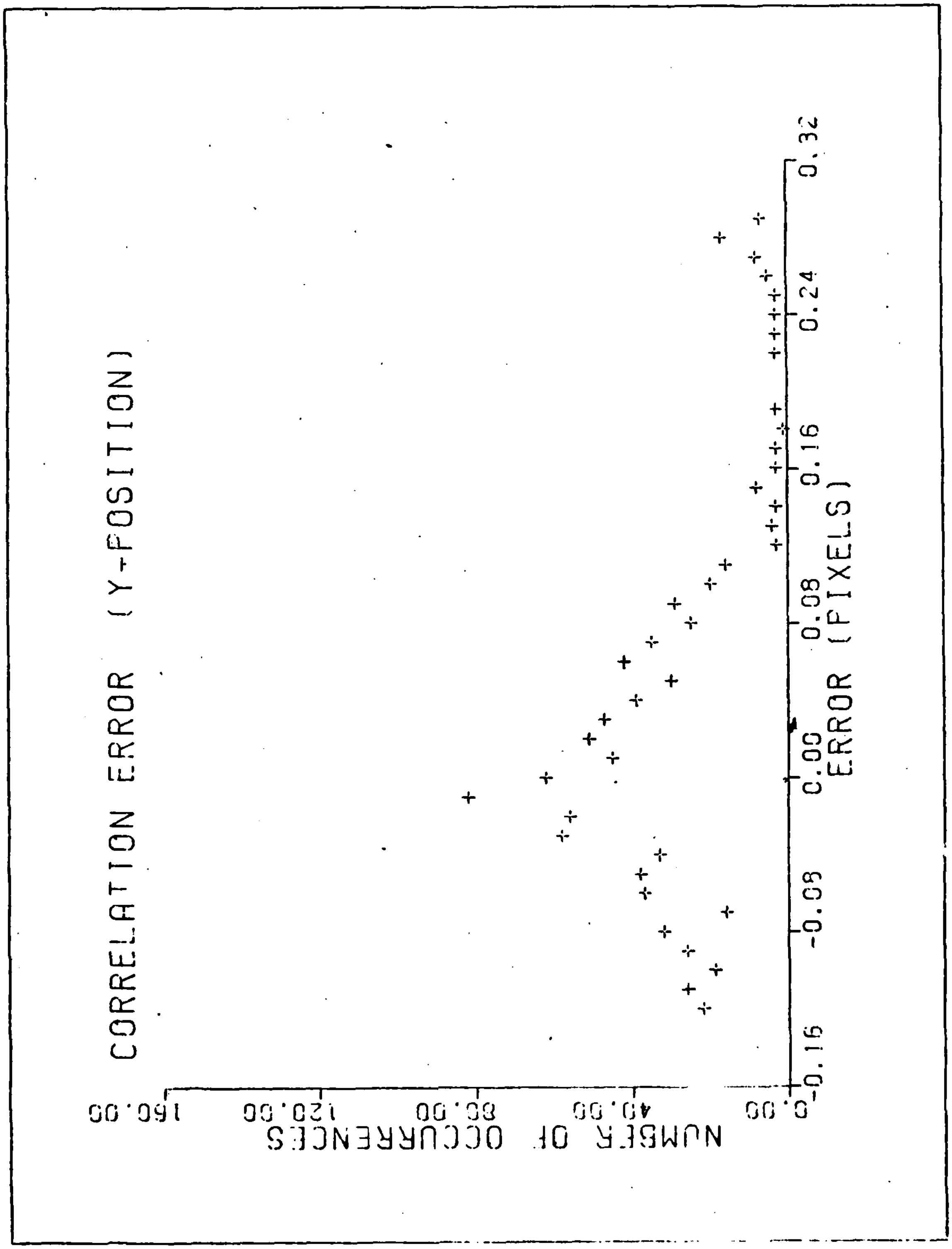

Figure 26. FFT Correlation
(Threshold = .3)

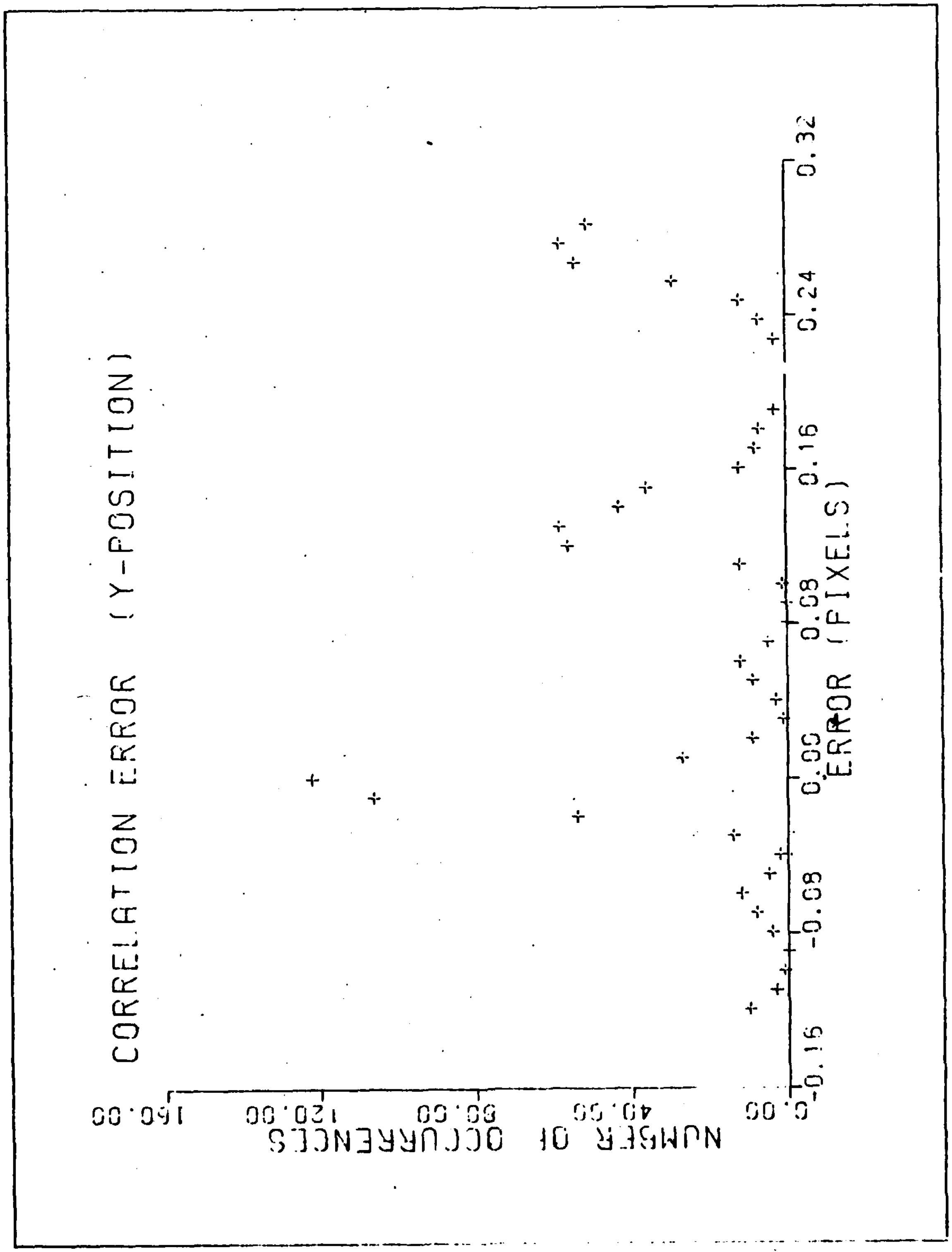

Figure 27. FFT Correlation (Threshold = .5)

assume Figure 28 is the result of a correlation using the FFT method.

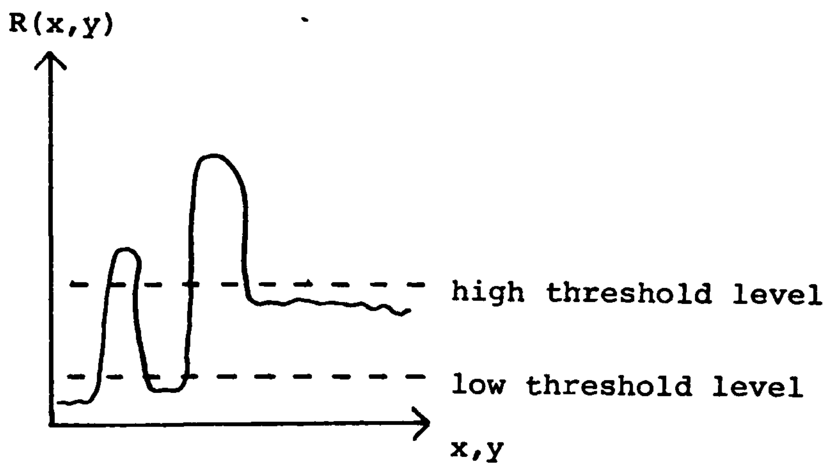

Figure 28. Thresholding (FFT Correlation Method)

As shown, a high degree of correlation lies to the right of the main peak. However, as the theshold is raised, this information is deweighted because the thresholding procedure sets these values to zero and the smaller peak to the left of the main peak becomes weighted more heavily. When the center of mass calculation is used to determine the peak of the correlation function the result will be an estimate which is incorrectly biased to the left. Thus, when using the FFT method the threshold must be set low enough to avoid this effect. However, due to the normalization process the correlation function generated by the phase correlation method would be as shown in Figure 29.

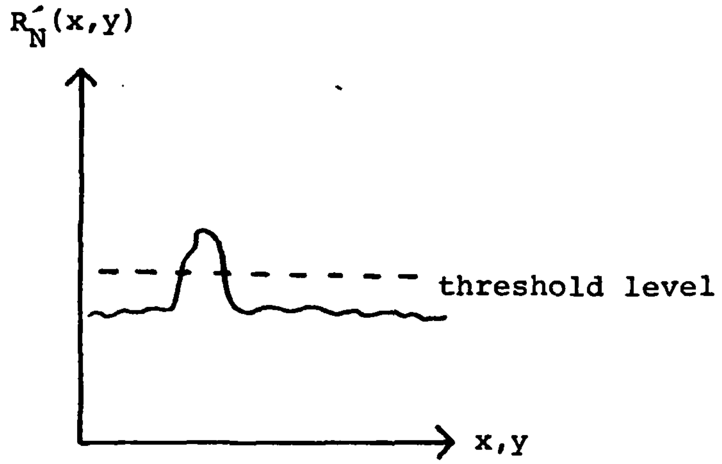

Figure 29. Thresholding (Phase Correlation Method)

Therefore, using this method, a better estimate of the true peak of the correlation function can be obtained by raising the threshold level and then calculating the center of mass.

Once the thresholding method has edited the results of the correlation, the point of maximum correlation must be located. Derivative-based peak detectors, i.e. a method which locates the point of zero slope can be used for this purpose. However, because the location of the point of maximum intensity could be rapidly changing on the FLIR image plane, as when the aircraft being tracked executes a snap roll, it was felt that these type detectors might often misinterpret a local peak as the global peak. Therefore, a centroid summation

AD-A124 884 ENHANCED TRACKING OF AIRBORNE TARGETS USING A CORRELATOR/KALMAN FILTER(U) AIR FORCE INST OF TECH WRIGHT-PATTERSON AFB OH SCHOOL OF ENGINEERING 2/4

UNCLASSIFIED P P MILLNER DEC 82 AFIT/GE/EE/82D-50 F/G 12/1 NL

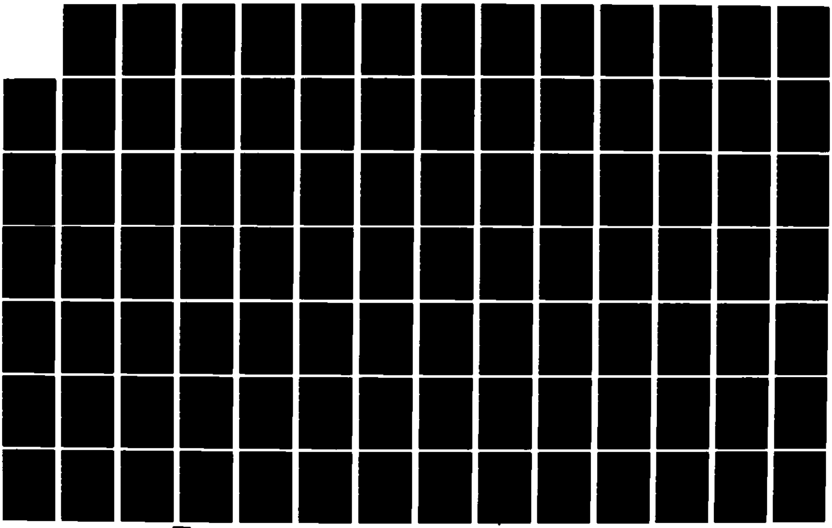

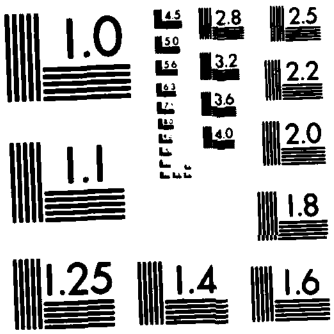

MICROCOPY RESOLUTION TEST CHART
NATIONAL BUREAU OF STANDARDS-1963-A

technique was selected to locate the center of mass of the edited two-dimensional cross-correlation sequence, $R_T(x,y)$ or $R_N(p,q)$. This method assumes that the center of mass of the thresholded or quantized correlation function is a good indication of the global peak location. The centroid summation used is defined in either the vertical or horizontal direction as (8:63):

$$C = \frac{\sum_{i=1}^{N} i \cdot Amp_i}{\sum_{i=1}^{N} Amp_i} \qquad (4\text{-}14)$$

where

i = vertical or horizontal pixel coordinate

Amp = amplitude value for that element

N = total number of pixels in the array

For example, to locate the center of mass of the correlation function in the horizontal direction, the horizontal coordinates of all of the elements of the $R_T(x,y)$ sequence would be multiplied by their respective amplitudes and their products summed. The centroid's horizontal coordinate is then achieved by dividing that summation by the sum of all the amplitudes in the $R_T(x,y)$ sequence. The same procedure is then applied in the vertical direction. The result is that the coordinates of the center of the correlation function in both directions from the center of the template is produced.

4.5 Analysis of Correlation Methods

This section analyzes the errors in the position estimates generated by the four correlation methods previously discussed. The statistical data for the one and three hot spot cases is presented first, followed by a discussion of each methods's performance. The position estimate generated by the correlation algorithm will be the measurements provided to the linear Kalman filter which will provide a better estimate of the target's position. The two-dimensional discrete measurement vector, $\underline{z}(t_i)$, is incorporated by the Kalman filter using the Equation (3-14).

Software was developed to test each of the correlation algorithm's position estimate, and statistical data and histograms of the resulting errors were gathered. For the cases to be discussed the centroid of the intensity was offset from the template by .15 pixels where this distance was selected as being representative of the propagation error. Simulated background and FLIR noise was added as described in section 2.4, and 1000 runs were made to gather the error statistics. As previously described, the errors were calculated so that if the correct offset was estimated a zero error is shown on the histogram, and any deviation from zero is the error in the estimate in pixels. The estimated offset errors were placed into bins .01 pixels wide, and the plots show the number of times the estimated position fell into a particular bin. (The bins were calculated from the mean error to a distance of the mean error $\pm$ .2 pixels where it was assumed the majority of the errors would fall.) Thus, while the area under all the curves has to be 1000 pixels, the total area will not appear on the histogram if the calculated offset was more than .2 pixels from the mean offset error. Table 1 shows the correlator errors for single hot spot targets where the centroid of the intensity function was truly offset from the template by

.15 as previously discussed, and the histograms for these cases are presented in Figures 30-33. (Note the scale in Figure 33 is times 10.)

Table I. Correlation Errors (Single Hot Spot Target)

Correlation Method	$\overline{x}_{err}$	$\sigma_{x\ err}$	$\overline{y}_{err}$	$\sigma_{y\ err}$	Time (sec)
Direct 2-level	-.00283	.14995	-.01012	.14875	255.939
Direct 6-level	-.06730	.13697	-.07024	.13510	365.109
FFT Thresh=.3	-.00113	.13262	-.00117	.13374	271.862
Phase Thresh=.7	-.00091	.27046	.00166	.27581	281.344

where

$\overline{x}_{err}, \overline{y}_{err}$ - mean error in the estimated offset in the x and y FLIR directions respectively

$\sigma_{x\ err}, \sigma_{y\ err}$ - standard deviation of the errors in the x and y FLIR directions respectively

Time - total computer simulation time for 1000 runs where all parameters were identical except the correlation method employed

The threshold values used for the FFT and phase correlation

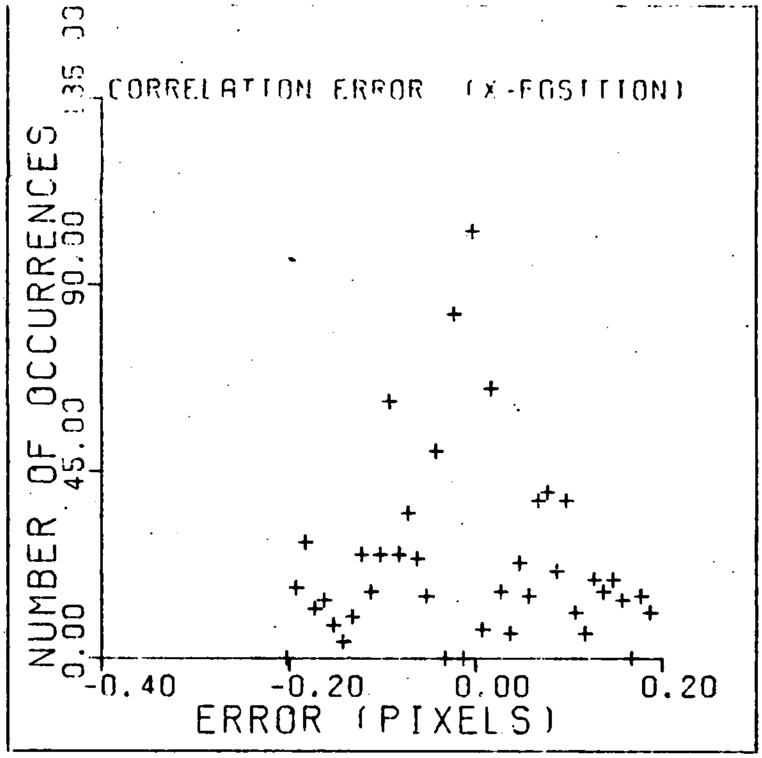

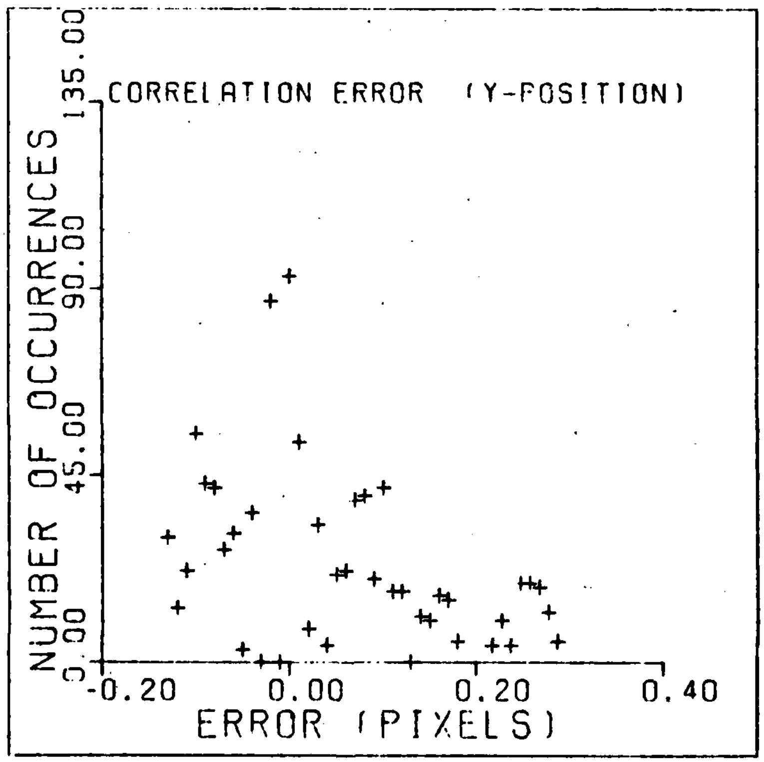

Figure 30. Histogram of Errors-Direct Method (2-level quantization, 1 hot spot)

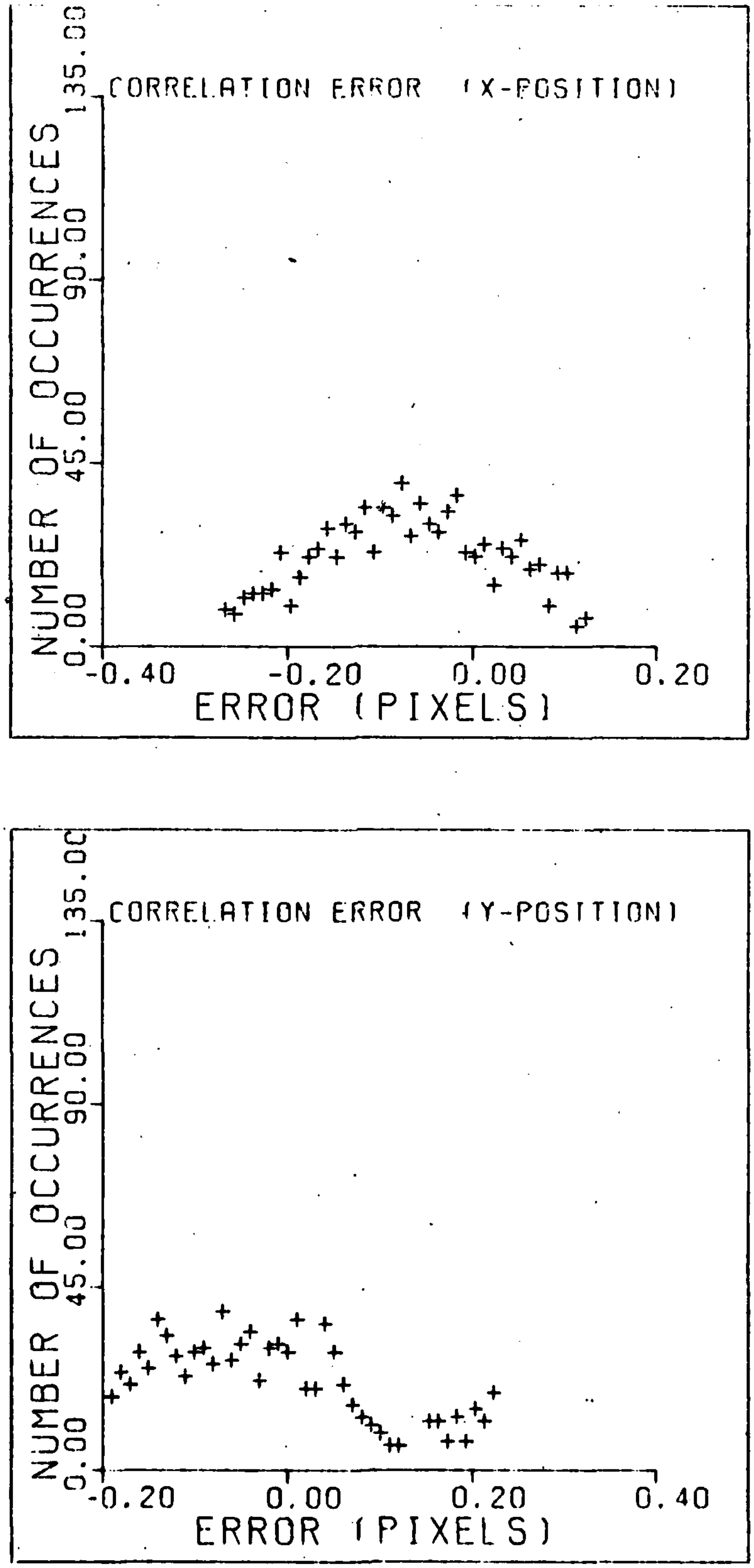

Figure 31. Histogram of Errors-Direct Method (6-level quantization, 1 hot spot)

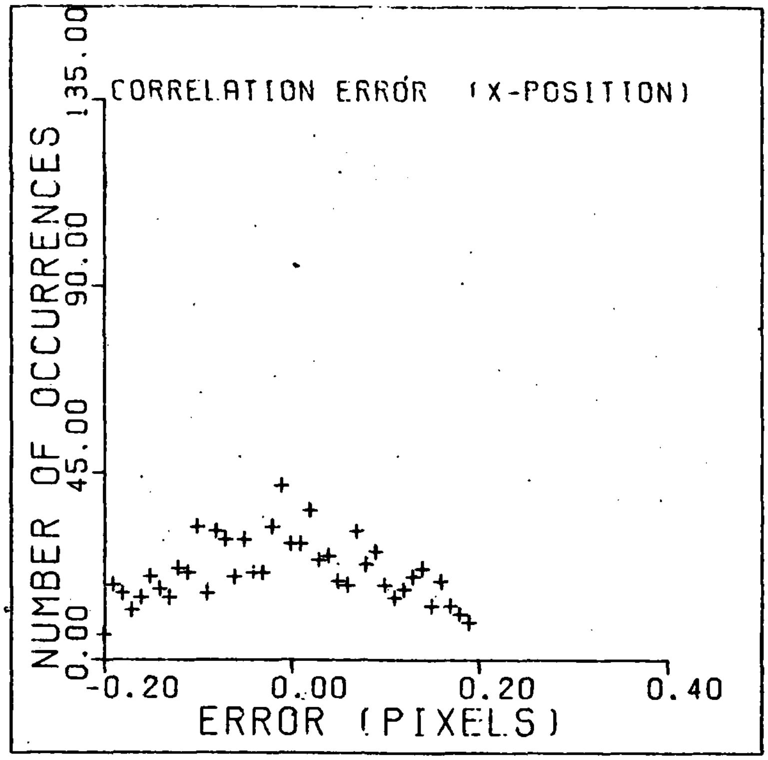

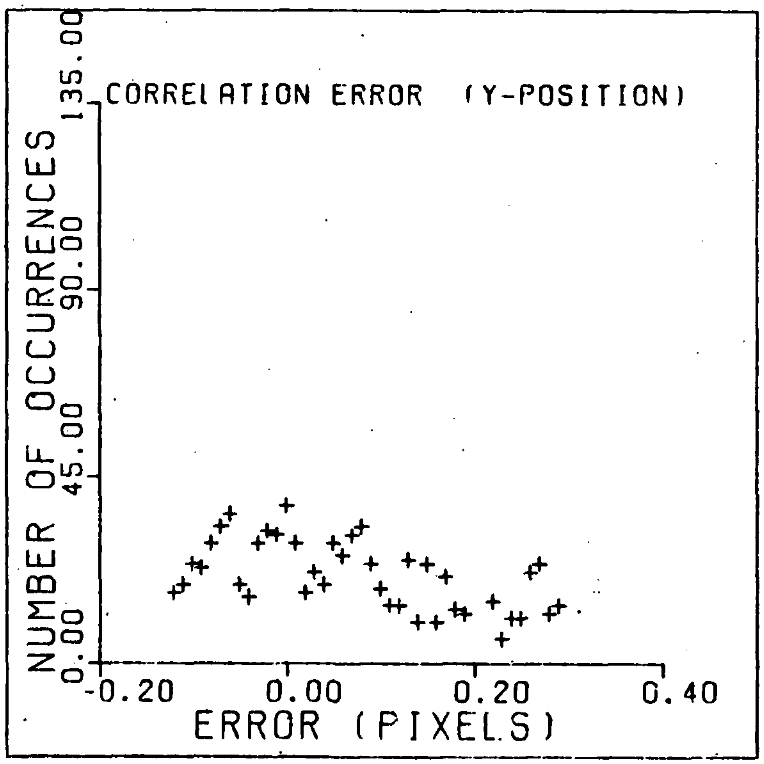

Figure 32. Histogram of Errors-FFT Method (threshold = .3, 1 hot spot)

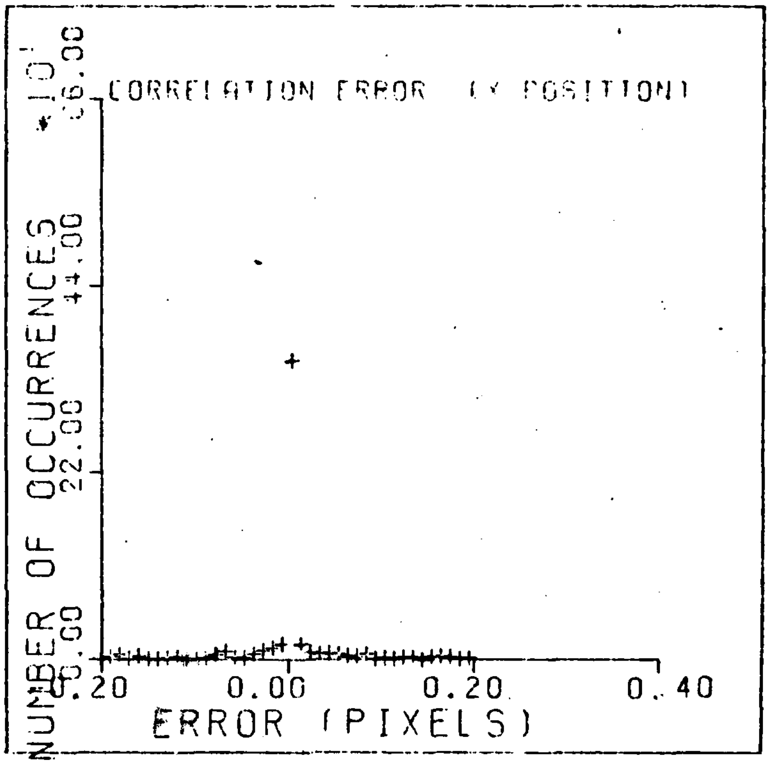

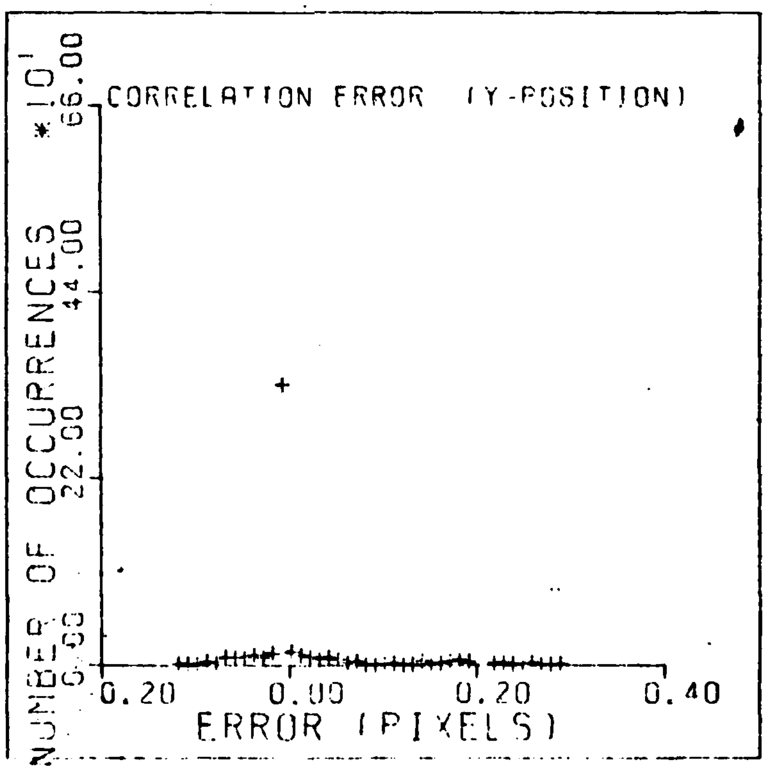

Figure 33. Histogram of Errors-Phase Method (threshold = .7, 1 hot spot)

methods were chosen as the best values to implement based on a comparison with other trials where various thresholds were used. The threshold value which produced the smallest rms error was chosen.

An error analysis was also conducted for the three hot spot target case. As in the previous simulations, 1000 runs were used to gather the statistical information. The results of the three hot spot cases are shown in Table II.

Table II. Correlation Errors (Three Hot Spot Target)

Correlation Method	$\bar{x}_{err}$	$\sigma_{x\ err}$	$\bar{y}_{err}$	$\sigma_{y\ err}$	Time (sec)
Direct 2-level	-.03304	.04116	-.01798	.10846	306.268
Direct 6-level	-.08426	.04770	.01754	.03696	400.785
FFT Thresh=.3	-.00053	.03858	.00225	.05428	319.056
Phase Thresh=.7	.00058	.09854	-.00422	.27691	325.461

The histograms of the three hot spot cases are shown in Figures 34-37. (Again, in Figure 37 the scale is times 10.) For the three hot spot cases, the difference in errors in the x and y direction is due to the location of the three target intensity profiles. The centroids of the intensity

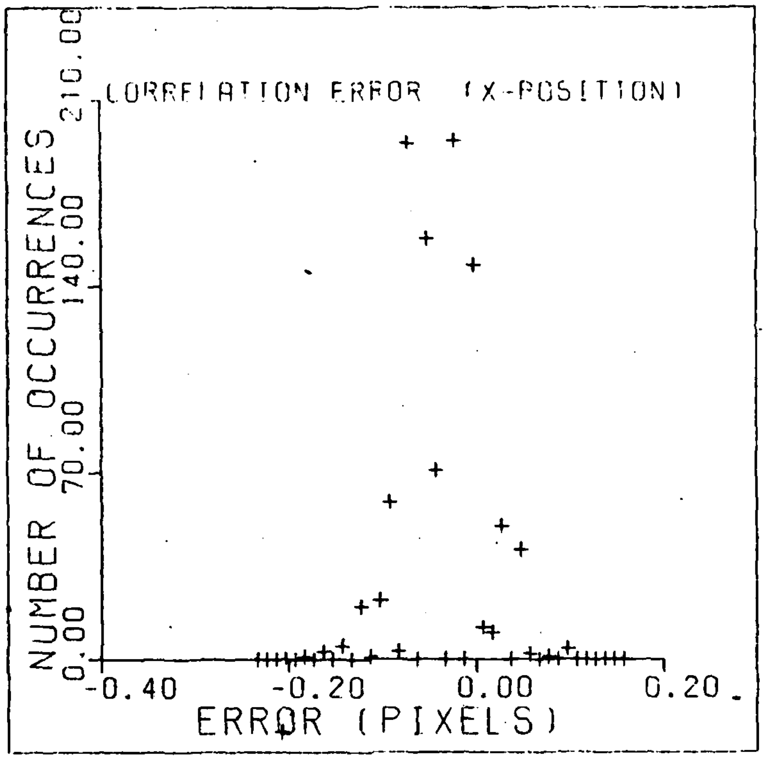

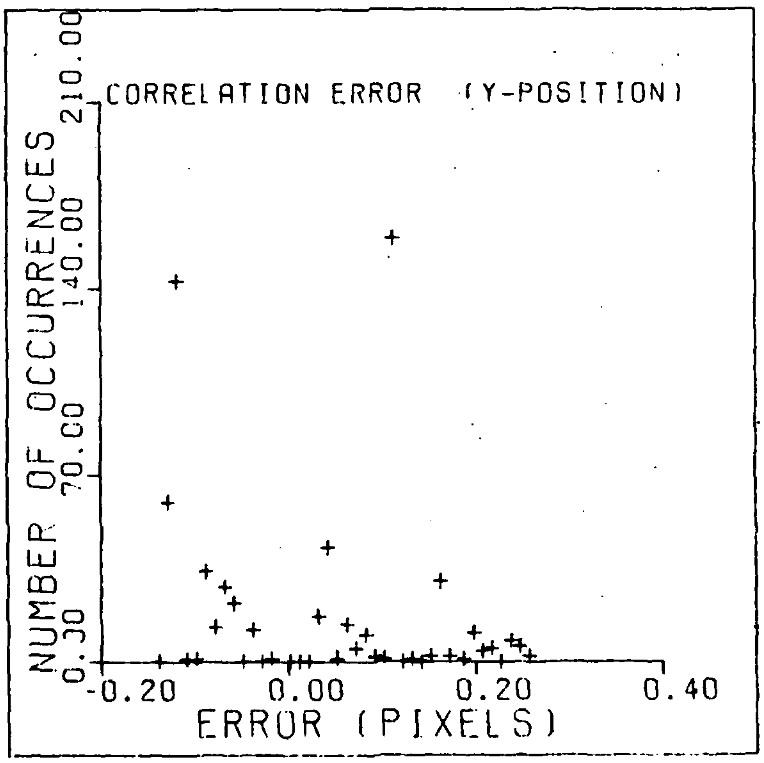

Figure 34. Histogram of Errors-Direct Method (2-level quantization, 3 hot spots)

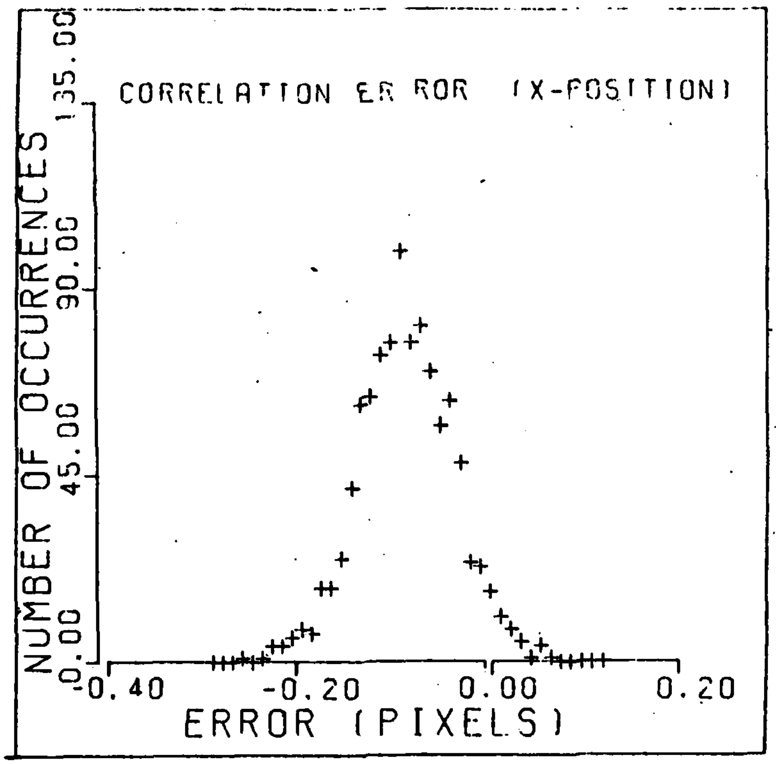

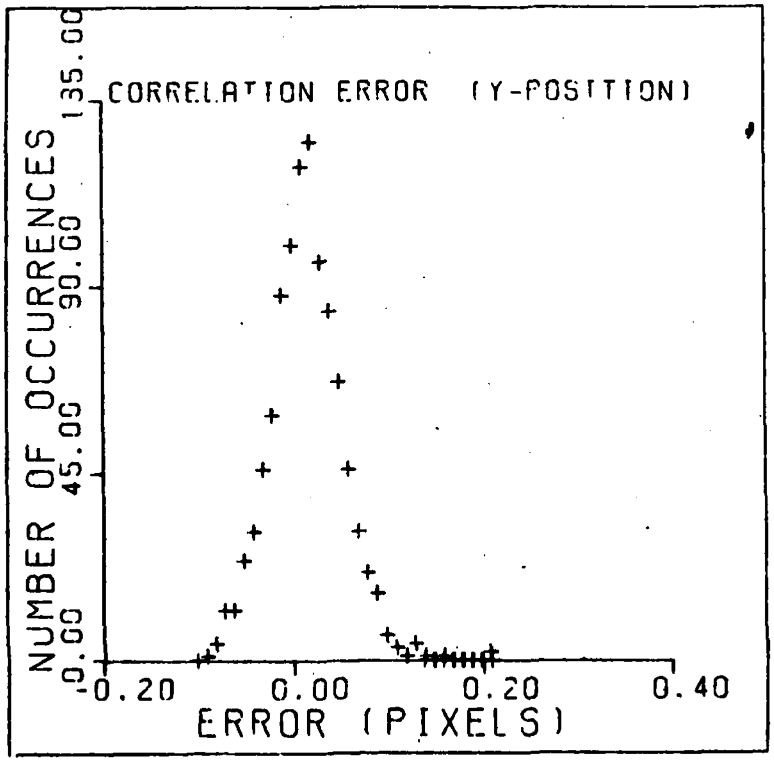

Figure 35. Histogram of Errors-Direct Method -level quantization, 3 hot spots)

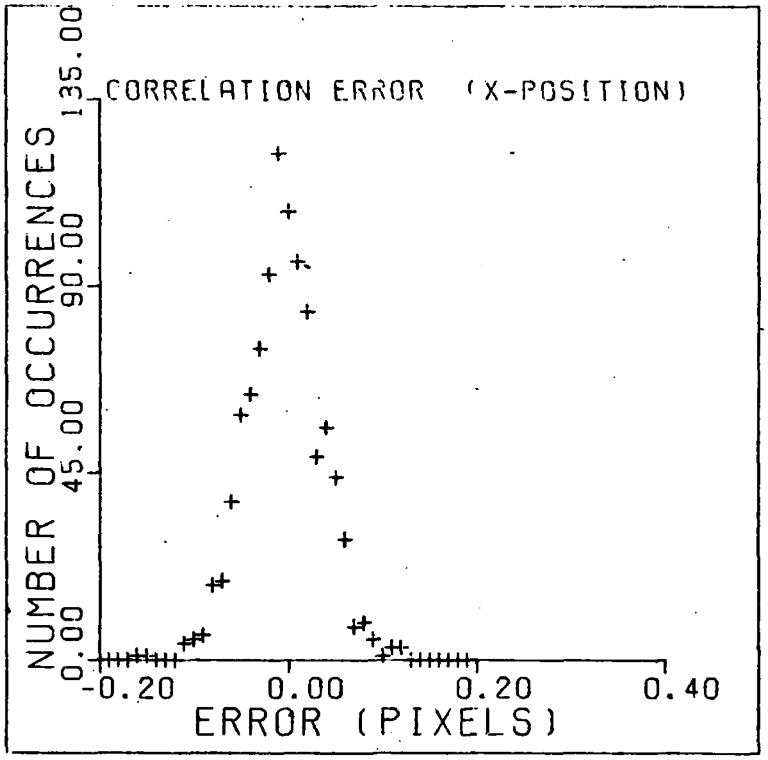

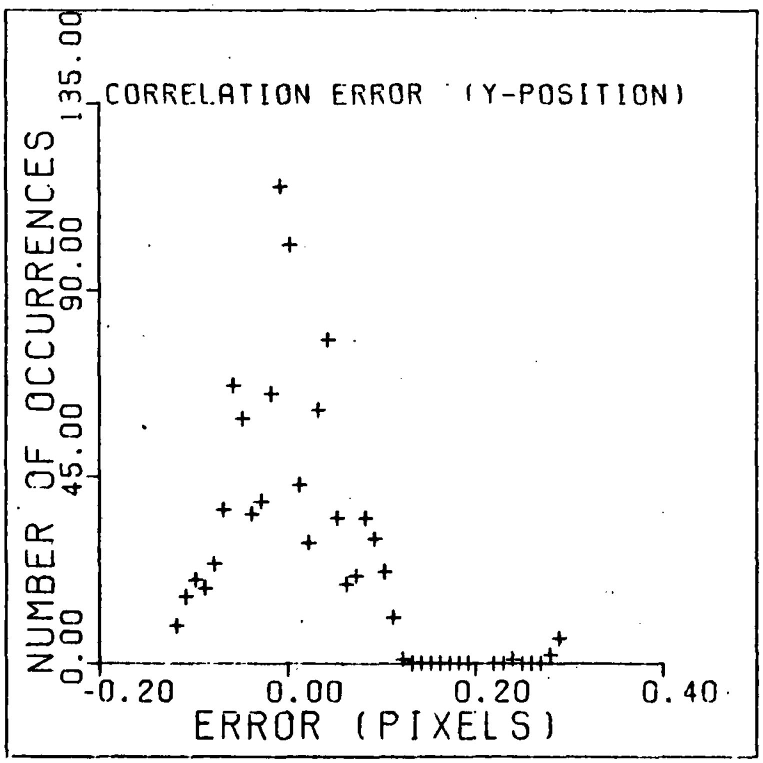

Figure 36. Histogram-FFT Method (threshold = .3, 3 hot spots)

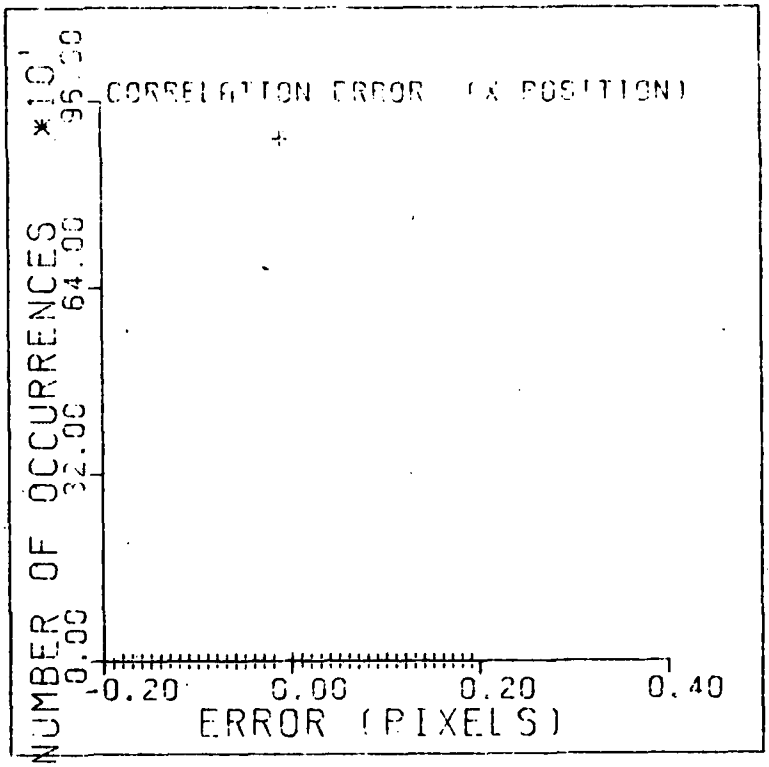

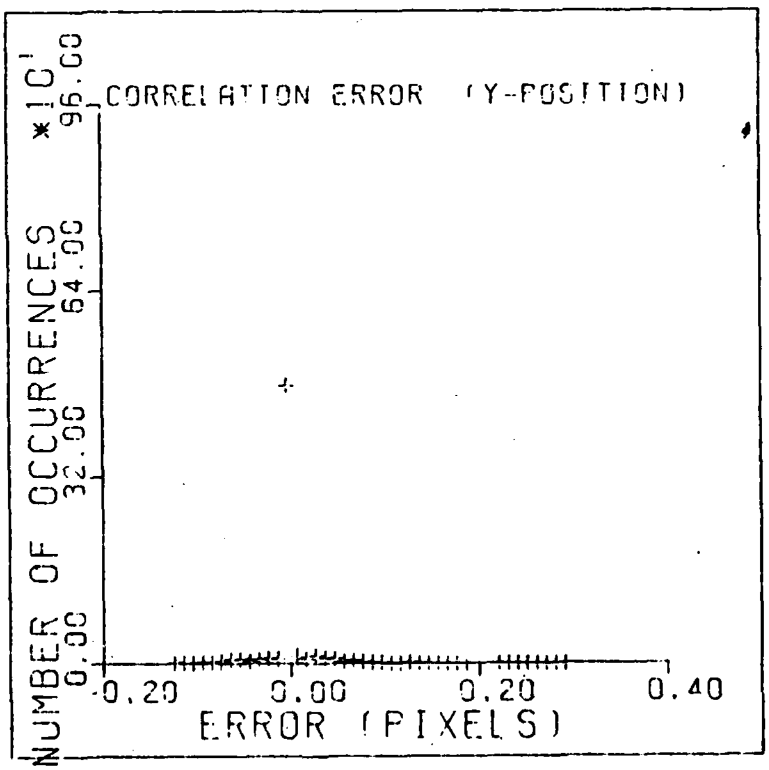

Figure 37. Histogram of Errors-Phase Method (threshold = .7, 3 hot spots)

profiles were located so that if the center of the 8x8 pixel FLIR tracking window was located at coordinates (0,0) then the target centroids would be at (0,-2,667), (-2,1.33), and (2,1.33). This spacing means the center of mass of the intensity profiles is at (0,0) but the resultant intensity profile is not radially symmetric about (0,0). In order to insure these statistics were representative of the true correlator errors and not of just one particular offset distance chosen, which may have enhanced or degraded the performance of a particular correlation method, evaluations were conducted for other offset distances between the target and the template. The error statistics for these cases, not shown, verified that the cases presented in Tables 1 and 2 were representative of the performance of the correlation methods.

Tables 1 and 2 and Figures (30-37) were analyzed to determine which correlation methods were best suited for implementation with the Kalman filter:

a. Direct Method: (two-level quantization): This is clearly the fastest of the four correlation methods considered. For the one hot spot case its performance is comparable to the other methods with errors which could be modeled as Gaussian. However, the mean error of this method increases from the one to three hot spot case, which is not surprising since this method only catagorizes the intensity values as above or below the mean intensity levels. Thus, when there are three hot spots of the same maximum intensity on the FLIR plane, this method has difficulty determining the global peak. This accounts for the erratic nature of the errors in Figure 34. In the x-direction, where the intensity pattern is symmetric, the method performs well. However, in the asymmetric y-direction, there are peaks around 0.0 and ±.15 pixels indicating the method is finding the global peak at times and is misinterpreting the peak of one of three hot spots as the global peak at other times. To model these errors as Gaussian would be questionable. Based on the performance degradation in the three hot spot case, this method was not implemented. However, if computational loading is the driving factor, this method could become more attractive.

b. Direct Method (six-level quantization): The performance of this method is comparable to FFT and phase correlation method with errors which are well modeled as Gaussian. The correlator performs extremely well in determining the peak in the asymmetric y-direction in the three hot spot case. However, the computational loading associated with this method, while gaining no real performance enhancement over the FFT and phase correlation methods, is too great for this method to be considered for implementation.

c. FFT Method (Threshold = .3): The threshold was set low while using this method to avoid the appearance of false peaks which lead to a biased estimate (Figure 27). This correlator performs well with errors, in both the single and multiple hot spot cases, which are well modeled as Gaussian, and in almost all instances, has the smallest standard deviation. The results of this analysis are consistent with the analyses performed by Rogers (8: Chapter V) and this method was implemented with the Kalman filter.

d. Phase Correlation Method (Threshold = .7): As expected, this method substantially reduced the biasing which can occur in the FFT method with the histograms appearing as a spike. However, the computational increase is not substantial. Noting the large standard deviation of this method, the errors committed cannot be well represented as Gaussian which may potentially cause problems. However, because this method does consistently locate the true global peak of the intensity function, it was implemented with the Kalman filter and a comparison of the tracking performance of this correlation method and the FFT method is presented in Chapter 5.

V. Performance Analysis

5.1 Introduction

This chapter presents the tracking performance of the correlator/Kalman filter when evaluated against the trajectories described in Chapter 2. The first section of the chapter gives an explanation of how the statistics used to evaluate the tracker's performance are computed. The next section of the chapter discusses those parameters within the computer simulation which were changed to evaluate the tracker's performance under various conditions. The third section of the chapter discusses those parameters within the correlator/Kalman filter which can be adjusted off-line in order to enhance the tracking ability of the filter. The final section of the chapter condenses the results of the tracking performance into tables. The statistical information of this chapter was generated using Monte Carlo techniques (12:329). Based on previous variance convergence analyses (6,7), 10 Monte Carlo runs were determined to be sufficient to generate sample statistics that are representative of the true process statistics, and therefore, 10 runs constitute one Monte Carlo study. Each single run consisted of a 5 second, or 150 sample period, simulation.

5.2 Tracking Ability

The errors of primary interest, with respect to the tracking ability of the filter, are errors in the estimated values of $\hat{x}_d(t_i^-)$, $\hat{y}_d(t_i^-)$, $\hat{x}_d(t_i^+)$, and $\hat{y}_d(t_i^+)$. Additionally, since the propagated estimate of the intensity centroid's location, $x_{peak}(t_{i+1}^-)$ and $y_{peak}(t_{i+1}^-)$, will affect the correlation process, it is important to estimate this position accurately. The mean error in the correlator/Kalman filter's estimate for the x-dynamic position can be calculated at any time t_i by

$$\bar{E}_{x_d}(t_i) = \frac{1}{N} \sum_{k=1}^{N} \{\hat{x}_{df_k}(t_i) - x_{dt_k}(t_i)\} = \frac{1}{N} \sum_{k=1}^{N} e_{xd_k}(t_i) \qquad (5\text{-}1)$$

where

$\bar{E}_{x_d}(t_i)$ = mean error (i.e. ensemble average error over all simulations) in the x-dynamic position at time t_i

$\hat{x}_{df_k}(t_i)$ = filter estimated x-dynamics value at time t_i for simulation k

$x_{dt_k}(t_i)$ = truth model, x-dynamics value at time t_i for simulation k

N = number of Monte Carlo runs

and the variance of the error is calculated as

$$\sigma^2_{xd}(t_i) = \frac{1}{N-1} \sum_{k=1}^{N} e^2_{xd_k}(t_i) - \frac{N}{N-1} \bar{E}^2_{x_d}(t_i) \qquad (5\text{-}2)$$

Equations (5-1) and (5-2) can be generalized to calculate the errors in the other quantities of interest previously discussed. Additionally, time averages of the mean error and variance were calculated over the last 1.5 seconds of the simulation. This time averaging interval was selected so that any transient effects caused by changes in the target dynamics would have decayed. This provides 45 sample runs, to serve as an indicator of the tracker's performance: time averaging these allows for a compact presentation in tabular form.

5.3 Variation of Truth Model Parameters

Parameters within the truth model are changed to analyze the sensitivity of the correlator/Kalman filter to changes in the "real world". The primary goal of the research was to evaluate the performance of the tracker against targets displaying the various dynamic profiles described in Chapter 2. Thus, the 4 trajectories previously described were the primary truth model factors varied to evaluate the tracker performance. In addition, variations were also considered in parameters defining the target intensity profile itself. To evaluate the performance of the tracker when the strength of the maximum target intensity value changes relative to the background noise, the signal-to-noise ratio (SNR) defined as

$$\frac{S}{N} = \frac{I_{max}}{\sigma_B} \tag{5-3}$$

where

I_{max} = maximum target intensity value

σ_B = rms value of background noise, including FLIR noise contributions

is varied. For the multiple hot spot cases, the values of the three Gaussian intensities were equal. Signal to noise ratios of 20 (standard) and 10 were considered as representative of realistic tracking scenarios.

The spread parameter, σ^2_{pv}, of the target's Gaussian intensity profile(s) can be varied to evaluate the performance of the tracker against sharply peaked (small σ^2_{pv}) or broad (large σ^2_{pv}) Gaussian target intensities. However, because the effects of varying this parameter were previously investigated by Rogers (8:Chapter 6), a standard value of 2.0 was used throughout this research (of course, σ_{pv} changed as a function of range to the target within a given simulation). However, the target aspect ratio (AR)

$$AR = \frac{\sigma_v}{\sigma_{pv}}$$

was varied to evaluate the tracker's performance against targets exhibiting different intensity profiles due to varying the aspect angle.

5.4 Variation of Data Processing Parameters

Several parameters are available within the data processing algorithm, upper path of Figure 1, which can be varied to improve the estimate of the intensity function. The 8x8 FLIR tracking window can be padded with zeros if the intensity spread parameters, σ_v and σ_{pv}, are such that the target intensity height is approaching zero near the edge of the 8x8 tracking window. However, if these parameters are such that significant intensity magnitudes exist outside the 8x8 tracking windows, then padding with zeros would induce an artifical edge (see Chapter 4). Therefore, the algorithm was structured so the 8x8 FLIR window could be padded with noise-corrupted data when necessary. Based on the results of Roger's research (8:Chapter 6), and because in a dynamic tracking environment significant intensity values may exist near the edge of the tracking widnow, the FLIR tracking window was padded with noise-corrupted data in this study.

Alpha, the relative weighting parameter for the exponential smoothing process is the next parameter which may be varied within the data processing algorithm. Equation (1-4) displays the role of this parameter in the algorithm.

The standard value used in this research was .05. This value, which indicates that the target intensity profile is essentially averaged over the most recent 20 sample periods, was considered appropriate for targets whose intensity projection was relatively constant. However, if the intensity pattern on the FLIR image plane is varying so that significant changes could occur within a 20-sample period interval of time, such as for a target performing a roll maneuver, increased emphasis should be placed on the more recent measurements. The effects of increasing alpha in this situation are explored.

5.5 Variation of Filter Parameters

Design parameters within the Kalman filter structure are varied either off-line during a filter tuning process or adaptively in real-time in an attempt to improve the quality of the state estimates. The parameters in the linear Kalman filter, developed in Chapter 3, which may be varied during the off-line filter tuning process, and the values of which may change for different target trajectories are the target acceleration and atmospheric jitter time constants, τ_{df} and τ_{af}, the discrete-time noise covariance matrix, $\underline{Q}_{fd}$, the strength of which may be interpreted as a measure of the uncertainity in the dynamics model being used, (i.e. how adequately the assumed model represents the "real world"), the measurement uncertainity covariance matrix, $\underline{R}$, and the initial filter covariance matrix, $\underline{P}(t_0)$.

Based upon previous research efforts (6,8,10) the assumed correlation time for the atmospheric jitter position was set at .0707 sec. Using this value assumes the effects of repeated poles shown in Equation (2-2) are considered negligible. The variance of the atmospheric jitter process was set at a constant .2 (pixels^2). The diagonal terms for the $\underline{R}(t_i)$ matrix were based on the statistical analysis of the correlation process detailed in Chapter 4. The cross-correlation between the errors in each of the FLIR image plane directions in the correlation process was calculated and proved to be small enough to assume that the correlation position uncertainty estimate in one direction is independent of the uncertainty of the position estimate in the other direction, resulting in a diagonal $\underline{R}(t_i)$. Thus, the parameters which were used to tune the filter to optimize filter tracking performance were τ_{df} and σ^2_{df}.

For the type of targets being tracked in this research, target acceleration time constants ranging from 1 to 4 secs were used where a lower τ_{df} is more appropriate for a highly dynamic tracking environment. Values of σ^2_{df} ranged from 150 (pixels^2/sec^5) to 500 (pixels^2/sec^5) depending on the type of trajectory being tracked, where σ^2_{df} was increased for highly dynamic targets. The wide disparity in the values used for σ^2_{df} and σ^2_{af} directly reflects the range of rms accelerations between benign versus harshly maneuvering targets and their relationship with the jitter rms value.

In the filter tuning process, the $\underline{P}(t_0)$ matrix is set to reflect the knowledge of the conditions under which the estimation process is to be initiated. Since in realistic scenarios, the filter may very well receive inaccurate handoff information from the target acquisition source (such as a multi-target search radar), the diagonal entries of $\underline{P}(t_0)$ were purposefully set high to reflect this handoff uncertainty. The appropriate values at which to initialize variances on the main diagonal were determined by observing the peak values of each of these terms during the filter transient period. The variances on the main diagonal, for position, velocity, and acceleration, were 10 (pixels^2), 2000 (pixels^2/sec^2), and 100 (pixels^2/sec^4) respectively. The initial values of the $\underline{P}(t_0)$ matrix will be the dominant factor in the initial transient characteristics of the filter (12:337). When tuning the filter, a useful technique is to compare the value of the actual rms errors committed by the filter to the filter's own representation of the error covariance. The time histories of these errors are available as the output of the Monte Carlo simulation process used. By "matching" the filter's rms estimation of its errors to the true rms errors committed by the filter, an attempt is made to insure that the proper relative weighting is given to the internal dynamics model and the measurements (12:338-339).

5.6 Plotting Results

An explanation of the plots generated to depict the filter's tracking errors are given in this section, with the plots which served as the baseline case for the correlator/Kalman filter being shown. The remainder of the performance plots are given in Appendix C. For each run, ten plots were generated. The first two plots show the filter-computed rms errors versus the actual rms errors in the x and y dynamics positions. The next four plots show the mean errors in the x and y dynamics position estimates ± one standard deviation, beginning with the first plot showing the filter's estimate at time minus and the second plot showing the filter's estimate at time plus. Similarly, the next four plots give the errors in the filter's estimates of the centroid position at times minus and plus. The case number on each plot is used to match each run with the tables shown in the next section. By referring to these tables, the trajectory, truth model parameters, and filter parameters can be cross-referenced. Additionally, a summary of the parameter values for each case is given at the end of the chapter.

Referring to Figure 38a, it is seen that the filter was intentionally set to overestimate its own errors,

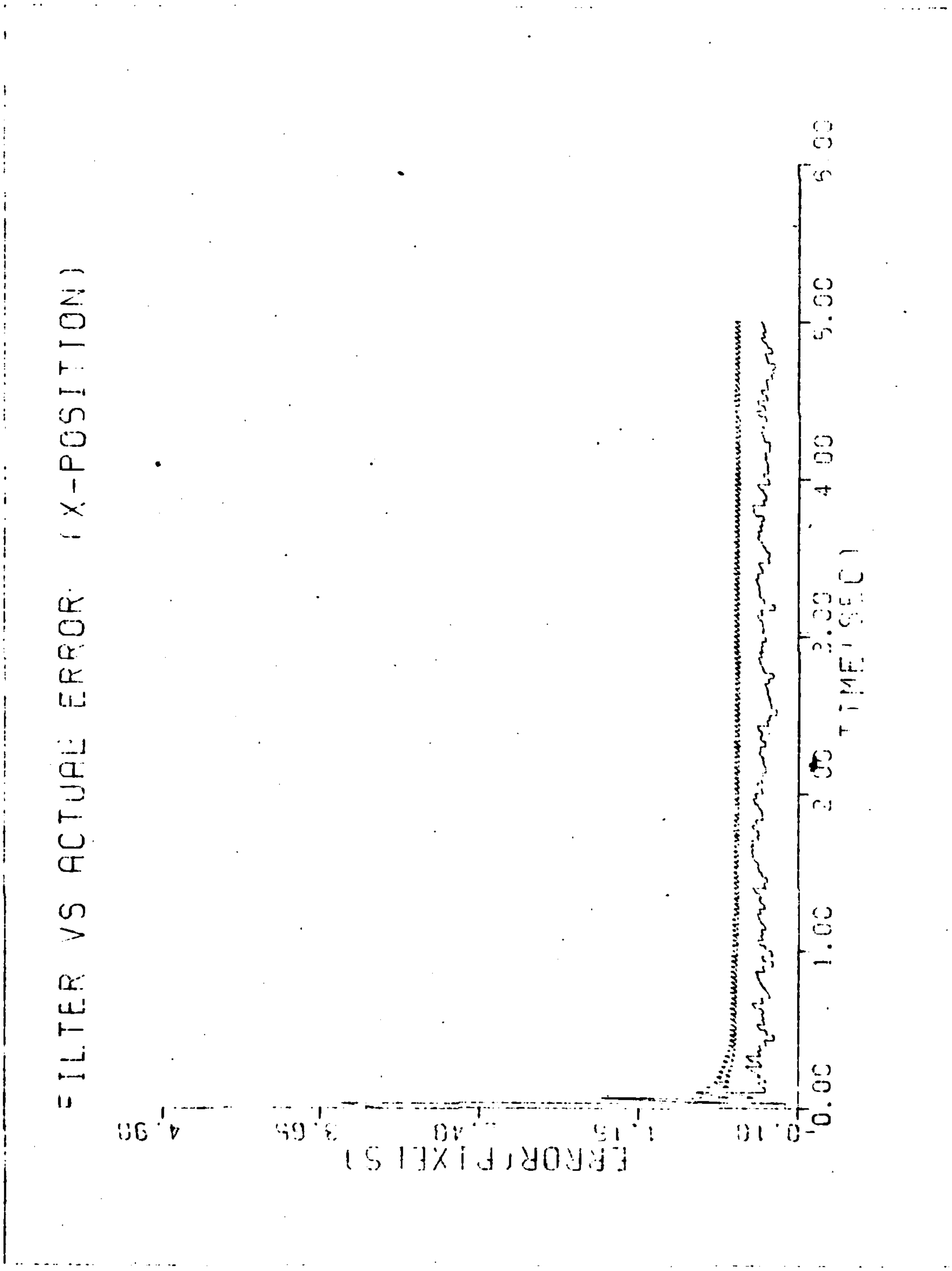

Figure 38a. Case 1

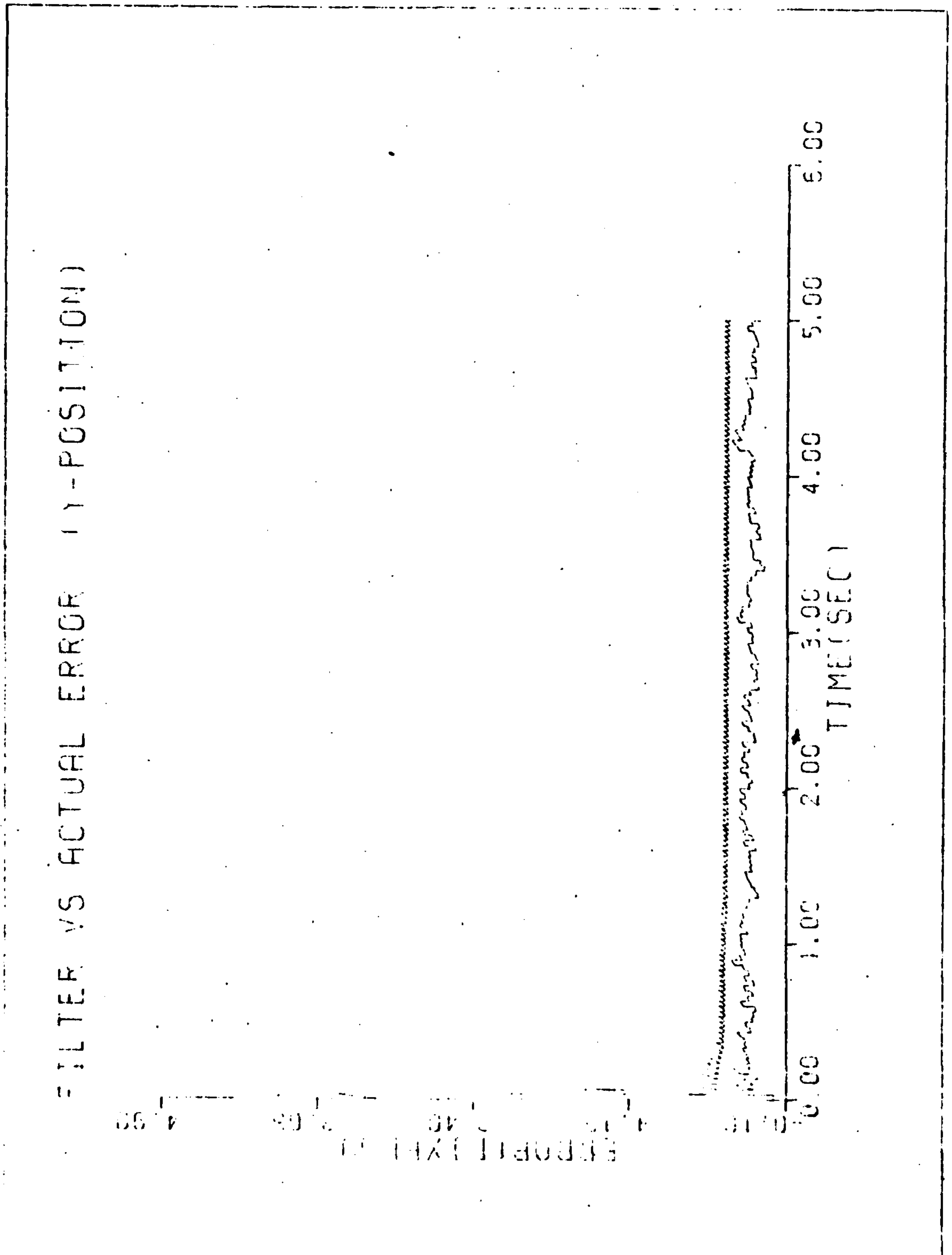

Figure 38b. Case 1

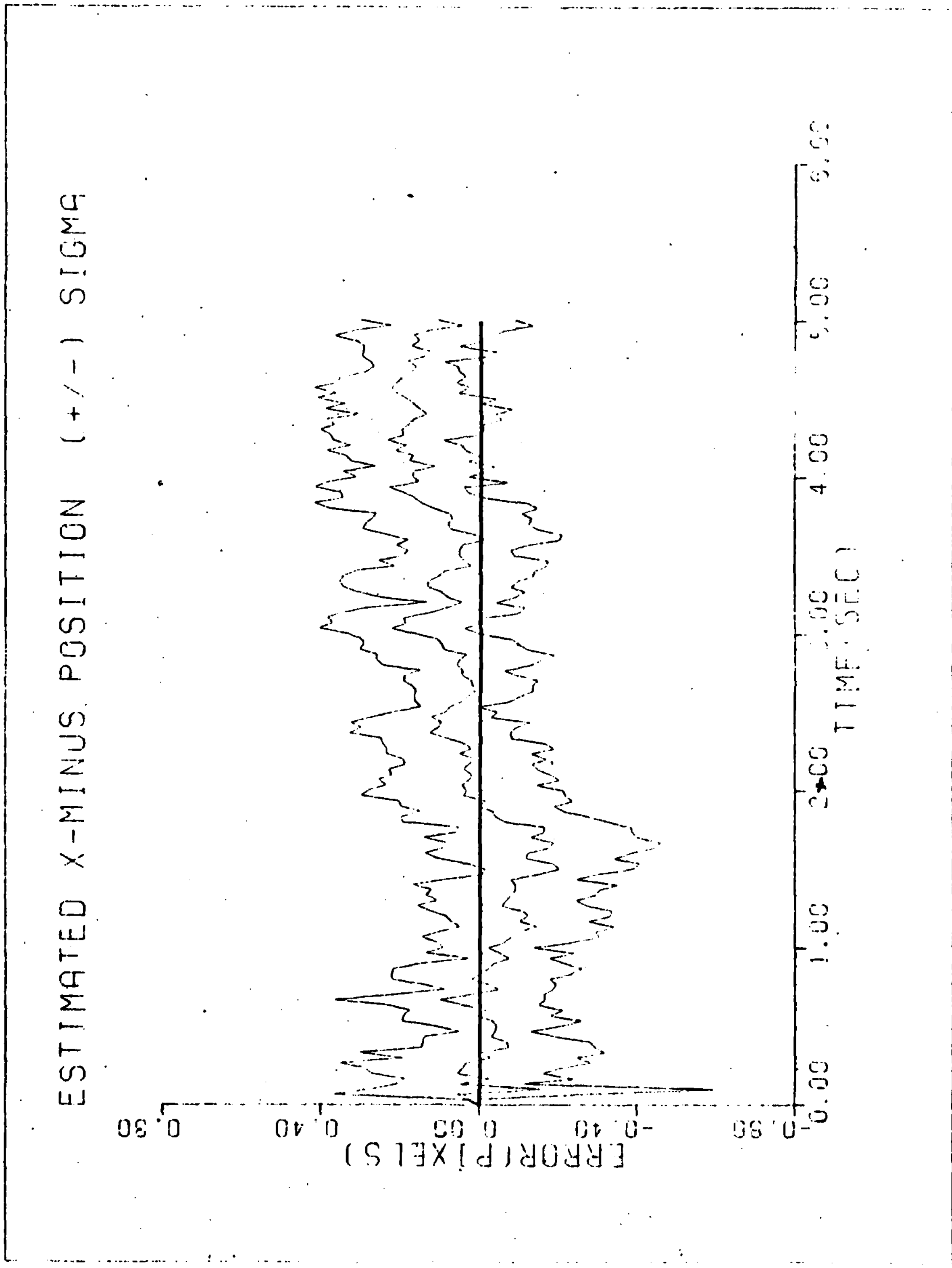

Figure 38c. Case 1

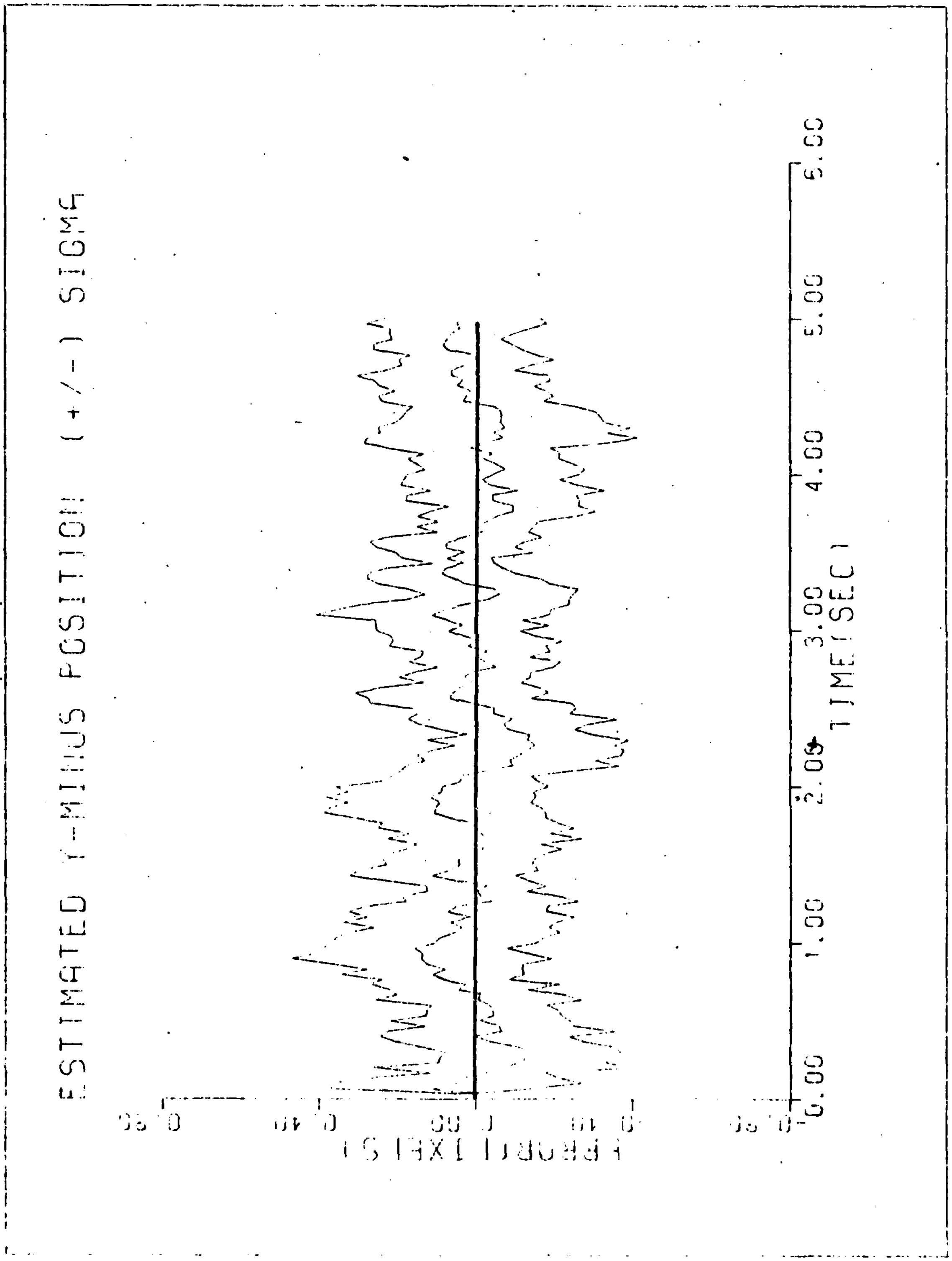

Figure 38d. Case 1

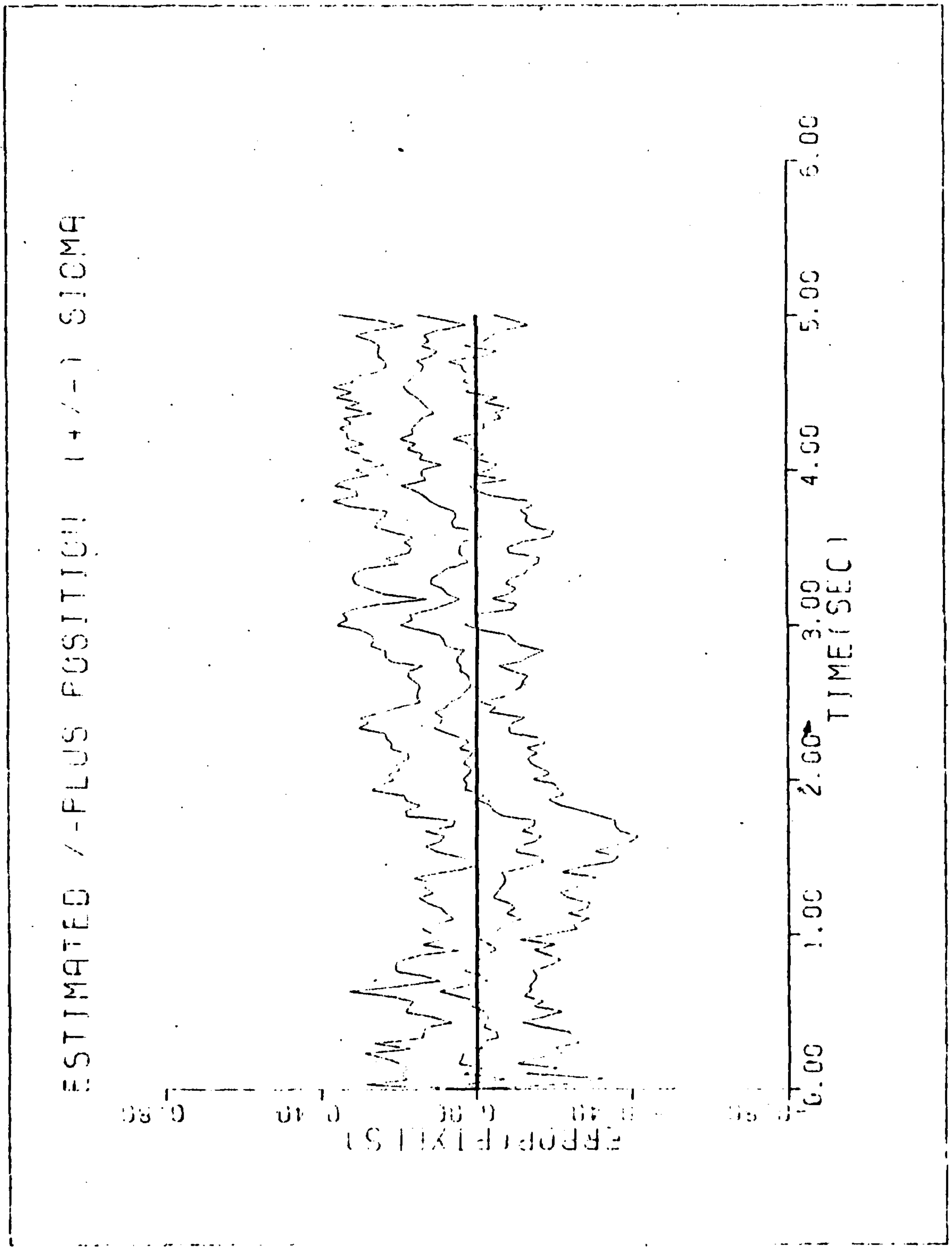

Figure 38e. Case 1

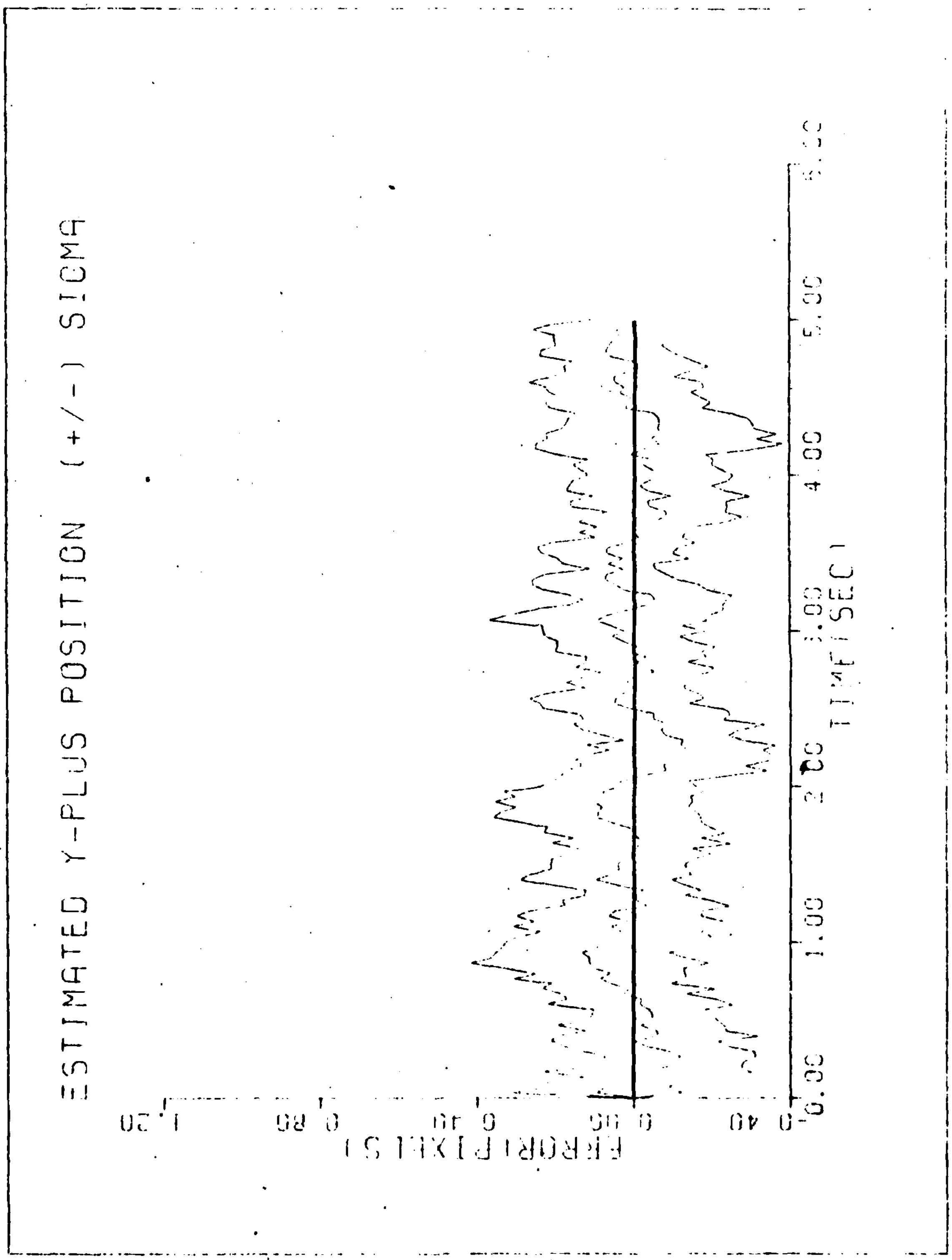

Figure 38f. Case 1

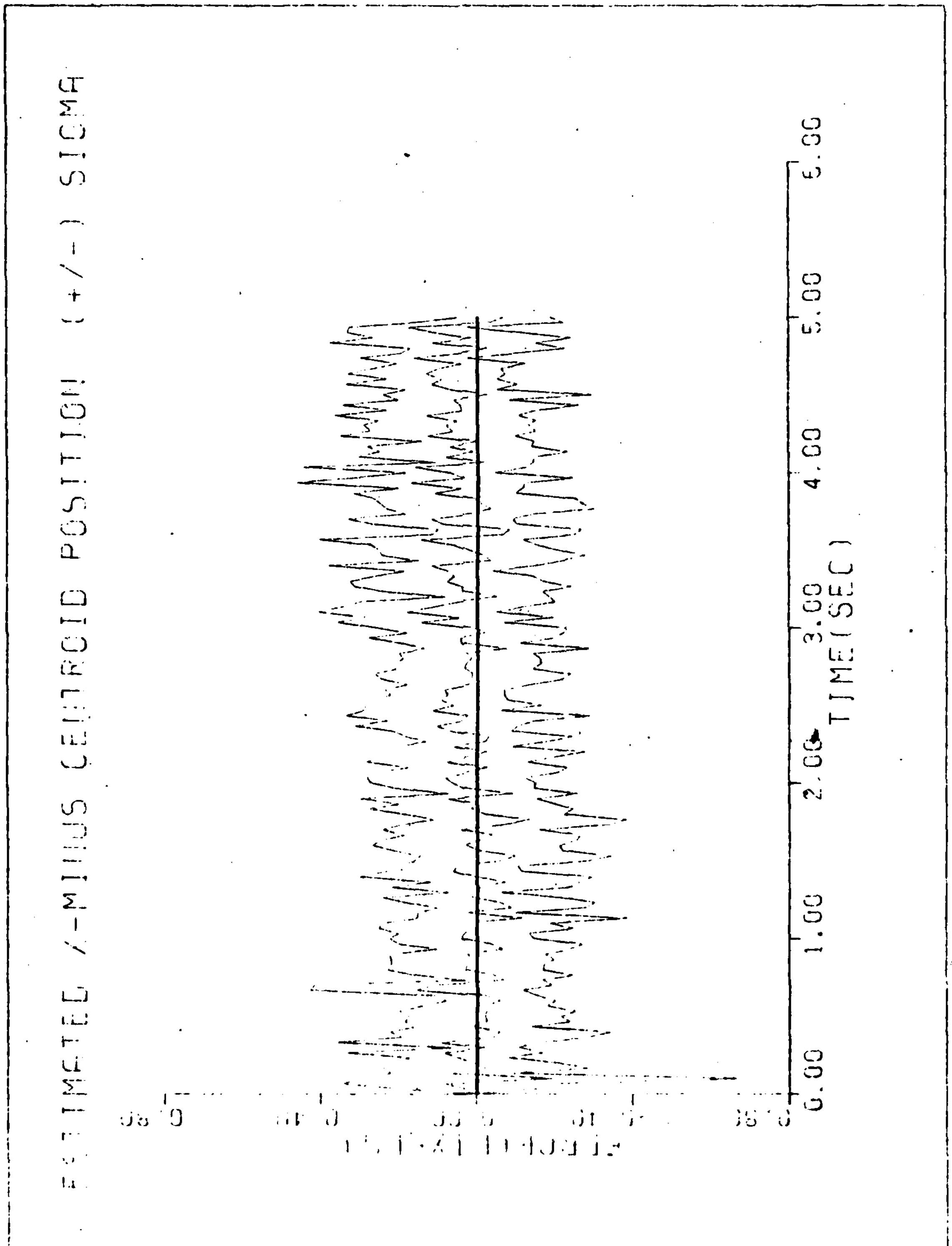

Figure 38g. Case 1

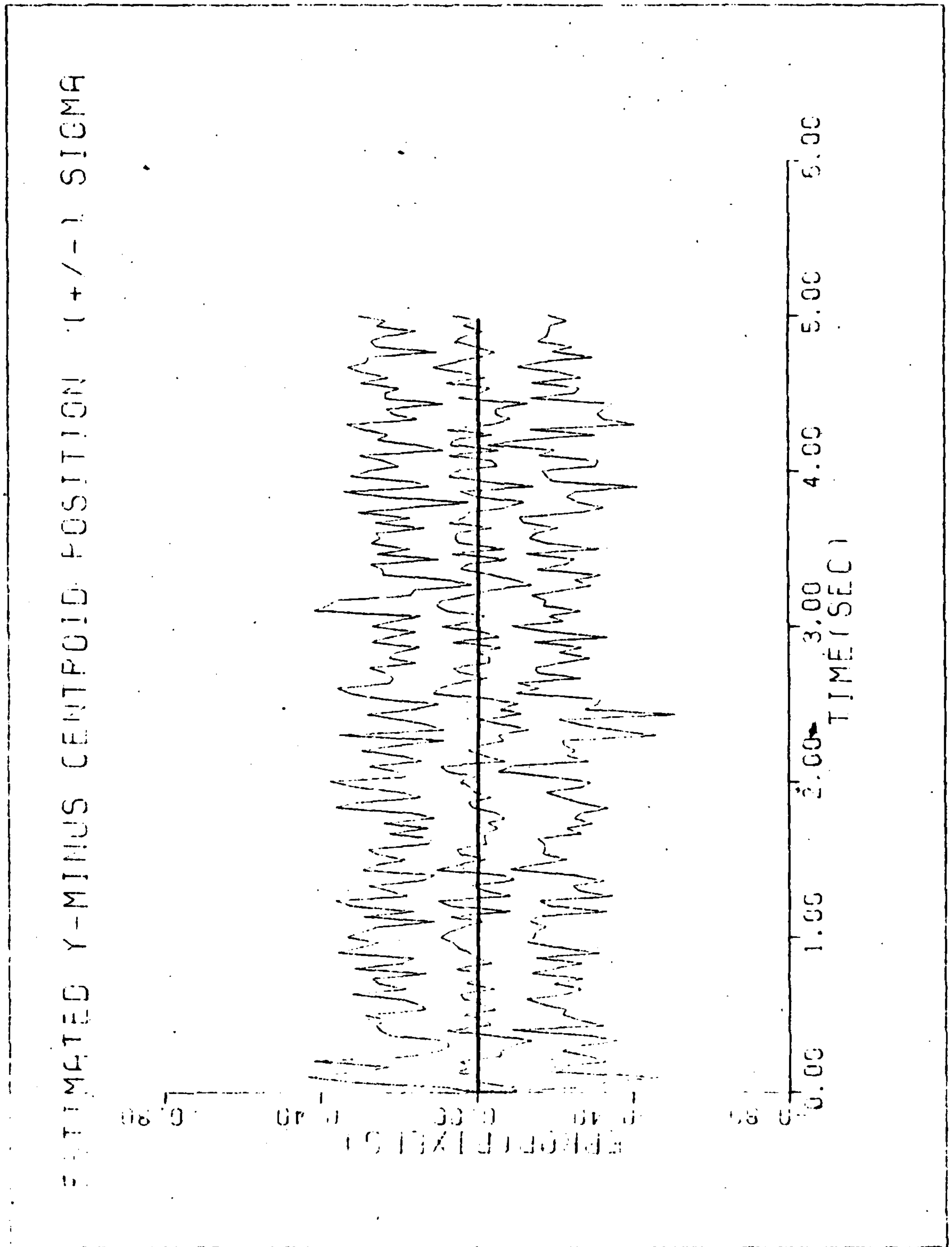

Figure 38h. Case 1

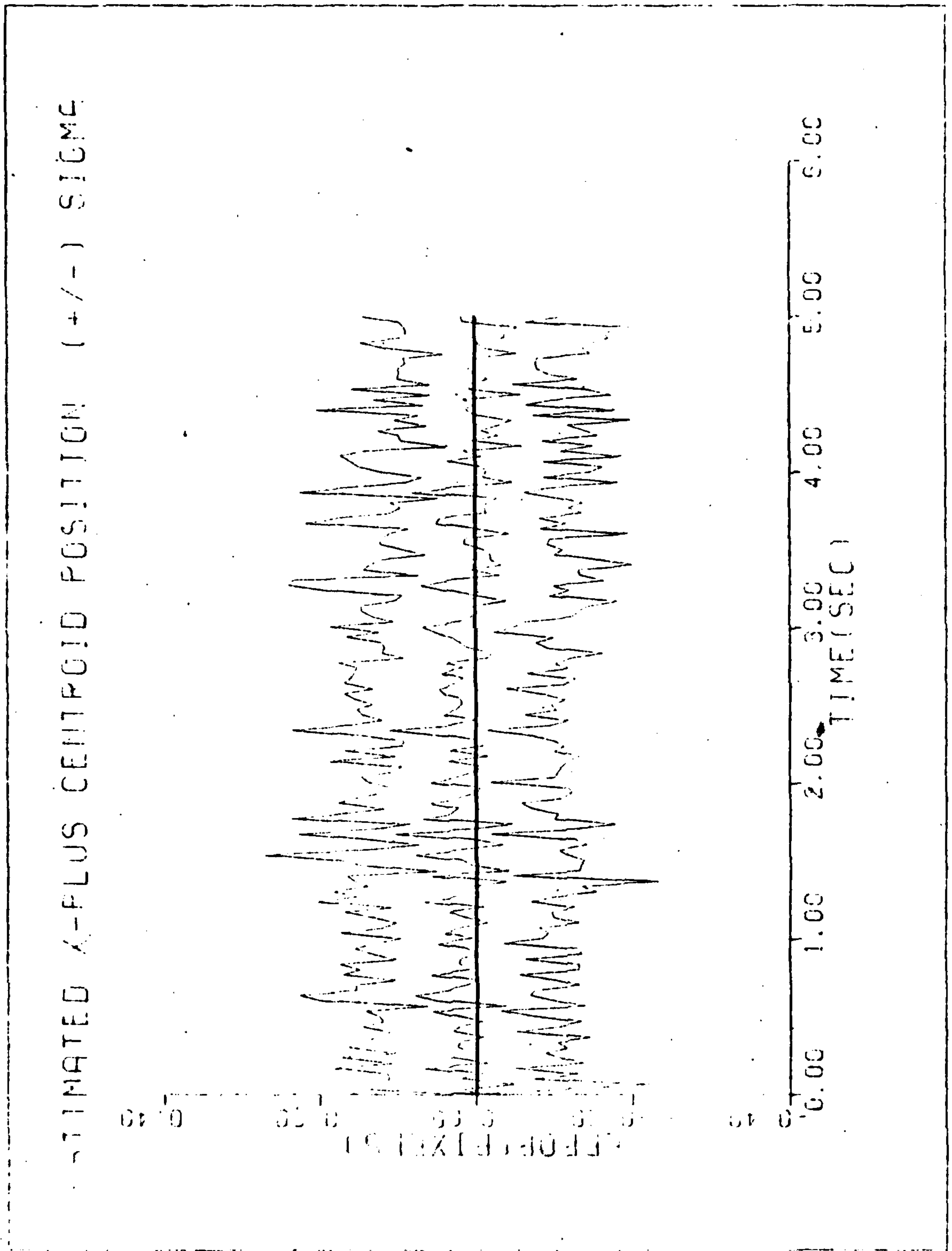

Figure 38i. Case 1

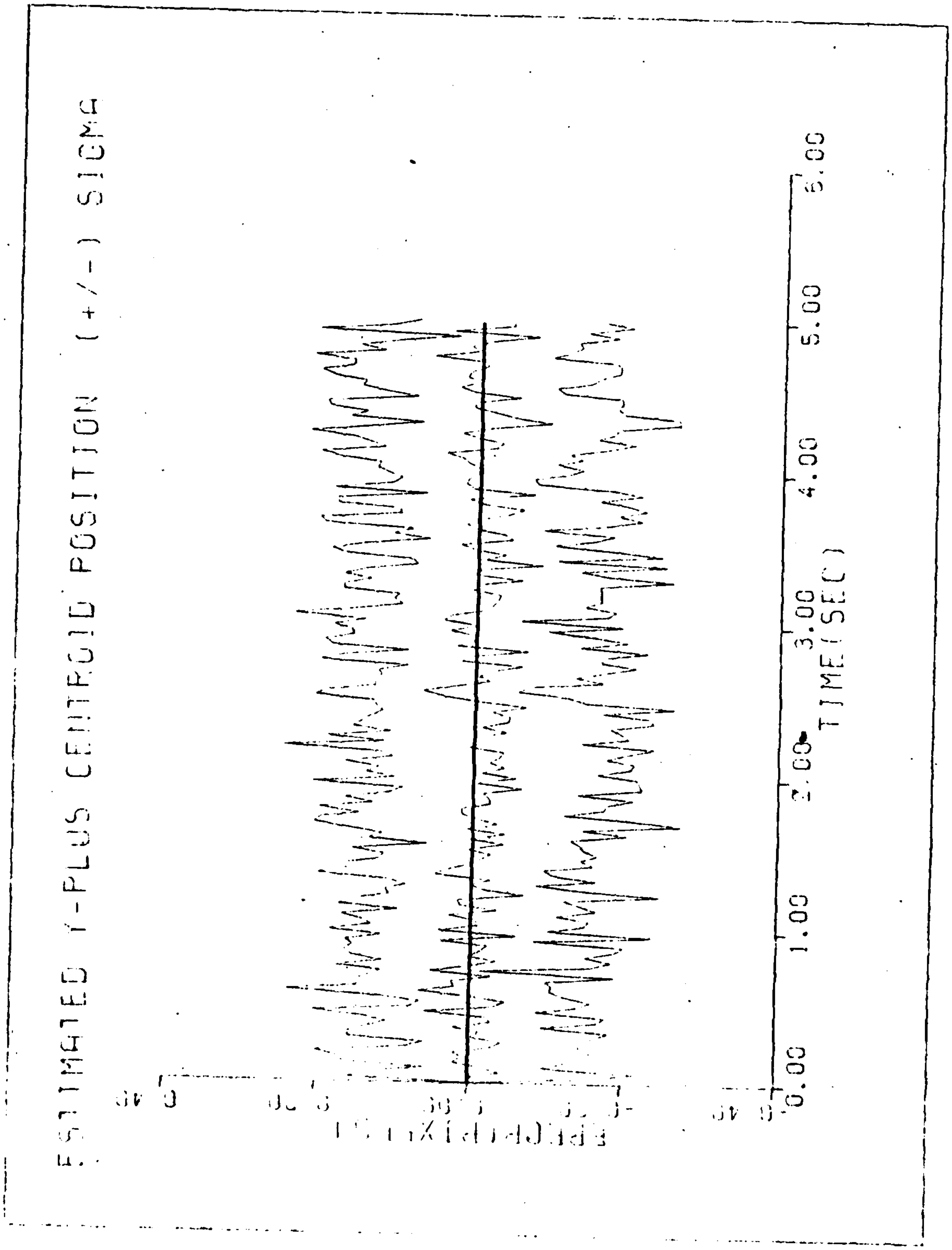

Figure 38j. Case 1

i.e., it was "conservatively" tuned. The reason for this conservative tuning which is used to guard against possible filter divergence is explained by referring to Figure 35c. As shown, the filter mean error has a transient characteristic which lasts for approximately two seconds. In an attempt to minimize this transient, the conservative tuning was used. The reason for this unexpected transient characteristic is not completely understood. However, a discussion of possible causes is included in the next chapter. Also note the filter was given perfect knowledge of the initial conditions through $\hat{\underline{x}}_f(t_0^+)$.

5.7 Analysis of Filter Performance

The results of the filter's performance will be presented in tabular form in this chapter and in graphical form in Appendix C. The error statistics shown in the tables are the temporal averages of the mean errors and standard deviations from t = 3.5 to t = 5.0. For the truth model parameters, the following standard values were used unless specifically noted in the comments section of the table:

a) Aspect Ratio (AR) = 1

b) Intensity Function Spread Parameter (σ^2_{pv}) = 2

c) Signal to Noise Ratio (SNR) = 20

d) Maximum Hot Spot Intensity (I_{max}) = 20

Thus, combining c and d above yields a rms background noise value = 1.

The first line in the header entry for each of the tables gives those parameters which were used for filter tuning where τ_{df} and σ^2_{df} are as previously defined and α is the exponential smoothing parameter shown in Equation (1-4). The truth model parameters which were often varied from one Monte Carlo run to another are given in the second line of the header column. The first entry references the trajectories defined in section 2.3. For trajectory 2 which is the pullup maneuver, the dynamics of the turn (g-factor) are shown in the comments column. The second entry gives the roll rate, ω, for the run in rad/sec. The final truth model entry in the header column gives the number of hot spots (NUMHS) used for the run. The statistics presented in the tables are defined as:

$\overline{x_e}$ = average of the mean error for the true position in the x-direction from t = 3.5 to t = 5.0 at times minus and plus (similarly for $\overline{y_e}$)

$\overline{\sigma x_e}$ = average of the standard deviation of the true position in the x-direction from t = 3.5 to t = 5.0 at times minus and plus (similarly for $\overline{\sigma y_e}$)

$\overline{cx_e}$ and $\overline{\sigma cx_e}$ = errors as defined above for the centroid position (similarly for $\overline{cy_e}$ and $\overline{\sigma cy_e}$)

5.8 Evaluation of Correlation Methods

Based on the analysis of the correlation methods detailed in Chapter 4, the FFT and phase correlation methods were incorporated into the tracking algorithm, to evaluate the performance of each in a tracking environment. The correlators were evaluated under a benign tracking environment, trajectory 1, against targets exhibiting both single and multiple hot spots. The results of the performance evaluation are shown in Table III. For the single hot spot case, the FFT method has a smaller mean error the the y-position, while the phase correlation method produces better mean estimates in the x-direction.

Table III. Correlator Performance Results

$$\text{Header} = \begin{matrix}(\tau_{df}, \sigma^2_{df}, \alpha) \\ (\text{Trajectory, Roll Rate, NUMHS})\end{matrix}$$

Comments	Header	$\bar{x}_e(-)/$ $\overline{\sigma x}_e(-)$	$\bar{x}_e(+)/$ $\overline{\sigma x}_e(+)$	$\overline{cx}_e(-)/$ $\overline{\sigma cx}_e(-)$	$\overline{cx}_e(+)/$ $\overline{\sigma cx}_e(+)$	$\bar{y}_e(-)/$ $\overline{\sigma y}_e(-)$	$\bar{y}_e(+)/$ $\overline{\sigma y}_e(+)$	$\overline{cy}_e(-)/$ $\overline{\sigma cy}_e(-)$	$\overline{cy}_e(+)/$ $\overline{\sigma cy}_e(+)$
Case 1 FFT Cor	3.5,150,.05 1,0,1	.142/ .177	.104/ .162	.053/ .207	-.005/ .116	-.006/ .203	-.010/ .190	.000/ .222	-.009/ .154
Case 2 Phase Cor	3.5,150,.05 1,0,1	-.043/ .344	-.070/ .331	-.134/ .405	-.190/ .388	.112/ .326	.1081 .317	.118/ .367	.108/ .352
Case 3 FFT Cor	3.5,150,.05 1,0,3	.142/ .160	.113/ .148	.052/ .179	-.007/ .056	.010/ .170	.005/ .156	.015/ .178	.006/ .066
Case 4 Phase Cor	3.5,150,.05 1,0,3	.286/ .315	.258/ .302	.198/ .339	.139/ .292	.063/ .292	.058/ .281	.068/ .331	.059/ .292

However, the FFT method produces the best position estimates in both directions in the three hot spot cases. The data presented in Table III can be used to calculate the rms error, defined as rms = $\sqrt{m^2+\sigma^2}$. A calculation of this statistic revealed that in all cases the phase correlation method had a rms error which was approximately 50% greater than the FFT rms error. Additonally, the standard deviation of the FFT method is substantially smaller in all cases, as expected based on the analysis of the correlation methods. Therefore, the FFT method was chosen as the correlation method to be used in the remainder of the evaluations. Since the mean tracking errors were slightly larger in the three hot spot case for the FFT method, the remainder of the evaluations were made for three hot spot targets, with case 1 to serve as the baseline for the correlator/Kalman filter performance.

5.9 Evaluation of Harnly and Jensen EKF

With case 1 of Table III established as the performance baseline for the correlator/Kalman filter in the single hot spot case, the 8-state EKF designed by Harnly and Jensen (6), which uses a Brownian motion acceleration model and a bivariate Gaussian measurement model, was evaluated to provide a performance benchmark. The Harnly-Jensen cases are referred to by letters whereas the correlator/Kalman filter cases are numbered. The first case, case A, was conducted with the same truth model parameters used in case 1. As shown in Figures 39a and 39b, the filter is well-tuned for this scenario. Although not accomplished, extended Kalman filters are often tuned by comparing the filter computed covariance to the actual rms error instead of the actual standard deviation to minimize any bias effects. As in the previous cases, the filter was initialized with perfect state knowledge so no recovery

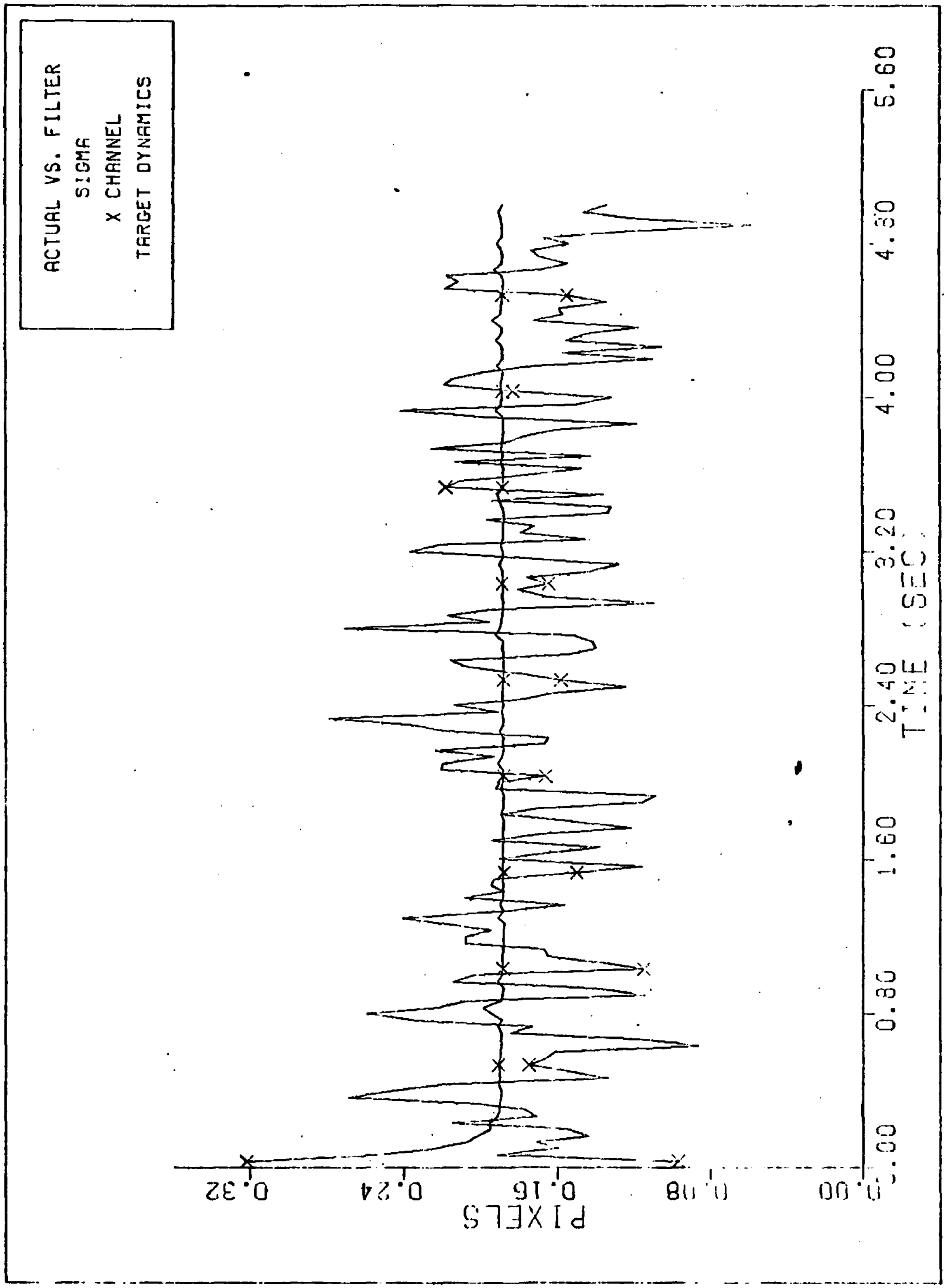

FILTER VS. ACTUAL SIGMA PLOT (S/N = 20)

Figure 39a. Case A

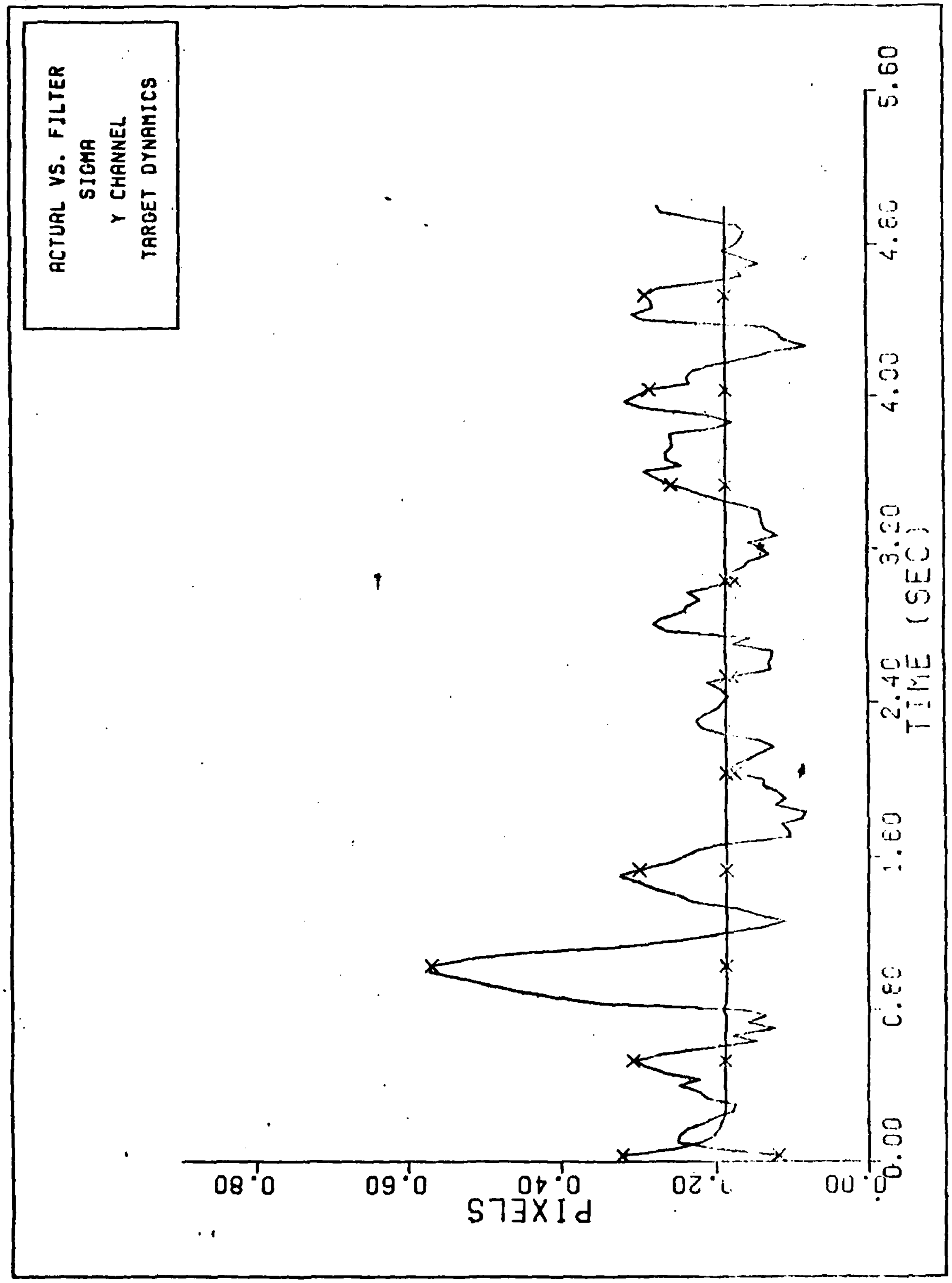

FILTER VS. ACTUAL SIGMA PLOT (S/N = 20)

Figure 39b. Case A

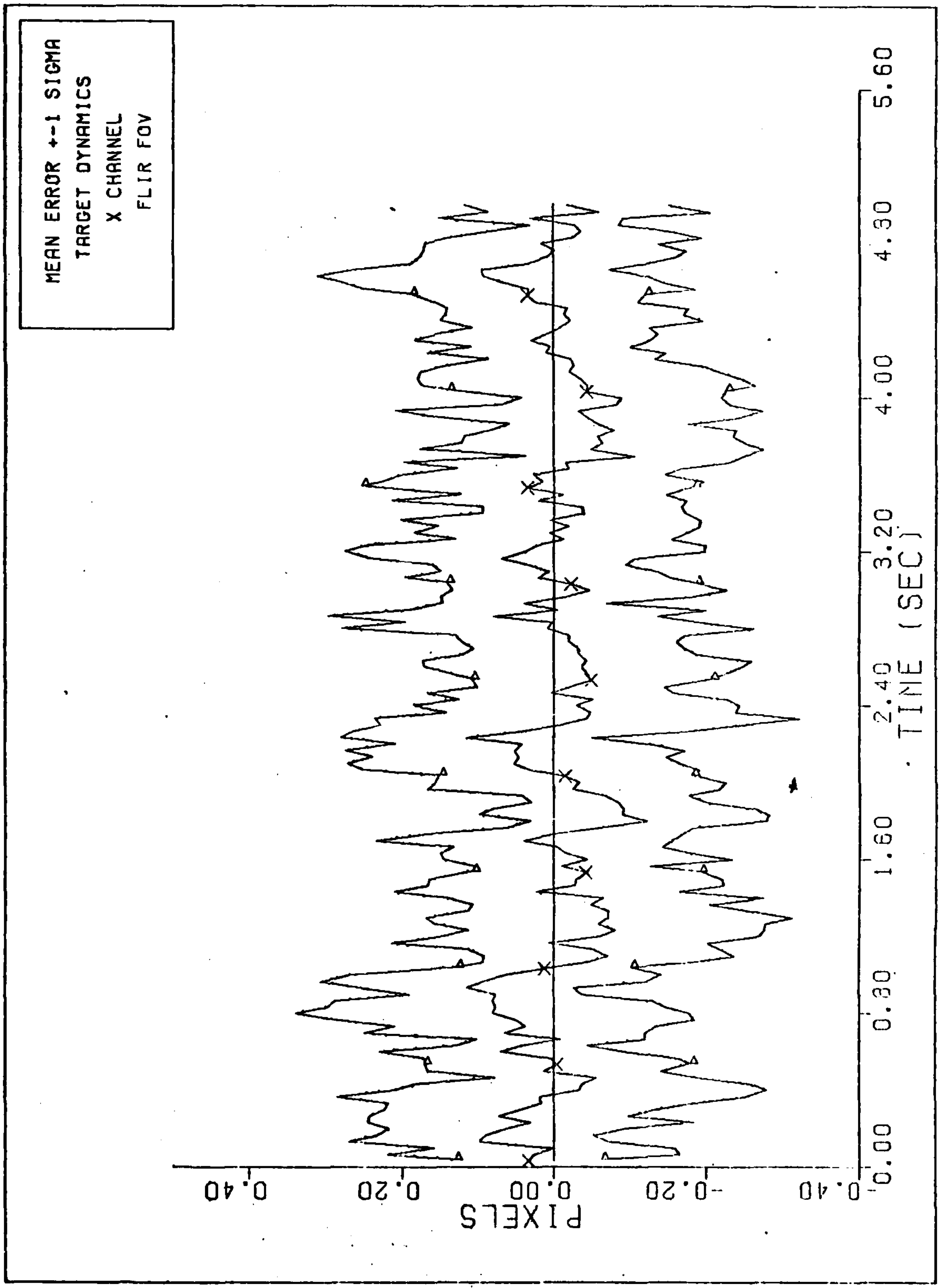

X CHANNEL DYNAMICS ERROR (S/N=)

Figure 39c. Case A

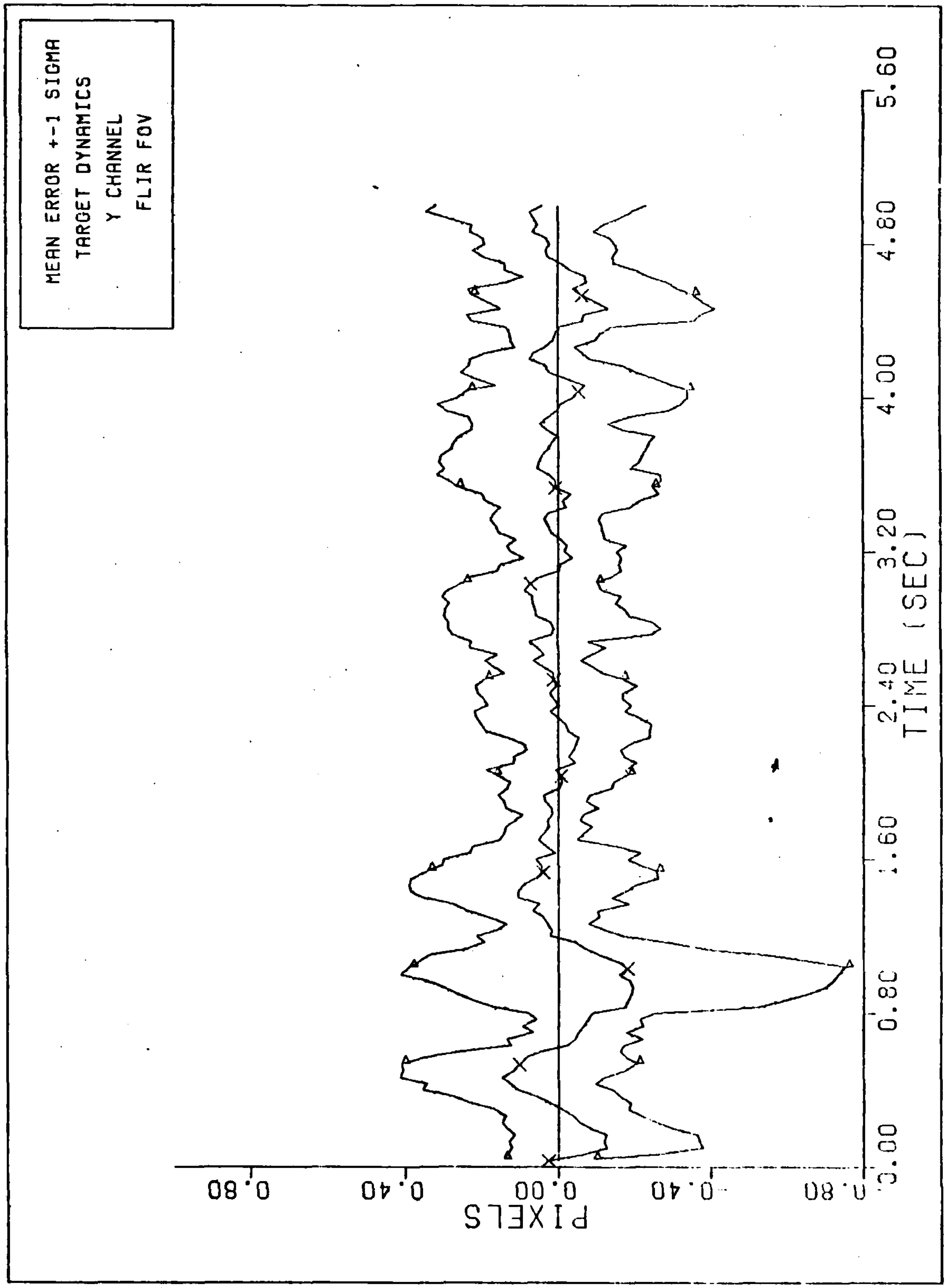

Y CHANNEL DYNAMICS ERROR (S/N 20)
Figure 39d. Case A

period is observed. (Note: The position plots are for the errors at time plus.) The statistics for the run were averaged as before from t = 3.5 to 5.0 and are shown in Table IV. (Note: The statistics shown are the only position calculations available from the Harnly-Jensen routine.) When this case is compared to case 1, it is seen that in the x-direction the mean error bias present in the correlator/Kalman filter is not present in the EKF, with which excellent tracking is obtained. However, the EKF has a slightly larger standard deviation. In the y-direction similar error characteristics are noted with the EKF having the smaller mean error and the correlator/ Kalman filter having the smaller standard deviation. Calculation of the rms errors from the table data shows the rms error for the Harnly-Jensen EKF is .06 pixel less in the x-direction and .01 pixel greater in the y-direction.

Table IV. Harnly-Jensen EKF Performance
Header (σ^2_{df})
(Trajectory)

Comments	Header	$\overline{x}_{ERR}(+)$/ $\overline{\sigma x}_{ERR}(+)$	$\overline{y}_{ERR}(+)$/ $\overline{\sigma y}_{ERR}(+)$	Remarks
Case A	150 1	-.012/ .165	.006/ .221	
Case C	200	-.000/ .164	.015/ .184	Special Trajectory

Note: Case B statistics not given due to filter divergence at the end of simulation.

The next run with the filter, case B, was a 2-g pullup maneuver using trajectory 2. The performance plots for this case are shown in Figures 40a-d. When this case is compared to cases 12 and 13 for the correlator/Kalman filter, which are presented in section 5.12, it is seen that the EKF responds better at maneuver initiation with the mean tracking error being 0.5 pixel at the maximum point as compared to a 1.0 mean pixel error for the correlator/Kalman filter (see Figures 40d and C-12d of Appendix C). Additionally, the EKF recovers to essentially a zero mean error in 0.75 sec whereas the correlator/Kalman filter has a transient of 1.0 sec. Note in the Harnly-Jensen cases the mean errors are calculated by subtracting the filter estimated states from the true states, opposite of Equation (5-1), which accounts for the plot differences. However, at the end of this simulation the Harnly-Jensen filter estimates in the y-direction begin to diverge. At this point, the target is approaching the position of closest approach, where it will transition from closing on the tracker location to receding from the tracker location. Therefore, the FLIR frame and its reference system must rotate at a greater rate than at any other point in the simulation to keep the target centered in the FOV. This rotation creates a non-inertial acceleration, and appeared in a 6-state filter which did not model acceleration employed by Harnly-Jensen in a manner very similar to case B. However, when Harnly-Jensen added the two acceleration states to the EKF, this divergent characteristic was not observed. Since many of the truth model parameters are not the same as in the Harnly-Jensen simulations a direct comparison cannot be made. It is also noted that even at the end of case A, the filter's standard deviation in the y-direction becomes larger which may have been caused by the same source.

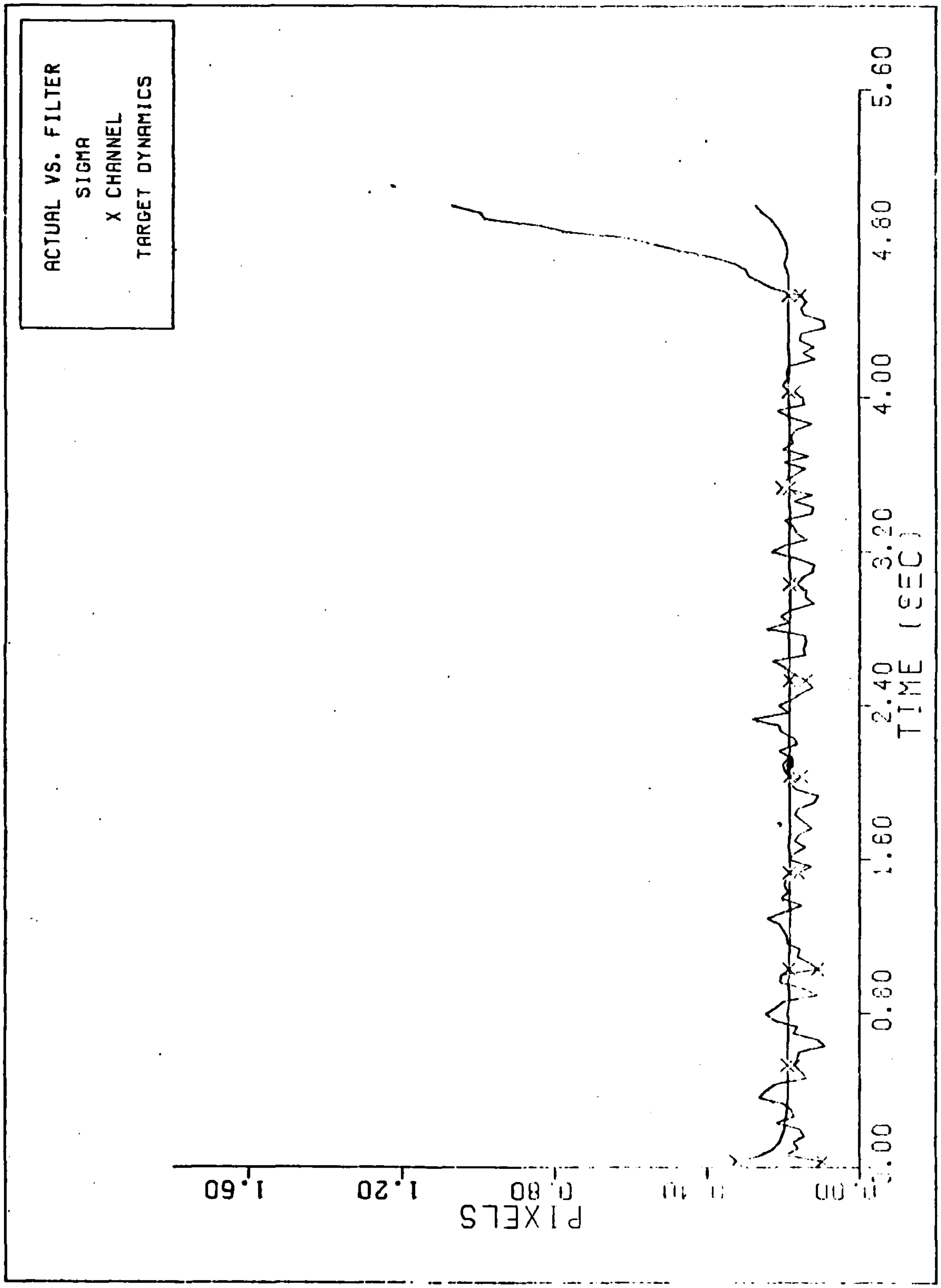

FILTER VS. ACTUAL SIGMA PLOT (S/N = 20)
Figure 40a. Case B

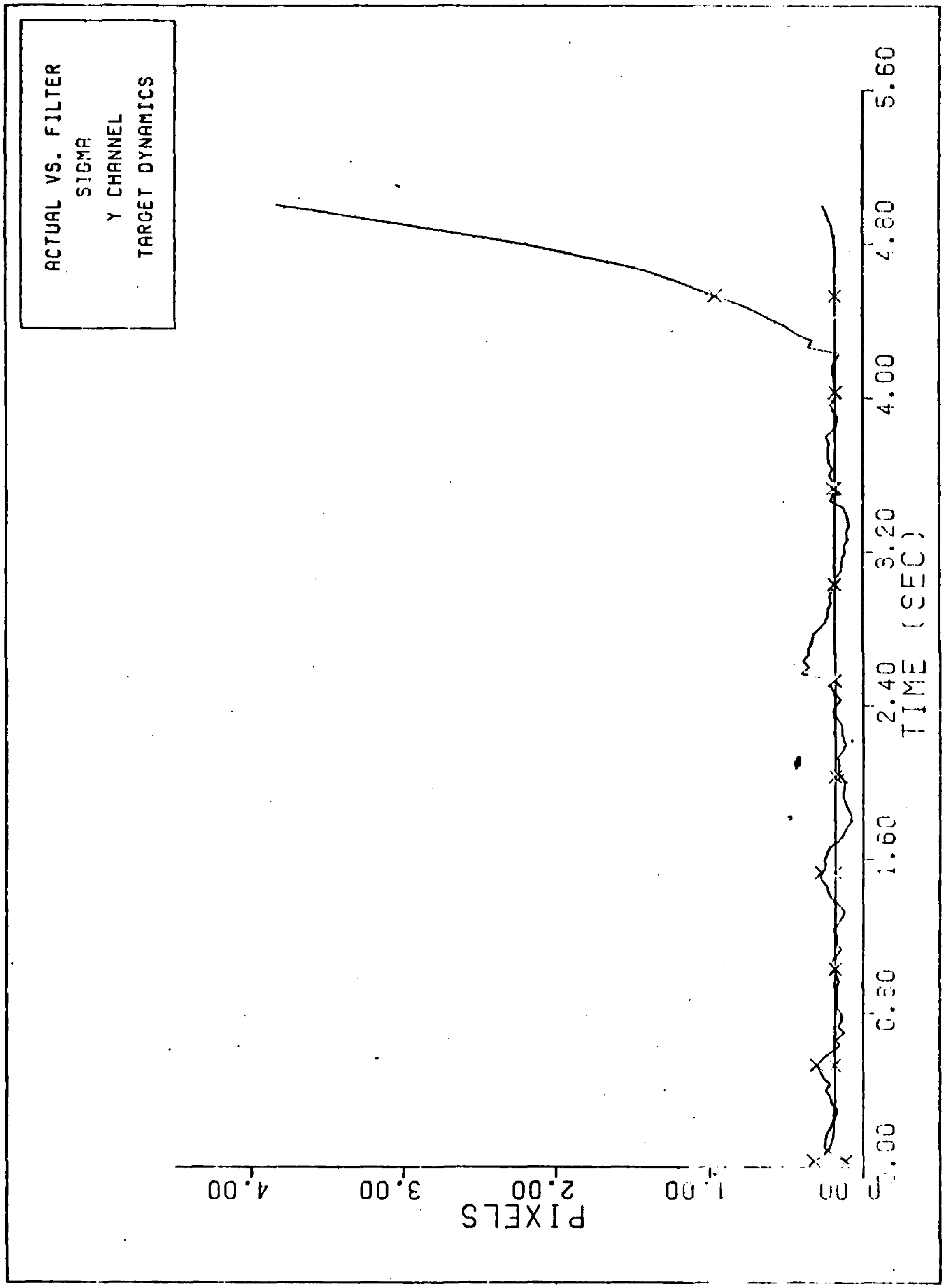

FILTER VS. ACTUAL SIGMA PLOT (S/N = 20)

Figure 40b. Case B

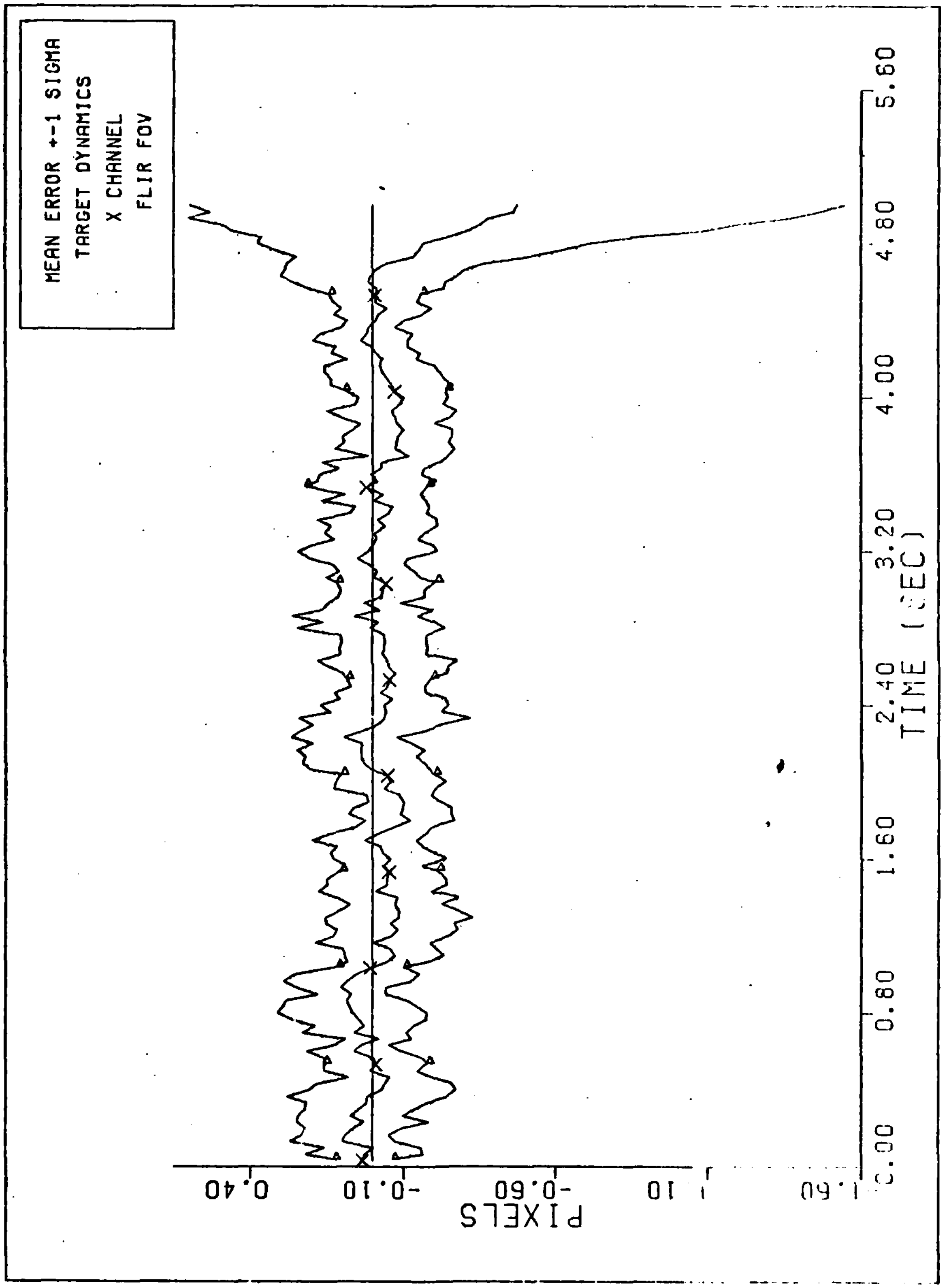

X CHANNEL DYNAMICS ERROR (S/N 20)
Figure 40c. Case B

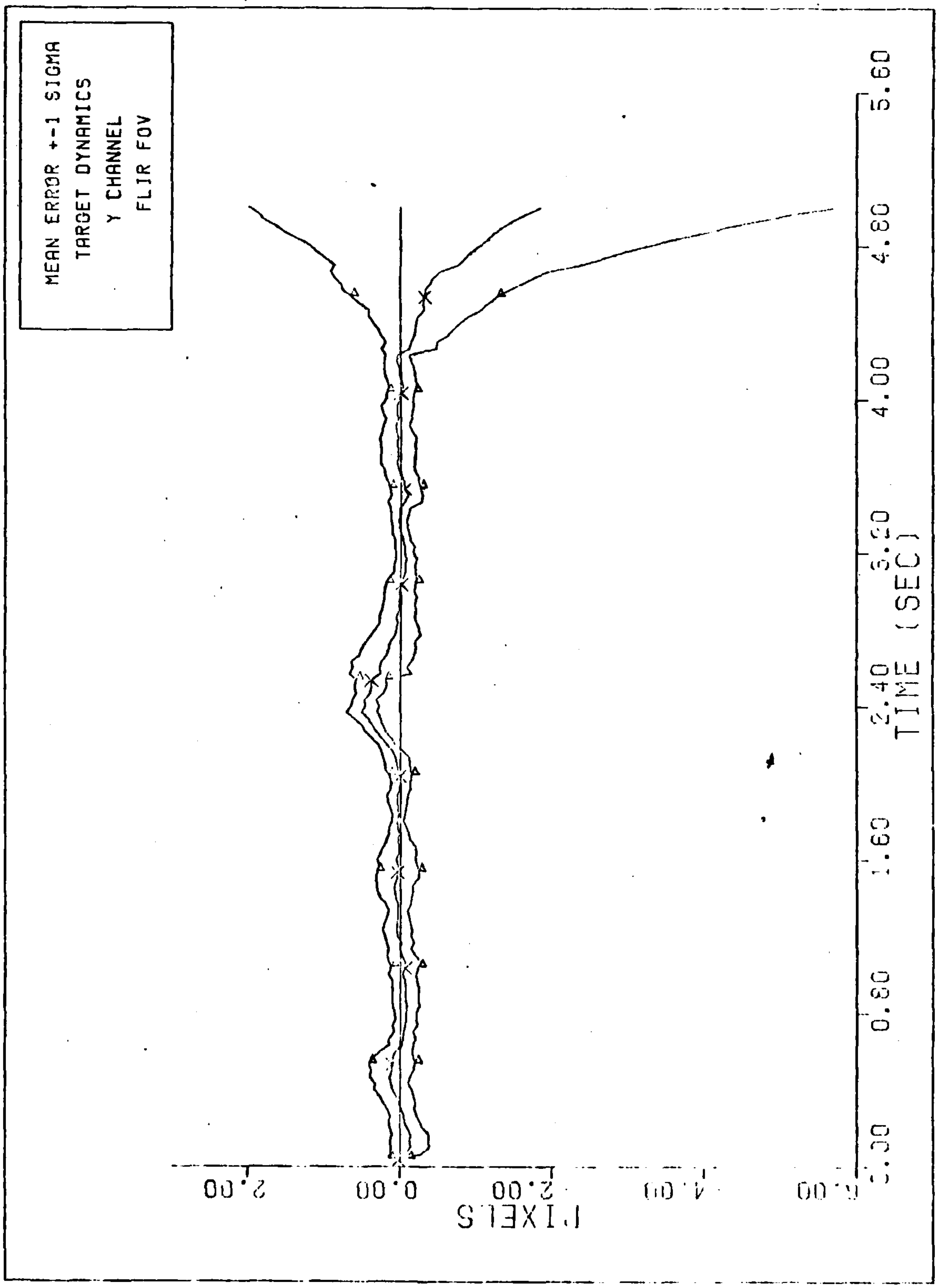

Y CHANNEL DYNAMICS ERROR (S/N 20)

Figure 40d. Case B

In order to determine if the geometry of trajectories 1 and 2 had a bearing on the increase in y-position errors, a special trajectory was designed which avoided the crossover situation. For this special trajectory, the simulation was initiated with inertial coordinates

$$x_I(t_0) = 20000.\ \text{m}$$
$$y_I(t_0) = 10000.\ \text{m}$$
$$z_I(t_0) = 30000.\ \text{m}$$

and the constant velocity used during the entire simulation was

$$\dot{x}_I(t) = -500.\ \text{m/sec}$$
$$\dot{y}_I(t) = -300.\ \text{m/sec}$$
$$\dot{z}_I(t) = 0.\ \text{m/sec}$$

This presents a more benign flight profile than before and the crossover point is avoided. Figures 41c and d show that in this situation the filter tracks the target very well for the entire simulation, indicating that the cause of the filter difficulties in the prior cases may be attributable to the trajectory geometry. The error statistics for this simulation are given as case C in Table IV. Also, while not indentical this simulation is very similar to case 36 in the Harnly-Jensen thesis, and the observed tracking performance between these two cases are analogous. Due to the difficulties encountered with this filter, the 5-g case was not evaluated because of the similarity in the trajectory geometry. However, for future studies this case could be evaluated in a situation where the crossover geometry is avoided.

Simulations were conducted with the EKF to determine

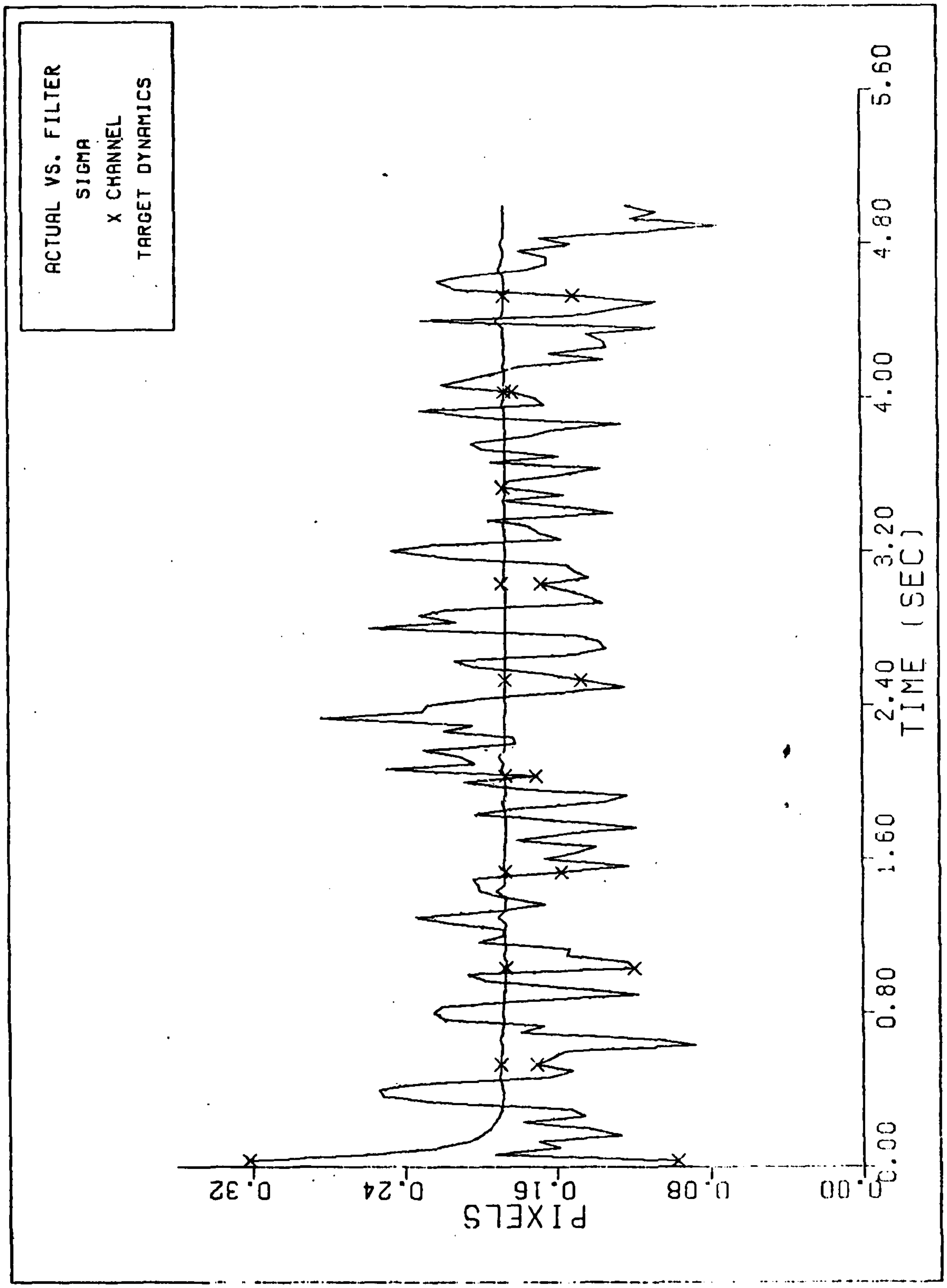

FILTER VS. ACTUAL SIGMA PLOT (S/N = 20)
Figure 41a. Case C

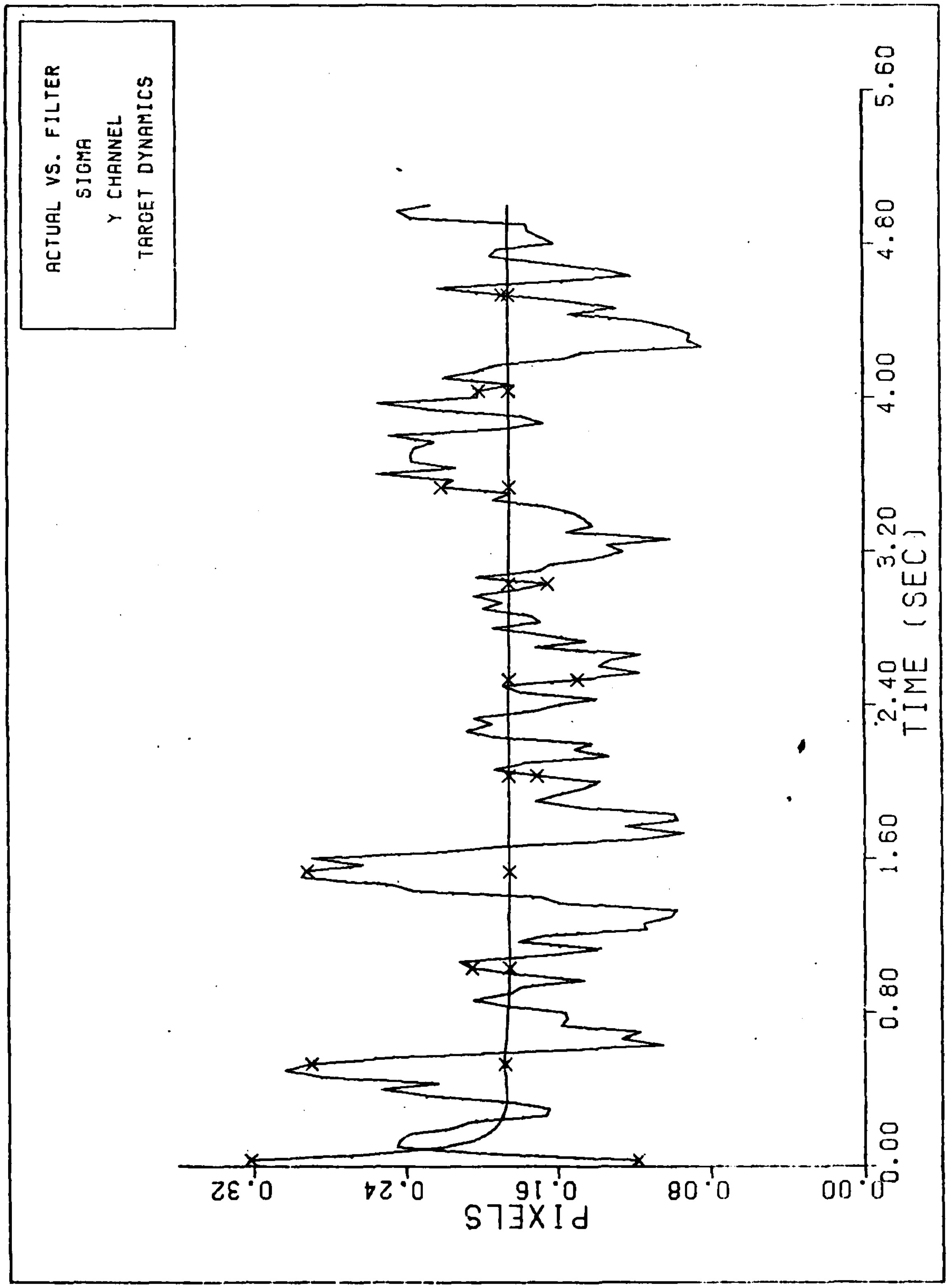

FILTER VS. ACTUAL SIGMA PLOT (S/N = **20**)
Figure 41b. Case C

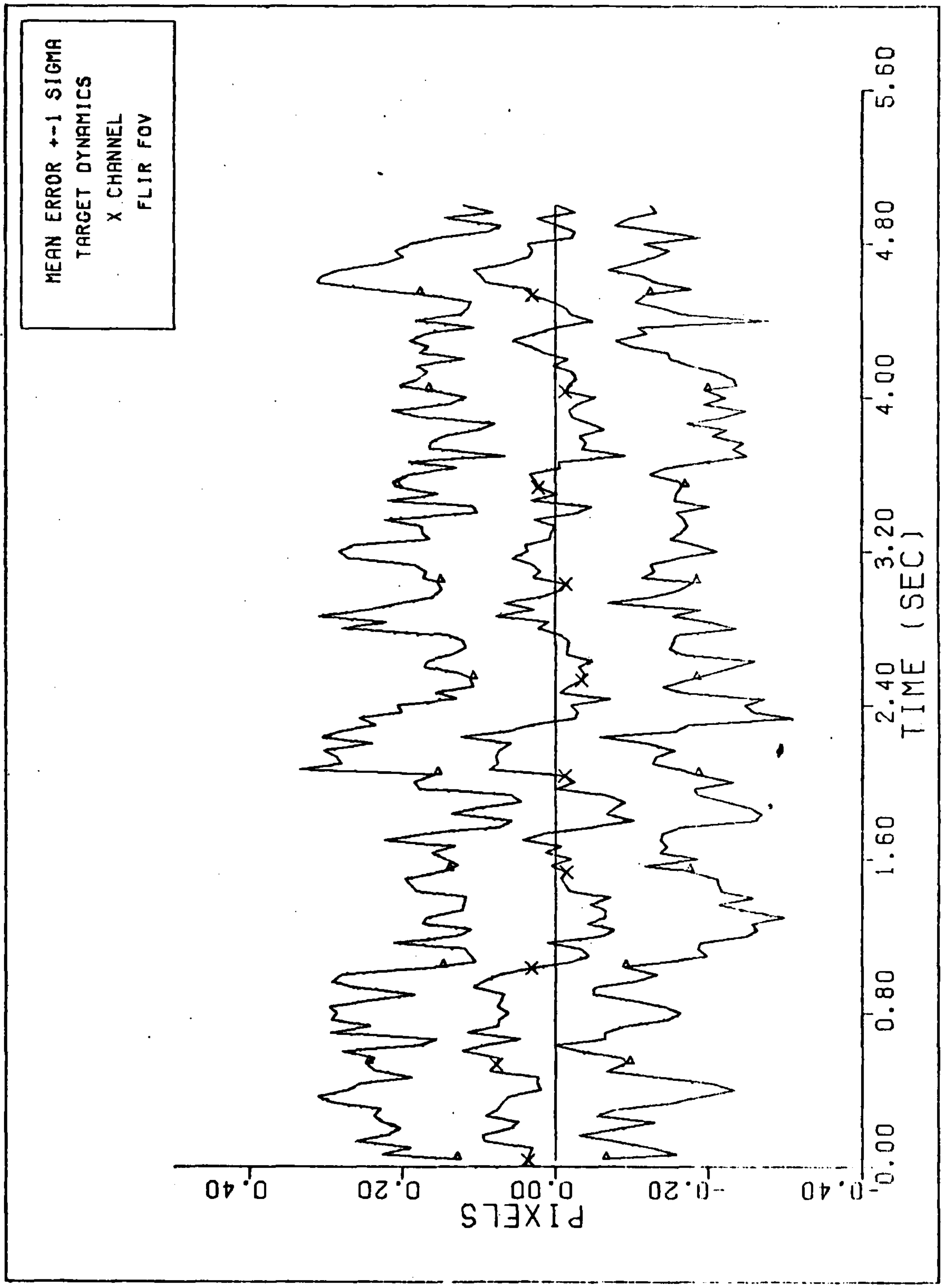

X CHANNEL DYNAMICS ERROR (S/N=20)
Figure 41c. Case C

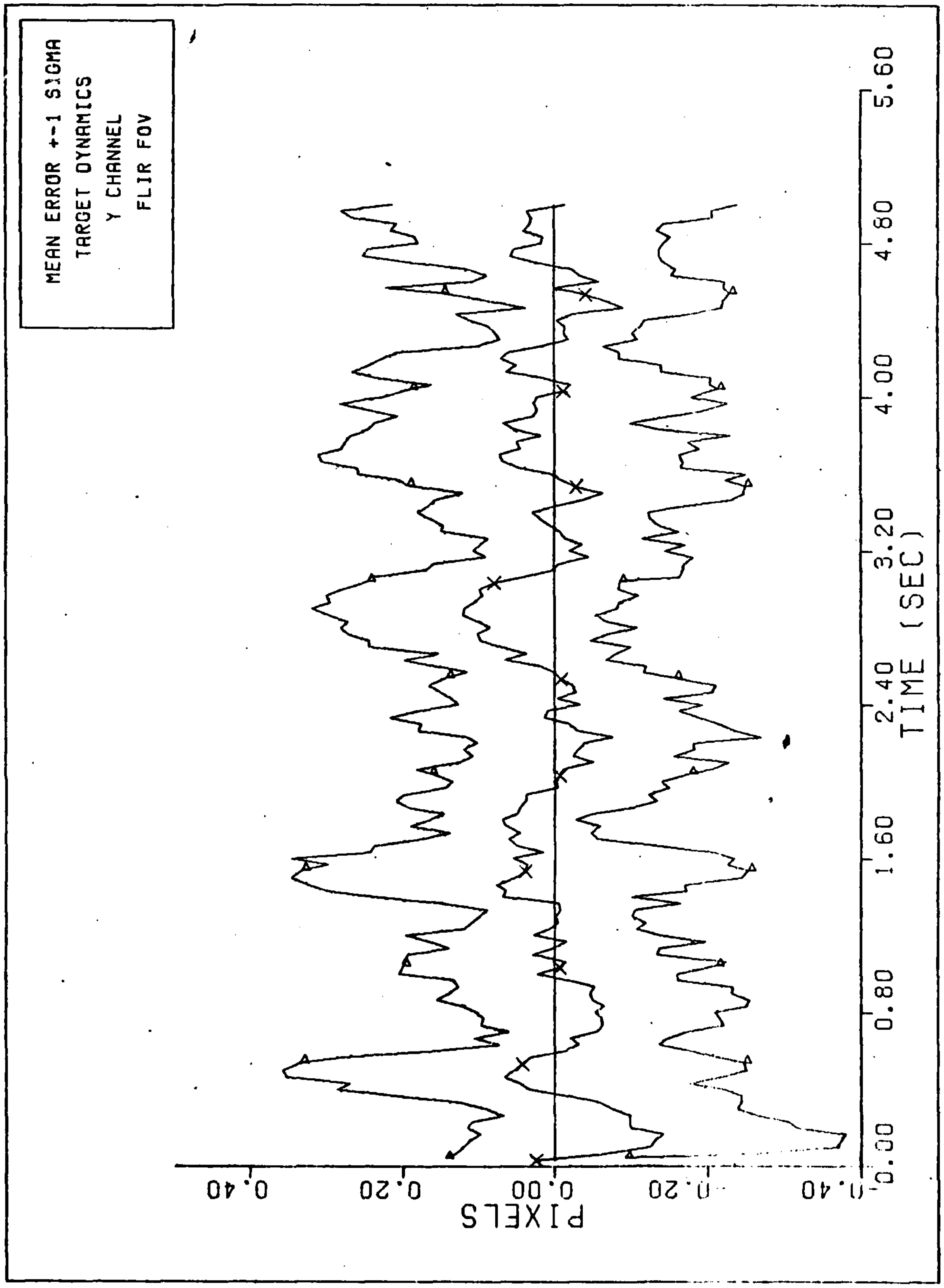

Y CHANNEL DYNAMICS ERROR (S/N 20)
Figure 41d. Case C

how the filter would respond in a muliple hot spot environment. The hot spots were intentionally spaced so that their projection onto the FLIR image plane could be approximated as bivariate Gaussian, which is the form used in the measurement model of the EKF employed by Harnly-Jensen. To achieve this spacing, the centroid of one hot spot was initially placed at the center of the overall target centroid while the other hot spots were symmetric about the centroid at a distance of $\pm$ 1 pixel. The spread parameter, σ_g^2, was 2. Initially, the filter tracked the target but as the simulation progresses the hot spot orientation changes. Due to this effect which results in an intensity pattern no longer well approximated as bivariate Gaussian the Monte Carlo simulations were not successful as the filter repeatedly lost target track 2 to 3 seconds into the simulations. During the phase of the simulation prior to loss of target track, the position estimates in both directions oscillated between a $\pm$ 2 pixel error which roughly corresponds to the displacement distances between the hot spot centroids on the FLIR plane. (The hot spot separation distance increases as the target approaches the FLIR location.) It appears the filter was moving from hot spot to hot spot during the estimation process.

5.10 Evaluations Using Trajectory 1.

With the baseline cases established for the one and three hot spot cases, trajectory 1 was used to evaluate how changes in α, SNR, and AR, would affect the tracking performance. The results of these runs are shown in Table V. Changing α from .05 as in case 3 to 0.1 as in case 5 results in only slight changes in the tracker's performance. In general, case 5 has slightly smaller mean errors while case 3 has slightly smaller standard deviations. The rms error is .01 pixel less for case 5 in the x-direction,

Table V. Trajectory 1 Evaluations

$$\text{Header} = \begin{matrix} (\tau_{df},\ \sigma^2_{df},\ \alpha) \\ (\text{Trajectory, Roll Rate, NUMHS}) \end{matrix}$$

Comments	Header	$\bar{x}_e(-)$/ $\overline{\sigma x}_e(-)$	$\bar{x}_e(+)$/ $\overline{\sigma x}_e(+)$	$\overline{cx}_e(-)$/ $\overline{\sigma cx}_e(-)$	$\overline{cx}_e(+)$/ $\overline{\sigma cx}_e(+)$	$\bar{y}_e(-)$/ $\overline{\sigma y}_e(-)$	$\bar{y}_e(+)$/ $\overline{\sigma y}_e(+)$	$\overline{cy}_e(-)$/ $\overline{\sigma cy}_e(-)$	$\overline{cy}_e(+)$/ $\overline{\sigma cy}_e(+)$
Case 5	3.5,150,.1 1,0,3	.113/ .168	.084/ .156	.023/ .182	-.037/ .065	-.001/ .174	-.005/ .160	.004/ .182	-.004/ .077
Case 6 SN = 10	3.5,150,.05 1,0,3	.134/ .168	.105/ .155	.044/ .185	-.016/ .066	.003/ .177	-.001/ .163	.009/ .187	.000/ .088
Case 7 AR = 2	3.5,150,.05 1,0,3	.265/ .146	.236/ .137	.175/ .194	.114/ .125	.007/ .172	.002/ .158	.012/ .176	.003/ .054

while in the y-direction the rms error for the two cases is approximately the same. Since increasing the α for the case does not clearly improve or degrade the performance of the tracker, it appears that for cases where the intensity pattern is not rapidly varying, an α in the range of .05 - 0.1 is appropriate. These values will be investigated later when the intensity pattern does show motion on the FLIR image plane. For case 6, the true signal to noise ratio was changed from the standard value of 20 to 10 while the filter was told the SNR was 20. The performance of the tracker is relatively unaffected by this signal-to-noise change, as was previously shown by Mercier (10). Although the case was not tested, Mercier and Harnly-Jensen showed that while going from a SNR of 20 to 10 has very little effect on the tracker's performance, going from a SNR of 10 to 1 results in a definite degradation in the filter's performance.

The last case in Table V shows the result of changing the aspect ratio from 1 to 2. For this particular scenario, this means the spread of the intensity pattern is twice as great in the x_{FLIR} direction as in the y_{FLIR} direction. As a result, the tracking ability is relatively unaffected in the y_{FLIR} direction, while in the x_{FLIR} direction an appreciable increase in the mean tracking error is noted. Thus, it appears that when the spread of the intensity function is increased, the tracker, and most probably the correlator, has difficulty determining the location of the centroid of the intensity function.

5.11 Evaluation for Rolling Maneuvers.

To evaluate the performance of the tracker when the intensity patterns were rapidly changing on the FLIR image plane a.. to evaluate how changing α affected the tracker's performance under this circumstance, a roll maneuver was used. Trajectory 1 was used for the target flight path to provide a benign trajectory to minimize possible errors due to trajectory effects and to concentrate on how the changing target shape effects are handled by the tracker. Roll rates of 0.5 rad/sec and 1.0 rad/sec were used. In both instances, the roll maneuver was initiated at t_i = .5 sec so the filter would have acquired the target prior to roll initiation, and the roll maneuver continued at a constant rate for the remainder of the simulation. This results in a total roll angle of 128.9° and 258.0° for the two cases respectively. The results of these runs are shown in Table VI.

A general observation on the tracking performance against the rolling maneuver is that the mean errors are slightly less in the x-direction and slightly greater in the y-direction when compared to the non-rolling cases. For the crossing trajectory with no roll, the intensity profiles are more symmetric in the y_{FLIR} direction than in the x_{FLIR} direction, and recalling the correlator performance analysis (Figure 36), the correlator performs much better in the symmetric case. This plus the fact that there is very little motion in the y-direction helps to account for the difference in the mean errors. However, in the rolling case, the intensity profiles will be more symmetric in the x-direction at times, and in the y-direction at other times, which accounts for the general trend in the mean error changes.

For the 0.5 rad/sec roll maneuver, cases 8 and 9, the α = 0.1 has the smaller mean errors in both the x and y position estimates as expected. This is because, for a changing intensity profile, more emphasis should be placed on the newer measurements which are more representative of the current intensity pattern. In cases 10 and 11, where a 1 rad/sec roll rate was used, a greater performance enhancement was expected for α = 0.1 than had been seen for the previous case, as the intensity pattern is varying

Table VI. Roll Manuever Evaluations

Header = $(\tau_{df}, \sigma^2_{df}, \alpha)$

(Trajectory, Roll Rate, NUMHS)

Comments	Header	$\bar{x}_e(-)/\overline{\sigma x}_e(-)$	$\bar{x}_e(+)/\overline{\sigma x}_e(+)$	$\overline{cx}_e(-)/\overline{\sigma cx}_e(-)$	$\overline{cx}_e(+)/\overline{\sigma cx}_e(+)$	$\bar{y}_e(-)/\overline{\sigma y}_e(-)$	$\bar{y}_e(+)/\overline{\sigma y}_e(+)$	$\overline{cy}_e(-)/\overline{\sigma cy}_e(-)$	$\overline{cy}_e(+)/\overline{\sigma cy}_e(+)$
Case 8	3.5,150,.05 1,.5,3	.109/ .161	.081/ .146	.020/ .184	-.038/ .058	.019/ .173	.014/ .160	.025/ .181	.016/ .081
Case 9	3.5,150,.1 1,.5,3	.097/ .163	.069/ .145	.008/ .185	-.051/ .060	.011/ .181	.007/ .168	.017/ .185	.009/ .088
Case 10	3.5,150,.05 1,1.0,3	.137/ .156	.108/ .141	.047 .179	-.011/ .049	.016/ .165	.012/ .152	.022/ .177	.013/ .078
Case 11	3.5,150,.1 1,1.0,3	.144/ .155	.114/ .139	.053/ .183	-.006/ .054	.009/ .172	.005/ .160	.015/ .181	.007/ .083

at a faster rate. Additionally, it was expected that because of the increased motion on the FLIR image plane, a performance degradation would be observed. However, upon analyzing the results these expectations were not met. In the x-direction, the mean errors did in fact increase slightly but the α = .05 case shows a mean error of .01 pixel less than for the α = 0.1 case. In the y-direction, the mean errors showed a slight decline with the α = 0.1 case having the smallest mean errors. At this point it can be concluded that the tracker's performance may be enhanced somewhat by a judicious choice of α, with α's in the ranges chosen being appropriate for the trajectories of concern. However, the symmetry of the intensity profiles on the FLIR image plane affects the tracker's performance more appreciably than anticipated. This problem could possibly be rectified by modifying the means of extracting the target position offsets from the correlation function and warrents further investigation (see Recommendations, section 6.3).

5.12 Evaluation for a Two-G Pullup Maneuver

The next cases were designed to evaluate the performance of the tracker when the target performs a constant 2-g pullup maneuver in the inertial y-direction (trajectory 2). Here attention is focused on how the dynamic trajectory effects are handled by the tracker, while the intensity shape function is essentially constant (it rotates about its principle axis slowly to remain aligned with the velocity vector.) The pullup maneuver was initiated at t = 2.0 sec and contiuned for the remainder of the simulation. Under this situation, the effects of varying the smoothing parameter, α, on the tracker's performance were evaluated. Additionally, to evaluate how the filter performance would respond to a relatively small deviation from that achieved on the straight crossing trajectory without retuning, the acceleration time constant, and the strength of the dynamic

Table VII. Trajectory 2 (two-g pullup) Evaluations

$$\text{Header} = \begin{matrix}(\tau_{df},\ \sigma^2_{df},\ \alpha) \\ (\text{Trajectory, Roll Rate, NUMHS})\end{matrix}$$

Comments	Header	$\bar{x}_e(-)/\overline{\sigma x}_e(-)$	$\bar{x}_e(+)/\overline{\sigma x}_e(+)$	$\overline{cx}_e(-)/\overline{\sigma cx}_e(-)$	$\overline{cx}_e(+)/\overline{\sigma cx}_e(+)$	$\bar{y}_e(-)/\overline{\sigma y}_e(-)$	$\bar{y}_e(+)/\overline{\sigma y}_e(+)$	$\overline{cy}_e(-)/\overline{\sigma cy}_e(-)$	$\overline{cy}_e(+)/\overline{\sigma cy}(+)$
Case 12 2-G	3.5,150,.05 2,0,3	.146/ .167	.115/ .152	.055/ .180	-.006/ .059	-.135/ .170	-.099/ .154	-.063/ .180	.010/ .062
Case 13 2-G	3.5,150,.1 2, 0, 3	.115/ .174	.084/ .160	.024/ .186	-.038/ .072	-.149/ .176	-.113/ .160	-.076/ .184	-.003/ .075

noise were left unchanged from the previous cases. Table VII shows the statistics for the 2-g maneuver cases. Once again, varying α does not significantly affect the filter's performance. While the larger α produces smaller mean errors in the x-direction, an almost equal decrease in the mean error is seen in the y-direction for the smaller α. Also, without changing the assumed target correlation time or increasing the Kalman filter gain through increasing σ^2_{df}, the filter's estimate of the dynamic target position trails the true target position, as shown by the negative errors in the $\overline{y}_{ERR}(+)$ columns, but the filter does track the target through the maneuver. Performance enhancement could be achieved, however, by allowing τ_{df} and/or σ^2_{df} to be adjusted, as shown in section 5.13 for the 5-g case.

5.13 Evaluation for a Five-g Pullup Maneuver

A 5-g pullup maneuver was selected to evaluate the performance of the filter in a highly dynamic tracking environment. The effects of changing the acceleration time constant from the 3.5 sec value used for the benign trajectories to a correlation time more representative of a dynamic environment, 1.5 sec, was evaluated. Additionally, the strength of the dynamic noise was increased to model higher possible rms acceleration levels and to place more emphasis (through the filter gain calculations) on the measurements and less on the dynamics model. The value for σ^2_{df} found by this tuning process to yield the best performance was 300 pixels^2/sec^4. The results of the 5-g pullup maneuver cases are shown in Table VIII. For these cases, the plots of the tracker's performance are a better indicator of the response of the filter than the simple temporal averages. As shown in Figure C-14f, the filter with the 3.5 sec correlation time does not respond well at maneuver

Table VIII. Trajectory 2 (five-g pullup) Evaluations

$$\text{Header} = \frac{(\tau_{df}, \sigma^2_{df}, \alpha)}{(\text{Trajectory, Roll Rate NUMHS})}$$

Comments	Header	$\overline{x}_e(-)$/ $\overline{\sigma x}_e(-)$	$\overline{x}_e(+)$/ $\overline{\sigma x}_e(+)$	$\overline{cx}_e(-)$/ $\overline{\sigma cx}_e(-)$	$\overline{cx}_e(+)$/ $\overline{\sigma cx}_e(+)$	$\overline{y}_e(-)$/ $\overline{\sigma y}_e(-)$	$\overline{y}_e(+)$/ $\overline{\sigma y}_e(+)$	$\overline{cy}_e(-)$/ $\overline{\sigma cy}_e(-)$	$\overline{cy}_e(+)$/ $\overline{\sigma cy}_e(+)$
Case 14 5-G	3.5,300,.1 2, 0, 3	.143/ .184	.094/ .169	.030/ .191	-.063/ .077	-.374/ .177	-.287/ .161	-.235/ .186	-.068/ .080
Case 15 5-G	1.5,300,.1 2, 0, 3	-.023/ .193	-.055/ .174	-.103/ .191	-.161/ .070	-.602/ .174	-.441/ .157	-.3801 .182	-.092/ .078

initiation, dropping off to a -2 pixel error in 0.5 sec. Figure C-15f shows the filter with the 1.5 sec correlation time tracks the maneuver initiation much better, with the y-error only dropping to -1.5 pixels. However, as can be seen in Table VIII, since the target continues on the constant-g pullup trajectory after the maneuver is initiated, the longer correlation time is a more accurate portrayal of the target dynamics during this phase of the trajectory and yields a filter that recovers to a better estimate of the target position. Thus, a target performing jinking maneuvers in the dynamic range shown rather than a simple constant-g pullup would be better represented by the shorter correlation time.

5.14 Adaptive $\underline{Q}_{fd}$ Estimation Evaluation

At this point, the self-tuning $\underline{Q}_{fd}$ adaptation procedure was evaluated to determine if reasonable performance could be obtained using this method. It is not expected that this method will perform better than the cases in which the parameter values were tuned off-line to optimize performance for specific trajectories. However, it is hoped that adequate performance across a wider dynamic range of scenarios can be achieved. The $\underline{Q}_{fd}$ estimation procedure was initiated at t = 0.5 secs. This time was selected so the filter would have sufficient time to acquire the target, where the $\underline{Q}_{fd}$ value is purposefully set to a large value to prevent the filter gains from decreasing to early in the tracking phase. Thus, at t = 0.5 sec, the filter is in a relatively stable tracking mode, and the adaption procedure began and continued for the remainder of the simulation. The performance was evaluated against the crossing trajectory and the 2-g pullup trajectory. The results of the $\underline{Q}_{fd}$ estimation are shown in Table IX.

Table IX. $\underline{Q}_{df}$ Estimation Evaluation

$$\text{Header} = \frac{(\tau_{df},\ \sigma^2_{df},\ \alpha)}{(\text{Trajectory, Roll Rate, NUMHS})}$$

Comments	Header	$\bar{x}_e(-)$/ $\overline{\sigma x}_e(-)$	$\bar{x}_e(+)$/ $\overline{\sigma x}_e(+)$	$\overline{cx}_e(-)$/ $\overline{\sigma cx}_e(-)$	$\overline{cx}_e(+)$/ $\overline{\sigma cx}_e(+)$	$\bar{y}_e(-)$/ $\overline{\sigma y}_e(-)$	$\bar{y}_e(+)$/ $\overline{\sigma y}_e(+)$	$\overline{cy}_e(-)$/ $\overline{\sigma cy}_e(-)$	$\overline{cy}_e(+)$/ $\overline{\sigma cy}_e(+)$
Case 16	3.5,150,.1 1, 0, 3	.117/ .195	.017/ .187	.058/ .184	-.052/ .061	.018/ .198	-.073/ .189	.025/ .179	-.004/ .068
Case 17 2-G	3.5,150,.1 2, 0, 3	.220/ .233	.108/ .227	.165 .232	.042 .133	-1.35/ .298	-.893 .291	-1.16/ .315	-.613/ .262

When case 16 is compared to cases 3 and 5, it is seen that in the x-direction the estimation process has a substantially smaller mean error while in the y-direction comparable performance is achieved. This is not surprising since a conservative tuning was used in the other cases to reduce the transient effects in the x-direction. Case 17 illustrates the major problem with this estimation technique. While the adaptive filter will converge to a reasonable estimation of the states, under benign trajectory conditions it reduces its gains to a point where it cannot respond quickly to harsh trajectory deviations. Referring to the Filter vs. Actual Error Plot, Figure C-17b, where the major velocity change occurs, it is clearly seen that while the maneuver is initiated at t = 2 sec, almost .5 sec elapses before the filter begins to respond to the maneuver. However, the gains are not increased rapidly enough and track of the target is lost. Also, note in the x-direction, Figures C-17c and e, the filter overestimates the target position due to the velocity decrease in that direction; similarly in the y-direction, Figures C-17d and f, the filter underestimates the target position due to the velocity increase. These results, consistent with the results found by Harnly-Jensen (6), show that while in cases where the estimated process is slowly changing, this estimation technique may be useful, it is not robust enough for useful application in a strongly dynamic environment.

5.15 Maneuvers Out of the x-y Plane

Trajectory 4 as described in Chapter II was motivated by the desire to evaluate the performance of the filter when the target turns in toward the FLIR plane, thereby projecting three distinct and separate ellipsoids onto the FLIR image plane. Thus, substantial trajectory offsets are combined with large target intensity shape changes, in a single and realistic scenario. However, because of the short length of the simulation, the out-of-plane angle is very small unless a very highly dynamic flight profile is used. The performance against a target flying a 2-g out-of-plane maneuver is shown in case 18. The resulting flight profile is very similar to the 2-g pullup maneuver previously discussed. Based on this, trajectory 2 was modified so that instead of initiating a 2-g pullup in the inertial y-direction, the maneuver is performed in the minus inertial z-direction. Thus, the target turns in towards the FLIR plane. Additionally, a roll rate of .25 rad/sec was used to simulate the rolling motion associated with this type of maneuver. A 10-g maneuver was used to insure the three separated target ellipsoids were projected onto the FLIR plane, yet because of the geometry of the trajectory, this is not a highly dynamic maneuver as seen in the FLIR image plane and the filter should have little difficulty tracking the target through the manuever. The results of these two cases are presented in Table X.

For reasons previously discussed, the results of case 18 are very similar to the other 2-g trajectory cases. In case 19, the effects of the hot spot symmetry on the correlator/Kalman filter performance are seen. For this trajectory, when the target turns in towards the FLIR plane, three distinct and relatively symmetric ellipsoids are projected onto the FLIR image plane. The result can be seen in the reduced mean errors in the x-position, again emphasizing the dependence of accurate target tracking on hot spot symmetry. Also, the plots of Figure C-19a and c show that when the velocity in the x-direction is reduced, the filter slightly overestimates the movement of the target initially but quickly recovers.

The final evaluation, case 20, was made using

Table X. Out of Plane Maneuvers

$$\text{Header} = \frac{(\tau_{df},\ \sigma^2_{df},\ \alpha)}{(\text{Trajectory, Roll Rate, NUMHS})}$$

Comments	Header	$\overline{x}_e(-)$/ $\overline{\sigma x}_e(-)$	$\overline{x}_e(+)$/ $\overline{\sigma x}_e(+)$	$\overline{cx}_e(-)$/ $\overline{\sigma cx}_e(-)$	$\overline{cx}_e(+)$/ $\overline{\sigma cx}_e(+)$	$\overline{y}_e(-)$/ $\overline{\sigma y}_e(-)$	$\overline{y}_e(+)$/ $\overline{\sigma y}_e(+)$	$\overline{cy}_e(-)$/ $\overline{\sigma cy}_e(-)$	$\overline{cy}_e(+)$/ $\overline{\sigma cy}_e(+)$
Case 18 2-G OP	3.5,250,.1 4, 0, 3	.101/ .177	.073/ .163	.018/ .186	-.035/ .073	-.148/ .174	-.114/ .158	-.082/ .180	-.015/ .066
Case 19 z-dir	3.5,150,.1 2, .25, 3	.045/ .141	.051/ .128	.017/ .183	.029/ .078	-.044/ .160	-.051/ .148	-.026/ .179	-.020/ .080

trajectory 3 to test the performance of the filter when the target initiated and terminated a maneuver. A 2-g pullup was initiated at t = 2 sec, and at t = 3.5 sec the maneuver was terminated and the target continued at a constant velocity. Because of the transient over the last 1.5 seconds of this simulation, no time-averaged statistics were calculated for a tabulation. Instead, a discussion of the performance shown in the plots is given. Figures C-20c and e show very little effects of the maneuver in the x-direction, which is expected since the change in the velocity in this channel is very small. Figures C-20f and f show the filter under-estimating the target position when the maneuver begins, and then when the velocity increase is terminated at t = 3.5, the filter overestimates the target movement. However, after a second transient period the filter recovers to good position estimates.

5.16 Summary of Test Cases

This section presents a brief recapitulation of the 20 test cases in tabular form. These cases are presented in Table XI, where deviations from the standard truth model parameters given in section 5.3 as well as the filter tuning parameters are shown. Major trends observed in these cases as well as conclusions drawn from these trends and recommendations for possible performance enhancement measures are discussed in Chapter VI.

Table XI. Summary of Test Cases

Case	Traj	Pullup Rate	Roll Rate	NUMHS	τ_{df}	σ^2_{df}	Alpha	Misc.
1	1	0	0	1	3.5	150	.05	
2	1	0	0	1	3.5	150	.05	phase corr.
3	1	0	0	3	3.5	150	.05	
4	1	0	0	3	3.5	150	.05	phase corr.
5	1	0	0	3	3.5	150	.1	
6	1	0	0	3	3.5	150	.05	SN=10
7	1	0	0	3	3.5	150	.05	AR= 2
8	1	0	.5	3	3.5	150	.05	
9	1	0	.5	3	3.5	150	.1	
10	1	0	1.0	3	3.5	150	.05	
11	1	0	1.0	3	3.5	150	.1	
12	2	2-g	0	3	3.5	150	.05	
13	2	2-g	0	3	3.5	150	.1	
14	2	5-g	0	3	3.5	300	.1	
15	2	5-g	0	3	1.5	300	.1	
16	1	0	0	3	3.5	150	.1	$\hat{\underline{Q}}_{fd}$
17	2	2-g	0	3	3.5	150	.1	$\hat{\underline{Q}}_{fd}$
18	4	2-g	0	3	3.5	250	.1	
19	2	10-g	0	3	3.5	150	.1	z-dir.
20	3	2-g	.25	3	3.5	150	.1	

VI. Conclusions and Recommendations

6.1 Introduction

This chapter presents the conclusions drawn from this research project and presents recommendations into other research efforts which could be pursued to enhance the performance of the correlator/Kalman filter and the realism of the truth model for performance evaluation purposes.

6.2 Conclusions

a. Data Processing Algorithm. The data processing algorithm which generated the estimated intensity function for use as the template in the correlation algorithm was shown to perform well in this research. With this method, almost identical performance was achieved in both the single and multiple hot spot cases. This is in direct contrast to the Harnly-Jensen EKF, which experienced difficulty when the target intensity function was not of the assumed bivariate Gaussian form. The extra computational loading incurred with implmenting this algorithm, which makes no assumptions about the intensity function shape, is well justified. However, it is possible that the bias which the tracker exhibited could be caused by the algorithm's reconstruction of the target intensity function. A discussion of a possible research approach to determine the cause of this bias will be deferred until the recommendations section. Varying the exponential smoothing parameter, alpha, to address changing target shapes did not significantly enhance or degrade the performance of the tracker. An alpha in the range of 0.05 to 0.1 consistently resulted in acceptable performance.

b. Correlation Methods. Based on the results of the analysis of the four correlation methods and a tracker evaluation of two methods, the FFT method clearly yielded the best tracking performance when implemented with the Kalman filter. This method performed well in both the single and multiple hot spot cases. However, the errors observed from the correlator/Kalman filter were closely tied to the symmetry of the target intensity pattern as projected onto the FLIR image plane which directly relates to the chosen method of deriving the peak offsets from the correlation function. In the asymmetric case,the center of mass calculation which was used to approximate the peak of the correlation function gives biased results which are readily apparent in the tracker's performance. Alternatives to the center of mass method will be considered in the recommendations section.

c. Kalman Filter. The first-order Gauss-Markov model chosen to represent target acceleration provided acceptable tracking performance, and thus the compuational savings associated with utilizing a linear filter over an extended Kalman filter or other non-linear filters were realized. The filter proved to be robust enough to track a benign target and a five-g target, which at the ranges considered is a very dynamic maneuver, without changing the acceleration time constant and with only a slight increase in the dynamics driving noise. However, better performance was realized when the acceleration time constant selected was more representative of the maneuver being tracked. Thus, the concept of implementing a correlation algorithm in cascade with a linear Kalman filter in a dynamic environment is a viable alternative to other non-linear approaches.

d. Adaptive Q_{fd} Estimation. The adaptive Q_{fd} estimation technique did not prove robust enough to be used throughout an entire simulation in a very dynamic environment. However, as detailed by Harnly and Jensen (6), this routine does contain indicators which could be monitored to detect when the target initiated a maneuver. Based on these indicators, the gain values within the filter could be changed to other preselected vaules, as an alternative to implementing more computationally burdensome maximum likelihood estimation techniques or multiple modeling schemes to provide the desired adaptation (13: Chapter 10).

e. Harnly and Jensen EKF. Assuming the divergence problem which appeared in the simulations in this research could be readily solved, the Harnly-Jensen designed EKF performed well in the single hot spot case where the target intensity function was well represented as bivariate Gaussian. However, the filter did not perform well when the target intensity pattern was not well represented as bivariate Gaussian, as expected. While this method may not readily adapt from the single to the multiple hot spot case, the performance in the single hot spot case was very similar to the correlator/Kalman filter without the increased computational loading incurred by using the data processing algorithm of this thesis. Therefore, for the single hot spot case, such as an air-to-air missile where information as to the target type could be readily obtained from the acquisition source, this may be the preferred filter.

6.3 Recommendations

a. Data Processing Algorithm. A possible cause of the bias observed in the correlator/Kalman filter is the data processing algorithm that generates the target intensity shape function. To determine if this algorithm is the cause of the bias, a comparison between this research and the research conducted concurrently by Lieutenant Mark Kozemchak, who used the same data processing algorithm in an extended Kalman filter, should be made. If the same characteristic bias is noted, a further confirmation could be obtained by replacing the estimated target intensity function with the true target intensity function in the correlation algorithm. If the bias is noted in the Kozemchak thesis and replacing the estimated intensity function with the true intensity function removes the bias then the data processing algorithm would have to be analyzed to determine where a phase shift in the transformed domain could occur which would cause this effect. If the bias is not observed in the Kozemchak thesis, then the bias is almost certainly due to the correlation method.

b. Correlation Methods. The center of mass calculation used in this research as an approximation to the point of maximum correlation yields a bias when the intensity pattern is not symmetric. This effect noticeably degraded the performance of the tracker. An alternative formulation could be developed whereby the center of mass calculation is used to determine the approximate peak of the correlation function and then a precise peak finding routine would be employed to provide a more precise estimate. (The reason for initially using the center of mass calculation is to get in the vicinity of the peak location prior to implementing the precise peak finder. This should help avoid locking onto local peaks as a basic peak finder might.)

c. Kalman Filter. The filter showed enough robustness to track the targets of interest with only small changes to the filter parameter values. To achieve high precision performance over a wide dynamic range, this filter could be implemented in a multiple model algorithm (13:Chapter 10) in which a small number of Kalman filters with varying parameter values would be capable of adequately modeling the dynamic profiles of concern, as an alternative to adaptive estimation of $\underline{Q}_{fd}$ in a single Kalman filter. Initial investigation of this concept conducted by Flynn (6) proved somewhat disappointing, but is possibly worth further exploration.

d. Truth Model. The truth model changes made in this research resulted in a fairly accurate portrayal of the real world processes of interest. The simulation is structured so that changes from one trajectory to another and from the single to multiple hot spot case are readily made. The truth model simulation could be enhanced by modeling the cases where the target fuselage is between the intensity function and the FLIR image plane, thereby either blocking out completely or blocking out portions of the intensity function. Realistically, when the target is receding from the tracker location the entire infrared source will be exposed to the FLIR image plane resulting in a hotter target while the converse is true for an incoming target. By varying the value of the intensity based on considerations such as these, the realism of the truth model would be improved. The unit vectors which are currently calculated for the multiple hot spot simulation could be used as the foundation upon which these more precise models could be based.

Bibliography

1. Robinson, Clarence A., Jr., "Beam-Target Interaction Testbed," Aviation Week and Space Technology, 114:14-17 (October 8, 1979).

2. Robinson, Clarence A., Jr., "Laser Technology Demonstrated," Aviation Week and Space Technology: 16-19 (February 16, 1981).

3. Singletery, James, Jr., "Adaptive Laser Pointing and Tracking Problem," M.S. Thesis, Air Force Institute of Technology, Wright-Patterson AFB, Ohio, December 1980.

4. Westinghouse Defense and Electronics System Center. Digital Correlation Tracker, Phase I Computer Simulations, TR-74-170. Prepared for the Air Force Weapons Laboratory, Kirtland AFB, New Mexico, March 1975.

5. Maybeck, Peter S. and Daniel E. Mercier, "A Target Tracker Using Spatially Distributed Infrared Measurements," IEEE Transactions on Automatic Control, AC-25(2): 222-225 (April 1980).

6. Harnly, Douglas A. and Robert L. Jensen, "An Adaptive Distributed-Measurement Extended Kalman Filter for a Short Range Tracker," M.S. Thesis, Air Force Institute of Technology, Wright-Patterson AFB, Ohio, December 1978.

7. Flynn, Patrick M., " Alternative Dynamics Models and Multiple Model Filtering for a Short Range Tracker," M.S. Thesis, Air Force Institute of Technology, Wright-Patterson AFB, Ohio, December 1981.

8. Rogers, Steven K., "Enhanced Tracking of Airborne Targets Using Forward Looking Infrared Measurements," M.S. Thesis, Air Force Institute of Technology, Wright-Patterson AFB, Ohio, December 1981.

9. Maybeck, Peter S. and Steven K. Rogers, "Adaptive Tracking of Multiple Hot-Spot Target IR Images," unpublished article, Air Force Institute of Technology, Wright-Patterson AFB, Ohio.

10. Mercier, Daniel E. "An Extended Kalman Filter for Use in a Shared Aperture Medium Range Tracker," M.S. Thesis, Air Force Institute of Technology, Wright-Patterson AFB, Ohio, December 1978.

11. Maybeck, Peter S., et al. "Investigation of Constant Turn Rate Dynamics Models in Filters for Airborne Vehicle Tracking," unpublished article, Air Force Institute of Technology, Wright-Patterson AFB, Ohio.

12. Maybeck, Peter S., Stochastic Models, Estimation, and Control Volume I. New York: Academic Press Incorporated. 1979.

13. Maybeck, Peter S., Stochastic Models, Estimation, and Control Volume II. New York: Academic Press Incorporated. 1982.

14. Boland, J.S., et al. "Automatic Target Hand-Off Using Correlation Techniques," Auburn University, Auburn, Alabama, January 1977. (AD-A036 435).

15. Shine, James A. and Eugene A. Margerum, "Correlation of Noisey Images," Engineer Topographic Laboratories, Fort Belvoir, Virginia, September 1980. (AD-A088 659).

16. Landau, Mark I., "Radar Tracking of Airborne Targets," presented at National Aerospace and Electronics Conference, Dayton, Ohio, May 19, 1976.

Appendix A

Intensity Centroid Projection Model for Multiple Hot Spots

In this appendix, the equations required to implement the multiple hot spot projection model, described in section 2.5, are detailed.

As depicted in Figure 13, a unit vector in the $\vec{e}_{z\alpha}$ direction can be defined by

$$\vec{e}_{z\alpha} = \cos\alpha\,\vec{k} - \sin\alpha\,\vec{i} \qquad \text{(A-1)}$$

where

$\vec{i}$, $\vec{j}$, $\vec{k}$, represent unit vectors along the inertial x, y, and z, axes respectively.

To determine the direction of a unit vector in the $\vec{e}_\beta$ direction, first rotate about the inertial y-axis. The coordinate transformation is:

$$\begin{bmatrix} \vec{e}_{x\alpha} \\ \vec{e}_{y\alpha} \\ \vec{e}_{z\alpha} \end{bmatrix} = \begin{bmatrix} \cos\alpha & 0 & \sin\alpha \\ 0 & 1 & 0 \\ -\sin\alpha & 0 & \cos\alpha \end{bmatrix} \begin{bmatrix} \vec{i} \\ \vec{j} \\ \vec{k} \end{bmatrix} \qquad \text{(A-2)}$$

Now rotate about the $\vec{e}_{z\alpha}$ axis to obtain:

$$\begin{bmatrix} \vec{e}_{\beta y} \\ \vec{e}_{\beta y} \\ \vec{e}_{\beta z} \end{bmatrix} = \begin{bmatrix} \cos\beta & \sin\beta & 0 \\ -\sin\beta & \cos\beta & 0 \\ 0 & 0 & 1 \end{bmatrix} \begin{bmatrix} \vec{e}_{x\alpha} \\ \vec{e}_{y\alpha} \\ \vec{e}_{z\alpha} \end{bmatrix} \qquad \text{(A-3)}$$

Substituting (A-2) into (A-3) yields

$$\begin{bmatrix} \vec{e}_{\beta x} \\ \vec{e}_{\beta y} \\ \vec{e}_{\beta z} \end{bmatrix} = \begin{bmatrix} \cos\beta & \sin\beta & 0 \\ -\sin\beta & \cos\beta & 0 \\ 0 & 0 & 1 \end{bmatrix} \begin{bmatrix} \cos\alpha & 0 & \sin\alpha \\ 0 & 1 & 0 \\ -\sin\alpha & 0 & \cos\alpha \end{bmatrix}$$

$$\cdot \begin{bmatrix} \vec{i} \\ \vec{j} \\ \vec{k} \end{bmatrix} \qquad \text{(A-4)}$$

Performing the indicated multiplication where $\vec{e}_{\beta y}$ in Equation (A-4) will henceforth be referred to as $\vec{e}_{\beta}$, see Figure 13, the desired vector is

$$\vec{e}_{\beta} = (\cos\alpha)(-\sin\beta)\vec{i} + \cos\beta\vec{j} + (-\sin\beta)(\sin\alpha)\vec{k} \qquad \text{(A-5)}$$

The relationship between these unit vectors and FLIR plane unit vectors is

$$\vec{e}_{\beta} = \vec{e}_{y\ \mathrm{FLIR}}$$

$$\vec{e}_{z\alpha} = -\vec{e}_{x\ \mathrm{FLIR}}$$

With the $\vec{e}_{\beta}$-$\vec{e}_{z\alpha}$ plane translated in inertial space to coincide with the aircraft COM, Figure 14, and since the velocity vector is assumed to lie along the aircraft centerline, a unit vector out the nose of the aircraft can be determined:

$$\vec{e}_{HX} = \frac{v_x\vec{i}+v_y\vec{j}+v_z\vec{k}}{|v|} \qquad \text{(A-6)}$$

where

v_x, v_y, v_z - refer to velocity components in the inertial frame

$\vec{e}_{HX}$ - unit vector along aircraft velocity vector $|v| = (v_x^2+v_y^2+v_z^2)^{\frac{1}{2}}$

Since $\vec{e}_{HX}$ will always pass through the aircraft COM, this unit vector is used to form the first axis of a coordinate system referred to as the H frame, with its origin at the aircraft COM.

To determine the orientation of the second H-frame axis the following cross-product was used

$$\vec{v}x\vec{j}$$

This cross-product produces a vector normal to $\vec{v}$ and $\vec{j}$. Explicitly,

$$\vec{v}x\vec{j} = \begin{vmatrix} i & j & k \\ v_x & v_y & v_z \\ 0 & 1 & 0 \end{vmatrix} = -v_z\vec{i}+v_x\vec{k} \qquad \text{(A-7)}$$

This vector is normalized to produce a unit vector in the direction of the second H-frame axis;

$$\vec{e}_{Hy} = \frac{-v_z i+v_x K}{(v_x^2+v_z^2)^{\frac{1}{2}}} \qquad \text{(A-8)}$$

Note that this axis will always lie in the horizontal inertial plane thus the H, or horizontal, frame notation.

To find the direction of the third H-frame axis, cross the vectors which define the first two H-frame axes:

$$\begin{vmatrix} \vec{i} & \vec{j} & \vec{k} \\ v_x & v_y & v_z \\ -v_z & 0 & v_x \end{vmatrix} = v_x v_y \vec{i} - (v_x^2 + v_z^2)\vec{j} + v_y v_z \vec{k} \qquad \text{(A-9)}$$

Equation (A-9) is normalized to produce a unit vector in the third H-frame direction:

$$\vec{e}_{HZ} = \frac{v_x v_y \vec{i} - (v_x^2 + v_z^2)\vec{j} + v_y v_z \vec{k}}{\left[(v_x^2 + v_z^2)(v_x^2 + v_y^2 + v_z^2)\right]^{1/2}} \qquad \text{(A-10)}$$

Thus, a coordinate system relative to the velocity vector is defined, see Figure 15.

For trajectories where a roll about the $\vec{e}_{HY}$ axis is desired, the two hot spots located on the $\vec{e}_{HY}$ axis will move out of the $\vec{e}_{HX}$-$\vec{e}_{HY}$ plane, whereas the hot spot 1, as defined in Figure 16, will remain along the $\vec{e}_{HX}$ axis. To determine the location of hot spots 2 and 3, a body axis with the x-axis out the aircraft nose, the y-axis out the right wing, and the z-axis out the belly is used. As depicted in Figure 17, the direction of hot spots 2 and 3 can be determined by

$$\vec{e}_{BY} = \cos\phi \; \vec{e}_{HY} + \sin\phi \; \vec{e}_{HZ} \qquad \text{(A-11)}$$

where

$$\phi(t_0) = 0$$

$$\phi(t) = \omega t$$

An example is used to demonstrate how these coordinate frames are used to project the locations of the ellipsoid centers onto the FLIR image plane. Referring to Figure 18, the offset distance, δ, along the $\vec{e}_{BY}$ axis can be projected onto the translated $\vec{e}_{\beta}$ axis by:

$$\delta_{\beta T} = \delta\left[\vec{e}_{BY} \cdot \vec{e}_{\beta}\right] \qquad \text{(A-12)}$$

Performing the dot product in Equation (A-12) yields

$$\delta_{\beta T} = \delta\left[\frac{(\cos\phi)(-v_z)(\cos\alpha)(-\sin\beta)+(\cos\phi)(v_x)(-\sin\beta)(\sin\alpha)}{A}\right.$$

$$+\ \frac{(\sin\phi)(v_x v_y)(-\sin\beta)(\cos\alpha)-(v_x^2+v_z^2)(\sin\phi)(\cos\beta)}{B}$$

$$\left.+\ \frac{(\sin\phi)(v_y\ v_z)(-\sin\beta)(\sin\alpha)}{B}\right] \qquad \text{(A-13)}$$

where

A = denominator of Equation (A-8)

B = denominator of Equation (A-10)

In the $\vec{e}_{z\alpha}$ direction, the projection is

$$\delta_{z\alpha T} = \delta\left[\vec{e}_{BY} \cdot \vec{e}_{z\alpha}\right] \qquad \text{(A-14)}$$

or explicitly,

$$\delta_{z\alpha T} = \delta\left[\frac{(\cos\phi)(-v_z)(-\sin\alpha)+(\cos\phi)(v_x)(\cos\alpha)}{A}\right.$$

$$\left. + \frac{(\sin\phi)(v_x v_y)(-\sin\alpha)+(\sin\phi)(v_y v_z)(\cos\alpha)}{B}\right] \tag{A-15}$$

The equations for the projection of the hot spot located along the $\vec{e}_{BX}$ axis onto the translated $\vec{e}_\beta$-$\vec{e}_{z\alpha}$ plane are:

$$\delta_{\beta T} = \delta\left[\vec{e}_{BX}\cdot\vec{e}_\beta\right] = \delta\left[\frac{(v_x)(-\sin\beta)(\cos\alpha)+(v_y)(\cos\beta)}{|v|}\right.$$

$$\left. + \frac{(v_z)(-\sin\beta)(\sin\alpha)}{|v|}\right] \tag{A-16}$$

and

$$\delta_{z\alpha T} = \delta\left[\vec{e}_{BX}\cdot\vec{e}_{z\alpha}\right] = \delta\left[\frac{(v_x)(-\sin\alpha)+(v_z)(\cos\alpha)}{|v|}\right] \tag{A-17}$$

The final step is to convert the offset distance on the translated $\vec{e}_\beta$ -$\vec{e}_{z\alpha}$ plane into distance on the FLIR image plane. The hot spot displacements in the translated $\vec{e}_\beta$ -$\vec{e}_{z\alpha}$plane are normal to line of sight from the FLIR image plane and with the range known from the trajectory model, the angular displacement of the hot spots will be used to approximate linear distance on the FLIR image plane. The geometry in the $\vec{e}_\beta$ direction is shown in Figure A-1.

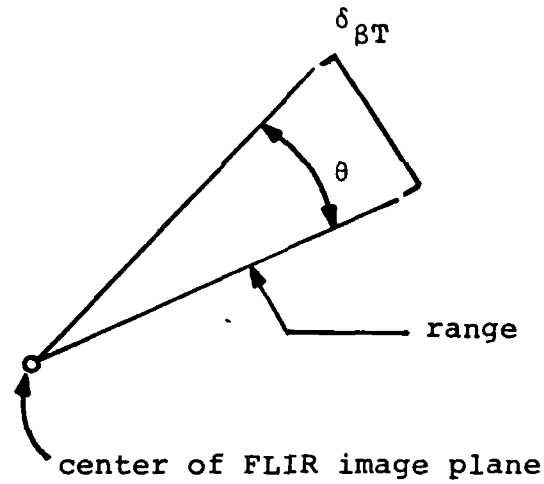

Figure A-1. Projection onto the FLIR Plane

Equation (A-18) gives the approximate displacement in the $\vec{e}_\beta$, direction, δ_β, which coincides with the y_{FLIR} direction, in radians:

$$\delta_\beta = \tan\theta \simeq \theta \simeq \frac{\delta_{BT}}{r} \qquad \text{(A-18)}$$

This distance is converted to pixels by dividing by .00002 and added to the coordinates of the aircraft COM in the FLIR plane. Thus, the offset distance in the y_{FLIR} direction for each hot spot is determined. The offset distance in the x_{FLIR} direction is determined in the same manner except the distance must be subtracted from the aircraft COM since $\vec{e}_{z\alpha} = (-)\vec{e}_{x\ FLIR}$.

Appendix B

Derivation of $\underline{Q}_{fd}$ for the Kalman Filter, Chapter III

The derivation of $\underline{Q}_{fd}$, Equation (3-12), for the filter state equation which was briefly described in Chapter 3 will be fully detailed in this appendix. From Chapter 3, $\underline{\Phi}_f$, $\underline{G}_f$, and $\underline{Q}_f$ are:

$$\underline{\Phi}_f(t_{i+1},t_i) = \begin{bmatrix} 1 & 0 & \Delta t & 0 & A & 0 & 0 & 0 \\ 0 & 1 & 0 & \Delta t & 0 & A & 0 & 0 \\ 0 & 0 & 1 & 0 & B & 0 & 0 & 0 \\ 0 & 0 & 0 & 1 & 0 & B & 0 & 0 \\ 0 & 0 & 0 & 0 & e^{\frac{-\Delta t}{T_{df}}} & 0 & 0 & 0 \\ 0 & 0 & 0 & 0 & 0 & e^{\frac{-\Delta t}{T_{df}}} & 0 & 0 \\ 0 & 0 & 0 & 0 & 0 & 0 & e^{\frac{-\Delta t}{T_{af}}} & 0 \\ 0 & 0 & 0 & 0 & 0 & 0 & 0 & e^{\frac{-\Delta t}{T_{af}}} \end{bmatrix} \tag{B-1}$$

where

$$A = T_{df}^{2}\left[\left(\frac{1}{T_{df}}\right)(\Delta t)-1+e^{\frac{-\Delta t}{T_{df}}}\right]$$

$$B = T_{df}\left[1-e^{\frac{-\Delta t}{T_{df}}}\right]$$

$\Delta t = (t_{i+1} - t_i)$

$$\underline{G}_f = \begin{bmatrix} 0 & 0 & 0 & 0 \\ 0 & 0 & 0 & 0 \\ 0 & 0 & 0 & 0 \\ 0 & 0 & 0 & 0 \\ 1 & 0 & 0 & 0 \\ 0 & 1 & 0 & 0 \\ 0 & 0 & 1 & 0 \\ 0 & 0 & 0 & 1 \end{bmatrix} \qquad \text{(B-2)}$$

and

$$\underline{Q}_f = \begin{bmatrix} 2\frac{\sigma_{df}^2}{T_{df}} & 0 & 0 & 0 \\ 0 & 2\frac{\sigma_{df}^2}{T_{df}} & 0 & 0 \\ 0 & 0 & 2\frac{\sigma_{af}^2}{T_{af}} & 0 \\ 0 & 0 & 0 & 2\frac{\sigma_{af}^2}{T_{af}} \end{bmatrix} \qquad \text{(B-3)}$$

where

σ_{df}^2 = assumed target acceleration process variance

σ_{af}^2 = assumed atmospheric jitter process variance

Thus, $\underline{Q}_{fd}$ may be evaluated using (12:171)

$$\underline{Q}_{fd} = \int_{t_i}^{t_{i+1}} \underline{\Phi}_f(t_{i+1},\tau)\underline{G}_f(\tau)\underline{Q}_f(\tau)\underline{G}^T(\tau)\underline{\Phi}_f^T(t_{i+2},\tau)\,d\tau \qquad \text{(B-4)}$$

Performing the matrix multiplication inside the integral of Equation (B-4) yields:

$$\underline{\Phi}_f\underline{G}_f\underline{Q}_f\underline{G}_f^T\underline{\Phi}_f^T = \begin{bmatrix} A^2Q_{11} & 0 & ABQ_{11} & 0 & ACQ_{11} & 0 & 0 & 0 \\ 0 & A^2Q_{22} & 0 & ABQ_{22} & 0 & ACQ_{22} & 0 & 0 \\ ABQ_{11} & 0 & B^2Q_{11} & 0 & BCQ_{11} & 0 & 0 & 0 \\ 0 & ABQ_{22} & 0 & B^2Q_{22} & 0 & BCQ_{22} & 0 & 0 \\ ACQ_{11} & 0 & BCQ_{11} & 0 & C^2Q_{11} & 0 & 0 & 0 \\ 0 & ACQ_{22} & 0 & BCQ_{22} & 0 & C^2Q_{22} & 0 & 0 \\ 0 & 0 & 0 & 0 & 0 & 0 & D^2Q_{33} & 0 \\ 0 & 0 & 0 & 0 & 0 & 0 & 0 & D^2Q_{44} \end{bmatrix}$$

(B-5)

where

A, B = are as in Equation (B-1)

$$C = e^{\frac{-\Delta t}{T_{df}}}$$

$$D = e^{\frac{-\Delta t}{T_{af}}}$$

Q_{11}-Q_{44} = matrix elements of Equation (B-3)

Since the integral of the matrix shown in Equation (B-5) equals a matrix of integrals of each element, the remaining demonstration of the computation of $\underline{Q}_{fd}$ will follow the integration of the 11-element of Equation (B-5). Substituting for A and Q_{11} yields:

$$A^2Q_{11} = \left[(T_{df}^2)\left(\frac{\Delta t}{T_{df}} - 1 + e^{\frac{-\Delta t}{T_{df}}}\right)^2\right]\left[2\,\frac{\sigma_{df}^2}{T_{df}}\right] =$$

$$= 2T_{df}^3\,\sigma_{df}^2\left[\frac{\Delta t^2}{T_{df}{}^2} - \frac{2\Delta t}{T_{df}} + \frac{2\Delta t}{T_{df}}\,e^{\frac{-\Delta t}{T_{df}}} + 1 - 2e^{\frac{-\Delta t}{T_{df}}} + e^{\frac{-2\Delta t}{T_{df}}}\right]$$

Thus,

$$\int_{t_i}^{t_{i+1}} A^2(\tau)Q_{11}(\tau)d\tau = \{2T_{df}^3\,\sigma_{df}^2\}\left[\int_{t_i}^{t_{i+1}} \frac{(t_{i+1}-\ )^2}{T_{df}^2}d\tau\right.$$

$$-\int_{t_i}^{t_{i+1}} \frac{2(t_{i+1}-\tau)}{T_{df}}d\tau + \int_{t_i}^{t_{i+1}} \frac{2(t_{i+1}-\tau)}{T_{df}}\,e^{\frac{-(t_{i+1}-\tau)}{T_{df}}}d + \int_{t_i}^{t_{i+1}} d\tau$$

$$\left. - \int_{t_i}^{t_{i+1}} 2e^{\frac{(t_{i+1}-\tau)}{T_{df}}}d\tau + \int_{t_i}^{t_{i+1}} e^{\frac{-2(t_{i+1}-\tau)}{T_{df}}}d\tau \right] \qquad \text{(B-6)}$$

After performing the indicated integrations and combining terms, the result is:

$$\int_{t_i}^{t_{i+1}} A^2(\tau)Q_{11}(\tau)d\tau = \sigma_{df}^2\left[\frac{(2)(T_{df})(\Delta t)^3}{3} - (2)(T_{df})^2(\Delta t)^2\right.$$

$$\left. -(4)(T_{df})^3(\Delta t)\left(e^{\frac{-\Delta t}{T_{df}}}\right) + (2)(T_{df})^3(\Delta t) + (T_{df})^4\left(e^{\frac{-2\Delta t}{T_{df}}}\right) + T_{df}^4\right]$$

(B-7)

The remainder of the terms of Equation (B-5) are evaluated in a similiar manner with the results being as expressed in Equation (3-12).

Appendix C

Plots of Tracking Errors

This appendix gives the sequence of plots described in Chapter 5. The figures are numbered so as to correspond directly to the case numbers used in Chapter 5, i.e. Figures C-2a thru C-2j are the plots which correspond to case 2 in Chapter 5. For a description of the truth model and filter paramters refer to the appropriate table in Chapter 5 or the summary table which is given in section 5.16. (Note: In order for the case and figure numbers to correspond, Figure C-1 is not used). For the cases where the filter tuning plots are not shown, the tuning employed was similar to case 1 for single and case 3 for multiple hot spot targets.

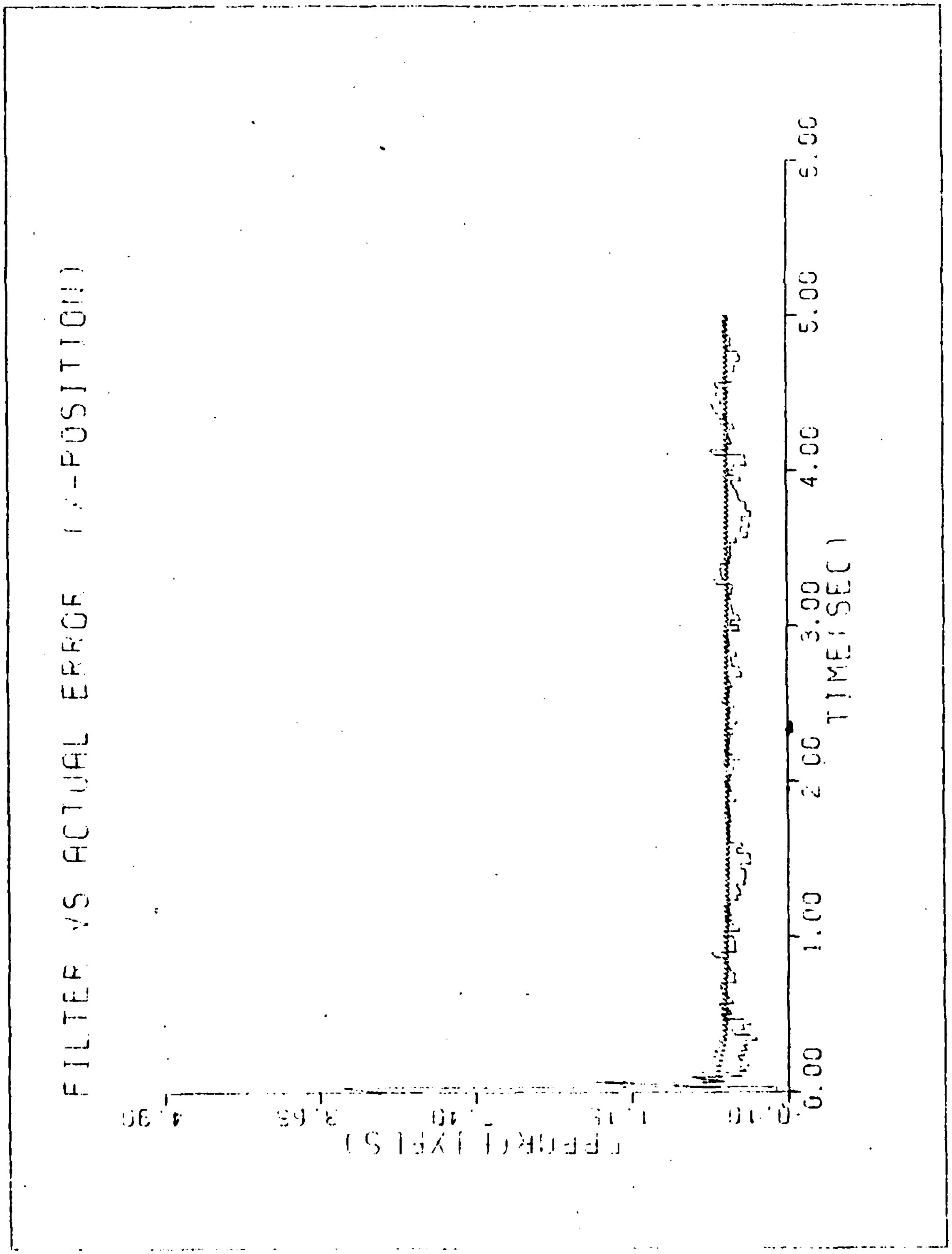

Figure C-2a. Case 2

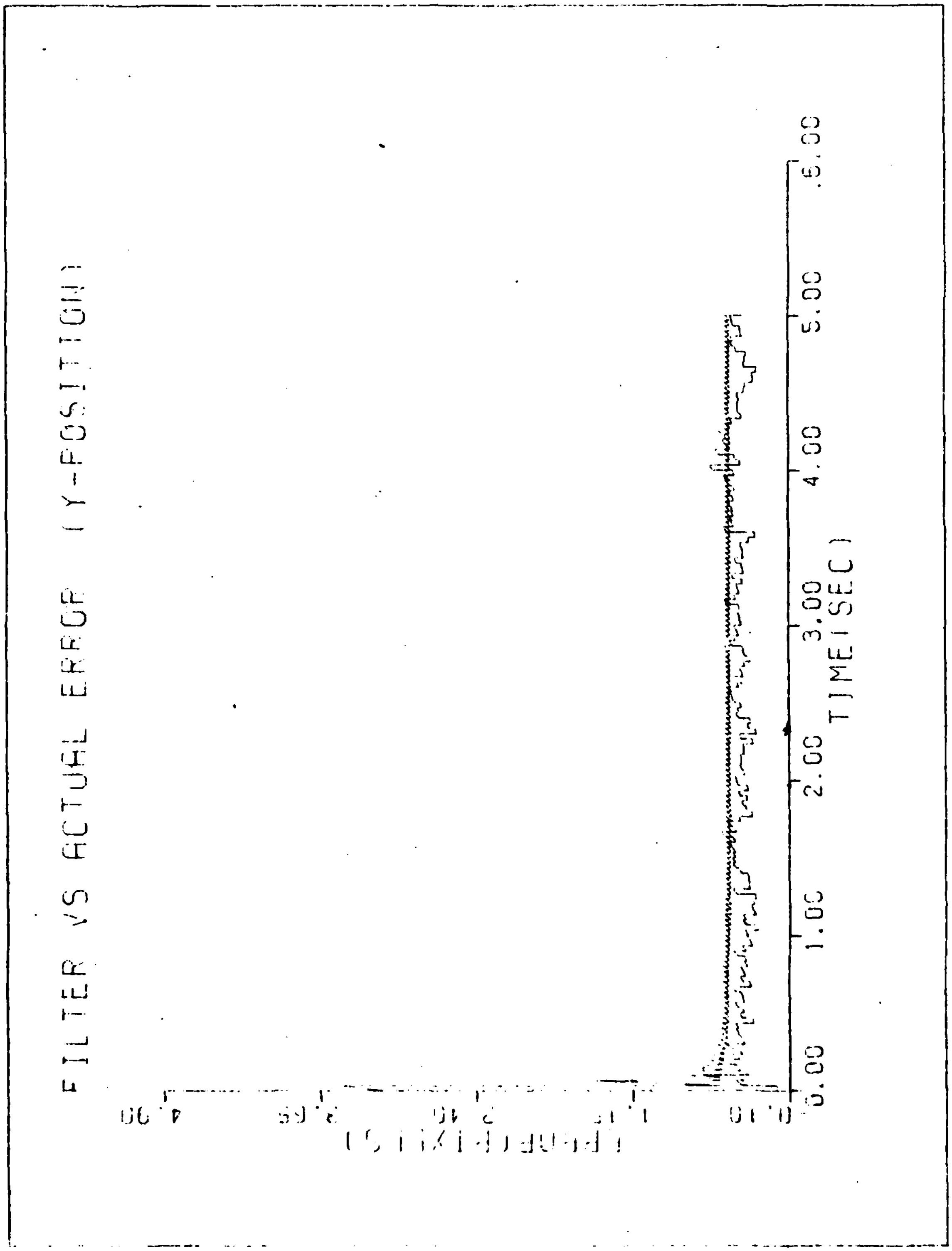

Figure C-2b. Case 2

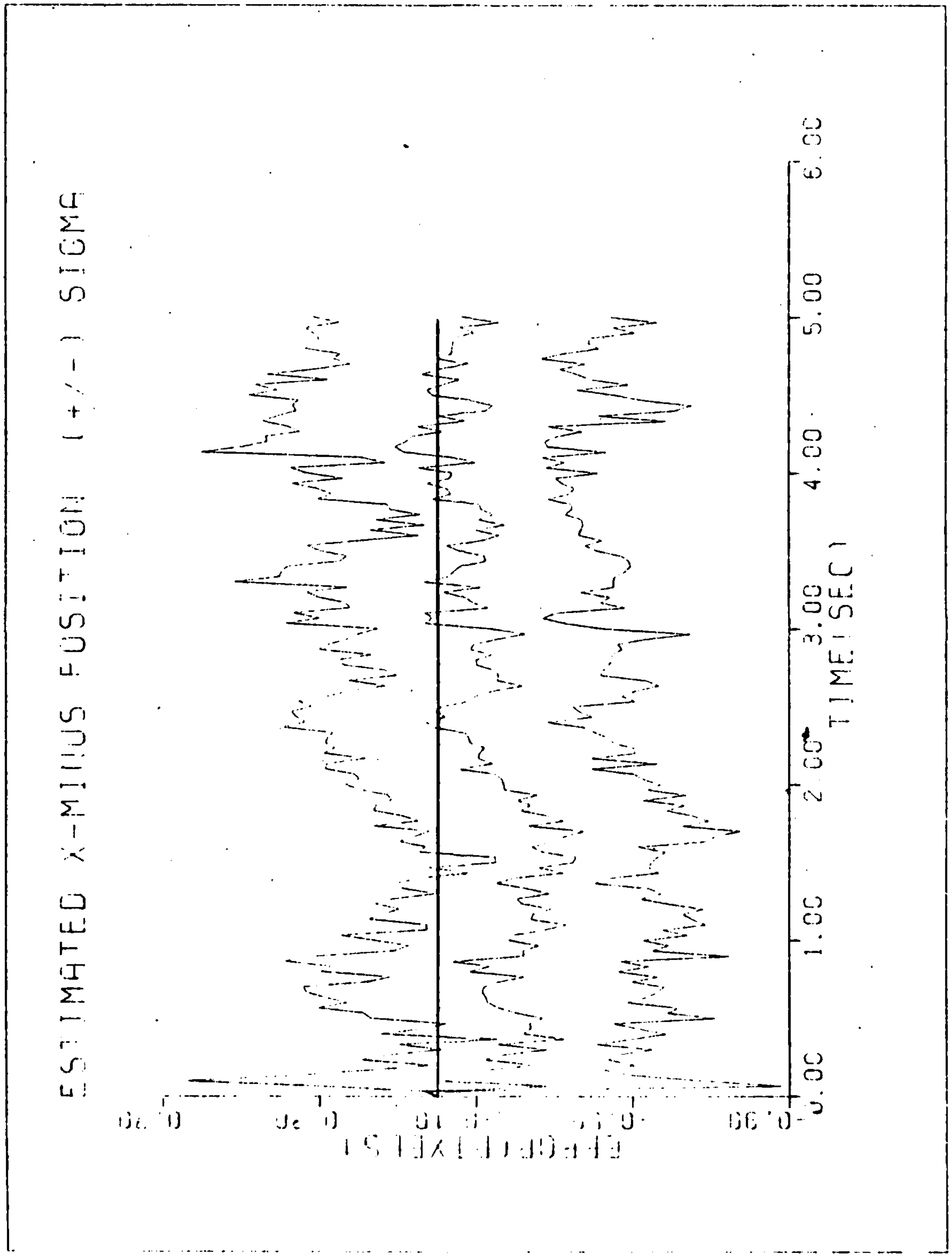

Figure C-2c. Case 2

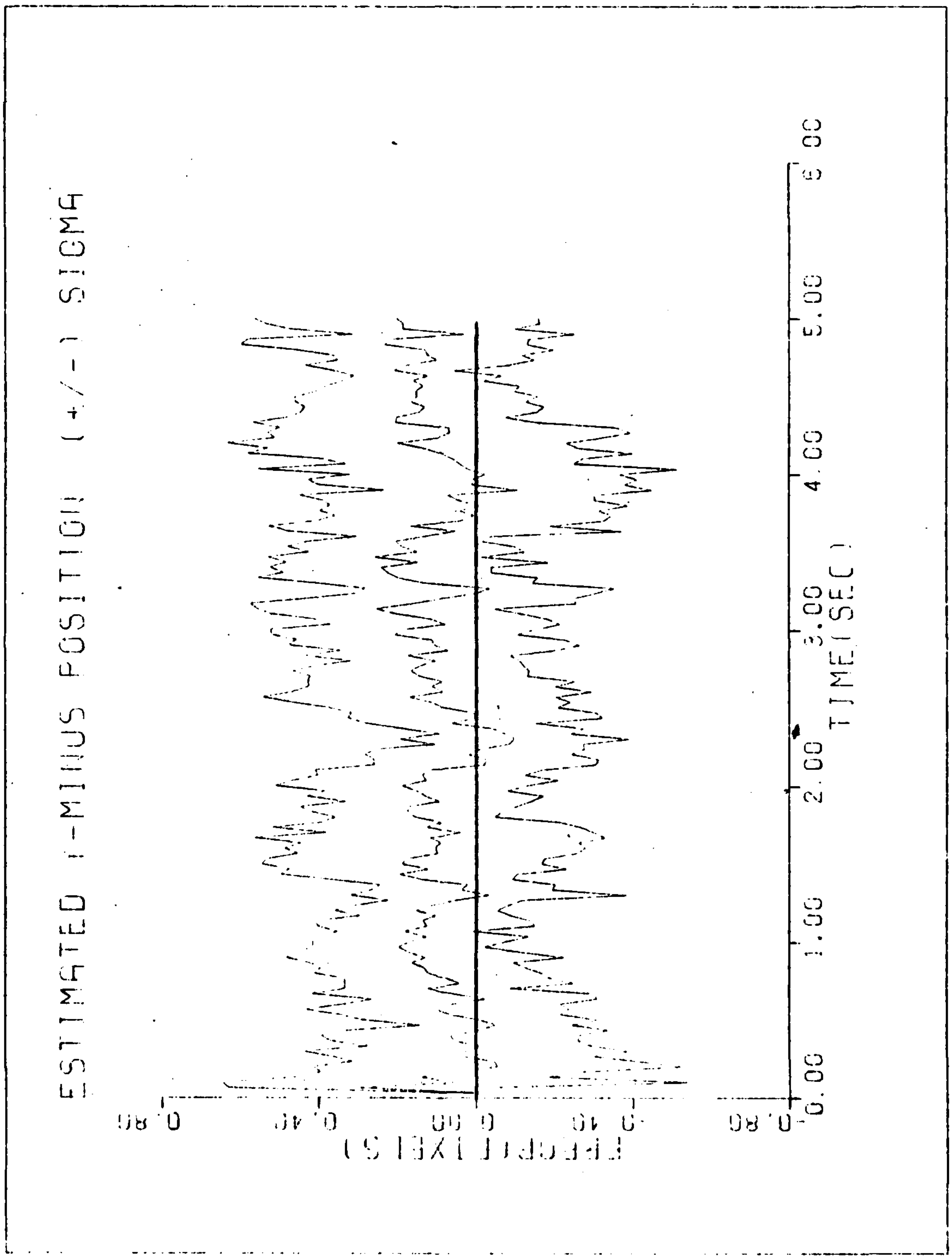

Figure C-2d. Case 2

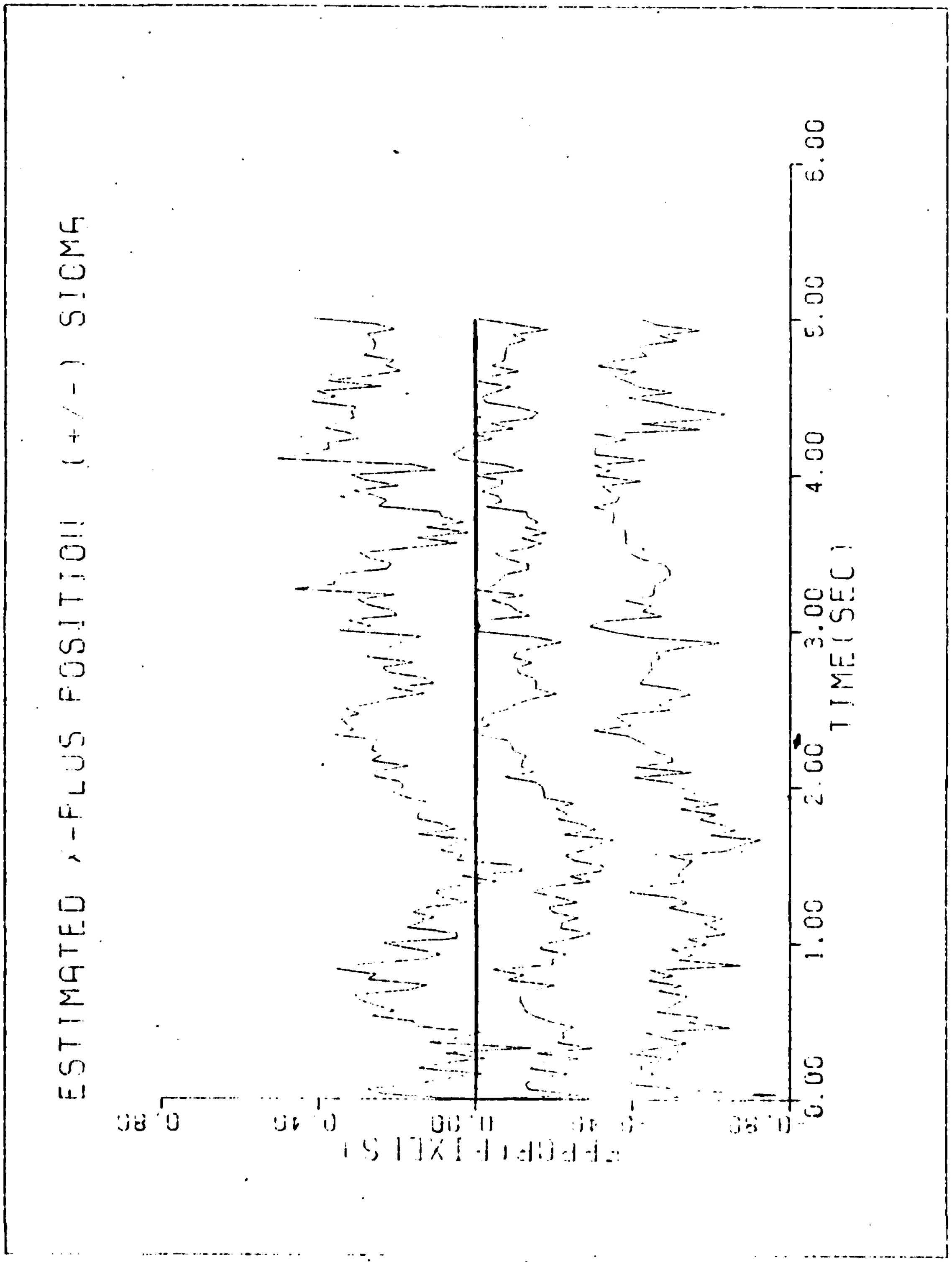

Figure C-2e. Case 2

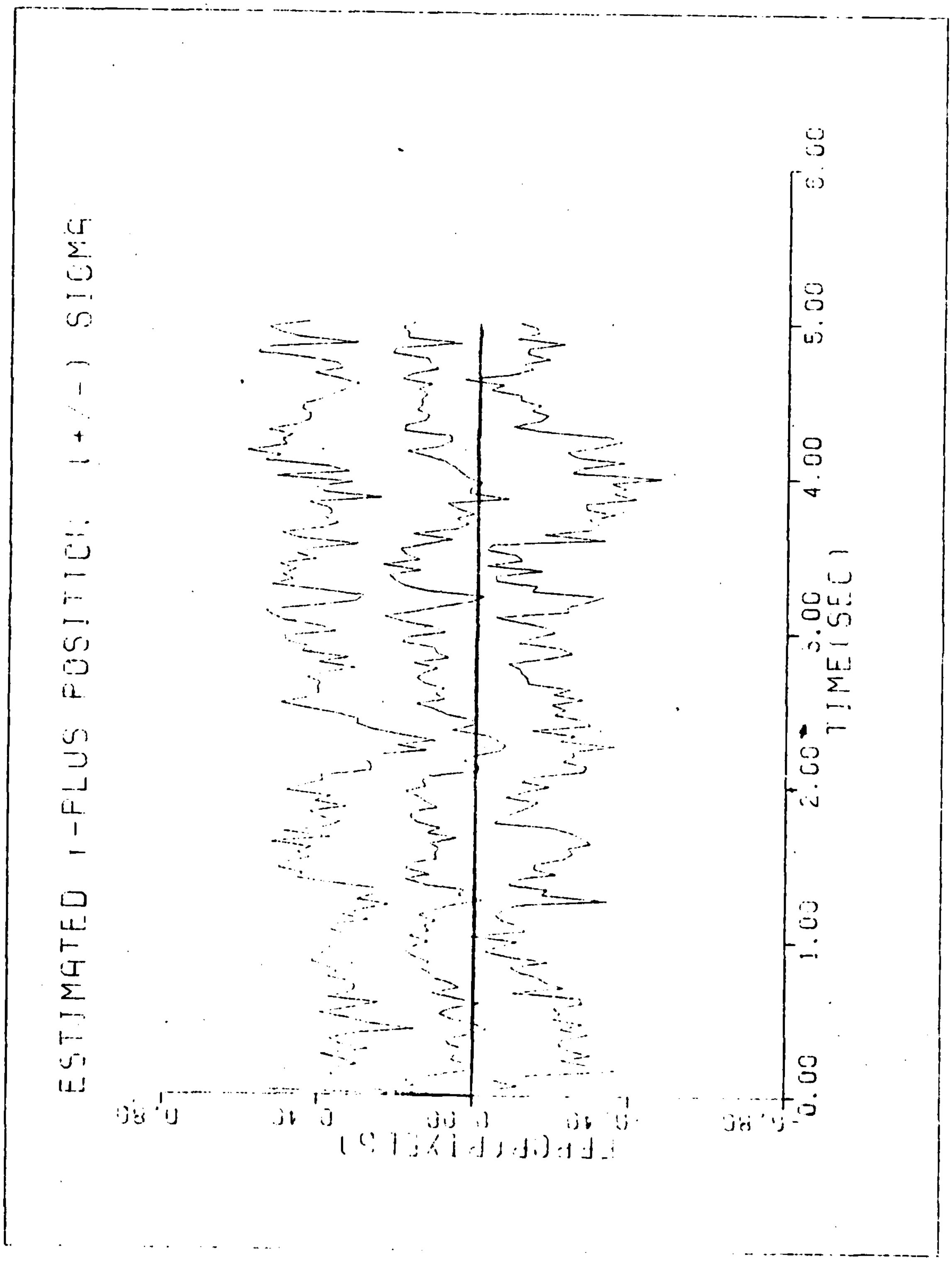

Figure C-2f. Case 2

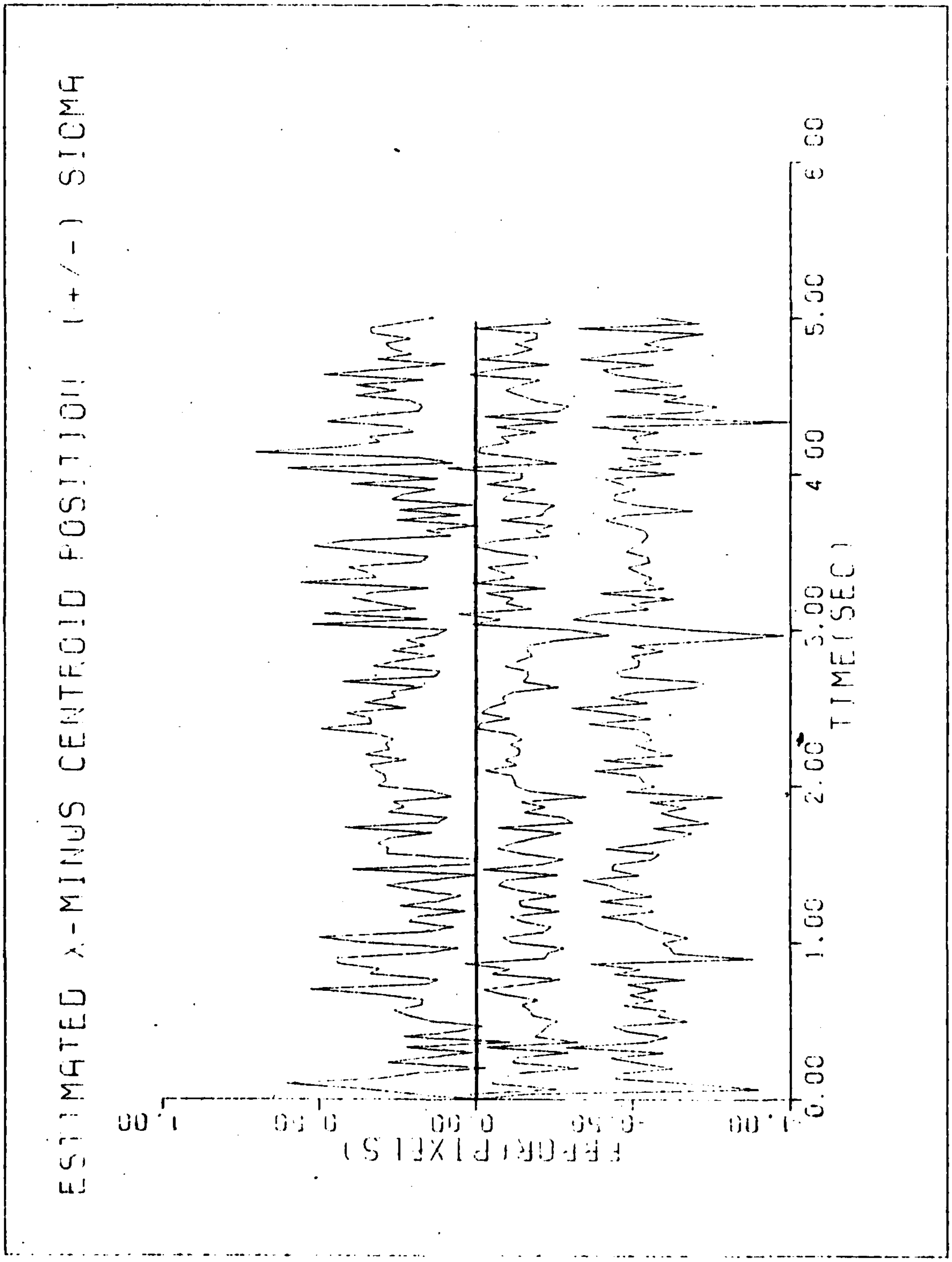

Figure C-2g. Case 2

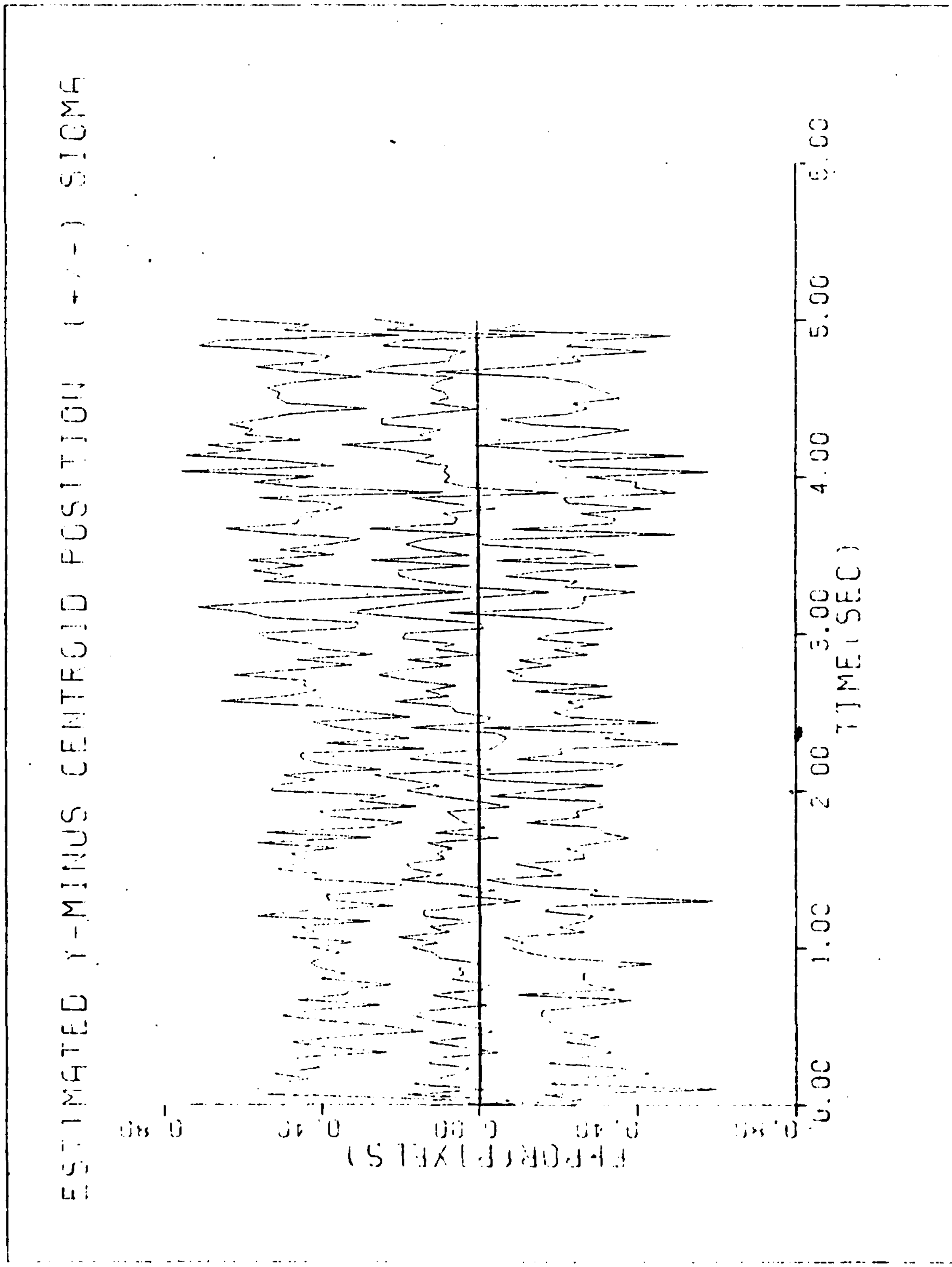

Figure C-2h. Case 2

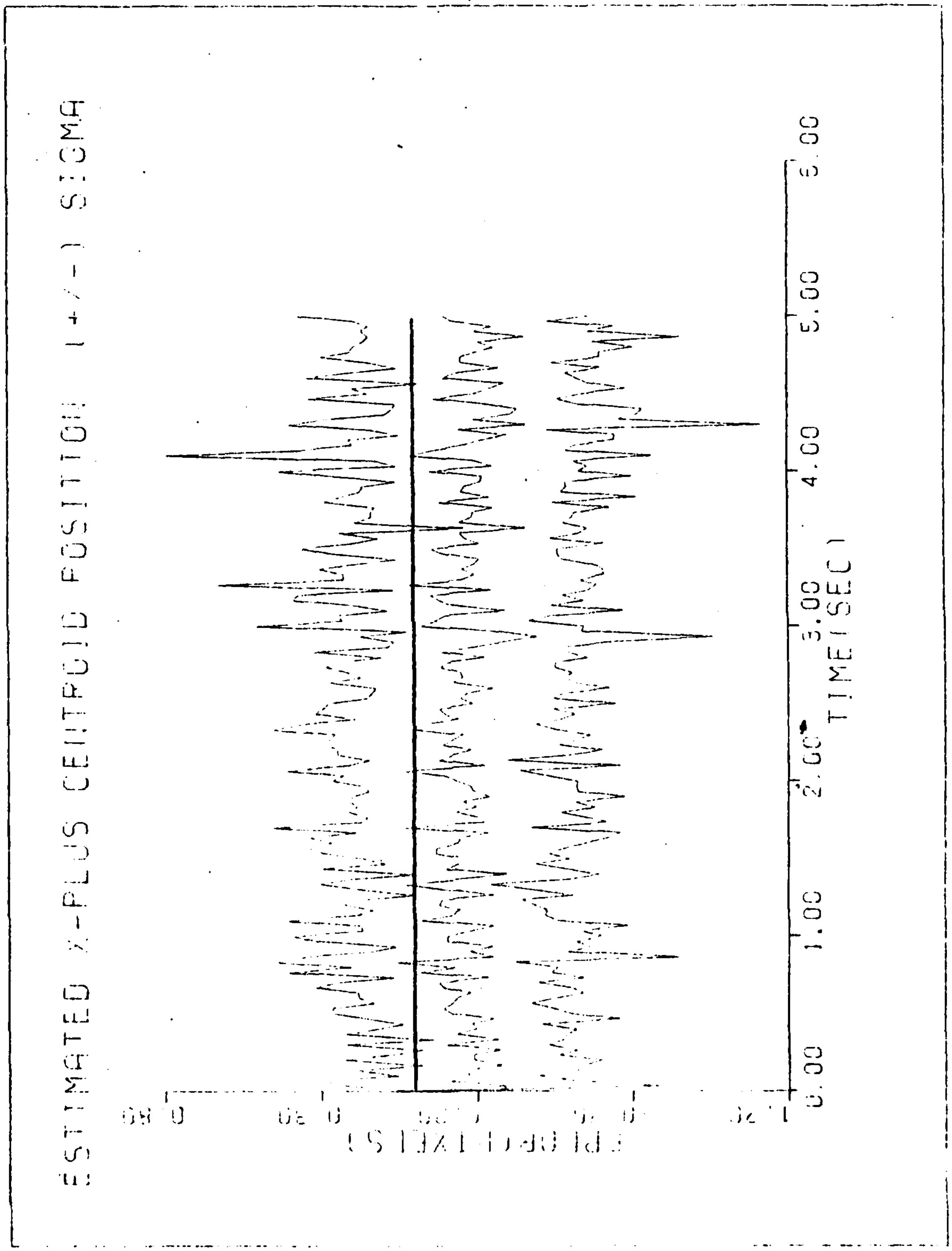

Figure C-2i. Case 2

AD-A124 884 ENHANCED TRACKING OF AIRBORNE TARGETS USING A CORRELATOR/KALMAN FILTER(U) AIR FORCE INST OF TECH WRIGHT-PATTERSON AFB OH SCHOOL OF ENGINEERING 3/4

UNCLASSIFIED P P MILLNER DEC 82 AFIT/GE/EE/82D-50 F/G 12/1 NL

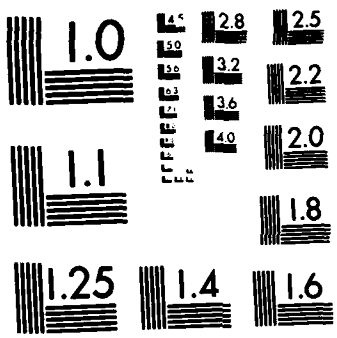

MICROCOPY RESOLUTION TEST CHART
NATIONAL BUREAU OF STANDARDS-1963-A

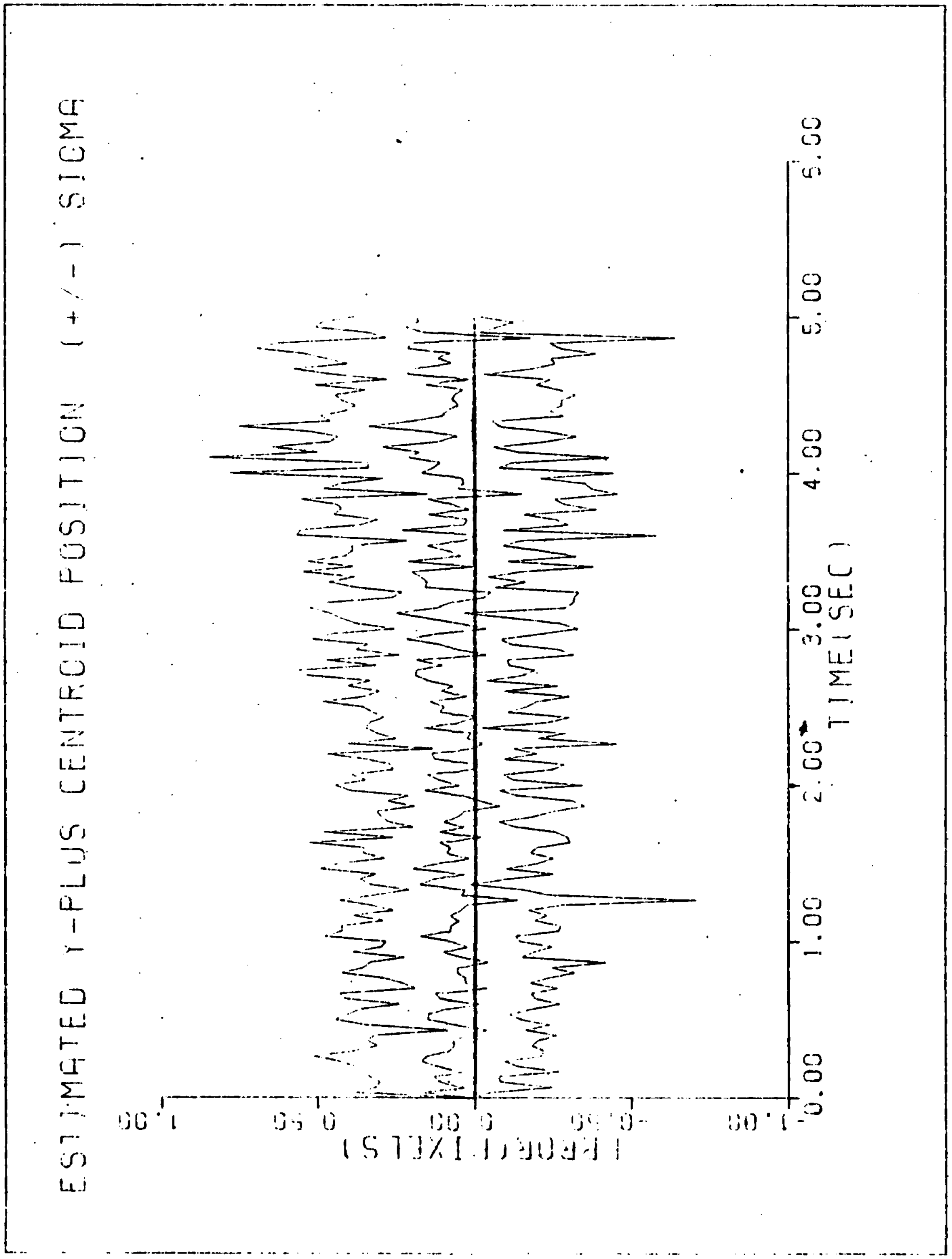

Figure C-2j. Case 2

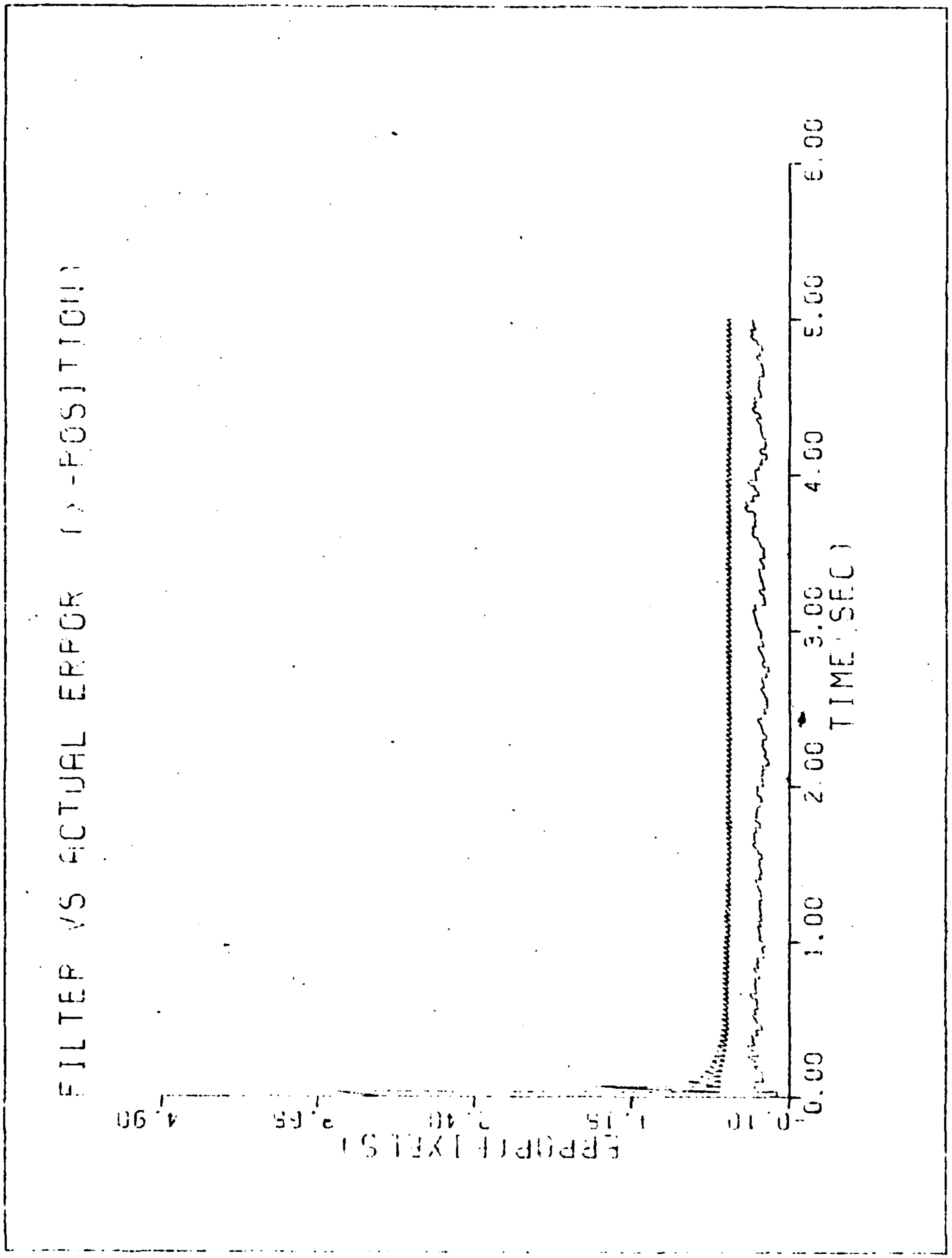

Figure C-3a. Case 3

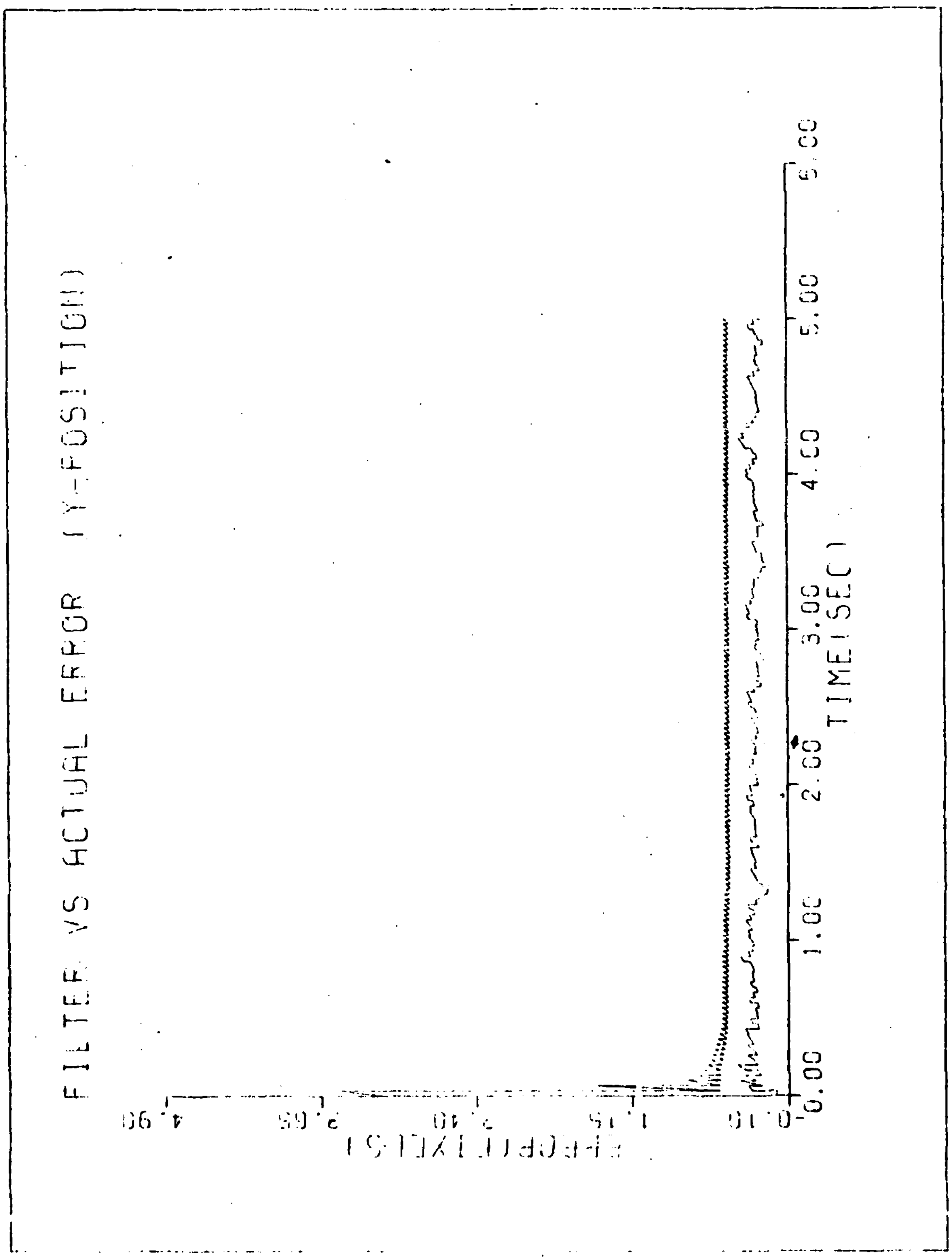

Figure C-3b. Case 3

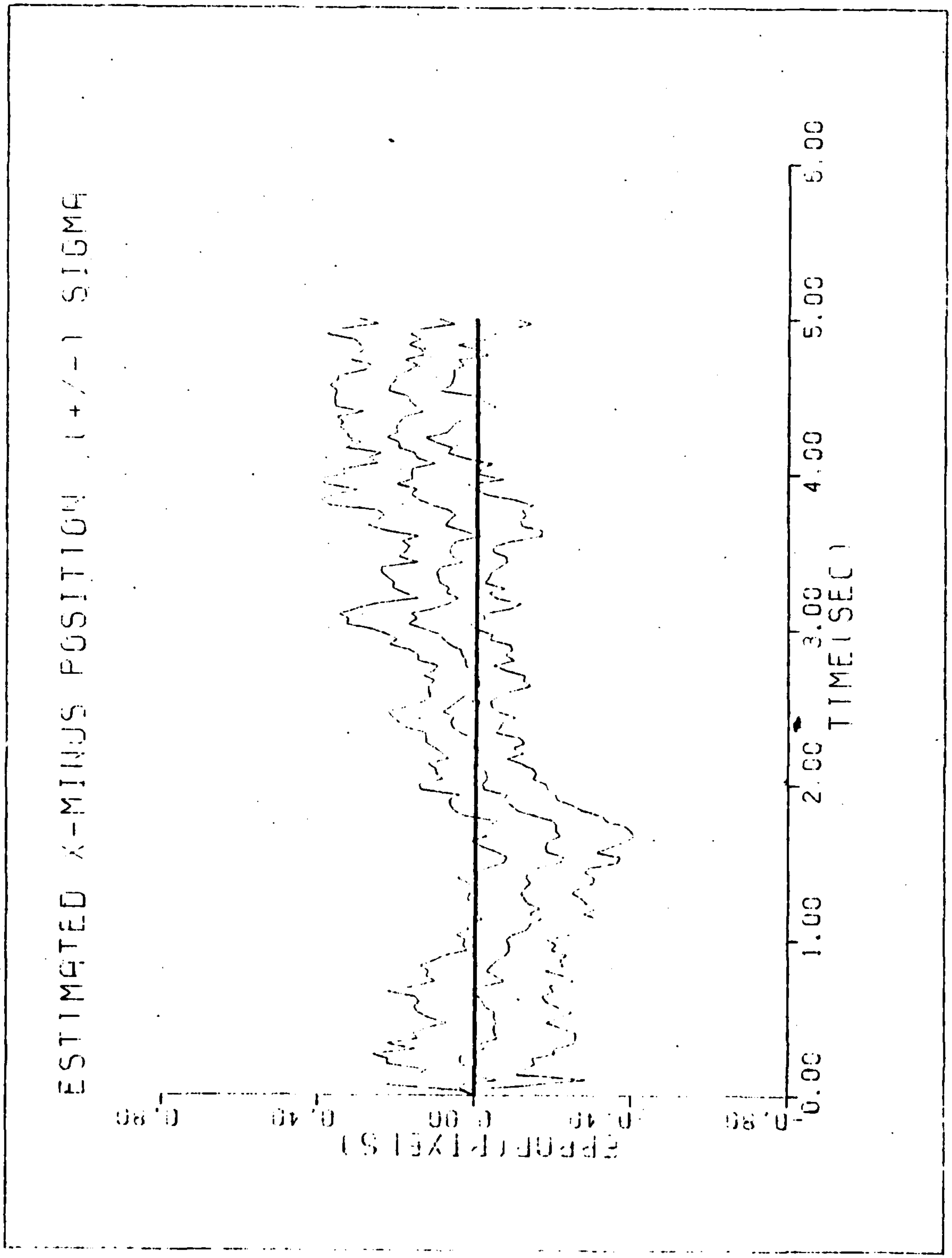

Figure C-3c. Case 3

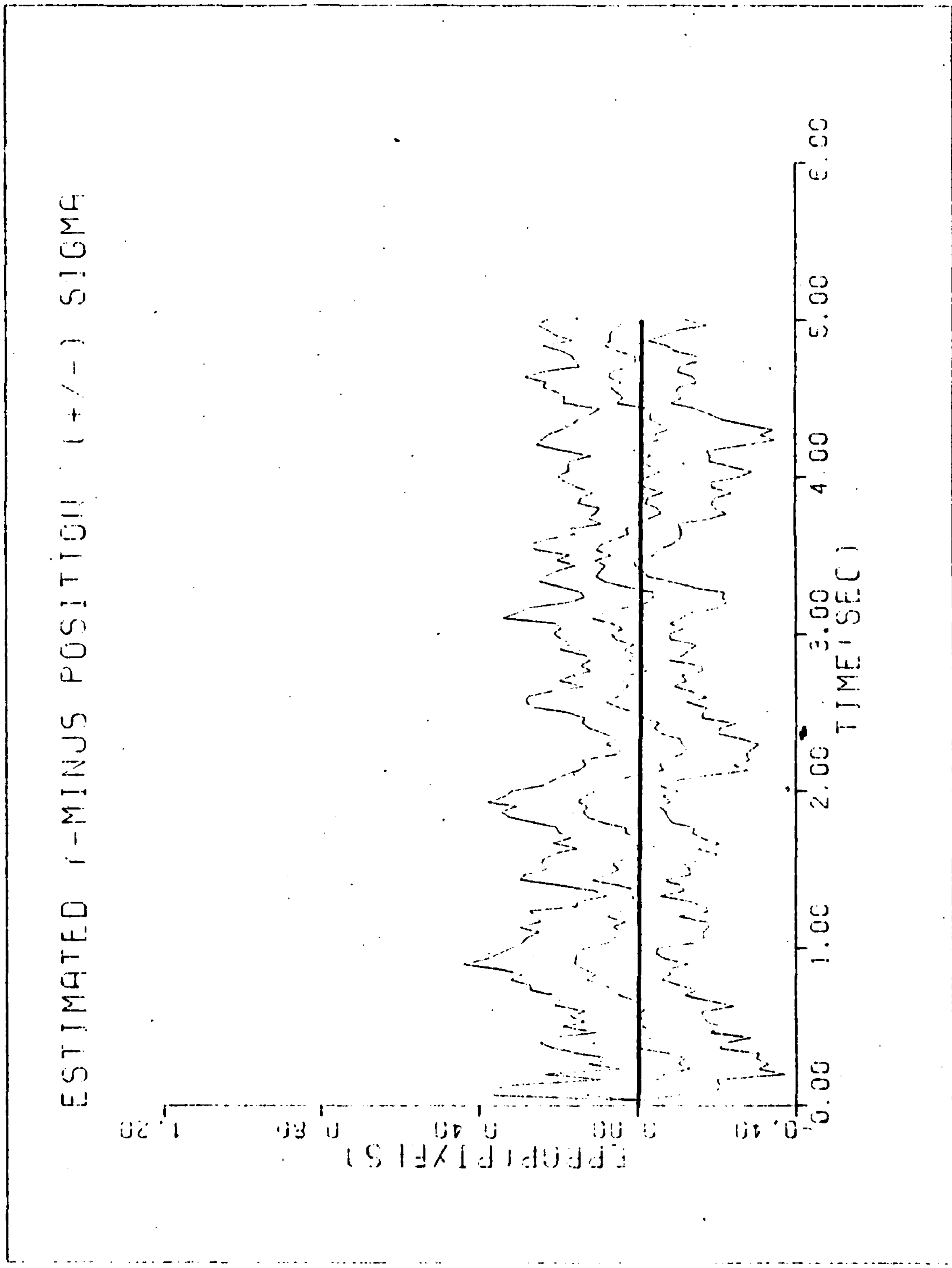

Figure C-3d. Case 3

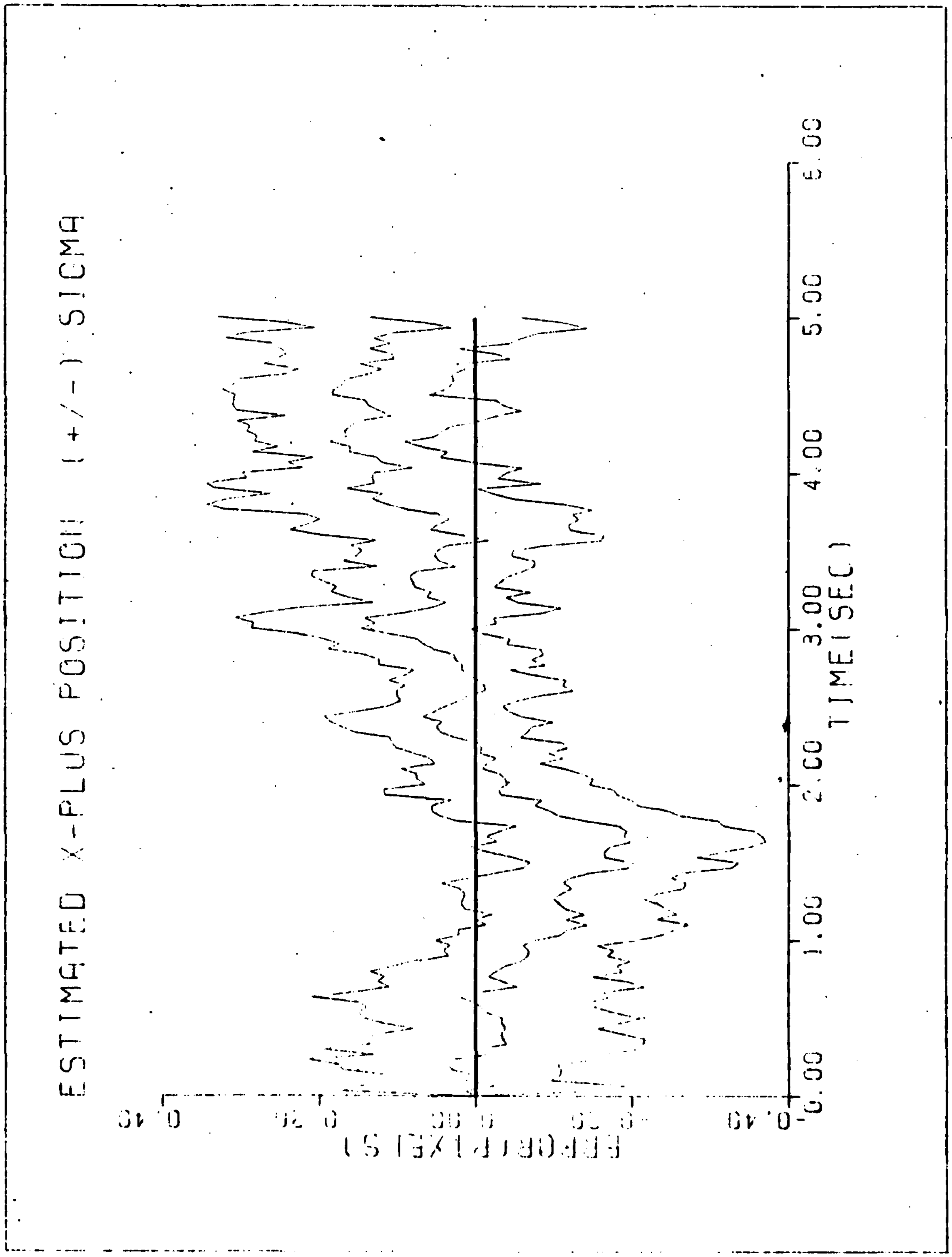

Figure C-3e. Case 3

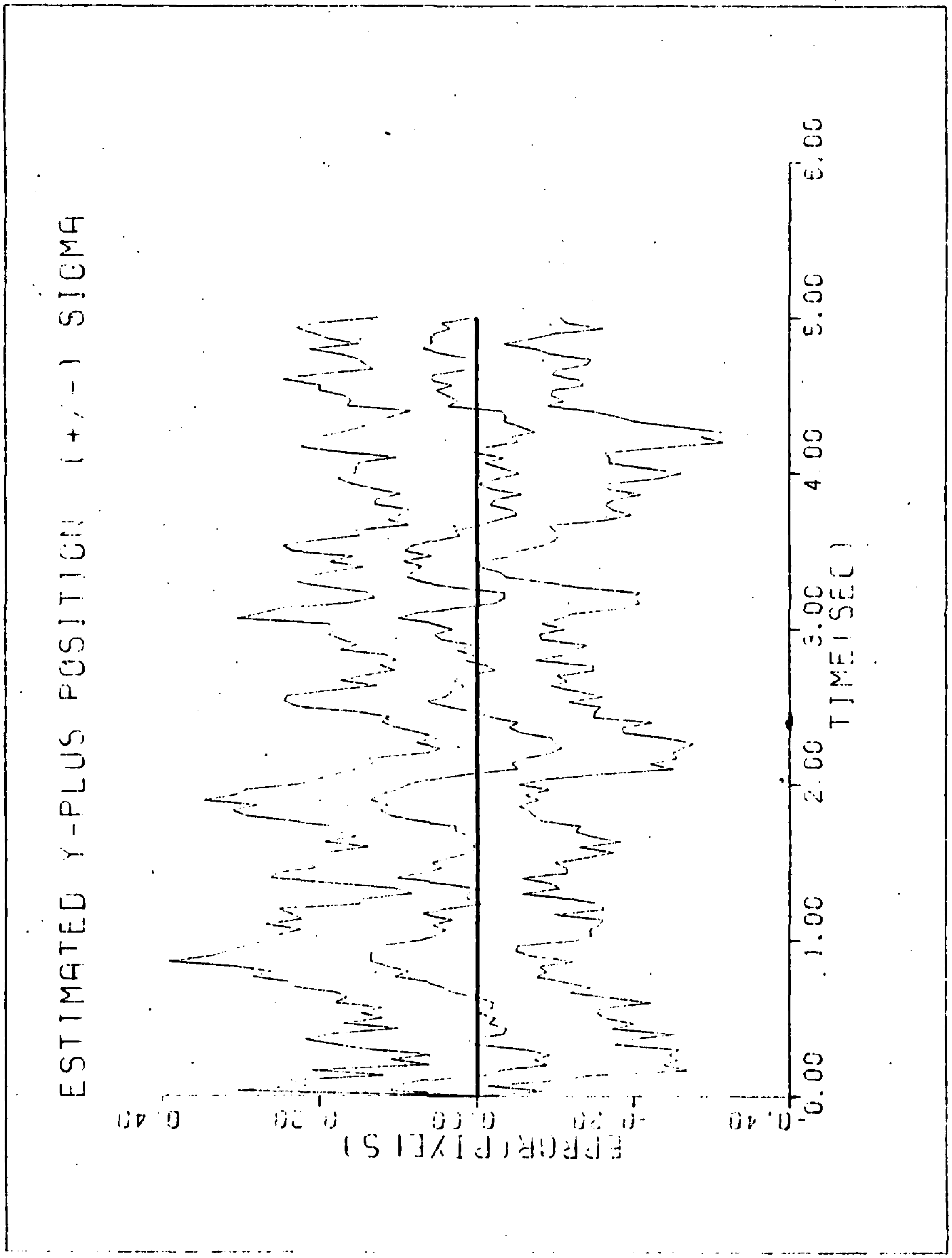

Figure C-3f. Case 3

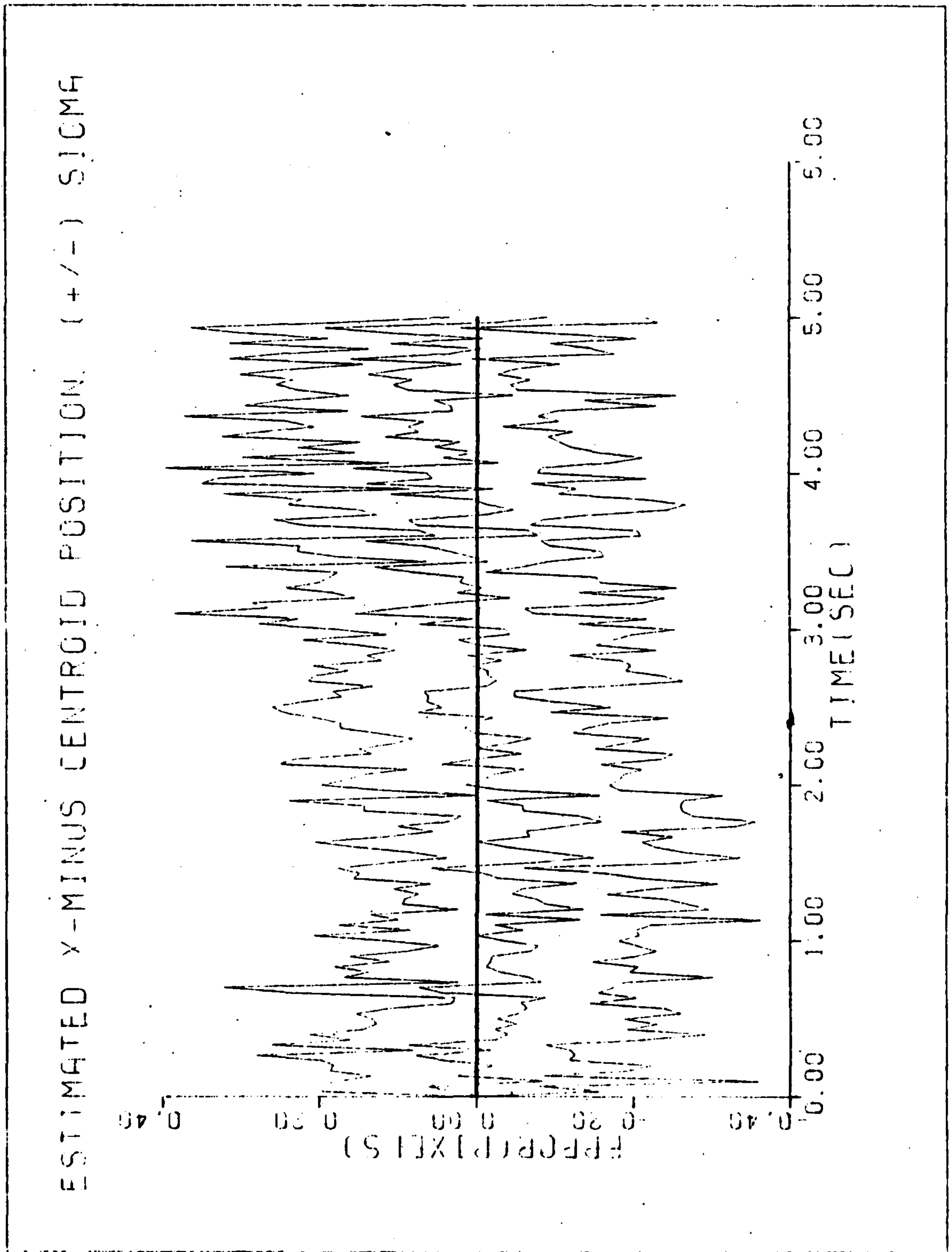

Figure C-3g. Case 3

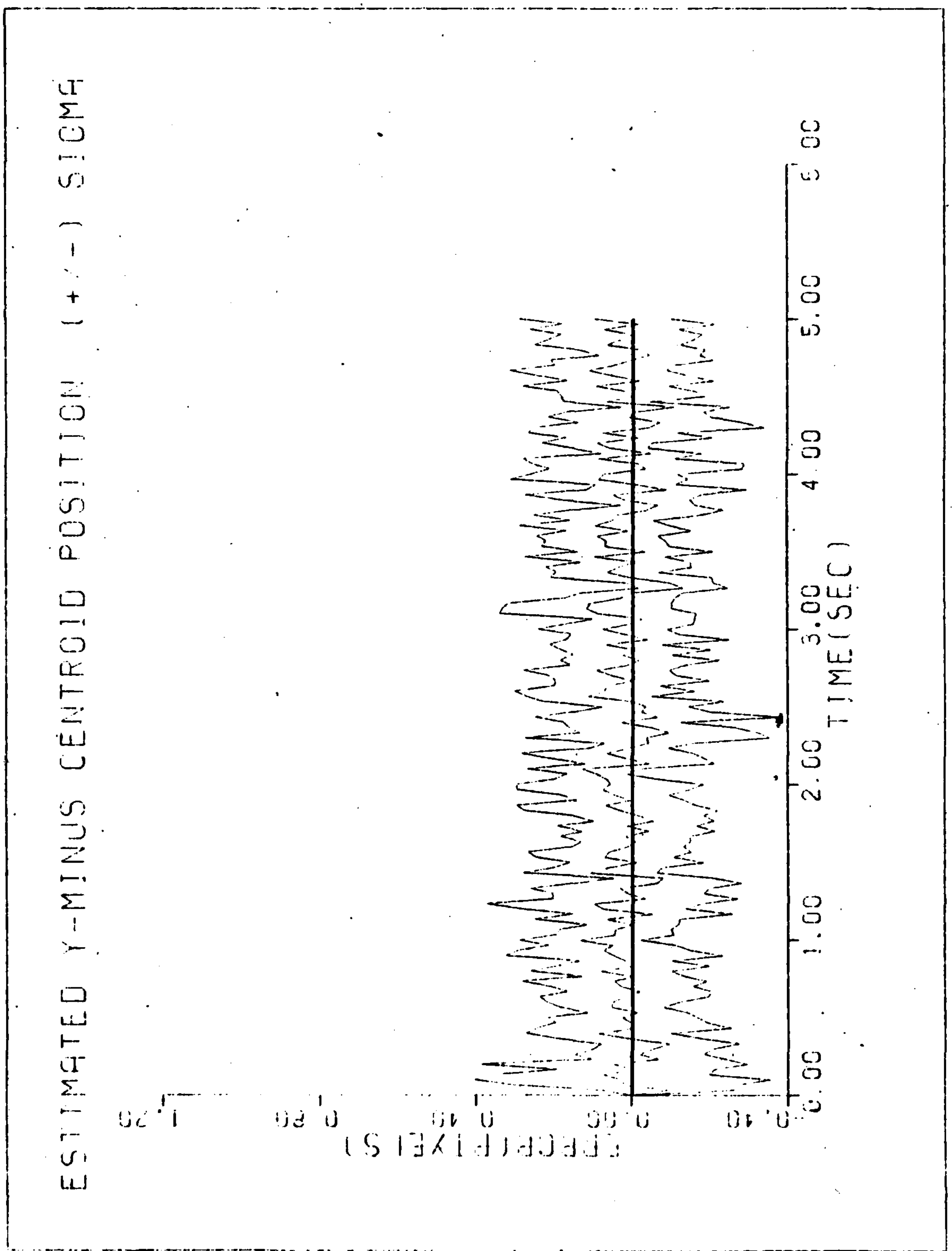

Figure C-3h. Case 3

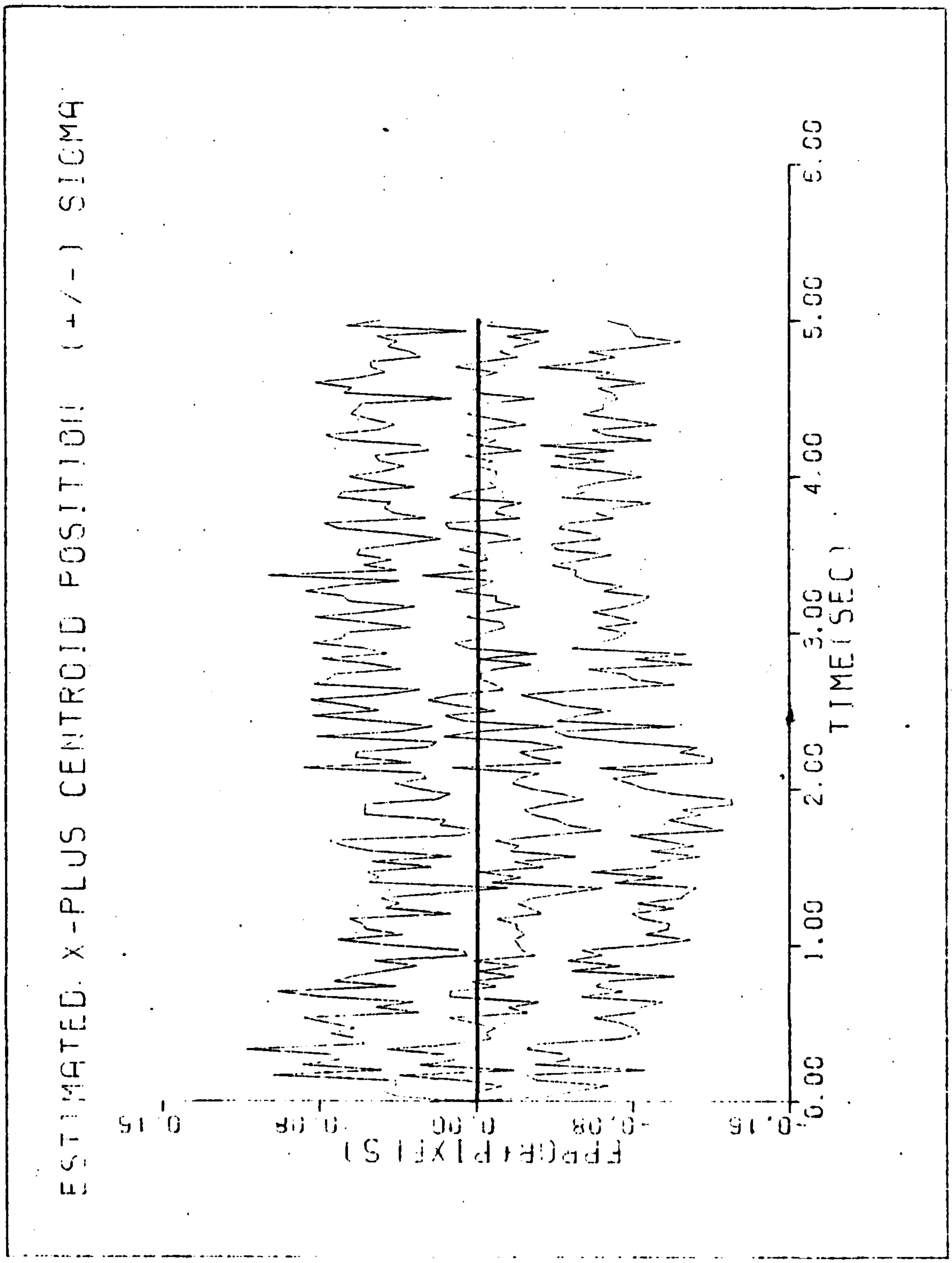

Figur: C-31. Case 3

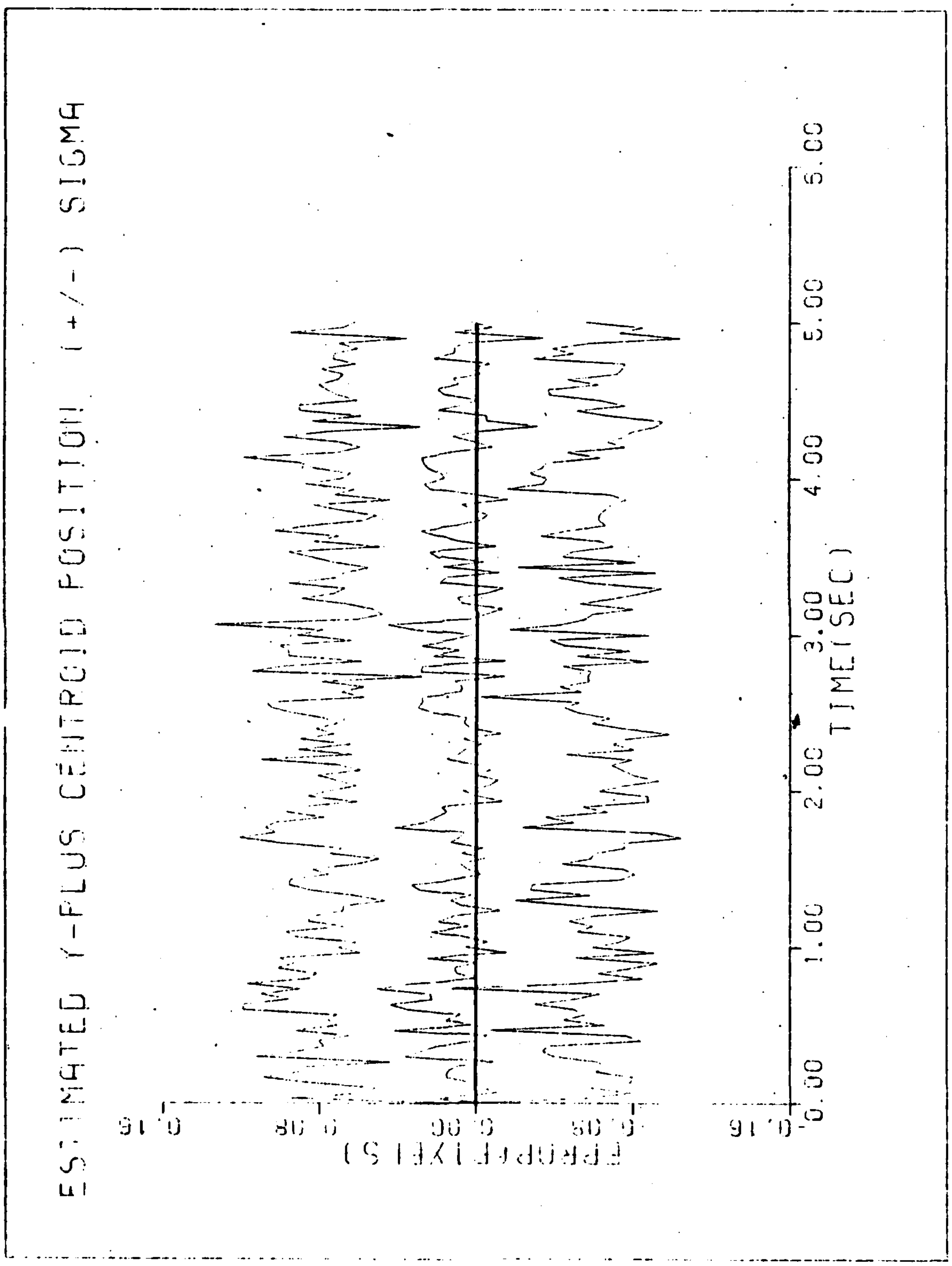

Figure C-3j. Case 3

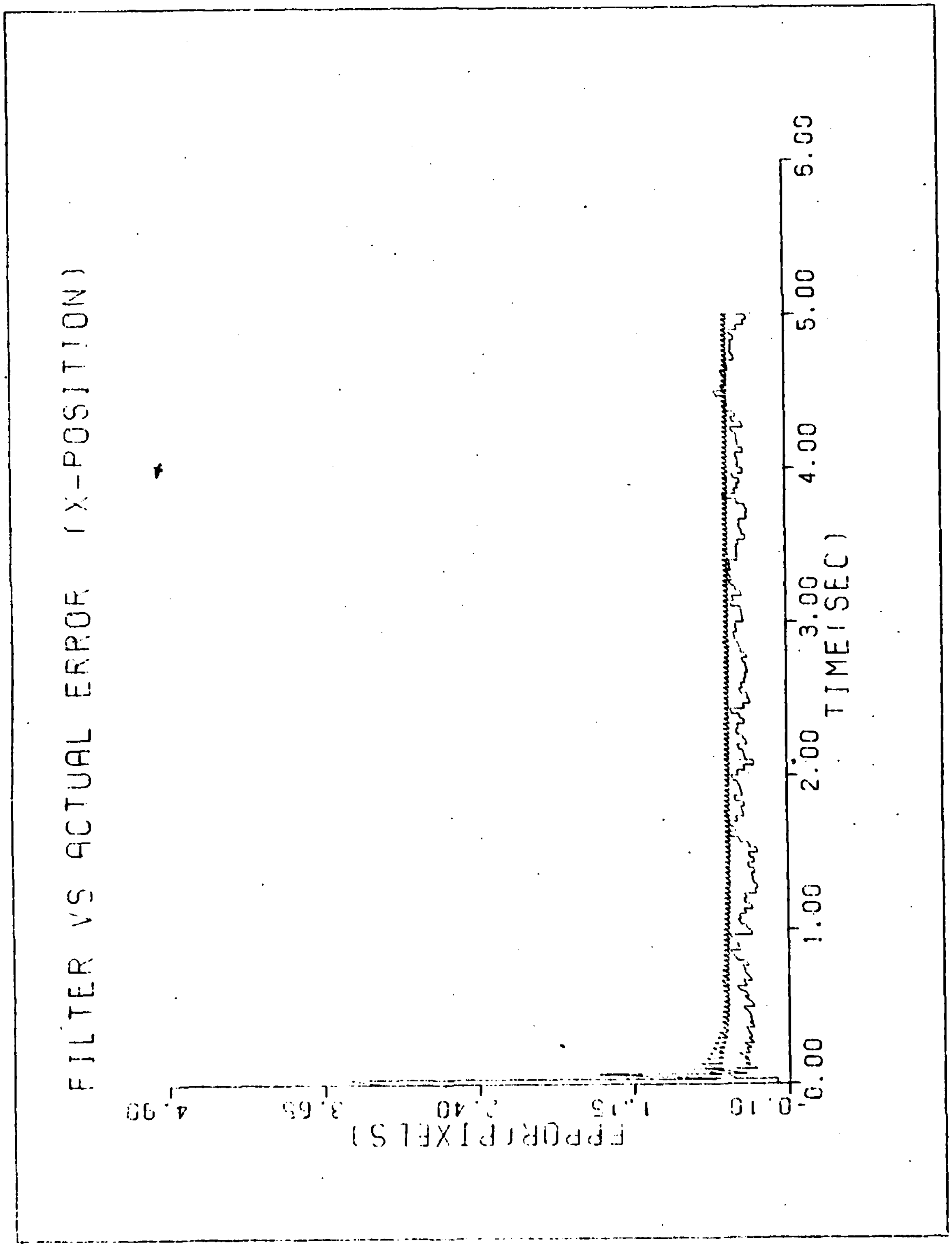

Figure C-4a. Case 4

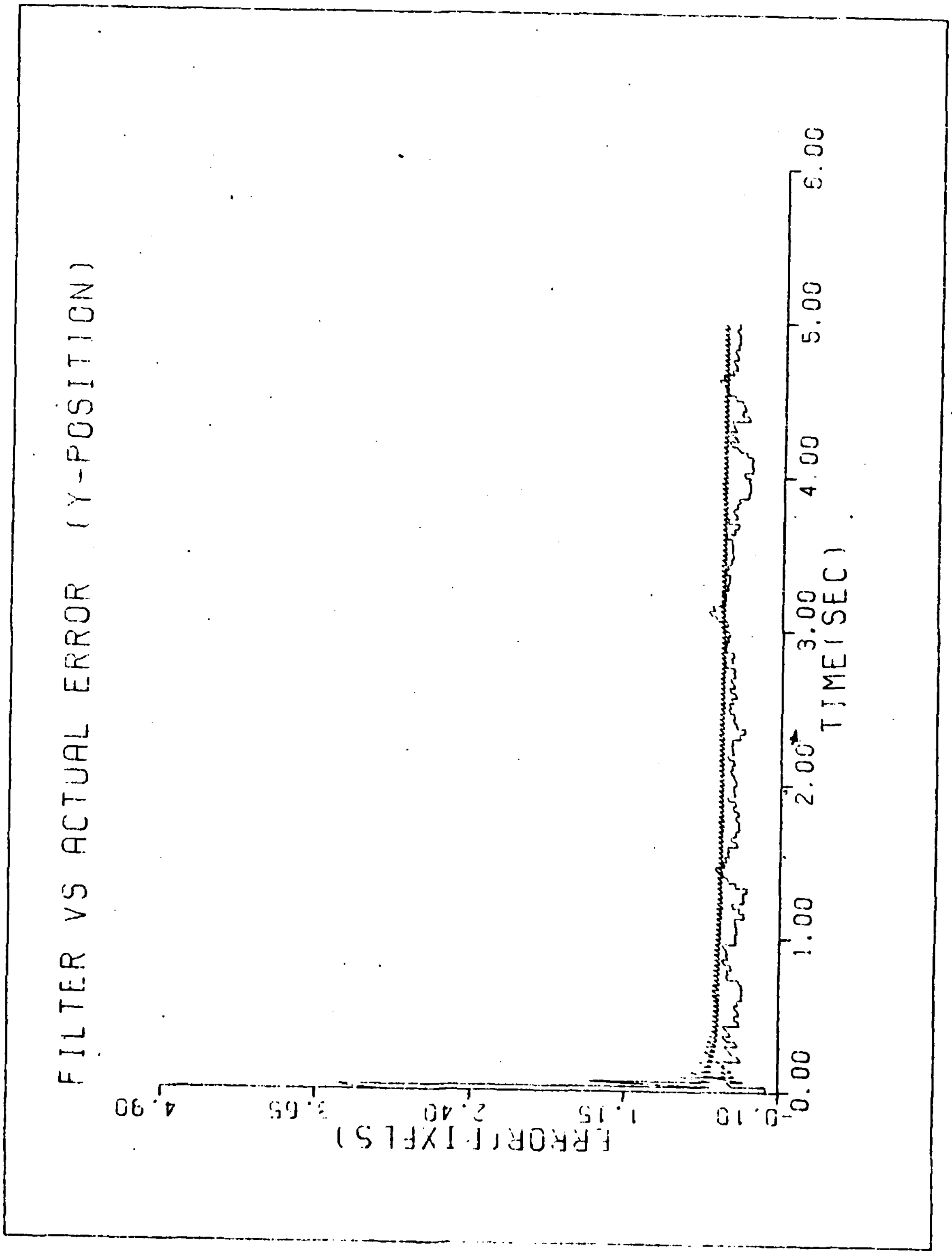

Figure C-4b. Case 4

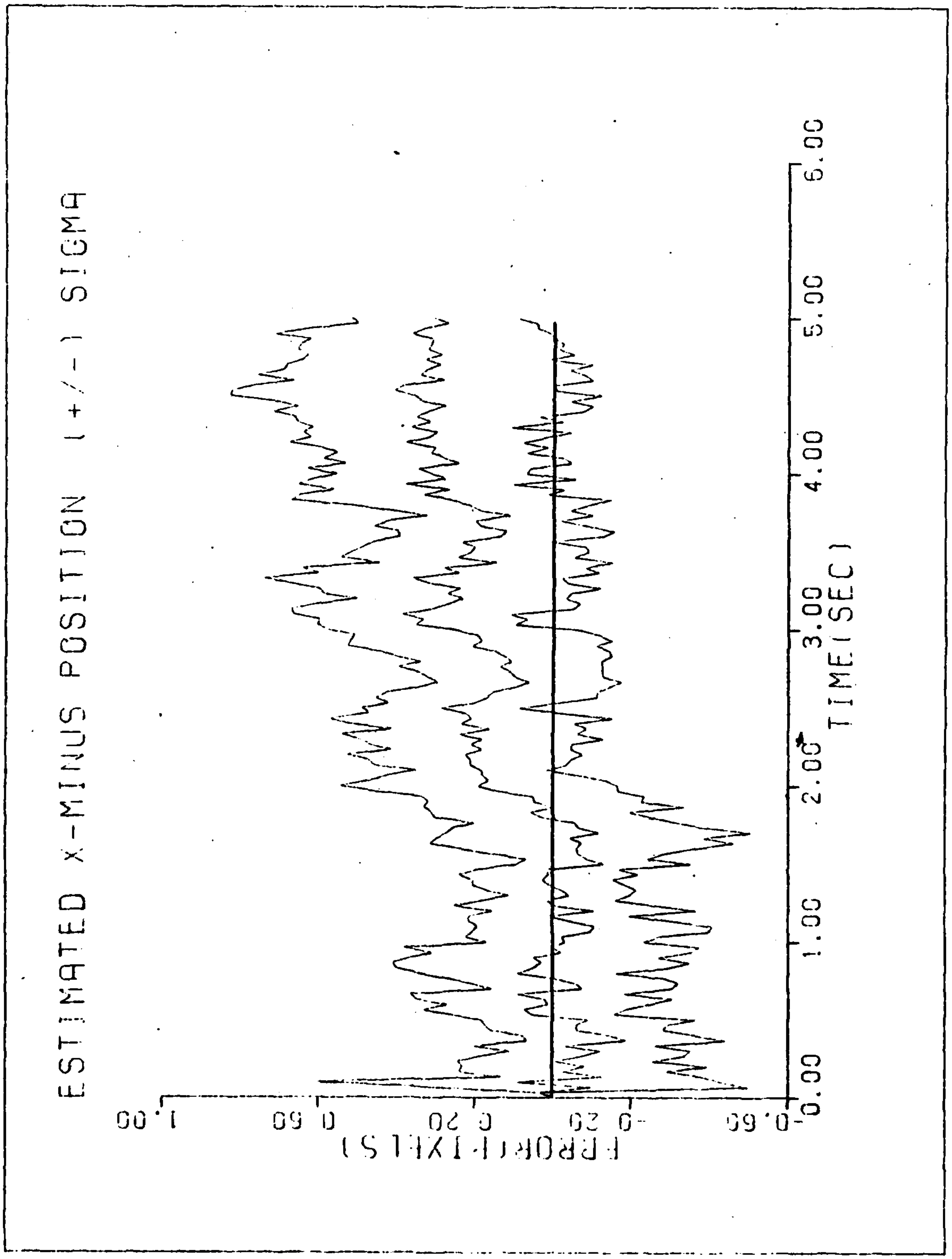

Figure C-4c. Case 4

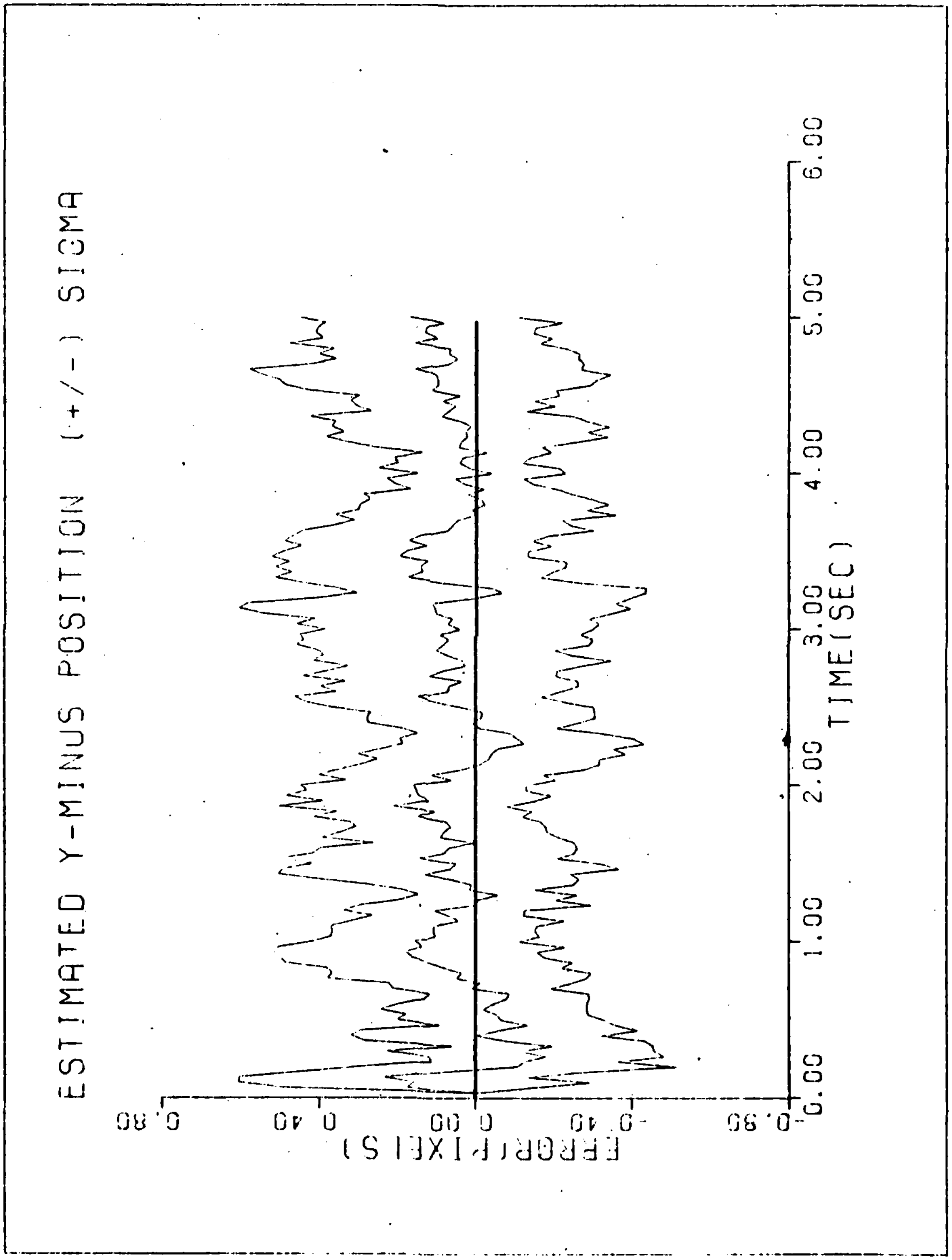

Figure C-4d. Case 4

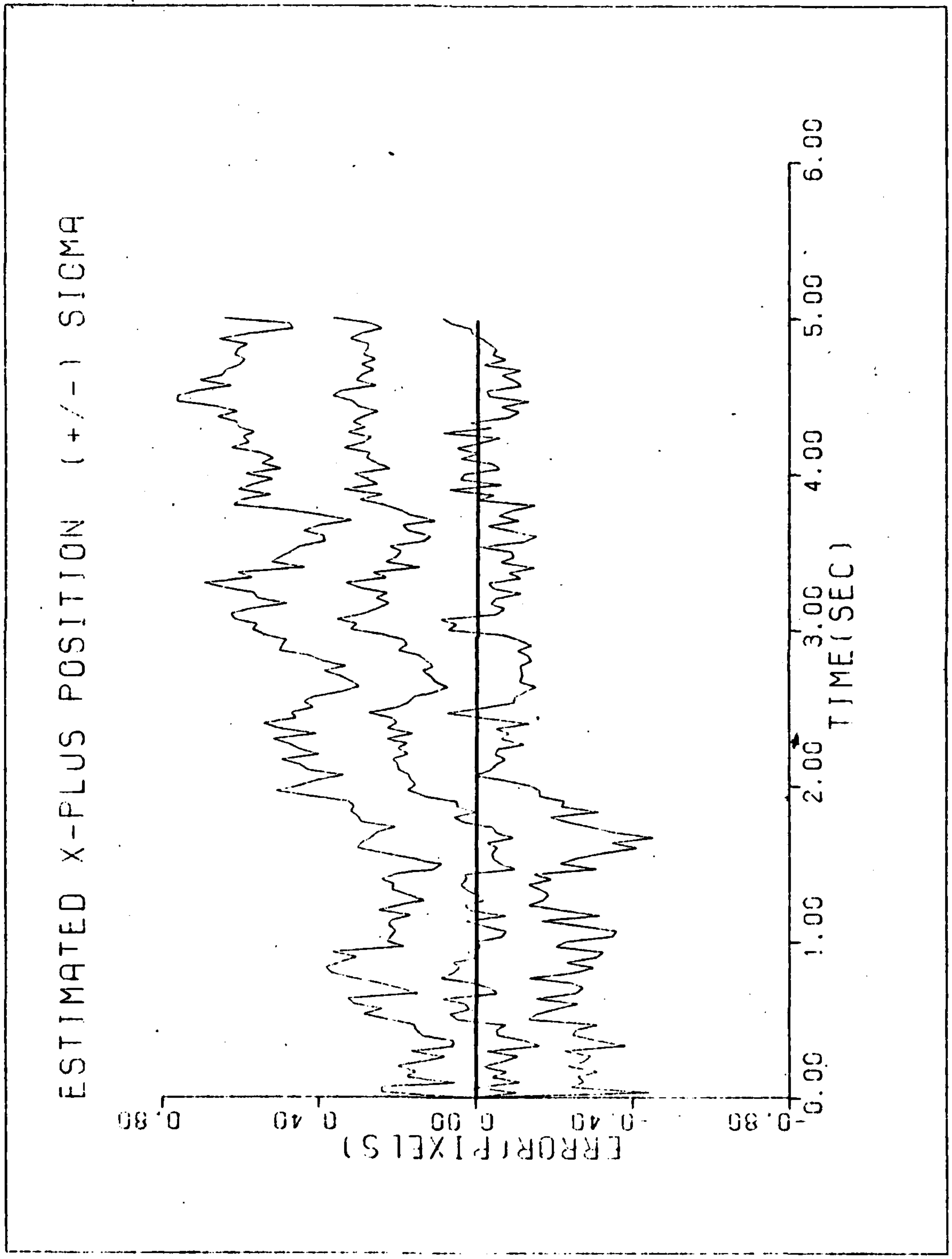

Figure C-4e. Case 4

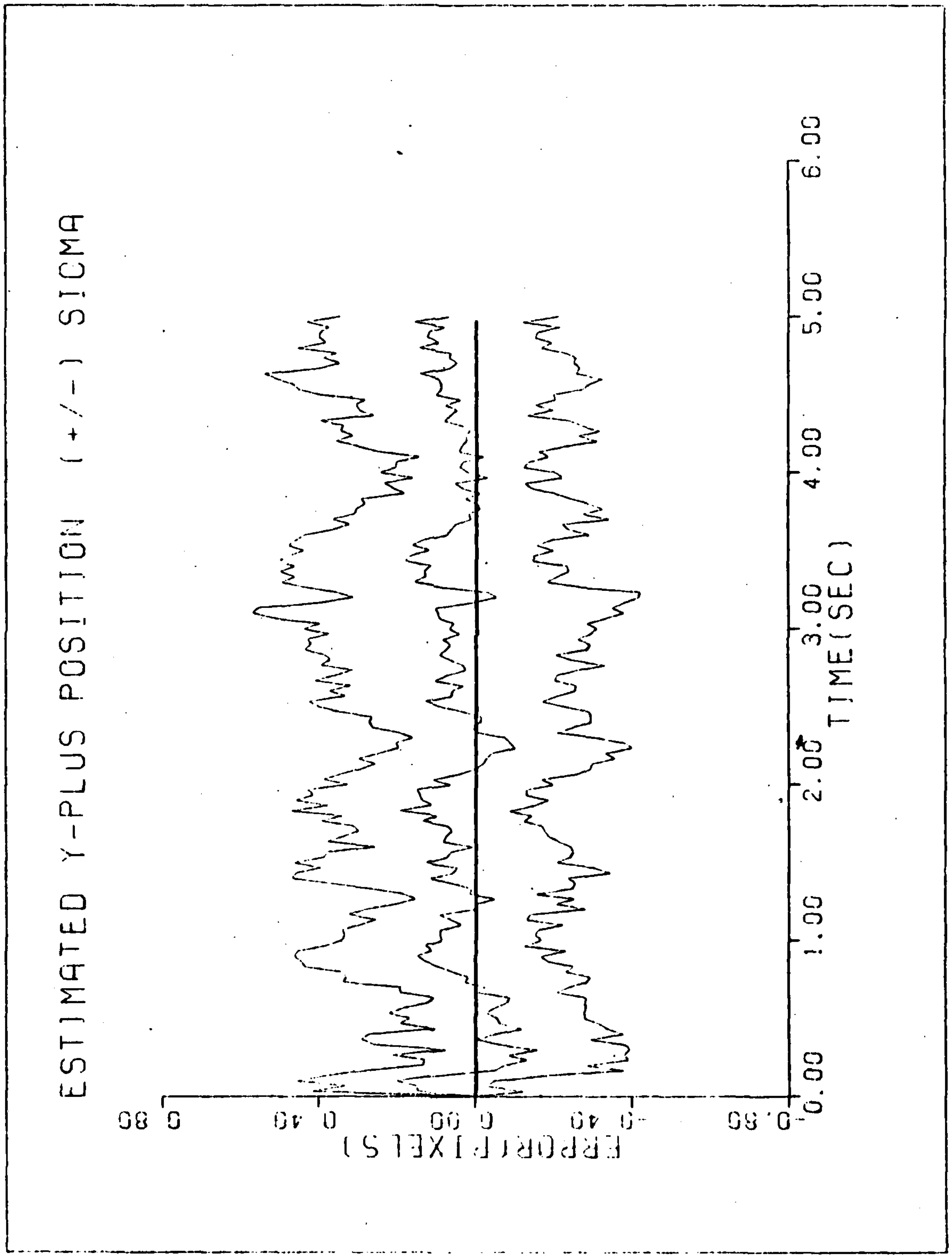

Figure C-4f. Case 4

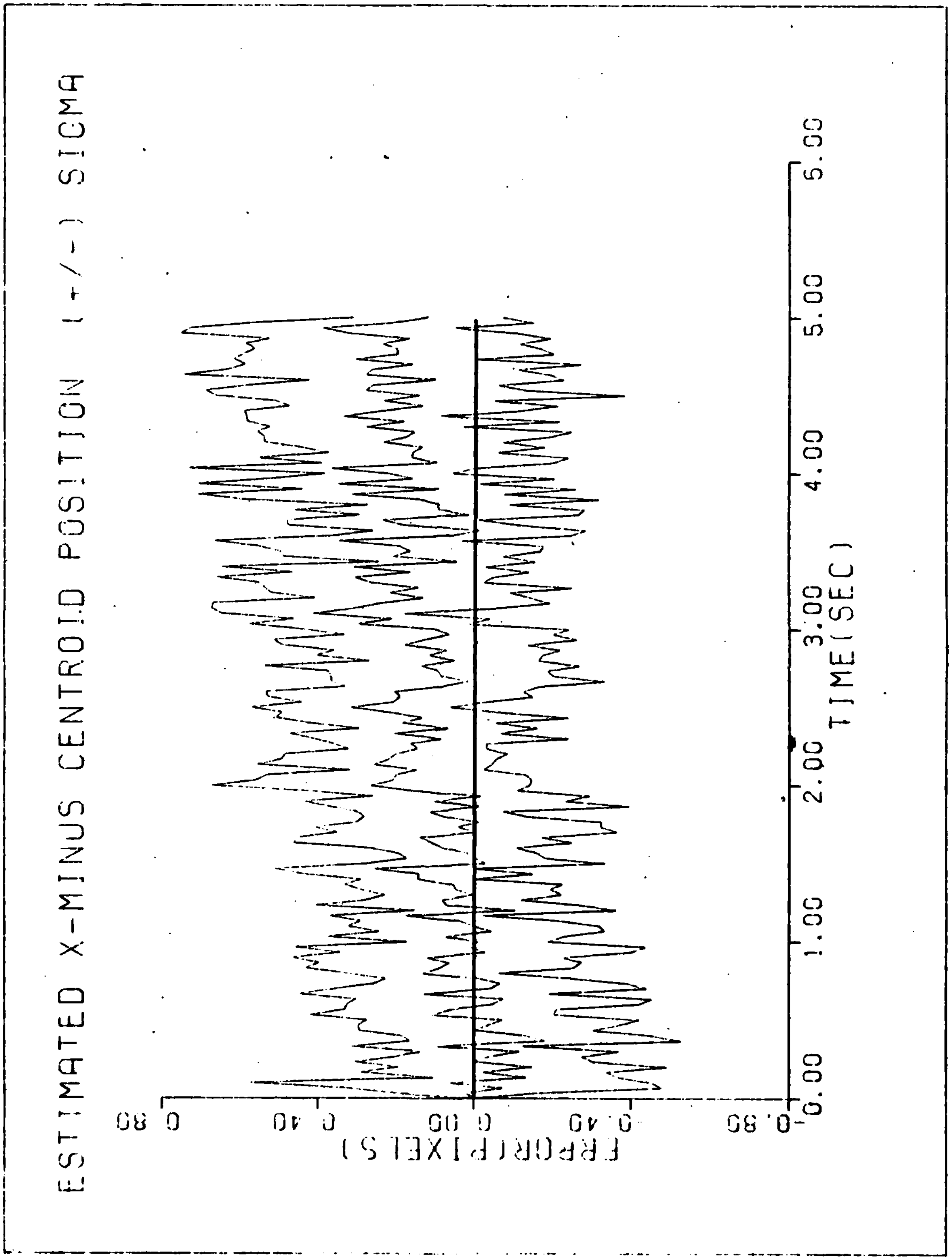

Figure C-4g. Case 4

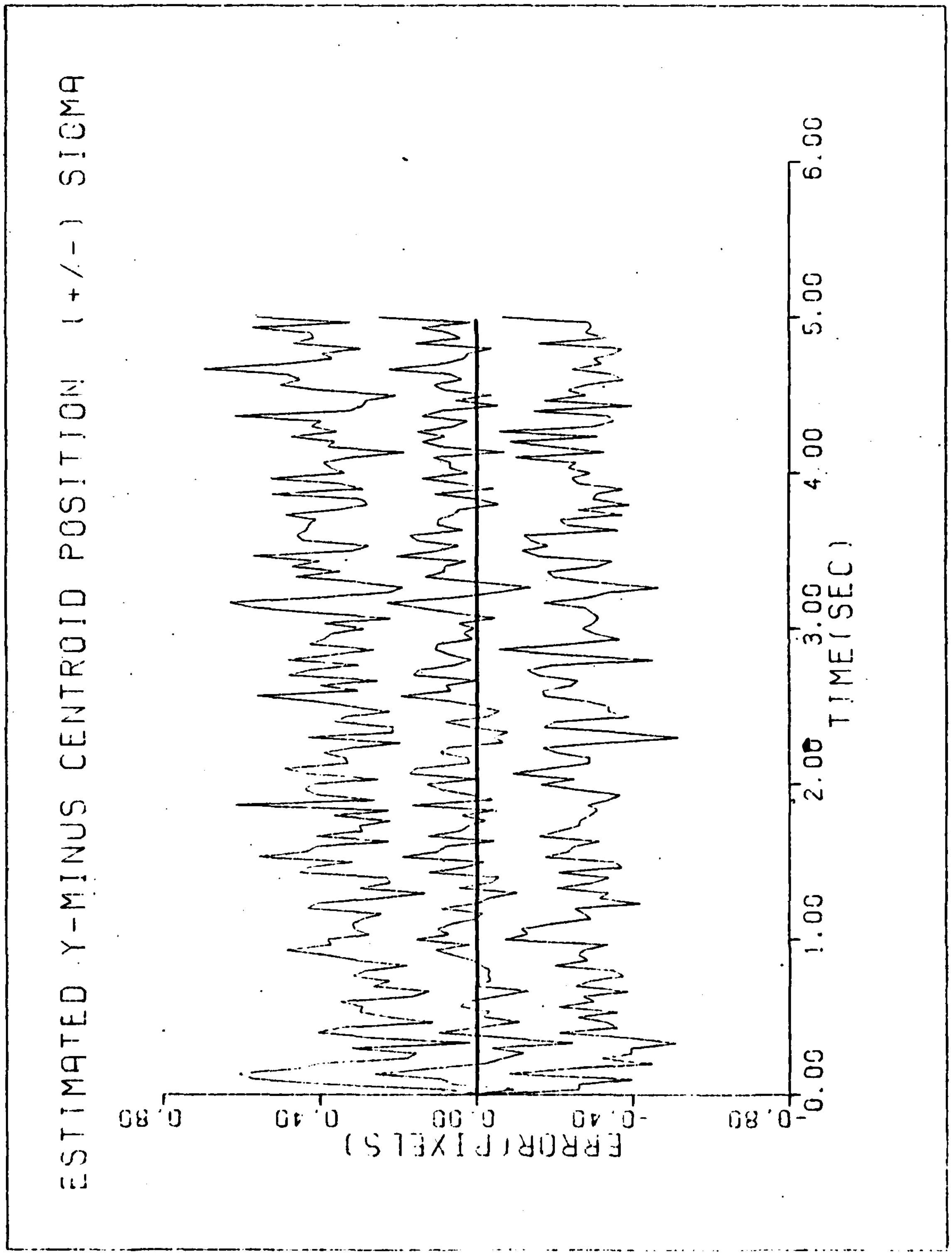

Figure C-4h. Case 4

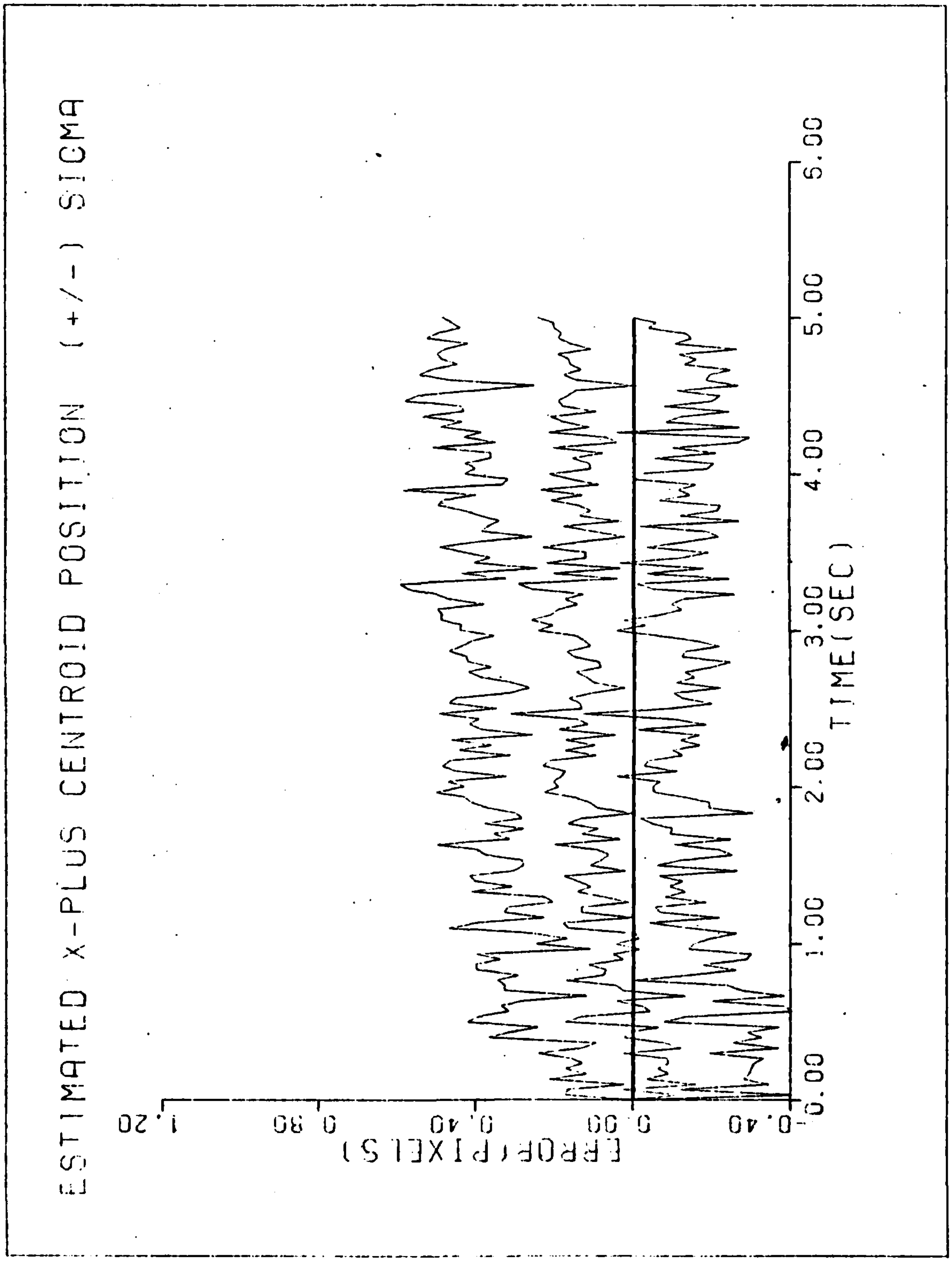

Figure C-4i. Case 4

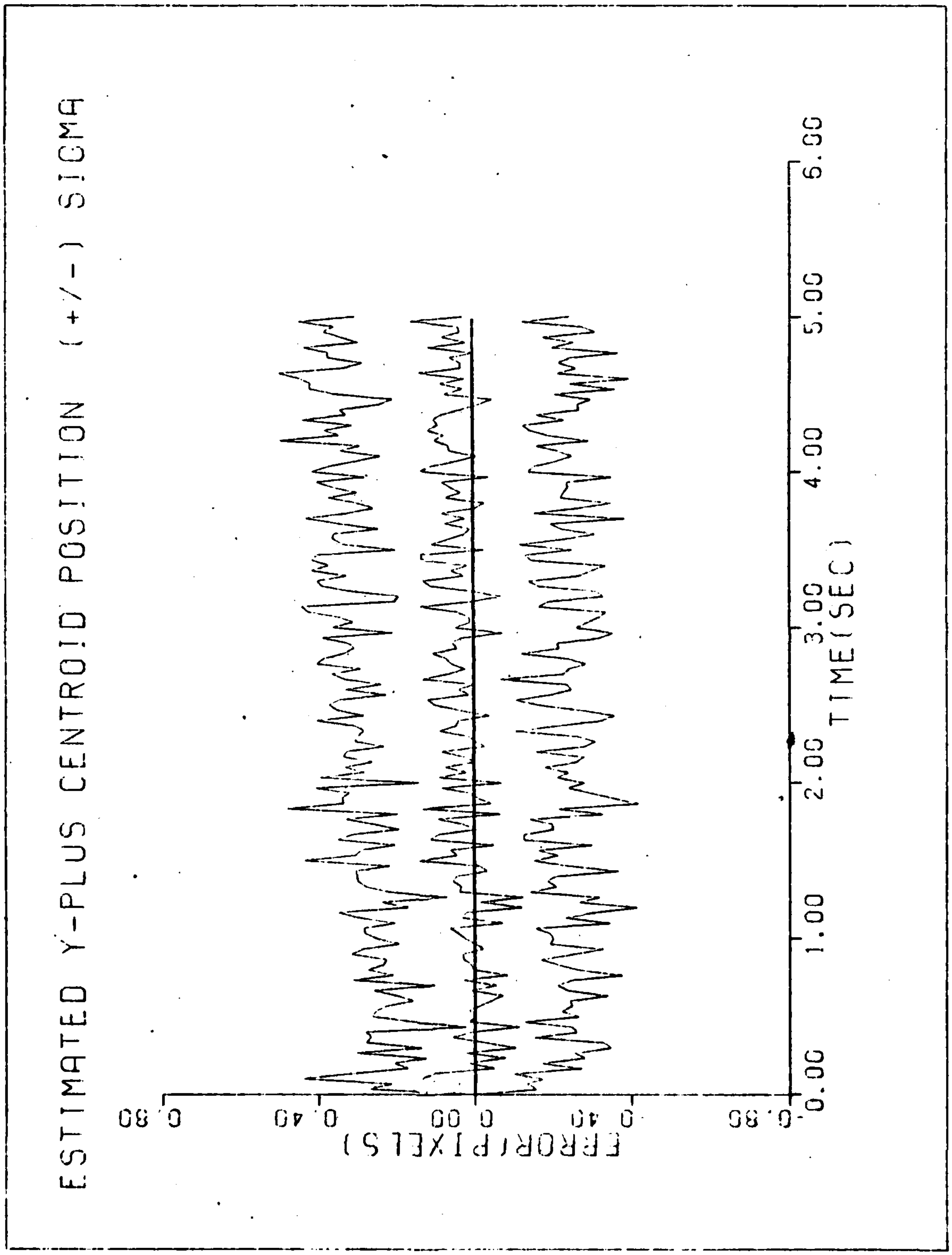

Figure C-4j. Case 4

The performance plots for this case were similar to the plots shown for case 3 and thus are omitted.

Figure C-5. Case 5

The performance plots for this case were similar to the plots shown for case 3, and thus are omitted.

Figure C-6. Case 6

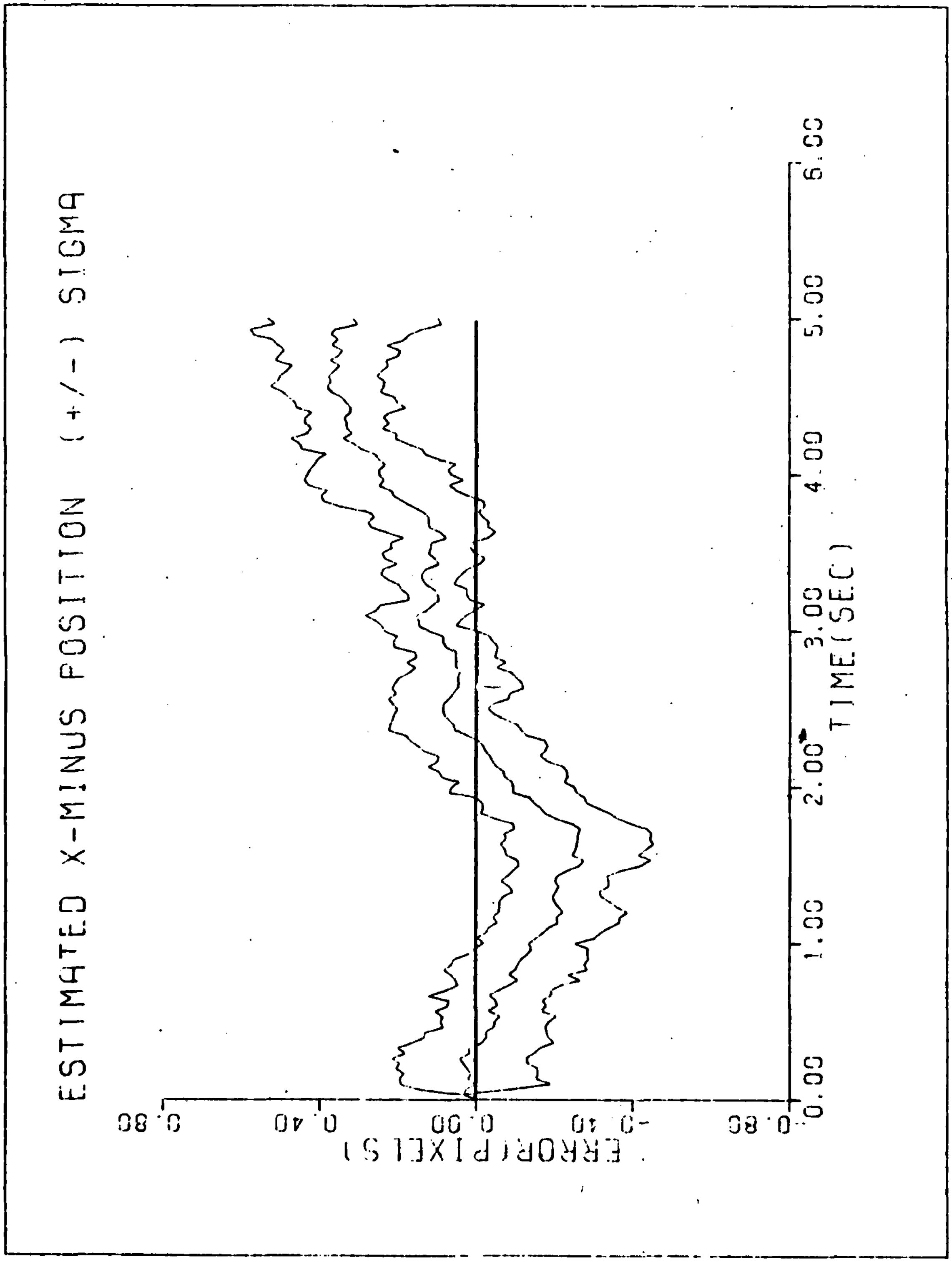

Figure C-7a. Case 7

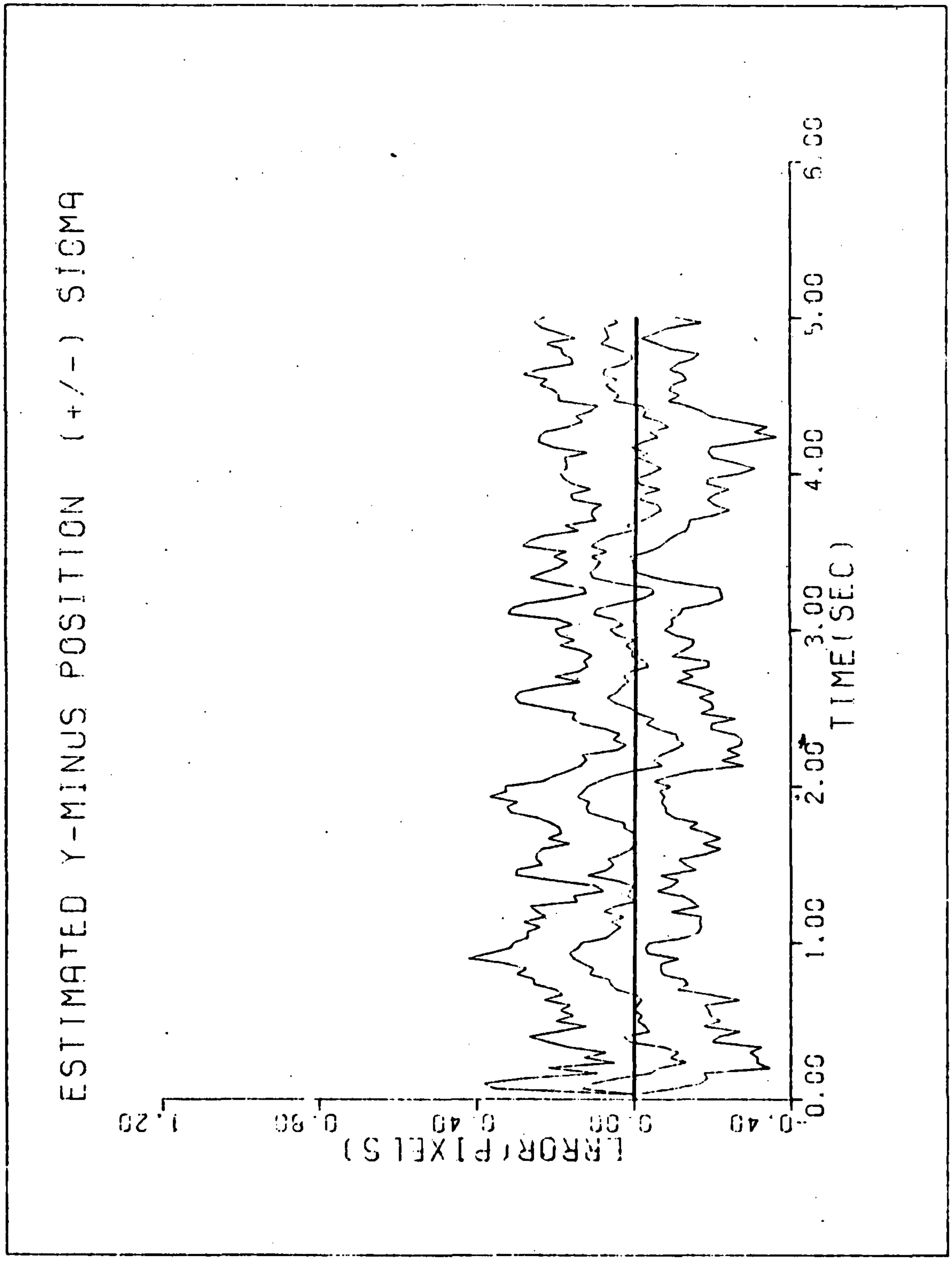

Figure C-7b. Case 7

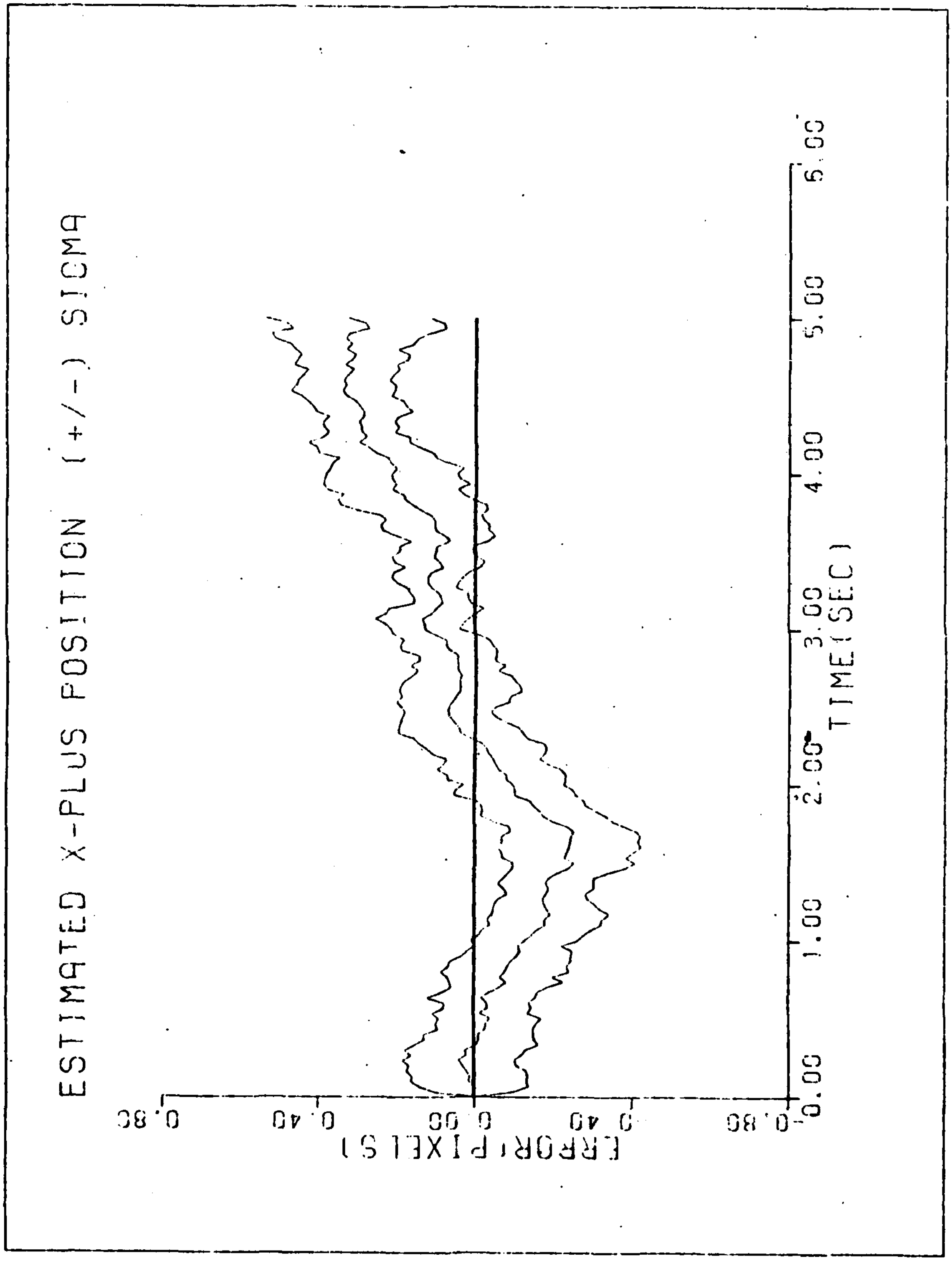

Figure C-7c. Case 7

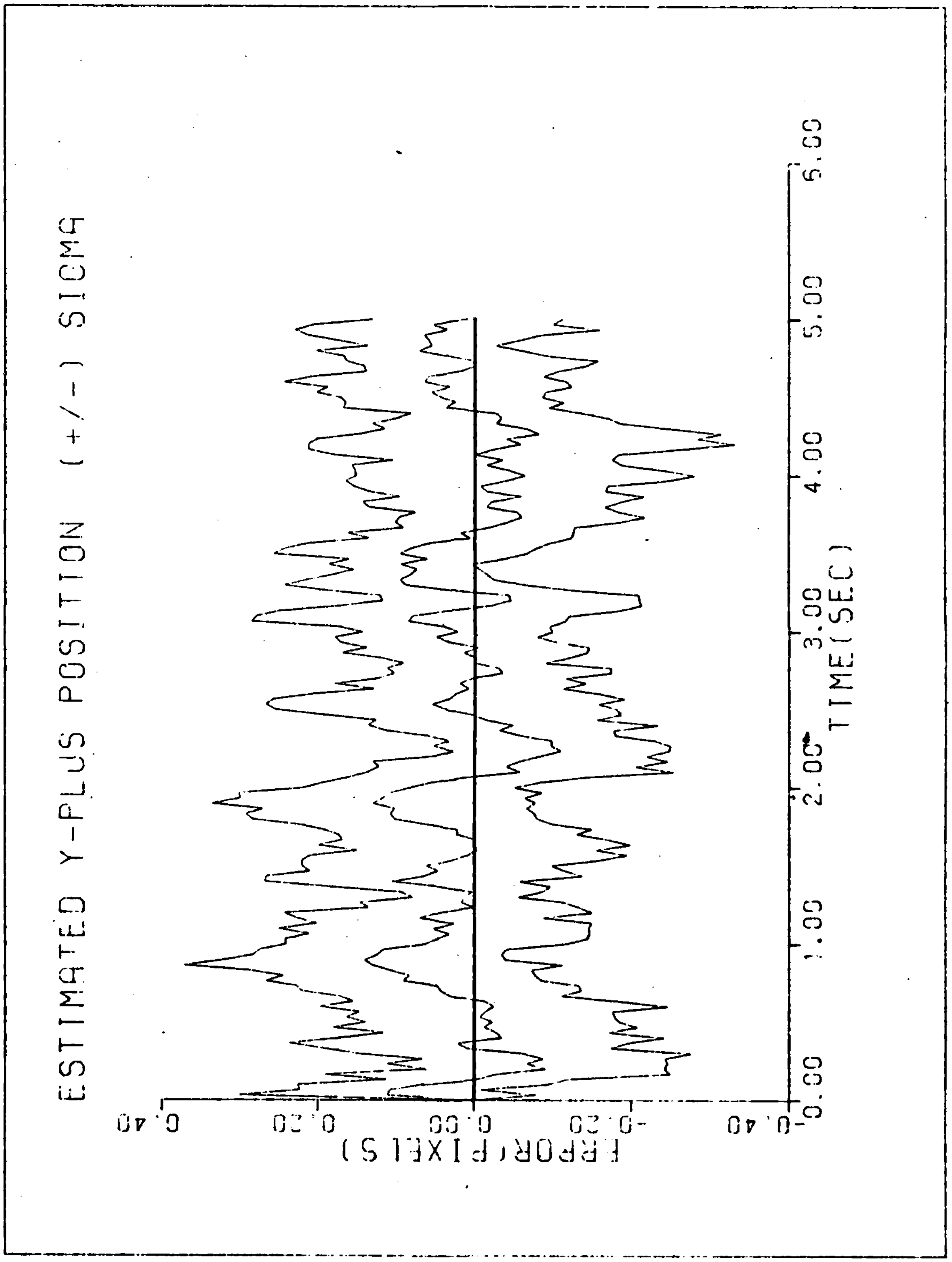

Figure C-7d. Case 7

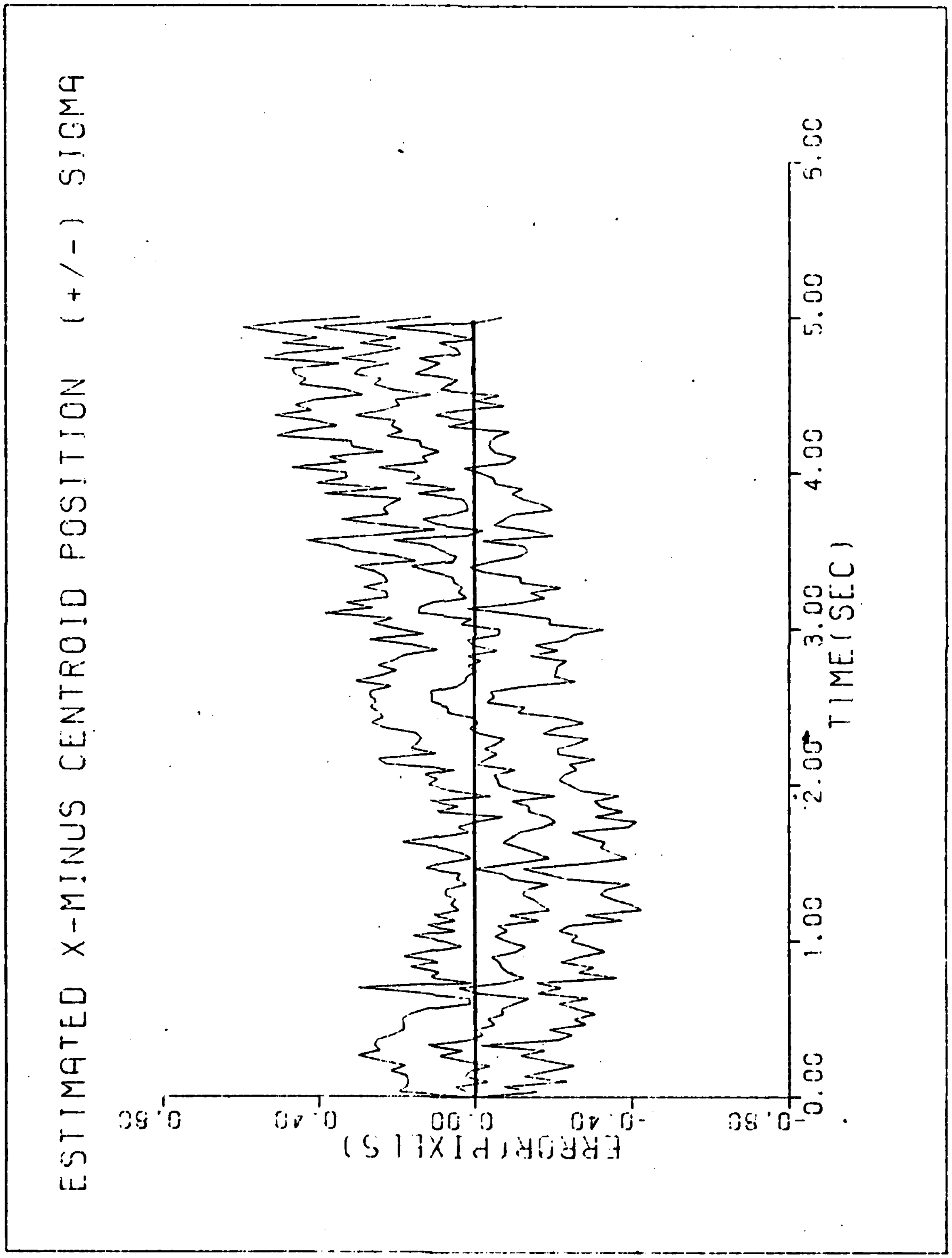

Figure C-7e. Case 7

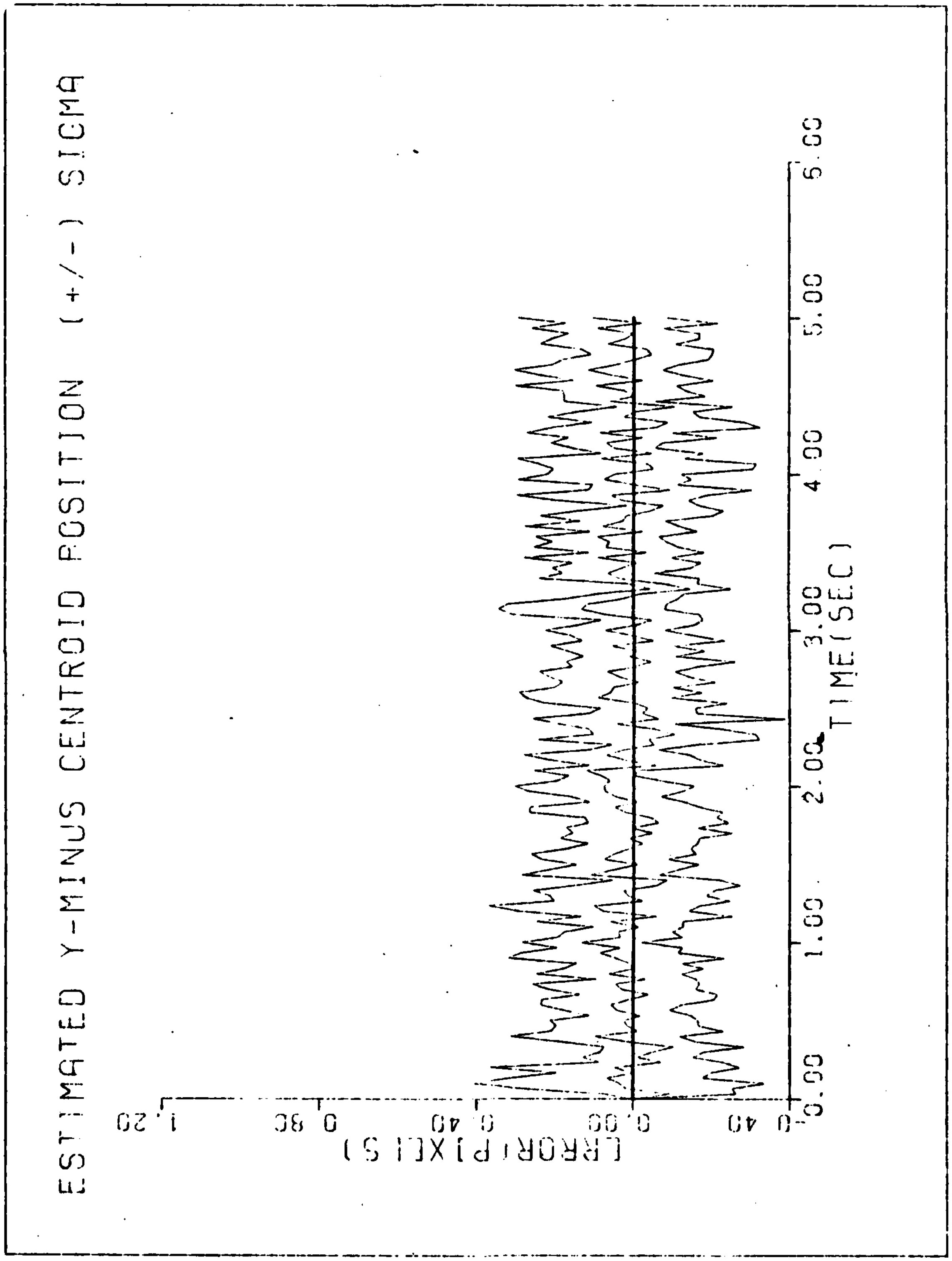

Figure C-7f. Case 7

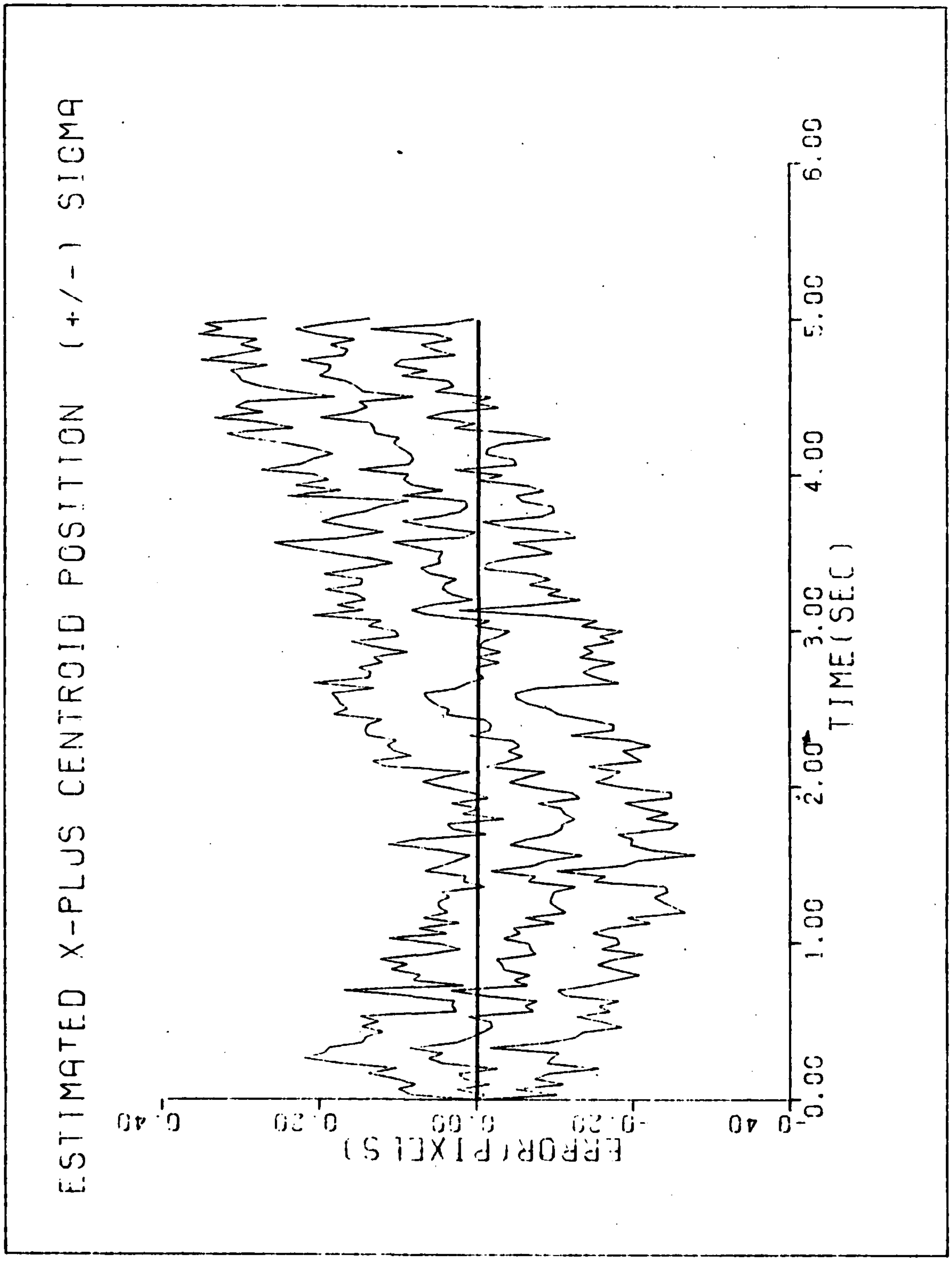

Figure C-7g. Case 7

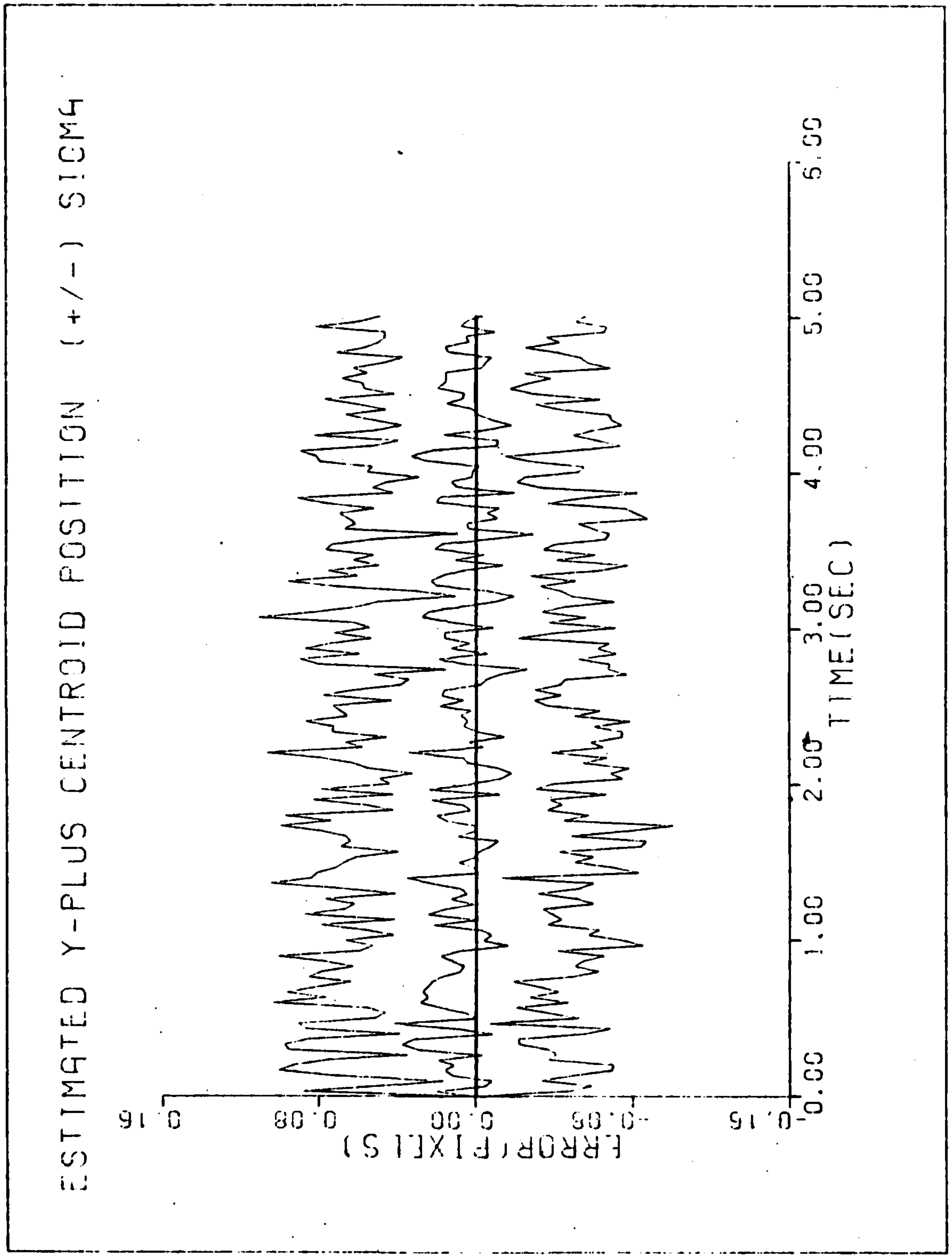

Figure C-7h. Case 7

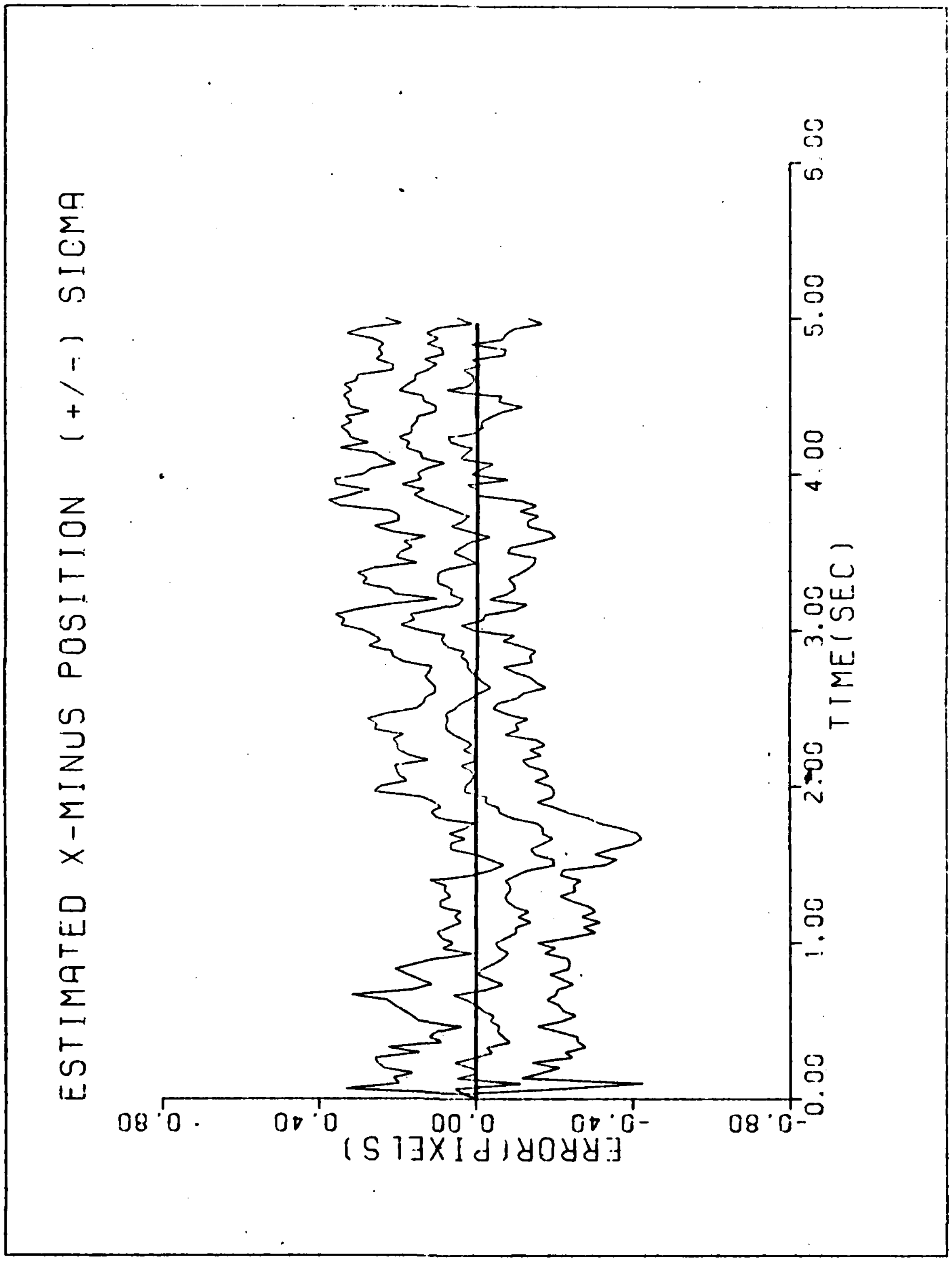

Figure C-8a. Case 8

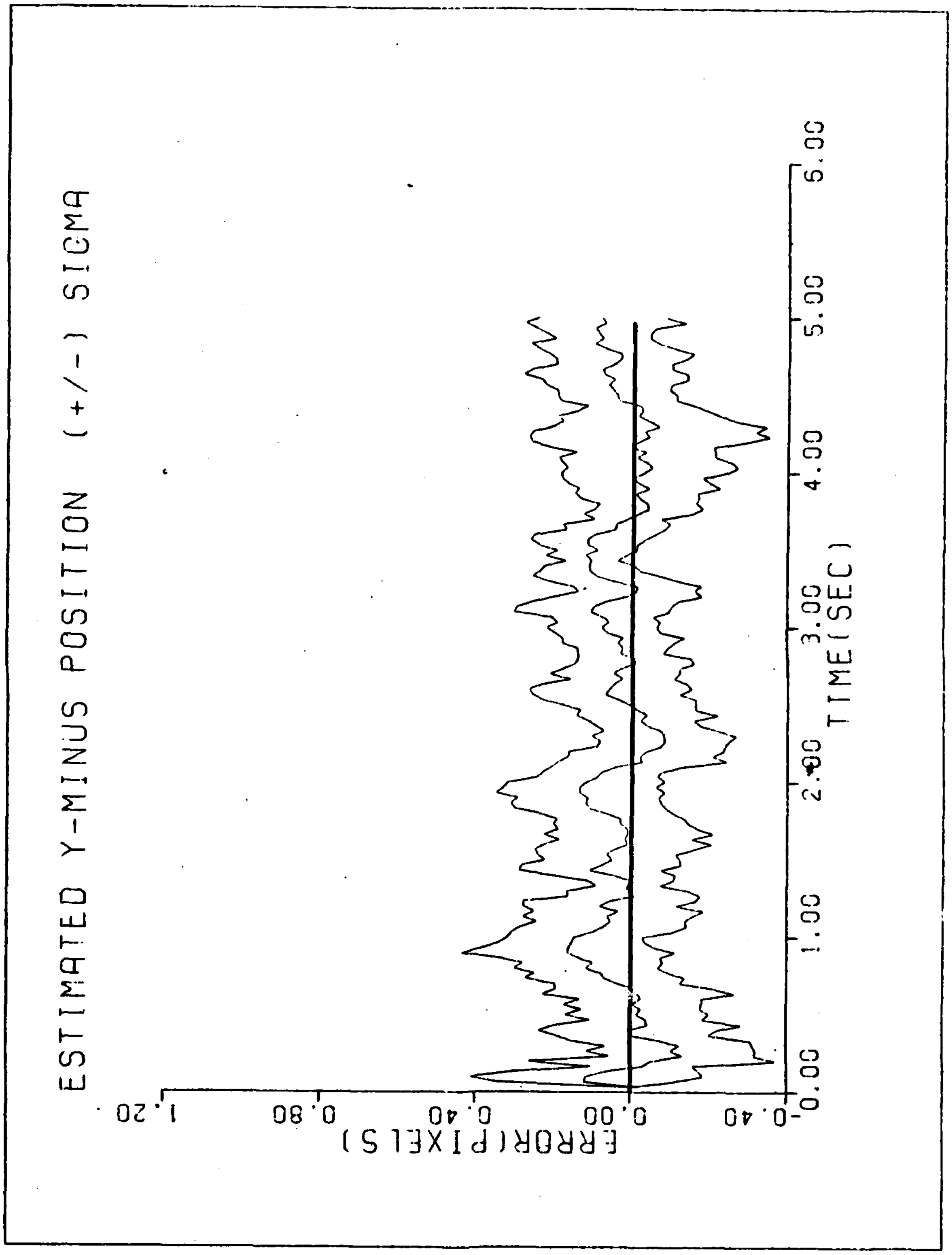

Figure C-8b. Case 8

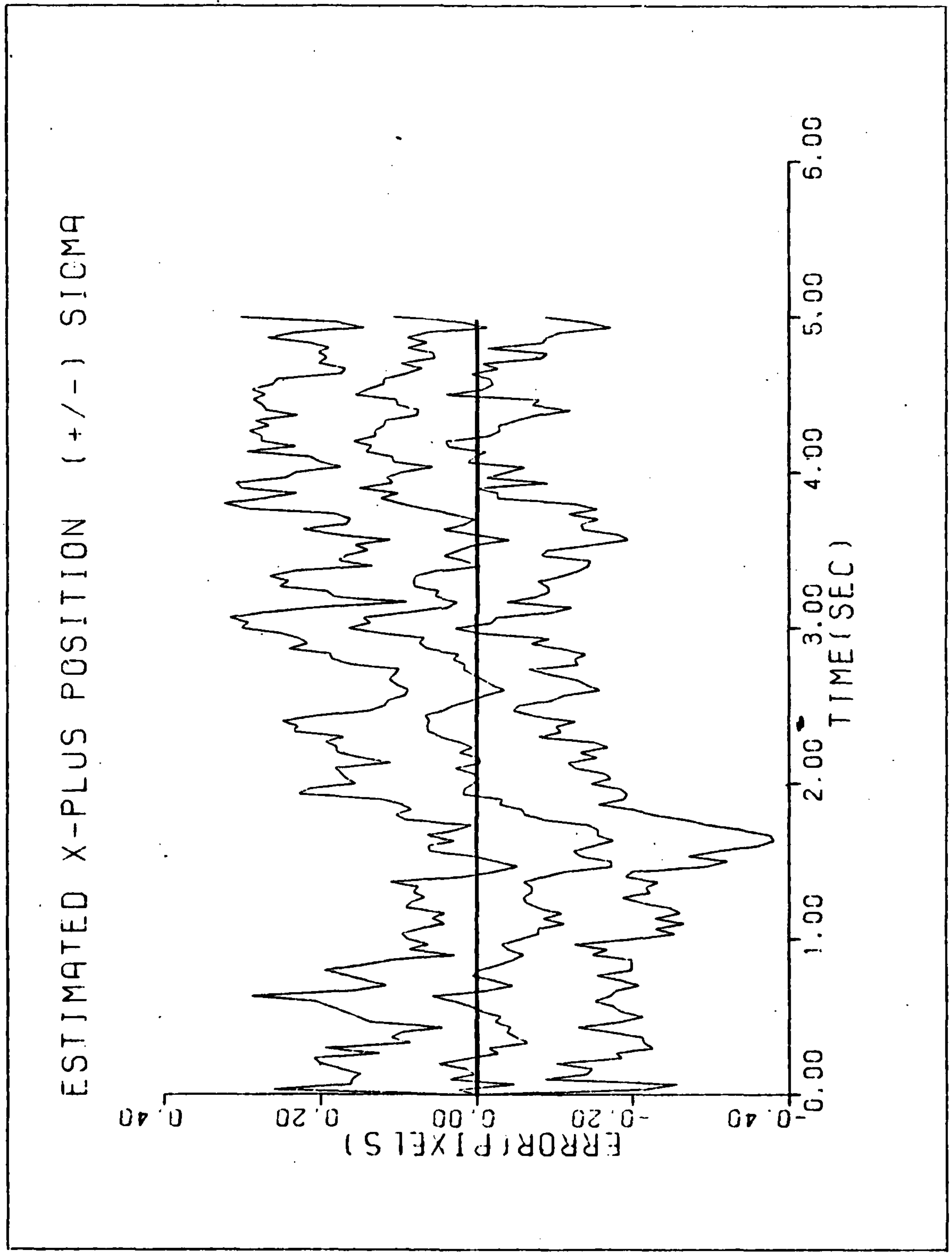

Figure C-8c. Case 8

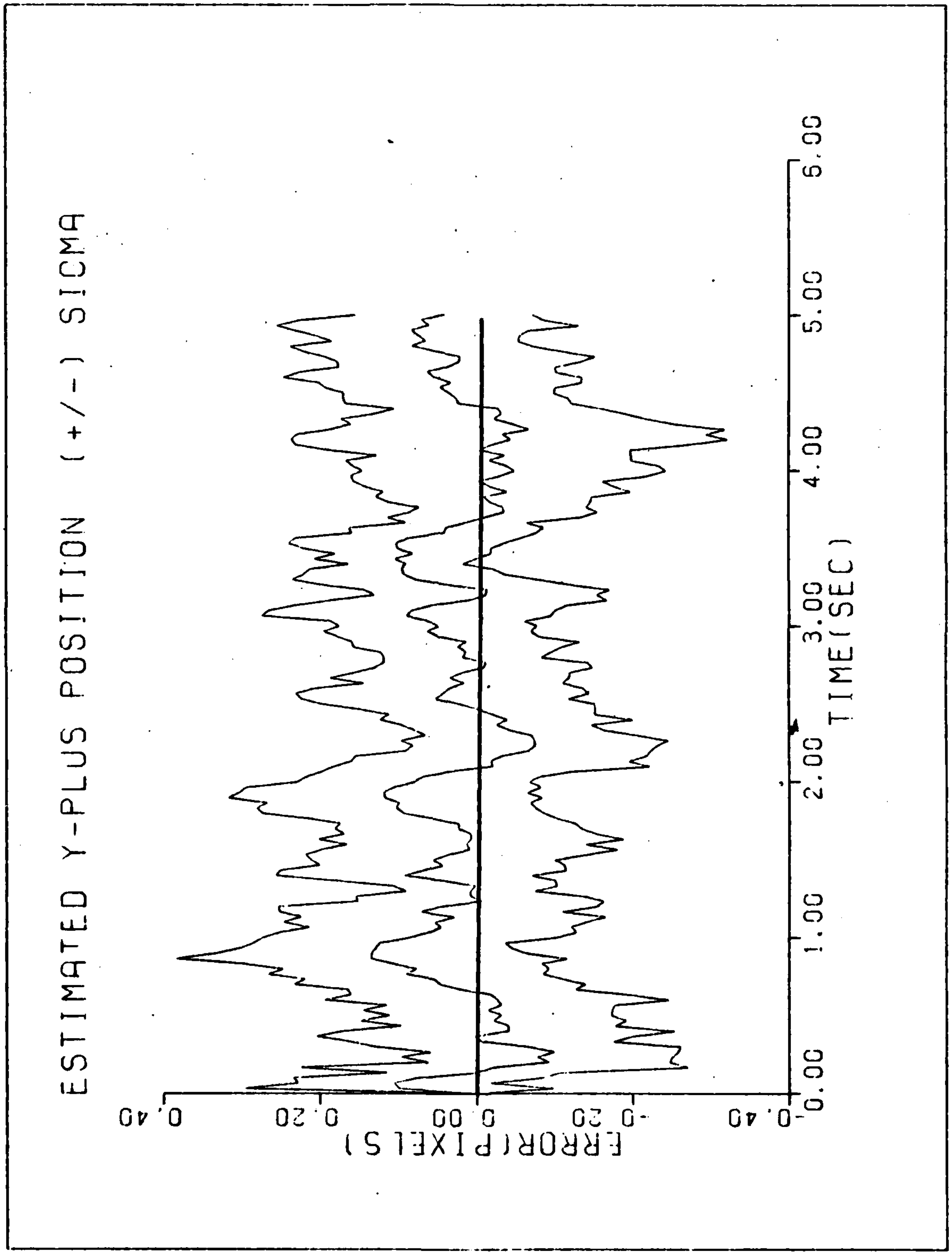

Figure C-8d. Case 8

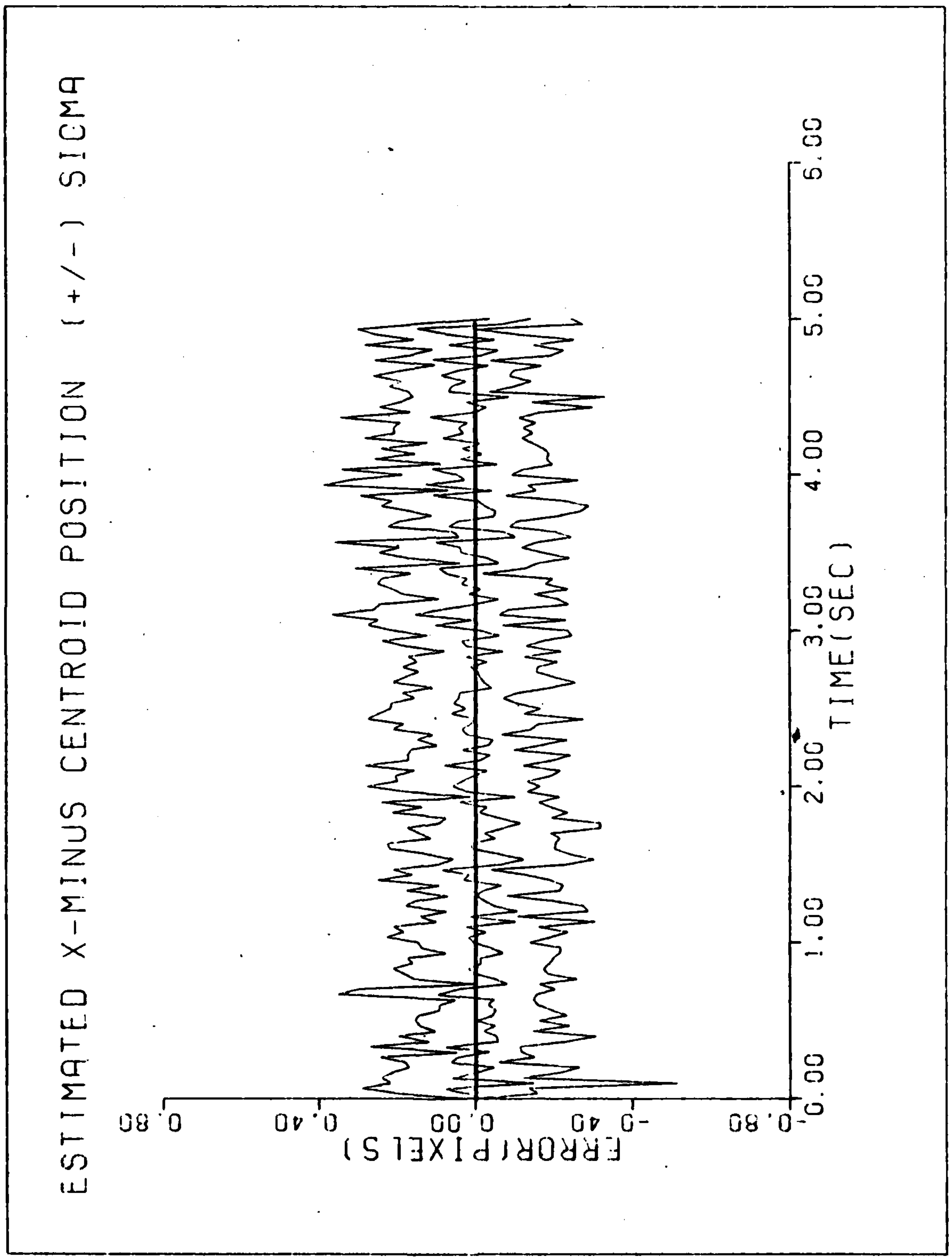

Figure C-8e. Case 8

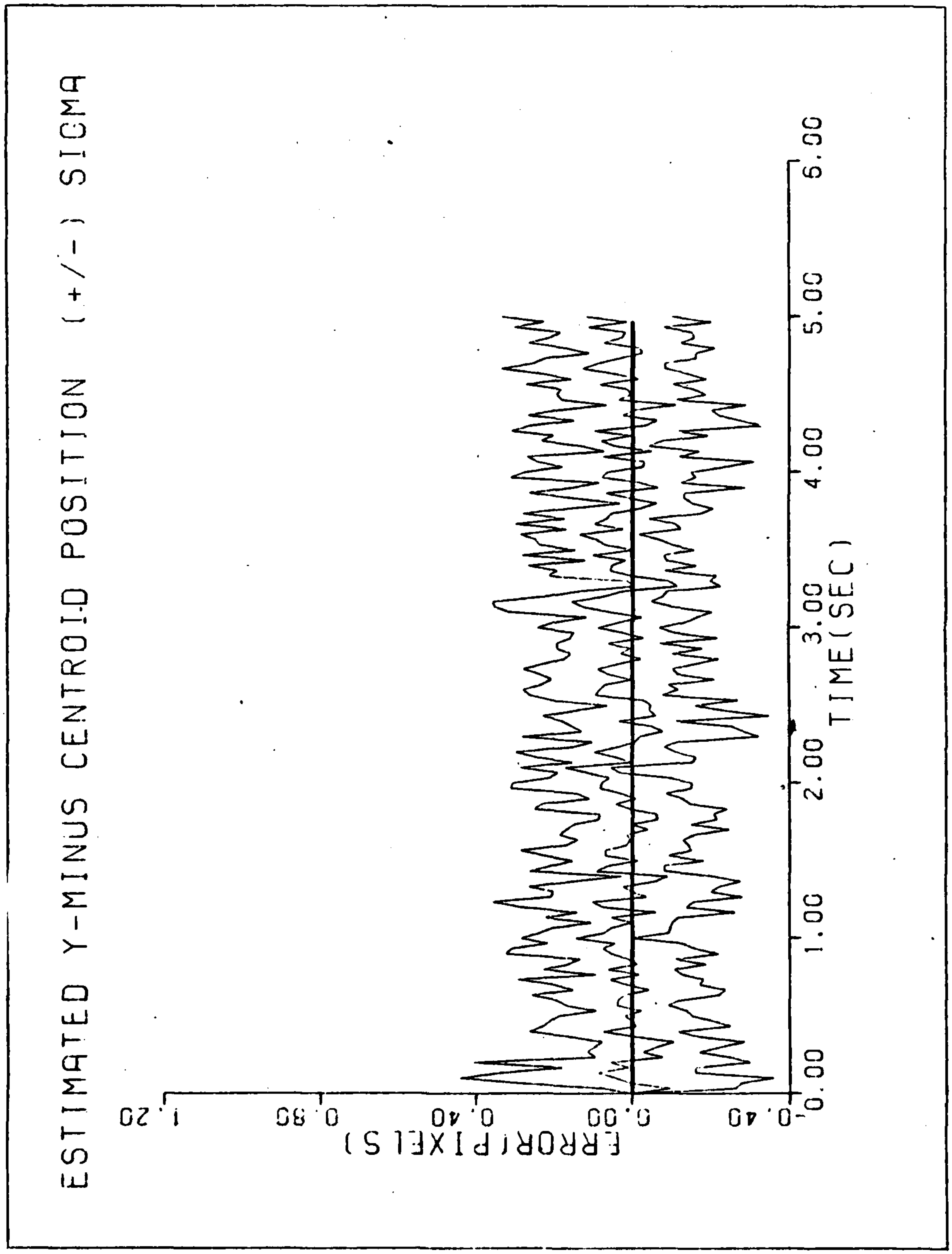

Figure C-8f. Case 8

The performance plots for this case were similar to the plots shown for case 8, and thus are omitted.

Figure C-9. Case 9

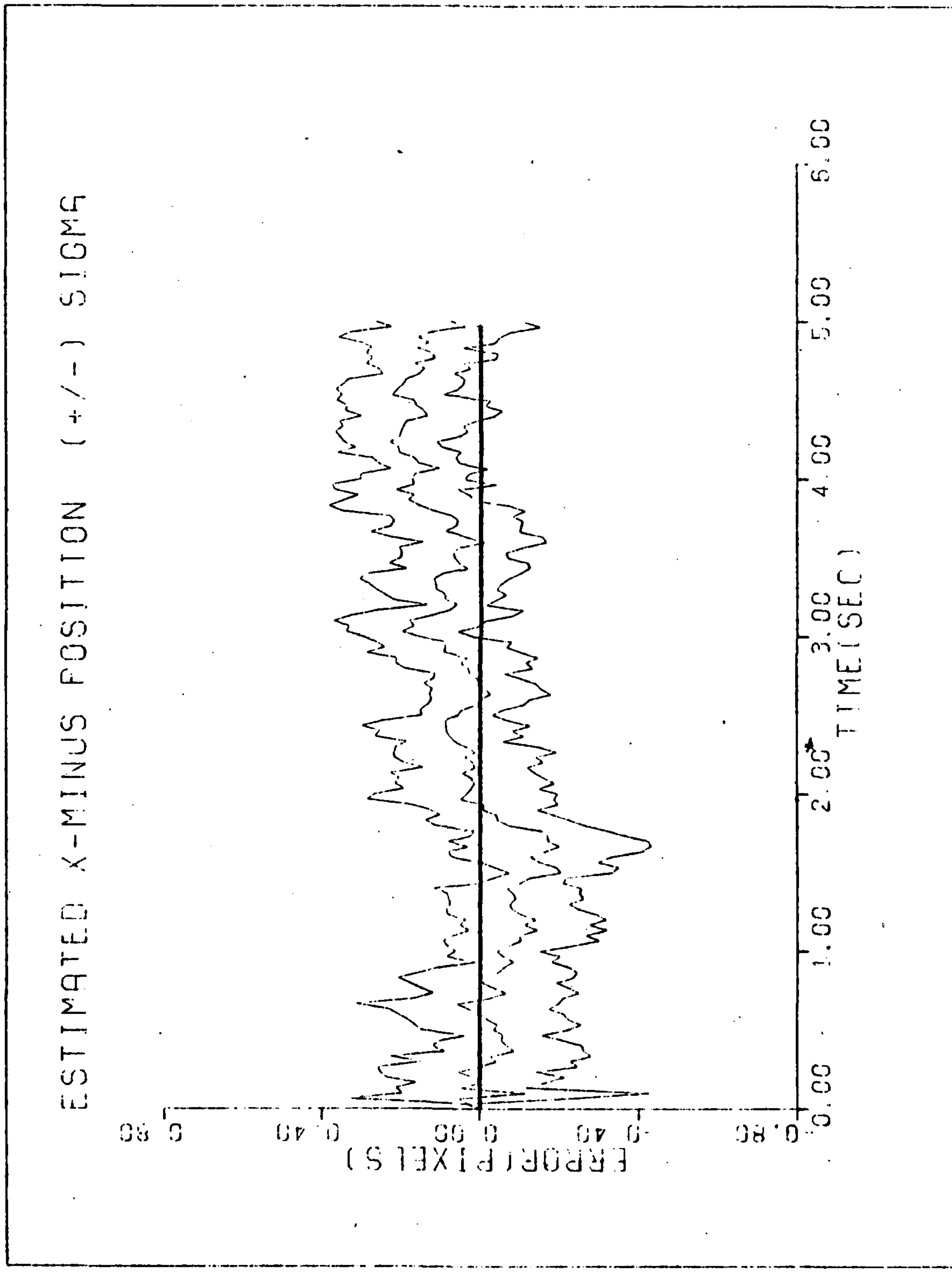

Figure C-10a. Case 10

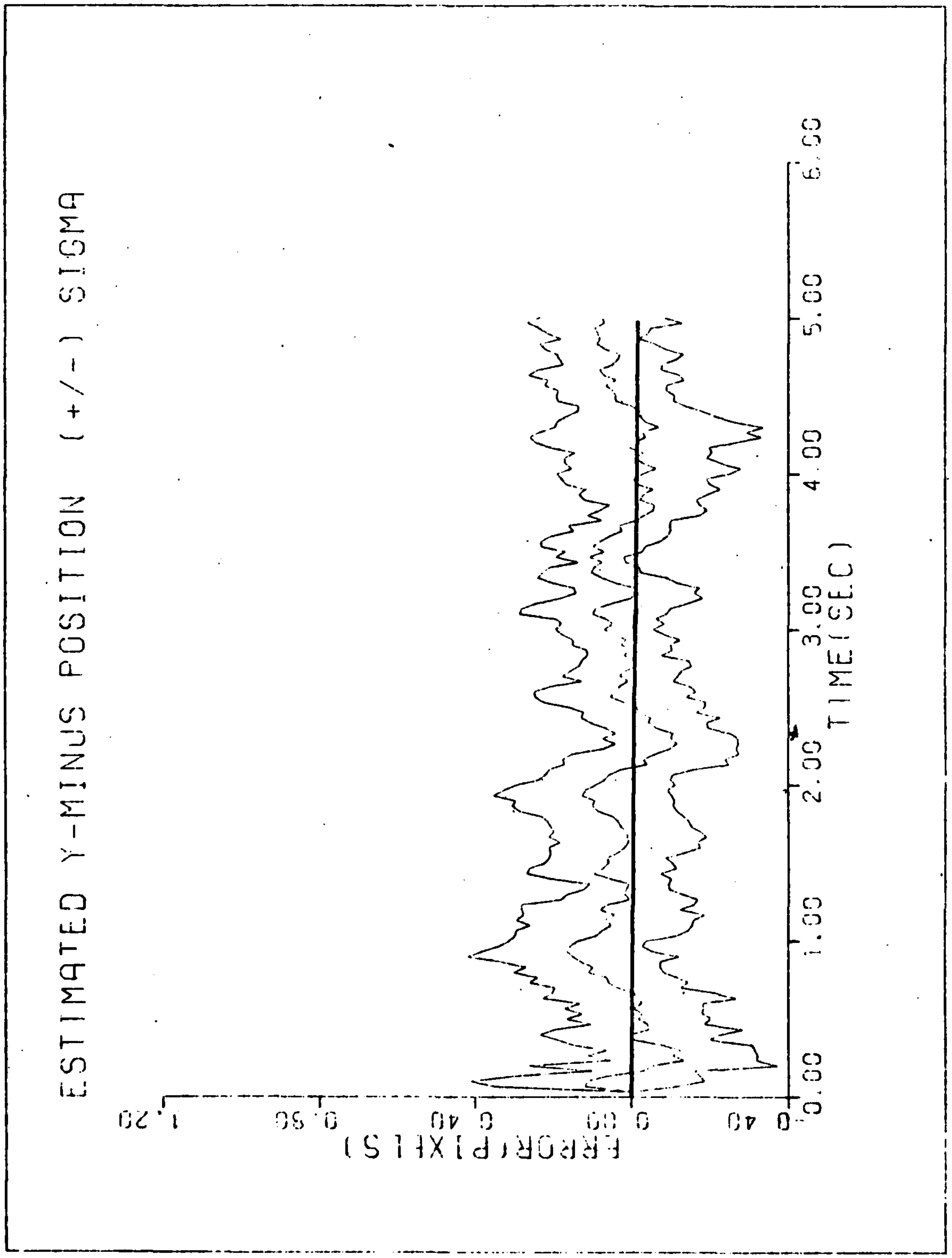

Figure C-10b. Case 10

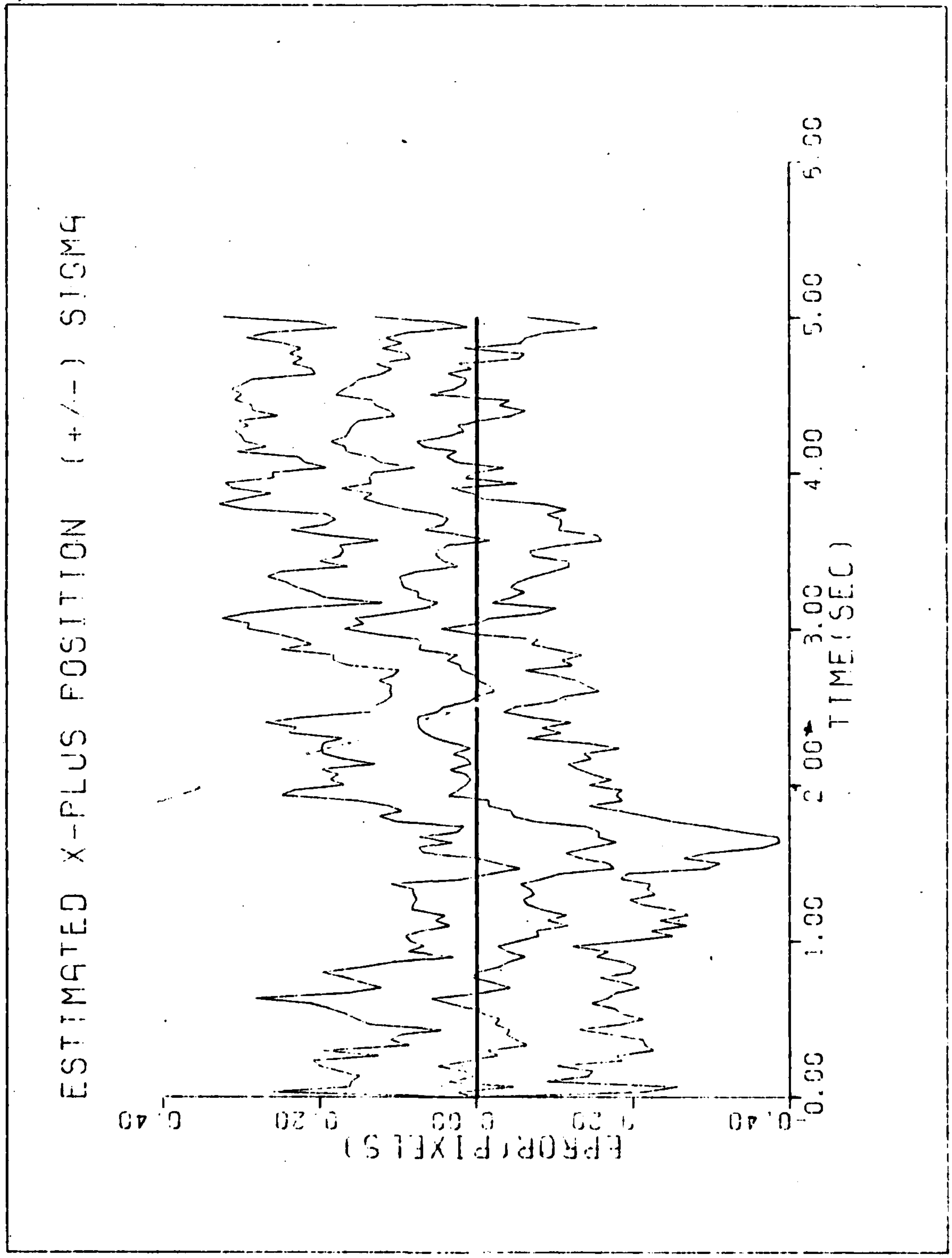

Figure C-10c. Case 10

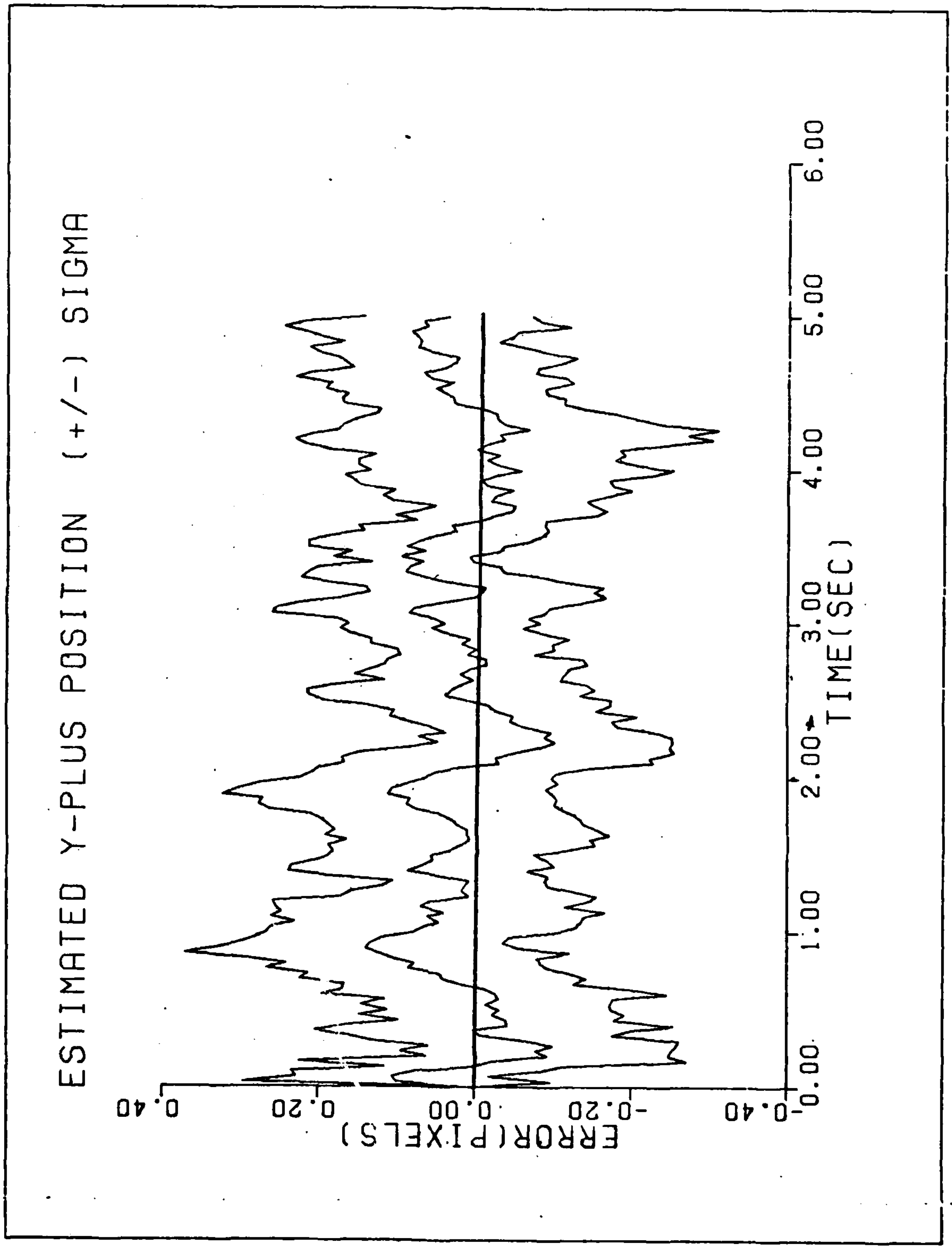

Figure C-10d. Case 10

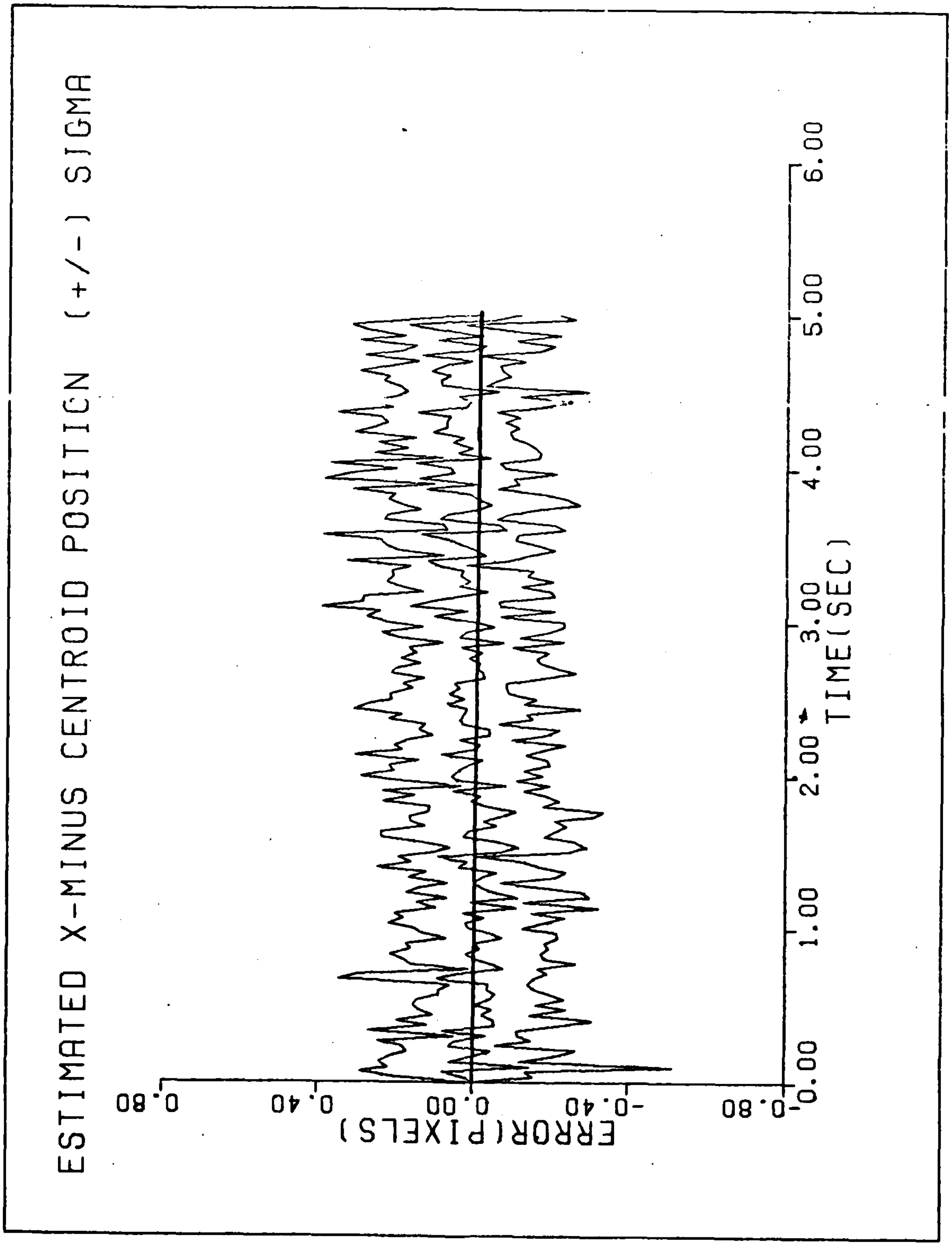

Figure C-10e. Case 10

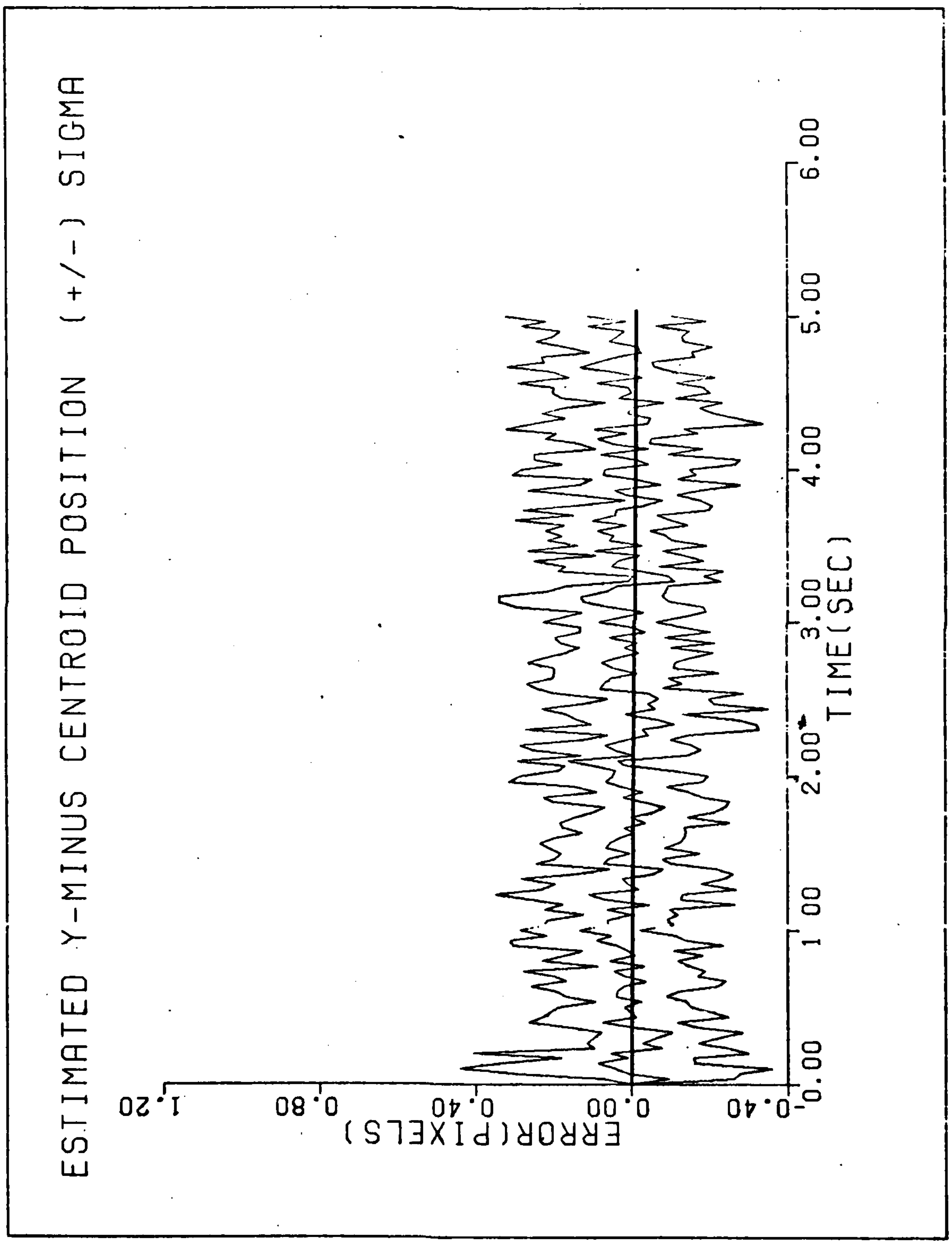

Figure C-10f. Case 10

The performance plots for this case were similar to the plots shown for case 10, and thus are omitted.

Figure C-11. Case 11

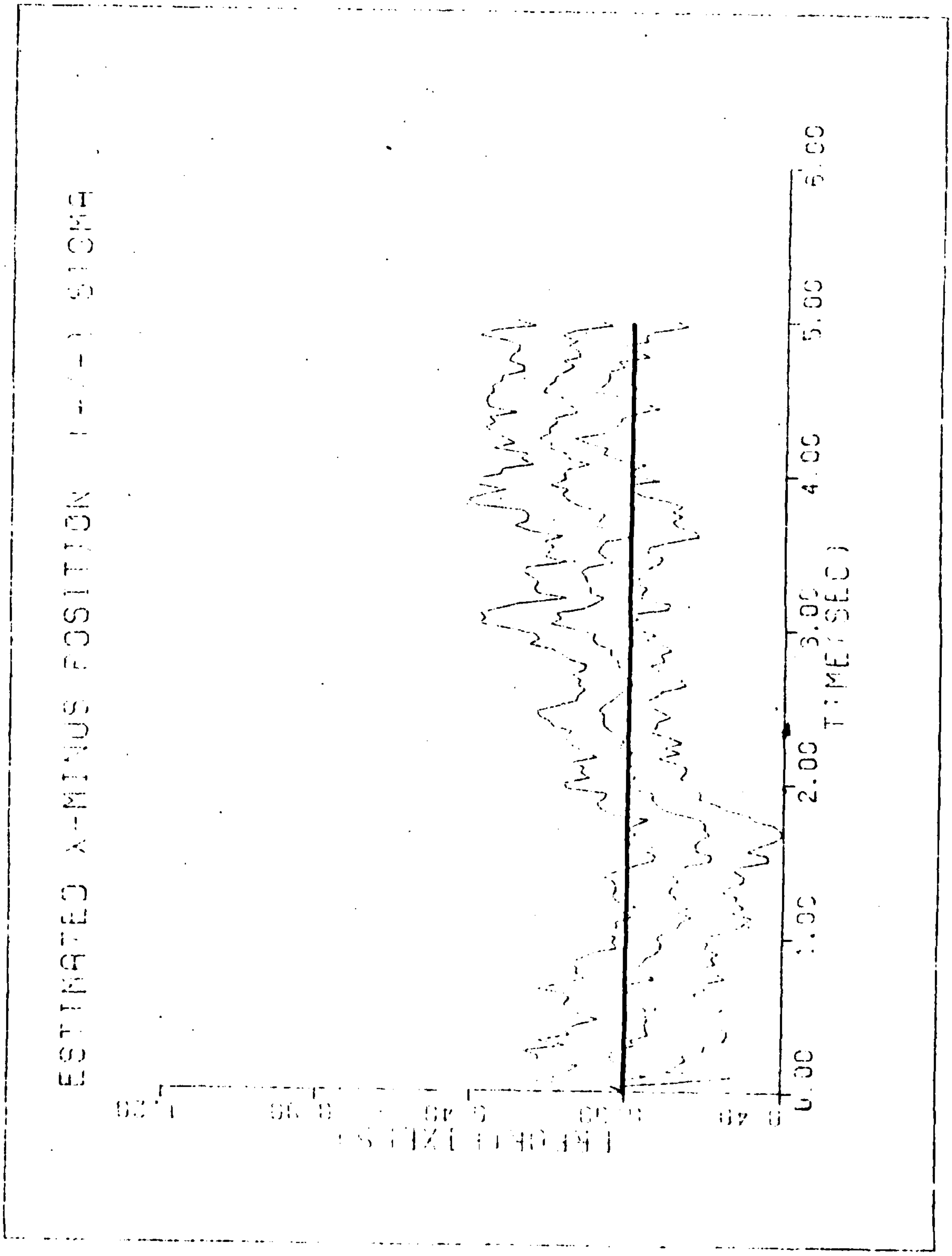

Figure C-12a. Case 12

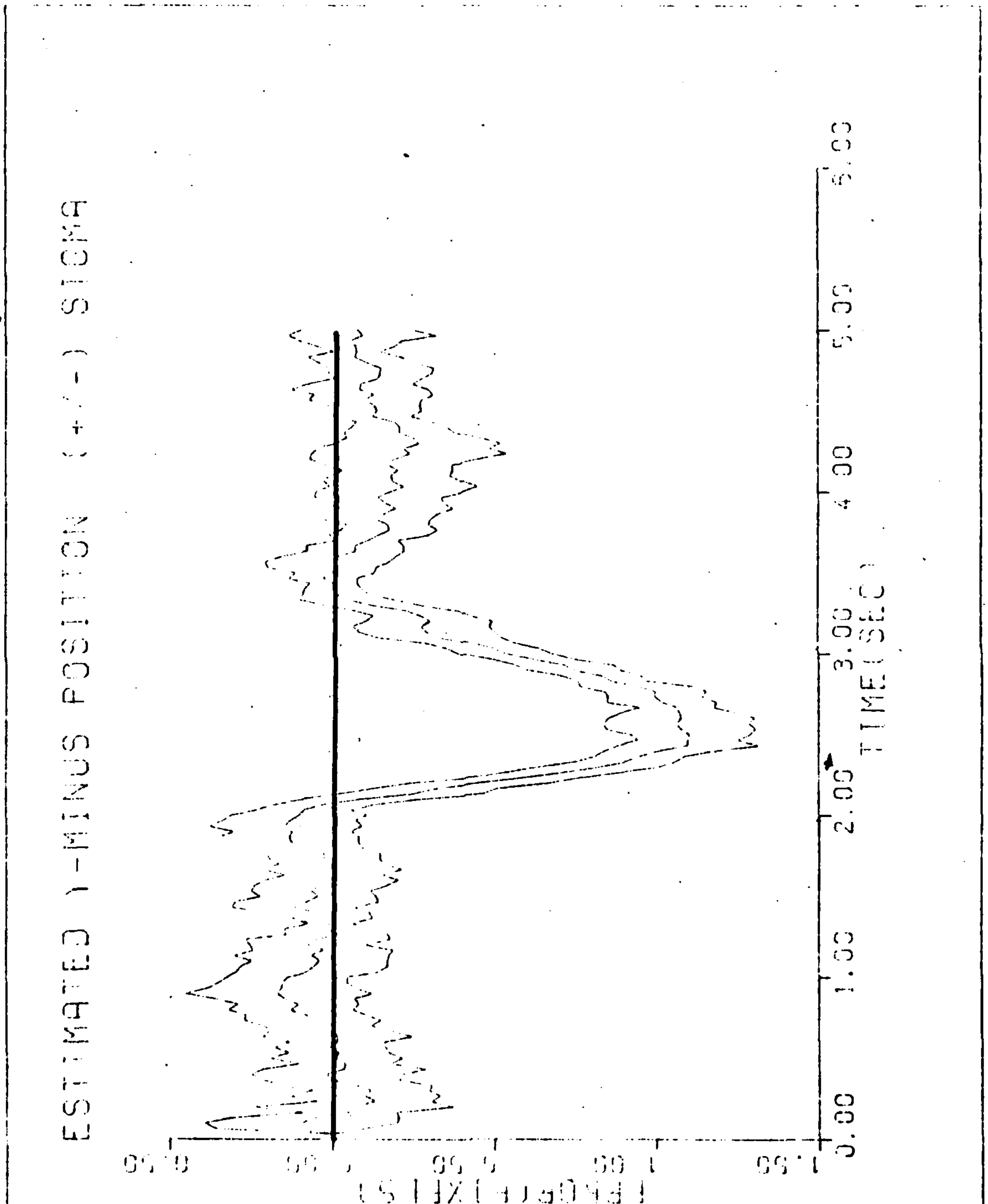

Figure C-12b. Case 12

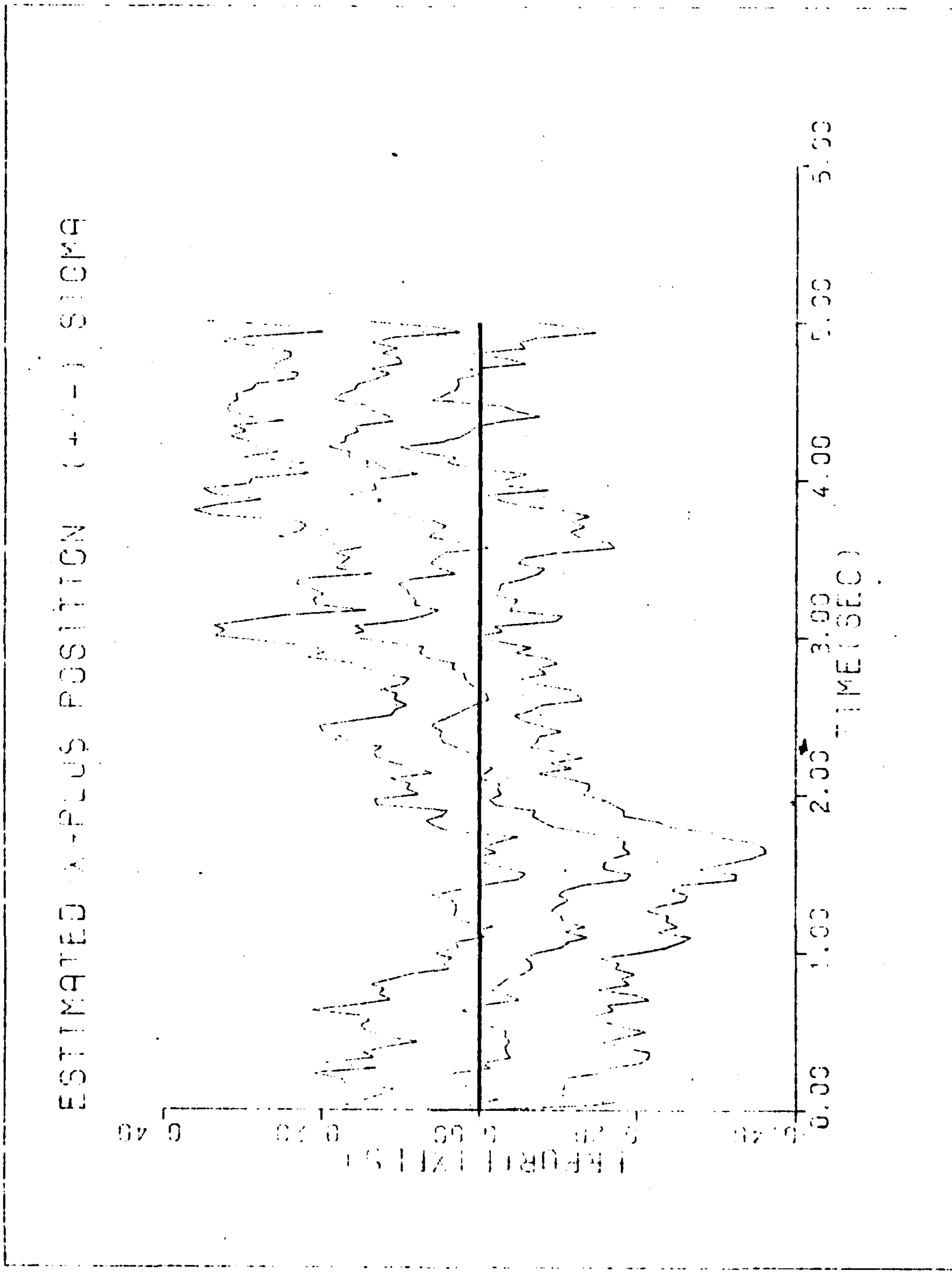

Figure C-12c. Case 12

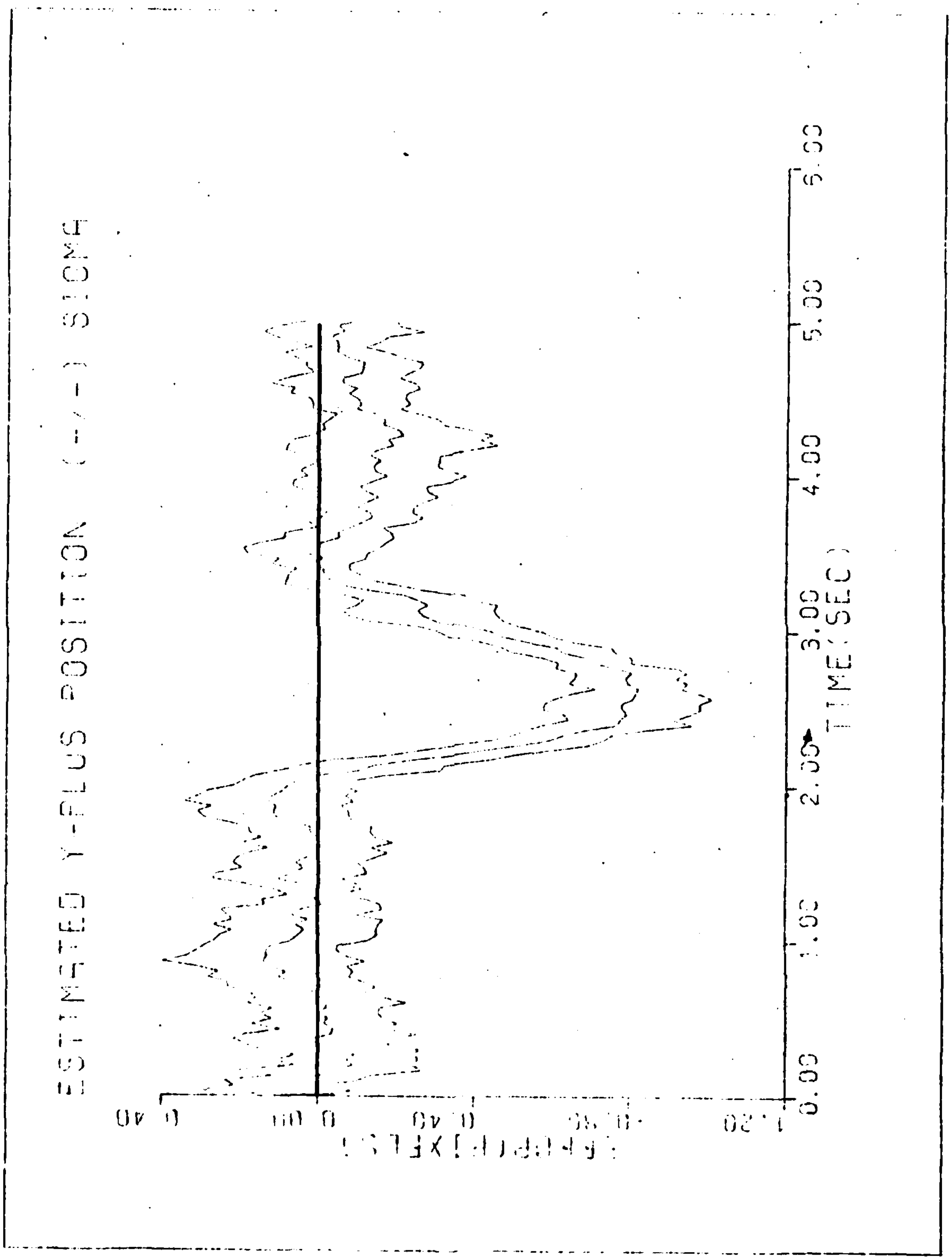

Figure C-12d. Case 12

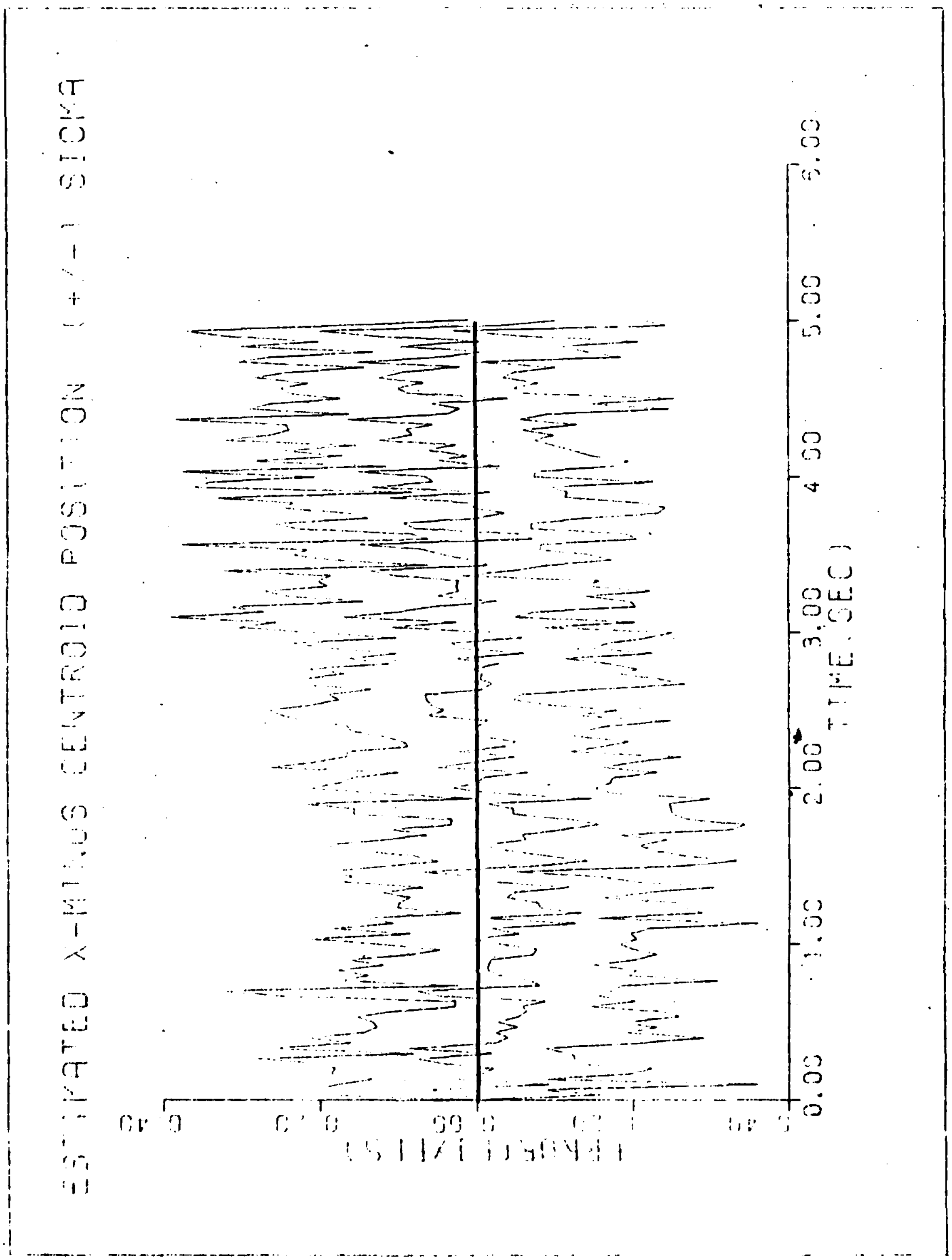

Figure C-12e. Case 12

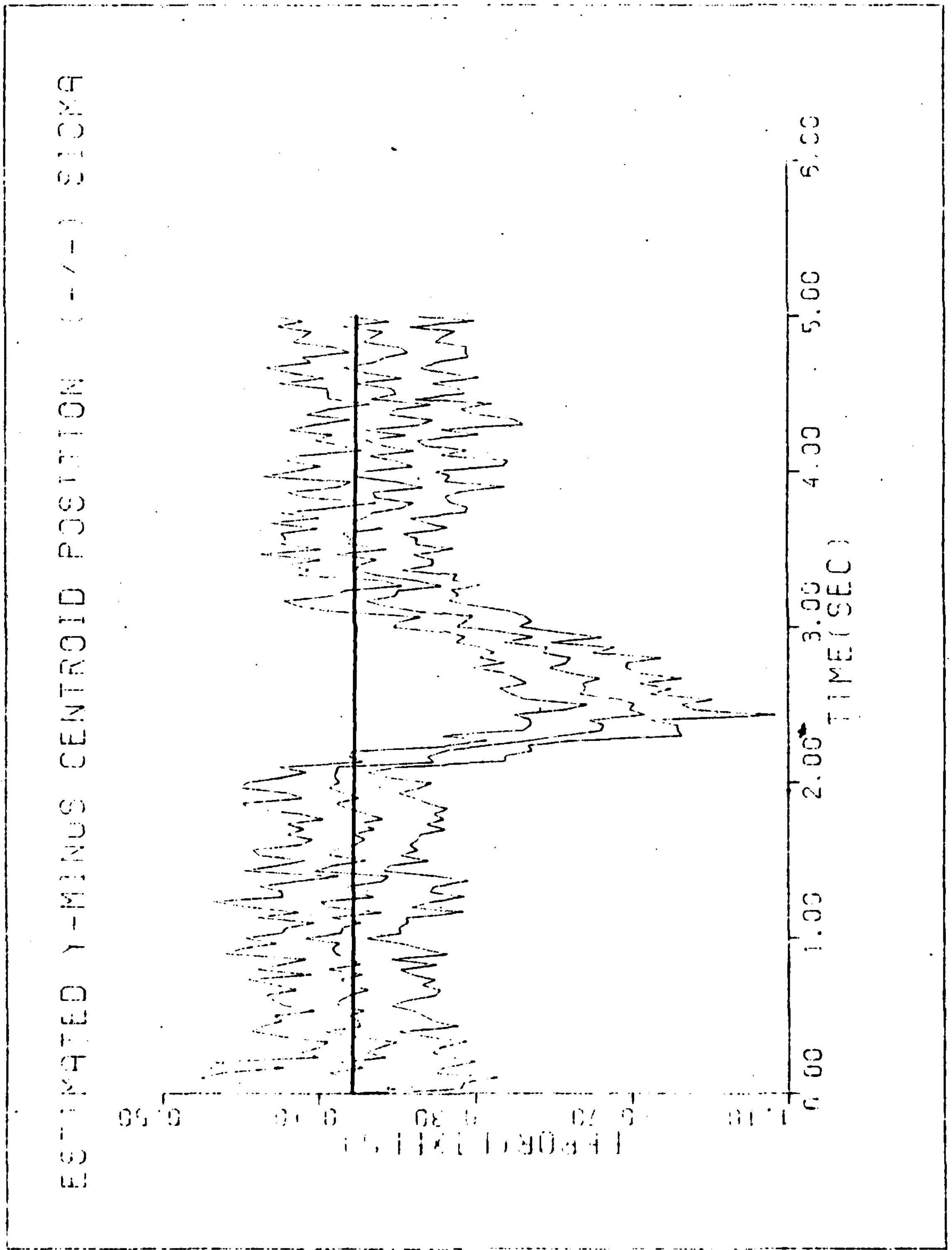

Figure C-12f. Case 12

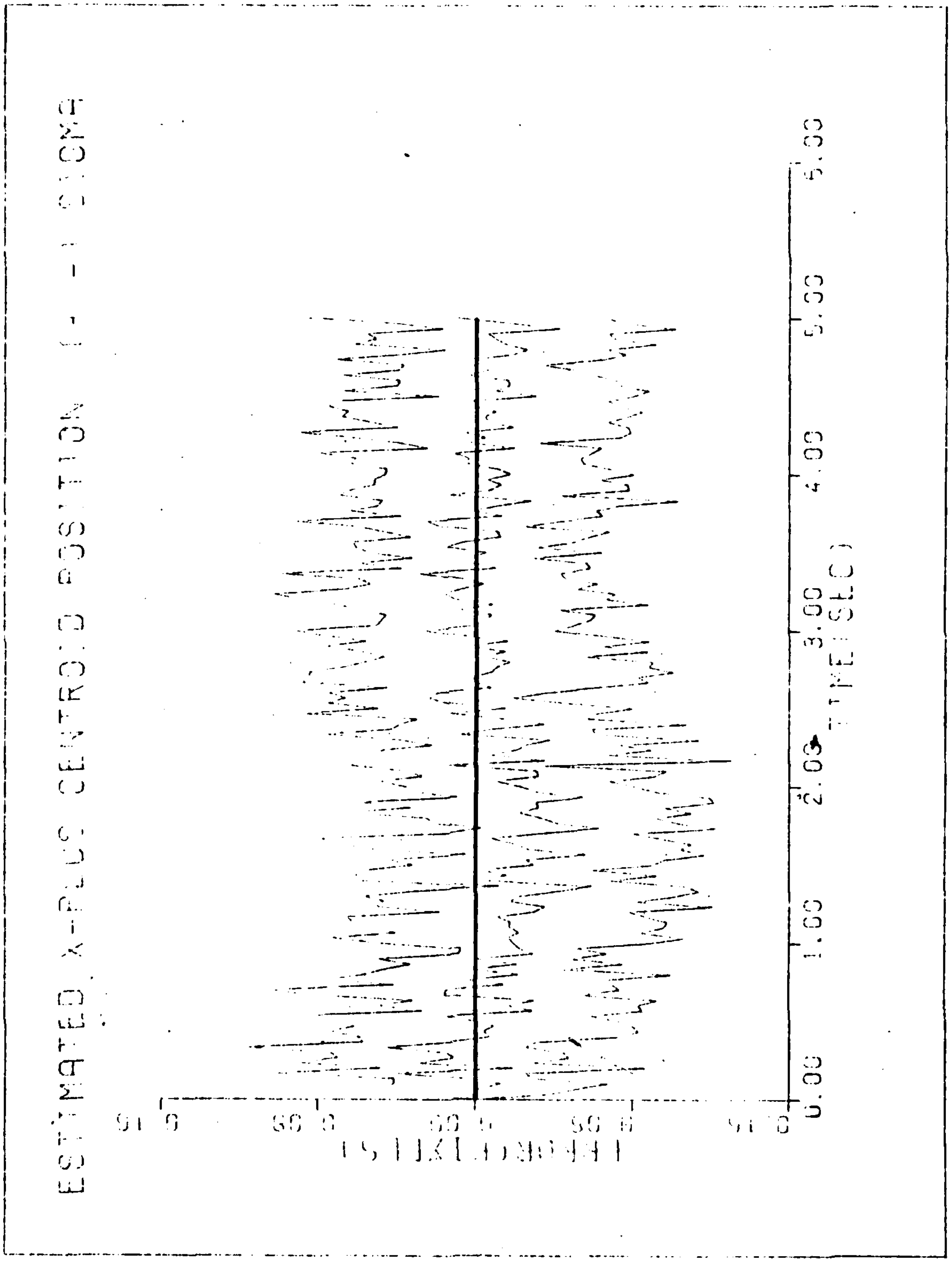

Figure C-12g. Case 12

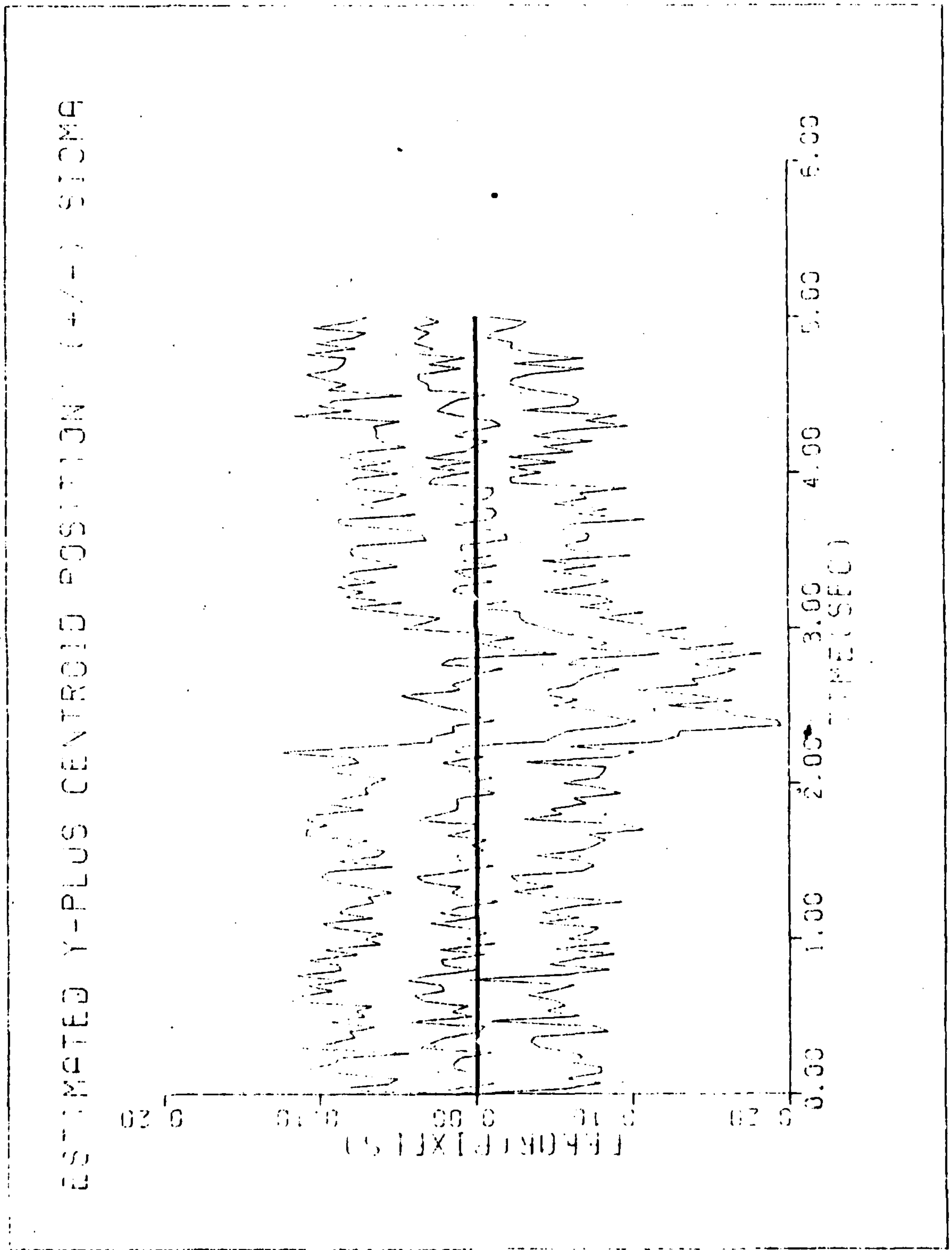

Figure C-12h. Case 12

The performance plots for this case were similar to the plots shown for case 12, and thus are omitted.

Figure C-13. Case 13

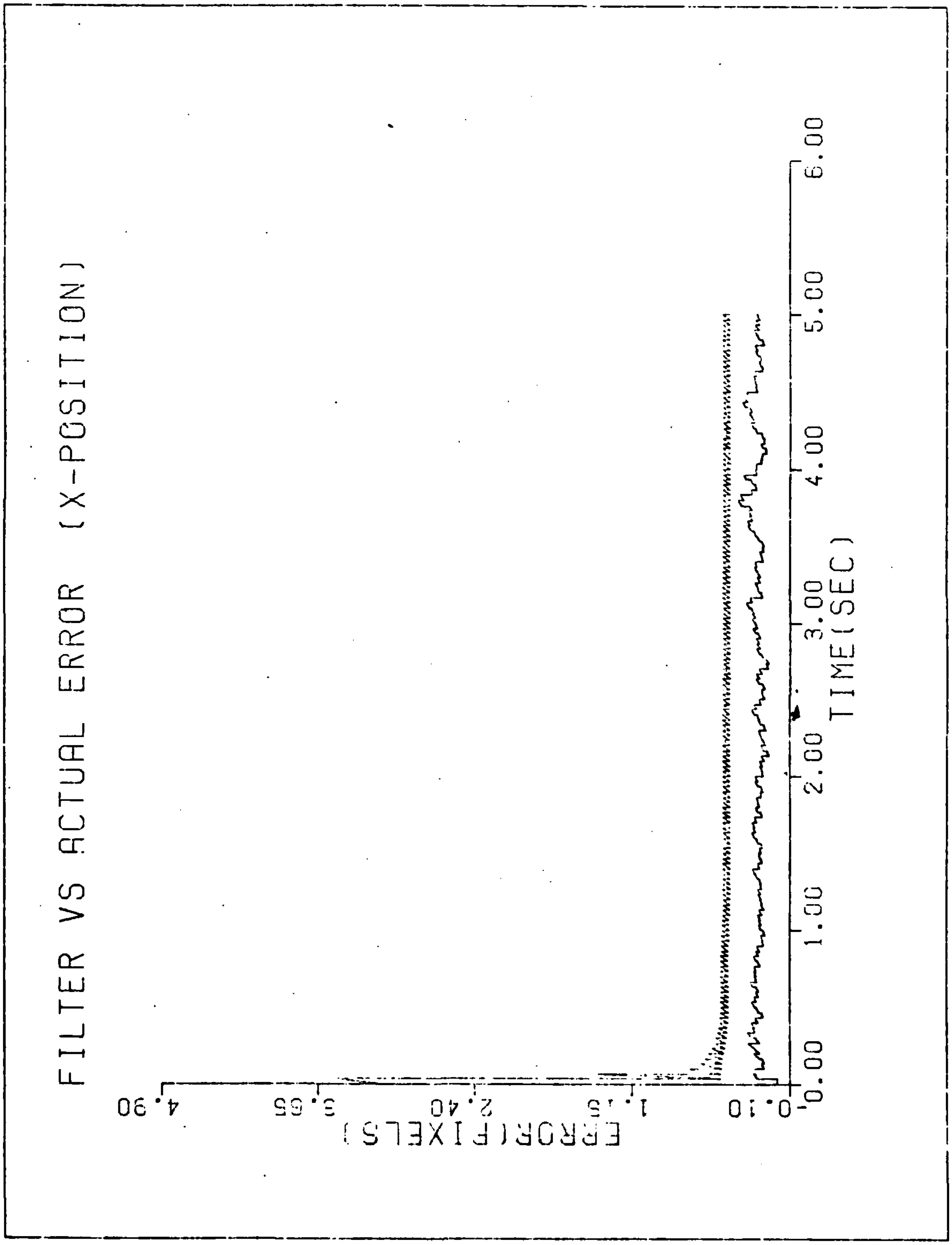

Figure C-14a. Case 14

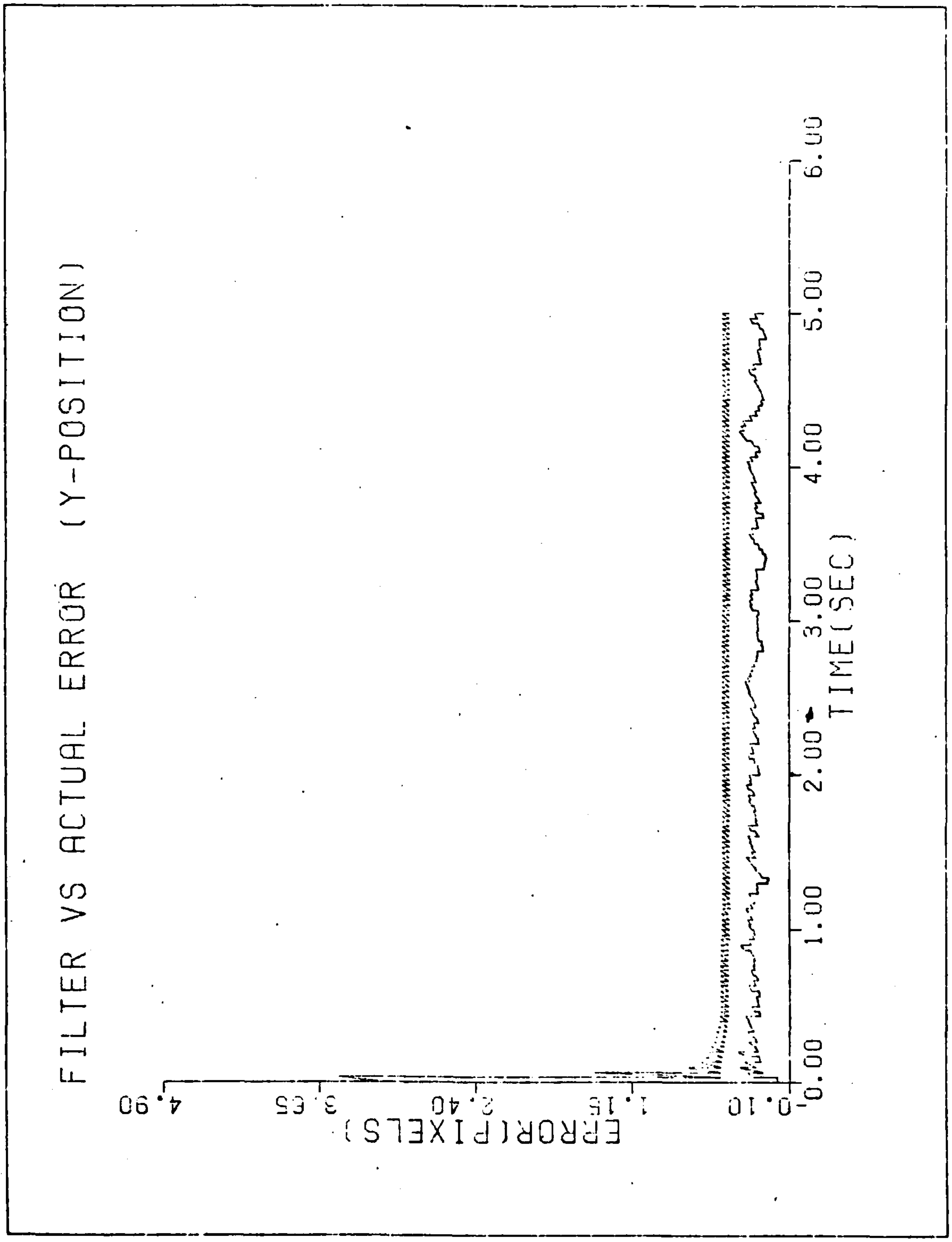

Figure C-14b. Case 14

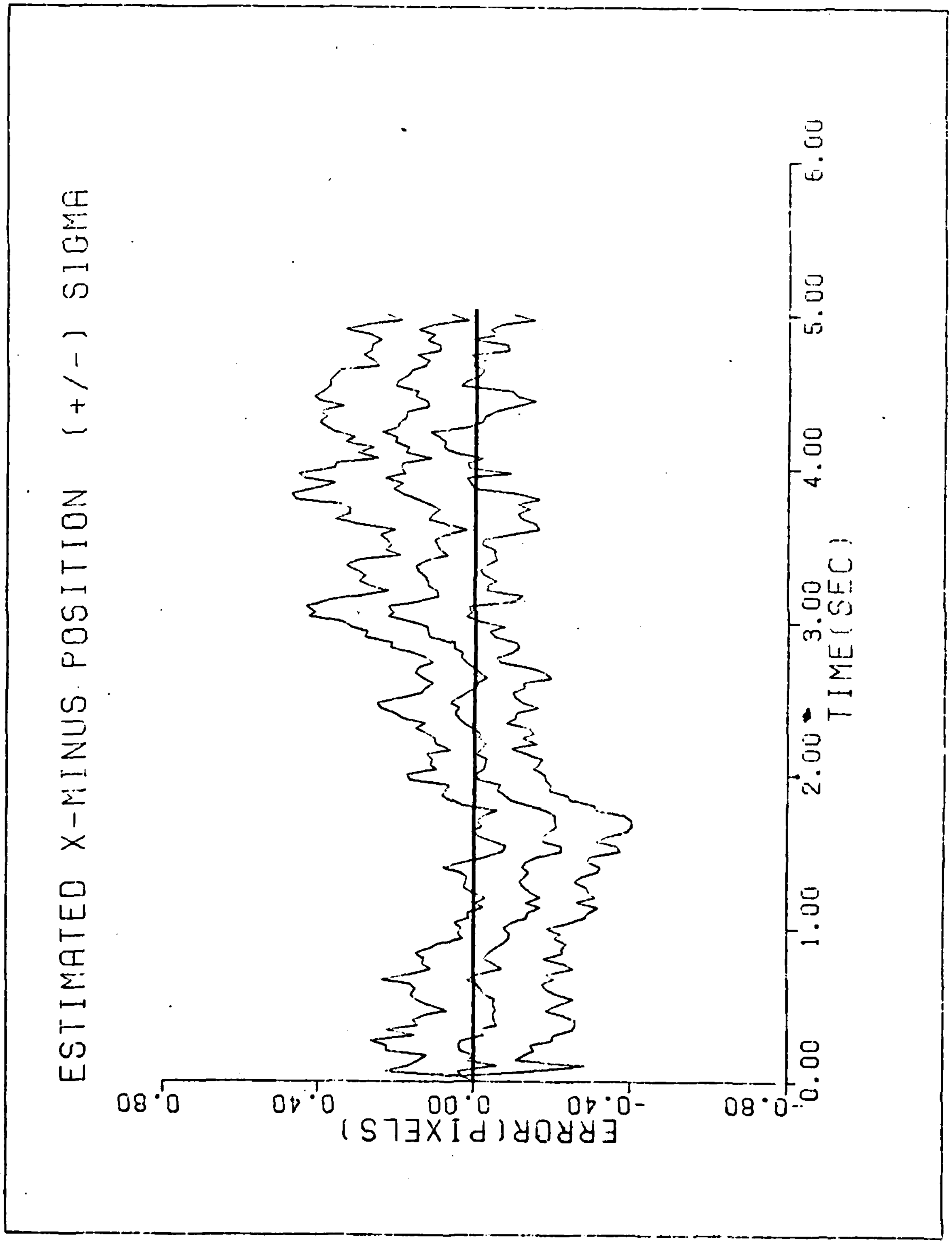

Figure C-14c. Case 14

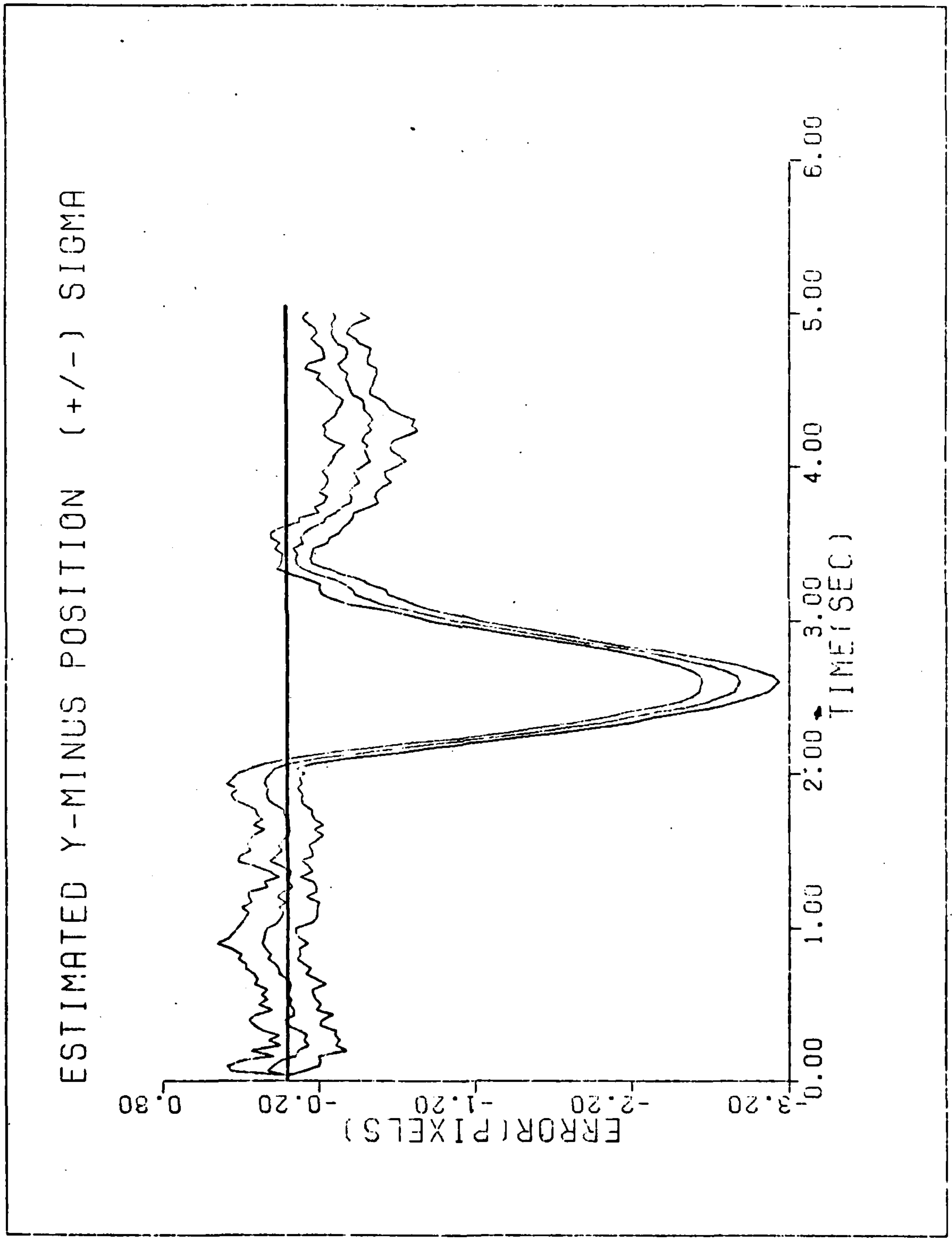

Figure C-14d. Case 14

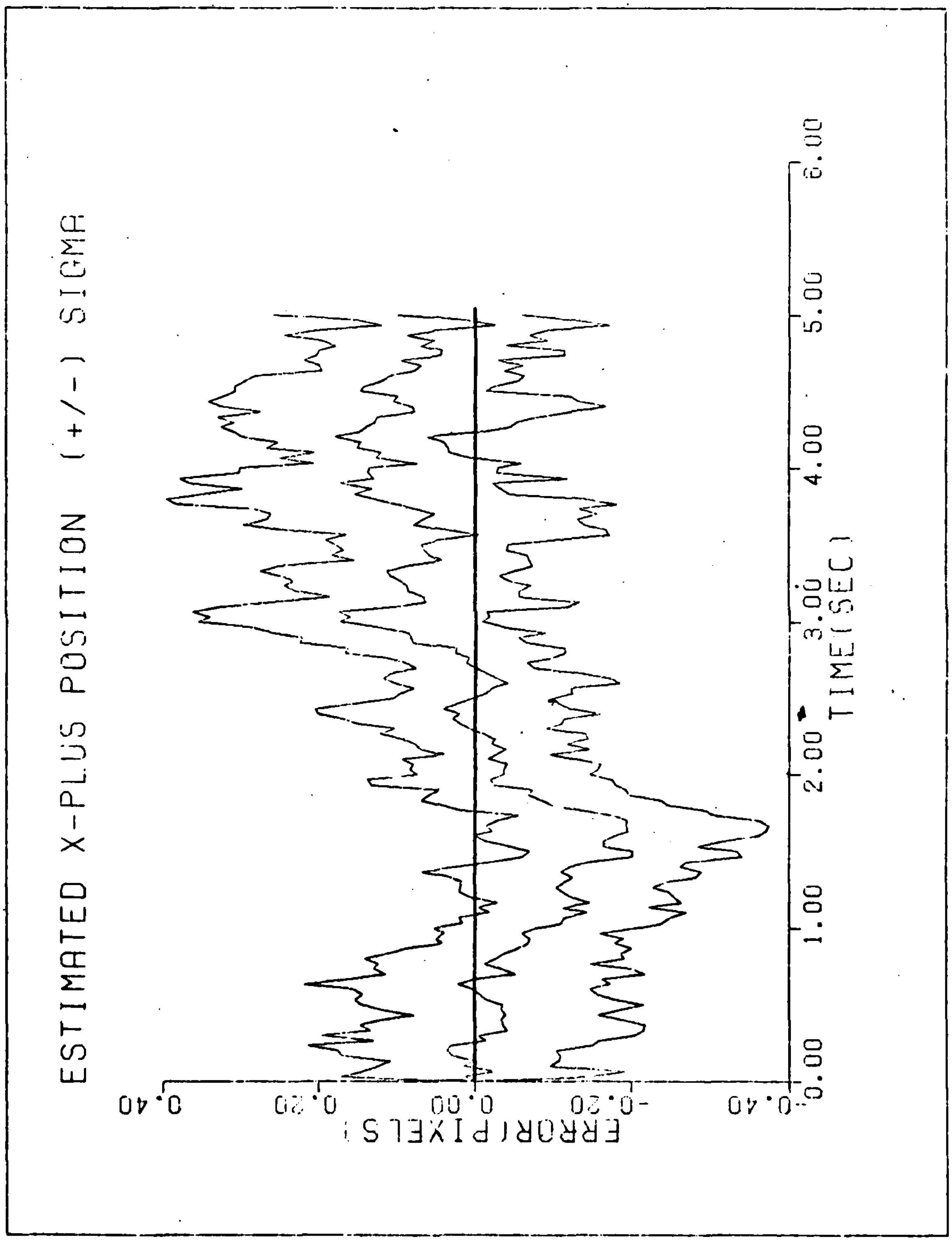

Figure C-14e. Case 14

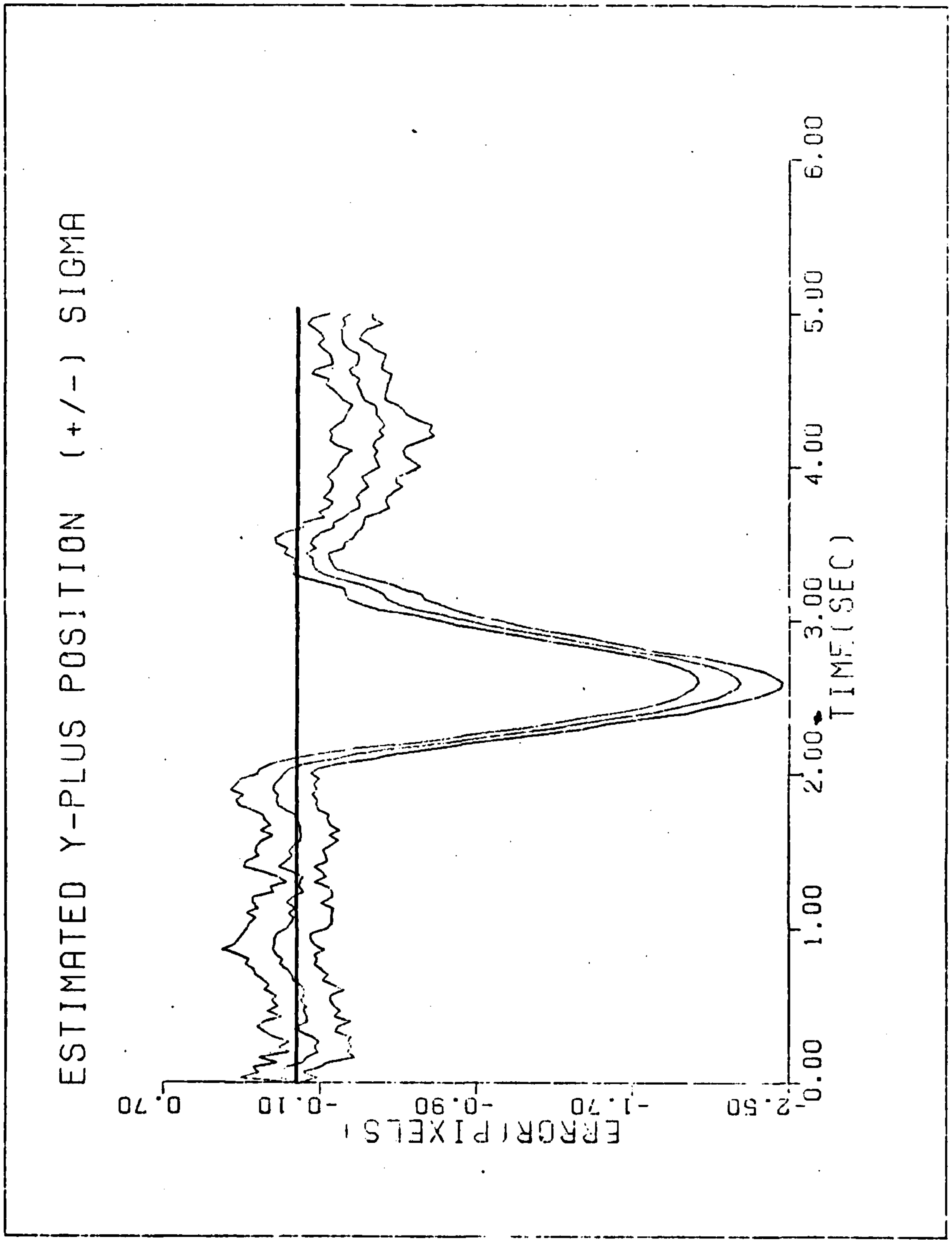

Figure C-14f. Case 14

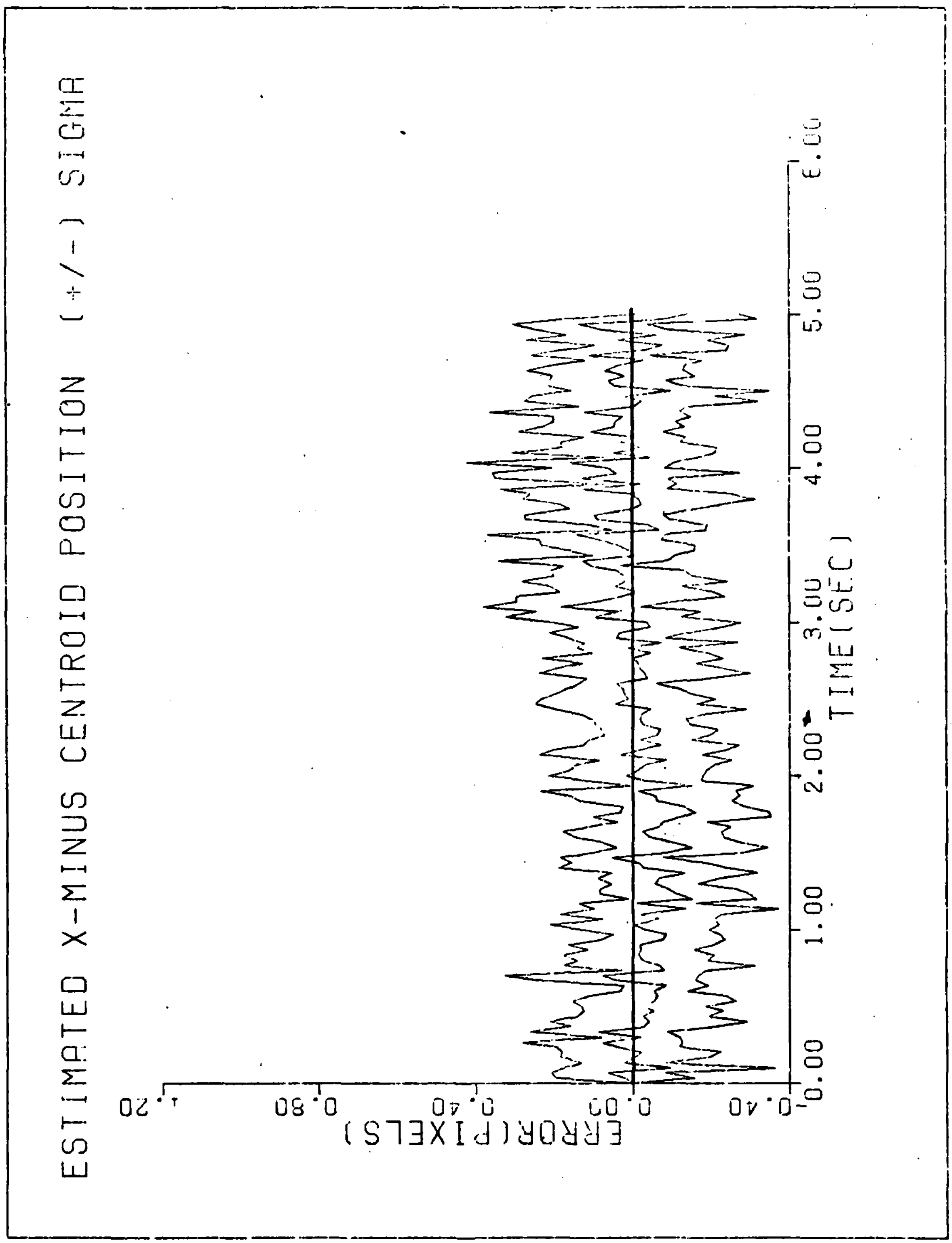

Figure C-14g. Case 14

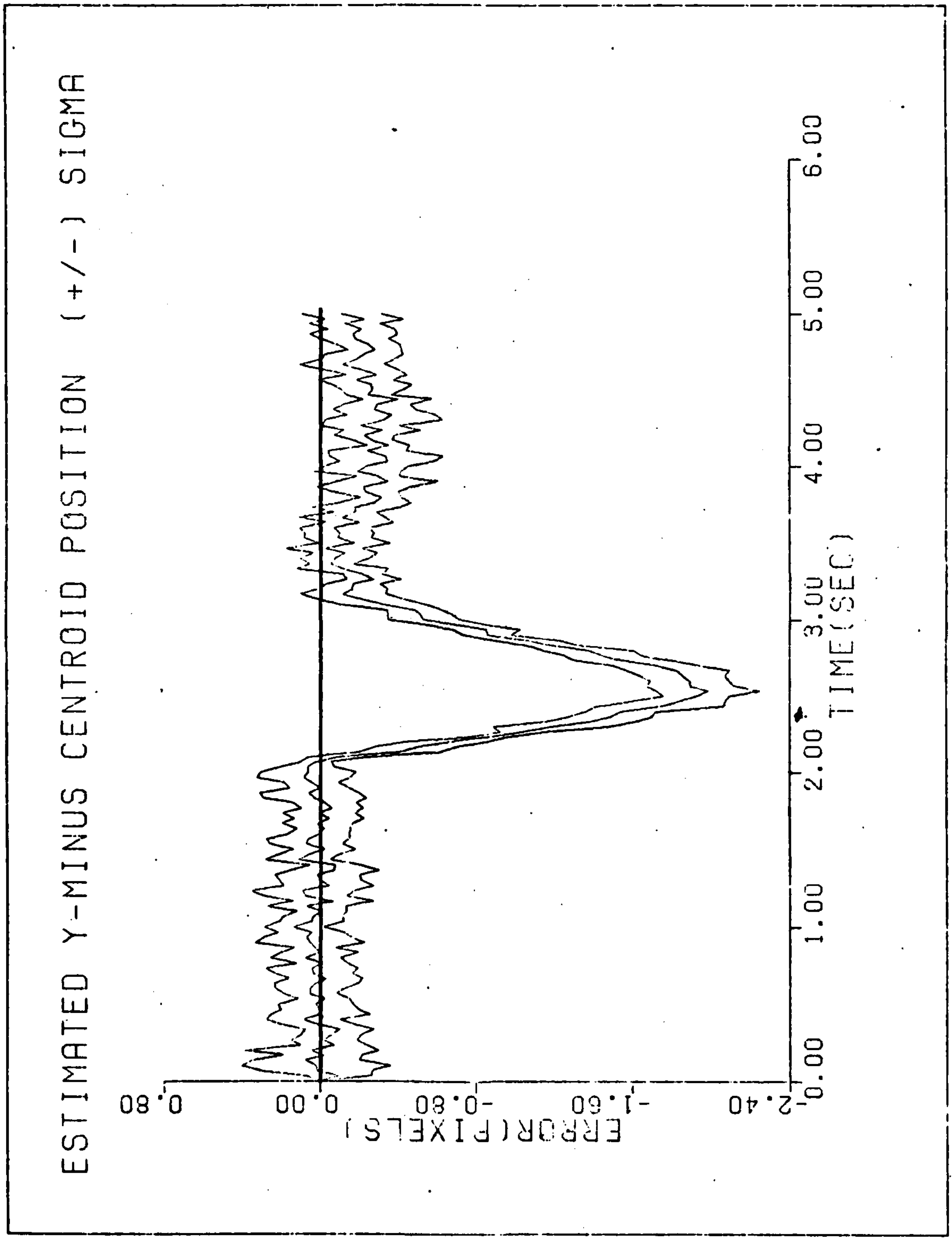

Figure C-14h. Case 14

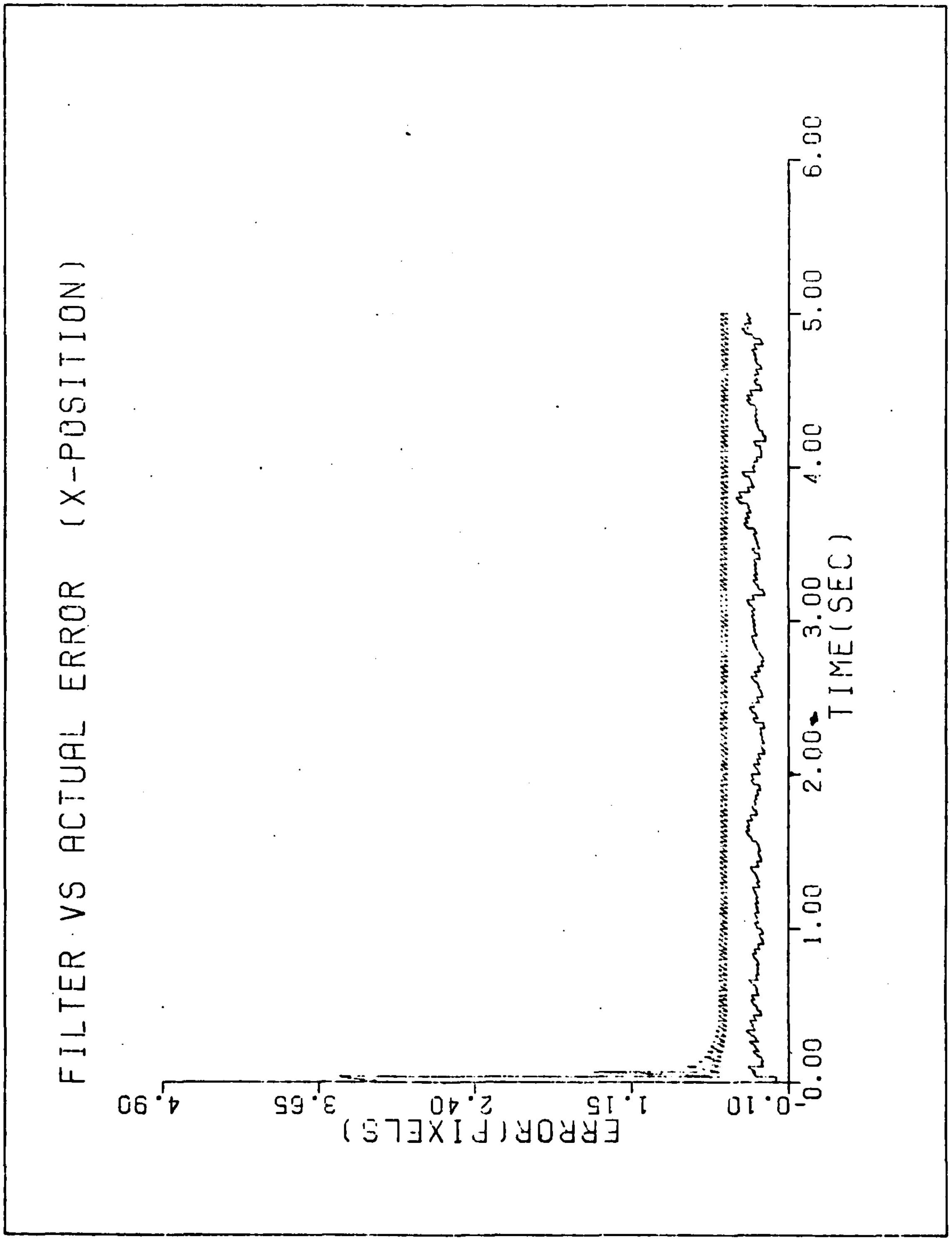

Figure C-15a. Case 15

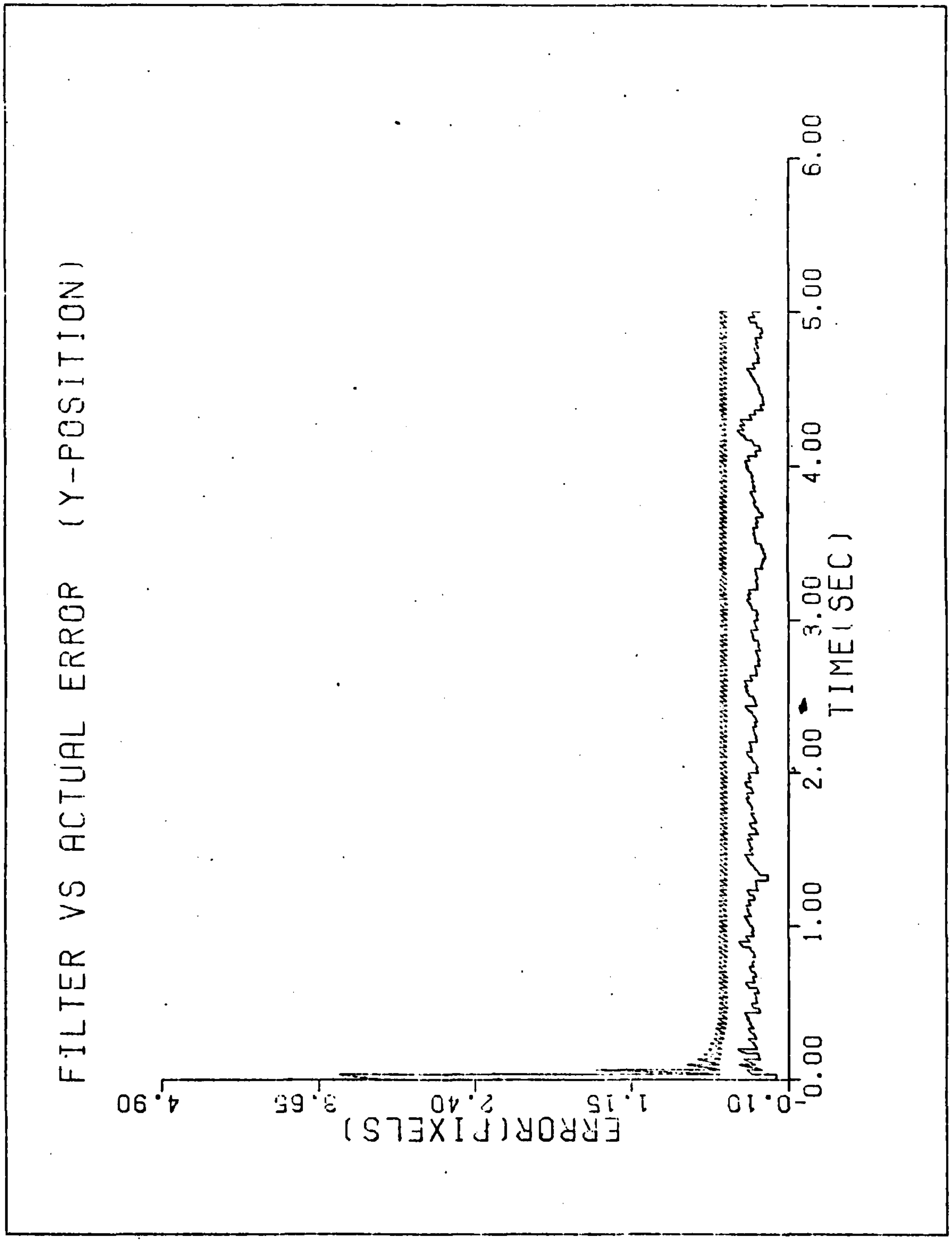

Figure C-15b. Case 15

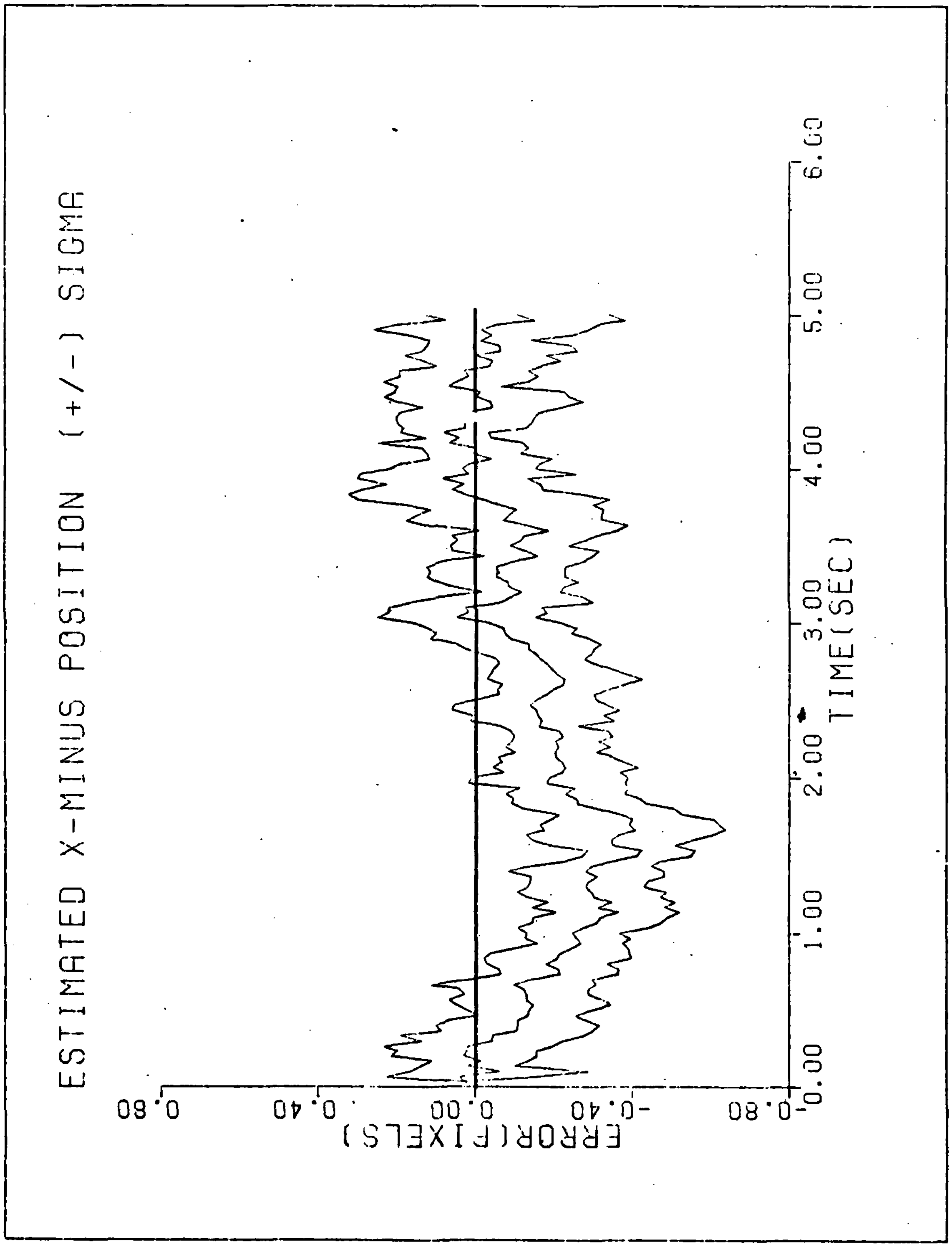

Figure C-15c. Case 15

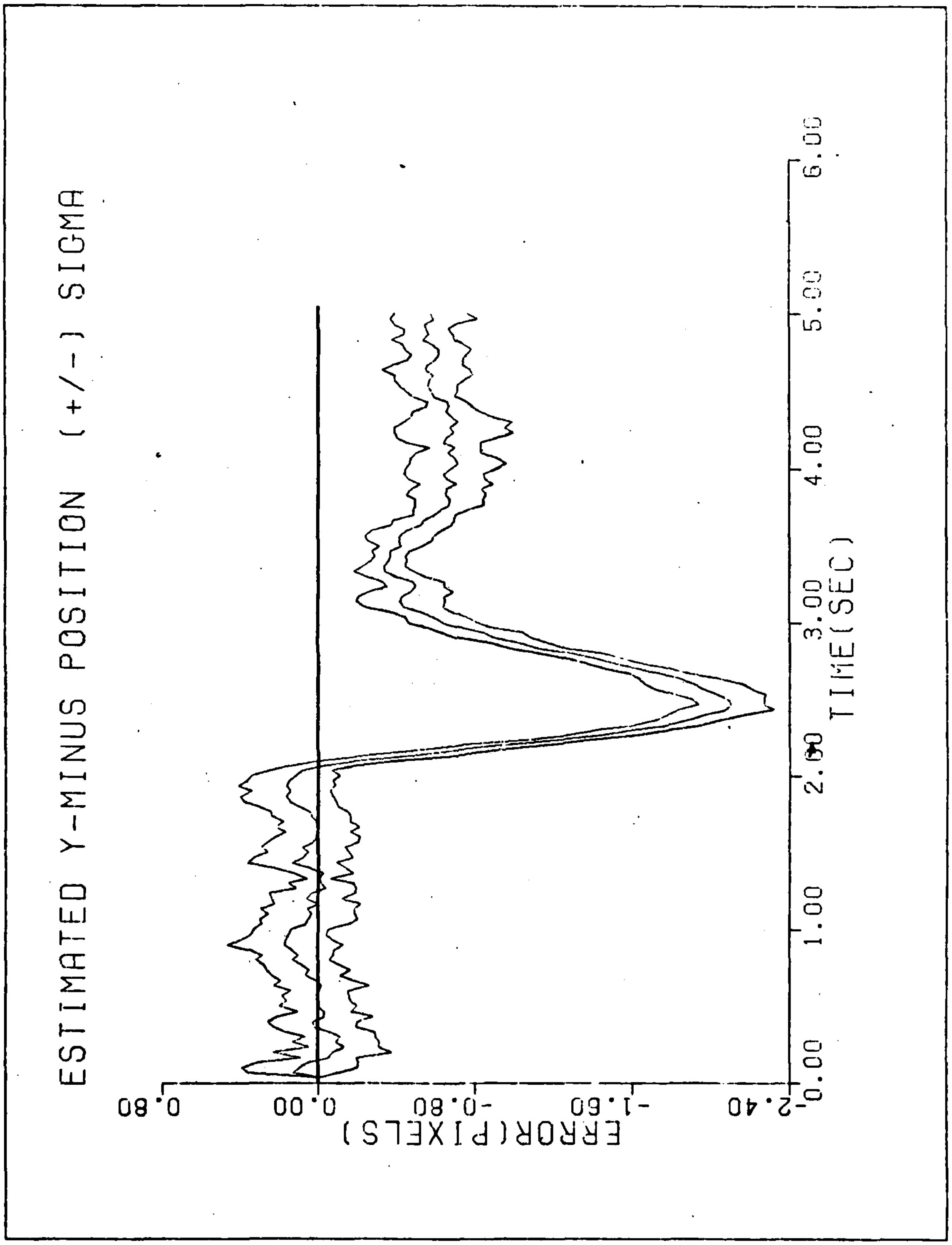

Figure C-15d. Case 15

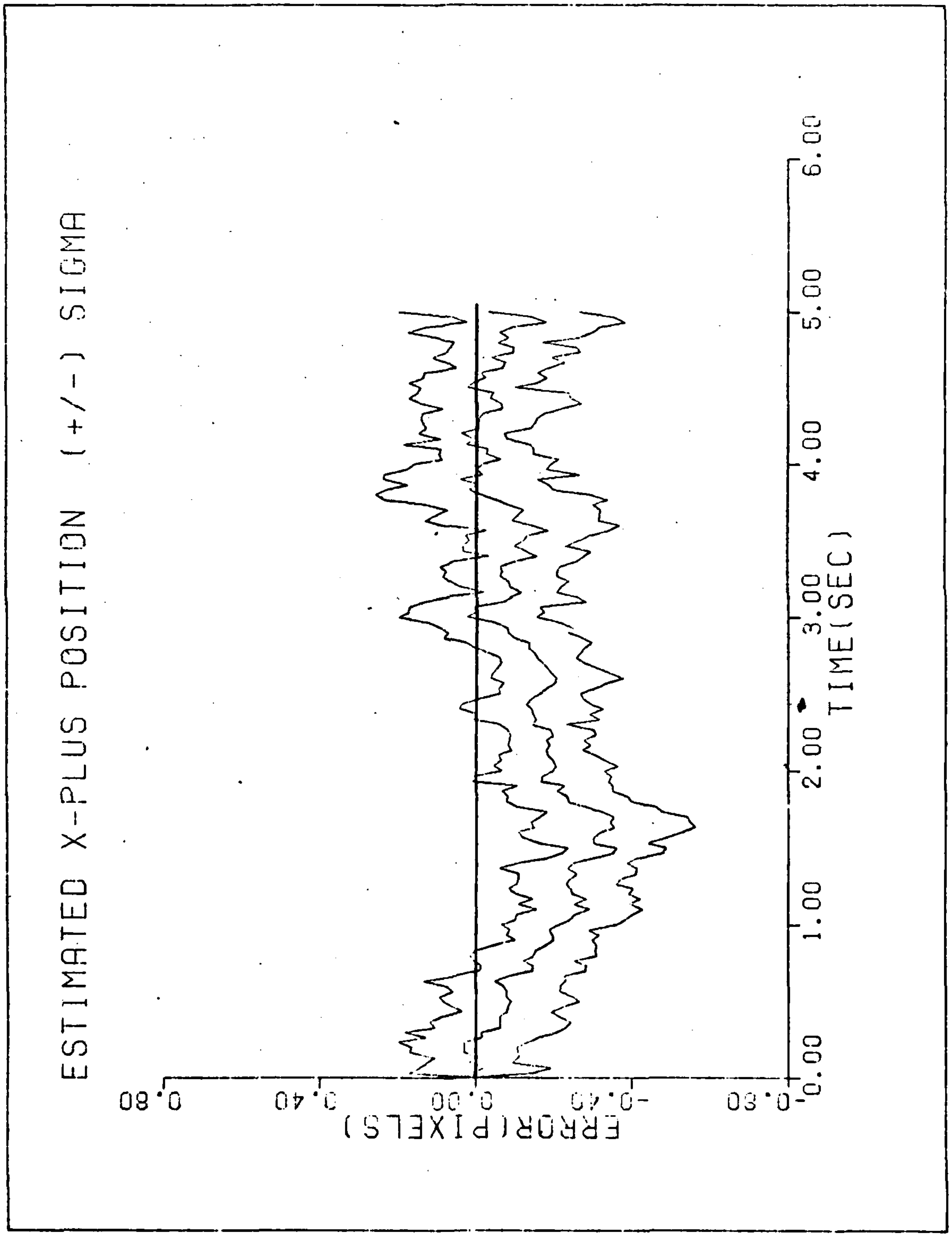

Figure C-15e. Case 15

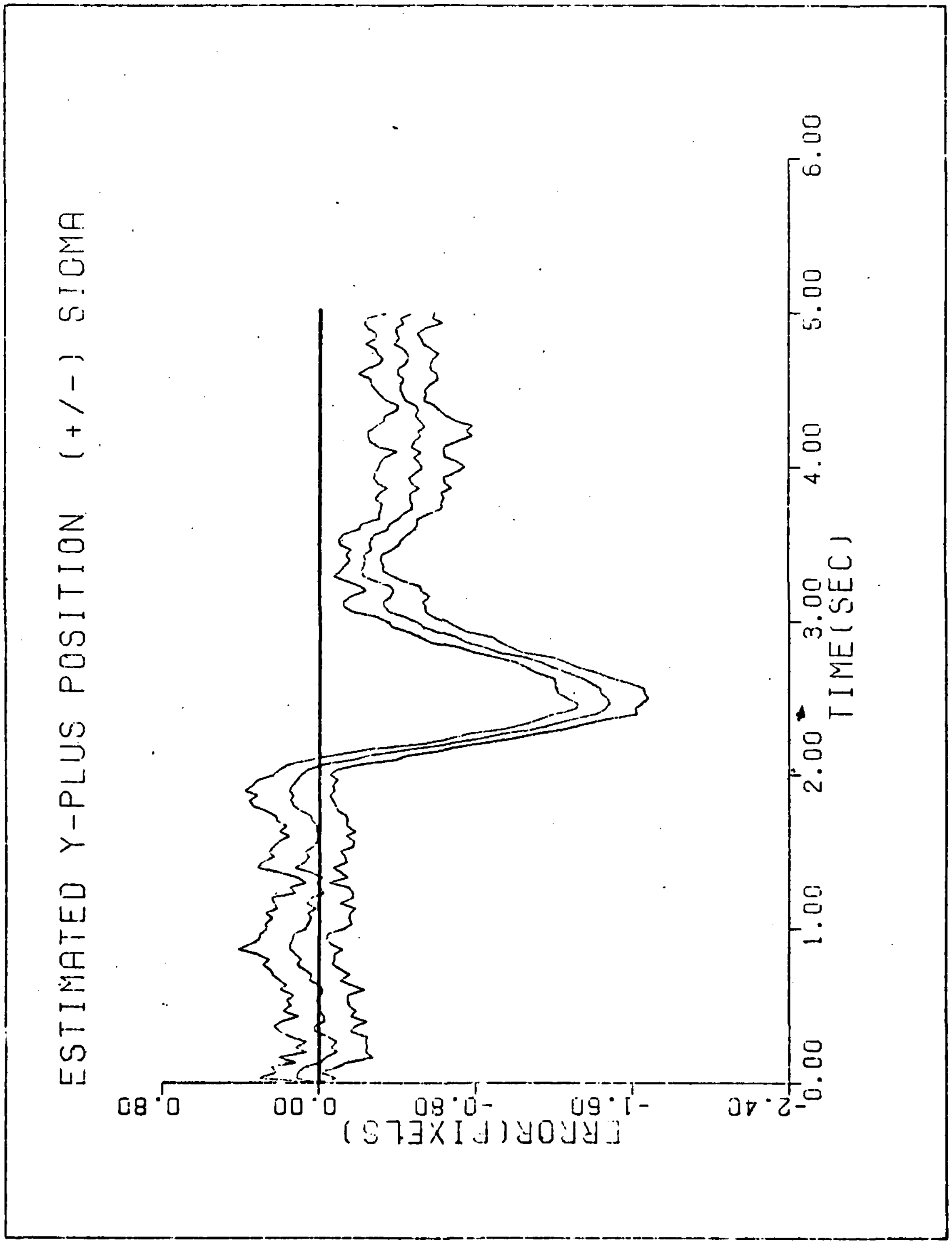

Figure C-15f. Case 15

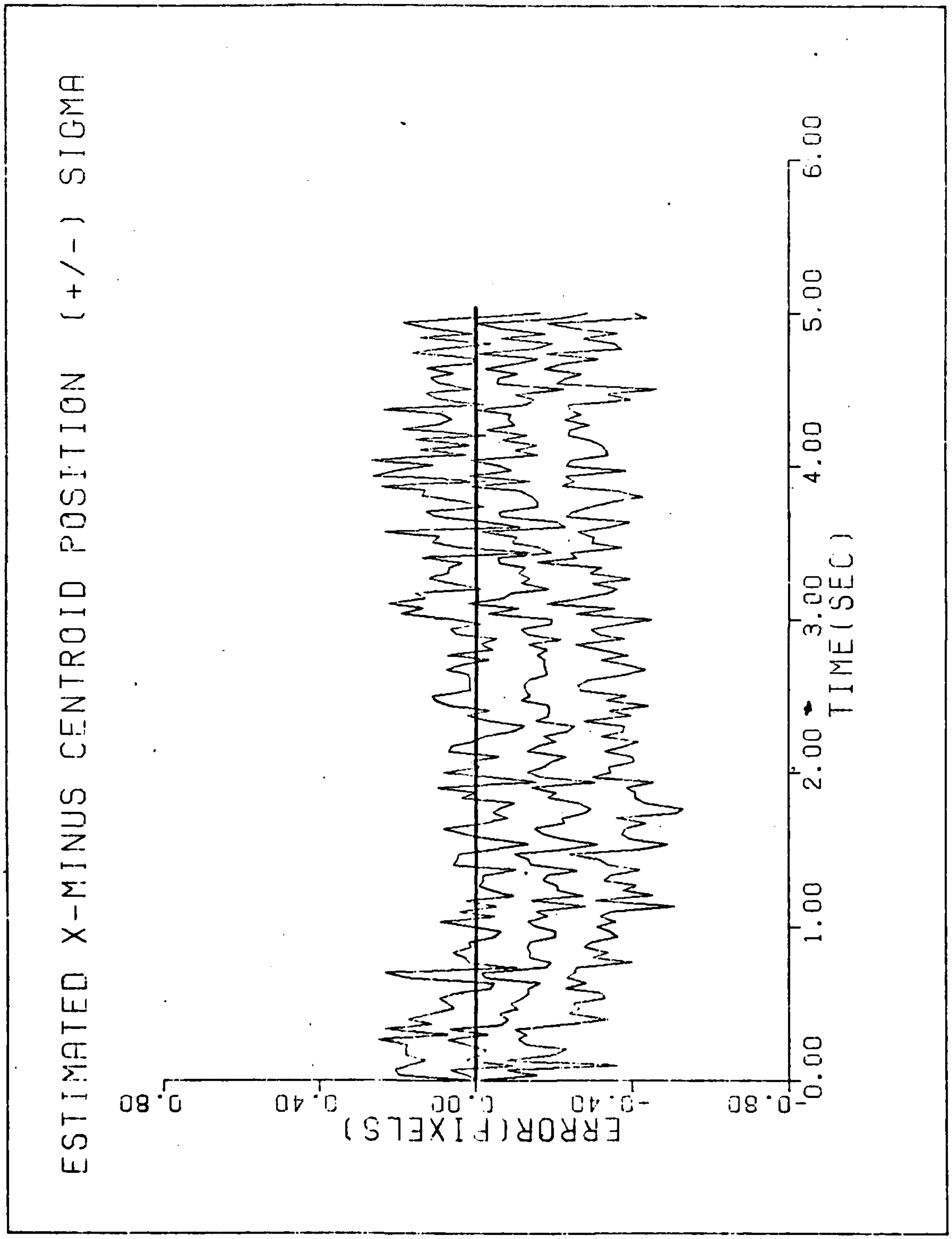

Figure C-15g. Case 15

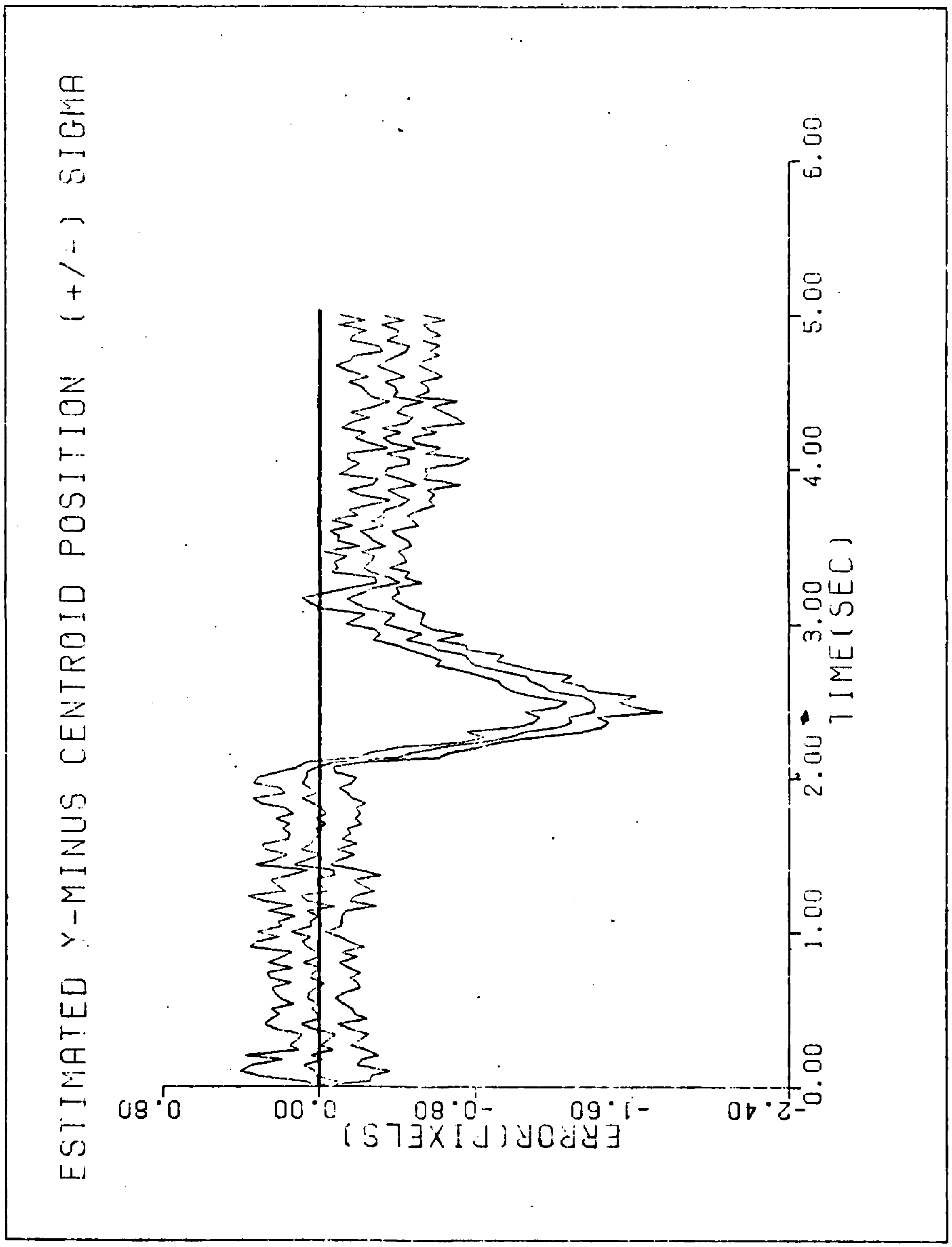

Figure C-15h. Case 15

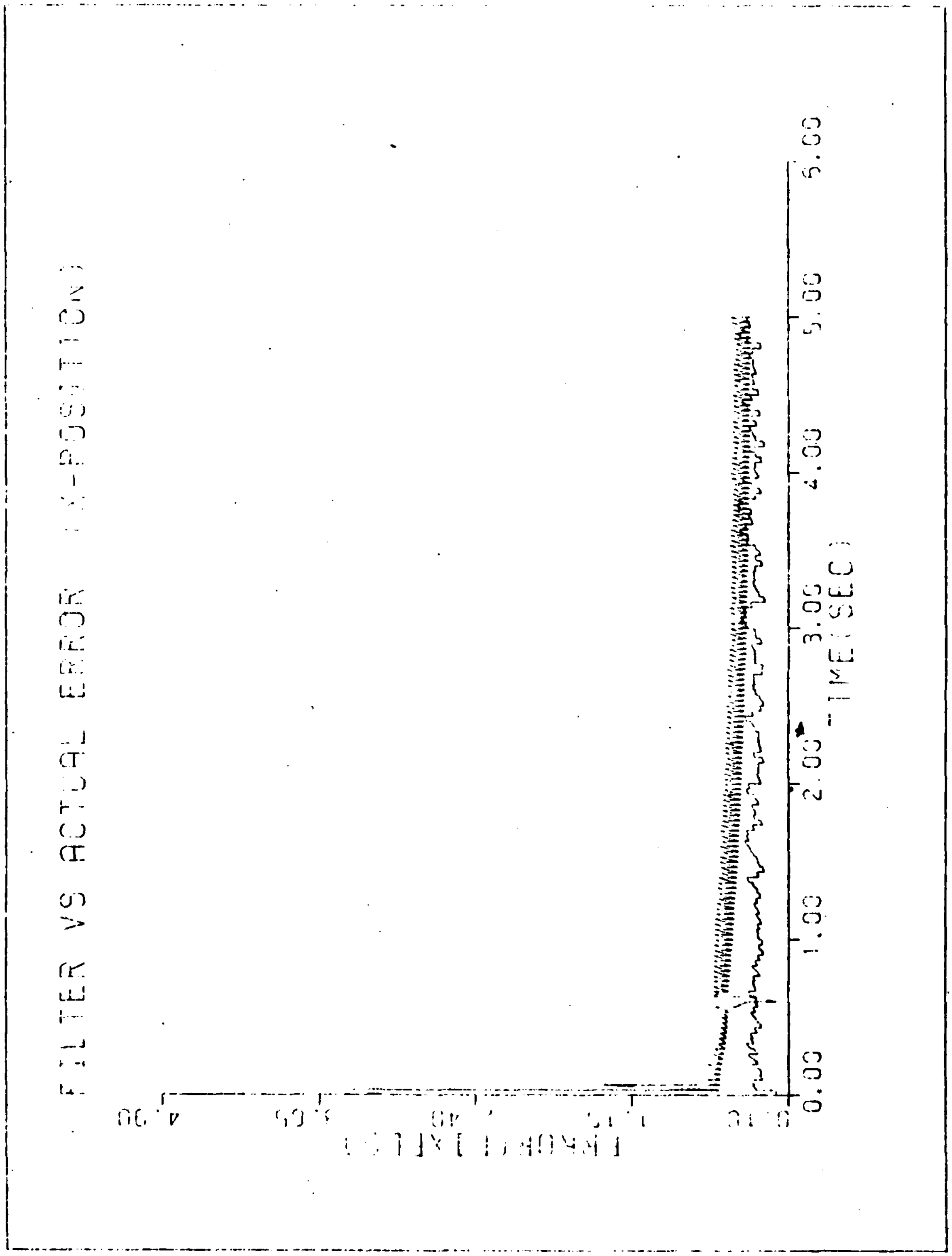

Figure C-16a. Case 16

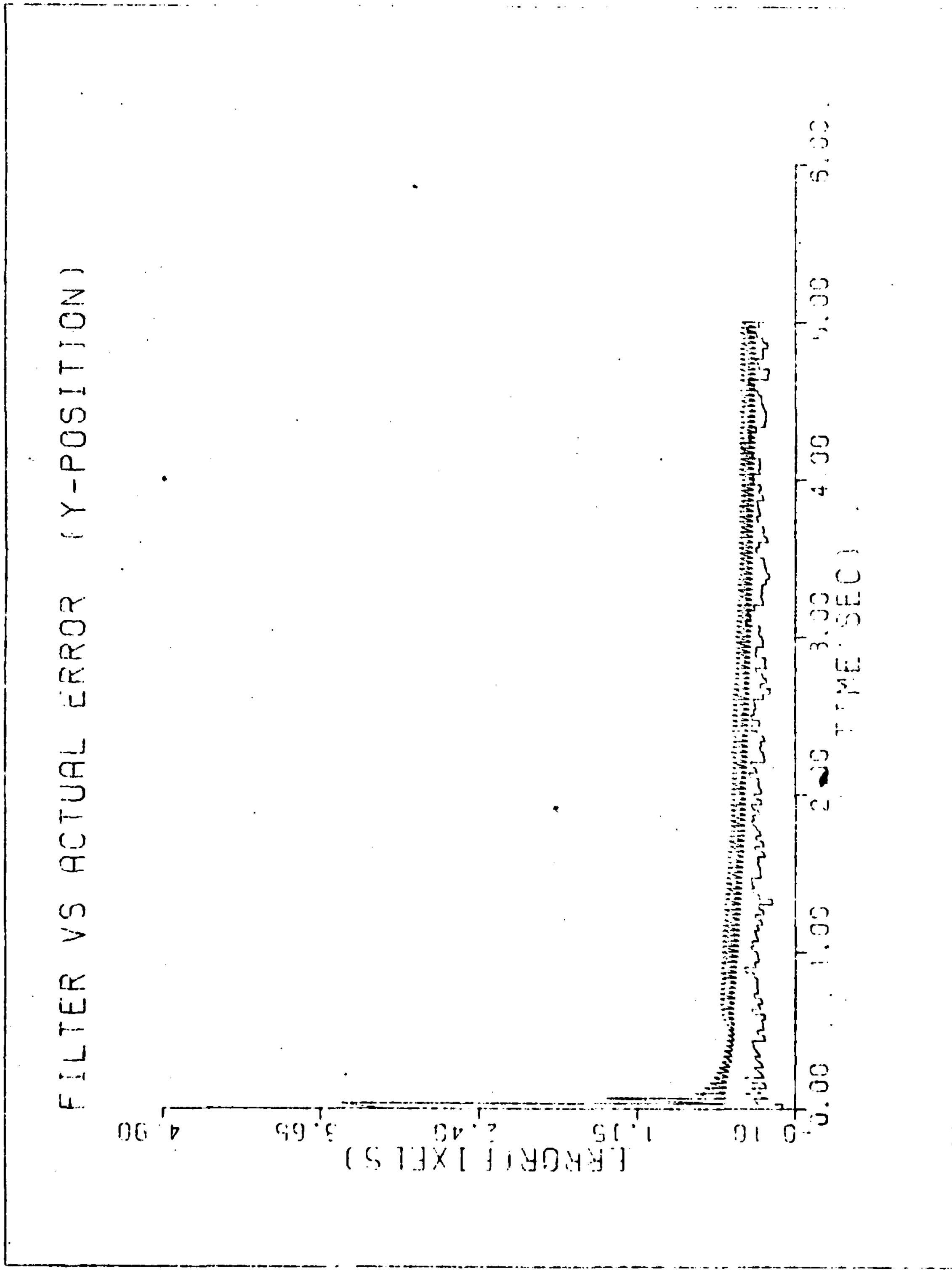

Figure C-16b. Case 16

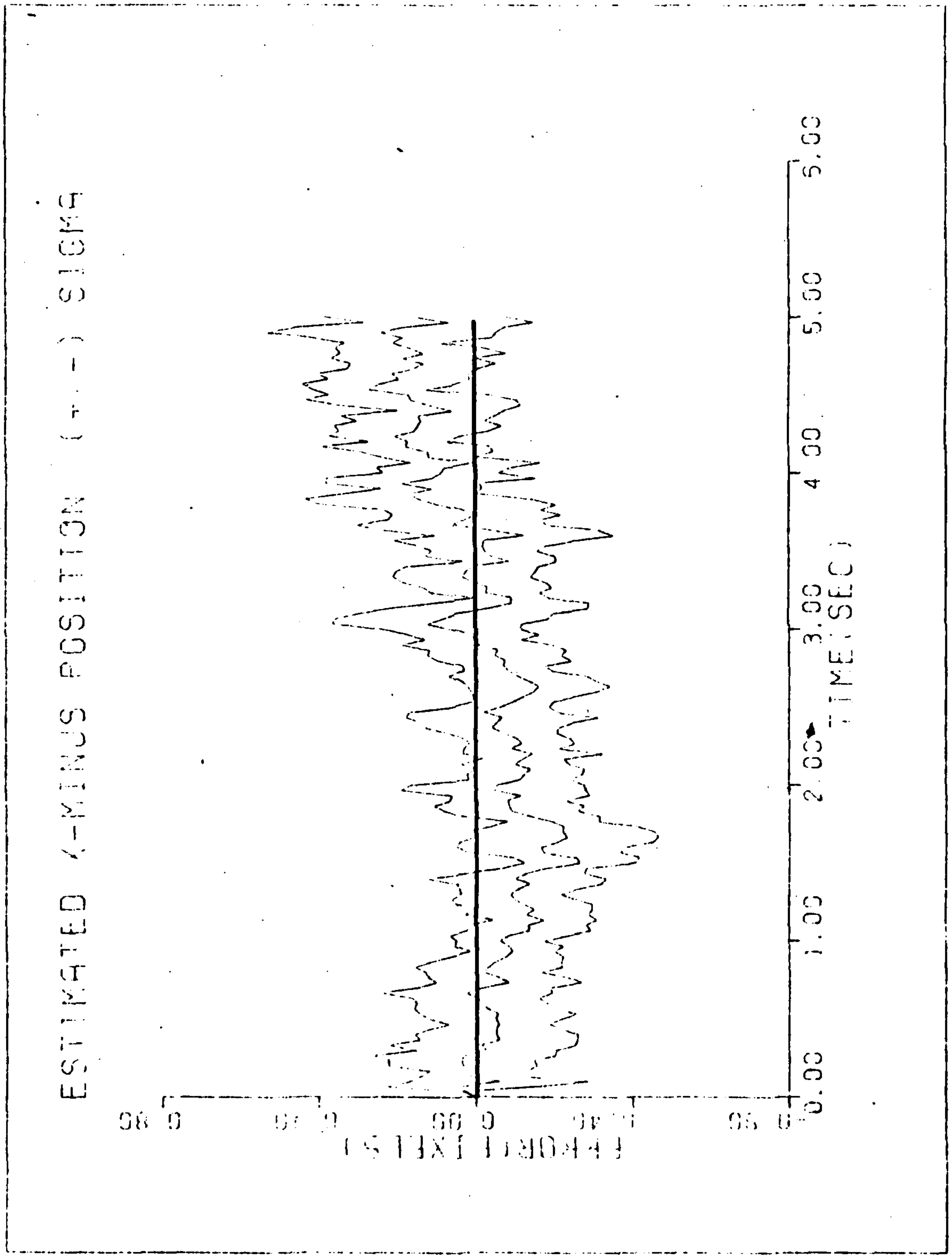

Figure C-16c. Case 16

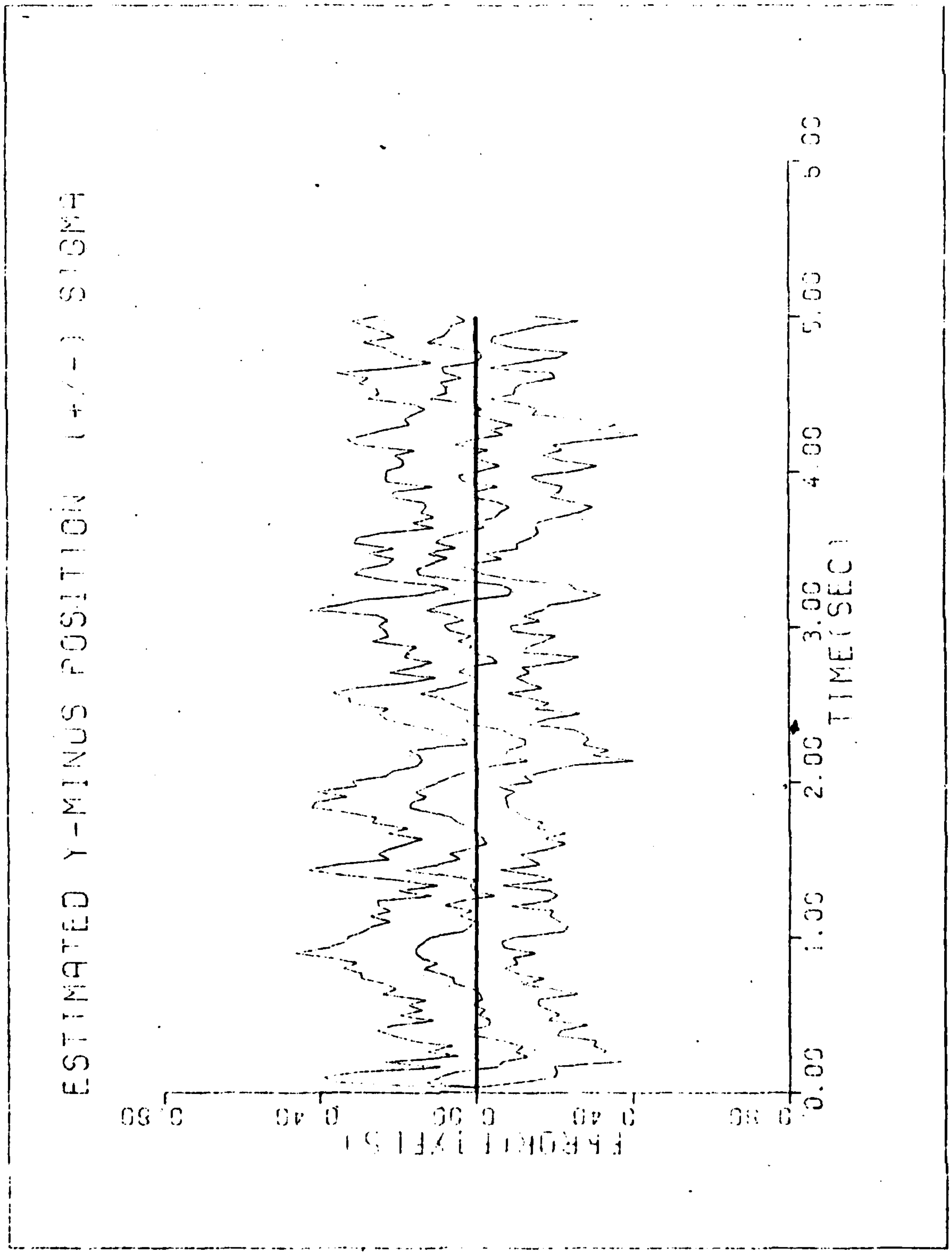

Figure C-16d. Case 16

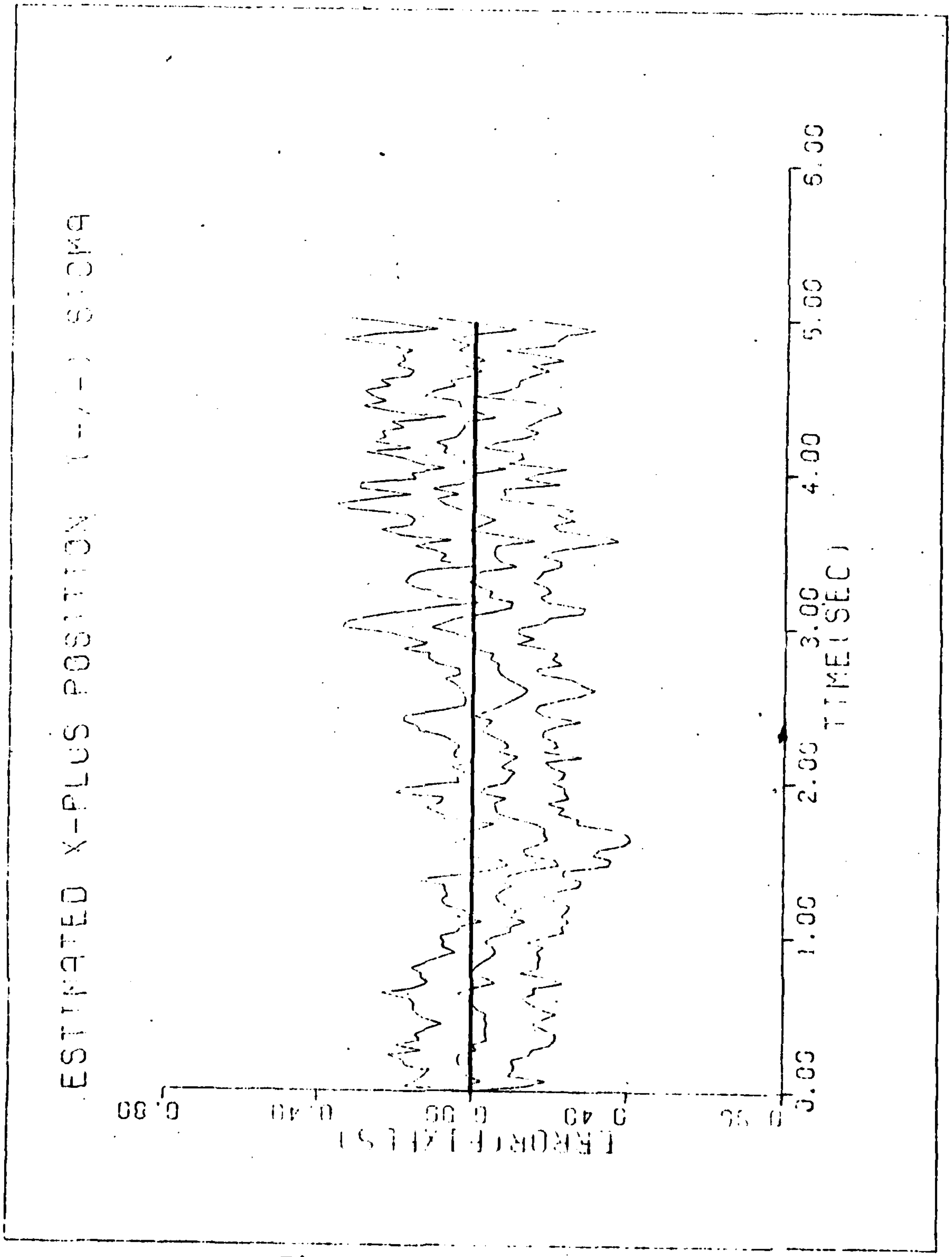

Figure C-16e. Case 16

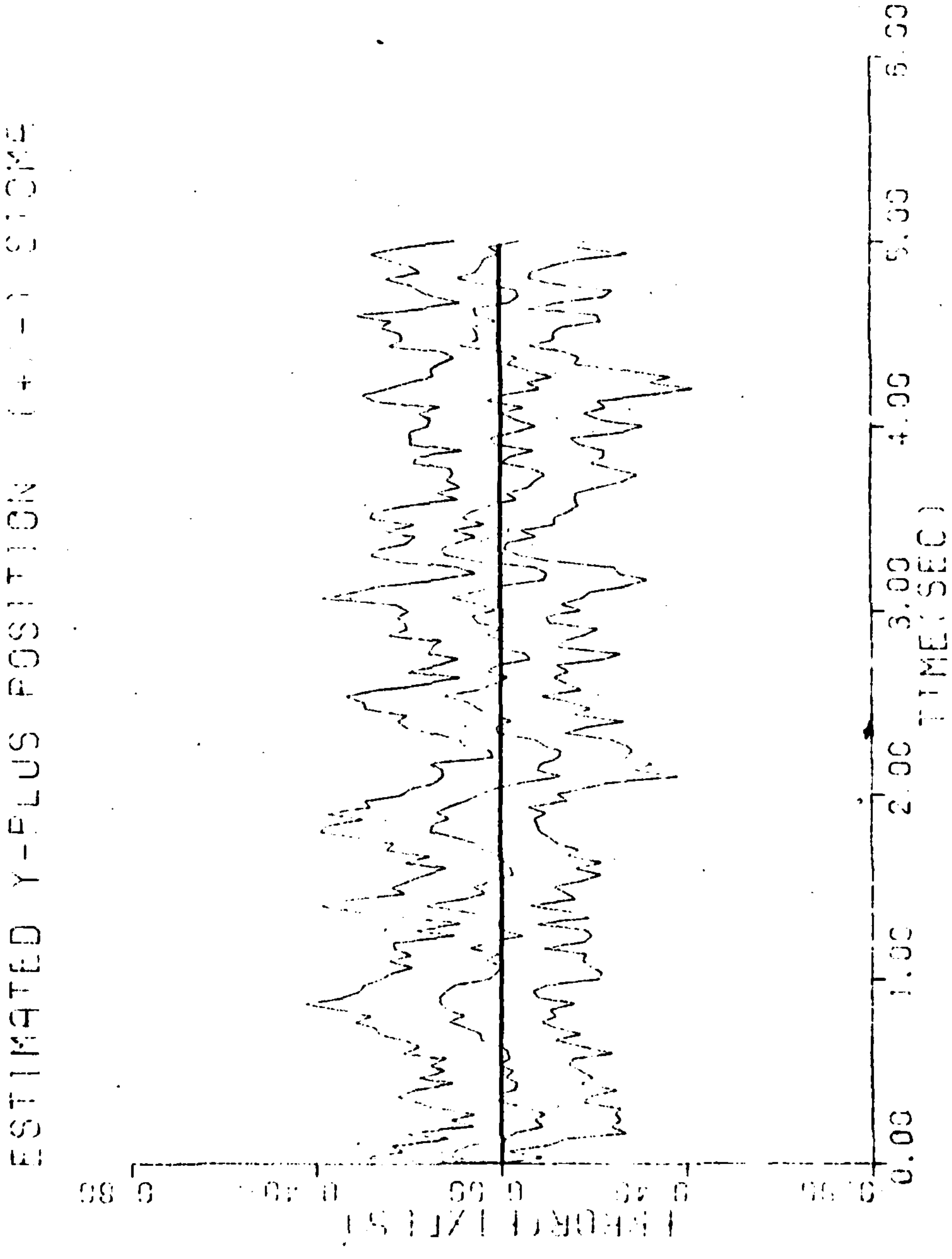

Figure C-16f. Case 16

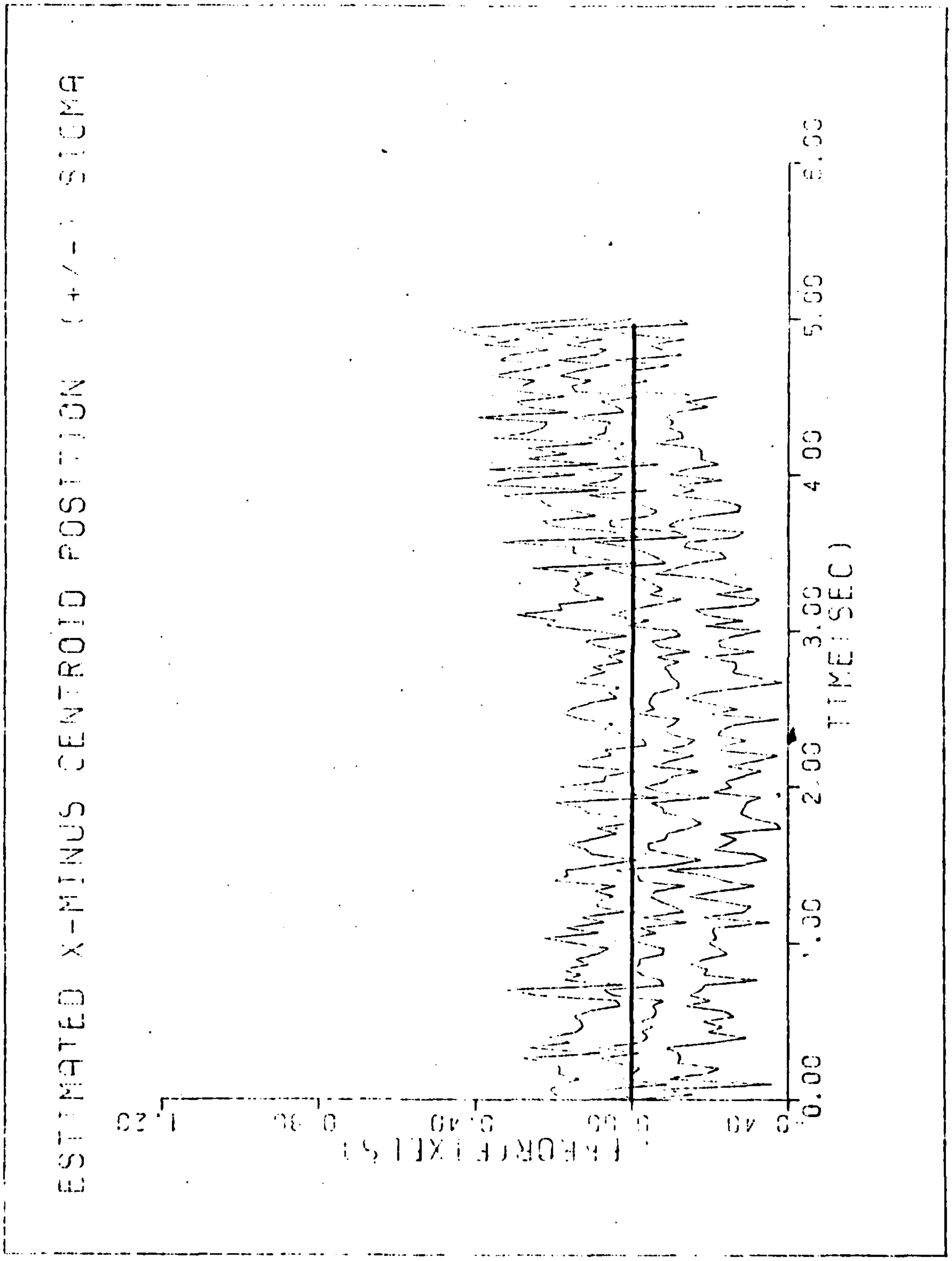

Figure C-16g. Case 16

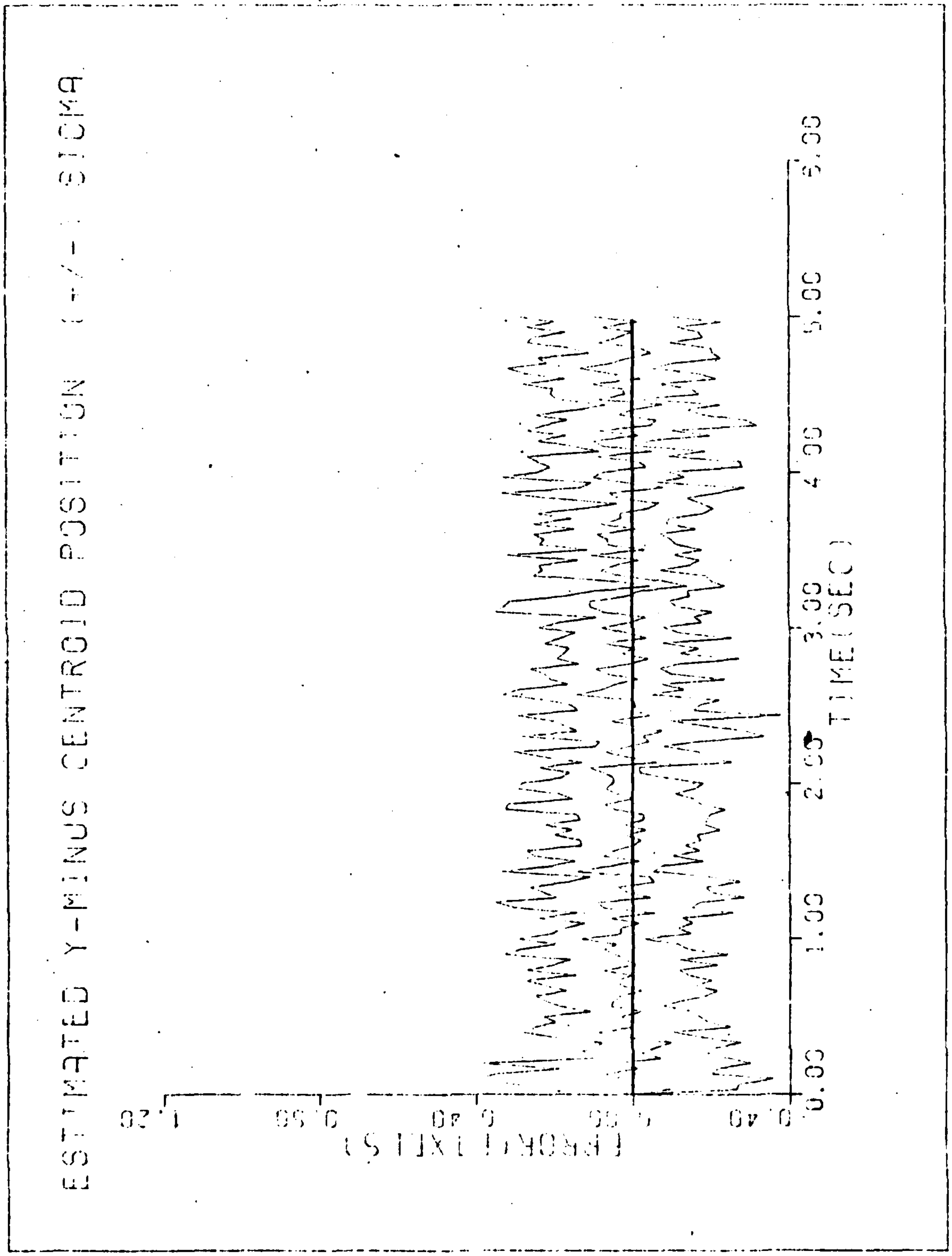

Figure C-16h. Case 16

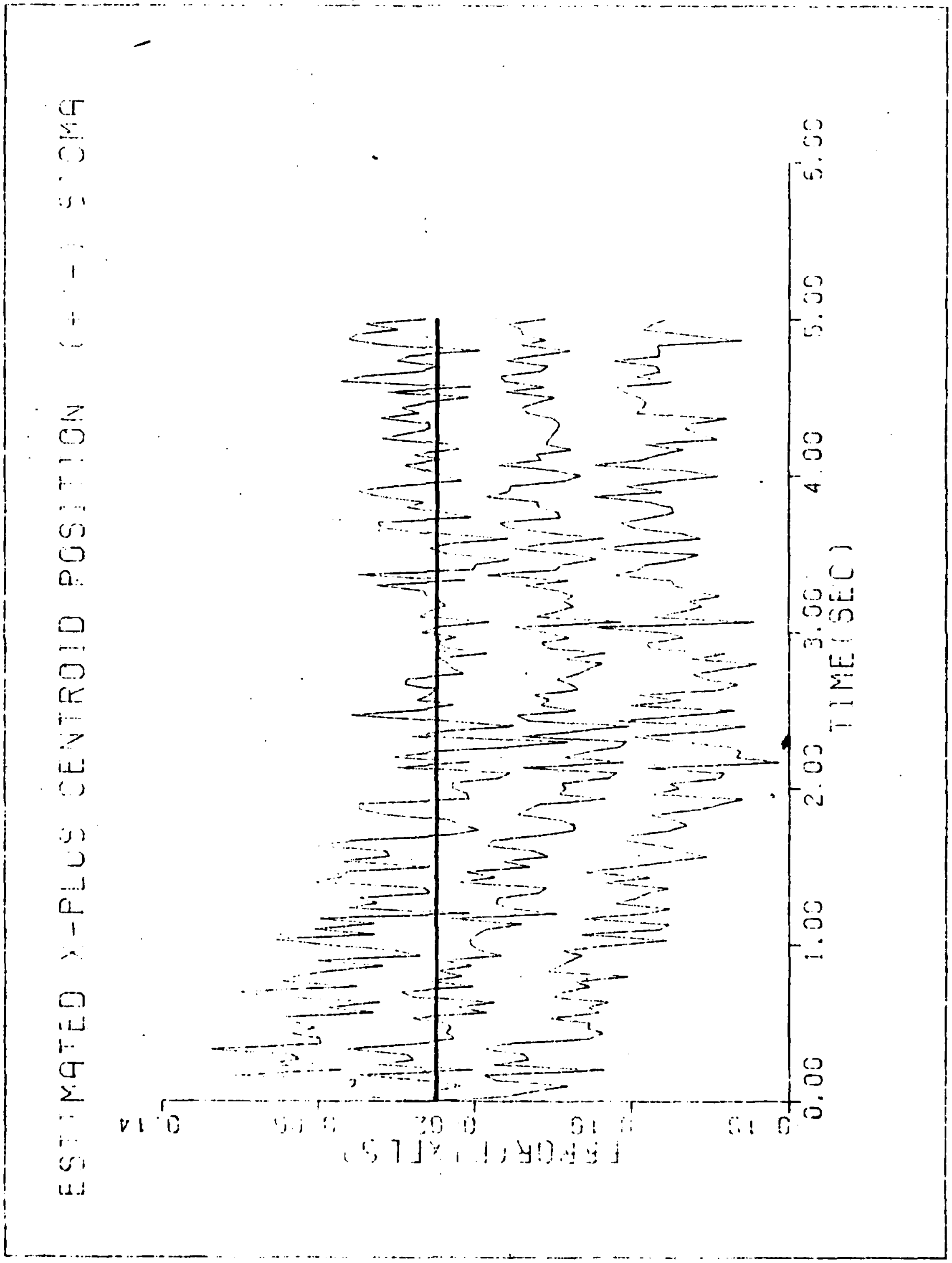

Figure C-16i. Case 16

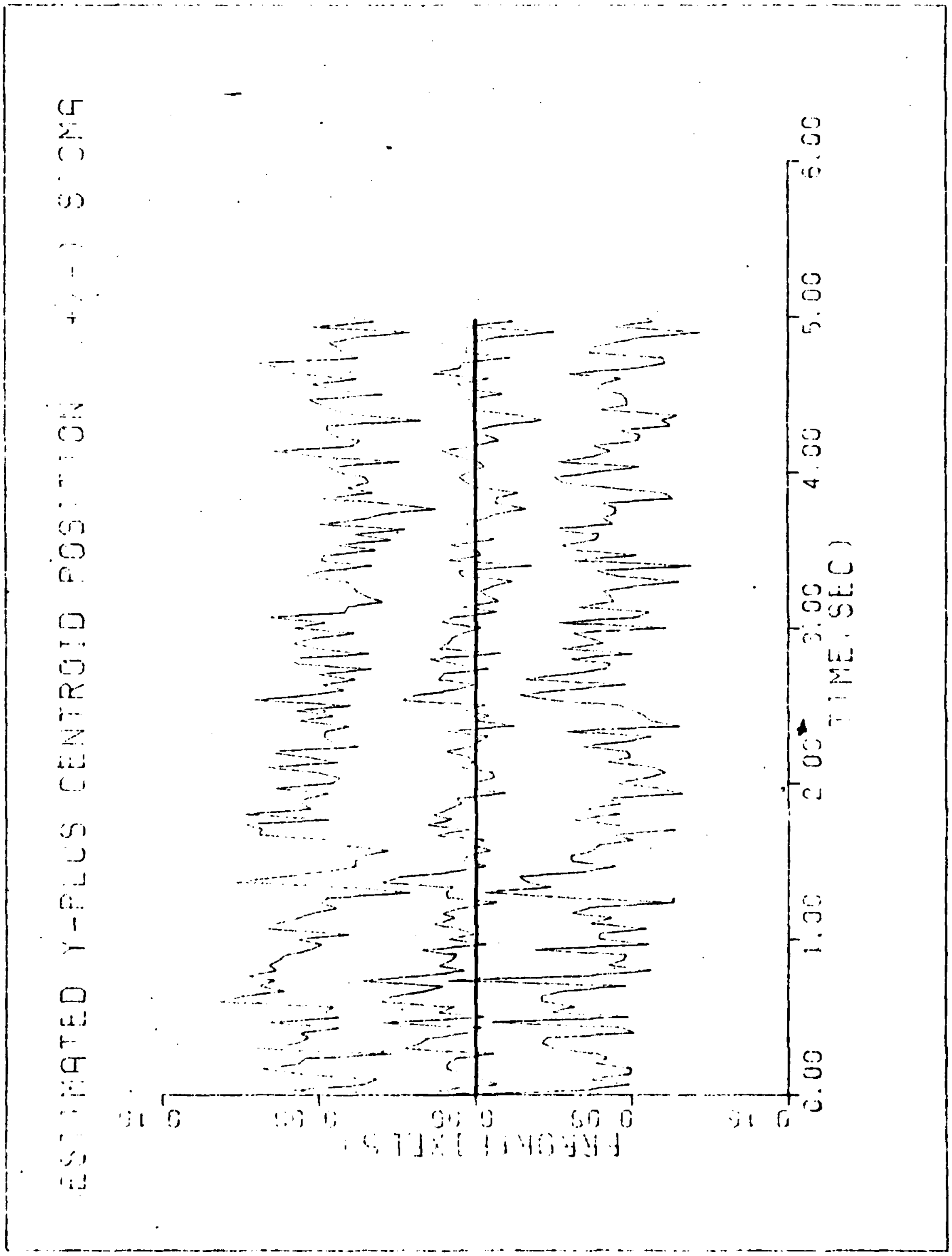

Figure C-16-j. Case 16

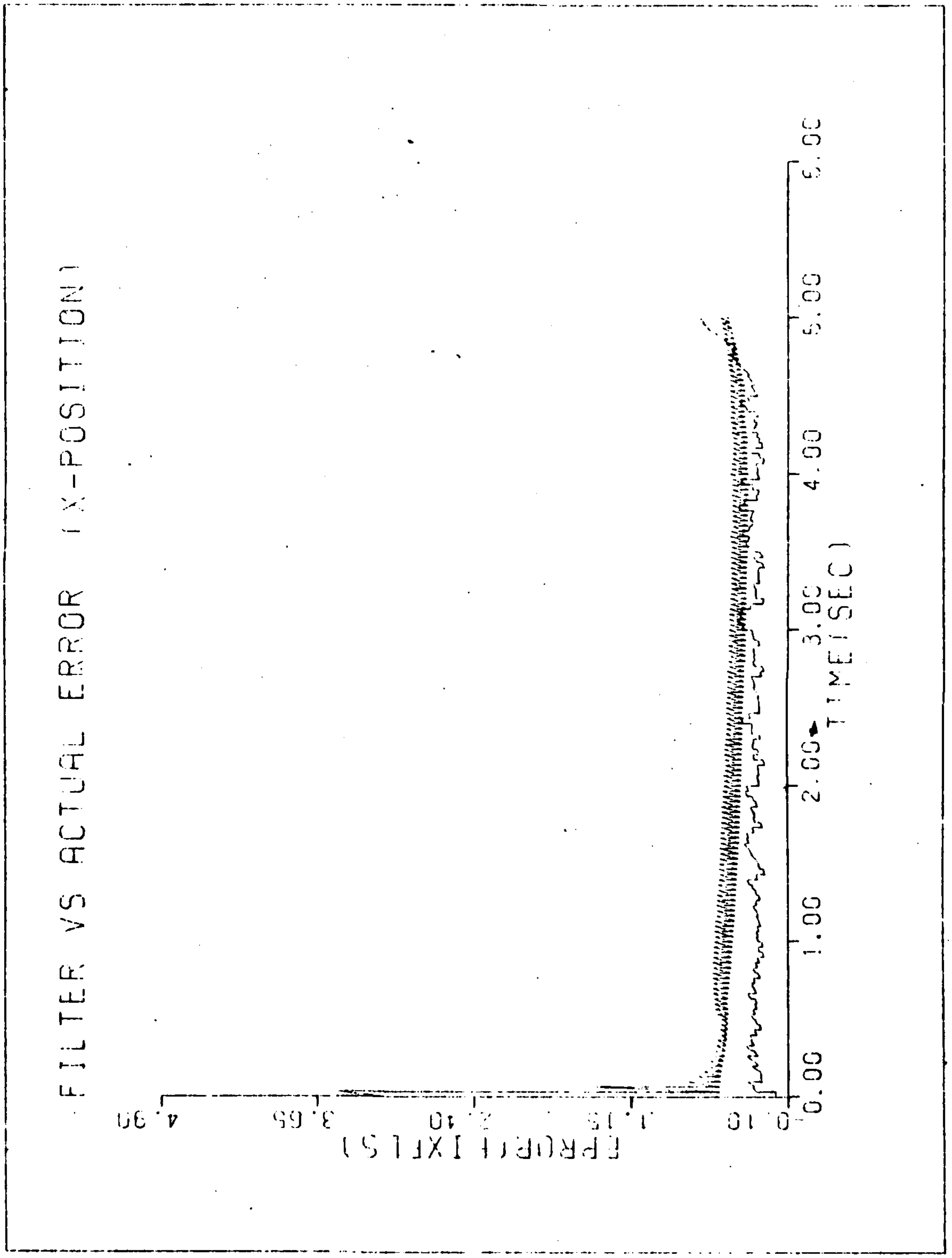

Figure C-17a. Case 17

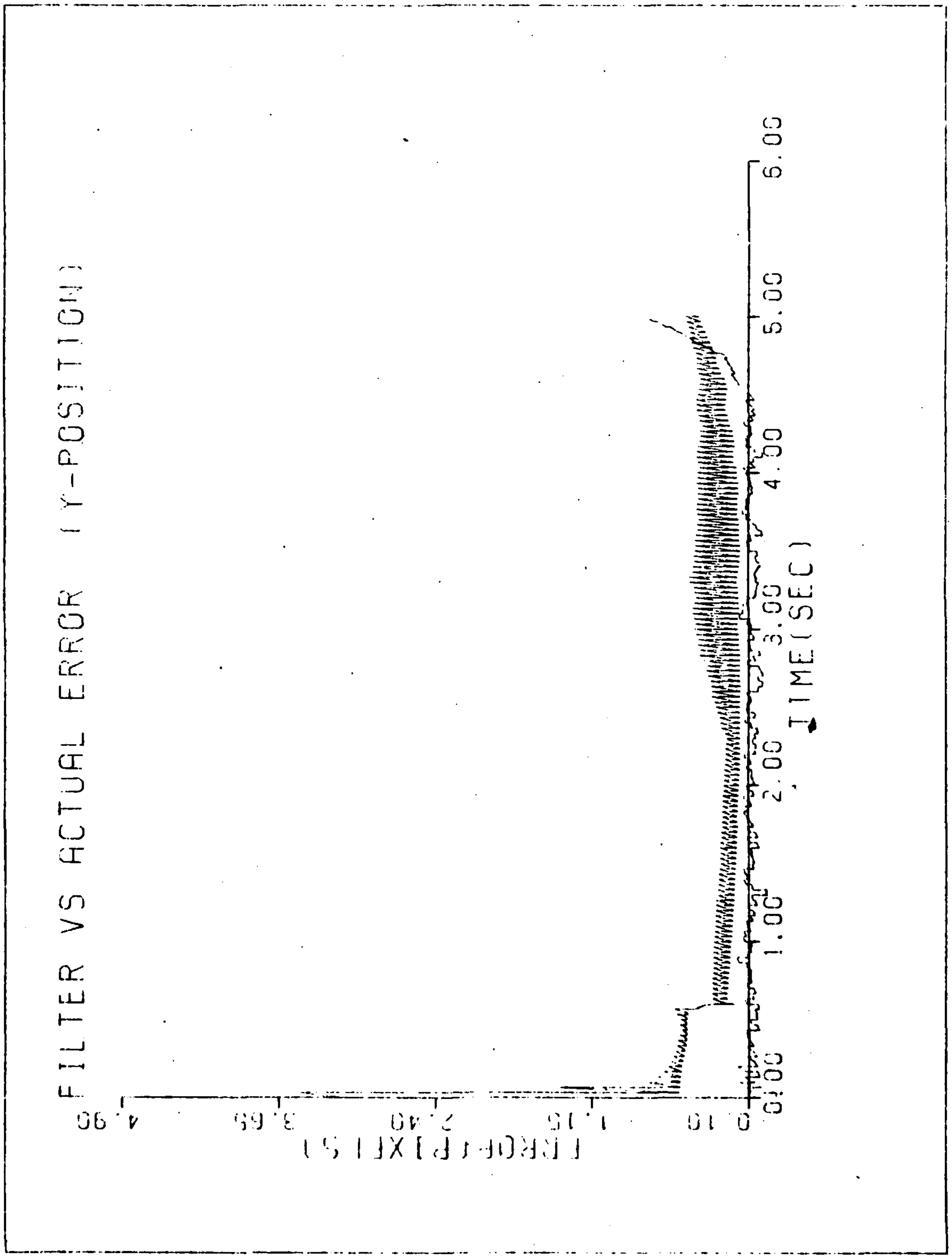

Figure C-17b. Case 17

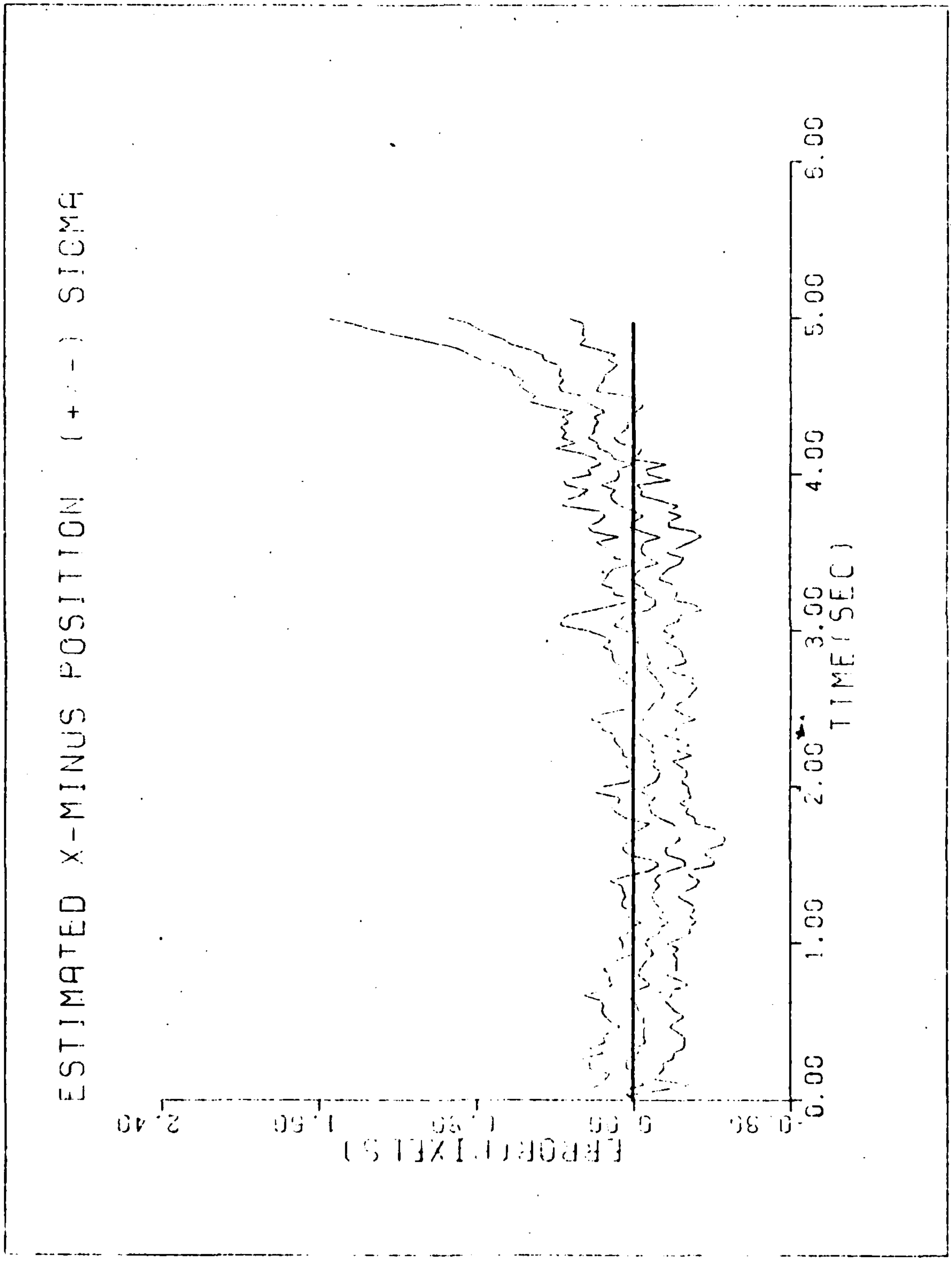

Figure C-17c. Case 17

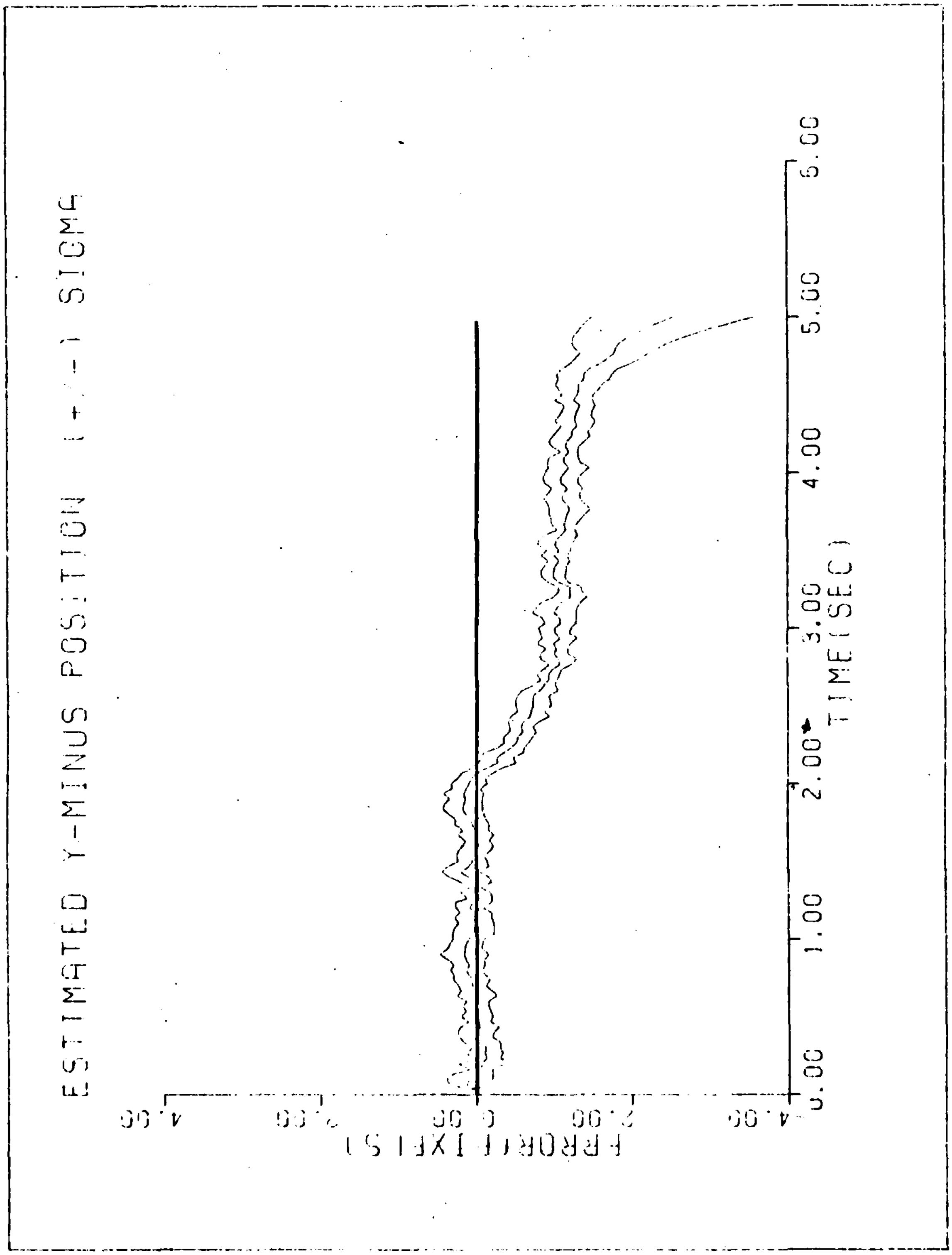

Figure C-17d. Case 17

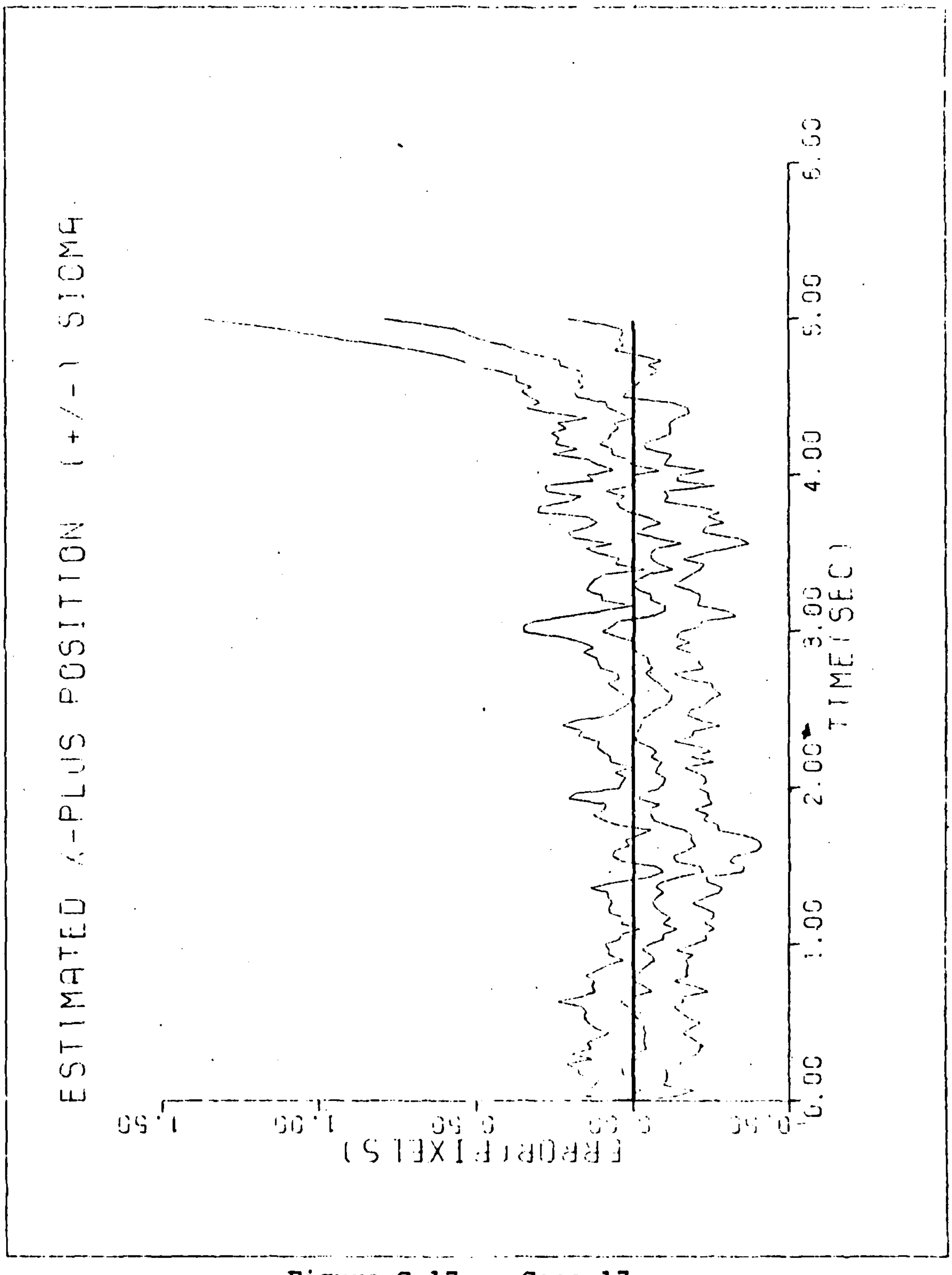

Figure C-17e. Case 17

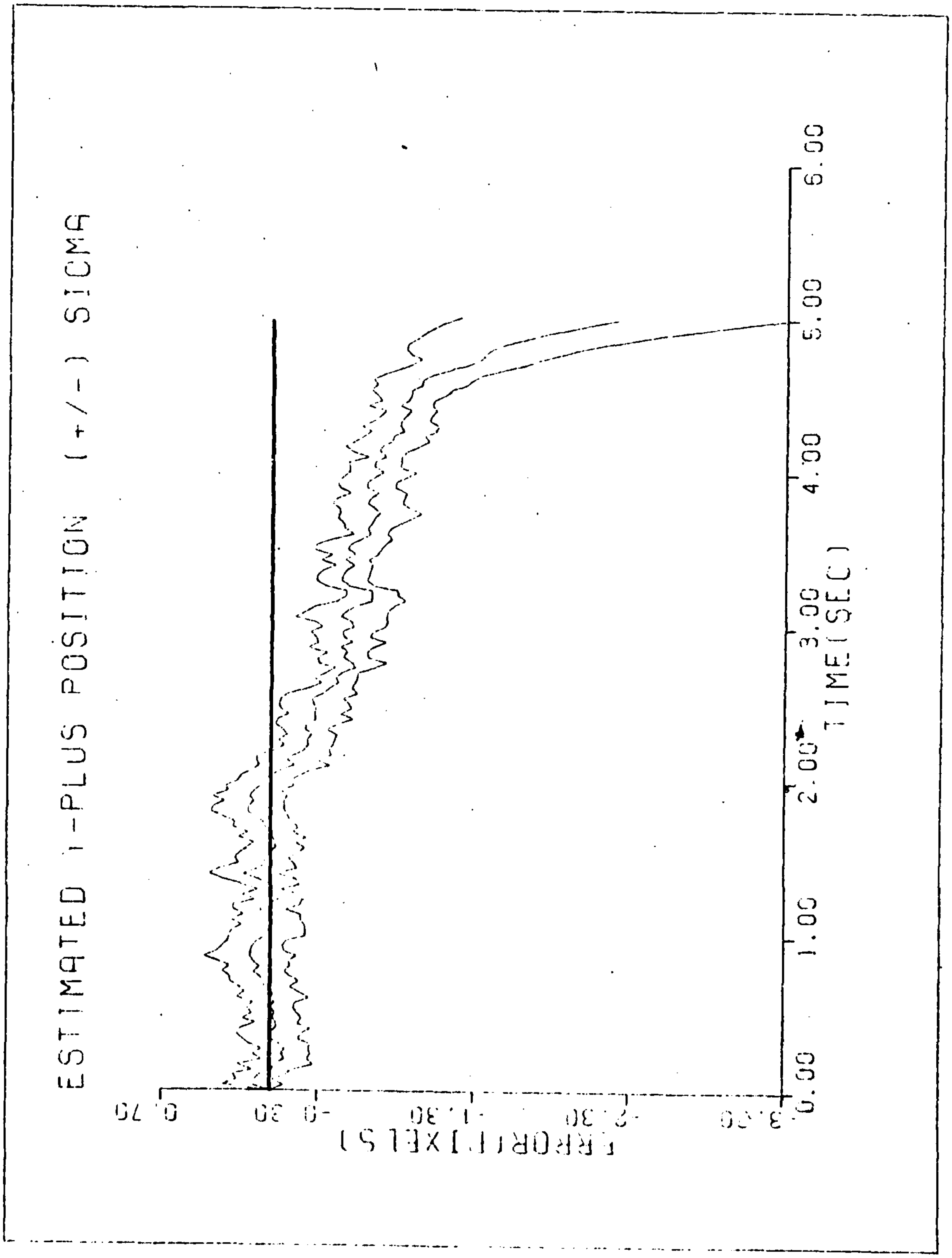

Figure C-17f. Case 17

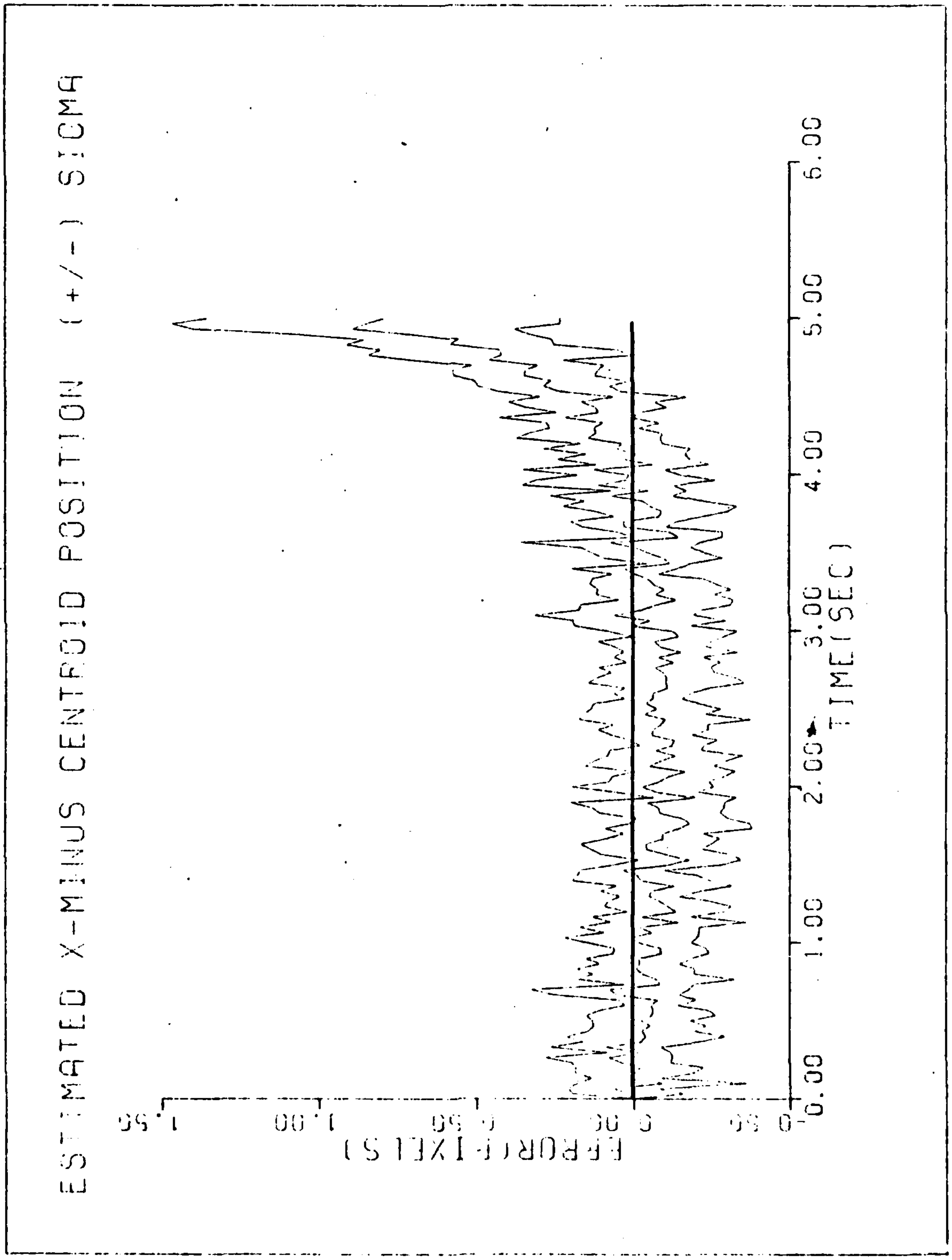

Figure C-17g. Case 17

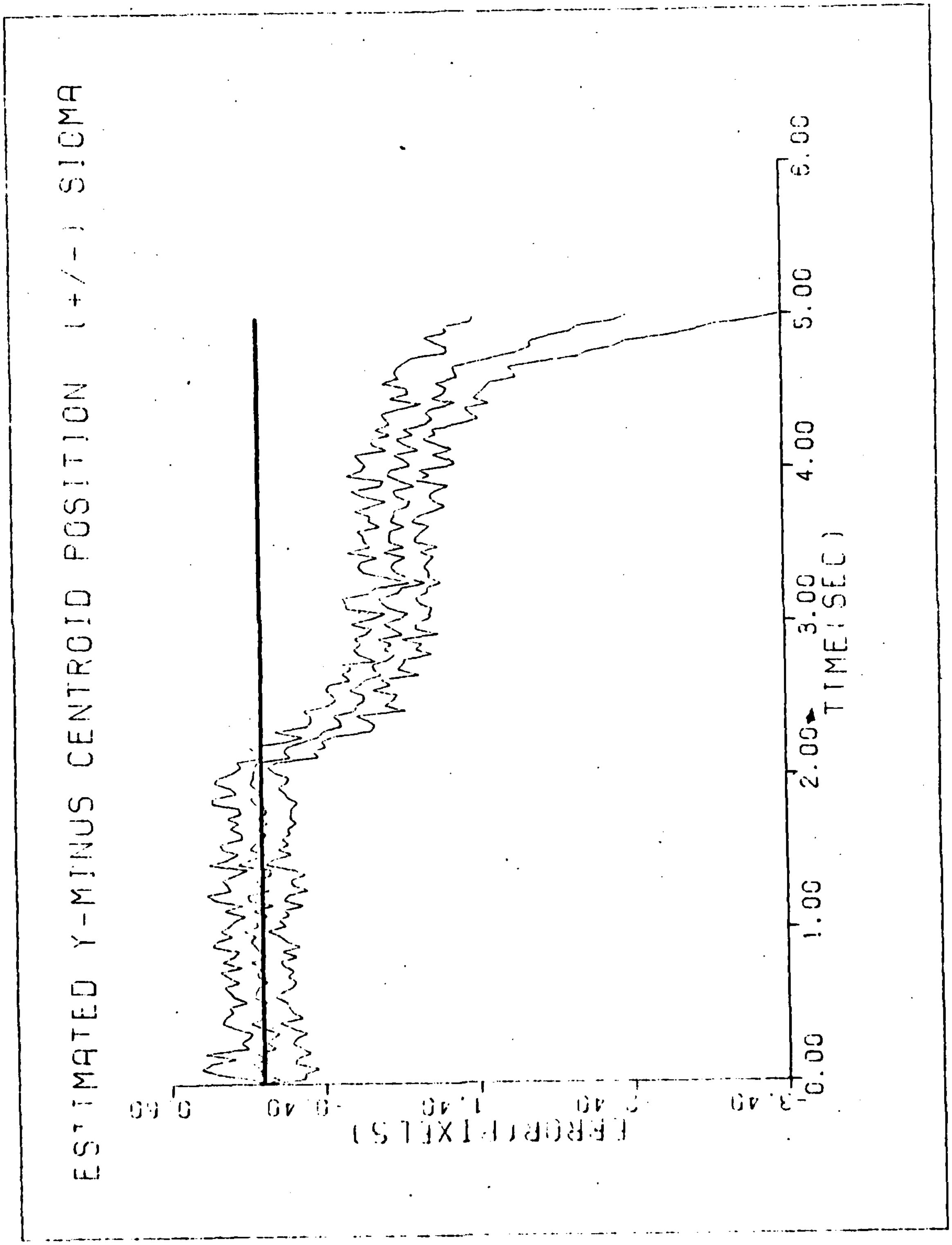

Figure C-17h. Case 17

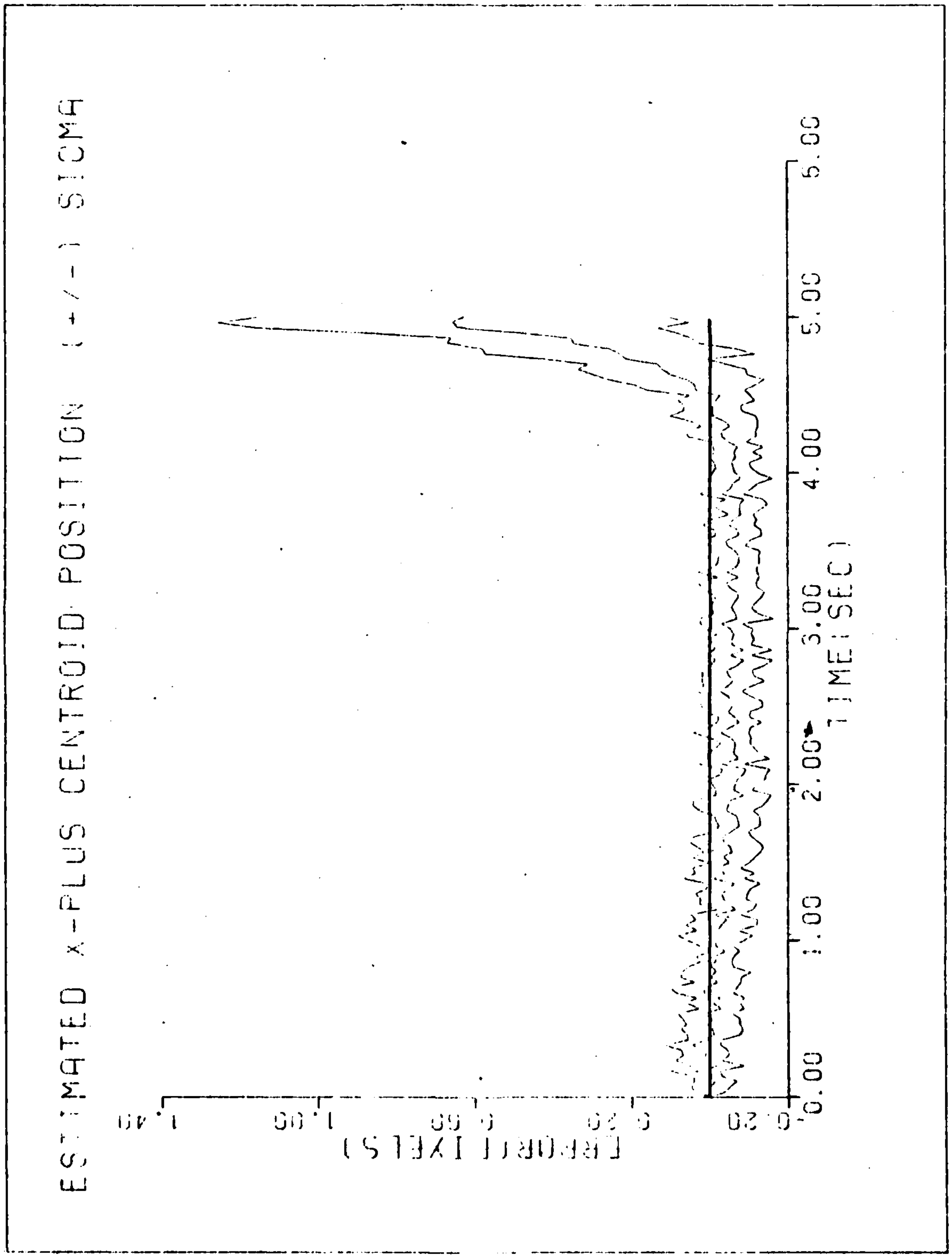

Figure C-17i. Case 17

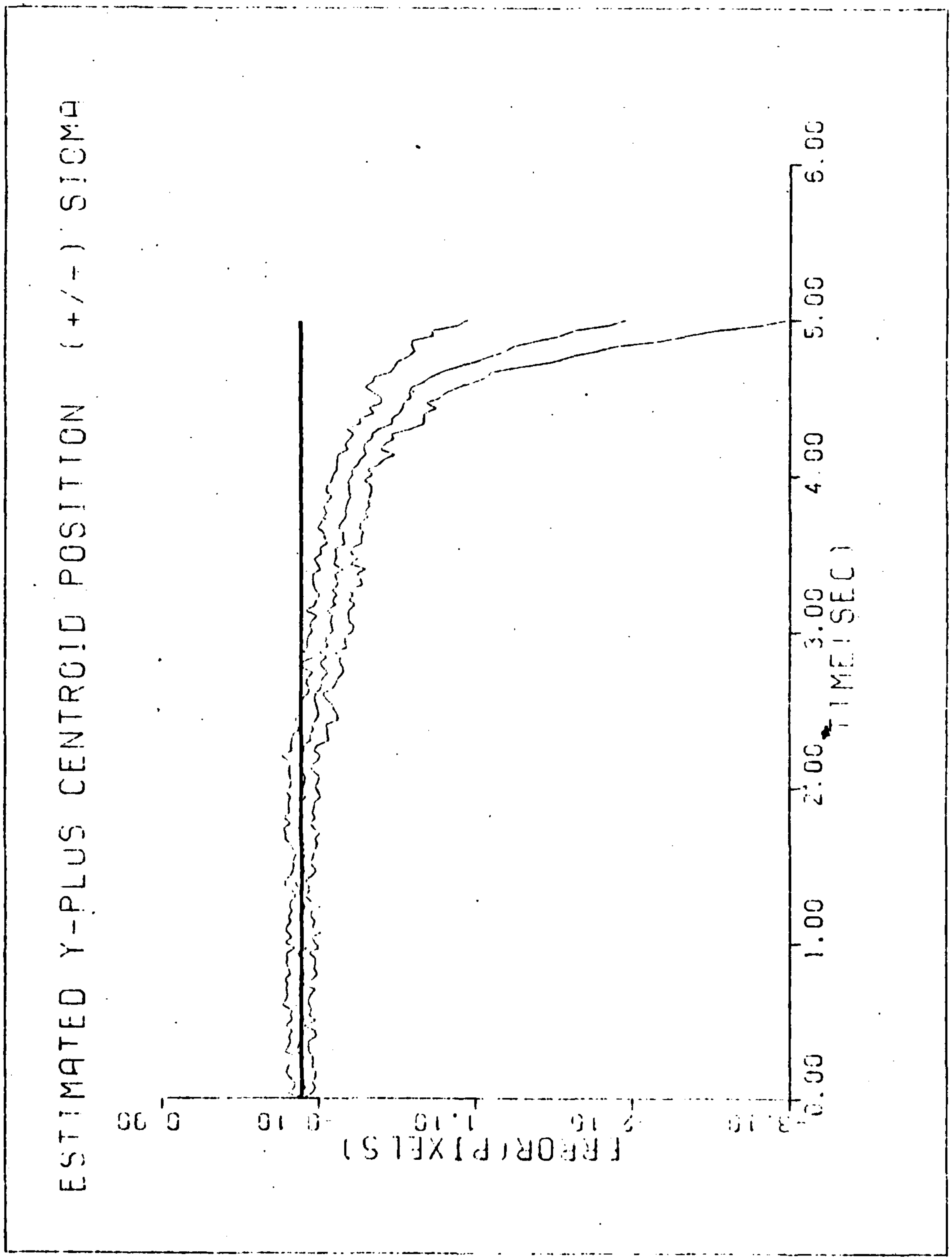

Figure C-17j. Case 17

The performance plots for this case were similar to the plots shown for case 12, thus they are omitted.

Figure C-18. Case 18

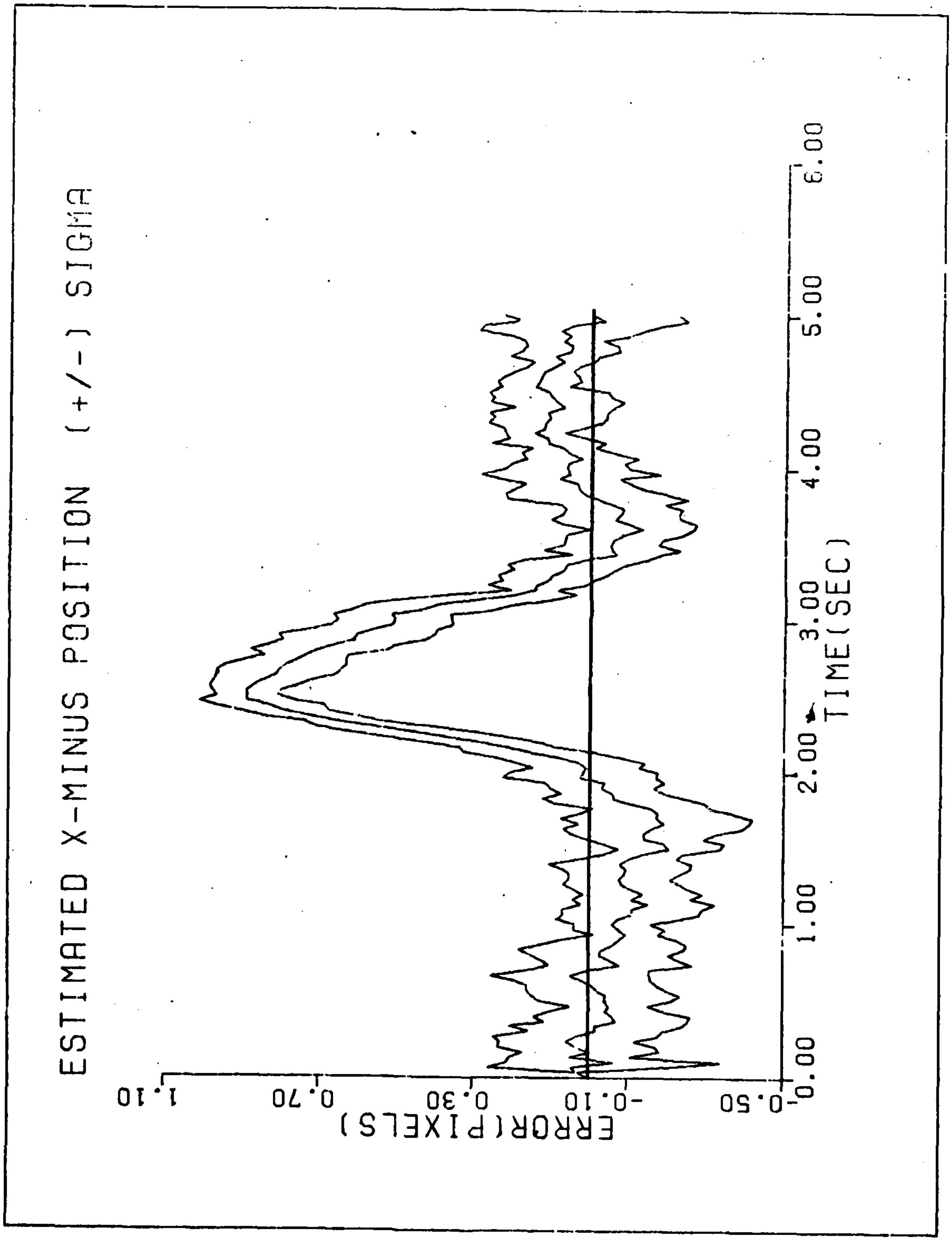

Figure C-19a. Case 19

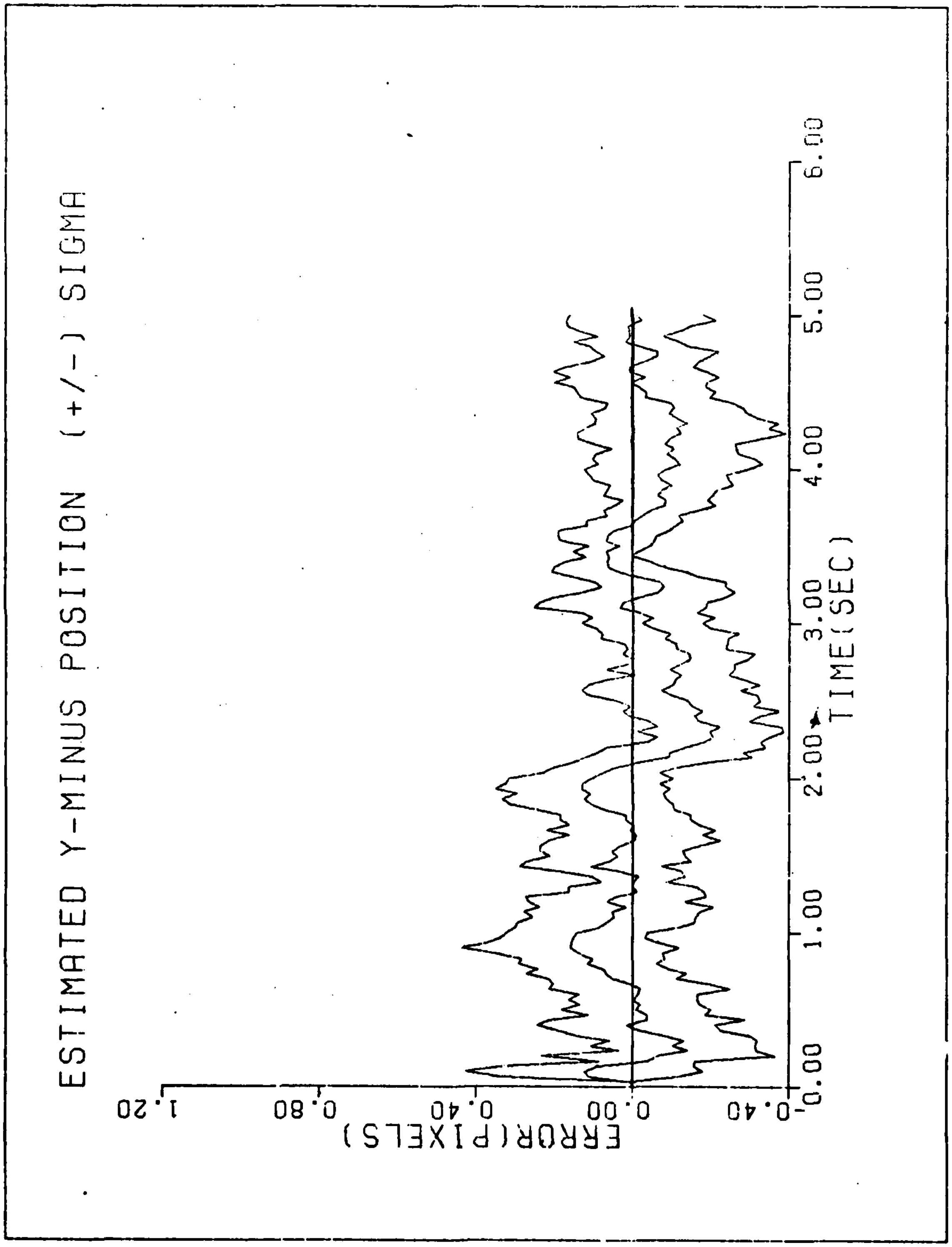

Figure C-19b. Case 19

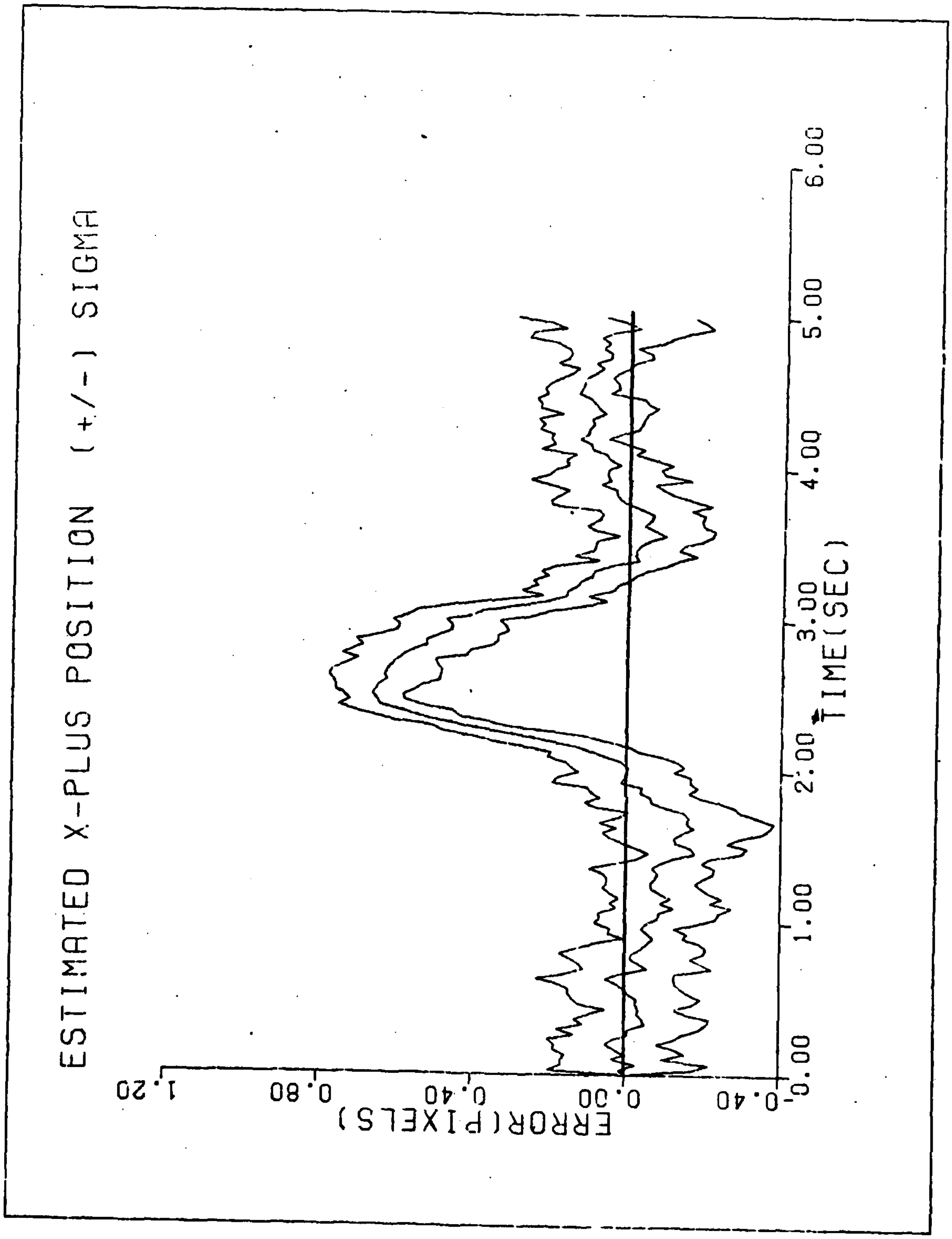

Figure C-19c. Case 19

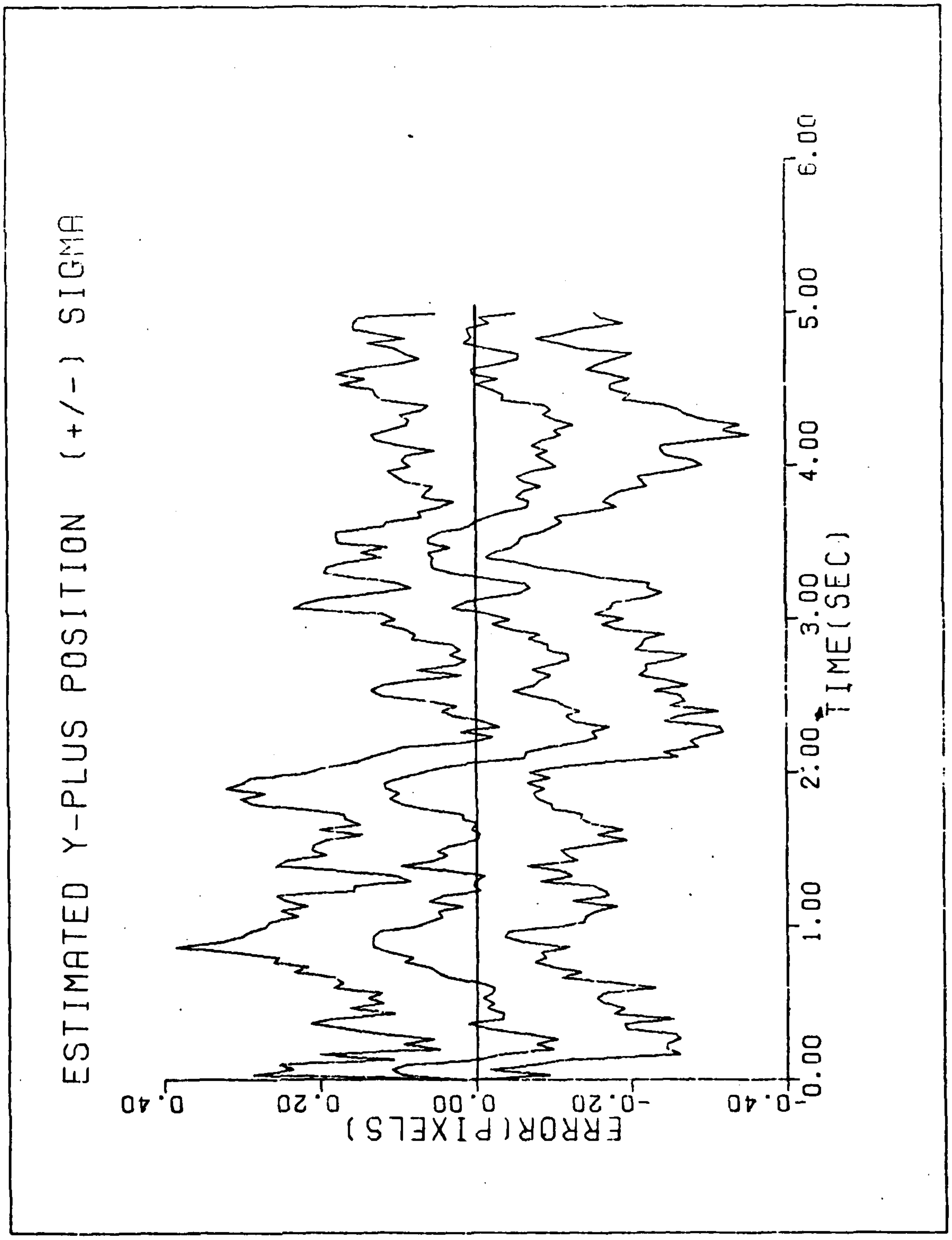

Figure C-19d. Case 19

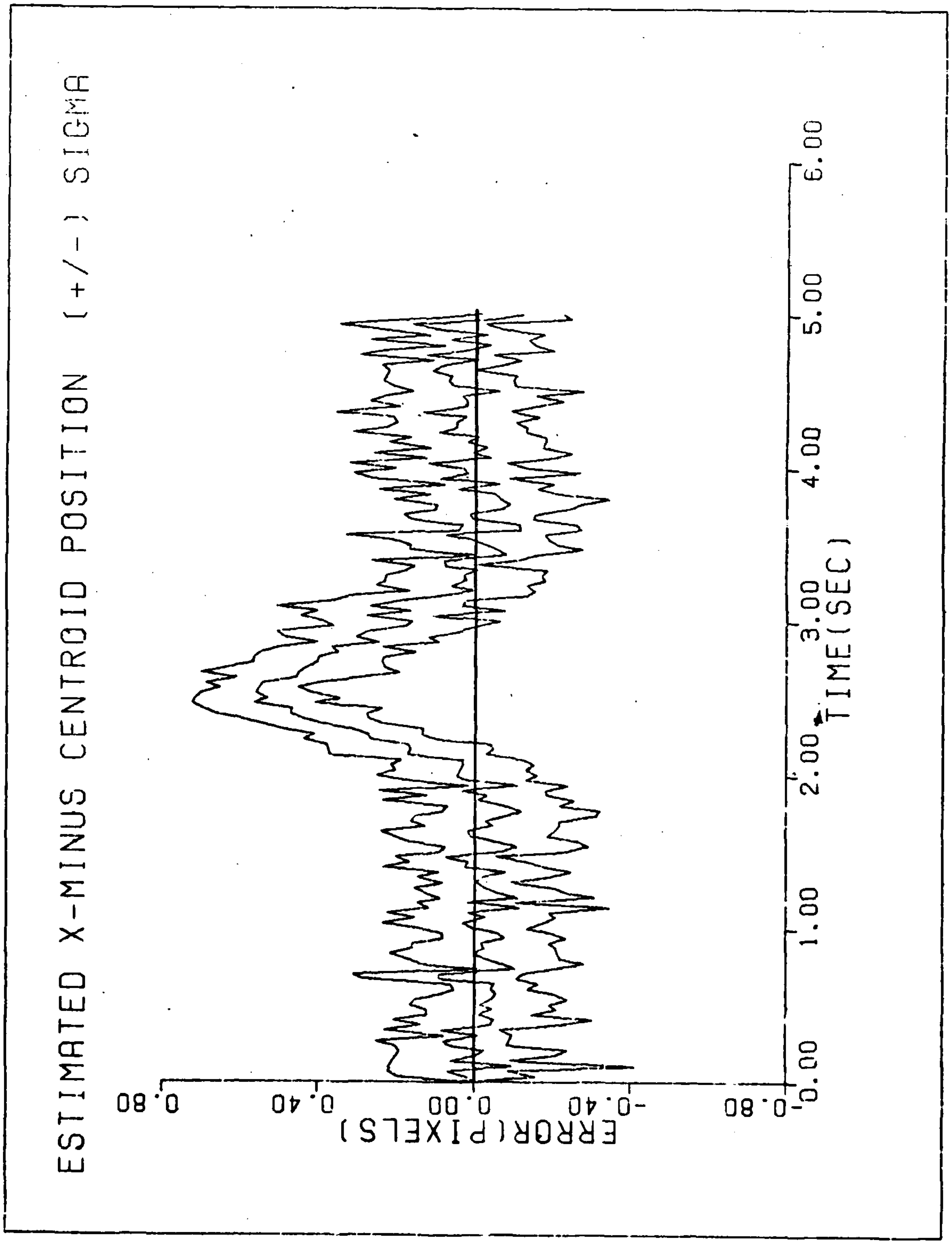

Figure C-19e. Case 19

AD-A124 884 ENHANCED TRACKING OF AIRBORNE TARGETS USING A 4/4
CORRELATOR/KALMAN FILTER(U) AIR FORCE INST OF TECH
WRIGHT-PATTERSON AFB OH SCHOOL OF ENGINEERING
UNCLASSIFIED P P MILLNER DEC 82 AFIT/GE/EE/82D-50 F/G 12/1 NL

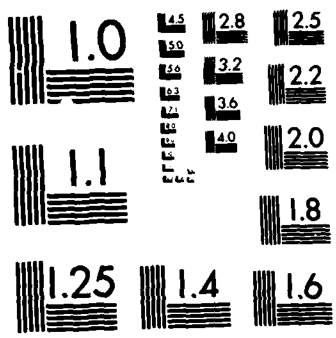

MICROCOPY RESOLUTION TEST CHART
NATIONAL BUREAU OF STANDARDS-1963-A

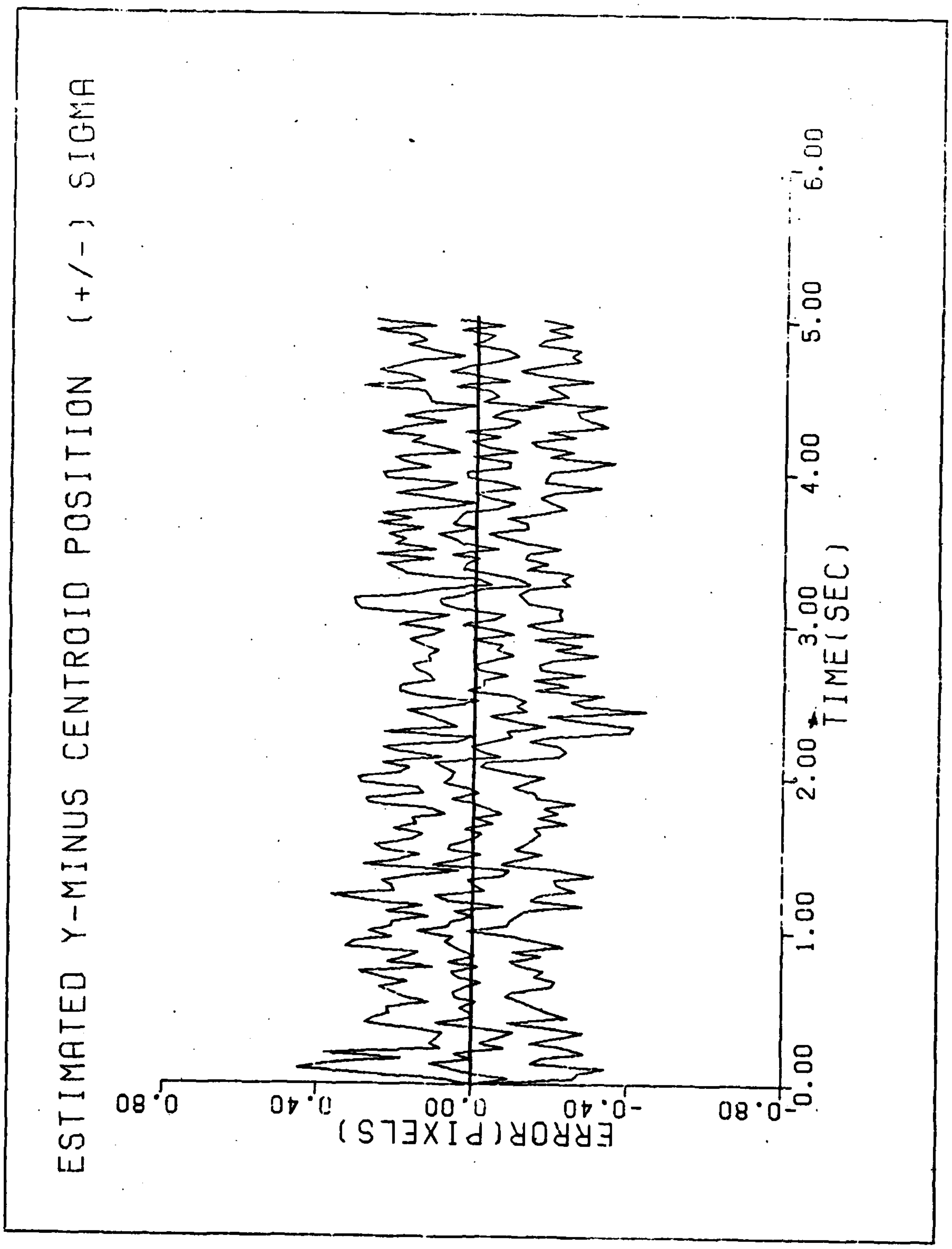

Figure C-19f. Case 19

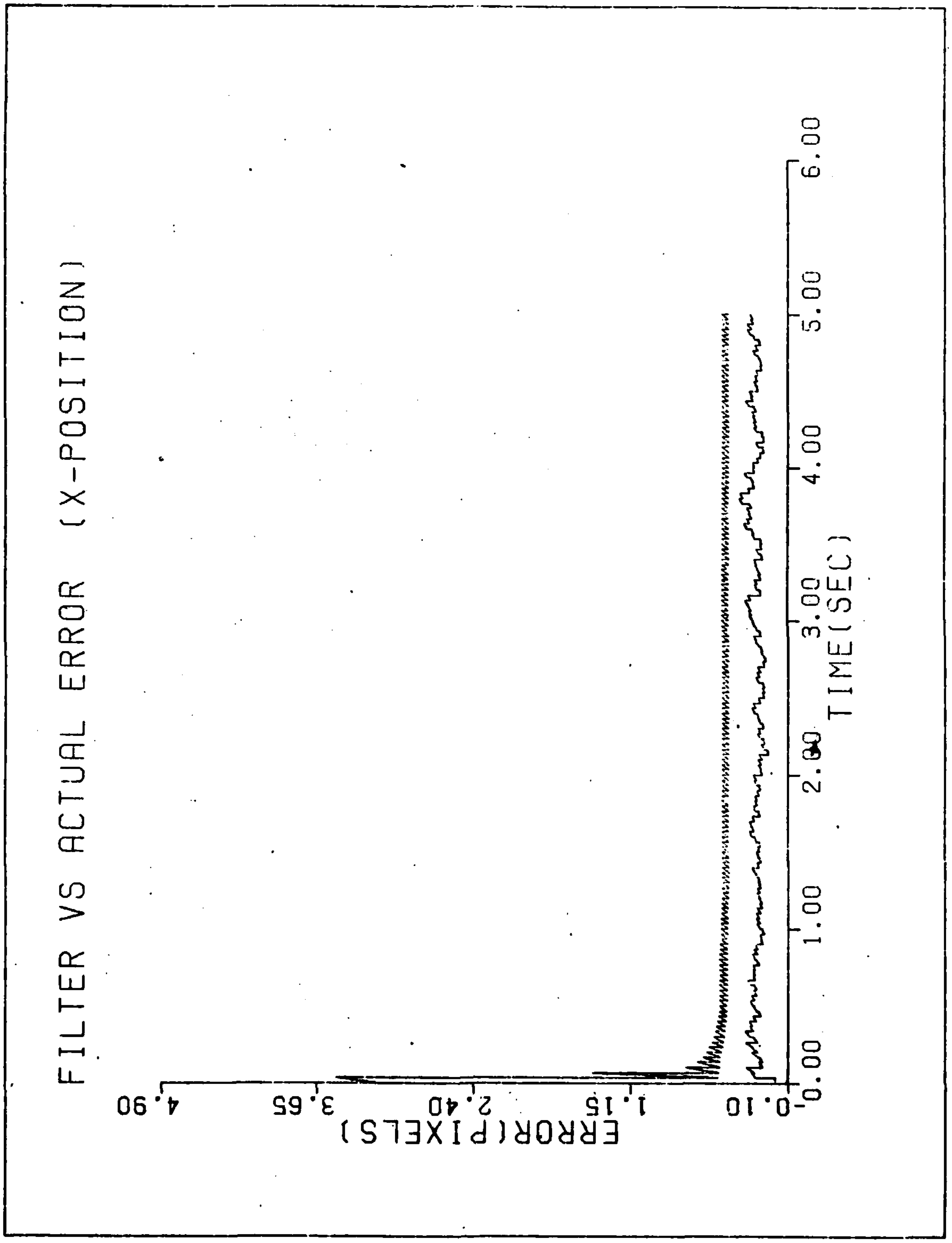

Figure C-20a. Case 20

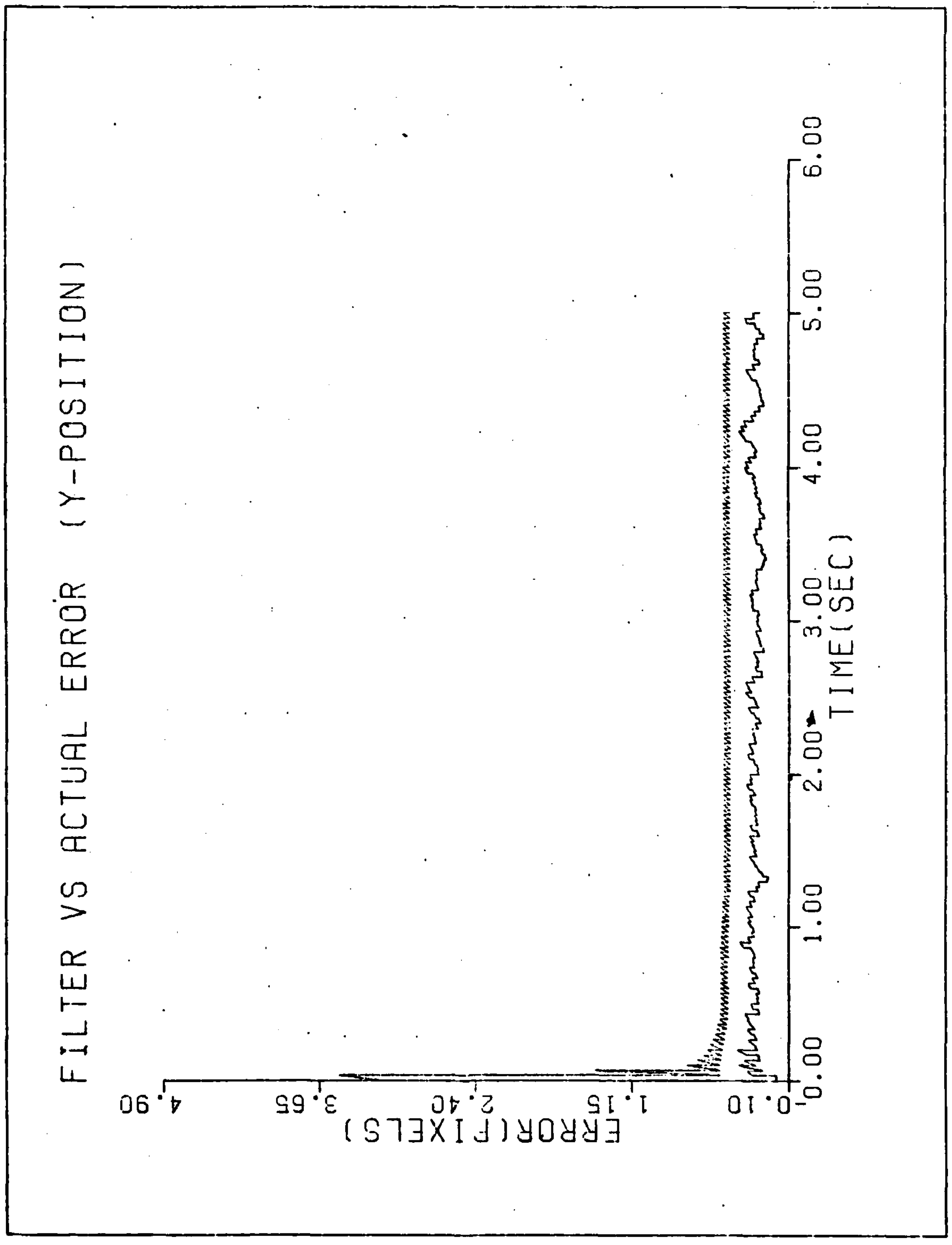

Figure C-20b. Case 20

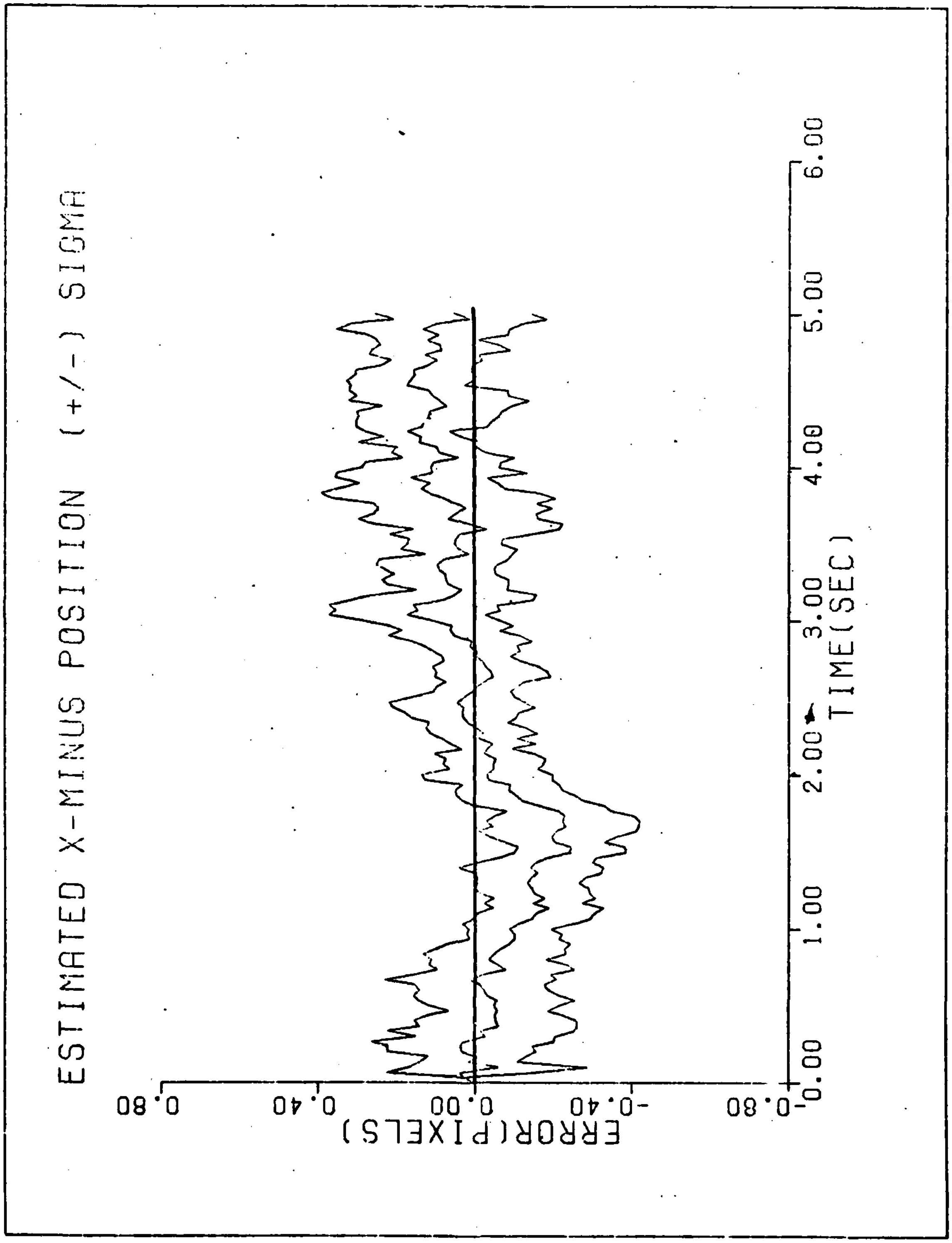

Figure C-20c. Case 20

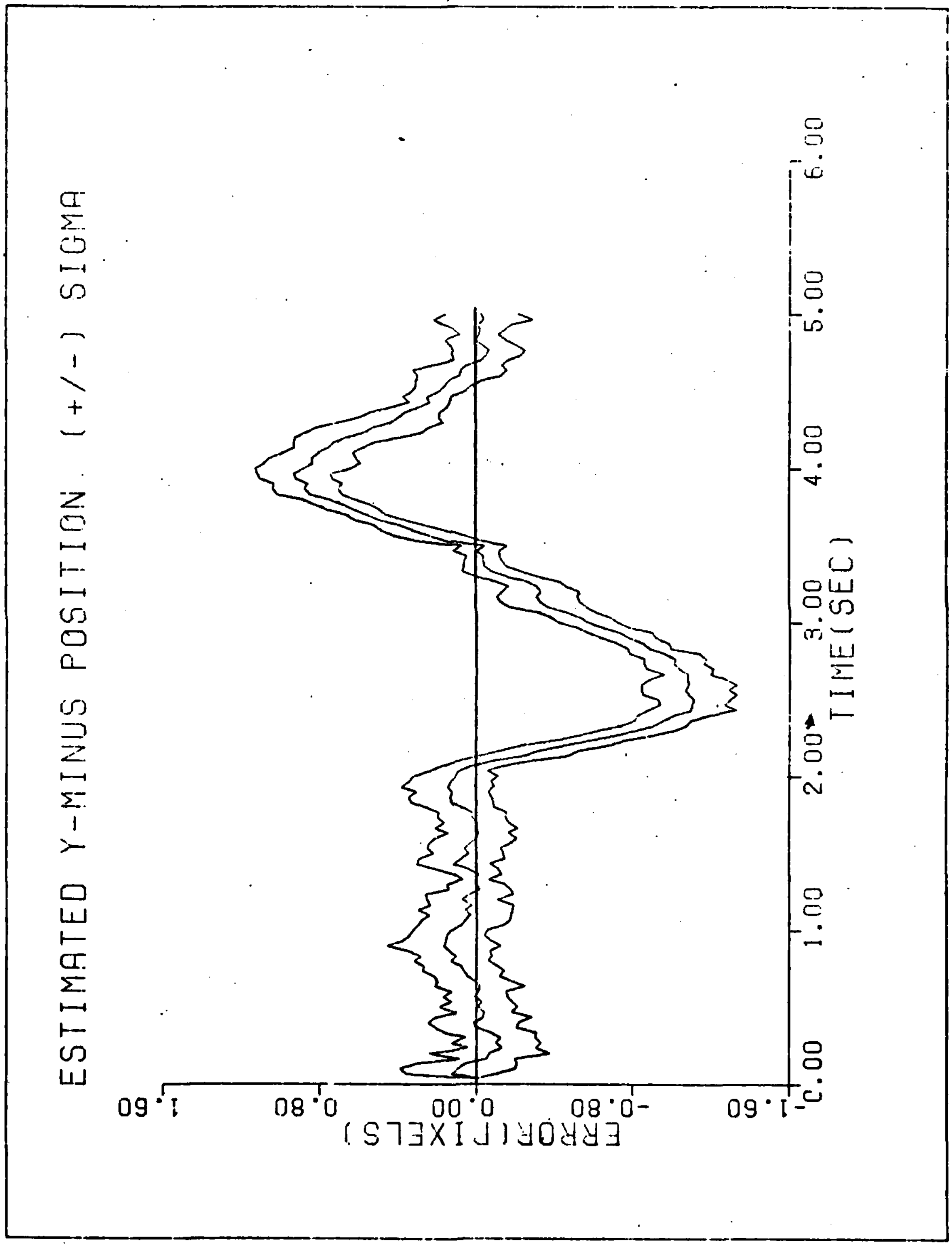

Figure C-20d. Case 20

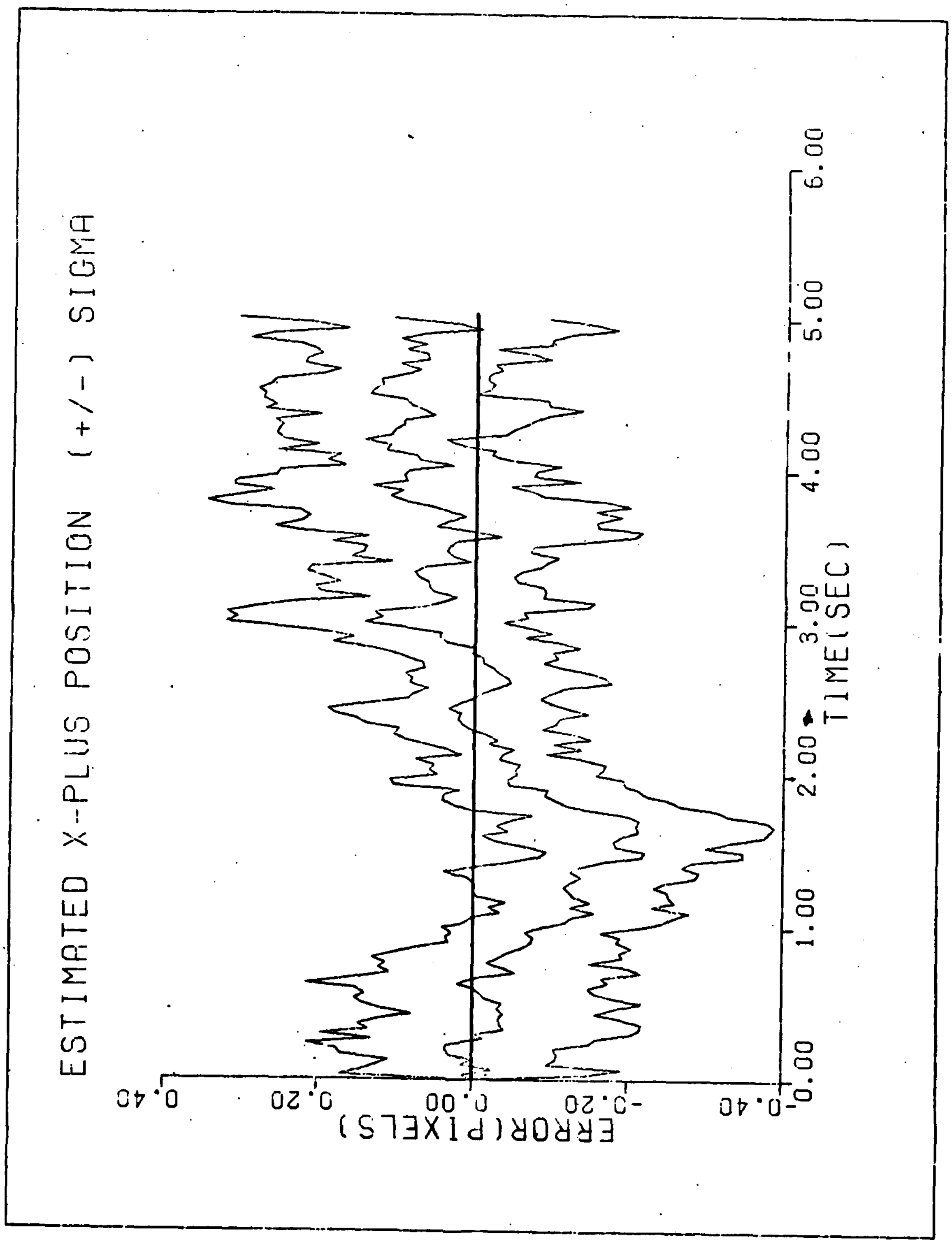

Figure C-20e. Case 20

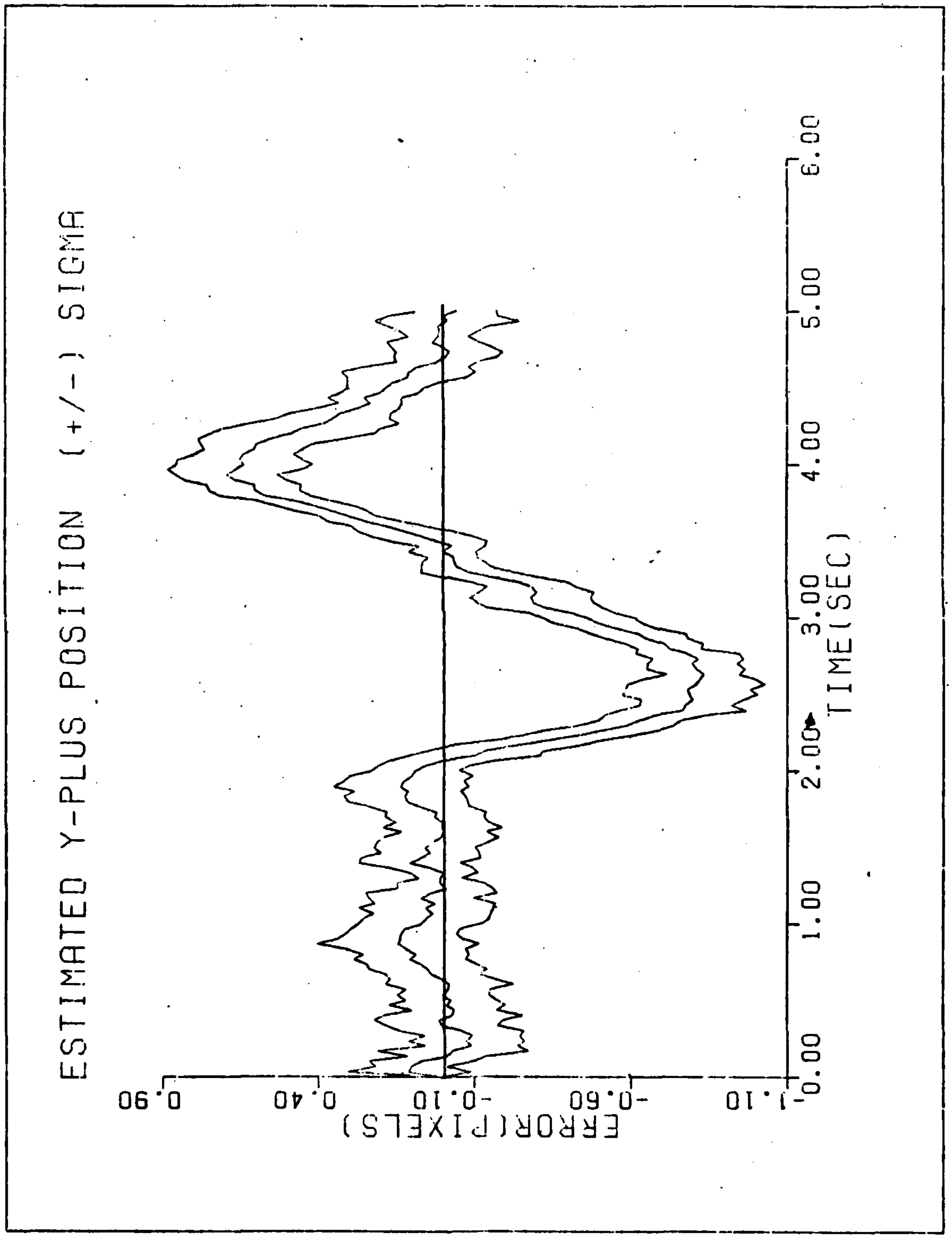

Figure C-20f. Case 20

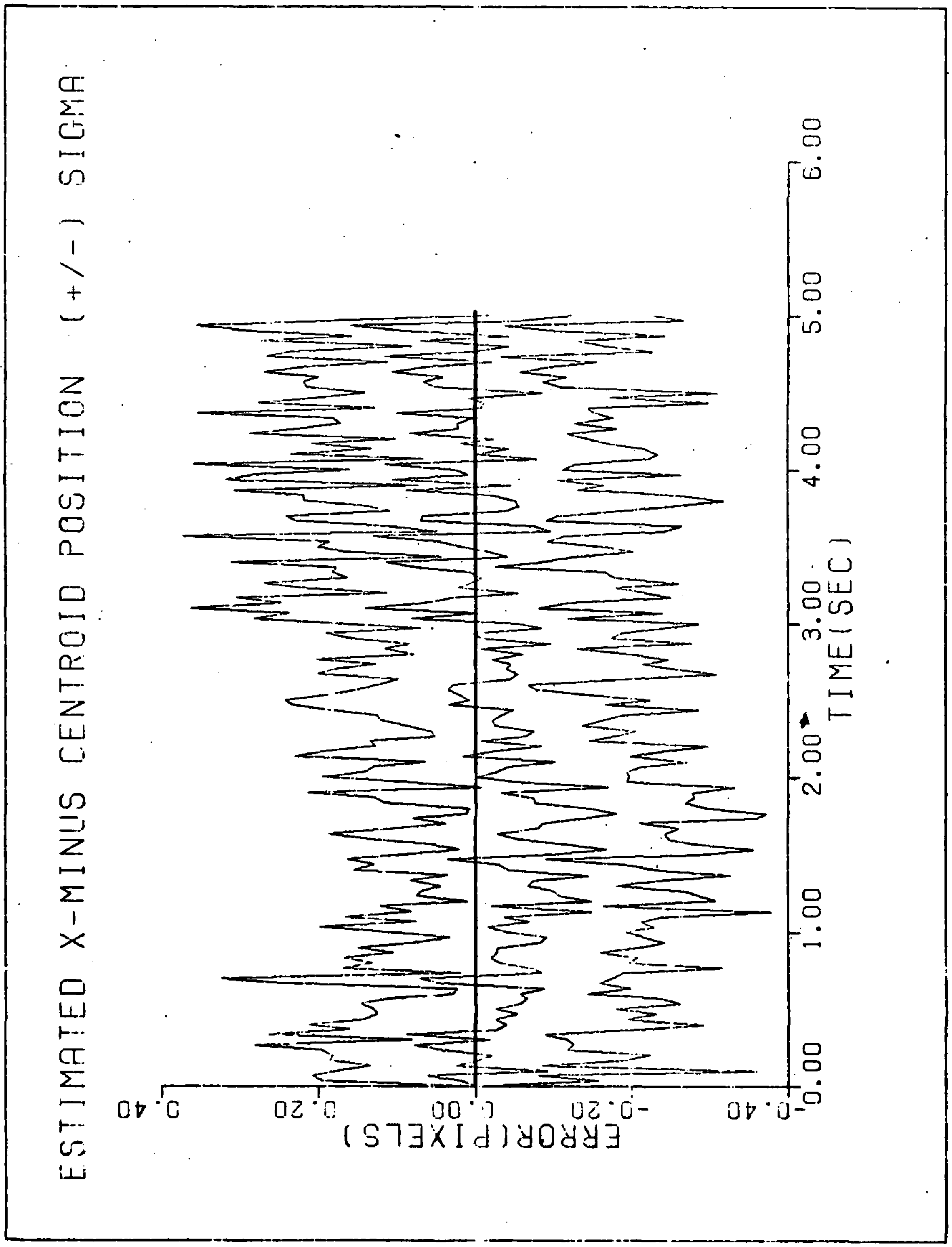

Figure C-20g. Case 20

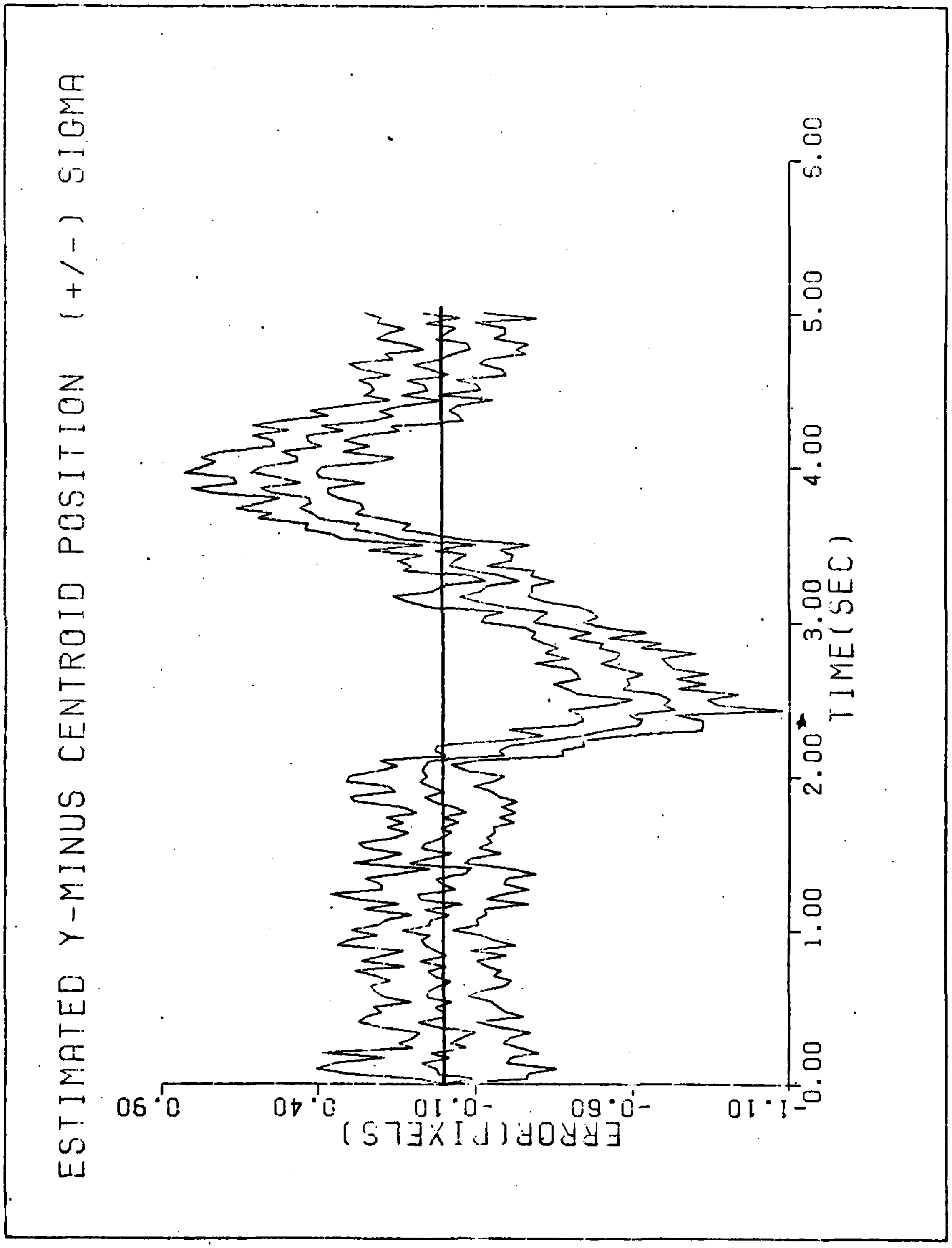

Figure C-20h. Case 20

Appendix D

Computer Software (Correlator/Kalman Filter)

This appendix contains the Fortran source code for the implementation of the algorithm of Figure 1. The program also contains the truth model described in Chapter 2 where the trajectory can be generated either with the model internal to this program or using the trajectory program given in Appendix E. (Note: For the multiple hot spot model the program given in Appendix E is used). Finally, this program contains the routines to calculate and plot the tracking errors of the algorithm which are presented in Chapter 5 and Appendix C. The program was written for use on the CDC Fortran IV compiler.

```
      PROG AM MAI (I PUT,OUTPUT,TAPE5=INPUT,TAPE6=OUTPUT,TAPE ,
     1 DEBUG=OUTPUT, APE )
      REAL IMAX(3),S(12),XMAX(3),YMAX(3),P(64,64)
      REAL ZI( )
      REAL RFIL(2, )
      REAL XT(8,1),PHIT( , ),ODPCCT(8,8),H(2, ),YT(2,1)
      REAL W(64),V(64),UC(576)
      INTEGER  (2),NFRAMES,NUMHS,TRAGEN,STRUN,NIMI
      COMPLEX DATA(24,24),WORK(50),SAVE(24,24),DX(24,24),DY(24,24)
      COMPLEX SDA A(24,24)
      REAL UT(2,1),BD( ,2)
      REAL FILPL(400),ACTPL(400),FILPY(400),ACTPY(400)
      REAL TIMPL(400),TIM (200)
      REAL PTA(400),PTB(400),PTC(400),PTD(400)
      REAL SIGMS,ASP O
      REAL UPD(8), VPFP(8, )
      INTEGER OPRINT,ICHO
      REAL EXUT(2,200),HS1A(200),HS1B(200),HS2A(200),HS2B(200)
      REAL HS3A(200),HS3B(200),VMAXEX(200),RANEX(200),TIMEX(200)
      REAL COSW(200)
      INTEGER CORRL,IPLOT
C
C
C     THE FOLLOWING IS A LIST OF THE MAJOR PROGRAM SUBROUTINES
C     AND A BRIEF DESCRIPTION OF THE SUBROUTINES ROLE IN THE
C     ALGORITHM
C
C     CHOLY-IMPLEMENTS THE CHOLESKY SQUARE ROOT ROUTINE
C     CENTRD-PERFORMS THE CENTER OF MASS CALCULATION FOR THE CORRELATOR
C     CORREL-IMPLEMENTS THE CORRELATION ROUTINE FOR THE FFT AND
C            PHASE CORRELATION ROUTINES
C     CORL2-IMPLEMENTS THE DIRECT CORRELATION METHOD (2 AND 6
C           LEVEL QUANTIZATION)
C     FILPT-ARRANGES THE DATA FOR THE FILTER VS. ACTUAL RMS ERROR PLOTS
C     FILST-CALCULATES THE ERROR STATISTICS
C     FILTER-DEFINES THE FILTER STATE TRANSITION AND QFD MATRICES
C     FOUR -IMPLEMENTS THE FFT
C     INITF-GIVES THE INITIAL FILTER VALUES FOR TDF AND TAF
C     INPUT3-CREATES THE MEASUREMENT ARRAY FOR INCORPORATION INTO THE
C            KALMAN FILTER
C     PLTA-PLOTS THE FILTER VS. ACTUAL ERROR DATA
C     PLTB-PLOTS THE MEAN ERRORS +/- 1 STANDARD DEVIATION
C     PROP-PROPAGATES THE TRUTH MODEL STATES
C     PROPF-PROPAGATES THE FILTER STATES
C     QDEST-IMPLEMENTS THE QFD ESTIMATION ROUTINE
C     SHIFT-IMPLEMENTS A SPATIAL PHASE SHIFT IN THE FREQUENCY DOMAIN
C     SMOOTH-PERFORMS THE EXPONENTIAL SMOOTHING OF THE INTENSTIY PATTERN
C     SPTN-SETS UP THE SPATIAL NOISE CORRELATION COEFFICIENT MATRIX
C     STATFM-CALCULATES THE ERRORS AT T(I-) FOR USE BY FILST
C     STATFP-CALCULATES THE ERRORS AT T(I+) FOR USE BY FILST
C     TRUTH-DEFINES THE TRUTH MODEL STATE TRANSITION AND QD MATRIX
C     UPCOKF-IMPLEMENTS THE KALMAN FILTER MEASUREMENT UPDATE EQUATION
C
C            DATA STRUCTURES TO GATHER STATISTICS ON FILTER
C                           TRACKER CAPIBILITY
C      XEMC   IS THE ERROR BETWEEN THE PREDICTED X DYNAMIC LOCATION
C             AT A PARTICULAR MINUS TIME AND THE TRUTH MODEL TRUE
```

```
      C                  X DYNAMIC LOCATION
      CF
      C       XFME2  IS THE SQUARE OF THE XFME
      C
      C       NOTE THAT XFME AND XFME2 ARE ARRAYS WHICH ARE DIMENSIONED TO
              REAL XFME(4,200),XFME2(4,200),CNME(4,200)
              REAL CNME2(4,200),XFMMS(4,200),XFMPS(4,200)
              REAL CNMMS(4,200),CNMPS(4,200)
      C                     BE 2X20 THE FIRST ROW IN EACH IS USED FOR THE X
      C                     DIRECTION WHILE THE SECOND ROW IS FOR THE Y DIRECTION
      C
      C       CNME    IS THE ERROR IN THE PREDICTED LOCATION OF THE CENTROID AT
      C                 A PARTICULAR MINUS TIME COMPARED TO THE TRUTH MODEL
      C       CNME2  IS THE SQUARE OF CNME
      C
      C       NOTE AGAIN THE DIMENSION OF CNME AND CNME2C
      C
      C       XFPE    IS THE ERROR BETWEEN THE UPDATED DYNAMIC LOCATION AT A
      C                 PARTICULAR PLUS TIME AND THE TRUTH MODEL TRUE DYNAMIC
      C       XFPE2  IS THE SQUARE OF XFPE
      C
      C       NOTE THE DIMENSIONALITY OF XFPE,XFPE2 FOR THE SAME REASONS AS
             REAL XFPE(4,200),XFPE2(4,200),CNPE(4,200)
             REAL CNPE2(4,200)
             REAL XFPMS(4,200),XFPPS(4,200),CNPMS(4,200),CNPPS(4,200)
             REAL PFPST(8,200),PFMST(8,200)
      C
      C
      C       CNPF    IS THE CENTROID ERROR AT THE PLUS TIME
      C
      C               FILTERS DATA STRUCTURES
      C
      C       PHIF  IS THE STATE TRANSITION MATRIX FOR THE KALMAN FILTER
      C               -SEE SUBROUTINE FILTER
      C       QFD     IS THE RESULT OF THE INTEGRAL TERM IN THE PROPAGATION
      C               -OF THE COV MATRIX  SEE SUBROUTINE PROPF
      C       PFP     IS THE FILTERS COVARIANCE MATRIX PLUS- AFTER INCORPORATION
      C               -OF A MEASUREMENT
      C       PFM     IS THE FILTERS COVARIANCE MATRIX MINUS AFTER PROPAGATION
      C               -BUT PRIOR TO MEASUREMENT INCORPORATION
      C       XFP     IS THE FILTER STATE VECTOR PLUS
      C       XFM     IS THE FILTER STATE VECTOR MINUS
      C
             REAL PHIF(8,8),QFD(8,8),PFP(8,8),PFM(8,8),XFP(8),XFM(8),TIME
      C
      C       Z       IS THE KALMAN FILTER MEASUREMENT VECTOR
      C
             REAL Z(64)
      C
             DIMENSION NAME(45)
      C
      C      ARRAY NAME STORES THE PLOT TITLES
      C
             DATA NAME(1)/40HFILTER V  ACTUAL ERROR  (X-POSITION)    /
             DATA NAME(5)/40HFILTER VS ACTUAL ERROR  (Y-POSITION)    /
             DATA NAME(9)/40HESTIMATED X-MINUS POSITION  (+/-) SIGMA /
             DATA NAME(13)/40HESTIMATED Y-MINUS POSITION  (+/-) SIGMA /
```

```
      DATA NAME(17)/40HESTIMATED Y-PLUS POSITION  (+/-) SIGMA  /
      DATA NAME(21)/40HESTIMATED Y-PLUS POSITION  (+/-) SIGMA  /
      DATA NAME(25)/50HESTIMATED X-MINUS CENTROID POSITION  (+/-) SIGMA
     +  /
      DATA NAME(30)/50HESTIMATED Y-MINUS CENTROID POSITION  (+/-) SIGMA
     +  /
      DATA NAME(35)/50HESTIMATED X-PLUS CENTROID POSITION  (+/-) SIGMA
     +  /
      DATA NAME(40)/50HESTIMATED Y-PLUS CENTROID POSITION  (+/-) SIGMA
     +  /
C
C
C
       DATA NN/24,24/
C
C
C      INITIALIZE THE FILTERS DATA STRUCTURES
C
      XVELTO=-1000.
      YVELTO=0.
       ZVELTO=0.
      DT=(1./30.)
      ASPRO=1.
      SIGM3=SQRT(2.)
C
C     FOR A ONE HOT SPOT SIMULATION SET NUMHS=1
      NUMHS=3
      WRITE(6,576)NUMHS
576   FORMAT(1X,* NUMBER OF HOT SPOTS=*,I4)
C
C     IF USING THE EXTERNAL TRAJECTORY SET TRAGEN=2
       RAGEN=1
      IF(TRAGEN.EQ.2)WRITE(6,551)
551   FORMAT(1X,* EXTERNAL TRAJECTORY*)
C
C
C     SELECT THE POINT IN THE EXTERNAL TAPE TO START THE RUN
C
      IF (TRAGEN.NE.2)GO TO 553
C     STRUN IS THE PARAMETER WHICH SETS THE START POINT
      STRUN=1
      WRITE(6,552)STRUN
552   FORMAT(1X,* RUN STARTED AT *,I4)
553   CONTINUE
C
C     THE FOLLOWING IS A LIST OF THE CORRELATION METHODS USED
C     CORRL=1  FFT METHOD
C     CORRL=2 PHASE CORRELATION METHOD
C     CORRL=3 DIRECT METHOD 2-LEVEL QUANTIZATION
C     CORRL=4 DIRECT METHOD 6-LEVEL QUANTIZATION
C
      CORRL=1
C
      WRITE(6,564)CORRL
564   FORMAT(1X,*CORRELATOR=*,I4)
C
C     IF PLOTS ARE DESIRED SET IPLOT = 2
```

```
      IPLOT=1
C
      WRITE(6,41)
41    FORMAT(/,1X,* CASE 000 *)
CM
C
C     SET THE CORRELATOR THRESHOLD
      THRESH=.3
C
C
C     IF THE INTERNAL TRAJECTORY IS BEING USED TRATE SETS THE
C     DESIRED G MANEUVER
C     A TURN RATE(TRATE) = .0196 YIELDS A 2-G TURN
C     A TURN RATE = .098 YIELDS A 10-G TURN
C     A TURN RATE = .196 YIELDS A 20-G TURN
      TRATE= .0196
      WRITE(6,550) TRATE
550   FORMAT(1X,* THE TURN RATE IS *,F8.4//)
C
C     TDF IS THE FILTER ACCELERATION TIME CONSTAN
      DATA TDF/3.5/
      WRITE(6,31)TDF
31    FORMAT(1X,*  TDF=*,E14.6)
C
C     THE FILTER MEASUREMENT COVARIANCE MATRIX (RFIL) IS DEFINED
C     ACCORDING TO THE CORRELATION METHOD STATISTICS
      DATA RFIL/.00436,0.,0.,.00578/
C     IF(CORRL.EQ.2)RFIL(1,1)=.472
C      IF(CORRL.EQ.2)RFIL(2,2)=.374
       IF(CORRL.EQ.3)RFIL(1,1)=.0343
      IF(CORRL.EQ.3)RFIL(2,2)=.00540
      IF(CORRL.EQ.4)RFIL(1,1)=.00733
      IF(CORRL.EQ.4)RFIL(2,2)=.0071
C
C*********************************************************************
C**                       I N I T I A L I Z A T I O N               **
C*********************************************************************
C
        CALL RANSET(12345)
54321   WRITE(6,3707)
3707    FORMAT(1X,*GAUSSIAN TARGET COVARIANCE VALUE*)
      READ(5,560) COV
560     FORMAT(F6.2)
      IF(EOF(5).NE.0) GO TO 6421
        WRITE(6,3701)
3701    FORMAT(1X,*NUMBER OF ZEROES TO PAD*)
        READ(5,561) NZ
561     FORMAT(I2)
        NZM=25-NZ
        WRITE(6,3702)
3702    FORMAT(1X,*NUMBER OF FRAMES*)
        READ(5,563) NFRAMES
563    FORMAT(I3)
        WRITE(6,4023)
4023    FORMAT(1X,*NUMBER OF SIMULATIONS*)
        READ(5,561) NRUNS
        WRITE(6,3703)
```

```
 37 3    FORMAT( X,*ALPHA FOR SMOOTHING*)
         READ(5,560) ALPHA
  3794    WRITE(6,3795)
 3795    FORMAT(1X,*NUMBER OF HIGH FREQ COMPONENTS TO ZERO*)
         READ(5,561) NFREQ
         ISF=14-NFREQ
         IEF=12+NFREQ
         WRITE(6,3796)
 3796    FORMAT(1X,*INPUT MEASUREMENT ERROR VARIANCE*)
         READ(5,560) VARM
 562     FORMAT(2F6.3)
        READ(5,563)X0
        WRITE(6,3797)X0
 3797   FORMAT(1X,*INITIAL X POSITION*,E16.7)
 563    FORMAT(F10.2)
        READ(5,563)Y0
        WRITE(6,3798)Y0
 3798   FORMAT(1X,*INITIAL Y POSITION*,E16.7)
        READ(5,563)Z0
        WRITE(6,3799)Z0
 3799   FORMAT(1X,*INITIAL Z POSITION*,E16.7)



C
        CALL INITF(TAF,VARDF,VARAF)
C
C    DEFINE TRUE TARGET AS 3 INDEPENDENT GAUSSIAN FUNCTIONS WITH
C    VARIANCE=COV.
C
         S(1)=1./COV
         S(2)=0.
         S(3)=0.
         S(4)=S(1)
         S(5)=S(1)
         S(6)=0.
         S(7)=0.
         S(8)=S(1)
         S(9)=S(1)
         S(10)=0.
         S(11)=0.
         S(12)=S(1)
C
C        INITIALIZE TARGET INTENSITY ASSUMING
C        3 CIRCULAR CROSS-SECTION GAUSSIAN TARGET.
C
         IMAX(1)=20.
         IMAX(2)=20.
         IMAX(3)=20.
C        DEFINE TRUTH MODEL DYNAMICS
C
         WRITE(6,965)
 965     FORMAT(2X,*STD. DEV OF TRUTH MODEL ATMOSPHERIC JITTER*)
         READ(5,6666) SIGDT
 6666    FORMAT(F5.3)
C
```

```
C  IF ICHQ = 1 QFD IS ADAPTIVELY ESTIMATED
      READ(5,561)ICHQ
      IF(ICHQ.NE.1)GO TO 570
      WRITE(6,571)
571   FORMAT(1X,/,' ADAPTIVELY ESTIMATE QFD',//)
570   CONTINUE
C
       CALL TRUTH(PHIT,QDROOT,H,SIGDT,DT)
C
C SET THE EXTERNAL MATRICES TO ZERO
C
      DO 554 I=1,200
      HS1A(I)=0.
        HS1B(I)=0.
        HS2A(I)=0.
        HS2B(I)=0.
        HS3A(I)=0.
        HS3B(I)=0.
        VMAXEX(I)=0.
      RANEX(I)=0.
      COSW(I)=0.
        TIMEX(I)=0.
        EXUT(1,I)=0.
        EXUT(2,I)=0.
554     CONTINUE
C
C
C      INITIALIZE THE FILTER ERROR MATRICES TO ZERO
C
      DO 21 I=1,4
      DO 21 J=1,NFRAMES
      XFME(I,J)=0.
      XFME2(I,J)=0.
      CNME(I,J)=0.
      CNME2(I,J)=0.
      XFPE(I,J)=0.
      XFPE2(I,J)=0.
      CNPE(I,J)=0.
 21    CNPE2(I,J)=0.
C
      DO 22 I=1,8
      DO 22 J=1,NFRAMES
         PFPS (I,J)=0.
         PFMSF(I,J)=0.
22    CONTINUE
C USING FIRST AND SECOND NEAREST NEIGHBOR DETERMINE THE CHOLESKY
C SQUAREROOT, R, OF THE MEASUREMENT COVARIANCE MATRIX, R
C
       CALL SPTN(VARM,R,8)
C     THIS LOOP MAKES SPATIALLY CORRELATED/UNCORRELATED NOISE
C          COMMENT THE NEXT FOUR LINES IF WANT SPATIAL CORRELATION
C      DO 6428 I=1,64
C      DO 6428 J=1,64
C      R(I,J)=0.
C      IF(I.EQ.J) R(I,J)=VARM
6428   CONTINUE
C     MODCOMP VERSION OF CHOLESKY PUTS ROOT BACK INTO CALLING MATRIX
```

```
      CALL CHOLY(?,64)
C
C     READ IN THE INITIAL DATA FROM THE EXTERNAL TRAJECTORY TAPE
C
      IF(TRAGEN.NE.2)GO TO 555
555   CONTINUE
      READ(9,*)ITER,EXUT(1,1),EXUT(2,1),VMAXEX(1),
     +COSW(1),RAMEX(1),TIMEX(1)
557   FORMAT(I4,6E14.5)
      READ(9,*)HS1A(1),HS1B(1),HS2A(1),HS2B(1),HS3A(1),
     +HS3B(1)
55?   FORMAT(6E14.5)
      READ(9,*)XPOS,YPOS,ZPOS,XVELTO,YVELTO,ZVELTO,TRATE
556   FORMAT(7E14.5)
C
C     LOOP UNTIL THE START POINT IS REACHED
C
      IF(ITER.NE.STRUN)GO TO 559
      XO=XPOS
      YO=YPOS
      YO=YPOS
      XDOT=XVELTO
      YDOT=YVELTO
      ZDOT=ZVELTO
      WRITE(6,541)
541   FORMAT(T2,* INITIAL STARTING CONDITIONS*)
      WRITE(6,542)
542   FORMAT(T4,*TIME*,T15,*XPOS*,T29,*YPOS*,T44,*ZPOS*,
     +T57,*TURN RATE*,T71,*HS1A*,T85,*HS2A*,T99,*HS3A*,
     +T112,*ROLL ANGLE*)
      WRITE(6,543)TIMEX(1),XO,YO,ZO,TRATE
     +,HS1A(1),HS2A(1),HS3A(1),COSW(1)
543   FORMAT(T1,F8.3,8E14.5)
559   CONTINUE
C
C
C*********************************************************************
C**                E N D   I N I T I A L I Z A T I O N             **
C*********************************************************************
C
C*********************************************************************
C**      B E G I N   M O N T E C A R L O   S I M U L A T I O N      **
C*********************************************************************
C
C      MAKE NRUNS SIMULATIONS OF NFRAMES EACH FOR MONTE-CARLO ANALYSIS
C
       DO 80 NS=1,NRUNS
C
      WRITE(6,544)NS
544   FORMAT(/,1X,* SIMULATION NUMBER*,I4)
C
      TIME=0.
       XSHIFT=0.
       YSHIFT=0.
C INITIALIZE SMOOTHED DATA ARRAY
C
       DO 7 I=1,24
```

```
      DO 7 J=1,24
 7     SDATA(I,J)=CMPLX(0.,0.)
C
C      INITIALIZE TRUTH MODEL STATE VECTOR
C
       DO 71 I=1,
71     XT(I,1)=0.
       XT(1,1)=X0
       XT(2,1)=Y0
       YT(1,1)=X0
       YT(2,1)=Y0
C
C      INITIALIZE THE FILTERS MATRICES DEFINITION
      CALL FILTER(TDF,VARDF,TAF,VARAF,DT,PHIF,QFD,NS)
C     ZERO THE FILTER MATRICES FOR THE NEXT RUN
C
      DO 106 I=1,8
      DO 106 J=1,8
      PFM(I,J)=0.0
      PFP(I,J)=0.0
      XFP(I)=0.0
106   XFM(I)=0.0
C
C     SET UP THE FILTER COVARIANCE MATRIX INITIAL CONDITIONS
      PFP(1,1)=10.
      PFP(2,2)=10.
      PFP(3,3)=2000.
      PFP(4,4)=2000.
      PFP(5,5)=100.
      PFP(6,6)=100.
      PFP(7,7)=.2
      PFP(8,8)=.2
      PFM(1,1)=PFP(1,1)
      PFM(2,2)=PFP(2,2)
      PFM(3,3)=PFP(3,3)
      PFM(4,4)=PFP(4,4)
      PFM(5,5)=PFP(5,5)
      PFM(6,6)=PFP(6,6)
      PFM(7,7)=PFP(7,7)
      PFM(8,8)=PFP(8,8)
C
C
      DO 43 I=1,8
      PFPST(I,1)=PFP(I,I)+PFPST(I,1)
43    CONTINUE
C
C
C     INITIAL CONDITIONS ON DYNAMIC STATES
C
C
      XFP(1)=X0
      XFP(2)=Y0
      XFM(1)=XFP(1)
      XFM(2)=XFP(2)
      RANGED= SQRT(X0**2+Y0**2+Z0**2)
      RHOR=(X0**2+Z0**2)
      RANGE=(RHOR+Y0**2)
```

```
      XFP(3)=(-ZO*XVELTO+XO*ZVELTO)/(RHO**.00002)
      RHOR=SQRT(RHO )
      XFP(4)=(RHOR*YVELTO-YO*((XO*XVELTO+ZO*ZVELTO)/RHOR))/(RANGE*
     +.00002)
      RANGE=SQRT(RANGE)
      VMAX=SQRT(XVELTO**2+YVELTO**2+ZVELTO**2)/(RANGE*.00002)
      XFM(3)=XFP(3)
      XFM(4)=XFP(4)
      XFP(5)=55.3
      XFP(6)=-2.0
C
      DO 15 I=1,8
         BD(I,1)=0.
         BD(I,2)=0.
15    CONTINUE
C
C
      BD(1,1)=DT
      BD(2,2)=DT
      UT(1,1)=XFP(3)
      UT(2,1)=XFP(4)
C      DEFINE UPPER-LEFT CORNER OF FOV
C
       X=XFP(1)-4.
       Y=XFP(2)-4.
C
C  ZERO THE VALUES NEEDED TO ESTIMATE QFD
      TRXXT=0.
      TRXXTO=0.
      QPRINT=0
C
C      TRACK TARGET FOR NFRAME FRAMES (TIME SLICES)
C*************************************************************************
       DO 90 NR=1,NFRAMES
C
C*************************************************************************
C
C      DEFINE GAUSSIAN PEAK LOCATIONS BASED ON CENTROID POSITION, YT
C
      YMAX(1)=YT(2,1)
      XMAX(1)=YT(1,1)
      IF(NUMHS.EQ.1)GO TO 72
      YMAX(1)= YT(2,1) + HS1B(NR)
      XMAX(1)=YT(1,1)-HS1A(NR)
       XMAX(2)=YT(1,1)-HS2A(NR)
       XMAX(3)=YT(1,1) - HS3A(NR)
       YMAX(2)=YT(2,1)+HS2B(NR)
       YMAX(3)=YT(2,1)+HS3B(NR)
72    CONTINUE
C
C      GET MEASUREMENT NOISE ARRAY
C
       CALL NOISE(W,64)
       CALL MULT(P,W,64,64,1,V)
C
C      GET MEASUREMENT DATA
C
```

```
C       CALL IDEAL(IMAX,XMAX,YMAX,N,NZ,X,Y,DATA,DX,DY,SIGMS,RANGED,RANGE,
C      +UT,VMAX,ASPRO)
        CALL INPUT3(IMAX,S,XMAX,24,X,Y,DATA,CENX,CENY,YMAX,
       +SIGMS,RANGED,RANGE,UT,VMAX,ASPRO,NUMHS)
C
C        ADD CORRELATED MEASUREMENT NOISE TO CENTER 8X8 PIXEL DATA
C
         DO 4 I=1,8
         DO 4 J=1,8
         DATA(I+8,J+8)=DATA(I+8,J+8)+CMPLX(V(8*(I-1)+J),0.0)
4        CONTINUE
C
C        ADD UNCORRELATED NOISE TO MEASUREMENT DATA OUTSIDE CENTER
C        8X8 PIXEL AREA.
C
         CALL NOISE(UC,576)
         DO 6 I=1,24
         DO 6 J=1,24
         IF(I.GE.9.AND.I.LE.16.AND.J.GE.9.AND.J.LE.16) GO TO 6
         IF((I.LE.NZ).OR.(J.LE.NZ).OR.(I.GE.NZM).OR.(J.GE.NZM)) GO TO 6
         DATA(I,J)=DATA(I,J)+CMPLX(UC(24*(I-1)+J),0.)*SQRT(VARM)
6        CONTINUE
C
C        CREATE THE MEASUREMENT VECTOR FOR THE FILTER UPDATE
C
        K=0
        DO 101 I=9,16
        DO 101 J=9,16
        K=K+1
101     Z(K)=REAL(DATA(I,J))
C
        IF(NN.NE.1) CALL CORREL(NN,DATA,SDATA,XCENT,YCENT,X,Y,THRESH,
       +CORL)
         Z1(1)=XCENT
        Z1(2)=YCENT
C
C        GO CALCULATE THE ERRORS OF THE FILTERS ESTIMATE PRIOR TO
C             MEASUREMENT INCORPORATION
        CALL STATFM(XFME,XFME2,CVME,CVME2,XFM,XT,YT,NR,NFRAMES,
       +PFM,PFMST,UT)
C
C        INCORPORATE MEASUREMENT
C
        IF(NR.EQ.1) GO TO 164
         CALL UPCOKF(Z1,XFP,XFM,PFP,PFM,RFIL,UPD)
C
        IF(NS.NE.1)GO TO 697
         WRITE(6,696)(XFP(I),I=1,8)
696      FORMAT(1X,* XFP*,8F14.6)
697     CONTINUE
C        CALCULATE THE ERRORS FOR THE FILTER AFTER THE INCORPORATION
C                OF THE MEASUREMENT
        CALL STATFP(XFPE,XFPE2,CVPE,CVPE2,XT,YT,XFP,NR,NFRAMES,
       +PFP,PFPST,UT)
C
C
C        SET THE TIME FOR THE ADAPTATION TO START
```

```
C
      IF(TIME.LT.?.5)GO TO 44
      IF(ICHQ.EQ. )CALL QDEST(SVPFP,PFP,U'D,TPXXT,TRXXTO
     +,QFD,TIME,QPRINT,NP)
44    CONTINUE
C
C      COMPUTE THE SHIFT INFORMATION FROM THE CENTER OF FOV
      XSHIFT=X-XFP(1)+4.-XFP(7)
      YSHIFT=Y-XFP(2)+4.-XFP(?)
C
C      SHIFT THE DATA ARRAY APPROPRIATELY
C
C      GET FORWARD FFT
C
164    CALL FOURT(DATA,NN,2,-1,1,WORK)
C
C      FILTER DESIRED FREQUENCY COMPONENTS OUT
C
       IF(NFREQ.GT.12) NFREQ=12
       IF(NFREQ.LE.0) GO TO 3796
       DO 6 I=ISF,IEF
       DO 8 J=1,24
       DATA(I,J)=CMPLX(0.,0.)
8       DATA(J,I)=CMPLX(0.,0.)
3796   CONTINUE
C
C      ASSUME IF NP=1 THAT THE DATA IS CENTERED
       IF(NP.NE.1) CALL SHIFT(DATA,24,XSHIFT,YSHIFT)
       CALL SMOOTH(DATA,SDATA,ALPHA,24,NP)
      TIME=TIME + DT
      CALL PROPF(PHIF,QFD,FFP,PFM,XFP,XFM,NS,SVPFP,ICHQ)
       X=XFM(1)-4.
      Y=XFM(2)-4.
C      PROPAGATE TRUTH MODEL STATE ONE FRAME
      CALL PROP(PHIT,QDROOT,H,XT,YT,8,2,UT,BD,
     +TIME,DT,TRAFF,XO,YO,ZO,VMAX,RANGE,TRAGEN,NR,NS,EXUT,
     +HS1A,HS1B,HS2A,HS2B,HS3A,HS3B,VMAXEX,RANEX,TIMEX,COSW)
C
      IF(NS.NE.1)GO TO 90
      WRITE(6,694)(XFM(I),I=1,8)
694   FORMAT(/,1X,* XFM*,8E14.6)
      WRITE(6,695)(XT(I,1),I=1,8)
695   FORMAT(1X,* XT *,8E14.6)
C
90     CONTINUE
C*************************************************************************
C**        E N D   M O N T E C A R L O   S I M U L A T I O N            **
C*************************************************************************
C
C      CALCULATE MEAN AND VARIANCE STATISTICS
C
      CALL FILST(XFME,XFME2,CNME,CNME2,XFPE,XFPE2,CNPE,CNPE2,NRUNS,
     #NFRAMES,PFPST,PFMST,XFMMS,XFMPS,XFPMS,XFPPS,CNMMS,CNMPS,CNPMS,CNPP
     + S)
C
      CALL FILPT(PFPST,PFMST,XFPE2,XFME2,NFRAMES,TIMPL,ACTPL,
     +FILPL,FILPY,ACTPY,TIMR)
```

```
C
      NIM1=NFRAMES+2
      NIM=2*NFRAMES+2
C
      IF(IPLOT.NE.1)GO TO 565
      CALL PLOTS(0.,0.,9)
      CALL PLOT(3.,3.,-3)
C
C     A 1 IN PLTB YIELDS X STATISTICS A 2 YIELDS Y
C
      CALL PLTA(TIMPL,ACTPL,FILPL,NFRAMES,NIM,1,NAME)
      CALL PLTA(TIMPL,ACTPY,FILPY,NFRAMES,NIM,5,NAME)
C
      CALL PLTB(TIMR,XFMMS,XFMPS,XFME,NIM1,NFRAMES,1,NAME,9,NIM,
     +PTA,PTB,PTC,PTD)
      CALL PLTB(TIMR,XFMMS,XFMPS,XFME,NIM1,NFRAMES,2,NAME,13,NIM,
     +PTA,PTB,PTC,PTD)
      CALL PLTB(TIMR,XFPMS,XFPPS,XFPE,NIM1,NFRAMES,1,NAME,17,NIM,
     +PTA,PTB,PTC,PTD)
      CALL PLTB(TIMR,XFPMS,XFPPS,XFPE,NIM1,NFRAMES,2,NAME,21,NIM,
     +PTA,PTB,PTC,PTD)
      CALL PLTB(TIMR,CNMMS,CNMPS,CNME,NIM1,NFRAMES,1,NAME,25,NIM,
     +PTA,PTB,PTC,PTD)
      CALL PLTB(TIMR,CNMMS,CNMPS,CNME,NIM1,NFRAMES,2,NAME,30,NIM,
     +PTA,PTB,PTC,PTD)
      CALL PLTB(TIMR,CNPMS,CNPPS,CNPE,NIM1,NFRAMES,1,NAME,35,NIM,
     +PTA,PTB,PTC,PTD)
      CALL PLTB(TIMR,CNPMS,CNPPS,CNPE,NIM1,NFRAMES,2,NAME,40,NIM,
     +PTA,PTB,PTC,PTD)
C
C     CALL SYMBOL(0.,0.,0.25,8HCASE P1 ,0.,8)
      CALL PLOTE
565   CONTINUE
C
      WRITE(6,9987) NRUNS,NFRAMES,NZ,NFREQ,COV,VARM,ALPHA,
     #                SIGDT
9987  FORMAT(1H1,T10,*RUNS=*,I2,T38,*FRAMES=*,I4,T73,*NUMBER ZERO PAD=*
     #   I1,T10?,*NUMBER FREQ ZEROED=*,I2,/,T10,*GAUSSIAN COVARIANCE=*,
     # F5.2,T38,*MEASUREMENT NOISE VARIANCE=*,F5.1,T73,*SMOOTHING ALPHA
     # =*,F7.3,/,T10,
     # *TRUTH MODEL UNCERTAINTY=*,F7.3,///)
      WRITE(6,45)THRESH
45    FORMAT(1X,* THE CORRELATOR THRESHOLD IS *,F6.2)
       GO TO 54321
6421   STOP
       END
```

```
RITY  DETAILS    DIAGNOSIS OF PROBLEM

I     FILTER V   HOLLERITH CONSTANT .GT. 10 CHARACTERS, EXCESS CHARACTERS INITIAL
I     FILTER V   HOLLERITH CONSTANT .GT. 10 CHARACTERS, EXCESS CHARACTERS INITIAL
I     ESTIMATE   HOLLERITH CONSTANT .GT. 10 CHARACTERS, EXCESS CHARACTERS INITIAL
I     ESTIMATE   HOLLERITH CONSTANT .GT. 10 CHARACTERS, EXCESS CHARACTERS INITIAL
I     ESTIMATE   HOLLERITH CONSTANT .GT. 10 CHARACTERS, EXCESS CHARACTERS INITIAL
```

```
      SUBROUTINE UPCOKF(Z1,XFP,XFM,PFP,PFM,RFIL,UPD)
      REAL Z1(2),XFP(8),XFM(8),PFP(8,8),PFM(8,8),RFIL(2,2)
      REAL TEMP1(8,2),TEMP2(2,2),TEMINV(2,2),TEMP3(2,8),TEMP4(8,8)
      REAL RESI(2),UPD(8)
      REAL HT(8,2),H(2,8),GACOK(8,2)
C
C     THIS SUBROUTINE IMPLEMENTS THE KALMAN FILTER MEASUREMENT
C     UPDATE EQUATION.
C     X(TI+)=X(TI-)+K(TI)(Z(TI)-HX(TI-))
C     P(TI+)=P(TI-)   -   K H P(TI-)
C     WHERE
C     K(TI)= P(TI-)HT(HP(TI-)HT+R)-1
C
      DO 5 I=1,8
      DO 5 J=1,2
         H(J,I)=0.
C
 5    CONTINUE
      H(1,1)=1.
      H(1,7)=1.
      H(2,2)=1.
      H(2,8)=1.
      DO 6 I=1,8
      DO 6 J=1,2
         HT(I,J)=H(J,I)
 6    CONTINUE
      CALL MULT(PFM,HT,8,8,2,TEMP1)
      CALL MULT(H,TEMP1,2,8,2,TEMP2)
      DO 1 I=1,2
      DO 1 J=1,2
 1    TEMP2(I,J)=TEMP2(I,J)+RFIL(I,J)
      CALL INVERT(TEMP2,2,TEMINV)
      CALL MULT(HT,TEMINV,8,2,2,TEMP1)
      CALL MULT(PFM,TEMP1,8,8,2,GACOK)
      CALL MULT(H,PFM,2,8,8,TEMP3)
      CALL MULT(H,XFM,2,8,1,RESI)
      CALL MULT(GACOK,TEMP3,8,2,8,TEMP4)
      DO 2 I=1,8
      DO 2 J=1,8
         PFP(I,J)=PFM(I,J)-TEMP4(I,J)
 2    CONTINUE
      DO 3 I=1,2
 3    RESI(I)=Z1(I)-RESI(I)
      CALL MULT(GACOK,RESI,8,2,1,UPD)
      DO 4 I=1,8
 4    XFP(I)=XFM(I)+UPD(I)
C
C
C
      RETURN
      END
```

```
      SUBROUTINE QDEST(SVPFP,PFP,UPD,TRXXT,TRXXTO,QFDN,
     +TIME,QPRINT,NS)
C
      REAL SVPFP(8,8),PFP(8,8),UPD(8,8),DXDXT(8,8)
      REAL QDMAX(8)
      REAL QFDN(8,8),QFDO(8,8),SAVE(8,8)
      REAL NTRXXT,TRXXTO,QFACTOR
      INTEGER NFRAMES,QPRINT
C
C THIS ROUTINE ESTIMATES QFD USING:
C QD=(X(TI+)-X(TI-))*(X(TI+)-X(TI-))T+P(TI+)-PHIF*P(TI-1+)*PHIFT
C
C THE FIRST TERM IS APPROXIMATED BY
C (X(TI+)-X(TI-))*(X(TI+)-X(TI-))T=K(TI)R(TI)R(TI)TK(TI)T
C   WHERE:
C    K(TI)= THE KALMAN FILTER GAIN
C    R(TI)= THE FILTER RESIDUAL
C    SVPFP= THE LAST TERM IN THE QD EQUATION
C
C  A FADING MEMORY TECHNIQUE IS USED INSTEAD OF TIME AVERAGING
C
C    FROM THE FILTER UPDATE UPD=K(TI)*R(TI)
C    USING THIS DELTA X * DELTA X (T) IS OBTAINED
C
      DO 80 I=1,8
      DO 80 J=1,8
        QFDO(I,J)=0.
80    CONTINUE
      QDMAX(1)=2.
      QDMAX(2)=2.
      QDMAX(3)=14.
      QDMAX(4)=14.
      QDMAX(5)=20.
      QDMAX(6)=20.
      QDMAX(7)=.5
      QDMAX(8)=.5
C
C
      NTRXXT=0.
      DO 10 I=1,8
      DO 10 J=1,8
        DXDXT(I,J)=UPD(I)*UPD(J)
10    CONTINUE
C
      DO 20 I=1,8
        NTRXXT= NTRXXT + DXDXT(I,I)
20    CONTINUE
C
      TRXXTO= TRXXT
      TRXXT=.8*TRXXTO+.2*NTRXXT
C
C  STORE QFD FROM THE PREVIOUS ESTIMATION
C
      DO 30 I=1,8
      DO 30 J=1,8
        QFDO(I,J)=QFDN(I,J)
30    CONTINUE
```

```
C
C   FORM THE NEW ESTIMATE OF QFD
C
      DO 40 I=1,8
      DO 40 J=1,8
        SAVE(I,J)= PFP(I,J) + DXDXT(I,J)
        QFDN(I,J)= SAVE(I,J) - SVPFP(I,J)
40    CONTINUE
C
C   INSURE THAT THE NEW QFD IS BOUNDED
C
      DO 50 I=1,8
        QFACTOR=1.
        IF(QFDN(I,I).GT.0.)GO TO 51
        QFACTOR=0.
        QFDN(I,I)=.1
        GO TO 52
51    CONTINUE
        IF(SQRT(QFDN(I,I)).GT.QDMAX(I)) QFACTOR=QDMAX(I)/SQRT(
     +QFDN(I,I))
        IF(QFACTOR.GE.1.)GO TO 50
        QFDN(I,I)=QFACTOR**2*QFDN(I,I)
52    CONTINUE
      DO 54 J=1,8
        IF(I.EQ.J) GO TO 54
        QFDN(I,J)=QFDN(I,J)*QFACTOR
54    CONTINUE
C
      DO 55 K=1,8
        IF(I.EQ.K)GO TO 55
        QFDN(K,I)= QFDN(K,I)*QFACTOR
55    CONTINUE
50    CONTINUE
C
C   COMBINE THE OLD AND NEW INFORMATION
C
      DO 56 I=1,8
      DO 56 J=1,8
        QFDN(I,J)=.2*QFDN(I,J)+.8*QFDO(I,J)
56    CONTINUE
      IF(NS.NE.1)GO TO 70
      IF(QPRINT.NE.5)GO TO 70
C
      QPRINT=0
      WRITE(6,61)TIME
61    FORMAT(1X,//,* AT TIME=*,F10.4)
      WRITE(6,62)((QFDN(I,J),J=1,8),I=1,8)
62    FORMAT(1X,/,* ESTIMATED QFD IS*,/,(1X,8E14.5))
      WRITE(6,63)TRXXT
63    FORMAT(1X,/,* TRXXT = *,E14.5)
C
70    CONTINUE
      QPRINT=QPRINT+1
      RETURN
      END
```

```
      SUBROUTINE STATFM(XFME,XFME2,CNME,CNME2,XFM,XT,YT,NR,NFRAMES,
     +PFM,PFMST,UT)
      INTEGER NR,NFRAMES
      REAL XFME(4,NFRAMES),XFME2(4,NFRAMES),CNME(4,NFRAMES)
      REAL CNME2(4,NFRAMES)
      REAL XFM(8),XT(3,1),YT(2,1)
      REAL PFMST(8,200),PFM(8,8)
      REAL UT(2,1)
C
C      THIS ROUTINE GATHERS THE INFORMATION THAT WILL BE
C           REQUIRED TO COMPUTE THE STATISTICS OF THE PREDICTIONS
C           OF THE FILTER PRIOR TO MEASUREMENT INCORPORATION
C
C     FIRST COLLECT THE ERROR IN THE PREDICTED DYNAMIC LOCATION
C
      XFME(1,NR)=XFME(1,NR)+XFM(1)-XT(1,1)
      XFME(2,NR)=XFME(2,NR)+XFM(2)-XT(2,1)
      XFME(3,NR)=XFME(3,NR)+XFM(3)-UT(1,1)
      XFME(4,NR)=XFME(4,NR)+XFM(4)-UT(2,1)
C
C      NOW COLLECT THE SQUARE OF THAT ERROR
C
       XFME2(1,NR)=XFME2(1,NR)+(XFM(1)-XT(1,1))**2
      XFME2(2,NR)=XFME2(2,NR)+(XFM(2)-XT(2,1))**2
      XFME2(3,NR)=XFME2(3,NR)+(XFM(3)-UT(1,1))**2
      XFME2(4,NR)=XFME(4,NR)+(XFM(4)-UT(2,1))**2
C
C      COLLECT ERROR IN CENTROID PREDICTED LOCATION MINUS
C
      CNME(1,NR)=CNME(1,NR)+(XFM(1)+XFM(7)-YT(1,1))
      CNME(2,NR)=CNME(2,NR)+(XFM(2)+XFM(8)-YT(2,1))
      CNME(3,NR)=CNME(3,NR)+XFM(3)-XT(3,1)
      CNME(4,NR)=CNME(4,NR)+XFM(4)-XT(4,1)
C
C      COLLECT THE SQUARE OF THE ERROR
C
      CNME2(1,NR)=CNME2(1,NR)+(XFM(1)+XFM(7)-YT(1,1))**2
      CNME2(2,NR)=CNME2(2,NR)+(XFM(2)+XFM(8)-YT(2,1))**2
      DO 10 I=1,8
         PFMST(I,NR)= PFMST(I,NR) + PFM(I,I)
10    CONTINUE
      RETURN
      END
```

```
      SUBROUTINE STATFP(XFPE,XFPE2,CNPE,CNPE2,XT,YT,XFP,NR,NFRAMES,
     +PFP,PFPST,UT)
      INTEGER NR,NFRAMES
      REAL XFPE(4,NFRAMES),XFPE2(4,NFRAMES),CNPE(4,NFRAMES)
      REAL CNPE2(4,NFRAMES)
      REAL UT(2,1)
      REAL XT(8,1),YT(2,1),XFP(8)
      REAL PFPST(8,200),PFP(8,8)
C
C       THIS ROUTINE GATHERS THE INFORMATION THAT WILL BE
C            REQUIRED TO COMPUTE THE STATISTICS ON THE FILTERS
C            UPDATED STATE ESTIMATES
C
C       COMPUTE DIFFERENCES THAT WILL BE NEEDED
C
      DIF1=XFP(1)-XT(1,1)
      DIF2=XFP(2)-XT(2,1)
      DIF3=XFP(1)+XFP(7)-YT(1,1)
      DIF4=XFP(2)+XFP(8)-YT(2,1)
      DIF5=XFP(3)-UT(1,1)
      DIF6=XFP(4)-UT(2,1)
C
C
C        FIRST COLLECT THE ERROR IN THE DYNAMIC LOCATION ESTIMATES
C
      XFPE(1,NR)=XFPE(1,NR)+DIF1
      XFPE(2,NR)=XFPE(2,NR)+DIF2
      XFPE(3,NR)=XFPE(3,NR)+DIF5
      XFPE(4,NR)=XFPE(4,NR)+DIF6
C
C       NOW COLLECT THE SQUARE OF THAT ERROR
C
       XFPE2(1,NR)=XFPE2(1,NR)+DIF1**2
      XFPE2(2,NR)=XFPE2(2,NR)+DIF2**2
      XFPE2(3,NR)=XFPE2(3,NR)+DIF5**2
      XFPE2(4,NR)=XFPE2(4,NR)+DIF6**2
C
C       NOW COLLECT THE ERROR IN THE CENTROID UPDATE
C
      CNPE(1,NR)=CNPE(1,NR)+DIF3
      CNPE(2,NR)=CNPE(2,NR)+DIF4
C
C       NOW COLLECT THE ERROR SQUARED
C
      CNPE2(1,NR)=CNPE2(1,NR)+DIF3**2
      CNPE2(2,NR)=CNPE2(2,NR)+DIF4**2
      DO 10 I=1,8
         PFPST(I,NR)= PFPST(I,NR) + PFP(I,I)
 10   CONTINUE
       RETURN
      END
```

```
      SUBROUTINE FILST(XFME,XFME2,CNME,CNME2,XFPE,XFPE2,CNPE,CNPE2,
     #NRUNS,NFRAMES,PFPST,PFMST,XFMMS,XFMPS,XFPMS,XFPPS,CNMMS,CNMPS,
     +CNPMS,CNPPS)
      REAL TIME(200)
      REAL TIMEM(200)
      INTEGER NRUNS,NFRAMES
      REAL XFME(4,NFRAMES),XFME2(4,NFRAMES),CNME(4,NFRAMES)
      REAL CNME2(4,NFRAMES)
      REAL XFPE(4,NFRAMES),XFPE2(4,NFRAMES),CNPE(4,NFRAMES)
      REAL CNPE2(4,NFRAMES)
      REAL XFMMS(4,200),XFMPS(4,200),XFPMS(4,200)
      REAL XFPPS(4,200)
      REAL CNMPS(4,200),CNMMS(4,200),CNPMS(4,200)
      REAL CNPPS(4,200)
      REAL PFPST(8,NFRAMES),PFMST(8,NFRAMES)
C
C       EXPLANATION OF DATA STRUCTURES
C         XFME IS THE XPOS OF THE FILTER AT MINUS TIME ERROR
C         THESE ARE ALL COMPATIBLE WITH THE ABOVE ROUTINES
C         XFMMS IS THE XPOS MEAN ERROR AT MINUS TIME MINUS SIGMA
C         XFMPS IS THE XPOS MEAN ERROR AT PLUS  TIME PLUS  SIGMA
C         ALL NAMES FOLLOW THIS CODE
C
C
C       THIS ROUTINE COMPUTES THE STATISTICS ON THE FILTER ERRORS
C
      DO 1 I=1,4
       DO 1 J=1,NFRAMES
      XFME(I,J)=XFME(I,J)/FLOAT(NRUNS)
      XFPE(I,J)=XFPE(I,J)/FLOAT(NRUNS)
      CNME(I,J)=CNME(I,J)/FLOAT(NRUNS)
      CNPE(I,J)=CNPE(I,J)/FLOAT(NRUNS)
      DIV=FLOAT(NRUNS-1)
      XFME2(I,J)=SQRT((ABS(XFME2(I,J)-FLOAT(NRUNS)*(XFME(I,J)**2)))/DIV)
      XFPE2(I,J)=SQRT((ABS(XFPE2(I,J)-FLOAT(NRUNS)*(XFPE(I,J)**2)))/DIV)
      CNME2(I,J)=SQRT((ABS(CNME2(I,J)-FLOAT(NRUNS)*(CNME(I,J)**2)))/DIV)
1     CNPE2(I,J)=SQRT((ABS(CNPE2(I,J)-FLOAT(NRUNS)*(CNPE(I,J)**2)))/DIV)
       DO 1001 I=1,4
      DO 1001 J=1,NFRAMES
      XFMMS(I,J)=XFME(I,J)-XFME2(I,J)
      XFMPS(I,J)=XFME(I,J)+XFME2(I,J)
      XFPMS(I,J)=XFPE(I,J)-XFPE2(I,J)
      XFPPS(I,J)=XFPE(I,J)+XFPE2(I,J)
      CNMMS(I,J)=CNME(I,J)-CNME2(I,J)
      CNMPS(I,J)=CNME(I,J)+CNME2(I,J)
      CNPMS(I,J)=CNPE(I,J)-CNPE2(I,J)
1001  CNPPS(I,J)=CNPE(I,J)+CNPE2(I,J)
      DO 12 I=1,8
      DO 12 J=1,NFRAMES
         PFPST(I,J)=SQRT( PFPST(I,J)/FLOAT(NRUNS))
         PFMST(I,J)=SQRT(PFMST(I,J)/FLOAT(NRUNS))
12    CONTINUE
      WRITE(6,2)
2     FORMAT(T2,*FRAME*,T10,*XERR(-)*,T22,*SXERR(-)*,T34,*YERR(-)*,
     #T46,*SYERR(-)*,T58,*XVELERR(-)*,T70,*SXVELERR(-)*,T82
     #,*YVELERR(-)*,T94,*SYVELERR(-)*)
C
```

```
      TIMXX=0.
      DO 3 I=1,NFRAMES
      WRITE(6,4) TIMXX,XFME(1,I),XFME2(1,I),XFME(2,I
     #),XFME2(2,I),XFME(3,I),XFME2(3,I),XFME(4,I),XFME2(4,I)
4     FORMAT(T1,F8.3,8E12.5)
      TIMXX=TIMXX+(1./30.)
3     CONTINUE
      TIMYY=0.
      WRITE(6,5)
5     FORMAT(T2,*FRAME*,T10,*XERR(+)*,T22,*SXERR(+)*,T34,*YERR(+)*,
     #T46,*SYERR(+)*,T58,*XVELERR(+)*,T70,*SXVELERR(+)*,
     #T82,*YVELERR(+)*,T94,*SYVELERR(+)*)
      DO 6 I=1,NFRAMES
      WRITE(6,7) TIMYY,XFPE(1,I),XFPE2(1,I),XFPE(2,I),XFPE2(2,I)
     #,XFPE(3,I),XFPE2(3,I),XFPE(4,I),XFPE2(4,I)
7     FORMAT(T1,F8.3,8E12.5)
      TIMYY=TIMYY+(1./30.)
6     CONTINUE
      TIMXX=0.
      WRITE(6,101)
101   FORMAT(T2,*FRAME*,T12,*CNER(-)*,T30,*SCNER(-)*,T55,*YCER(-)*,
     #T68,*SYCER(-)*)
      DO 102 I=1,NFRAMES
      WRITE(6,103) TIMXX,CNME(1,I),CNME2(1,I),CNME(2,I),CNME2(2,I)
103   FORMAT(T1,F8.3,T10,E12.5,T23,E12.5,T52,E12.5,T66,E12.5)
      TIMXX=TIMXX+(1./30.)
102   CONTINUE
      TIMXX=0.
      WRITE(6,10)
10    FORMAT(T2,*FRAME*,T12,*CNER(+)*,T30,*SCNER(+)*,T55,*YCER(+)*,
     #T68,*SYCER(+)*)
      DO 8 I=1,NFRAMES
      WRITE(6,9) TIMXX,CNPE(1,I),CNPE2(1,I),CNPE(2,I),CNPE2(2,I)
9     FORMAT(T1,F8.3,T10,E12.5,T23,E12.5,T52,E12.5,T66,E12.5)
      TIMXX=TIMXX+(1./30.)
8     CONTINUE
      TIMXX=0.
      WRITE(6,17)
17    FORMAT(//,T2,*FRAME*,T14,*SQRT PFP(1,1)*,T30,*SQRT PFP(2,2)*,
     +T53,*SQRT PFP(3,3)*,T66,*SQRT PFP(4,4)*)
      DO 13 J=1,NFRAMES
      WRITE(6,14) TIMXX,PFPST(1,J),PFPST(2,J),PFPST(3,J),PFPST(4,J)
14    FORMAT(T1,F8.3,T12,E12.5,T23,E12.5,T52,E12.5,T66,E12.5)
      TIMXX=TIMXX+(1./30.)
13    CONTINUE
      WRITE(6,18)
18    FORMAT(//,T2,*FRAME*,T14,*SQRT PFM(1,1)*,T30,*SQRT PFM(2,2)*,
     +T53,*SQRT PFM(3,3)*,T66,*SQRT PFM(4,4)*)
      TIMXX=0.
      DO 15 I=1,NFRAMES
      WRITE(6,16)TIMXX,PFMST(1,I),PFMST(2,I),PFMST(3,I),PFMST(4,I)
16    FORMAT(T1,F8.3,T10,E12.5,T23,E12.5,T52,E12.5,T66,E12.5)
      TIMXX=TIMXX+(1./30.)
15    CONTINUE
C
      ISTART=15
      IFIN=60
```

```
      GO TO 837
      DO 80 K=1,2
      TIMXX=FLOAT(ISTART)*(1./30)
      TIMMM=FLOAT(IFIN)*(1./30.)
      WRITE(6,84)TIMXX,TIMMM
84    FORMAT(//,1X,* FROM TIME*,F8.3,* TO TIME*,F8.3)
      WRITE(6,85)
85    FORMAT(/,T4,* X/Y ERRM*,T18,* X/Y ERRP*,T32,* X/Y CERRM*,
     +T46,* X/Y CERRP*,T60,* X/Y SERRM*,T74,* X/Y SERRP*,
     +T88,* X/Y SCERRM*,T102,* X/Y SCERRP*)
C
C     THE FOLLOWING CALCULATIONS ARE USED TO FIND THE
C     AVERAGE ERRORS OVER A GIVEN PERIOD
C     SET ISTART AND IFIN FOR THE DESIRED RANGE
C
      DO 81 I=1,2
      ERRM=0.
      ERRP=0.
      CERRM=0.
      CERRP=0.
      SERRP=0.
      SERRM=0.
      SCERRM=0.
      SCERRP=0.
C
      DO 82 J=ISTART,IFIN
        ERRM=ERRM+XFME(I,J)
        ERRP=ERRP+XFPE(I,J)
        CERRM=CERRM+CNME(I,J)
        CERRP=CERRP+CNPE(I,J)
        SERRM=SERRM+XFME2(I,J)
        SERRP=SERRP+XFPE2(I,J)
        SCERRM=CNME2(I,J)+SCERRM
        SCERRP=SCERRP+CNPE2(I,J)
82    CONTINUE
C
      ERRM=ERRM/FLOAT(IFIN-ISTART+1)
      ERRP=ERRP/FLOAT(IFIN-ISTART+1)
      CERRM=CERRM/FLOAT(IFIN-ISTART+1)
      CERRP=CERRP/FLOAT(IFIN-ISTART+1)
      SERRM=SERRM/FLOAT(IFIN-ISTART+1)
      SERRP=SERRP/FLOAT(IFIN-ISTART+1)
      SCERM=SCERM/FLOAT(IFIN-ISTART+1)
      SCERP=SCERP/FLOAT(IFIN-ISTART+1)
C
      WRITE(6,83)ERRM,ERRP,CERRM,CERRP,SERRM,SERRP,SCERM,SCERP
83    FORMAT(1X,(8E14.5))
81    CONTINUE
      IF(NFRAMES.GT.149)ISTART=135
      IF(NFRAMES.GT.149)IFIN=150
80    CONTINUE
837   CONTINUE
C
C
C
C
C
```

```
      DO 110 I=1,NFRAMES
C     TIMEM IS THE TIME MINUS ARRAY SET FOR MULTIPLE PLOTS
      TIMEM(I)=FLOAT(I)-.2
        IF(I. EQ .1 )  T I M E M( I ) = 1.
       TIME(I)=FLOAT(I)
110   IF(I.EQ.1) TIME(I)=1.001
C
C      NOTE THE ORDER OF OUTPUT TO TAPE
C
C        MEAN ERROR AT MINUS X POS FOLLOWED BY PLUS X POS
C        MEAN ERROR AT MINUS X POS MINUS SIGMA FOLLOWED BY X POS
C         MEAN ERROR AT MINUS X POS PLUS SIGMA FOLLOWED BY PLUS XPOS
C        MEAN ERROR AT MINUS Y POS FOLLOWED BY PLUS Y POS
C        MEAN ERROR AT MINUS Y POS MINUS SIGMA FOLLOWED BY PLUS Y POS
C        MEAN ERROR AT MINUS Y POS PLUS  SIGMA FOLLOWED BY PLUS Y POS
C        MEAN ERROR AT MINUS X CEN POS FOLLOWED BY PLUS XCEN
C         MEAN ERROR AT MINUS X CEN POS MINUS SIGMA FOLLOWED BY PLUS X
C        MEAN ERROR AT MINUS X CEN POS PLUS  SIGMA FOLLOWED BY PLUS X
C        MEAN ERROR AT MINUS Y CEN POS FOLLOWED BY PLUS Y CEN
C        MEAN ERROR AT MINUS Y CEN POS MINUS SIGMA FOLLOWED BY PLUS Y
C        MEAN ERROR AT MINUS Y CEN POS PLUS  SIGMA FOLLOWED BY PLUS Y
C
C        WRITTEN WITH A 6E12.5 RECORDS WHICH IMPLIES EACH PLOTTABLE
C             SET OF POINTS CONSIST OF 14 RECORDS WITH THE LAST RECORD
C             ONLY CONTAINING 2 POINTS INSTEAD OF 6
C
C     WRITE(1,1000) ((TIMEM(I),XFME(1,I),TIME(I),XFPE(1,I)),I=1,20)
C     WRITE(1,1000) ((TIMEM(I),XFMMS(1,I),TIME(I),XFPMS(1,I)),I=1,20)
C     WRITE(1,1000) ((TIMEM(I),XFMPS(1,I),TIME(I),XFPPS(1,I)),I=1,20)
C     WRITE(1,1000) ((TIMEM(I),XFME(2,I),TIME(I),XFPE(2,I)),I=1,20)
C     WRITE(1,1000) ((TIMEM(I),XFMMS(2,I),TIME(I),XFPMS(2,I)),I=1,20)
C      WRITE(1,1000) ((TIMEM(I),XFMPS(2,I),TIME(I),XFPPS(2,I)),I=1,20)
C     WRITE(1,1000) ((TIMEM(I),CNME(1,I),TIME(I),CNPE(1,I)),I=1,20)
C     WRITE(1,1000) ((TIMEM(I),CNMMS(1,I),TIME(I),CNPMS(1,I)),I=1,20)
C     WRITE(1,1000) ((TIMEM(I),CNMPS(1,I),TIME(I),CNPPS(1,I)),I=1,20)
C     WRITE(1,1000) ((TIMEM(I),CNME(2,I),TIME(I),CNPE(2,I)),I=1,20)
C     WRITE(1,1000) ((TIMEM(I),CNMMS(2,I),TIME(I),CNPMS(2,I)),I=1,20)
C     WRITE(1,1000) ((TIMEM(I),CNMPS(2,I),TIME(I),CNPPS(2,I)),I=1,20)
1000  FORMAT(6F12.5)
      RETURN
      END
```

VERITY DETAILS DIAGNOSIS OF PROBLEM

THERE IS NO PATH TO THIS STATEMENT.

```
      SUBROUTINE FILPT(PFP T,PFMST,XFPE2,XFME2,NFRAMES,TIMPL,ACTPL,
     +FILPL,FILPY,ACTPY,TIMR)
      REAL TIMPL(400),FILPL(400),ACTPL(400),FILPY(400),ACTPY(400)
      REAL PFPST( ,NFRAMES),PFMST(3,NFRAME )
      REAL XFME2(4,NFRAMES),XFPE2(4,NFRAME )
      REAL TIM (200)
C
C     THIS SUBROUTINE COMBINES PFP AND PFM ,AND XFME2
C     AND XFPE2 FOR PLOTTING PURPOSES
C
      KOUNT=1
      KOUNT1=1
      KOUNT2=3
      KOUNT3=1
      KOUNT4=1
      TIM=0.
C
C
      DO 10 I=1,NFRAMES
      FILPL(KOUNT)= (PFMST(1,I))
      FILPL(KOUNT+1)=(PFPST(1,I))
      KOUNT=KOUNT+2
10    CONTINUE
C
C
      DO 20 I=1,NFRAMES
      ACTPL(KOUNT1)=XFME2(1,I)
      ACTPL(KOUNT1+1)=XFPE2(1,I)
      KOUNT1=KOUNT1+2
20    CONTINUE
C
      DO 30 I=1,NFRAMES
      IF(I.LT.1.5)GO TO 40
      TIMPL(KOUNT2)=TIM
      TIMPL(KOUNT2+1)=TIMPL(KOUNT2) + .000001
      TIMR(I)=TIM
      KOUNT2=KOUN 2+2
      TIM=TIM+(1./30.)
      GO TO 41
40    TIMPL(I)=0.
      TIM (1)=0.
      TIMPL(2)=.000001
      TIM=TIM + 1./30.
41    CONTINUE
30    CONTINUE
C
C
      DO 50 I=1,NFRAMES
        FILPY(KOUNT3)=PFMST(2,I)
        FILPY(KOUNT3+1)=PFPST(2,I)
        KOUNT3=KOUNT3+2
50    CONTINUE
C
      DO 60 I=1,NFRAMES
        ACTPY(KOUNT4)=XFME2(2,I)
        ACTPY(KOUNT4+1)=XFPE2(2,I)
        KOUNT4=KOUNT4+2
```

```
   6?     CONTINUE
   C
   C
          RETURN
          END
```

```
      SUBROUTINE TRUTH(PHIT,QD,CDT,H,SIGDT,DT)
        REAL PHIT(8,8),QD(8, ),<,QDROOT(8,8),H(2, )
      REAL QD (6,6)
C
C
C     THE   STATE SPACE MODEL IS:
C
C     D(XD)/DT=FT*XD+BU+GT*WT      AND     YD=H*XD
C      WHERE
C
C                    :  1    0    0    0    0    0    0    0   :
C                   :  0    1    0    0    0    0    0    0   :
C                    :  0    0   -A    0    0    0    0    0   :
C       FT=         :  0    0    0   -B    1    0    0    0   :
C                     :  0    0    0    0   -B    0    0    0   :
C                   :  0    0    0    0    0   -A    0    0   :
C
C                   :  0    0    0    0    0    0   -B    1   :
C                    :  0    0    0    0    0    0    0   -B   :
C
C
C      GT=          : 1    0    0    0 :
C                    : 0    1    0    0 :
C                   : 0    0   G1    0 :
C                   : 0    0   G2    0 :
C                   : 0    0   G3    0 :
C                      : 0    0    0   G1 :
C                   : 0    0    0   G2 :
C                   : 0    0    0   G3 :
C
C
C       AND    HT=  : 1    0    1    1    0    0    0    0 :
C                     : 0    1    0    0    0    1    1    0 :
C
C
C                XD=  : XT   :
C                     : YT   :
C                    : X1A :
C                     : X2A :
C                     : X3A :
C                     : Y1A :
C                    : Y2A :
C                       : Y3A :
C
C
C         THE SOLUTION OF THE DYNAMIC EQUATIONS IS
C
C
C          XD(I+1)= PHIT*XD(I) + SQRT(QD)*WT
C
C          WHERE PHIT=STATE TRANSITION MATRIX
C                SIGDT= ATMOS NOISE STANDARD DEVIATION
C                   WT= GAUSSIAN NOISE VECTOR
C                   QD= COVARIANCE MATRIX
C
C
      NSTATE=8
```

```
      K=.36210?544*CIGOT
      TD=1.
      A=14.14
      B=659.5
      DO 1 I=1,NSTATE
      DO 1 J=1,NSTATE
       PHIT(I,J)=0.
1     QD(I,J)=0.
C     PHIT(1,1)=EXP(-DT/TD)
C     PHIT(2,2)=EXP(-DT/TD)
     PHIT(1,1)=1.
     PHIT(2,2)=PHIT(1,1)
      PHIT(3,3)=EXP(-A*DT)
      PHIT(4,5)=DT*EXP(-B*DT)
      PHIT(5,5)=EXP(-B*DT)
      PHIT(6,6)=EXP(-A*DT)
      PHIT(7,7)=EXP(-B*DT)
      PHIT(7,8)=DT*EXP(-B*DT)
      PHIT(8,8)=EXP(-B*DT)
       FACT=(K**2)*(A**2)*(B**4)
      FACT1=A-B
       FACT2=A+B
      FACT3=2.*B
      G1=FACT/(FACT1**4)
      G2=FACT/(FACT1**3)
      G3=FACT/(FACT1**2)
      P1=1.-EXP(-2.*A*DT)
      P2=1.-EXP(-FACT2*DT)
      P3=1.-EXP(-2.*B*DT)
      P4=DT*EXP(-FACT2*DT)
      P5=DT*EXP(-2.*B*DT)
      QD(1,1)=0.
      QD(2,2)=QD(1,1)
      QD(3,3)=(G1*P1)/(2.*A)
      QD(3,4)=P2*(G2/FACT2**2-G1/FACT2)-P4*G2/FACT2
      QD(3,5)=G2*P2/FACT2
      QD(4,3)=QD(3,4)
      QD(4,4)=P3*(G1/FACT3-2.*G2/FACT3**2+2.*G3/FACT3**3)-
     1        P5*(-G2/B+G3*DT/FACT3+2.*G3/FACT3**2)
      QD(4,5)=P3*(G3/FACT3**2-G2/FACT3)-P5*G3/FACT3
      QD(5,3)=QD(3,5)
      QD(5,4)=QD(4,5)
       QD(5,5)=P3*G3/FACT3
      DO 2 I=3,5
      DO 2 J=3,5
      QD(I+3,J+3)=QD(I,J)
2     CONTINUE
      DO 964 I=1,6
      DO 964 J=1,6
964    QDP(I,J)=QD(I+2,J+2)
     CALL CHOLY(QDP,6)
      DO 965 I=1,6
      DO 965 J=1,6
965   QD(I+2,J+2)=QDP(I,J)
      DO 5 I=1,6
      DO 5 J=1,6
5      QDROOT(I,J)=QD(I,J)
```

```
      1267   FORMAT(1X,*F5.2)
             DO 3 I=1,2
             DO 3 J=1,8
      3      H(I,J)=0.
             H(1,1)=1.
             H(1,3)=1.
             H(1,4)=1.
             H(2,2)=1.
             H(2,6)=1.
             H(2,7)=1.
             RETURN
             END
```

```
      SUBROUTINE PROP(PHIT,QDROOT,H,XT,YT,N,M,UT,BD,
     +TIME,DT,TRATE,X0,Y0,Z0,VMAX,RANGE,TRAGEN,NP,NS,EXUT,
     +HS1A,HS1B,HS2A,HS2B,HS3A,HS3B,VMAXEX,RANEX,TIMEX,COSW)
        REAL PHIT(N,N),QDROOT(N,N),XT(N,1),YT(M,1),H(M,N)
       REAL TEMP1(8,1),TEMP2(8,1),TEMP3(2,1)
      REAL UT(2,1),BD(8,2)
      INTEGER TRAGEN,NR,NS
      REAL EXUT(2,200),HS1A(200),HS1B(200),HS2A(200),HS2B(200)
      REAL HS3A(200),HS3B(200),VMAXEX(200),RANEX(200)
      REAL TIMEX(200),COSW(200)
C
C
C      THIS ROUTINE IMPLEMENTS THE STATE TRANSITION EQUATION.
C
C            XT(I+1)=PHIT*XT(I) + QDROOT*WD
C
C      WHERE     XT= STATE VECTOR (NX1)
C                PHIT= STATE TRANSITION MATRIX (NXN)
C                QDROOT= STATE UNCERTAINTY COVARIANCE MATRIX (NXN)
C                WD= GAUSSIAN DISTRIBUTED NOISE VECTOR (NX1)
C
C        AND THE OUTPUT EQUATION
C
C                YT=H*XT
C
C       WHERE     YT=MEASUREABLE OUTPUT VECTOR (MX1)
C                H= STATE TO OUTPUT MAXTRIX (MXN)
C
      NP=N +1
      IF (TRAGEN.EQ.2)GO TO 400
C
C
      XDOT= -1000.
      YDOT= 0.
      ZDOT= 0.
      XPOS= X0 + XDOT*TIME
      YPOS= Y0
      ZPOS= Z0
      VTIME=TIME-(DT/2.0)
      IF(TIME.LT.2.0)GO TO 310
      XDOT= -1000.*COS(TRATE*(VTIME-2.))
      YDOT= 1000.*SIN(TRATE*(VTIME-2.))
      XPOS= X0-2000.-((1000./TRATE)*SIN(TRATE*(TIME-2.)))
      YPOS= Y0 + ((1000/TRATE)*(1.-COS(TRATE*(TIME-2.))))
      ZPOS= Z0
  310 CONTINUE
      RHOR= XPOS**2 + ZPOS**2
      RANGE= RHOR + YPOS**2
      UT(1,1)= (-ZPOS*XDOT+XPOS*ZDOT)/(RHOR*.00002)
      RHOR= SQRT(RHOR)
      UT(2,1)=(RHOR*YDOT-YPOS*((XPOS*XDOT+ZPOS*ZDOT)/RHOR))/(RANGE
     +*.00002)
      RANGE= SQRT(RANGE)
      VMAX=SQRT(XDOT**2+YDOT**2+ZDOT**2)/(RANGE*.00002)
      GO TO 401
C
  400 CONTINUE
```

```
C     READ IN THE DATA FROM THE EXTERNAL TAPE
C     AND STORE THE DATA FOR THE NEXT RUN
C
      IF(NI.NE.1)GO TO 402
      READ(9,*)ITER,EXUT(1,NP),EXUT(2,NP),VMAXEX(NP)
     +,COSW(NP),RANEX(NP),TIMEX(NP)
403   FORMAT(I4,6E14.5)
      READ(9,*)HS1A(NP),HS1B(NP),HS2A(NP),HS2B(NP),HS3A(NP),HS3B(NP)
404   FORMAT(6E14.5)
      READ(9,*)XPOS,YPOS,ZPOS,XDOT,YDOT,ZDOT,TRATE
405   FORMAT(7E14.5)
C
      WRITE(6,411)
411   FORMAT(//,T1,* FRAME*,T12,* ADOT*,T26,* BDOT*,T40,* VMAX*,
     +T51,*ROLL ANGLE*,T68,*RANGE*,T82,* EX TIME*)
      WRITE(6,406)ITER,EXUT(1,NP),EXUT(2,NP),VMAXEX(NP),COSW(NP)
     +,RANEX(NP),TIMEX(NP)
406   FORMAT(1X,I4,6E14.5)
C
      WRITE(6,412)
412   FORMAT(T6,* HS1A*,T21,* HS1B*,T35,*HS2A*,T49,*HS2B*,T63,
     +* HS3A*,T77,* HS3B*)
      WRITE(6,407)HS1A(NP),HS1B(NP),HS2A(NP),HS2B(NP),HS3A(NP),HS3B(NP)
407   FORMAT(1X,6E14.5)
402   CONTINUE
C
      UT(1,1)=EXUT(1,NP)
      UT(2,1)=EXUT(2,NP)
      VMAX=VMAXEX(NP)
      RANGE=RANEX(NP)
C
401   CONTINUE
C
C
C
       CALL NOISE(TEMP1,N)
       CALL MULT(QDROOT,TEMP1,N,N,1,TEMP2)
       CALL MULT(PHIT,XT,N,N,1,TEMP1)
      CALL MULT(BD,UT,5,2,1,TEMP3)
       DO 1 I=1,N
1     XT(I,1)=TEMP1(I,1) + TEMP2(I,1) + TEMP3(I,1)
       CALL MULT(H,XT,M,N,1,YT)
       RETURN
       END
```

```
      SUBROUTINE INITF(TAF,VARDF,VARAF)
C
C
C       THIS ROUTINE CONTROLS INPUTING VALUES NEEDED FOR THE KALMAN
C           - FILTER
C
C
      AF=.07072
C
C        THIS IS THE CORRELATION TIME FOR THE ATMOSPHERIC MODEL FOR THE
C              - FILTER
C
C
C       THE VARIANCE OF THE DYNAMICS FOR THE FILTER
C
C
      READ(5,2)VARDF
      WRITE(6,1)VARDF
1     FORMAT(1X,*VARIANCE OF FILTER DYNAMICS*,E14.5)
      WRITE(6,3)
3     FORMAT(1X,*VARIANCE OF FILTER ATMOSPHERICS*)
      READ(5,2) VARAF
2     FORMAT(F7.4)
C
C
C       THE VARIANCE OF THE ATMOSPHERIC JITTER FOR THE FILTER
C
C
      RETURN
      END
```

```
      SUBROUTINE FILTER(TDF,VARDF,TAF,VARAF,DT,PHIF,QFD,NS)
      REAL PHIF(8,8),QFD(8,8)
      INTEGER NS
C
C     THIS SUBROUTINE DEFINES THE FILTER STATE TRANSITION
      DO 1 I=1,8
      DO 1 J=1,8
           PHIF(I,J)=0.
           QFD(I,J)=0.
1     CONTINUE
C
      PHIF(1,1)=1.
      PHIF(1,3)=DT
      PHIF(1,5)=(TDF**2)*((DT/TDF)-1.0+(EXP(-DT/TDF)))
      PHIF(2,2)=1.
      PHIF(2,4)=PHIF(1,3)
      PHIF(2,6)=PHIF(1,5)
      PHIF(3,3)=1.
      PHIF(3,5)=TDF*(1.-EXP(-DT/TDF))
      PHIF(4,4)=1.
      PHIF(4,6)=PHIF(3,5)
      PHIF(5,5)=EXP(-DT/TDF)
      PHIF(6,6)=PHIF(5,5)
      PHIF(7,7)=EXP(-DT/TAF)
      PHIF(8,8)=PHIF(7,7)
C     MATRIX(PHIF) AND THE DISCRETE NOISE COVARIANCE
C     MATRIX (QFD)
      QFD(1,1)=((2*VARDF*TDF*(DT**3))/3.)-(2*VARDF*(TDF**2)*(DT**2)
     +)-(4*VARDF*(TDF**3)*DT*EXP(-DT/TDF))+(2*VARDF*(TDF**3)*DT)-VARDF*(
     +TDF**4)*EXP(-2.*DT/TDF)+(VARDF*(TDF**4))
      QFD(1,3)=(VARDF*TDF*(DT**2))+(2*VARDF*(TDF**2)*DT*EXP(-DT/TDF))+(V
     +ARDF*(TDF**3))-(2*VARDF*(TDF**3)*EXP(-DT/TDF))-(2*VARDF*(TDF**2)*D
     +T)+(VARDF*(TDF**3)*EXP(-2.*DT/TDF))
      QFD(1,5)=(-2.*TDF*VARDF*DT*EXP(-DT/TDF))+(VARDF*(TDF**2))-(VARDF*(
     +TDF**2)*EXP(-2.*DT/TDF))
      QFD(2,2)=QFD(1,1)
      QFD(2,4)=QFD(1,3)
      QFD(2,6)=QFD(1,5)
      QFD(3,1)=QFD(1,3)
      QFD(3,3)=(2.*VARDF*TDF*DT)-(3.*(TDF**2)*VARDF)+(4.*(TDF**2)*VARDF*
     +EXP(-DT/TDF))-((TDF**2)*VARDF*EXP(-2.*DT/TDF))
      QFD(3,5)=(VARDF*TDF)-(2.*VARDF*TDF*EXP(-DT/TDF))+(VARDF*TDF*EXP(-2
     +.*DT/TDF))
      QFD(4,2)=QFD(2,4)
      QFD(4,4)=QFD(3,3)
      QFD(4,6)=QFD(3,5)
      QFD(5,1)=QFD(1,5)
      QFD(5,3)=QFD(3,5)
      QFD(5,5)=VARDF*(1.-EXP(-2.*DT/TDF))
      QFD(6,2)=QFD(2,6)
      QFD(6,4)=QFD(4,6)
      QFD(6,6)=QFD(5,5)
      QFD(7,7)=VARAF*(1.-EXP(-2.*DT/TAF))
      QFD(8,8)=QFD(7,7)
C
C     WRITE THE MATRIX DEFINITIONS TO THE OUTPUT TAPE
      IF(NS.NE.1)GO TO 20
```

```
      WRITE(6,200) ((PHIF(I,J),J=1,8),I=1,8)
200   FORMAT(1X,*PHIF*,/,(1X,8E14.5))
      WRITE(6,201) ((QFD(I,J),J=1,8),I=1,8)
201   FORMAT(1X,//* QFD*,/,(1X,8E14.5))
20    CONTINUE
C
      RETURN
      END
```

```
      SUBROUTINE PROPF(PHIF,QFD,PFP,PFM,XFP,XFM,NS,SVPFP,ICHQ)
      REAL PHIF(8,8),QFD(8,8),PFP(8,8),PFM(8,8),XFP(8),XFM(8)
      REAL PHIFT(8,8),TEMP1(8,8),TEMP2(8,8)
      REAL SVPFP(8,8)
      INTEGER ICHQ
C
C
C
C       THIS ROUTINE IMPLEMENTS THE STATE TRANSITION
C               -EQUATIONS FOR THE FILTER
C
C
C       XF(I+1)=PHIF*XF(I)
C
C
C      PM=PHIF*PFP*PHIFT +QFD
C
C
C       WHERE                 PHIF=FILTER STATE TRANSITION MATRIX
C                              XF  =FILTER STATE VECTOR
C                             PFM =COV FILTER STATES MINUS
C                             PFP =COV FILTER STATES PLUS
C                             QFD=NOISE COVARIANCE MATRIX
C
C
C
C
C          PERFORM FILTER STATE PROPAGATION
C
C
      CALL MULT(PHIF,XFP,8,8,1,XFM)
      CALL MULT(PHIF,PFP,8,8,8,TEMP1)
      DO 1 I=1,8
      DO 1 J=1,8
         PHIFT(I,J)=PHIF(J,I)
1     CONTINUE
      CALL MULT(TEMP1,PHIFT,8,8,8,TEMP2)
C
C SAVE PHIF*PFP*PHIFT FOR QFD ESTIMATION
C
      IF(ICHQ.NE.1)GO TO 377
      DO 376 I=1,8
      DO 376 J=1,8
        SVPFP(I,J)=TEMP2(I,J)
376   CONTINUE
377   CONTINUE
C      WRITE(6,360)
360   FORMAT(* TEMP2*)
C      CALL MPRINT(TEMP2,8,8,10)
C      WRITE(6,370)
370   FORMAT(* QFD*)
C      CALL MPRINT(QFD,8,8,10)
      IF(NS.NE.1) GO TO 374
C     WRITE(6,371) ((PFP(I,J),J=1,8),I=1,8)
371   FORMAT(1X,*PFP*,/,(1X,8E14.5))
374   CONTINUE
      DO 2 I=1,8
```

```
          DO 2 J=1,6
             PFM(I,J)=TEMP2(I,J)+QFD(I,J)
    2     CONTINUE
          IF(NS.NE.1) GO TO 375
C         WRITE(6,373) ((PFM(I,J),J=1,9),I=1,9)
  373     FORMAT(1X,//,* PFM*,/,(1X,9E14.5))
  375     CONTINUE
          RETURN
          END
```

```
      SUBROUTINE INPUT3(IMAX,S,XMAX,N,X,Y,DATA,CENX,CENY,YMAX,
     +SIGMS,RANGED,RANGE,UT,VMAX,ASPRO,NUMHS)
       REAL IMAX(3),S(12),XMAX(3),YMAX(3)
       COMPLEX DATA(N,N)
      REAL SIGMS,RANGED,RANGE,VMAX,ASPRO
      REAL UT(2,1)
      INTEGER GNEH
C
C          THIS ROUTINE DETERMINES REAL MODEL INTENSITY AND CENTROID
C       VALUES FOR AN 8X8 PIXEL FOV. ZERO PADDING IS ACCOMPLISHED BY
C       CENTERING THE 8X8 PIXEL FOV WITHIN A NULL NXN SPACE.
C          THE COORDINATE SYSTEM IS AS DEFINED BELOW:
C
C
C            (0,0).......................
C                 .                     .
C                 .                     .
C                 .          N          .
C                 .    GAUSSIAN         .
C                 .                     .
C                 .                     .
C                 .    (X,Y).......     .
C                 .         . FOV  .    .
C                 .    N    .     N.    .
C                 .         ........    .
C                 .......................
C
C
C       THE INTENSITY PATTERN IS DEFINED TO BE 3 GAUSSIAN DISTRIBUTIONS
C       OF INTENSITY IMAX(I),I=1,3 LOCATED AT XMAX(I),YMAX(I),I=1,3
C       WITH COVARIANCE S(I),I=1,3. THE UPPER LEFT CORNER OF THE 8X8 PIXEL
C       FOV IS DEFINED TO BE LOCATION X,Y MICRORAD.
C         THE INTENSITY AT EACH PIXEL IS DETERMINED BY INTEGRATING THE
C       INTENSITY OF 25 EQUALLY SPACED SPOTS WITHIN THE PIXEL.
C
      SIGPV=SIGMS*(RANGED/RANGE)
      PLVEL=SQRT(UT(1,1)**2+UT(2,1)**2)
      SNTH=UT(2,1)/PLVEL
      CSTH=UT(1,1)/PLVEL
      SIGV=(1.+(ASPRO-1.)*PLVEL/VMAX)*SIGPV
C
C
C
C       ZERO OUT FOV SPACE.
        DO 10 I=1,N
        DO 10 J=1,N
10      DATA(I,J)=0.
        SUMX=0.
        SUMY=0.
        SUMAVG=0.
        LM=N/2-3
        LP=N/2+4
        DO 1 I=LM,LP
        DO 2 J=LM,LP
        AVG=0.
C       DIVIDE PIXEL I,J INTO 25 SEGMENTS
        DO 3 K1=1,5
```

```
      DO 4 K2=1,5
      DELY=(I-9)*1.0+(K1-1)*.2
      DELX=(J-9)*1.0+(K2-1)*.2
      XP=X+DELX
      YP=Y+DELY
      CX1=(XP-XMAX(1))*CSTH
      SX1=(XP-XMAX(1))*SNTH
      CY1=(YP-YMAX(1))*CSTH
      SY1=(YP-YMAX(1))*SNTH
      X1=CX1+SY1
      Y1=CY1-SX1
      ARG1=-.5*((X1/SIGV)**2+(Y1/SIGPV)**2)
      IF (NUMHS.EQ.1)GO TO 70
      CX2=(XP-XMAX(2))*CSTH
      CY2=(YP-YMAX(2))*CSTH
      SX2=(XP-XMAX(2))*SNTH
      SY2=(YP-YMAX(2))*SNTH
      CX3=(XP-XMAX(3))*CSTH
      CY3=(YP-YMAX(3))*CSTH
      SX3=(XP-XMAX(3))*SNTH
      SY3=(YP-YMAX(3))*SNTH
      X2=CX2+SY2
      Y2=CY2-SX2
      X3=CX3+SY3
      Y3=CY3-SX3
      ARG2=-.5*((X2/SIGV)**2+(Y2/SIGPV)**2)
      ARG3=-.5*((X3/SIGV)**2+(Y3/SIGPV)**2)
      FXY=IMAX(1)*EXP(ARG1)+IMAX(2)*EXP(ARG2)+IMAX(3)*EXP(ARG3)
      GO TO 71
70    FXY=IMAX(1)*EXP(ARG1)
71    CONTINUE
      AVG=AVG+FXY
      SUMX=SUMX+XP*FXY
      SUMY=SUMY+YP*FXY
4     CONTINUE
3     CONTINUE
      DATA(I,J)=AVG/25.
C     WRITE(6,100) I,J,DATA(I,J)
100   FORMAT(2X,2I4,2X,E12.5)
      SUMAVG=SUMAVG+AVG
2     CONTINUE
1     CONTINUE
      CENX=SUMX/SUMAVG
      CENY=SUMY/SUMAVG
      RETURN
      END
```

```
      SUBROUTINE CORREL(NN,DATA,TMPLAT,XCENT,YCENT,X,Y,THRESH,CORRL)
      COMPLEX TMPLAT(24,24),DATA(24,24)
      COMPLEX TEMP(24,24)
       COMPLEX WORK(50)
       REAL RDATA(24,24)
       EAL MAG
      INTEGER CORRL
        INTEGE  NN(2)
C
C     THIS SUBROUTINE IMPLEMENTS THE CORRELATION METHODS IN
C     FREQUENCY DOMAIN,I.E.THE FFT AND PHASE CORRELATION
C     METHOD. IF THE DIRECT METHOD IS BEING USED SUBROUTINE
C
      IF(CORRL.GT.2)CALL CCRL2(NN,DATA,TMPLAT,XCENT,YCENT,X,Y,CORRL)
      IF(CORRL.GT.2)GO TO 20
       CALL FOURT(DATA,NN,2,-1,1,WORK)
       DO 1 I=1,24
       DO 1 J=1,24
      TEMP(I,J)=CONJG(TMPLAT(I,J))*DATA(I,J)
      IF(CORRL.NE.2)GO TO 1
      XM=REAL(TEMP(I,J))**2
      YM=AIMAG(TEMP(I,J))**2
      MAG=SQRT(XM+YM)
C
C     IN ORDER TO AVOID NUMERICAL DIFFICULTIES THE MAGNITUDE
C     IS CHECKED BEFORE THE DIVISION
      IF(MAG.LT..000000001)GO TO 101
C
      TEMP(I,J)=TEMP(I,J)/MAG
      GO TO 1
101   TEMP(I,J)=CMPLX(0.,0.)
1     CONTINUE
       CALL FOURT(DATA,NN,2,1,1,WORK)
       CALL FOURT(TEMP,NN,2,1,1,WORK)
C     IF(CORRL.EQ.2)GO TO 22
       DO 35 I=1,24
      DO 35 J=1,24
      TEMP(I,J)=TEMP(I,J)/576.
35    DATA(I,J)=DATA(I,J)/576.
22    CONTINUE
C      CALL DISPLAY(24,24,DATA)
       CALL  CHAQUAD(TEMP,24)
C      CALL DISPLAY(24,24,DATA)
       DO 31 I=1,24
      DO 31 J=1,24
31    RDATA(I,J)=REAL(TEMP(I,J))
C      WRITE(6,112) ((RDATA(I,J),J=1,24),I=1,24)
112    FORMAT(4(1X,6E12.5,/),//)
      CALL CENTRD(X,Y,TEMP,24,XCENT,YCENT,THRESH)
C     CALL DISPLAY(24,24,DATA)
20    CONTINUE
       XCENT=XCENT-.5
      YCENT=YCENT-.5
C      WRITE(6,110) XCENT,YCENT
110    FORMAT(1X,*CENTROID=(*,F7.2,*,*,F7.2,*)*)
C     XCUM=XCUM+(XCENT-XSHIFT)
C     YCUM=YCUM+(YCENT-YSHIFT)
```

```
C       XCUM2=XCUM2+(XCENT-XSHIFT)**2
C       YCUM2=YCUM2+(YCENT-YSHIFT)**2
1000    CONTINUE
C       CALL STATC(XCUM,YCUM,XCUM2,YCUM2,N1)
        RETURN
         END
```

```
      SUBROUTINE CORL2(NN,DATA,TMPLAT,XCENT,YCENT,X,Y,CORPL)
C
      COMPLEXTMPLAT(24,24),WORK(50),DATA(24,24),HOLDT(24,24)
      REAL COR(24,24),QNT(24,24),QND(24,24),TEMP(24,24),SUMM(17,17)
      REAL VA(24,24),MEANT(24,24),VART(24,24)
      REAL A(24,24)
      INTEGER NN(2)
      INTEGER CORPL,PMAX,QMAX
      INTEGER P,Q,P3,Q3,N1
      REAL Q1,Q2
      INTEGER Q5,P5
      REAL MEAND
C
C     THIS SUBROUTINE IMPLEMENTS THE DIRECT CORRELATION METHOD;
C
C
      N1=4
      HOLD1=0.
      HD1=0.
      HD2=0.
      TOTAL=0.
      HOLD2=0.
      SUMX=0.
      SUMY=0.
      SUMA=0.
      DO 31 I=1,24
      DO 31 J=1,24
      A(I,J)=0.
      VART(I,J)=0.
      VA(I,J)=0.
31    CONTINUE
      VA=0.
      VB=0.
      DO 26 I=1,17
      DO 26 J=1,17
      II=I-1
      JJ=J-1
      SUMM(II,JJ)=0.
26    CONTINUE
      DO 25 I=1,24
      DO 25 J=1,24
        HOLDT(I,J)=TMPLAT(I,J)
25    CONTINUE
C
      CALL FOURT(HOLDT,NN,2,1,1,WORK)
      DO 27 I=1,24
      DO 27 J=1,24
        HOLDT(I,J)=HOLDT(I,J)/575.
27    CONTINUE
C
C     THE MEAN FOR THE DATA IS CALCULATED ONE TIME
C     THE MEAN FOR THE TEMPLATE IS CALCULATED FOR EACH P,Q VALUE
C     THE VARIANCE CALCULATIONS ARE ONLY REQUIRED FOR THE
C     THE 6-LEVEL QUANITIZZER
C
      DO 30 P3=5,13
      DO 30 Q3=5,13
```

```
      Q=Q3-1
      P=P3-1
      DO 1 I=1,8
      DO 1 J=1,8
C
        A(P,Q)=A(P,Q)+(REAL(HOLDT(I+P,J+Q)))
      IF(CORRL.EQ.4)VA(P,Q)=VA(P,Q)+REAL(HOLDT(I+P,J+Q))**2
      IF(N1.NE.4)GO TO 121
      B=B+(REAL(DATA(I+8,J+8)))
      IF(CORRL.EQ.4)VB=VB+(REAL(DATA(I+8,J+8)))**2
121   CONTINUE
C
1     CONTINUE
C
      MEANT(P,Q)=A(P,Q)/64.0
      IF(CORRL.EQ.4)VART(P,Q)=SQRT(ABS((VA(P,Q)/64.0)-(MEANT(P,Q)**2)))
      IF(N1.NE.4)GO TO 122
      MEAND=B/64.0
      IF(CORRL.EQ.4)VARD=SQRT(ABS((VB/64.0)-(MEAND**2)))
122   CONTINUE
      N1=N1+1
30    CONTINUE
C
      IF(CORRL.EQ.4)GO TO 90
C
C     CALCULATE THE QUANITIZED VALUES BASED ON THE MEAN
C     CALCULATIONS FOR THE 2-LEVEL QUNATIZER
C
      DO 15 Q3=5,13
      DO 15 P3=5,13
      Q=Q3-1
      P=P3-1
      DO 16 J=1,8
      DO 16 I=1,8
C
      QNT(I+P,J+Q)=-1.0
      IF(REAL(HOLDT(I+P,J+Q)).GT.MEANT(P,Q))QNT(I+P,J+Q)=1.0
      QND(I+8,J+8)=-1.0
      IF(REAL(DATA(I+8,J+8)).GT.MEAND)QND(I+8,J+8)=1.0
        SUMM(P,Q)=SUMM(P,Q)+QNT(I+P,J+Q)*QND(I+8,J+8)
16    CONTINUE
C     CHECK FOR THE MAX CORRELATION VALUE
      IF(SUMM(P,Q).LT.TOTAL)GO TO 51
        PMAX=P
        QMAX=Q
      TOTAL=SUMM(P,Q)
      DO 3 I=1,8
      DO 3 J=1,8
        COR(I+PMAX,J+QMAX)=(QNT(I+PMAX,J+QMAX)*QND(I+8,J+8))/64.0
3     CONTINUE
51    CONTINUE
15    CONTINUE
      GO TO 89
90    CONTINUE
C
C     PERFORM THE CALCULATIONS FOR THE 6-LEVEL QUANTIZER
C
```

```
      DO 17 Q5=5,13
      DO 17 P5=5,13
      HD1=0.
      HD2=0.
      P=P5-1
      Q=Q5-1
      DO 18 J=1,8
      DO 18 I=1,8
      Q1=(REAL(HOLDNT(P+I,Q+J))-MEANNT(P,Q))/VARNT(P,Q)
        IF(Q1.GT.0.0)GO TO 81
      QNT(I+P,J+Q)=-1.0
C
        IF(Q1.LT.-0.6)QNT(I+P,J+Q)=-3.0
        IF(Q1.LT.-1.4)QNT(I+P,J+Q)=-6.0
      GO TO 82
81    QNT(I+P,J+Q)=1.0
        IF(Q1.GT..6)QNT(I+P,J+Q)=3.0
        IF(Q1.GT.1.4)QNT(I+P,J+Q)=6.0
82    CONTINUE
C
        Q2=(REAL(DATA(I+8,J+8))-MEAND)/VARD
      IF(Q2.GT.0.0)GO TO 83
      QND(I+8,J+8)=-1.0
        IF(Q2.LT.-0.6)QND(I+8,J+8)=-3.0
        IF(Q2.LT.-1.4)QND(I+8,J+8)=-6.0
      GO TO 84
83    QND(I+8,J+8)=1.0
      IF(Q2.GT.0.6)QND(I+8,J+8)=3.0
        IF(Q2.GT.1.4)QND(I+8,J+8)=6.0
84    CONTINUE
      HD1=HD1+QNT(I+P,Q+J)**2
      HD2=HD2+QND(I+8,J+8)**2
C
C
18    CONTINUE
      DO 36 I=1,8
      DO 36 J=1,8
      SUMM(P,Q)=SUMM(P,Q)+(QNT(I+P,J+Q)*QND(I+8,J+8))/SQRT(HD1*HD2)
36    CONTINUE
      IF(SUMM(P,Q).LT.TOTAL)GO TO 52
C
      TOTAL=SUMM(P,Q)
      PMAX=P
      QMAX=Q
      HOLD1=HD1
      HOLD2=HD2
C
      DO 5 I=1,8
      DO 5 J=1,8
        COR(I+PMAX,J+QMAX)=(QNT(I+PMAX,J+QMAX)*QND(I+8,J+8))/(SQRT(HOLD1
     **HOLD2))
5     CONTINUE
52    CONTINUE
17    CONTINUE
89    CONTINUE
89    CONTINUE
C     WRITE(6,62)PMAX,QMAX
```

```
62      FORMAT(1X,* PMAX=*,I4,* QMAX=*,I4)
        DO 6 I=1,8
        DO 6 J=1,8
          SUMX=SUMX+FLOAT(I+PMAX)*COR(I+PMAX,J+QMAX)
          SUMY=SUMY+FLOAT(J+QMAX)*COR(I+PMAX,J+QMAX)
          SUMA=SUMA+COR(I+PMAX,J+QMAX)
6       CONTINUE
        XCENT=SUMX/SUMA+X-8.0
        YCENT=SUMY/SUMA+Y-8.0
C
        RETURN
         END
```

```
      SUBROUTINE CENTRD(X,Y,DATA,N,XCENT,YCENT,THRESH)
       COMPLEX DATA(N,N)
C
C     THIS SUBROUTINE PERFORMS THE CORRELATOR THRESHOLDING
C
      AMAX=-1.E30
      DO 10 I=1,N
      DO 10 J=1,N
10    AMAX=AMAX1(AMAX,REAL(DATA(I,J)))
       SUMA=0.
       SUMX=0.
        SUMY=0.
       DO 1 I=1,N
       DO 1 J=1,N
      IF(REAL(DATA(I,J)).LT.THRESH*AMAX) DATA(I,J)=0.
       SUMA=SUMA+REAL(DATA(I,J))
       SUMX=SUMX+FLOAT(J)*REAL(DATA(I,J))
1      SUMY=SUMY+FLOAT(I)*REAL(DATA(I,J))
       XCENT=SUMX/SUMA+X-8.5
       YCENT=SUMY/SUMA+Y-8.5
       RETURN
       END
```

```
      SUBROUTINE CHAQUAD(DA A,N)
      COMPLEX DATA(N,N),SAVE1,SAVE2
       N2= /2
      DO 1 I=1,
       DO 1 J=1,
      SAVE1=DATA(I,J)
      DATA(I,J)=DATA(12+I,12+J)
      DATA(12+I,12+J)=SAVE1
      SAVE2=DATA(12+I,J)
       DATA(12+I,J)=DATA(I,12+J)
      DATA(I,12+J)=SAVE2
    1 CONTINUE
      RETURN
      END
```

```
      SUBROUTINE SMOOTH(DATA,SDATA,ALPHA,N,ITERAT)
      COMPLEX DATA(N,N),SDATA(N,N)
C       THIS ROUTINE SMOOTHS RAW DATA ARRAY DATA USING EXPONENTIAL
C      SMOOTHING. WEIGHTING FACTOR ALPHA IS USED TO GENERATE THE
C      SMOOTHED DATA IN ARRAY SDATA. THE PARAMETER ITERATION IS
C      USED TO DETERMINE THE WEIGHTING FACTOR WHEN FEWER THEN
C      1/ALPHA ITERATIONS HAVE BEEN DONE.
     A=1./ITERAT
      IF(A.LT.ALPHA) A=ALPHA
1       DO 3 I=1,N
      DO 3 J=1,N
3     SDATA(I,J)=A*DATA(I,J)+(1.-A)*SDATA(I,J)
      RETURN
      END
```

```
      SUBROUTINE SPTN(SIGMAB, ,M)
      DIMENSION  (64,64),C(5)
      DATA C/.3679,.2431,.1353,.1069,.0591/
C
C        SET UP SPATIAL NOISE CORRELATION COEFFICIENT MATRIX
C        USING SECOND NEAREST NEIGHBOR CORRELATION.
C
C
C        C IS THE ARRAY CONTAINING THE NON-ZERO ELEMENTS
C        CORRESPONDING TO THE DISTANCES TO NEIGHBORING PIXELS.
C        THE ARRAY VALUES ARE EXP(-DISTANCE IN PIXELS)
C
C        SIGMAB IS THE BACKGROUND VARIANCE
C
C        R IS THE M**2 BY M**2 CORRELATION MATRIX
C
      N=M**2
      DO 30 I=1,N
      DO 30 J=1,N
      R(I,J)=0.0
 30   CONTINUE
      DO 36 I=1,N
      R(I,I)=1.
      IF (I.GE.64) GO TO 36
      R(I,I+1)=C(1)
      IF (I.GE.63) GO TO 36
       (I,I+2)=C(3)
      IF(I.GE.59) GO TO 36
       (I,I+6)=C(4)
      IF(I.GE.5   GO TO 36
      R(I,I+7)=C(2)
       IF(I.GE.57) GO TO 36
       (I,I+8)=C(1)
      IF(I.GE.56) GO TO 36
      R(I,I+9)=C(2)
      IF(I.GE.55) GO TO 36
      R(I,I+10)=C(4)
      IF(I.GE.51) GO TO 36
      R(I,I+14)=C(5)
      IF(I.GE.50) GO TO 36
      R(I,I+15)=C(4)
      IF(I.GE.49) GO TO 36
      R(I,I+16)=C(3)
      IF(I.GE.48) GO TO 36
      R(I,I+17)=C(4)
       IF(I.GE.47) GO TO 36
      R(I,I+18)=C(5)
 36   CONTINUE
      DO 37 I=1,M
      R(8*I-7,8*I)=0.0
      R(8*I-7,8*I-1)=0.0
      R(8*I-6,8*I)=0.0
       IF (I.GE.8) GO TO 37
      R(8*I,8*I+1)=0.0
      R(8*I,8*I+2)=0.0
      R(8*I-1,8*I+1)=0.0
      R(8*I-7,8*I+7)=0.0
```

```
      B(8*I-7,8*I+ )=0.0
      B(8*I-6,8*I+ )=0.0
      IF (I.GE.7) GO TO 37
      B(8*I,8*I+9)=0.0
      B(8*I,8*I+10)=0.0
      B(8*I-1,8*I+9)=0.0
      IF (I.GE.6) GO TO 37
      B(8*I,8*I+17)=0.0
      B(8*I,8*I+1 )=0.0
      B(8*I-1,8*I+17)=0.0
37    CONTINUE
      DO 38 I=1,N
      L=I+1
      DO 38 J=L,N
      IF(L.GT.N) GO TO 38
      B(J,I)=B(I,J)
38    CONTINUE
      DO 39 I=1,N
      DO 39 J=1,N
39    B(I,J)=SIGMAB*B(I,J)
      RETURN
      END
```

```
      SUBROUTINE NOISE(W,N)
      REAL W(N)
      IA=1
 1    DO 2 I=1,N
      CALL GAUSS(IA,IY,VAL)
      W(I)=VAL
      IA=IY
 2    CONTINUE
       RETURN
      END
```

```
      SUBROUTINE SHIFT(DATA,N,XSHIFT,YSHIFT)
      COMPLEX DATA(N,N),TEMP1,TEMP2,TEMP3,TEMP4,FX,FXC,FY,FYC
C         THIS ROUTINE IMPLEMENTS A SPATIAL PHASE SHIFT
C     IN THE FREQUENCY DOMAIN. THE ARRAY DATA IS ASSUMED TO BE THE
C     NXN ARRAY OF FOURIER TRANSFORM COMPONENTS AS GENERATED BY THE
C     TRANSFORM ROUTINE FOURT. FOR EXAMPLE, FOR A 6X6 ARRAY DATA
C
C               ------------------------------------------------
C               [ X0  Y0 [ X1  Y0 [ X2  Y0 [ X3  Y0 [X2*  Y0 [X1*  Y0 [
C               ------------------------------------------------
C               [ X0  Y1 [ X1  Y1 [ X2  Y1 [ X3  Y1 [X2*  Y1 [X1*  Y1 [
C               ------------------------------------------------
C               [ X0  Y2 [ X1  Y2 [ X3  Y2 [ X3  Y2 [X2*  Y2 [X1*  Y2 [
C               ------------------------------------------------
C               [ X0  Y3 [ X1  Y3 [ X2  Y3 [ X3  Y3 [X2*  Y3 [X1*  Y3 [
C               ------------------------------------------------
C               [ X0  Y2*[ X1  Y2*[ X2  Y2*[ X3  Y2*[X2*  Y2*[X1*  Y2*[
C               ------------------------------------------------
C               [ X0  Y1*[ X1  Y1*[ X2  Y1*[ X3  Y1*[X2*  Y1*[X1*  Y1*[
C               ------------------------------------------------
C
C                 PHASE SHIFTING IS IMPLEMENTED BY MULTIPLYING THE
C               FOURIER TRANSFORM COMPONENTS BY
C                        EXP(J*2*PI(FX*XSHIFT+FY*YSHIFT))
C
C               XSHIFT AND YSHIFT ARE THE SHIFTS IN THE X AND Y COORDINATE
C                DIRECTIONS.
C
C
7     PI=3.141592654
      DEM=FLOAT(N)
      NCENT=N/2+1
      DO 1 I=1,NCENT
      DO 1 J=1,NCENT
      FX=CMPLX(0.,-2.*PI*(J-1)*XSHIFT/DEM)
      FY=CMPLX(0.,-2.*PI*(I-1)*YSHIFT/DEM)
      FXC=CONJG(FX)
      FYC=CONJG(FY)
      TEMP1=DATA(I,J)
      DATA(I,J)=TEMP1*CEXP(FX+FY)
       IF(I.EQ.1) GO TO 10
      IF(J.EQ.1.OR.J.EQ.NCENT) GO TO 20
      TEMP2=DATA(I,N+2-J)
      TEMP3=DATA(N+2-I,J)
      TEMP4=DATA(N+2-I,N+2-J)
      DATA(I,N+2-J)=TEMP2*CEXP(FXC+FY)
      DATA(N+2-I,J)=TEMP3*CEXP(FX+FYC)
      DATA(N+2-I,N+2-J)=TEMP4*CEXP(FXC+FYC)
      GO TO 1
10    IF(J.EQ.1.OR.J.EQ.NCENT) GO TO 1
      TEMP2=DATA(I,N+2-J)
      DATA(I,N+2-J)=TEMP2*CEXP(FXC+FY)
      GO TO 1
20    TEMP3=DATA(N+2-I,J)
       DATA(N+2-I,J)=TEMP3*CEXP(FX+FYC)
1     CONTINUE
      RETURN
```

```
      UBROUTINE FOURT(DATA,NN,NDIM,ISIGN,IFORM,WORK)
C     FOR INFORMATION CONTACT MR. MARK HALLER 4950/ADD /56244
C
C     THE COOLEY-TUKEY FAST FOURIER TRANSFORM IN USASI BASIC FORTRAN
C
C
C     TRANSFORM(K1,K2,...) = SUM(DATA(J1,J2,...)*EXP(ISIGN*2*PI*SQRT(-1)
C     *((J1-1)*(K1-1)/NN(1)+(J2-1)*(K2-1)/NN(2)+...))), SUMMED FOR ALL
C     J1, K1 BETWEEN 1 AND NN(1), J2, K2 BETWEEN 1 AND NN(2), ETC.
C     THERE IS NO LIMIT TO THE NUMBER OF SUBSCRIPTS.  DATA IS A
C     MULTIDIMENSIONAL COMPLEX ARRAY WHOSE REAL AND IMAGINARY
C     PARTS ARE ADJACENT IN STORAGE, SUCH AS FORTRAN IV PLACES THEM.
C     IF ALL IMAGINARY PARTS ARE ZERO (DATA ARE DISGUISED REAL), SET
C     IFORM TO ZERO TO CUT THE RUNNING TIME BY UP TO FORTY PERCENT.
C     OTHERWISE, IFORM = +1.  THE LENGTHS OF ALL DIMENSIONS ARE
C     STORED IN ARRAY NN, OF LENGTH NDIM.  THEY MAY BE ANY POSITIVE
C      INTEGERS, THO THE PROGRAM RUNS FASTER ON COMPOSITE INTEGERS, AND
C     ESPECIALLY FAST ON NUMBERS RICH IN FACTORS OF TWO.  ISIGN IS +1
C     OR -1.  IF A -1 TRANSFORM IS FOLLOWED BY A +1 ONE (OR A +1
C     BY A -1) THE ORIGINAL DATA REAPPEAR, MULTIPLIED BY NTOT (=NN(1)*
C     NN(2)*...).  TRANSFORM VALUES ARE ALWAYS COMPLEX, AND ARE RETURNED
C     IN ARRAY DATA, REPLACING THE INPUT.  IN ADDITION, IF ALL
C     DIMENSIONS ARE NOT POWERS OF TWO, ARRAY WORK MUST BE SUPPLIED,
C     COMPLEX OF LENGTH EQUAL TO THE LARGEST NON 2**K DIMENSION.
C     OTHERWISE, REPLACE WORK BY ZERO IN THE CALLING SEQUENCE.
C     NORMAL FORTRAN DATA ORDERING IS EXPECTED, FIRST SUBSCRIPT VARYING
C     FASTEST.  ALL SUBSCRIPTS BEGIN AT ONE.
C
C     RUNNING TIME IS MUCH SHORTER THAN THE NAIVE NTOT**2, BEING
C     GIVEN BY THE FOLLOWING FORMULA.  DECOMPOSE NTOT INTO
C     2**K2 * 3**K3 * 5**K5 * ....  LET SUM2 = 2*K2, SUMF = 3*K3 + 5*K5
C     + ... AND NF = K3 + K5 + ....  THE TIME TAKEN BY A MULTI-
C     DIMENSIONAL TRANSFORM ON THESE NTOT DATA IS T = T0 + NTOT*(T1+
C     T2*SUM2+T3*SUMF+T4*NF).  ON THE CDC 3300 (FLOATING POINT ADD TIME
C     OF SIX MICROSECONDS), T = 3000 + NTOT*(500+43*SUM2+68*SUMF+
C     320*NF) MICROSECONDS ON COMPLEX DATA.  IN ADDITION, THE
C     ACCURACY IS GREATLY IMPROVED, AS THE RMS RELATIVE ERROR IS
C     BOUNDED BY 3*2**(-B)*SUM(FACTOR(J)**1.5), WHERE B IS THE NUMBER
C     OF BITS IN THE FLOATING POINT FRACTION AND FACTOR(J) ARE THE
C     PRIME FACTORS OF NTOT.
C
C     PROGRAM BY NORMAN BRENNER FROM THE BASIC PROGRAM BY CHARLES
C     RADER.  RALPH ALTER SUGGESTED THE IDEA FOR THE DIGIT REVERSAL.
C     MIT LINCOLN LABORATORY, AUGUST 1967.  THIS IS THE FASTEST AND MOST
C     VERSATILE VERSION OF THE FFT KNOWN TO THE AUTHOR.  SHORTER PRO-
C     GRAMS FOUR1 AND FOUR2 RESTRICT DIMENSION LENGTHS TO POWERS OF TWO.
C     SEE-- IEEE AUDIO TRANSACTIONS (JUNE 1967), SPECIAL ISSUE ON FFT.
C
C     THE DISCRETE FOURIER TRANSFORM PLACES THREE RESTRICTIONS UPON THE
C     DATA.
C     1.  THE NUMBER OF INPUT DATA AND THE NUMBER OF TRANSFORM VALUES
C     MUST BE THE SAME.
C     2.  BOTH THE INPUT DATA AND THE TRANSFORM VALUES MUST REPRESENT
C     EQUISPACED POINTS IN THEIR RESPECTIVE DOMAINS OF TIME AND
C     FREQUENCY.  CALLING THESE SPACINGS DELTAT AND DELTAF, IT MUST BE
C     TRUE THAT DELTAF=2*PI/(NN(I)*DELTAT).  OF COURSE, DELTAT NEED NOT
C     BE THE SAME FOR EVERY DIMENSION.
```

```
C      3.  CONCEPTUALLY AT LEAST, THE INPUT DATA AND THE TRANSFORM OUTPUT
C      REPRESENT SINGLE CYCLES OF PERIODIC FUNCTIONS.
C
C      EXAMPLE 1.  THREE-DIMENSIONAL FORWARD FOURIER TRANSFORM OF A
C      COMPLEX ARRAY DIMENSIONED 32 BY 25 BY 13 IN FORTRAN IV.
C      DIMENSION DATA(32,25,13),WORK(50),NN(3)
C      COMPLEX DATA
C      DATA NN/32,25,13/
C      DO 1 I=1,32
C      DO 1 J=1,25
C      DO 1 K=1,13
C    1 DATA(I,J,K)=COMPLEX VALUE
C      CALL FOURT(DATA,NN,3,-1,1,WORK)
C
C      EXAMPLE 2.  ONE-DIMENSIONAL FORWARD TRANSFORM OF A REAL ARRAY OF
C      LENGTH 64 IN FORTRAN II.
C      DIMENSION DATA(2,64)
C      DO 2 I=1,64
C      DATA(1,I)=REAL PART
C    2 DATA(2,I)=0.
C      CALL FOURT(DATA,64,1,-1,0,0)
C
        DIMENSION DATA(1),NN(1),IFACT(32),WORK(1)
C      CDC 6600 INITIALIZATION
C      WRITE(6,9000)
       WR=0.
       WI=0.
       WSTPR=0.
       WSTPI=0.
       TWOPI=6.283185307
       IF(NDIM-1)920,1,1
1      NTOT=2
       DO 2 IDIM=1,NDIM
       IF(NN(IDIM))920,920,2
2      NTOT=NTOT*NN(IDIM)
C
C      MAIN LOOP FOR EACH DIMENSION
C
       NP1=2
       DO 910 IDIM=1,NDIM
       N=NN(IDIM)
       NP2=NP1*
       IF(N-1)920,900,5
C
C      FACTOR N
C
5      M=N
       NTWO=NP1
        IF=1
       IDIV=2
10     IQUOT=M/IDIV
       IREM=M-IDIV*IQUOT
       IF(IQUOT-IDIV)50,11,11
11     IF(IREM)20,12,20
12     NTWO=NTWO+NTWO
       M=IQUOT
       GO TO 10
```

```
 20     IDIV=3
 30     IQUOT=M/IDIV
        IREM=M-IDIV*IQUOT
        IF(IQUOT-IDIV)60,31,31
 31     IF(IREM)40,32,40
 32     IFACT(IF)=IDIV
        IF=IF+1
        M=IQUOT
        GO TO 30
 40     IDIV=IDIV+2
        GO TO 30
 50     IF(IREM)60,51,60
 51     NTWO=NTWO+NTWO
        GO TO 70
 60     IFACT(IF)=M
C
C       SEPARATE FOUR CASES--
C          1. COMPLEX TRANSFORM OR REAL TRANSFORM FOR THE 4TH, 5TH,ETC.
C             DIMENSIONS.
C          2. REAL TRANSFORM FOR THE 2ND OR 3RD DIMENSION.  METHOD--
C             TRANSFORM HALF THE DATA, SUPPLYING THE OTHER HALF BY CON-
C              JUGATE SYMMETRY.
C             JUGATE SYMMETRY.
C          3. REAL TRANSFORM FOR THE 1ST DIMENSION, N ODD.  METHOD--
C             TRANSFORM HALF THE DATA AT EACH STAGE, SUPPLYING THE OTHER
C             HALF BY CONJUGATE SYMMETRY.
C          4. REAL TRANSFORM FOR THE 1ST DIMENSION, N EVEN.  METHOD--
C             TRANSFORM A COMPLEX ARRAY OF LENGTH N/2 WHOSE REAL PARTS
C             ARE THE EVEN NUMBERED REAL VALUES AND WHOSE IMAGINARY PARTS
C             ARE THE ODD NUMBERED REAL VALUES.  SEPARATE AND SUPPLY
C             THE SECOND HALF BY CONJUGATE SYMMETRY.
C
 70     NON2=NP1*(NP2/NTWO)
        ICASE=1
        IF(IDIM-4)71,90,90
 71     IF(IFORM)72,72,90
 72     ICASE=2
        IF(IDIM-1)73,73,90
 73     ICASE=3
        IF(NTWO-NP1)90,90,74
 74     ICASE=4
         NTWO=NTWO/2
        N=N/2
        NP2=NP2/2
        NTOT=NTOT/2
        I=3
        DO 80 J=2,NTOT
        DATA(J)=DATA(I)
 80      I=I+2
 90     I1RNG=NP1
        IF(ICASE-2)100,95,100
 95     I1RNG=NP0*(1+NPREV/2)
C
C       SHUFFLE ON THE FACTORS OF TWO IN N.  AS THE SHUFFLING
C       CAN BE DONE BY SIMPLE INTERCHANGE, NO WORKING ARRAY IS NEEDED
C
 100    IF(NTWO-NP1)600,600,110
```

```
 110   NP2HF=NP2/2
       J=1
       DO 150 I2=1,NP2,NON2
       IF(J-I2)120,130,130
 120   I1MAX=I2+NON2-2
        DO 125 I1=I2,I1MAX,2
       DO 125 I3=I1,NTOT,NP2
       J3=J+I3- 2
       TEMPR=DATA(I3)
       TEMPI=DATA(I3+1)
       DATA(I3)=DATA(J3)
       DATA(I3+1)=DATA(J3+1)
       DATA(J3)=TEMPR
 125   DATA(J3+1)=TEMPI
 130   M=NP2HF
 140   IF(J-M)150,150,145
 145   J=J-M
       M=M/2
       IF(M-NON2)150,140,140
 150   J=J+M
C
C      MAIN LOOP FOR FACTORS OF TWO.  PERFORM FOURIER TRANSFORMS OF
C      LENGTH FOUR, WITH ONE OF LENGTH TWO IF NEEDED.  THE TWIDDLE FACTOR
C      W=EXP(ISIGN*2*PI*SQRT(-1)*M/(4*MMAX)).  CHECK FOR W=ISIGN*SQRT(-1)
C      AND REPEAT FOR W=ISIGN*SQRT(-1)*CONJUGATE(W).
C
       NON2T=NON2+NON2
       IPAR=NTWO/NP1
 310   IF(IPAR-2)350,330,320
 320   IPAR=IPAR/4
       GO TO 310
 330   DO 340 I1=1,I1RNG,2
       DO 340 J3=I1,NON2,NP1
        DO 340 K1=J3,NTOT,NON2T
       K2=K1+NON2
       TEMPR=DATA(K2)
       TEMPI=DATA(K2+1)
       DATA(K2)=DATA(K1)-TEMPR
       DATA(K2+1)=DATA(K1+1)-TEMPI
       DATA(K1)=DATA(K1)+TEMPR
 340   DATA(K1+1)=DATA(K1+1)+TEMPI
 350   MMAX=NON2
 360   IF(MMAX-NP2HF)370,600,600
 370   LMAX=MAX0(NON2T,MMAX/2)
       IF(MMAX-NON2)405,405,380
 380   THETA=-TWOPI*FLOAT(NON2)/FLOAT(4*MMAX)
       IF(ISIGN)400,390,390
 390   THETA=-THETA
 400   WR=COS(THETA)
       WI=SIN(THETA)
       WSTPR=-2.*WI*WI
       WSTPI=2.*WR*WI
 405   DO 570 L=NON2,LMAX,NON2T
       M=L
       IF(MMAX-NON2)420,420,410
 410   W2R=WR*WR-WI*WI
       W2I=2.*WR*WI
```

```
      W3R=W2R*WR-W2I*WI
      W3I=W2R*WI+W2I*WR
420   DO 530 I1=1,I1RNG,2
      DO 530 J3=I1,NON2,NP1
      KMIN=J3+IPAR*M
      IF(MMAX-NON2)430,430,440
430   KMIN=J3
440   KDIF=IPAR*MMAX
450   KSTEP=4*KDIF
       DO 520 K1=KMIN,NTOT,KSTEP
      K2=K1+KDIF
      K3=K2+KDIF
      K4=K3+KDIF
      IF(MMAX-NON2)460,460,480
460   U1R=DATA(K1)+DATA(K2)
      U1I=DATA(K1+1)+DATA(K2+1)
       U2R=DATA(K3)+DATA(K4)
      U2I=DATA(K3+1)+DATA(K4+1)
      U3R=DATA(K1)-DATA(K2)
      U3I=DATA(K1+1)-DATA(K2+1)
      IF(ISIGN)470,475,475
470   U4R=DATA(K3+1)-DATA(K4+1)
      U4I=DATA(K4)-DATA(K3)
      GO TO 510
475   U4R=DATA(K4+1)-DATA(K3+1)
      U4I=DATA(K3)-DATA(K4)
      GO TO 510
480   T2R=W2R*DATA(K2)-W2I*DATA(K2+1)
      T2I=W2R*DATA(K2+1)+W2I*DATA(K2)
      T3R=WR*DATA(K3)-WI*DATA(K3+1)
       T3I=WR*DATA(K3+1)+WI*DATA(K3)
      T4R=W3R*DATA(K4)-W3I*DATA(K4+1)
      T4I=W3R*DATA(K4+1)+W3I*DATA(K4)
      U1R=DATA(K1)+T2R
      U1I=DATA(K1+1)+T2I
      U2R=T3R+T4R
      U2I=T3I+T4I
      U3R=DATA(K1)-T2R
      U3I=DATA(K1+1)-T2I
      IF(ISIGN)490,500,500
490   U4R=T3I-T4I
      U4I=T4R-T3R
      GO TO 510
500   U4R=T4I-T3I
      U4I=T3R-T4R
510   DATA(K1)=U1R+U2R
      DATA(K1+1)=U1I+U2I
      DATA(K2)=U3R+U4R
      DATA(K2+1)=U3I+U4I
       DATA(K3)=U1R-U2R
      DATA(K3+1)=U1I-U2I
      DATA(K4)=U3R-U4R
520   DATA(K4+1)=U3I-U4I
      KMIN=4*(KMIN-J3)+J3
      KDIF=KSTEP
      KDIF=KSTEP
      IF(KDIF-NP2)450,530,530
```

```
  530   CONTINUE
        M=MMAX-M
        IF (ISIGN)540,550,550
  540   TEMPR=WR
        WR=-WI
        WI=-TEMPR
         GO TO 560
  550   TEMPR=WR
        WR=WI
        WI=TEMPR
  560   IF(M-LMAX)565,565,410
  565   TEMPR=WR
        WR=WR*WSTPR-WI*WSTPI+WR
  570   WI=WI*WSTPR+TEMPR*WSTPI+WI
        IPAR=3-IPAR
        MMAX=MMAX+MMAX
        GO TO 360
C
C       MAIN LOOP FOR FACTORS NOT EQUAL TO TWO.  APPLY THE TWIDDLE FACTOR
C       W=EXP(ISIGN*2*PI*SQRT(-1)*(J2-1)*(J1-J2)/(NP2*IFP1)), THEN
C       PERFORM A FOURIER TRANSFORM OF LENGTH IFACT(IF), MAKING USE OF
C       CONJUGATE SYMMETRIES.
C
  600   IF(NTWO-NP2)605,700,700
  605   IFP1=NON2
        IF=1
        NP1HF=NP1/2
  610   IFP2=IFP1/IFACT(IF)
        J1RNG=NP2
        IF(ICASE-3)612,611,612
  611   J1RNG=(NP2+IFP1)/2
        J2STP=NP2/IFACT(IF)
         J1RG2=(J2STP+IFP2)/2
  612   J2MIN=1+IFP2
        IF(IFP1-NP2)615,640,640
  615   DO 635 J2=J2MIN,IFP1,IFP2
        THETA=-TWOPI*FLOAT(J2-1)/FLOAT(NP2)
        IF(ISIGN)625,620,620
  620   THETA=-THETA
  625   SINTH=SIN(THETA/2.)
        WSTPR=-2.*SINTH*SINTH
        WSTPI=SIN(THETA)
        WR=WSTPR+1.
        WI=WSTPI
        J1MIN=J2+IFP1
        DO 635 J1=J1MIN,J1RNG,IFP1
         I1MAX=J1+I1RNG-2
        DO 630 I1=J1,I1MAX,2
        DO 630 I3=I1,NTOT,NP2
        J3MAX=I3+IFP2-NP1
        DO 630 J3=I3,J3MAX,NP1
        TEMPR=DATA(J3)
        DATA(J3)=DATA(J3)*WR-DATA(J3+1)*WI
  630    DATA(J3+1)=TEMPR*WI+DATA(J3+1)*WR
        TEMPR=WR
        WR=WR*WSTPR-WI*WSTPI+WR
  635   WI=TEMPR*WSTPI+WI*WSTPR+WI
```

```
640   THETA=-TWOPI/FLOAT(IFACT(IF))
      IF(ISIGN)650,645,645
645   THETA=-THETA
650    SINTH=SIN(THETA/2.)
      WSTPR=-2.*SINTH*SINTH
      WSTPI=SIN(THETA)
      KSTEP=2*N/IFACT(IF)
      KRANG=KSTEP*(IFACT(IF)/2)+1
      DO 698 I1=1,I1RNG,2
      DO 698 I3=I1,NTOT,NP2
      DO 690 KMIN=1,KRANG,KSTEP
      J1MAX=I3+J1RNG-IFP1
      DO 680 J1=I3,J1MAX,IFP1
      J3MAX=J1+IFP2-NP1
       DO 680 J3=J1,J3MAX,NP1
      J2MAX=J3+IFP1-IFP2
      K=KMIN+(J3-J1+(J1-I3)/IFACT(IF))/NP1HF
      IF(KMIN-1)655,655,665
655   SUMR=0.
      SUMI=0.
      DO 660 J2=J3,J2MAX,IFP2
       SUMR=SUMR+DATA(J2)
660   SUMI=SUMI+DATA(J2+1)
      WORK(K)=SUMR
      WORK(K+1)=SUMI
      GO TO 680
665   KCONJ=K+2*(N-KMIN+1)
      J2=J2MAX
       SUMR=DATA(J2)
      SUMI=DATA(J2+1)
      OLDSR=0.
      OLDSI=0.
      J2=J2-IFP2
670   TEMPR=SUMR
      TEMPI=SUMI
       SUMR=TWOWR*SUMR-OLDSR+DATA(J2)
      SUMI=TWOWR*SUMI-OLDSI+DATA(J2+1)
      OLDSR=TEMPR
      OLDSI=TEMPI
      J2=J2-IFP2
      IF(J2-J3)675,675,670
675   TEMPR=WR*SUMR-OLDSR+DATA(J2)
      TEMPI=WI*SUMI
      WORK(K)=TEMPR-TEMPI
      WORK(KCONJ)=TEMPR+TEMPI
      TEMPR=WR*SUMI-OLDSI+DATA(J2+1)
      TEMPI=WI*SUMR
      WORK(K+1)=TEMPR+TEMPI
      WORK(KCONJ+1)=TEMPR-TEMPI
680   CONTINUE
      IF(KMIN-1)685,685,686
685   WR=WSTPR+1.
       WI=WSTPI
      GO TO 690
686   TEMPR=WR
      WR=WR*WSTPR-WI*WSTPI+WR
      WI=TEMPR*WSTPI+WI*WSTPR+WI
```

```
690     TWOWR=WR+WR
        IF(ICASE-3)692,691,692
691     IF(IFP1-NP2)695,692,692
692     K=1
        I2MAX=I3+NP2-NP1
        DO 693 I2=I3,I2MAX,NP1
        DATA(I2)=WORK(K)
        DATA(I2+1)=WORK(K+1)
693     K=K+2
        GO TO 698
C
C        COMPLETE A REAL TRANSFORM IN THE 1ST DIMENSION, N ODD, BY CON-
C       JUGATE SYMMETRIES AT EACH STAGE.
C
695     J3MAX=I3+IFP2-NP1
        DO 697 J3=I3,J3MAX,NP1
        J2MAX=J3+NP2-J2STP
        DO 697 J2=J3,J2MAX,J2STP
         J1MAX=J2+J1RG2-IFP2
        J1CNJ=J3+J2MAX+J2STP-J2
        DO 697 J1=J2,J1MAX,IFP2
        K=1+J1-I3
        DATA(J1)=WORK(K)
        DATA(J1+1)=WORK(K+1)
         IF(J1-J2)697,697,696
696     DATA(J1CNJ)=WORK(K)
        DATA(J1CNJ+1)=-WORK(K+1)
697     J1CNJ=J1CNJ-IFP2
698     CONTINUE
        IF=IF+1
        IFP1=IFP2
         IF(IFP1-NP1)700,700,610
C
C       COMPLETE A REAL TRANSFORM IN THE 1ST DIMENSION, N EVEN, BY CON-
C       JUGATE SYMMETRIES.
C
700     GO TO (900,800,900,701),ICASE
701     NHALF=N
         N=N+N
        THETA=-TWOPI/FLOAT(N)
        IF(ISIGN)703,702,702
702     THETA=-THETA
703     SINTH=SIN(THETA/2.)
        WSTPR=-2.*SINTH*SINTH
         WSTPI=SIN(THETA)
        WR=WSTPR+1.
        WI=WSTPI
        IMIN=3
        JMIN=2*NHALF-1
        GO TO 725
710     J=JMIN
        DO 720 I=IMIN,NTOT,NP2
        SUMR=(DATA(I)+DATA(J))/2.
        SUMI=(DATA(I+1)+DATA(J+1))/2.
        DIFR=(DATA(I)-DATA(J))/2.
        DIFI=(DATA(I+1)-DATA(J+1))/2.
        TEMPR=WR*SUMI+WI*DIFR
```

```
      TEMPI=WI*SUMI-WR*DIFR
      DATA(I)=SUMR+TEMPR
      DATA(I+1)=DIFI+TEMPI
      DATA(J)=SUMR-TEMPR
      DATA(J+1)=-DIFI+TEMPI
  720 J=J+NP2
      IMIN=IMIN+2
      JMIN=JMIN-2
      TEMPR=WR
      WR=WR*WSTPR-WI*WSTPI+WR
      WI=TEMPR*WSTPI+WI*WSTPR+WI
  725 IF(IMIN-JMIN)710,730,740
  730 IF(I IGN)731,740,740
  731 DO 735 I=IMIN,NTOT,NP2
  735 DATA(I+1)=-DATA(I+1)
  740 NP2=NP2+NP2
      NTOT=NTOT+NTOT
      J=NTOT+1
      IMAX=NTOT/2+1
  745 IMIN=IMAX-2*NHALF
      I=IMIN
      GO TO 755
  750 DATA(J)=DATA(I)
      DATA(J+1)=-DATA(I+1)
  755 I=I+2
      J=J-2
      IF(I-IMAX)750,760,760
  760 DATA(J)=DATA(IMIN)-DATA(IMIN+1)
      DATA(J+1)=0.
      IF(I-J)770,780,780
  765 DATA(J)=DATA(I)
      DATA(J+1)=DATA(I+1)
  770 I=I-2
      J=J-2
      IF(I-IMIN)775,775,765
  775 DATA(J)=DATA(IMIN)+DATA(IMIN+1)
      DATA(J+1)=0.
      IMAX=IMIN
      GO TO 745
  780 DATA(1)=DATA(1)+DATA(2)
      DATA(2)=0.
      GO TO 900
C
C     COMPLETE A REAL TRANSFORM FOR THE 2ND OR 3RD DIMENSION BY
C     CONJUGATE SYMMETRIES.
C
  800 IF(I1RNG-NP1)805,900,900
  805 DO 860 I3=1,NTOT,NP2
      I2MAX=I3+NP2-NP1
      DO 860 I2=I3,I2MAX,NP1
      IMIN=I2+I1RNG
      IMAX=I2+NP1-2
      JMAX=2*I3+NP1-IMIN
      IF(I2-I3)820,820,810
  810 JMAX=JMAX+NP2
  820 IF(IDIM-2)850,850,830
  830 J=JMAX+NP0
```

```
      DO 840 I=IMIN,IMAX,2
      DATA(I)=DATA(J)
      DATA(I+1)=-DATA(J+1)
840   J=J-2
850   J=JMAX
      DO 860 I=IMIN,IMAX,NP0
      DATA(I)=DATA(J)
      DATA(I+1)=-DATA(J+1)
860   J=J-NP0
C
C     END OF LOOP ON EACH DIMENSION
C
900   NP0=NP1
      NP1=NP2
910   NPREV=N
920   RETURN
      END
```

```
RITY  DETAILS    DIAGNOSIS OF PROBLEM

      DATA       ARRAY REFERENCE OUTSIDE DIMENSION BOUNDS.
      DATA       ARRAY REFERENCE OUTSIDE DIMENSION BOUNDS.
```

```
      SUBROUTINE GAUSS(IA,IY,VAL)
C     THIS ROUTINE CALCULATE  A GAUSSIAN DISTRIBUTED RANDOM VARIABLE
C     VAL, WITH MEAN=0. AND STANDARD DEVIATION=1.
C
C     IA IS INITIALIZED BEFORE FIRST CALL TO ANY ODD INTEGER LESS THEN
C      10 DIGITS IN LENGTH.
C     IY IS GENERATED AND SHOULD BE USED FOR IA ON THE NEXT CALL  O
C     THIS ROUTINE.
      VAL=0.
      DO 1 I=1,12
      X=RANF(DUM)
      IA=IY
        VAL=VAL+X
1     CONTINUE
      VAL=VAL-6.
      RETURN
      END
```

```
      SUBROUTINE INVERT(A,N,B,IER)
      IMPLICIT REAL (A-H,O-Z)
       DIMENSION A(1),B(1)
       REAL L(128),M(128)
      NSQ=N*N
      DO 1000 I=1,NSQ
1000  B(I)=A(I)
      D=1.0
      NK=-N
       DO 80 K=1,N
      NK=NK+N
      L(K)=K
      M(K)=K
      KK=NK+K
       BIGA=A(KK)
      DO 20 J=K,N
       IZ=N*(J-1)
      DO 20 I=K,N
       IJ=IZ+I
10    IF(ABS(BIGA)-ABS(A(IJ))) 15,20,20
15     BIGA=A(IJ)
      L(K)=I
       M(K)=J
20    CONTINUE
      J=L(K)
      IF(J-K) 35,35,25
25    KI=K-N
       DO 30 I=1,N
      KI=KI+N
      HOLD=-A(KI)
      JI=KI-K+J
      A(KI)=A(JI)
30    A(JI)=HOLD
35    I=M(K)
       IF(I-K) 45,45,38
38    JP=N*(I-1)
      DO 40 J=1,N
      JK=NK+J
      JI=JP+J
      HOLD=-A(JK)
        A(JK)=A(JI)
40    A(JI)=HOLD
45    IF(BIGA) 48,46,48
46     D=0.0
      IER=129
       GO TO 150
48    DO 55 I=1,N
       IF(I-K) 50,55,50
50    IK=NK+I
       A(IK)=A(IK)/(-BIGA)
55    CONTINUE
      DO 65 I=1,N
        IK=NK+I
      IJ=I-N
      DO 65 J=1,N
60    IF(J-K) 62,65,62
62    KJ=IJ-I+K
```

```
         A(IJ)=A(IK)*A(KJ)+A(IJ)
   65    CONTINUE
         KJ=K-N
         DO 75 J=1,N
         KJ=KJ+N
         IF(J-K) 70,75,70
   70    A(KJ)=A(KJ)/BIGA
   75    CONTINUE
         D=D*BIGA
         A(KK)=1.0/BIGA
   80    CONTINUE
         K=N
   100   K=(K-1)
         IF(K) 150,150,105
   105   I=L(K)
         IF(I-K) 120,120,108
   108   JQ=N*(K-1)
         JR=N*(I-1)
         DO 110 J=1,N
         JK=JQ+J
         HOLD=A(JK)
         JI=JR+J
         A(JK)=-A(JI)
   110   A(JI)=HOLD
   120   J=M(K)
         IF(J-K) 100,100,125
   125   KI=K-N
         DO 130 I=1,N
         KI=KI+N
         HOLD=A(KI)
         JI=KI-K+J
         A(KI)=-A(JI)
   130   A(JI)=HOLD
         GO TO 100
   150   DO 1002 I=1,NSQ
         SAVE=A(I)
         A(I)=B(I)
         B(I)=SAVE
   1002  CONTINUE
         RETURN
         END
```

```
      SUBROUTINE MULT(A,B,L,M,N,C)
      REAL A(L,M),B(M,N),C(L,N)
      DO 300 I=1,L
       DO 200 J=1,N
      C(I,J)=0.
       DO 100 INDEX=1,M
      C(I,J)=C(I,J)+A(I,INDEX)*B(INDEX,J)
  100 CONTINUE
  200 CONTINUE
  300 CONTINUE
       RETURN
      END
```

```
      SUBROUTINE CHOLY(A,N)
C     THIS ROUTINE DETERMINES THE LOWER TRIANGULAR CHOLESKY SQUARE-
C     ROOT OF AN NXN MATRIX.
C     A IS THE INPUT MATRIX AND A IS THE CHOLESKY SQUARE-ROOT MATRIX.
      DIMENSION A(N,N)
      DO 123 I=1,N
       DO 123 J=1,N
      IF(ABS(A(I,J)).GT.1.E-36) GO TO 124
123   CONTINUE
      DO 125 I=1,N
      DO 125 J=1,N
125    A(I,J)=0.
      RETURN
124    A(1,1)=SQRT(A(1,1))
      DO 5 I=2,N
      IM1=I-1
      DO 3 J=1,IM1
      JM1=J-1
      SUM=0.
       IF(J.EQ.1) GO TO 3
      DO 2 K=1,JM1
2     SUM=SUM+A(I,K)*A(J,K)
3     A(I,J)=(A(I,J)-SUM)/A(J,J)
      SUM=0.
       DO 4 K=1,IM1
4     SUM=SUM+A(I,K)**2
5     A(I,I)=SQRT(A(I,I)-SUM)
     DO 6 I=1,N
     IP1=I+1
     DO 6 J=IP1,N
6    A(I,J)=0.
     RETURN
     END
```

```
      SUBROUTINE PLTA(TIMPL,A,B,NFRAMES,NIM,I,NAME)
C
C
      INTEGER I
      REAL B(NIM),A(NIM),TIMPL(NIM)
      DIMENSION NAME(45)
C
C     THIS SUBROUTINE PERFORMS THE PLOTTING CALLS REQUIRED
C     TO PLOT THE FILTER ESTIMATED RMS ERRORS VS.THE ACTUAL
C     ERRORS
C
C
      N2=NFRAMES*2
      CALL SCALE(TIMPL,6.,N2,1)
      B(N2+1)=-.1
      B(N2+2)=1.25
      CALL AXIS(0.,0.,9HTIME(SEC),-9,6.,0.,TIMPL(N2+1),TIMPL(N2+2))
      CALL AXIS(0.,0.,13HERROR(PIXELS),13,4.,90.,B(N2+1),B(N2+2)
     +)
      CALL LINE(TIMPL,B,N2,1,0,0)
      CALL PLOT(0.,0.,3)
      A(N2+1)=B(N2+1)
      A(N2+2)=B(N2+2)
      CALL LINE(TIMPL,A,N2,1,0,0)
      CALL PLOT(-1.,-1.,-3)
      CALL PLOT(8.,0.,2)
      CALL PLOT(8.,6.,2)
      CALL PLOT(0.,6.,2)
      CALL PLOT(0.,0.,2)
      CALL SYMBOL(1.0,5.5,0.15,NAME(I),0.,36)
      CALL PLOT(0.,0.,3)
      CALL PLOT(13.,1.,-3)
C
C
      RETURN
      END
```

```
      SUBROUTINE PLTR(TIMR,A,B,C,NIM1,NFRAMES,I,NAME,
     +K,NIM,PTA,PTB,PTC,PTD)
C
      INTEGER NIM,NIM1,NFRAMES,I,K,J,N2,COUNT
      REAL TIMR(NIM1),A(4,NFRAMES),B(4,NFRAMES),C(4,NFRAMES)
      REAL PTA(NIM),PTB(NIM1),PTC(NIM1),PTD(NIM1)
      DIMENSION NAME(45)
C
C     THIS SUBROUTINE PLOTS THE MEAN ERRORS (+/-)ONE SIGMA
C     USING THE DATA FROM THE FIRST ROUTINE. THE NAMES
C     FOR THE ARRAYS WERE PREVIOUSLY STORED IN ARRAY NAME.
C
      N2=NFRAMES*2
      COUNT=1
C
C
      DO 20 J=1,NFRAMES
        PTA(COUNT)=B(I,J)
        PTA(COUNT+1)=A(I,J)
       PTB(J)=A(I,J)
        PTC(J)=B(I,J)
        PTD(J)=C(I,J)
        COUNT=COUNT+2
20    CONTINUE
      CALL SCALE(PTA,4.,N2,1)
      PTB(NFRAMES+1)=PTA(N2+1)
      PTC(NFRAMES+1)=PTA(N2+1)
      PTD(NFRAMES+1)=PTA(N2+1)
      PTB(NFRAMES+2)=PTA(N2+2)
      PTC(NFRAMES+2)=PTA(N2+2)
      PTD(NFRAMES+2)=PTA(N2+2)
      CALL SCALE(TIMR,6.,NFRAMES,1)
      CALL AXIS(0.,0.,9HTIME(SEC),-9,6.,0.,TIMR(NFRAMES+1),
     +TIMR(NFRAMES+2))
      CALL AXIS(0.,0.,13HERROR(PIXELS),13,4.,90.,PTA(N2+1),PTA(N2+2))
      CALL LINE(TIMR,PTB,NFRAMES,1,0,0)
      CALL PLOT(0.,0.,3)
      CALL LINE(TIMR,PTC,NFRAMES,1,0,0)
      CALL PLOT(0.,0.,3)
      CALL LINE(TIMR,PTD,NFRAMES,1,0,0)
      CALL PLOT(-1.,-1.,-3)
C
      CALL PLOT(8.,0.,2)
      CALL PLOT(8.,6.,2)
      CALL PLOT(0.,6.,2)
      CALL PLOT(0.,0.,2)
      IF(K.GT.22)GO TO 30
      CALL SYMBOL(1.0,5.5,0.15,NAME(K),0.,40)
      GO TO 40
30    CALL SYMBOL(.40,5.5,0.15,NAME(K),0.,50)
40    CONTINUE
C
C
C
C     MOVE PENCIL BACK TO ORIGIN
C
      CALL PLOT(0.,0.,3)
```

```
C
C      POSITION THE PENCIL FOR THE NEXT PLOT
C
       CALL PLOT(15.,1.,-3)
C
C
C
       RETURN
       END
```

Appendix E

Computer Software (Trajectory Model)

This appendix contains the Fortran source code for the implementation of the various trajectories and the multiple hot spot projection model detailed in Chapter 2. The trajectories and hot spot locations were generated and saved on file for use in the computer simulation given in Appendix D. The program was written for use on the CDC Fortran IV compiler.

```
      PROGRAM  TRAJEC(INPUT,OUTPUT,TAPE3,TAPE6=OUTPUT,DEBUG=OUTPUT,TAPE8)
      REAL UT(2,1),SVHS2A(200),SVHS2B(200),SVHS3A(200),SVHS3B(200)
      REAL SVHS1A(200),SVHS1B(200)
      REAL PULLUP
      INTEGER NFRAMES
      INTEGER CONT ,OPLANE
C
C     SET III=1 IF A PLOT OF THE INTENSITY CENTRIOD IS DESIRED
      III=2
C
C     X0,Y0,AND Z0 ARE THE INITIAL INERTIAL COORDINATES
      X0=20000.
      Y0=10000.
      Z0=30000.
C
C     SET CONT = 1 FOR THE 2G PULLUP AND CONTINUATION MANEUVER
C     (TRAJECTORY 3)
      CONT=2
C
C      SET OPLANE = 1 FOR THE OUT OF PLANE MANEUVER
C     (TRAJECTORY 4)
      OPLANE=2
C
      DT=(1./30.)
C
C     TSTART AND TFIN SET THE TIME FOR A ROLL TO START AND END
      TSTART=10.
       FIN=11.
C
      NFRAMES=155
C
C     DISV IS THE DESIRED DISTANCE IN THE EBX DIRECTION FOR HOTSPOT
C     ONE IN METERS
C     DISVP2 AND 3 ARE THE OFFSETS FOR HOTSPOTS 2 AND 3 IN THE
C     EBY DIRECTION IN METERS
C
      DISV=.1
      DISVP2=.1
      DISVP3=-.1
       IME=0.
C
C     PULLUP SETS THE TIME FOR THE PULLUP MANEUVER TO START
C     (TRAJECTORY 2)
      PULLUP=10.0
C
C     TRATE SETS THE DEGREE OF THE PULLUP MANEUVER
C     2-G=.0196,5-G=.049,AND10-G=.098
      TRATE=0.0196
C
      DO 99 NN=1,NFRAMES
C
      XDOT= -300.
      YDOT= -300.
      ZDOT= 0.0
      XPOS= X0 + XDOT*TIME
      YPOS= Y0+YDOT*TIME
      ZPOS= Z0+ZDOT*TIME
```

```
      VTIME=TIME-(DT/2.0)
      IF(TIME.LT.PULLUP)GO TO 310
      IF(CONT.NE.1)GO TO 71
      IF(NR.LT.106)GO TO 71
      IF(NR.GE.106)XDOT=-999.530
      IF(NR.GE.106)YDOT=29.063
      IF(NR.EQ.106)TIMEA=0.
C     THE XO AND YO BELOW ARE VALID FOR A 2G PULLUP AT T=3.5SEC
C     WHERE THE TARGET CONTINUES AT A CONSTANT VELOCITY AFTER THAT POINT
C
      XO=1500.2
      YO=52.295
      XPOS=XO+XDOT*TIMEA
      YPOS=YO+YDOT*TIMEA
      TIMEA=TIMEA+DT
      GO TO 72
71    CONTINUE
      IF(OPLANE.NE.1)GO TO 73
      XDOT=-1000.*COS(TRATE*(VTIME-2.))
      YDOT=1000.*COS(TRATE*(VTIME-2.))*SIN(TRATE*(VTIME-2.))
      ZDOT=-1000.*(SIN(TRATE*(VTIME-2.))**2)
      XPOS=XO-2000.-((1000/TRATE)*SIN(TRATE*(TIME-2.)))
      YPOS=YO+(1000/(2*TRATE)*(SIN(TRATE*(TIME-2.))**2))
      ZPOS=ZO-1000.*(((TIME-2.)/2.)-((1./(4.*TRATE))*SIN(2*TRATE*(TIME-2
     #.))))
      GO TO 310
73    CONTINUE
      XDOT= -1000.*COS(TRATE*(VTIME-2.))
      YDOT= 1000.*SIN(TRATE*(VTIME-2.))
      XPOS= XO-2000.-((1000/TRATE)*SIN(TRATE*(TIME-2.)))
      YPOS= YO + ((1000/TRATE)*(1.-COS(TRATE*(TIME-2.))))
72    CONTINUE
      ZPOS= ZO
310   CONTINUE
      RHOR= XPOS**2 + ZPOS**2
      RANGE= RHOR + YPOS**2
      UT(1,1)= (-ZPOS*XDOT+XPOS*ZDOT)/(RHOR*.00002)
      RHOR= SQRT(RHOR)
      UT(2,1)=(RHOR*YDOT-YPOS*((XPOS*XDOT+ZPOS*ZDOT)/RHOR))/(RANGE
     +*.00002)
      RANGE= SQRT(RANGE)
      VMAG=SQRT(XDOT**2+YDOT**2+ZDOT**2)
      VMAX=(VMAG)/(RANGE*.00002)
      CALL HSPOT(HS1A,HS1B,HS2A,HS2B,HS3A,HS3B,TSTART,TFIN,TIME,COSW
     +,XPOS,YPOS,ZPOS,XDOT,YDOT,ZDOT,DISV,DISVP2,DISVP3,
     +NR,SVHS2A,SVHS2B,SVHS3A,SVHS3B,VMAG,RHOR,RANGE,SVHS1A,SVHS1B)
      WRITE(9,*)NR,UT(1,1),UT(2,1),VMAX,COSW,RANGE,TIME
90    FORMAT(I4,6E14.5)
      WRITE(9,*)HS1A,HS1B,HS2A,HS2B,HS3A,HS3B
91    FORMAT(6E14.5)
      WRITE(7,*)XPOS,YPOS,ZPOS,XDOT,YDOT,ZDOT,TRATE
93    FORMAT(7E14.5)
      WRITE(6,92)XPOS,YPOS,ZPOS,XDOT,YDOT,ZDOT,TRATE
92    FORMAT(1X,7E14.5)
      TIME=TIME+D
99    CONTINUE
C
```

```
      IF(III.EQ.1)CALL PLTO(SVHS2A,SVHS2B,SVHS3A,SVHS3B,NFRAMES,SVHS1A,S
     +VHS1B)
C
C
      END
```

```
      SUBROUTINE PLTD(SVHS2A,SVHS2B,SVHS3A,SVHS3B,NFRAMES,SVHS1A,SVHS1B)
C
      REAL SVHS2A(200),SVHS2B(200)
      REAL SVHS3A(200),SVHS3B(200)
      REAL SVHS1A(200),SVHS1B(200),HOLD1(600),HOLD(600)
      INTEGER CT,N3
C
      N=NFRAME
      N3=NFRAMES*3
      CT=1
C
      DO 10 I=1,NFRAME
        HOLD(CT)=SVHS1A(I)
        HOLD(CT+1)=SVHS2A(I)
        HOLD(CT+2)=SVHS3A(I)
        HOLD1(CT)=SVHS1B(I)
        HOLD1(CT+1)=SVHS2B(I)
        HOLD1(CT+2)=SVHS3B(I)
      CT=CT+3
10    CONTINUE
      CALL PLOTS(0.,0.,9)
      CALL PLOT(1.,1.,-3)
      CALL SCALE(HOLD,4.,N3,1)
      CALL SCALE(HOLD1,4.,N3,1)
      SVHS2A(N+1)=HOLD(N3+1)
      SVHS2A(N+2)=HOLD(N3+2)
      SVHS2B(N+1)=HOLD1(N3+1)
      SVHS2B(N+2)=HOLD1(N3+2)
      CALL AXIS(0.,0.,28HPROJECTION ON THE ALPHA AXIS,
     +-28,4.,0.,SVHS2A(N+1),SVHS2A(N+2))
      CALL AXIS(0.,0.,27HPROJECTION ON THE BETA AXIS,
     +27,4.,90.,SVHS2B(N+1),SVHS2B(N+2))
      SVHS3A(N+1)=SVHS2A(N+1)
      SVHS3B(N+1)=SVHS2B(N+1)
      SVHS3A(N+2)=SVHS2A(N+2)
      SVHS3B(N+2)=SVHS2B(N+2)
      SVHS1A(N+1)=HOLD(N3+1)
      SVHS1A(N+2)=HOLD(N3+2)
      SVHS1B(N+1)=HOLD1(N3+1)
      SVHS1B(N+2)=HOLD1(N3+2)
C
      CALL LINE(SVHS2A,SVHS2B,N,1,-1,3)
      CALL PLOT(0.,0.,3)
      CALL LINE(SVHS3A,SVHS3B,N,1,-1,2)
      CALL PLOT(0.,0.,3)
      CALL LINE(SVHS1A,SVHS1B,N,1,-1,4)
      CALL PLOT(-1.,-1.,-3)
      CALL PLOT(6.,0.,2)
      CALL PLOT(6.,6.,2)
      CALL PLOT(0.,6.,2)
      CALL PLOT(0.,0.,2)
      CALL SYMBOL(1.70,5.3,0.15,17HINTENSITY PATTERN,0.,17
     +)
C
      CALL PLOTE
C
      RETURN
```

```
      SUBROUTINE HCPOT(HS1A,HS1B,HS2A,HS2B,HS3A,HS3B,TSTART,TFIN,TIME
     +,COSW,XPOS,YPOS,ZPOS,XDOT,YDOT,ZDOT,DISV,DISVP2,DISVP3,
     +NR,SVHS2A,SVHS2B,SVHS3A,SVHS3B,VMAG,THOR,RANGE,SVHS1A,SVHS1B)
      REAL SVHS2A(200),SVHS2B(200),SVHS3A(200),SVHS3B(200)
      REAL SVHS1A(200),SVHS1B(200)
C
C
C     ROLL SETS THE RATE OF THE CONSTANT ROLL MANEUVER
C     FOR A 360 ROLL IN 5 SECS ROLL=1.2566
      ROLL=.5
C
      ALPHA=ATAN(ZPOS/XPOS)
      BETA=ATAN(YPOS/THOR)
      VXZ2=(XDOT**2+ZDOT**2)
      SQVXZ=SQRT(VXZ2)
      SINB=SIN(BETA)
      COSA=COS(ALPHA)
      SINA=SIN(ALPHA)
      COSB=COS(BETA)
C
C
      HS1B=((DISV/RANGE)*((XDOT*SINB*(-COSA))+(YDOT*COSB)+(ZDOT*SINB*
     #(-SINA))))/(VMAG*.00002)
      HS1A=((DISV/RANGE)*((XDOT*(-SINA))+(ZDOT*COSA)))/(((VMAG))*.00002)
      IF (TIME.GT.TFIN)GO TO 63
      IF (TIME.LT.TSTART)GO TO 60
      COSW=COS(ROLL*(TIME-TSTART))
      SINW=SIN(ROLL*(TIME-TSTART))
   63 DPPV=SQRT(XDOT**4+(YDOT**2)*(XDOT**2)+(2*(
     +XDOT**2)*(ZDOT**2))+(ZDOT**2)*(YDOT**2)+(ZDOT**4))
      GO TO 61
   60 SINW=0.
      COSW=1.
      DPPV=1.
C
   61 SAVEA=((COSW*(-ZDOT))/SQVXZ)+((SINW*YDOT*XDOT)/DPPV)
      SAVEB=((SINW*YDOT*ZDOT)/DPPV)+((COSW*XDOT)/SQVXZ)
      DELA=((SAVEA)*(-SINA))+(SAVEB*COSA)
      DELB=(SAVEA*SINB*(-COSA))+((-VXZ2*SINW*COSB)/DPPV)
     #+(SAVEB*SINB*(-SINA))
C
      HS2A=(((DISVP2/RANGE)*DELA)/.00002)
      HS2B=(((DISVP2/RANGE)*DELB)/.00002)
      HS3A=(((DISVP3/RANGE)*DELA)/.00002)
      HS3B=(((DISVP3/RANGE)*DELB)/.00002)
C
C
      SVHS1A(NR)=HS1A
      SVHS1B(NR)=HS1B
      SVHS2A(NR)=HS2A
      SVHS2B(NR)=HS2B
      SVHS3A(NR)=HS3A
      SVHS3B(NR)=HS3B
C
C
      RETURN
      END
```

Vita

Paul P. Millner was born on January 31, 1952 in Danville, Virginia. He graduated from West Mecklenburg High School in Charlotte, North Carolina in June 1970 and entered the United States Military Academy at West Point in July of the same year. In June 1974, he graduated from West Point with a Bachelor of Science degree and was commissioned as an Army Air Defense officer. Military assignments include: Vulcan platoon leader and executive officer, 2nd Armored Division, Fort Hood, Texas; Redeye platoon leader, 2nd Infantry Division, Korea; Improved HAWK battery commander, 11th Air Defense Artillery Brigade, and instructor, Department of Tactics, United States Army Air Defense Artillery School, Fort Bliss, Texas. Captain Millner is a graduate of the Air Defense Artillery Officers Basic and Advanced Course. In June 1981, Captain Millner was assigned to the Air Force Institute of Technology to pursue a Masters Degree in Electrical Engineering.

Permanent address: 4226 Westridge Drive
Charlotte, N.C. 28208

```
      DO 65 J=1,
60    IF(J-K) 62,65,62
62    KJ=IJ-I+K
```